The role of carbon nanotube structure in their retention and pathogenicity in the pleural cavity

Fiona A. Murphy

Presented for the degree of Doctor of Philosophy

University of Edinburgh

2012

Abstract

Carbon nanotubes (CNT) are hexagonal arrangements of carbon atoms built up to form fibres with diameters in the nanometre range but lengths which may extend up to hundreds of microns. The physiochemical properties of CNT are advantageous for a variety of industrial applications leading to CNT becoming one of the major products in the burgeoning field of nanotechnology. However their structural similarity to asbestos has raised concerns that they may also pose an occupational inhalation hazard and cause diseases of the lung or pleura. Several decades of fibre toxicology have lead to the development of a robust structure/activity model, the fibre pathogenicity paradigm (FPP), which identifies length, thinness and biopersistence as the critical properties a fibrous particle must possess if it is to be pathogenic. The purpose of this study was to examine the pathogenicity of CNT in relation to the FPP by examining the effect of CNT in the pleural space, a target tissue for asbestos-related disease.

In order to address this aim a method of injection directly into the pleura cavity of mice was employed. Direct instillation of long and short CNT into the pleural cavity produced length-dependent responses characterized by acute inflammation leading to progressive fibrosis on the parietal pleura which mirrored the pleura response to asbestos. Furthermore examination of the size-restricted clearance mechanisms from the pleural cavity confirmed the hypothesis that the pathogenicity of long CNT and other fibres, arises as a result of length-dependent retention at the stomata on the parietal pleura.

The cellular interactions leading to an inflammatory response in the pleural cavity were also examined in an *in vitro* study which tested the CNT for their ability to stimulate the release of the acute phase cytokines from both mesothelial cells and macrophages. Direct exposure to CNT resulted in significant cytokine release from the macrophages but not mesothelial cells. This pro-inflammatory response was length dependent but modest and was shown to be a function of frustrated phagocytosis. Furthermore the indirect actions of the CNT were examined by treating the mesothelial cells with conditioned media from CNT-treated macrophages. This resulted in dramatic amplification of cytokine release from the mesothelial cells. We therefore hypothesise that long fibres elicit an inflammatory response in the pleural cavity via frustrated phagocytosis in pleural macrophages. The activated macrophages then stimulate an amplified pro-inflammatory cytokine response from the adjacent pleural mesothelial cells.

A further aim was to investigate the relationship between the length-dependent pathogenicity of a fibre sample and the surface of the fibre. By using different forms of functional groups attached to the surface of a pathogenic CNT we tested if the level of inflammation and fibrosis triggered *in vivo* can be altered by simple alteration of the surface. Our results showed that, although the surface

modification of CNT did not alter the acute inflammogenicity of the CNT, the chronic fibrotic response was significantly attenuated. The specific role surface chemistry played in the modification of the CNT pathogenicity however was obfuscated by the apparent lack of biopersistence of the functionalised CNT compared with the pristine sample.

Although direct injection into the pleural space is a convenient model to assess the hazard of fibres to the mesothelium it is not a physiologically relevant route by which workers may be exposed to CNT. Therefore we examined the inflammatory potential of CNT on the lungs and pleural cavity following pharyngeal aspiration into the airspaces. A length-dependent inflammatory response in the lungs was observed where only the long CNT sample caused acute neutrophilic inflammation at one week and progressive interstitial thickening of the alveolar septa by six weeks post exposure. Furthermore we report the induction of a length-dependent inflammatory response in the pleural cavity after exposure to CNT via the lung airspaces with concomitant evidence for the translocation of CNT from the lung into in the pleural cavity and subsequent retention along the parietal pleura.

In summary the results presented here demonstrate the length-dependent pathogenicity of CNT in the pleural cavity and highlights the necessity for risk assessment for people likely to be exposed in the workplace. We also explored mechanistic aspects of the inflammatory response to long CNT which has implications for the general understanding of fibre-related pleural disease and may prove useful for the design of safe nanofibres.

Declaration

I hereby declare that the presented thesis has been composed only by me the undersigned. The work contained within this thesis has been performed wholly by me except in certain circumstances, for which the contributors and level of contribution are clearly indicated.

I also declare that the work presented herein has not been submitted for any other degree or professional qualification.

Fiona A. Murphy

Acknowledgements

First and foremost I would like to say a huge thank you to my supervisor, Prof. Ken Donaldson who throughout my PhD has been an amazing source of help, support and knowledge! I could not have wished for better! It was a great experience carrying out this project and I am grateful that Ken allowed me to do this.

I would also like to thank Dr. Craig Poland, who from the start gave me a great insight into the world of carbon nanotubes and without all his great work before this project would not have got very far. It was great being involved in the HARN story building on the work Craig had done before and seeing the exciting ways Anja Schinwald is now taking it forward. I also want to thanks Dr. Rodger Duffin for all his brilliant help with the in vivo work.

Thanks to everyone who worked in the ELEGI lab over the course of my project for both all the help and advice over the years but also for making the lab a lovely place to work!

There are a number of people at the University of Edinburgh who technical expertise helped immensely: Bob Morris and his team for the histology work, Steve Mitchell for the preparation of samples and help with scanning electron microscopy and Shona Johnston and Fiona Rossi for help with flow cytometry. Thanks to you all.

Thanks to our collaborations, Prof Vicky Stone and Matt Boyles (Napier University), Dr. Ian Kinloch (University of Manchester), Prof. Kostas Kostarelos and Dr. Khuloud Al-Jamal (University of London), Dr. Adriele Prina-Mello and Dr. Fiona Byrne (Trinity College Dublin) and Prof. James Tour and his lab. Working with all the above has allowed me the opportunity to work with some interesting people, particles or techniques that have added immeasurably to this project!

I want to thank all my family and friends but in particular my mam and dad, Ina and John Murphy who supported me emotionally and often financially throughout this experience and without whose encouragement throughout my life I would not have made it this far!

Finally I would like to thank Fraser without whose amazing support I could not have completed this. He was with me and there for me throughout all the highs and lows, gave me encouragement when experiments weren't going so well and when it seemed like the thesis was never going to end often providing a well needed distraction! I dedicate this to you!

Contents

Table Index

Figure Index

Abbreviations

AgNW	Silver nanowire
ANOVA	Analysis of variance
AP-1	Activator protein-1
ASC	apoptosis-associated speck-like protein containing a CARD
BAL	Broncheoalveolar lavage
BED	Biologically effective dose
BSA	Bovine serum albumin
BS-SEM	Back-scatter scanning electron microscopy
CBA	Cytometric bead array
Cd	Cadmium
CNT	Carbon nanotubes
Co	Cobalt
CO_2	Carbon dioxide
Cr	Chromium
Cu	Copper
CVD	Catalytic vapour discharge
D_{ae}	Aerodynamic diamter
DIEA	diisopropylethylamine
DMPO	5,5-Dimethyl-1-Pyrroline-N-Oxide
DNA	Deoxyribonucleic acid
DPI	Diphenyleneiodonium Chloride
DPPC	Dipalmitoylphosphatidycholine
DTPA	Diethylentriaminepentaacetic
ECM	Extracellular matrix
EDTA	Ethylenediaminetetraacetic acid
EGF	Epidermal growth factor
EGFR	Epidermal growth factor receptor
ELEGI	Edinburgh lung and environment group initiative
ELISA	Enzyme-linked immunosorbant assay

EPR	Electron paramagnetic resonance
ERK1/2	Extracellular signal-regulated kinases
FBGC	Foreign body giant cell
FBS	Foetal bovine serum
Fe	Iron
FGF	Fibroblast growth factor
FPP	Fibre pathogenicity paradigm
GRO	Growth-regulated protein
GSD	Geometric standard deviation
H_2O_2	Hydrogen peroxide
HARN	High aspect ratio nanoparticle
HCl	Hydrogen chloride
HGF	Hepatocyte growth factor
HiPCO	high-pressure carbon monoxide
IARC	International Agency for Research on Cancer
ICAM-1	Intercellular adhesion molecule-1
ICP-OES	Inductively coupled plasma atomic emission spectroscopy
IGF	Insulin growth factor
IL-1b	Interleukin 1b
IL-6	Interleukin-6
IL-8	Interleukin-8
IMIG	International mesothelioma interest group
KCl	Potassium chloride
KGF	Keratinocyte growth factor
LAL	Limulus amebocyte lysate
LDH	Lactate dehyrogenase
LFA	Long fibre asbestos
LPS	Lipposaccharide
MAPK	Mitogen-activated protein kinase
MCP-1	Monocyte chemoattractant protein-1
MM	Malignant mesothelioma

MMAD	Mass mean aerodynamic diameter
MMP-1	Matrix metalloproteinase-1
Mn	Manganese
MPPD	Multiple path particle dosimetry
mRNA	Messenger ribonucleic acid
MSU	Monosodium urate
MTT	3-(4,5-Dimethylthiazol-2-yl)-2,5-diphenyltetrazolium bromide
MWCNT	Multiwalled carbon nanotube
NADPH	Nicotinamide adenine dinucleotide phosphate
NALP3	NACHT, LRR and PYD domains-containing protein 3
NEAT	Nanoparticle exposure assessment technique
NFkB	Nuclear factor kappa B
Ni	Nickel
NiNW	Nickel nanowire
NIOSH	National institute of occupational safety and health
NOEL	No observable effect limit
NPCB	Nanoparticulate carbon back
OECD	Organisation for Economic Co-operation and Development
PAI	Plasminogen activator inhibitor
PARP	Poly (ADP-ribose) polymerase
PBS	Phosphate buffered saline
PDGF	Platelet derived growth factor
PMA	Phorbol myristate
PP2A	Protein phosphatase 2
PSR	Pico Sirius red
PVC	Polyvinyl chloride
RANTES	Regulated and normal T cell expressed and secreted
ROS	Reactive oxygen species
RPMI-1640	Roswell Park Memorial Institute-1640
SAR	Structure activity relationship
SEM	Scanning electron microscopy

SFA	Short fibre asbestos
SPECT	Single-photon emission computed tomography
SV40	Simian Virus 40
SWCNT	Single walled carbon nanotube
TEG	Triethyleneglycol
TEM	Transmission electron microscopy
TF	Tissue factor
TGFb	Transforming growth factor beta
TI	Alveolar type 1 cell
Ti	Titanium
TII	Alveoalr type 2 cell
TLC	Thin layer chromotography
TMB	3,3',5,5'-Tetramethylbenzidine
TNFa	Tumour necrosis factor alpha
tPA	Tissue plasminogen activator
uPA	Urokinase plasminogen activator
UT	Untreated control
V	Vanadium
VCAM-1	Vascular cell adhesion protein 1
VEGF	Vascular endothelial growth factor
WHO	World health organisation
Z	Atomic number
Zn	Zinc

Chapter 1: Introduction

1.1 The respiratory system

1.1.1 Structure

The function of the respiratory system is to facilitate the diffusion of oxygen into the blood and the removal of carbon dioxide waste.

The respiratory system is divided into two regions, the upper respiratory tract and the lower respiratory tract. The upper respiratory tract comprises the nasal cavity, continuing over the nasopharynx and oropharynx to the larynx and the proximal end of the trachea, and conducts air from the nose down to the lower respiratory tract cavity (Figure 1.1). The primary function of the upper respiratory tract is to warm, humidify and filter the inspired air.

The lower respiratory tract extends from the trachea to the alveoli where gas exchange occurs. At the inferior border of the superior mediastinum of the thorax, the trachea bifurcates into two primary bronchi. The designated subdivisions of the respiratory tree distal to the bronchus are the bronchiole, respiratory bronchiole, alveolar duct, alveolar sac and alveolus. As the bronchi undergo progressive reduction in size through dichotomous branching, the cartilage support is eventually lost at which point the passageway is termed a bronchiole. As a smaller subdivision of the conducting tube, the bronchiole varies in size from about 0.5 to 1 mm in diameter. Distal to the smallest bronchiole (terminal bronchiole) are the respiratory bronchioles which are not present in rodents (Warheit and Hartsky, 1990). These segments of the lung mark the transition from the conducting to the respiratory passages, where oxygen and CO_2 are exchanged. The respiratory bronchiole branches to form alveolar ducts which possess alveoli that appear as outpockets of the main wall. The terminal portion of the respiratory duct gives rise to the alveolar sacs, composed of a variable number of alveoli.

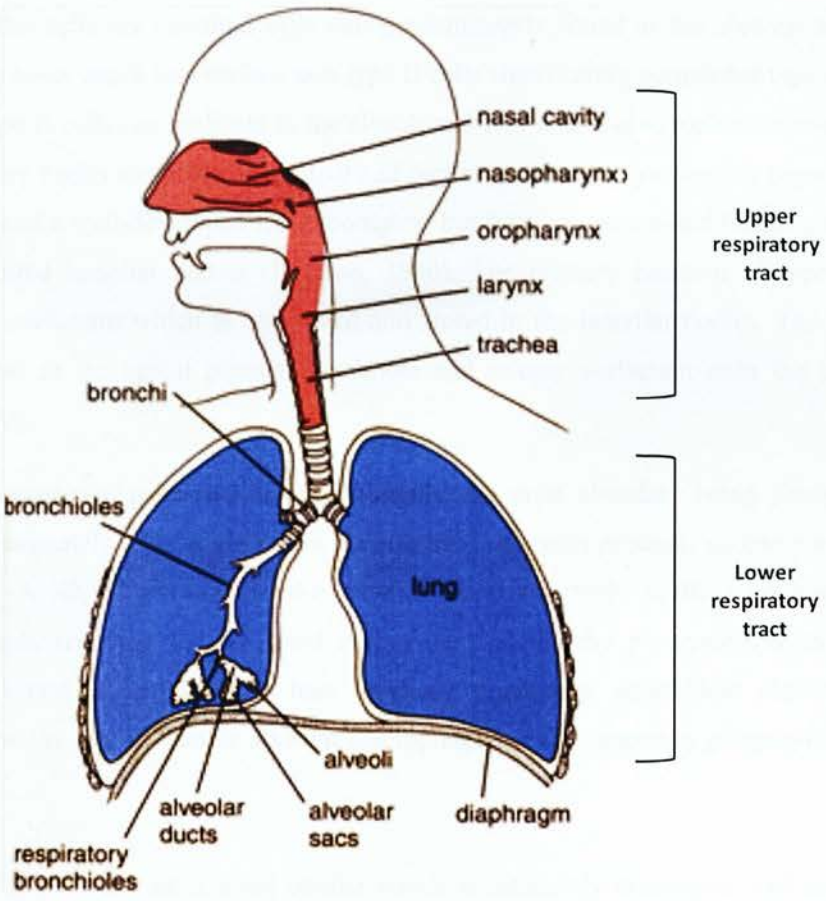

Figure 1.1: Gross anatomy of the respiratory system. Adapted from (www.anatomy.iupui.edu/respiratory.html.)

1.1.2 The alveolar region

The alveoli are the final branchings of the respiratory tree and act as the primary gas exchange units of the lung. The gas-blood barrier between the alveolar space and the pulmonary capillaries is extremely thin, allowing for rapid gas exchange. There are approximately 300 million alveoli in the human lung, which together account for 99% of the internal surface of the lung (Stone et al., 1992).

The alveoli are composed of type I and type II epithelial cells surrounded by a network of capillaries. Alveolar type I (TI) cells are very large squamous cells approximately 5400μm^2 in surface area (Stone et al., 1992). Although TI cells comprise only approximately 10% of the cells in the alveolar region, they cover 99% of the internal surface area of the lung with the remaining 2% accounted for by the type II epithelial cells (TII) (Crapo et al., 1982). The thin cytoplasmic extensions of the TI cells form the air-blood barrier essential for gas exchange. TI cells are terminally differentiated and commonly considered to be unreactive, however it has been recently been suggested that these cells may also play an important role in the regulation of cell proliferation, ion transport, modulation of macrophage function and signalling events in the peripheral lung (Berthiaume et al., 2006).

Type II alveolar cells are cuboidal cells and predominantly found at the alveolar septal junctions. Although they cover much less surface area type II cells significantly outnumber type I cells (Crapo et al., 1982). Type II cells can replicate in the alveoli and will replicate to replace damaged type I cells. Type II cells are highly metabolically active and contain numerous cytoplasmic organelles, including mitochondria and a well-developed Golgi complex, but they are most noted for the presence of large, membrane-limited lamellar bodies (Johnson, 1980). The primary function of type II cells is the production of surfactant which is assembled and stored in the lamellar bodies. The lamellar bodies carry surfactant to the apical plasma membrane and release surfactant onto the alveolar surface (Johnson, 1980).

Surfactant is composed primarily of phospholipids, the most abundant being phosphatidylcholine, although approximately 10% of surfactant is comprised of serum proteins, apoproteins and surfactant proteins (SP) –A, -B, -C and –D (Goerke, 1998; Pison et al., 1996). A film of pulmonary surfactant lines the alveoli, reducing the air-liquid surface tension thereby preventing alveolar collapse. In addition, surfactant plays a role in host defences, containing antioxidant activity and bacteria opsonising proteins which promote alveolar macrophage activity especially phagocytosis (Pison et al., 1996).

The TI and TII cells rest on a basal lamina which is intimately associated with capillaries of the pulmonary vascular system. The pulmonary artery conveys the venous blood to the lungs where it divides into branches which accompany the bronchial tubes and end in a dense capillary network in the walls of the alveoli. The pulmonary capillaries form plexuses which lie immediately beneath the lining epithelium where the thin walls allow the diffusion of gases. The minute capillaries coalesce forming pulmonary veins until finally they open into the left atrium of the heart, conveying oxygenated blood to be distributed to all parts of the body by the aorta. The bronchial arteries are derived from the thoracic aorta and supply blood for the nutrition of the lung.

Alveolar macrophages are the phagocytic cells that dwell in the surfactant layer in the alveoli. Alveolar macrophages make up approximately 5 % of the total lung cell population and occur at a frequency of approximately one macrophage per alveolus under resting conditions (Stone et al., 1992). Macrophages are the first line of defence in the lungs and play a critical role in homeostasis, host defence and the response to foreign substances, including particulates.

1.2 The Pleura

1.2.1 Structure

The lungs and inner surface of the chest wall and diaphragm are covered by a serous membrane known as the pleura. The main roles of the pleura are to reduce the friction created by the constantly

moving lungs against the chest wall and to form a coupling between the lung and chest to allow breathing.

The pleural lining covering the lungs is referred to as the visceral pleura which, at the root of the lung, folds back on itself to form the parietal pleura covering the chest wall and diaphragm. The tight fit of the lungs to the inside of the chest wall means that the two pleurae are closely apposed however they are prevented from contact by a thin film of fluid (Bouros.D, 2004). The parietal pleura can be further subdivided based on the area of the thoracic cavity it covers with the costal pleura covering the ribs and intercostal muscles, the diaphragmatic pleura associated with the diaphragm, the cervical pleura extending to the neck. The mediastinal pleura is the portion of the parietal pleural membrane that lines the mediastinum (Bouros.D, 2004).

The pleural surface is a smooth surface composed of 5 layers consisting of a single layer of mesothelial cells, a thin sub-mesothelial connective tissue layer, a thin superficial elastic layer, a loose connective tissue layer and a deep fibroelastic layer. The surface layer of mesothelial cells is referred to as the mesothelium and covers the entire surface of the three serosal cavities (pleural, pericardial and peritoneal) and, in the male, the testicular sac. The mesothelium is derived from the embryonic mesoderm around day 14 of gestation in humans (Mutsaers, 2004).

1.2.2 Pleural fluid

The pleural cavity formed between the parietal and visceral pleura is filled with a fluid layer forming a continuous barrier between the visceral and parietal pleura preventing their contact (Emilio Agostoni, 1986). Pleural fluid has several roles in the pleural cavity which are essential to health. It lubricates the pleura surface and allows the opposing pleural layers to slide against each other easily during ventilation. The pleural fluid also provides a liquid coupling between the chest wall and the lung surface enabling breathing to occur. The outward pull of the chest wall and the inward recoil of the lungs act to draw the visceral pleura away from the parietal pleura. However the pleural fluid provides the surface tension that keeps the lung surface in close apposition with the chest wall (Emilio Agostoni, 1986). As such any conditions which alter the dynamics of this pleural space can be potentially life threatening as it alters this transpulmonary pressure, potentially leading to collapsing of the lung or compressing it.

Generally pleural fluid thickness is uniform with respect to height in the thorax which is facilitated by the continuous flow of pleural fluid throughout the pleural space (Lai-Fook, 2004). Based on studies in rabbits using fluorescent micro beads a model of pleural liquid recirculation has been proposed characterised by a gravity-dependent downward flow of pleural liquid on the flat costal surfaces, an upward flow along lobar margins, and a transverse flow from lobar margins to the flat costal surfaces (Wang and Lai-Fook, 1993; Butler et al., 1995).

The normal volume of pleural fluid per unit body mass has been found to be between 0.1-0.2 ml/kg in a number of mammals (Agostoni and Zocchi, 2007). Consistent with these findings a study by Noppen et al estimated that the total pleural volume in normal, non-smoking humans is approximately 0.26 ml/kg (Noppen et al., 2000).

In all mammals, pleural liquid is generated as a filtrate from capillaries in the parietal pleura lining the chest wall (Lai-Fook, 2004). In small animals with thin visceral pleura a small amount of pleural liquid might be reabsorbed by pulmonary capillaries underlying the visceral pleura, otherwise drainage of pleural liquid from the pleural space occurs via lymphatic stomata in the parietal pleura (Lai-Fook, 2004). Stomata are between 2-8 μm in diameter and are predominately found in the dorsal caudal intercostal spaces and to a lesser degree in the ventro-cranial region of the pleura (Wang, 1975). There are limited recordings of the dimensions of human parietal pleural stomata (Li, 1993) but across mammalian species there is a remarkable constancy in the reported size of stomata (Shinohara, 1997; Wang, 1975; Miura et al., 2000). The stomata open to the sub-mesothelial lymphatic capillaries which terminate in dilations called lacunae. These lacunae are covered with a loose layer of connective tissue called the macula cribriformis, forming a sieve-like structure which supports covering mesothelial cells (Miura et al., 2000). The lymphatic stomata frequently possess valve-like structures which consist of projections of lymphatic endothelial flaps and prevent retrograde flow of fluid from the lymphatic channel (Lai-Fook, 2004). Pleural fluid volume is strictly controlled and maintained at a minimum, to ensure the maximum intrathoracic expansion of the lungs, by the ability of the draining lymphatics to markedly increase draining flow in response to increased filtration (Miserocchi, 2009).

The cellular content of normal pleural fluid is made up predominately of macrophages (75%) and lymphocytes (23%). Free-floating mesothelial cells and granulocytes may also be present albeit low in number (Noppen et al., 2000). Pleural fluid also contains a low concentration of protein, approximately 1.5g/dl which mostly consists of albumin (Lai-Fook and Houtz, 2007; Noppen et al., 2000).

1.2.3 Mesothelial cells

The mesothelium is predominately composed of flat squamous-like mesothelial cells up to 25 μm in diameter however mesothelial cells with a cuboidal morphology are also found in specific regions including 'milky spots' and overlaying the lymphatic lacunae (Mutsaers, 2004). Cuboidal mesothelial cells contain well-developed rough endoplasmic reticulum, well-developed Golgi complexes, rich mitochondrial complexes and numerous ribosomes suggesting these cells are metabolically active. Conversely squamous mesothelial cells have few mitochondria, poorly developed Golgi apparatus and

little endoplasmic reticulum (Mutsaers, 2004). Mesothelial cells are unique as although they are derived from the mesoderm and expresses the mesenchymal intermediate filaments vimentin and desmin, they also express cytokeratins which are intermediate filaments characteristic of epithelial cells (Larocca and Rheinwald, 1984).

Connections between adjacent mesothelial cells are mainly via tight junctions which are crucial for the development of cell surface polarity although other forms of junction such adherens junctions and desmosomes also occur (Mutsaers, 2002).

A primary function of mesothelial cells is to provide a protective barrier against abrasion and invading pathogens. The luminal surface of the mesothelium is lined with a carpet of microvilli which vary in size and density dependent on mesothelial cell phenotype and location. Microvilli serve to trap hyaluronan, a glycosaminoglycan produced by the mesothelial cells which acts as a boundary lubricant (Arai et al., 1975). An increase in secretion of hyaluronan is thought to occur in activated or damaged cells, potentially as a defence mechanism against the action of lymphocytes and prevents adhesion formation (Mutsaers, 2002). Similar to alveolar type II cells mesothelial cells also contain lamellar bodies and secrete phosphotidylcholine to aid lubrication between the serosal surfaces. The presence of layers of phospholipids on the mesothelium may also serve to prevent contact between the parietal and visceral pleurae as polar groups on the opposing surfaces repel each other (Miserocchi, 2009).

Mesothelial cells play an important role in the induction and resolution of inflammation and tissue repair in the pleural cavity through secretion of cytokines, growth factors, matrix, proteases, and other inflammatory mediators (Mutsaers, 2002).

1.3 Particle Lung Interactions

During the process of ventilation the respiratory system will inevitably come into contact with a considerable quantity of airborne particulate matter. The mechanisms by which inhaled particles are dealt with are largely determined by the region of the respiratory tract in which the particles deposit.

1.3.1 Deposition

There are five significant modes of particle deposition in the respiratory tract, namely impaction, sedimentation, diffusion, interception in the case of fibres, and in the case of charged particles, electrostatic precipitation (Gehr et al., 2000). Impaction is the inertial deposition of a particle onto an airway surface when the airflow changes course but particles maintain their trajectory and impact on the airway wall. Impaction is the main mechanism by which particles with an aerodynamic diameter ≥

0.5 μm deposit in the upper respiratory tract and tracheobronchial bifurcations. Sedimentation occurs in response to gravity where the particles settle due to their mass and is an important deposition mechanism for particles with diameters ≥ 0.5 μm which reach the respiratory zone where airflow is minimal. Particles with a diameter ≤ 0.5 μm are influenced by diffusion and are moved randomly by Brownian motion which may result in particle contact with the airway wall. The probability of deposition by diffusion increases with increasing particle residence time within the airway. Interception is important for fibres as whilst their centre of gravity may follow the airstream, their ends may contact the sides of the airway causing the fibre to deposit. Whilst the probability of deposition by interception increases with increasing fibre length, deposition by impaction or sedimentation is more influenced by fibre diameter.

The site and extent of particle deposition in the respiratory tract is dependent on a number of factors including physical characteristics of the particles, geometry of the respiratory tract and breathing pattern (Heyder, 2004). Figure 1.2 demonstrates the effect of particle size on the zone of deposition as the respiratory tract is subdivided into the head airways, the trachea-bronchial regions and the pulmonary region. There is a peak of deposition of large particle (~10μm) which represents the impaction of large particles in the naso-pharyngeal region of the respiratory tract (Heyder, 2004). As particle size decreases into the respirable range to a size which can penetrate the alveoli, deposition in the pulmonary region increases. The sub-micron size range shows the largest peak of deposition in the pulmonary region. Extremely small ultrafine particles show significant deposition in the trachea-bronchial region of due to turbulent diffusion. The deposition probability for particles with geometric diameters ≥ 0.5 μm is governed largely by their aerodynamic diameter whereas for smaller particles the probability of deposition is more closely related to the diffusion equivalent diameter (Gehr et al., 2000).

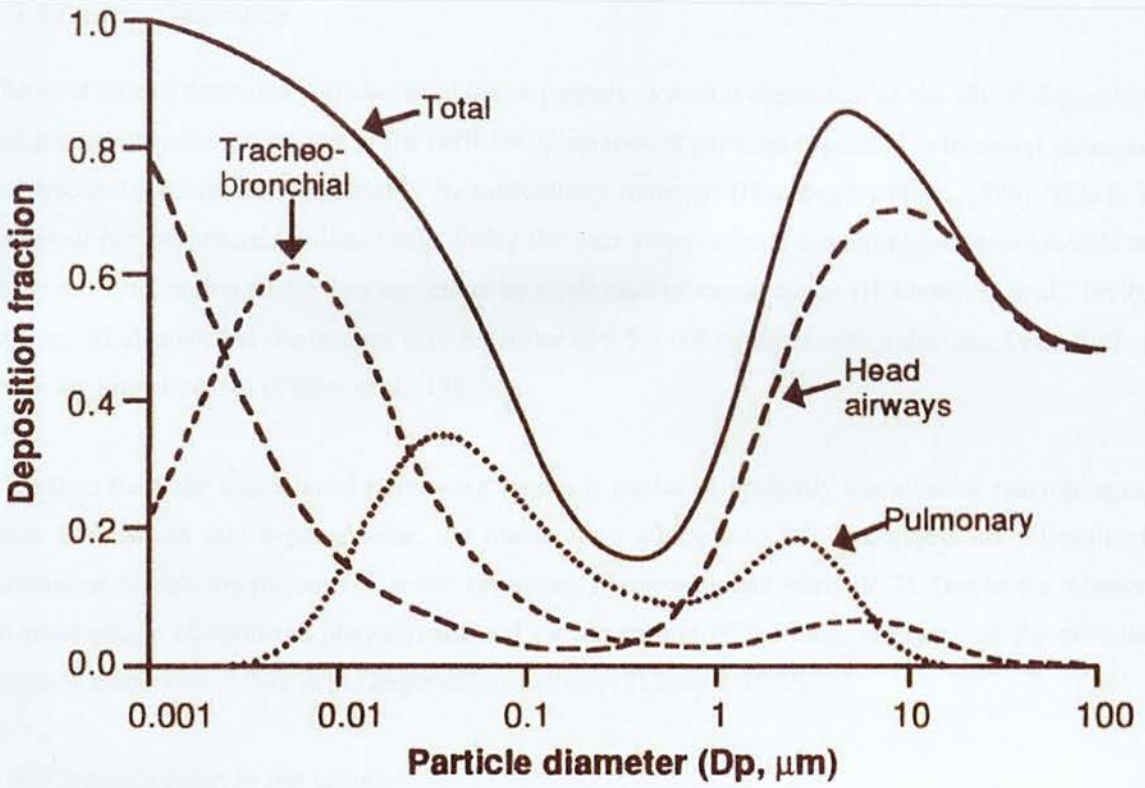

Figure 1.2: Deposition of particles in the human respiratory tract. The fractional particle deposition in the different regions of human respiratory tract based on particle size. Reproduced from Gehr, Brand & Heyder, 2000.

1.3.2 Deposition of a fibre

A fibre is defined by the WHO as a particle with a length greater than 5 μm, a diameter less than 3 μm and a length to width ratio of greater than 3:1 (WHO, 1997). The principal factor governing the respirability and deposition of a fibre is its aerodynamic diameter (D_{ae}) (Sturm and Hofmann, 2009). The aerodynamic diameter of a particle is defined as the diameter of a unit density (1 g/cm^3) sphere with the same settling speed as the particle of interest (Sturm and Hofmann, 2009). In simple terms the aerodynamic diameter of an irregularly shaped object is the same as the diameter of a perfect sphere with a density of 1 g/cm^3 which falls at the exact same rate as the irregularly shaped object.

In a laminar flow of air, a fibre aligns itself axially due to the airflow across the fibre surface allowing it to travel along aligned with the airways. Therefore the aerodynamic diameter of a fibre is dependent on the fibre's actual diameter with fibre length only playing a minor role as such length has little impact on the deposition of a fibre except which it is sufficient to cause interception. Because of this fibres with a small D_{ae} but many times longer than the cut-off diameter for a spherical particle can deposit in the alveolar region of the respiratory system. In a study by Jones the ratio of aerodynamic diameter to geometric diameter was determined to be approximately 2.5-3 over a wide range of aspect ratios (Jones, 1993).

1.3.3 Particle Clearance

The clearance of deposited particles from the respiratory system is dependent on the site of deposition and physicochemical properties of the particles. Clearance of particles deposited in the nasal passages and tracheobronchial tree is primarily by mucociliary transport (Houtmeyers et al., 1999). This is a continual process whereby ciliated cells lining the tract sweep mucus containing particles towards to the oropharynx region where they can either be swallowed or expectorated (Houtmeyers et al., 1999). The rate of clearance in the trachea is of the order of 5.5 ± 0.4 mm/min with a decreased rate further down the bronchial tree (Yeates et al., 1981).

Clearance from the non-ciliated pulmonary region is mediated primarily via alveolar macrophages. Once internalised into a phagosome, the macrophage attempts to kill and digest the internalised bacteria or particle via fusion with acidic lysosomes (Armstrong and Hart, 1971). Due to the reliance on macrophage chemotaxis, phagocytosis and movement out of the lung, clearance in the alveolar region is much slower than in the larger ciliated airways (Lehnert, 1992).

1.3.4 Translocation to the pleura

Although the exact mechanism of fibre translocation from the lung to the pleural space is unknown there is a body of literature which suggests a proportion of all particles that deposit in the distal regions of the lung translocate to the pleural space. A study carried out by Mitchev *et al* on healthy individuals showed the presence of 'black spots', benign areas of particle accumulation, on the parietal pleura in 92.7 % of a cohort of 150 urban dwellers examined at autopsy (Mitchev et al., 2002). A greater accumulation of black spots has been noted on the parietal pleural surface of miners reflecting their higher exposure levels to coal dust (Muller et al., 2002). Black spots represent areas of particle accumulation where a proportion of inhaled particles translocated from the lung to the pleural space and became interstitialised in the parietal pleura of the chest wall as they are in the process of being cleared.

The mechanism of translocation from the distal regions of the lung to the pleural space is not well understood. The penetration of subpleurally-deposited carbon nanotubes through the visceral pleura into the pleural space after aspiration exposure has been seen by Mercer *et al* suggesting a direct route of translocation (Mercer et al., 2010). This is supported by Bernstein *et al* who demonstrated the penetration of long asbestos fibres into the pleural space after inhalation exposure using a non-invasive, in situ examination of the lungs and pleural space obtained from freeze-substituted tissue in deep frozen rats (Bernstein et al., 2011). Alternative routes of translocation have also been proposed including the primary translocation of fibres into the blood or lymphatic system from where they can potentially move to any area of the body including the pleural space (Miserocchi et al., 2008). It has

been suggested that the translocation is possibly driven by the increased pulmonary interstitial pressure and aided by the enhanced permeability of the visceral pleura due to asbestos-induced inflammation (Miserocchi et al., 2008).

1.4 Asbestos

1.4.1 Structure

Asbestos is a generic term referring to six types of naturally occurring silicate mineral fibres that are or have been commercially exploited. These fibres belong to two mineral groups: serpentine and amphiboles. The serpentine group contains a single asbestiform variety: chrysotile, which has a fibrillar, thread-like appearance. The amphibole asbestos fibres consist of five forms of needle-shaped fibres namely anthophyllite asbestos, amosite asbestos (grunerite), crocidolite asbestos (riebeckite), tremolite asbestos, and actinolite asbestos. Of these derivations of asbestos, only crocidolite, amosite and chrysotile were industrially exploited to a significant degree with tremolite asbestos featuring as a common contaminant of other minerals such as chrysotile and talc (Virta, 2002).

The basic building blocks of asbestos fibres are the silicate tetrahedra. The structure of amphibole asbestos is that of two ribbons of silicate tetrahedra positioned back to back. The crystal structure has sixteen cationic sites that can host a large variety of metal cations without substantial disruption of the lattice (Virta, 2002). Chrysotile is in the form of a silicate sheet, rolled into a spiral shaped fibril. Between these sheets exists a layer of a magnesium hydroxide named brucite ($Mg_6O_4(OH)_8$) which shares oxygen atoms with the silicate layers. The diameter of the individual fibrils is 20-50 nm although these are commonly in groups and can be millimetres in diameter and up to 10 cm in length (Virta, 2002). The silicate nature of asbestos imbues the fibres with a number of physicochemical properties including high tensile strength, low electrical conductivity, flexibility and resistance to heat and chemical degradation.

All types of asbestos have associated iron cations which may promote the formation of highly reactive hydroxyl free radical ($HO^{\bullet}$) from hydrogen peroxide (H_2O_2) as described by the Fenton reaction.

$$Fe^{2+} + H_2O_2 \rightarrow Fe^{3+} + HO^- + HO^{\bullet}$$

Amphibole fibres such as crocidolite and amosite have high iron content present as an integral component of their crystalline structure. Chrysotile has a lower iron content which is primarily present as a surface contaminant (Kamp et al., 1992). Consequently crocidolite and amosite have a greater ability to produce $HO^{\bullet}$ than chrysotile (Shukla et al., 2003a).

1.4.2 History of asbestos

The history of asbestos usage can be traced as far back as approximately 2500 BC where it was used to reinforce clay utensils and pottery (Tweedale, 2002). However the modern era of asbestos usage began in the late 19th century when asbestos began to be exploited on an industrial scale. The insulating and fire-proof properties of asbestos were exploited for a vast array of applications including insulation for ships and brakes, clutches and gaskets for the newly developed automobile industry. Asbestos fibres were also widely used in domestic products including furnishings and ironing board covers. World War II supported the growth of asbestos fibre production for military applications, typically in thermal insulation and fire protection, applications which were subsequently extended into the areas of residential and industrial construction. The worldwide production of asbestos fibres reached a maximum in 1977 of 5 million tons however the identification of health risks associated with exposure to asbestos fibres lead to a large reduction in the usage of asbestos fibres and by the year 2000 the world production levels had decreased to less than 2 million tons (Virta, 2002).

The highest exposure to asbestos fibres is to those involved in the mining, milling and processing the raw asbestos and therefore asbestos exposure is largely considered an occupational hazard. However a number of environmental exposure pathways have also been identified with increases in airborne asbestos fibre counts found in areas surrounding asbestos mines or factories making asbestos-based products (Hillerdal, 1999; Hansell, 2008). There is also the potential for exposure during the renovation or demolition of buildings containing high levels of asbestos. The importance of non-occupational exposure routes is reflected in the numerous epidemiological studies which report the development of asbestos-related disease such as mesothelioma in populations with no known occupational exposure (Hillerdal, 1999).

The first definitive report on the development of disease due to asbestos exposure was published in the British Medical Journal in 1924 (Cooke, 1924). The condition described as type of severe pulmonary fibrosis was coined 'asbestosis' by Thomas Oliver in 1925 (Bartrip, 2004). In 1928 Edward Merewether, a medical inspector based in Glasgow, was instructed to perform a large scale investigation into the relationship between workers' exposure to asbestos and the development of pulmonary fibrosis and his final report concluded there was a 'definite occupational risk among asbestos workers as a class'(Bartrip, 2004). In the 1950s a causal link between lung cancer and asbestos exposure was confirmed by Richard Doll. In his study into the mortality of asbestos workers, Doll found that of a cohort of 105 asbestos workers, 18 developed lung cancer, 15 of which were associated with asbestosis (Doll, 1993). Even with the confirmed health risks it was believed that industrial hygiene measures would prove effective in preventing disease development. Indeed the implementation of health controls in asbestos factories and the subsequent reduction in the number of asbestosis cases suggested that this was a move which was effective in controlling the disease

(Bartrip, 2004). However it was soon realised that the hazards associated with asbestos dust were not confined to heavily exposed workers in asbestos factories but extended to insulation workers, other users of products containing asbestos and people who lived close to asbestos factories. It was the evidence for a causal relationship between asbestos exposure and the development of a previously rare cancer of the pleural and peritoneal mesothelium; mesothelioma, that eventually lead to the decline of the asbestos industry. In 1960 Wagner, Sleggs and Marchand published their first paper indicating a relationship between pleural mesothelioma and asbestos exposure which was based on the incidence of mesothelioma cases in the crocidolite mining district of Griqualand West, South Africa. The article connected asbestos with mesothelioma and also suggested that non-occupational exposure might cause the disease (Wagner et al., 1960). Papers published in 1964 and 1965 resulted in the general medical recognition of mesothelioma as an asbestos related disease (Tweedale, 2002). Regulations were subsequently introduced to limit the maximum exposure of airborne fibres in workplace environments (Asbestos Regulations Act, 1969). In 1987 IARC designated asbestos fibres as a Group 1 carcinogen for humans and consequently, a complete ban the import and use of all types of asbestos fibres was implemented in many Western countries in the 1990s (Bartrip, 2004).

1.5 Asbestos-related disease

Exposure to asbestos fibres may lead to the development of a number of pathologies affecting both the lungs and the pleural or the peritoneal cavities.

1.5.1 Asbestosis

Asbestosis is defined as bilateral diffuse interstitial fibrosis of the lungs and is associated with high levels of exposure to asbestos (Mossman and Churg, 1998). A fibre burden geometric mean of 10 $x10^6$ fibres/g of dry lung has been shown to be assosciated with asbestosis development in shipyard workers (Churg and Vedal, 1994). Pulmonary function tests in advanced disease reveal asbestosis is a restrictive condition characterised by a reduction of the vital capacity and lung compliance (Kilburn and Warshaw, 1991). The clinical and physiological symptoms of asbestos are similar to other forms of pulmonary fibrosis but a differential diagnosis can be made with the identification of asbestos fibres which are often surrounded by an iron-protein coating, so called asbestos bodies. In advanced asbestosis honeycombing is common.

Both inflammation and fibrosis occur in a dose-dependent fashion after inhalation exposure to asbestos and as such a number of cytokines and growth factors have been implicated in the pathogenesis of asbestosis (Mossman and Churg, 1998). Platelet-derived growth factor (PDGF) is a growth factor that stimulates the migration and proliferation of fibroblasts (Bonner et al., 1991). Levels of PDGF mRNA have been shown to be increased following inhalation exposure to chrysotile asbestos (Liu et al., 1997). Similarly levels of transforming growth factor beta (TGFβ) which

upregulates genes involved in collagen synthesis, have been shown to increase in at sites of developing fibrotic lesions (Perdue and Brody, 1994).

The generation of reactive oxygen species (ROS) by asbestos fibres has been shown in several systems including both cell-free production of ROS by asbestos fibres and phagocyte-derived oxidative stress as a result of uptake by cells (Liu et al., 2000). ROS generated by asbestos fibres has been demonstrated to convert latent TGFβ to its active form which is a potent upregulator of genes involved in collagen and fibronectin biosynthesis (Pociask et al., 2004). The presence of iron has been shown to increase oxidative stress within cells, both in culture and in vivo via the generation of hydroxyl radicals by Fenton chemistry as a consequence of redox cycling between ferrous and ferric states (Kamp and Weitzman, 1999). The use of an iron chelator, phytic acid, to reduce the iron content of a sample of amosite asbestos was shown to significantly reduce the inflammatory and fibrotic responses in rats two weeks after a single intratracheal instillation highlighting the importance of oxidative stress is the pathogenesis of asbestosis (Kamp et al., 1995).

1.5.2 Lung cancer

Lung cancer is also associated with exposure to pathogenic fibres and estimates place asbestos as being related to 2-3% of all lung cancer deaths between 1980 and 2000 in the UK (Darnton et al., 2006). The exact incidence of asbestos-related lung cancer is difficult to quantify due to the numerous other factors which are known to cause lung cancer, clinically indistinguishable from those not caused by asbestos.

There is an apparent relationship between the development of lung cancer and asbestosis attested to by numerous epidemiological studies suggesting that persons suffering from asbestosis are at excess risk of developing lung cancer (Hughes and Weill, 1991; Nurminen and Tossavainen, 1994). This link between fibrosis and lung cancer is also evident in animal studies where rats were exposed to asbestos and other mineral fibres by inhalation. It was noted that animals with pulmonary tumours had double the amount of fibrosis than animals that did not develop tumours (Davis and Cowie, 1990).

1.5.3 Malignant Mesothelioma

Malignant mesothelioma is a fatal tumour originating from the mesothelial lining of the pleural and to a lesser degree the peritoneal cavities. The main risk factor for mesothelioma development is asbestos exposure however in rare instances mesothelioma can occur in patients who have undergone radiation therapy, chronic pleural inflammation or infection (Carbone et al., 2002). Mesothelioma has a long latency period where clinical symptoms often only begin to manifest 20-40 years after exposure to asbestos (Carbone et al., 2002). In the UK, the number of cases of mesothelioma is projected to peak

in the year 2020 with somewhere between 2700 and 3300 cases per year reflecting the high exposure levels experienced by workers during the height of the asbestos industry in the 1960's and 1970's (Peto et al., 1995).

There are three classifications of mesothelioma dependent on the predominant mesothelioma cell phenotype, namely epithelioid, sarcomatoid and biphasic. Epithelioid tumours are the most common (50-70%) and have a less severe prognosis than sarcomatoid or biphasic types (Van Gelder et al., 1994).

The clinical staging of mesothelioma in the pleural cavity, as set out by the International Mesothelioma Interest Group (IMIG), describe early stage tumour development (T1a) as involving only the parietal pleura covering the chest wall and diaphragm with no involvement of the visceral pleural surrounding the lung. T1b describes a slightly more advanced tumour that involves all pleural surfaces but only minimal involvement of the visceral pleura (Rusch, 1996). The distinction between T1a and T1b is based on a study by Boutin et al who staged the development of mesothelioma by thoracoscopic examination and showed that involvement of the parietal pleura alone was associated with 32 months survival whereas when tumours were also seen on the visceral pleura survival time was shortened to 7 months (Boutin et al., 1993). The initiation of mesothelioma along the parietal pleural suggest the key fibre effects leading to mesothelioma development will take place at this site rather than the visceral pleural surrounding the lung which only becomes involved in the progression of the disease. Only at the end stage of disease is blood bore metastasis observed (Rusch, 1996).

Genetic analysis of mesothelioma have detected frequent deletions of specific regions in the short (p) arms of chromosomes 1, 3 and 9 and the long (q) arms of 6, 13, 15 and 22 (Murthy and Testa, 1999; Yang et al., 2008). Mutations is certain tumour suppressor genes located in these chromosomal regions have been implicated in the development and progression of mesothelioma. *CDKN2A/ARF* located at chromosome band 9p21 encodes the tumour suppressors p16INK4a, a cyclin-dependent kinase inhibitor, and p14ARF, a component of the p53 cell cycle checkpoint (Hirao et al., 2002). Therefore loss of *CDKN2A/ARF* may impair both the retinoblastoma (Rb) and p53 tumour suppression pathways. The NF2 gene, present on chromosome 22 is also frequently altered in mesothelioma. The NF2 product, Merlin, represses cyclin D1 expression so a loss of NF2 expression will lead to cell cycle progression due to an upregulation of cyclin D1 (Xiao et al., 2005).

The molecular mechanisms leading to mesothelial cell transformation and the development of mesothelioma are unclear. Fraire et al suggest that there may be a gradual progression from mesothelial hyperplasia to mesothelioma, with intermediate stages characterised by the presence of fibrous adhesions and pleural nodular lesions (Fraire et al., 1997) thus highlighting the likely role for chronic inflammation in mesothelioma carcinogenesis as discussed further below.

Simian virus 40 (SV40) is a DNA monkey virus that is considered a co-carcinogen with asbestos exposure in the development of mesothelioma (Carbone et al., 2002). A study carried out by Kroczynska exposed hamsters to asbestos and/or SV40 and assessed the development of mesothelioma (Kroczynska et al., 2006). SV40 alone did not cause mesothelioma whereas 20% of hamsters developed mesothelioma after treatment with asbestos alone. However upon treatment with both asbestos and SV40 mesothelioma was seen in 90% of the hamsters suggesting the fibres and SV40 can act as co-carcinogens (Kroczynska et al., 2006). SV40 produces two proteins namely Large T antigen (Tag) and small T antigen (tag). In human mesothelioma biopsies Tag was found to bind to and inhibit p53 and pRb tumour suppressor proteins (Bocchetta and Carbone, 2008). Tag has also been shown to activate the gene promoter for insulin growth factor I (IGF-I) thereby leading to enhanced cell growth (Bocchetta et al., 2008). Small tag inhibits the cellular phosphatase 2A (PP2A), an inhibitor of the mitogen-activated protein kinase (MAPK) pathway. Therefore through inhibition of PP2A, tag can activate MAPK signalling which may in turn induce the activator protein-1 (AP-1) transcription factor which regulates cell proliferation and survival (Yang et al., 2008).

Mesothelioma is extremely difficult to treat. Although single-modality therapy using traditional approaches of surgery, chemotherapy or radiotherapy alone has failed to improve patient survival significantly, multimodality approaches which involve pleurectomy with sequential chemotherapy and radiography have demonstrated improved survival (Jaklitsch et al., 2001). However regardless of treatment strategy, median survival time from initial presentation to death is only 9 to 17 months (van der et al., 2012). Novel therapies which focus on immune modulation, disruption of protein synthesis and process or gene therapy are currently being explored and may provide better therapeutic options for patients with mesothelioma in the future (Tsao et al., 2009).

1.5.4 Pleural plaque

Plaques are typically bilateral and are usually found on the lower portions of the posterior parietal pleura and on the diaphragm thus corresponding to regions with a high abundance of draining stomata (Roberts, 1971). Microscopically most plaques are acellular or sparsely cellular and demonstrate a basket-weave pattern of collagen. Plaques may become calcified over time. The surface of the plaque is sometimes covered by a single layer of mesothelial cells but can also appear uncovered (Roberts, 1971). Although plaques are generally confined to the same areas of the parietal pleura as where mesothelioma is believed to originate, pleural plaques are not considered a pre-malignant lesion. They remain benign and self-limiting and rarely cause morbidity (Chapman et al., 2003).

Fibrosis involving the visceral pleura is generally referred to as diffuse pleural thickening (Gevenois et al., 1998). In contrast to pleural plaques which are highly specific for asbestos exposure diffuse

pleural thickening can result from a variety of conditions affecting the pleura and often occurs as a consequence of pleural effusion (Gevenois et al., 1998).

1.5.5 Pleural effusion

Pleural effusion occurs when there is a build up of fluid within the pleural space, typically in excess of 15-20 ml due to an imbalance between the influx and efflux of pleural fluid (Owens and Milligan, 1995). Pleural effusions can occur as a benign pleural effusion which is sometimes bloody and may resolve spontaneously or be recurring (Peacock et al., 2000). Malignant pleural effusions can also occur as a complication of mesothelioma as well as other forms of cancer such as lung and breast cancer. Therefore pleural effusions are not restricted to asbestos exposure and can be as a result of other causes such as pulmonary embolism or complications from certain drug therapies (Kalomenidis and Light, 2004).

1.6 Inflammation in the pleural cavity

Inflammation and changes in the delicate homeostatic balance of the pleural space can be initiated by introduction of foreign cells, microbes or asbestos as well as by mechanical disruption of the mesothelial monolayer. The onset of pleural infections and injury is characterised by a massive influx of leukocytes from the vascular compartment into the pleural space which may be initiated by interaction of the inflammatory stimulus with the surface of the mesothelial cells or via activation of the patrolling pleural macrophages (Mutsaers et al., 2004). Mesothelial cells play a pivotal role in conducting the inflammatory response which is coordinated by an interconnected network of chemokines and cytokines such as interleukin-8 (IL-8), a potent neutrophil chemoattractant (Visser et al., 1995a). Activated macrophages also stimulate mesothelial cells to release factors which act as monocyte chemoattractants such as growth-related oncogene (GRO)-α, monocyte chemoattractant protein (MCP-1) and regulated-on-activation normal T-cell expressed and secreted (RANTES) (Mutsaers et al., 2004). Other early inflammatory mediators released by mesothelial cells include interleukin-1 beta (IL-1β) and tumour necrosis factor alpha (TNFα) which may act to enhance IL-8 and MCP-1 chemoattractants (van, V et al., 1998). By secreting chemokines in a polarized manner, mesothelial cells create a chemotactic gradient thereby promoting the influx of inflammatory leukocytes into the pleural cavity (Li et al., 1998). Movement of leukocytes from the circulation to the site of inflammation is further facilitated by the expression of integrins and adhesion molecules such as intercellular adhesion molecule (ICAM-1), vascular cellular adhesion molecule (VCAM-1), E-cadherin, N-cadherin, CD49a, CD49b and CD29 (Mutsaers, 2004). The primary function of both neutrophils and monocytes recruited to the site of inflammation is phagocytosis and neutralisation of the inciting agent which may involve the release of oxidants and proteases. The release of oxidants during an inflammatory response may cause tissue damage in the surrounding microenvironment further perpetuating the response. Oxidants play important roles in the initiation of numerous signal

transduction pathways that are linked to apoptosis, inflammation, and proliferation (Kamp and Weitzman, 1999).

In response to injury mesothelial cells can release a host of growth factors, including TGFβ, PDGF, fibroblast growth factor (FGF), hepatocyte growth factor (HGF) and epidermal growth factor (EGF), as well as extracellular matrix (ECM) proteins (Mutsaers, 2004). Proliferation of mesothelial cells to resurface a denuded mesothelium can occur from the edge of the wound as in epithelial wound healing but also from the incorporation of free-floating mesothelial cells onto the wound surface (Foley-Comer et al., 2002). Mesothelial regeneration requires factors expressed by macrophages (Mutsaers et al., 2002). As demonstrated by Mutsaers et al depletion of circulating monocytes significantly delayed serosal healing whereas addition of peritoneal exudate cells to the wound site 36 hours before injury increased the healing rate (Mutsaers et al., 2002).

During the early stages of normal wound repair the deposition and subsequent turnover of fibrin precedes complete regeneration of the mesothelial layer. However if the normal healing process is impaired fibrin persists and subserosal fibroblasts migrate into the fibrin matrix and deposit collagen eventually forming scar tissue. Mesothelial cells have both procoagulant and fibrinolytic activity (Mutsaers, 2002) controlling the fine balance between fibrin deposition and breakdown in serosal cavities. The pro-coagulant activity is due to tissue factor (TF) which along with activated factor VII initiates the formation of transitional fibrin. Fibrin deposition is also aided by the secretion of plasminogen activator inhibitors (PAI), PAI-1 and PAI-2. Fibrinolysis is mediated through secretion of the plasminogen activators, tissue plasminogen activator (tPA) and urokinase (uPA) which convert the inactive zymogen plasminogen into active plasmin which in turn enzymatically breaks down fibrin (Jantz and Antony, 2008). Both pro- and anti-fibrinolytic mediators can be regulated by inflammatory factors including TNFα, IL-1β and TGFβ which have been shown to induce increased PAI-1 and decreased tPA concentrations in an in vitro mesothelial cell assay (Whawell and Thompson, 1995; Falk et al., 2000). This modified PAI-1/tPA secretion profile will lead to a significant delay of fibrinolysis. TGFβ also plays an important role in extracellular matrix (ECM) production with overexpression of TGFβ found to be a consistent abnormality in most fibrotic disease (Jagirdar et al., 1996). Following stimulation by TGFβ, mesothelial cells can synthesize collagen and matrix proteins. In addition to enhanced ECM production, overexpression of TGFβ decreases the production of matrix degrading enzymes; matrix metalloproteinases (MMP-1). Mesothelial cells can also produce high levels of growth factors which are mitogenic for fibroblasts; TGFβ, FGFβ and PDGF which may also contribute to the development of fibrosis (Mutsaers, 2002).

1.6.1 Asbestos and chronic inflammation

The molecular mechanisms leading to the development of asbestos-related disease are not yet fully elucidated however disregulated inflammatory and repair processes are widely accepted to play an important role.

As discussed above, the generation of oxidants, either intrinsically by the fibres themselves or during phagocytosis by alveolar macrophages and other cell types, may be responsible for the initiation of cell signalling and inflammatory events (Kamp and Weitzman, 1999). In pleural mesothelial cells, crocidolite asbestos caused phosphorylation and activation of extracellular signal-regulated kinases (ERK 1/2) in an oxidant dependent manner (Zanella et al., 1996). ERK1/2 activation leads to the transactivation of multiple transcription factors such as AP-1 which promotes cellular responses such as proliferation, apoptosis or inflammation (Ramos-Nino et al., 2002b). Asbestos-induced ERK activation was shown to be due in part to oxidative stress as demonstrated by the blockage of signalling cascade activation by the antioxidants, catalase or Nacetyl- L-cysteine, and by chelation of surface iron from crocidolite fibres (Jimenez et al., 1997)

Asbestos fibres may interact directly with surface receptors triggering these pathways e.g. epidermal growth factor receptor (EGFR) (Pache et al., 1998). The asbestos-mediated auto-phosphorylation of EGFR activated the ERK signalling cascade leading to apoptosis, cell proliferation or inflammation. Furthermore the chronic asbestos induced activation of ERK1/2 has been linked to the induction of fra-1 a component of the AP-1 complex that is causally related to anchorage-independent growth in mesothelial cells (Ramos-Nino et al., 2002a) which may be important in mesothelial cell transformation.

Nuclear factor-kappa B (NF-κB) is another redox sensitive transcription factor that regulates expression of genes involved in inflammation and cell proliferation (Janssen-Heininger et al., 2000). Activation of the NFκB signalling pathway by asbestos-mediated oxidative stress regulates the expression of pro-inflammatory cytokines, IL-6 and IL-8 thereby contributing to the chronic inflammatory state (Shukla et al., 2003b). The NF-κB signalling pathway has also been shown to be activated in mesothelial cells by the asbestos-induced release of TNFα, which can act in an autocrine and paracrine fashion (Yang et al., 2006). This has led the authors to propose that the activation of NF-κB and subsequent activation of multiple prosurvival genes allows mesothelial cells with asbestos-induced DNA damage to divide and proliferate rather than die and, if key genetic alterations accumulate, to eventually develop into mesothelioma.

The generation of ROS either by the fibres themselves or during the pro-oxidant milieu can act as mutagens with the potential to cause multiple genotoxic effects including point mutations, DNA strand breaks and large chromosomal deletions. DNA damage induced by $HO^{\bullet}$ occurs either by

hydrogen abstraction or via addition of HO• to the DNA (Chatgilialoglu and O'Neill, 2001). The sensitivity of mesothelial cells to asbestos damage has been proposed to be due to their greater susceptibility than epithelial cells of the respiratory tract to DNA damage (Nygren et al., 2004). This, in turn has been suggested to be due possibly to lower levels of glutathione in mesothelial cells than alveolar epithelial cells (3.5 fold) making mesothelial cells less resistant to oxidative stress. These studies however were performed using cell lines which may have altered glutathione levels in comparison to primary cells (Puhakka et al., 2002).

A number of growth factors and cytokines have been implicated in asbestos carcinogenesis including TGF-β which binds to and activates EGFR, and PDGF, a potent mesothelial cell mitogen. Insulin-like growth factor (IGF), hepatocyte growth factor (HGF) and keratinocyte growth factor (KGF) function as autocrine growth factors in normal and MM cells, which may promote tumour proliferation, cell migration and tumour invasiveness (Liu and Klominek, 2004; Adamson et al., 2000). Vascular endothelial growth factor (VEGF) which plays an important role in tumour angiogenesis is also produced by mesothelioma cells (Shukla et al., 2003b).

1.7 The fibre pathogenicity paradigm

A structure/activity relationship (SAR) relates the physical or chemical structure of a test substance to its biological activity. The biological properties of a new material can therefore be inferred from properties of similar existing material whose hazards are already known (McKinney et al., 2000). A SAR describing the pathogenic characteristics of a fibre, known as the fibre pathogenicity paradigm (FPP), emerged late in the 20th century as a result of several decades of fibre research (Donaldson et al., 2010). The FPP identifies dose, fibre dimensions and biopersistence as the most important factors contributing to the toxicity of a fibre sample (Donaldson et al., 2010). The FPP is the most robust SAR in the field of particle toxicology as it has held true for every fibre type tested to date including different forms of asbestos, synthetic vitreous fibres and glass fibres. Therefore the FPP could similarly help to identify those CNT (as well as other high aspect ratio nanoparticles) that may pose a health hazard (Donaldson et al., 2011).

1.7.1 Dose

When contemplating the toxicity of fibres, as with all substances, the most important consideration is dose, as an absence of dose means an absence of effect.

Dose differs from exposure in that exposure may be defined as the presence of particles found in the external environment surrounding the body whereas the dose is the exposure of the internal environment of the body. The biological effective dose (BED) is a further subdivision and refers to

the fraction of a total dose to which the body is exposed that drives an adverse effect. In the field of particle toxicology the BED differs considerably depending on the particle of interest. For example the pathogenicity of quartz is dependent on its highly reactive surface therefore the BED relates to the surface area of the quartz particles to which a person is exposed rather than the mass or particle number (Duffin et al., 2001). In the case of pathogenic fibres the BED is the proportion of the total dose that is biopersistent and long enough to prevent clearance and stimulate a pathogenic response as discussed in detail below.

1.7.2 Fibre dimensions

Stanton performed some of the early experiments leading to the generation of the FPP by assessing the role of fibre characteristics in mesothelioma using implantation of fibres in gelatin, directly onto the pleural mesothelial surface. A range of 72 experiments were conducted using a wide variety of respirable and durable minerals ranging in fibre dimensions and chemical properties (Stanton et al., 1981). The resulting development of tumours correlated with fibre attributes based on length and biopersistence. Specifically they found that fibres that measured > 8 μm in length and < 0.25 μm in diameter correlated well with the formation of malignant mesothelioma whereas short fibres were not tumorigenic (Stanton et al., 1981). The importance of fibre length has also been identified in numerous experimental set-ups including the more physiologically relevant inhalation exposure. In a study by Davis et al rats were exposed in a chamber to clouds with equal airborne mass concentration of either long amosite asbestos fibre or short fibre amosite. After lifetime exposure there was substantial tumour formation and fibrotic response in those rats exposed to the long amosite but virtually no response in rats exposed to the short amosite (Davis et al., 1986a). Most recently studies by Schinwald et al have used nanofibres in tight length classes to demonstrate a threshold of 5 μm for retention and inflammation in the pleural space of mice (Schinwald et al., 2012a).

The mechanism by which long fibres elicit a pathogenic response is proposed to be via disruption of macrophage-mediated clearance from the lung or pleura space. The elutriating effects of the lung help to restrict the pulmonary deposition of foreign material to a size that can comfortably be phagocytosed by macrophages however fibres present an exception. As discussed above a low aerodynamic diameter will allow deposition of fibres beyond the ciliated airways in the pulmonary regions of the lung where clearance is mediated by alveolar macrophages. However if fibres exceed the maximal length a macrophage can enclose (~15 μm) the macrophage will be unable to successfully removed the fibre and become 'frustrated'. The act of becoming 'frustrated' leads to the release of various toxic components primarily involved in the microbiocidal activity of the cells as part of the innate immune defence (Brown et al., 2007).

An important mechanism by which macrophages kill invading pathogens is the formation of an oxidative burst. The oxidative burst is characterised by an increase in cellular oxygen consumption followed by the generation of superoxide free radicals (O_2^-) which results from the activation of NADPH oxidase that catalyses the one-electron reduction of oxygen to superoxide at the expense of NADPH.

$$2O_2 + NADPH \rightarrow 2 \cdot O_2^- + NADP^+ + H^+$$

The $\cdot O_2^-$ product is unstable and quickly undergoes another reduction to hydrogen peroxide (H_2O_2), either spontaneously or in a much faster reaction catalysed by superoxide dismutase:

$$2 \cdot O_2^- + 2H^+ \rightarrow H_2O_2 + O_2$$

O_2^- and H_2O_2 are used as starting materials for the production of oxidising halogens and free radicals which are microbiocidal. Whilst this process, in the case of bacterial killing, occurs internally with ROS being released into the bacteria containing phagosome, if the macrophage is 'frustrated' ROS may be released into the extracellular environment (Bergstrand, 1990).

Lysosomal enzymes can similarly be released from the macrophages under the conditions of frustrated phagocytosis. Lysosomal enzymes are synthesized in the endoplasmic reticulum and packaged by the Golgi apparatus into structures called primary lysosomes. These primary lysosomes fuse with phagosomes containing ingested materials to form phagolysosomes, however if the phagosome is not fully internalised as is the case in frustrated phagocytosis the lysosome contents will be release outside the cell (Hornung et al., 2008; Halle et al., 2008).

The activation of the NALP3 inflammasome has been implicated in the increased release of mature IL-1β during frustrated phagocytosis of asbestos, silica and monosodium urate crystals. The NALP3 inflammasome controls the maturation and release of IL-1β from activated cells by binding caspase-1 via an associated protein linker known as ASC (apoptosis-associated speck-like protein containing a carboxy-terminal CARD) which subsequently cleaves pro-IL-1β to produce the mature form which is then secreted (Tschopp and Schroder, 2010). Triggering of this event has been suggested to be caused by destabilisation of the formed phagolysosomes during the ingestion of material. This destabilisation can lead to the release of lysosomal enzymes such as cathepsin B which has been hypothesised to trigger the activation of the inflammasome (Halle et al., 2008). Combined, the increase in reactive oxygen species, the release lytic enzymes and the up-regulation of pro-inflammatory factors serves to generate a destructive and pro-inflammatory environment in the biological milieu surrounding the deposition of long fibres.

The retention of long fibres in the pleural and peritoneal cavities is also likely to be responsible for the selective pathogenicity of long fibres (Donaldson et al., 2010). There are two pathways by which particles or fibres may be cleared from the pleural cavity, passively in the flow of pleural fluid through the stomata in the parietal pleura to the lymphatics or by active uptake by pleural macrophages. Excessive fibre length can prevent efficient clearance by both mechanisms. Firstly as the stomata connecting the pleural space to the lymphatics are size restricted, fibres which exceed the calibre of the stomatal openings (2-8 μm) will be retained in the pleural space. Secondly the removal of long fibres by pleural macrophages will face the same difficulties as the alveolar macrophages and result in a state of 'frustrated phagocytosis'. Studies from Agnes Kane's group were the first to critically examine the role for size restricted clearance mechanisms in the pathogenesis of fibre-related pleural disease. Moalli et al demonstrated the retention of long fibres invoked an intense inflammatory reaction (Moalli et al., 1987). This was associated with mesothelial cytotoxicity and regeneration at the periphery of asbestos fibre clusters. It was hypothesised that repeated episodes of injury and regeneration might promote the development of mesothelioma.

1.7.3 Biopersistence

Clearance of a fibre from the lung or pleural space is also dependent on the potential of the fibres to dissolve away, in whole or in part, in biological fluid. A fibre that undergoes weakening and breakage in the lungs is termed non-biopersistent. This occurs if structural elements are leached from the fibre in the presence of lung fluids which results in breakage of long fibres into shorter fragments which are more easily cleared therefore causing a reduction of dose. If the rate of clearance exceeds deposition in the lung the dose experienced will not accumulate to the critical threshold for adverse effects to manifest.

There are a number of examples where a lack of biopersistence has rendered a long fibre sample low in hazard. Chrysotile asbestos is less biopersistent than the amphiboles and this may explain why chrysotile has been found to be low in pathogenicity in human epidemiological studies (Bernstein and Hoskins, 2006). The 'rolled sheet' structure of chrysotile is much more fragile than the silicate double chains of the amphiboles and can break. The brucite (Mg^{2+}) layer can dissolve in water or the lung fluid, and the remaining structure is attacked in an acid environment such as is encountered with the macrophage (Virta, 2002). Deterioration of the chrysotile surface can result in the loss of the structural integrity of the fibre and disintegration. The lack of durability of a chrysotile fibre is reflected in lung burden studies. In a study on a cohort of miners it was found that despite the main exposure being to chrysotile asbestos with only tremolite being a minor contaminant, chrysotile and tremolite were found in roughly equal quantities in the lung (McDonald et al., 1997). This suggests that exposure to low levels of biopersistent tremolite lead to a cumulative build up of dose whilst the dissolution of chrysotile led to a reduction in retained dose over time. Similarly studies examining the

potential toxicity of synthetic fibre show that even when the exposure cloud is rich in long fibres there is little or no pathogenicity provided the fibres are non-biopersistent (Donaldson, 2009). P-aramid is a manufactured fibre composed of synthetic polyamide which is used as an advanced composite and in fabrics. Although fibrils of p-aramid can be long and thin they are not biopersistent as demonstrated by a number of inhalation studies reporting an apparent increase in the short fibre pool in the lung accompanied by depletion of the long fibre pool (Donaldson, 2009). Thus the hazard associated with the inhalation of p-aramid is low which is supported by animal studies showing only a transient inflammatory response to the inhalation of p-aramid but no sustained pathological changes.

To fully examine the biopersistence of a fibre requires lengthy in vivo experiments. However, fibre durability, the chemical mimicking of fibre dissolution in vitro is more readily determined. Searl et al assessed the relative biopersistence of nine mineral fibre types in the lung up to one year after intratracheal instillation and also measured the ability of the test materials to resist dissolution in a parallel series of simple in vitro acellular experiments (Searl et al., 1999). Comparison between the in vivo and in vitro results showed that differences in persistence of long fibres in the lung were correlated with measured rates of dissolution in vitro (Searl et al., 1999).

Figure 1.3 summarises the requirement for both length and biopersistence for the build-up of dose in the body until a critical threshold is reached and harmful effects begin to manifest. If either length or biopersistence of the fibre is removed then the fibre can be cleared from the body resulting in a reduction of biologically effective dose.

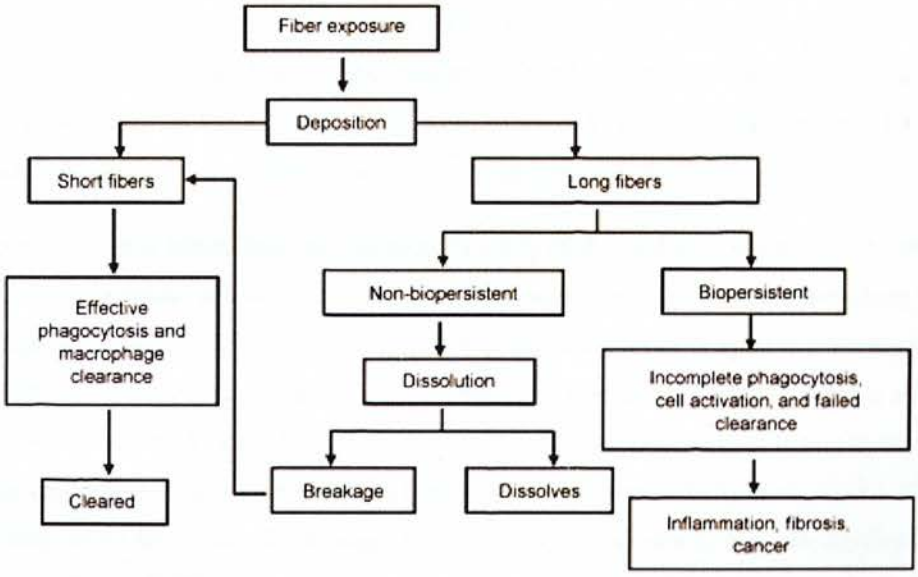

Figure 1.3: Paradigm for the role of long fibres and biopersistence in the pathogenic effects of fibres. Reproduced from Donaldson et al 2006.

1.7.4 Surface reactivity

The FPP describes fibre pathogenicity as being irrespective of chemical make-up of the fibre, except in so far as the composition makes a contribution to biopersistence. However the FPP only describes the basic requirements for pathogenicity; chemical composition or surface reactivity may have additive effects and increase fibre potency. There is evidence that some fibre samples such as erionite and silicon carbide whiskers have specially enhanced pathogenicity. Erionite, a naturally occurring fibrous zeolite, has been implicated in the high prevalence of mesothelioma in certain regions of Turkey (Carbone et al., 2007), and has been demonstrated in animal studies to have a greater carcinogenic potential than crocidolite and chrysotile. The increased surface area of erionite compared to crocidolite and the accumulation of iron on the surface of erionite resulting in the production of ROS are considered to play a role in the greater potency of erionite (Dogan et al., 2008).

1.8 Carbon Nanotubes

Carbon nanotubes are a form of engineered nanomaterial with unique properties making them desirable for a wide range of industrial applications. Although nanotubes have been identified as early as 1889 and visualised by a number of scientists since, the rediscovery of CNT by Ijima in 1991 (Iijima, 1991) lead to the current boom in the understanding of the properties of nanotubes and their potential as an industrially useful material.

1.8.1 Structure and properties

Carbon nanotubes are composed of a lattice of hexagonal carbon atoms rolled into a cylinder. They can be classified as one of three forms, single walled CNT (SWCNT), double-walled CNT or multi-walled CNT (MWCNT) dependent on the number of CNT cylinders concentrically stacked inside each other. In addition to variations in their wall number, CNT can differ in their length, shape, surface modification, purity and their propensity to form agglomerates and aggregates.

In the carbon nanotubes lattice each carbon atom is connected covalently to three other carbon atoms held at a 120° angle from each other in the XY plane resulting in a sp^2 bonding structure where each atom is connected evenly to three carbons in the XY plane and a weak pi bond is present in the Z axis. The free electrons in the pZ orbital move within this cloud and are no longer local to a single carbon atom. The associated weak Van der Waals forces cause weak interactions between adjacent CNT which cause difficulties in dispersing the CNT into individual fibres (Tasis et al., 2006). The strength of CNT results from the stable bond angle between the carbon atoms and the covalent sp^2 bonds formed between the individual carbon atoms. A MWCNT was tested to have a tensile strength of 63 gigapascals which translates to the ability to endure tension of a weight equivalent to 6422 kg on a cable with a cross section of $1mm^2$ (Yu et al., 2000).

A CNT can be imagined as a graphene sheet rolled at a certain 'chiral' angle with respect to a plane perpendicular to the tubes long axis. Tubes with a chiral angle of 30 are called 'armchair' and those with a chiral angle of 0 are known as zigzag (Figure 1.4). The chirality of the CNT determines the electrical properties of the CNT with the armchair form considered metallic and the zigzag form considered semi-conducting.

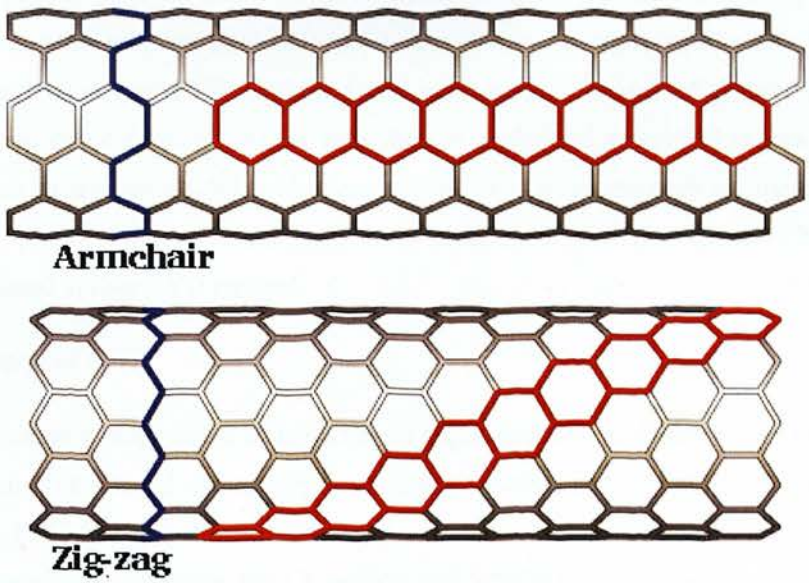

Figure 1.4: Schematic diagram of atomic arrangement of an armchair or zigzag CNT.

Topological defects in the hexagonal arrangement of carbon atoms, for example the Stone-Wales defect where four hexagons are changed into two pentagons and two heptagons, can cause weakening of the CNT mechanical strength (Tasis et al., 2006). The introduction of pentagon-heptagon pair defects into the hexagonal network can change the chirality of the CNT and fundamentally alter its electronic structure. Structural defects may also result in elongation or compression of one side of the CNT causing it to bend. This deformation may dictate how a CNT will present itself, as a fibre or a curled spherical particle and therefore will have implications for the toxicity testing of the CNT in relation to the FPP. Defects in the CNT backbone that result in the presence of free bonds may also be important in toxicity due to increased reactivity (Muller et al., 2008).

1.8.2 Synthesis

A number of methods are being employed in the synthesis of CNT (Awasthi et al., 2005). The Arc Discharge method involves striking an arc between graphite electrodes in an inert atmosphere (argon or helium). The formation of an arc in the current between the adjacent electrodes causes vaporisation of the carbon electrode leading to the self assembly of CNT on the opposite electrode. It is a discontinuous and unstable process and cannot produce large quantities of CNT. However it does

produce structurally excellent, high quality CNT. In the method known as laser ablation a piece of graphite target is vaporised by laser irradiation under high temperature in an inert atmosphere resulting in the formation of carbon atoms which condense to form structures such as carbon nanotubes as they rapidly cool. The quality and yield depend on the reaction temperature. This method is not considered economically advantageous due to the requirement for high purity graphite rods and high laser power. The chemical vapour deposition (CVD) method involves growing CNT by decomposing an organic gas over a substrate covered with metal catalyst particles. Rather than using a solid carbon feed stock the CVD method feeds in a gaseous source of carbon such as carbon monoxide. The use of a catalyst allows the formation of predefined arrays and shapes and lends itself well to formation of straighter CNT with more control over attributes such as diameter and length. This method is commonly used in the large scale production of CNT. All MWCNT used in this project are produced via the CVD method.

1.8.3 Applications of CNT

Due to their remarkable properties a wide variety of applications for CNT have been identified. These applications span a number of diverse fields including material science, electronics and biomedical science (Figure 1.5). The global CNT industry turned over $668.3 million in 2010 with MWCNT production value of approximately $631.5 million and SWCNT production value of $36.8 million. The market value is forecast to grow to $1.1 billion by 2016 (www.nanowerk.com). The exponential growth of the industry greatly increases the possibility of exposure to CNT.

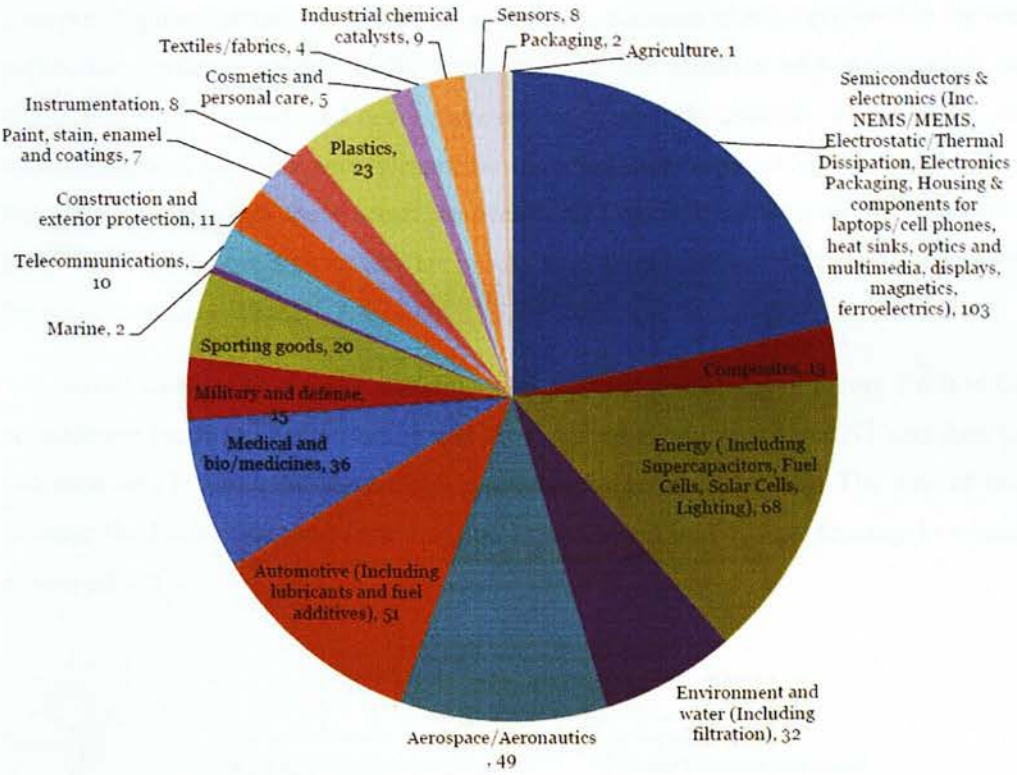

Figure 1.5: Current applications for CNT. The figures indicate the number of CNT companies developing products in that end user market. Future Markets, Inc 2011.

1.9 The toxicology of CNT

Although CNT are becoming more widely used in many applications, little is known to date with regards their potential to cause harm to human health. CNT have three properties that are clearly associated with particles pathogenicity: their large surface area, they are fibre-shaped and therefore have the potential to behave like pathogenic fibres and finally, they are graphitic in nature and so expected to be biopersistent (Donaldson et al., 2006). In light of the fibrogenic and carcinogenic potency of asbestos fibres and the health and socio-economical tragedies caused by unregulated asbestos utilization, the increasing development and uses of CNT have triggered concern about their potential toxicity, particularly in relation to the structural similarities to asbestos. This sentiment was summed up in the seminal Royal Society and Royal Academy of Engineering 2004 report, Nanoscience and nanotechnology: opportunities and uncertainties, which stated: 'Given previous experience with asbestos, we believe that nanotubes deserve special toxicological attention' (Royal Society and Royal Academy of Engineering, 2004). These concerns have stimulated researchers in the field of particle toxicology to critically assess the risks associated with exposure to CNT.

This pre-emptive approach is in contrast to the more common process involved in the identification of pathogenic particles which initially starts with the identification of a pathological condition in a workforce who handled and were exposed to a specific particle, followed by comprehensive epidemiological, exposure and mechanistic studies (Donaldson and Seaton, 2012). For the emerging field of nanotoxicology the process has been turned on its head with efforts focussed on predicting particle toxicity before the particles are produced in significant quantities and before there is evidence for particle-induced disease.

The overall strategy for the risk assessment of CNT as summarised in Figure 1.6 is to simultaneously examine the hazard to human health and the potential for exposure to CNT and then integrate these two data sets in order to characterise risk (Aschberger et al., 2010). The aim of this study is to increase the knowledge base regarding the hazard posed by CNT particularly in relation to adverse pleural effects.

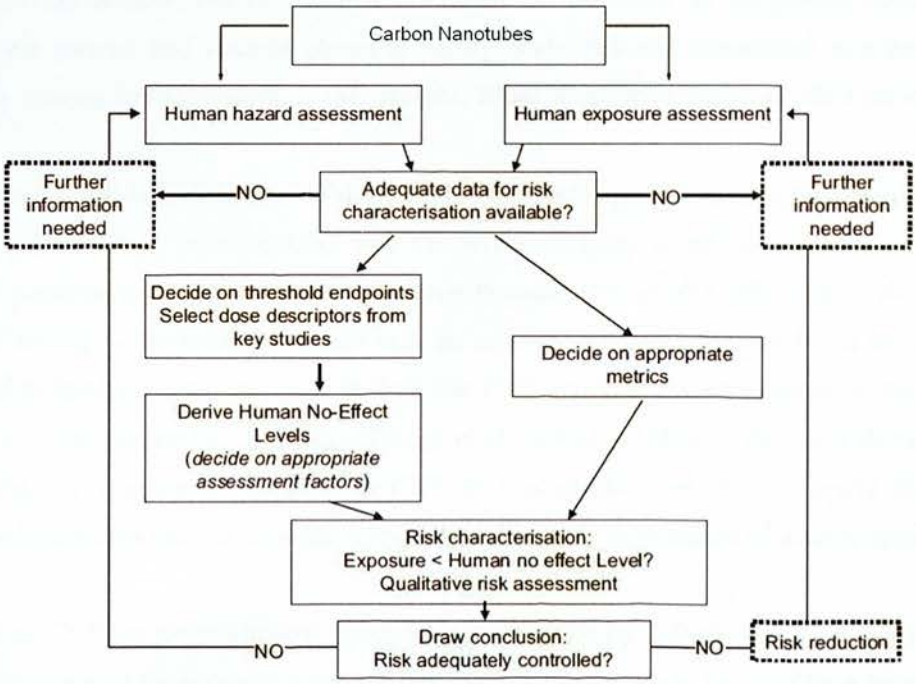

Figure 1.6: The overall process flow chart for the successful risk characterisation of CNT. Before adequate data for risk characterisation is available sufficient data on the particle hazard and potential for exposure is required. Reproduced and adapted from (Aschberger et al., 2010).

1.9.1 Hazard

The basis for comparison of CNT and asbestos is their morphological similarities. As described, carbon nanotubes are high aspect ratio nanomaterials that can be found in both fibrous and non-fibrous forms. Whilst the diameter is typically within the nanometre range, their length can reach up to tens of microns. The graphene nature of CNT means that they are likely to be very biopersistent and resistant to breakage or dissolution in the body. Therefore CNT may possess the physical characteristics that imbue a fibre with pathogenicity as laid out in the FPP.

To date only a limited number of studies have investigated the potential for CNT to cause mesothelioma or asbestos-like responses at the mesothelium. When assessing the biological activity of various forms of fibre, the peritoneal cavity of the mouse is commonly used as a surrogate for the thoracic mesothelium (Donaldson et al., 1989; Moalli et al., 1987). The peritoneal cavity is similarly lined with mesothelial cells, has a population of patrolling macrophages and a stomatal-mediated clearance mechanism which is consistent with the pleural cavity. Despite this, the two spaces do have fundamental differences, one of which is the nature of the space. In the pleural cavity, the space between the parietal and visceral pleura is tightly controlled and maintained at a minimum with constantly moving apposing surfaces (Miserocchi, 2009) which may impact on fibre pathogenicity.

A study carried out by Takagi *et al* (Takagi et al., 2008) attempted to address the potential of CNT to cause mesothelioma by injecting CNT into the peritoneal space of p53 deficient mice. This mouse model is particularly sensitive to carcinogenesis because loss of p53 affects their ability to repair genotoxic damage or to induce damaged cells to undergo apoptosis. Mesothelioma were observed 6 months after intraperitoneal injection in both the CNT and asbestos exposed mice but not in mice exposed to fullerenes (carbon spheres) (Takagi et al., 2008). Although the study demonstrated the development of tumours in response to CNT in susceptible mice, the extremely high doses (3 mg/mouse) used calls into question the relevance of this study to potential inhalation exposures.

Exposure to CNT via intraperitoneal injection was also used by Poland *et al* in a study designed to specifically compare the potential pathogenicity of CNT to asbestos in terms of fibre length (Poland et al., 2008). A panel of fibres of varied length, including long and short CNT and long and short asbestos were injected into mice at a dose of 50 μg/mouse. An acute inflammatory response followed by the formation of granulomas was observed only in mice injected with long asbestos and long CNT (Poland et al., 2008). The lack of response to the short tangled CNT used in this study or to nanoparticulate carbon black (NPCB) highlights the role of fibre length in initiating a pathogenic response. These results also show CNT display to a similar length dependent pathogenicity as is seen with asbestos fibres however further studies need to be carried out to assess the potential of CNT to cause mesothelioma. The importance of fibre length in the peritoneal assay was confirmed in a study by Muller et al in which non-fibrous CNT samples (0.7 μm), with or without structural defects, were

injected into the peritoneal cavity of rats that after 2 years were assessed for mesothelioma formation (Muller et al, 2009). The particulate nature of the CNT used and the lack of a sustained pathogenic response or mesothelioma formation lead the authors to conclude that the CNT may have been insufficiently long for a true estimation of the carcinogenicity using this model (Muller et al, 2009).

Sakamoto et al exposed wildtype rats to a single intrascrotal administration of 1 mg/kg MWCNT and examined the mesothelial response after 1 year (Sakamoto et al., 2009). MWCNT induced mesothelial hyperplasia and the development of nodular and papillary mesothelioma. The overall incidence of mesothelioma was 86% in MWCNT-treated rats while no mesothelioma were found in vehicle- or crocidolite-treated rats (Sakamoto et al., 2009). The unusual model of intrascrotal injection was chosen to increase sensitivity and specificity as it was expected that the dose would be largely retained in the small space of the scrotal cavity. Although this study demonstrates the carcinogenicity of CNT at the mesothelium the use of this highly artificial exposure model and single CNT fibre type tell us little about the fibre characteristics that may contribute to mesothelial cell transformation and whether this may be applicable in human exposures.

A recent paper by Nagai et al has proposed that CNT diameter rather than length is the critical factor in CNT-mediated fibrotic inflammation and carcinogenesis using the peritoneal model of mesothelial exposure (Nagai et al., 2011). They demonstrated that in their panel of CNT only the thin CNT sample (diameter 50 nm) caused fibrotic inflammation and tumour development after injection into the peritoneal cavity whereas rats treated with the thicker CNT (diameter 145 nm) showed negligible fibrosis (Nagai et al., 2011). This raises an interesting possibility for the role of diameter in mesothelial carcinogenesis which has not previously been identified to be directly responsible for asbestos pathogenicity.

From the available data it can be concluded that long, straight MWCNT can behave in a similar manner to asbestos and have the potential to induce mesothelioma following intraperitoneal or intrascrotal injection in mice and rats. Furthermore, in keeping with the FPP, the pathogenicity of CNT appears to be dependent on fibre dimensions. However no study has yet examined the pathogenicity of CNT in a model of pleural exposure which is the focus of this study.

As the lungs will be the primary organs affected by the inhalation exposure of CNT several studies have recently examined the cellular and pulmonary reactions after pharyngeal or intratracheal instillation of CNT in rats and mice. The first two such studies were published in the journal Toxicological Sciences in 2004 (Lam et al., 2004; Warheit et al., 2004). Lam et al demonstrated that a single intratracheal instillation in mice with three different types of SWCNT resulted in dose-dependent granuloma formation and interstitial inflammation. The different samples had different metal contents but this did not result in differences in their ability to produce granulomas (Lam et al.,

2004). In the study by Warheit, instillation of high doses of short SWCNT led to the formation of multifocal granulomas with foreign body giant cells (FBGC) which are typical of foreign body induced reaction (Warheit et al., 2004). However these granulomas were distributed in a non-uniform pattern and did not reflect the dose response. The study by Warheit also demonstrated the affect aggregation of CNT can have on experimental systems as the use of high doses (5 mg/kg) for intranasal instillation led to ~15% mortality in their instilled rats (Warheit et al., 2004). Ultimately the non-uniform deposition, lack of dose response relationship and asphyxiation of a significant proportion of instilled rats possibly stems from the high doses used, method of instillation and dispersion of the CNT rather than a nature of their toxicity.

In the years following these initial studies various pathological responses including acute neutrophilic inflammation (Muller et al., 2005; Shvedova et al., 2008), cytokine production (Shvedova et al., 2005; Shvedova et al., 2008), granulomatous inflammation (Shvedova et al., 2008; Lam et al., 2004; Porter et al., 2010), interstitial thickening (Porter et al., 2010) and fibrosis (Shvedova et al., 2005; Mercer et al., 2011) have been observed to varying degrees of severity in a number of rodent models exposed to both SWCNT and MWCNT. The data from these studies however is not easily comparable due to differences in exposure methods and variations in the morphology and physio-chemical features of different samples of CNT which may modulate their toxicity.

The mechanisms underlying effects induced by a bolus delivery are likely to be very different from those induced when the same dose is delivered by inhalation over a longer period. Large bolus doses are likely to overwhelm the clearance mechanisms, which are usually effective when the body is exposed to low doses. Therefore the results from inhalation studies are more appropriate for risk assessment. There have been few inhalation studies carried out to assess the pathogenicity of CNT due to the limitations such as the requirement for specialist facilities and expertise and the expense involved. In general the inhalation studies conducted with CNT have confirmed qualitatively the effects seen following intratracheal instillation but with lower potency (Johnston et al., 2010).

Recently two inhalation studies with MWCNT have been published that were designed to comply with OECD protocols and were intended to provide data to support risk assessment. A 90 day exposure to MWCNT at doses of 0.1 mg/m^3, 0.5 mg/m^3 and 2.5 mg/m^3 carried out by Ma-Hock *et al* (Ma-Hock et al., 2009) reported the formation of granulomatous lesions similar to those seen after intratracheal instillation of CNT. At the lowest exposure level of 0.1 mg/m^3 there was evidence of minimal granulomatous inflammation and therefore a no observable effects limit (NOEL) to CNT exposure could not be established (Ma-Hock et al., 2009). In the second study carried out by Pauluhn et al rats were similarly exposed for 6 hours/day, 5 days a week for 13 consecutive weeks but with doses ranging from 0.1 to 6 mg/m^3 (Pauluhn, 2010b). Histopathology revealed pathological changes in

the bronchoalveolar regions starting at the dose of 0.4 mg/m^3 which was characterised by an increase in interstitial collagen deposition. More severe granulomatous lesions were identified at the higher dose which the authors suggested were due to lung overload. In this study at the low dose of 0.1 mg/m^3 all endpoints examined were on par with the control treatment group and therefore suggested as a NOEL (Pauluhn, 2010b). The CNT used in the Pauluhn study have a strong tendency to aggregate and therefore present as 'densely coiled sphere-like' aggregates rather than fibrous structures.

Migration of MWCNT to the subpleural region of the lungs directly underlying the visceral pleural has been demonstrated after inhalation exposure by Ryman-Rasmussen et al (Ryman-Rasmussen et al., 2009) and penetration of MWCNT through the visceral pleura into the pleural space after aspiration exposure has been reported by Mercer et al (Mercer et al., 2010). These results are entirely consistent with the notion that a fraction of all particles deposited in the lung can reach the pleural space and highlight the necessity to evaluate the mesothelial hazard CNT may pose.

Numerous *in vitro* studies have been carried out on CNT using different models and cell lines to examine potential toxicity, however results and conclusions drawn from these studies are often contradictory depending on dose, dispersion, endpoints measured and also differences in the CNT themselves (Helland et al., 2007; Johnston et al., 2010).

1.9.2 Exposure

The main exposure routes in the occupational setting are anticipated to be inhalation and dermal contact. Human exposure is not expected during the synthesis phase of commercial production as this reaction is preformed in a closed reaction chamber. The highest exposures are likely to occur during handling of dry powder including activities such as collection, weighing, blending or transferring to containers. Various downstream applications of CNTs can also have the potential to result in exposure of workers for example drilling or sanding of CNT-containing composites may lead to release of CNT into the air (Aschberger et al., 2010).

Occupational inhalation exposure to CNT has been evaluated in a number of workplaces and laboratories. The first such investigation was carried out by Maynard et al who measured SWCNT aerosol concentration in a laboratory following SWCNT generation by both laser ablation and the HiPCO process (Maynard et al., 2004). Estimates of the SWCNT concentration in air samples taken ranged from 0.7 μg/m^3 in the ablation facility to 53 μg/m^3 in the HiPCO process however scanning electron microscopy analysis of the filter samples revealed that many of the particles appeared as compact particles rather than fibrous structures (Maynard et al., 2004). Han et al monitored the possible exposure to MWCNT in a research laboratory before and after the implementation of exposure controls (use of a fumehood and ventilation) and reported a reduction in airborne mass

concentration from 430 $\mu g/m^3$ to 40 $\mu g/m^3$ (Han et al., 2008). Based on these measurements the implementation of controls appears to be effective at limiting exposure to CNT during production. The effectiveness of engineering controls in the reduction of airborne particulate concentration was also demonstrated in a study carried out by Yeganeh et al at a commercial nanotechnology facility where fullerenes and CNT are produced (Yeganeh et al., 2008).

The National Institute for Occupational Safety and Health (NIOSH) recently described the development of a 'nanoparticle emission assessment technique' (NEAT) which employs portable direct-reading instrumentation to detect releases of airborne nanomaterial (Methner et al., 2010). This is supplemented by filter-based air sampling and microscopic evaluation which will allow for particle identification and also provide information on the physical form of the nanomaterials emitted. Field studies conducted at CNT facilities demonstrated the emission of nanomaterial during tasks such as opening the growth chamber, weighing, mixing and sonication however these levels were again reduced to near background control levels with the implementation of simple controls (Methner et al., 2010). From these studies it is clear that exposure to airborne CNT will depend both on the process being carried out and the effectiveness of exposure controls.

The limited number of studies carried out to date and the variety of measurements obtained depending on the processes and facilities of the CNT facilities means it is not yet possible to determine representative exposure values for specific activities. The determination of such values will be essential for both effective hazard assessments as more relevant doses can be examined and also importantly for risk assessment of the facilities themselves.

It is clear that for effective risk assessment for CNT more data are required for both better hazard and exposure assessment.

Hypothesis and Aims

The over-arching hypothesis for the project is that carbon nanotubes, because of their structural similarities to asbestos, will adhere to the fibre pathogenicity paradigm and therefore pose a hazard to the pleural mesothelium. The aims of this project designed to test the hypothesis were as follows:

1. Develop a method for direct injection of fibres into the pleural cavity of mice
2. Determine whether a panel of CNT administered by direct intrapleural injection cause pathogenic changes that reflect the response elicited by asbestos controls
3. Examine the translocation of CNT through the lung to the pleura and the subsequent effects in the pleural space after pulmonary exposure
4. Examine the interactions between CNT and mesothelial cells and macrophages in vitro as a potential predictive in vitro assay

Chapter 2: Materials and Methods

2.1 Particles

2.1.1 CNT panel

In order to evaluate the pathogenicity of CNT in terms of fibre length a panel of 5 CNT of varying lengths was assembled. All the CNT used in this project were multiwalled CNT produced by catalytic vapour discharge (CVD). The CNT panel comprised four commercially available CNT and one sample produced in an academic research laboratory. The NT_{long1} sample (Mitsui & Co. Ltd., Japan) was produced by CVD using the floating reaction method. The NT_{long2} sample was produced in an academic research laboratory (The Nanoscience Centre, University of Cambridge) using CVD method using a ferrocene-toluene feedstock to grow nanotubes from iron catalysts held on a silica plate. These nanotubes grew aligned as mats, meaning they were straight and un-entangled. The nanotubes were harvested from the mats using a razor blade, with some residual iron remaining within the nanotubes. We also included one commercially available short straight CNT (NT_{short}; Nanostructured and Amorphous Materials, Inc.) and two curled and tangled nanotubes of different lengths (NT_{tang1}, which was cut to form predominantly short NT fibres and the original length NT sample; NT_{tang2}) (NanoLab, Inc., MA, USA). These were produced by CVD with an iron and ceramic oxide (alumino-silicate) catalyst support which was removed using HCl and Hydrofluoric acid treatment.

2.1.2 Controls

A non-fibrous particle, nanoparticulate carbon black (NPCB) was included in the panel as a control particle for the effects of bulk carbon chemistry (Printex 90, Evonik Degussa GmbH, Düsseldorf, Germany).

Two amosite asbestos samples were also included as controls. The samples consisted of mixed length amosite asbestos enriched for long fibres (50.36% fibres >15 μm, 35.25% fibres >20 μm), hereafter referred to as long fibre asbestos (LFA). Shortened amosite asbestos (SFA) was prepared by grinding long fibres in a ceramic ball mill, and the resulting fibre preparation sedimented in water. The SFA sample consisted of 4.46% fibres >15 μm, 0.99% fibres >20 μm. Both LFA and SFA were created from the same batch of South African amosite (Davis et al., 1986a) obtained from the Manville Corporation (USA).

2.1.3 Synthesis of NT_{short}-DTPA conjugates

NT_{short}-DTPA conjugates were synthesized and radiolabelled by Dr. Khuloud Al-Jamal (University of London). NT_{short}-NH_3^+ were obtained following the procedure reported in reference (Li et al., 2008). Briefly, 150 mg of NT_{short} were heated in 15 mL of neat oxalyl chloride at 62 °C for 24 h. After evaporation *in vacuo* the resulting nanotubes were dispersed in a solution of Boc-monoprotected diamino-triethyleneglycol (TEG) (670 mg) in distilled THF (10 mL) and heated at reflux for 48 h. The nanotubes were re-precipitated several times from methanol/diethyl ether by successive sonication and centrifugation. The Boc protecting groups were removed overnight using 4 M HCl in dioxane (10 ml) to afford ammonium functionalized MWNT (110 mg) following evaporation of the acid solution and re-precipitation in diethyl ether. Kaiser test afforded a loading of 0.320 mmol/g. Aminated MWNT (10 mg) were dispersed in a mixture of dry DMSO/DMF (0.4:2.5 ml) and neutralized with DIEA (diisopropylethylamine) (50 µl). Diethylentriaminepentaacetic (DTPA) dianhydride (28.5 mg) was added and the mixture was stirred for 48 h at 50°C. The DMSO/DMF solution was partly evaporated and diluted with water. The NT_{short}-DTPA were recovered by centrifugation, re-dispersed in water and lyophilized. Kaiser test showed that only 0.034 mmol/g of free ammonium groups were still present.

2.1.4 Radiolabelling to produce NT_{short}-DTPA[^{111}In]

The radioactive tracer [^{111}In]Cl_3 was obtained from Amersham Pharmacia Biosciences (UK) as an aqueous solution and used without further purification. As a standard procedure, dispersions of NT_{short}-DTPA (80µl-400µl of 250µg/ml) were diluted with an equal volume of 0.2 M ammonium acetate buffer pH 5.5, to which 20-100MBq as indium chloride ($^{111}InCl_3$) was added. The indium was left to react with the NT_{short}-DTPA for 30 min at room temperature, after which the reaction was quenched by the addition of 0.1 M EDTA chelating solution (1/20 the reaction volume is added). $^{111}InCl_3$ alone, used as a control, was also subjected to the same conditions of the labelling reaction. Aliquots of each final product were diluted five-fold in PBS and then 1 µl spotted on silica gel impregnated glass fibre sheets (PALL Life Sciences, UK). The strips were developed with a mobile phase of 50 mM EDTA in 0.1 M ammonium acetate and allowed to dry before analysis. Autoradioactivity of the strips was quantitively counted using a Cyclone phosphor detector (Packard Biosciences, UK). The immobile spot on the TLC strips indicated the percentage of radiolabelled NT_{short}-DTPA[^{111}In] conjugate, while the free ^{111}In or [^{111}In]DTPA were shown by the mobile spot.

2.1.5 Compact particle panel

Quartz particles (DQ12), coal mine dust particles and two samples of commercially available polystyrene beads (10 µm, 3 µm beads, Polysciences, PA, USA) were also used in this study. Mean

particle diameter of DQ12 quartz and coalmine dust were measured by dynamic light scattering using 90 plus Particle Size Analyzer (Brookhaven Instruments Corp., NY, USA).

2.1.6 Nickel nanowires

Nickel nanowires (NiNW) were fabricated by Dr. Adriele Prina-Mello and Dr. Fiona Byrne using electrochemical template synthesis using alumina membranes (Anodisc 25, Whatman, UK) with an average pore diameter of 200 nm (Byrne et al., 2009; Prina-Mello et al., 2006). Once formed, NiNW were removed from the membrane by dissolving it in 1 M NaOH and re-suspending the solution in ddH_2O. This resulted in a wire consisting of metallic nickel which was rapidly oxidised to form a 3-4 nm thick layer of nickel oxide (Prina-Mello et al., 2006). The formation of short and long NiNW ($NiNW_{long}$, $NiNW_{short}$ respectively) was achieved via altering the deposition time and resulted in average (mean) lengths of 4.3 ± 1.0 μm and 24.0 ± 7.0 μm respectively. Size distributions were prepared and examined by scanning electron microscope (SEM, Carl Zeiss Ultra Plus, UK) by Dr. Fiona Byrne.

2.1 7 Functionalised CNT

Surface functionalisation of long MWCNT was performed on a sub-set of a long MWCNT sample produced by Matthew Boyles using the same methodology and reactor (The Nanoscience Centre, University of Cambridge) as those used in the synthesis of the NT_{long2} sample. The sample was sent to the laboratory of Prof. James Tour (Rice University, TX, USA) and functionalised in two separate ways by Amanda Higginbotham and Ashley Leonard prior to testing. The Arylation of MWCNT was performed using the aryl iodide isopathic acid as described by Chattopadhyay and colleagues (Chattopadhyay et al., 2005). Briefly the NT_{long} sample was mixed under an atmosphere of argon with ammonia followed by the addition of lithium metal in a 100 ml, three-neck, round-bottomed flask fitted with a dry ice condenser. Into the flask, 6.4 M aryl iodide was added and stirred at -33 °C for 12 h with the slow evaporation of ammonia. The reaction mixture was quenched by slow addition of ethanol followed by water, then acidified by the addition of 10% HCl. The mixture was filtered through a 0.2 μm filter membrane and washed with water and ethanol before drying in vacuum at 80 °C. Long carbon nanotubes were alkylated using octyl-iodide (Sigma-Aldrich) by the same method.

2.1.8 Size distributions

The size distribution measurements for 4 members of the CNT panel (NT_{tang1}, NT_{tang2}, NT_{long1}, NT_{long2}) were previously carried out by Craig A. Poland (ELEGI, University of Edinburgh) and reported in (Poland et al., 2008). Measurements were made from CNT samples visualized by transmission electron microscopy (TEM) and scanning electron microscopy (SEM). All measurements were taken using calibrated measurement software (Image-Pro Plus; Media Cybernetics Inc., MD, USA) based on

100 μm stage graticule (Graticules LTD, Kent, UK). In keeping with WHO guidelines (WHO 1997) we only considered those particles with a length to width ratio greater than 3:1 and a length more than 5 μm as a fibre. The size distribution of the NT_{short} CNT sample was measured from images of the sample prepared for TEM.

2.1.9 Transmission electron microscopy

Particles were suspended in propan-2-ol (Fisher Chemicals) and briefly sonicated using an ultra sonicating water bath (Fisherbrand FB11002, 40kHz). The sample suspensions were then diluted into 1.25 % propan-2-ol/ ddH_2O (Milli-Q Academic, Millipore, MA, USA) solution. A drop of the sample suspension was placed on a grid with a support film of Formvar/carbon, excess material was blotted off with a filter paper and the material was examined under a FEI CM120 BioTwin Transmission Electron Microscope (Philips, Eindhoven, Netherlands) using a Lab6 emitter. Images were captured using an AMT Digital Camera (AMT, MA, USA).

2.1.10 Soluble metal contamination

The levels and types of contaminating metals contained within the samples were established using an inductively coupled plasma optical emission spectrometer (ICP- OES) analysis using an iCAP 6500 (Thermo Scientific, MA, USA) by the Institute of Occupational Medicine. The degree of soluble metal contamination was established by preparation of a soluble fraction prepared by suspending each sample in dH_2O prior to mixing and filtration to remove particulates and the supernatant analysed.

2.1.11 Endotoxin contamination

The presence of bacterial contamination of the particle panel was established by measuring endotoxin levels. A 1 mg/ml solution of each particle was prepared using certified endotoxin free LAL reagent water (Cambrex Bio Science Walkersville, Inc, MD) and mixed on a rotating mixer at room temperature for 24 hrs prior to ultracentrifugation of the sample (13,800g) and removal of the extracted supernatant. The endotoxin level of the supernatant was established using limulus ameobocyte lysate (LAL) assay (Cambrex Bio Science Walkersville, Inc, MD). Comparison against a standard curve of known concentrations of endotoxin in the range of 0.1-1 EU/ml enabled the calculation of sample endotoxin concentration.

2.1.12 CNT durability

The durability of the functionalised CNT was analysed based on the use of a physiological extra cellular fluid describe by J.L. Gamble (GAMBLE, 1952). The composition of Gamble solution is described in Table 2.1.The pH of the Gambles solution was adjusted to pH 4.5 and the pH readjusted

24 hrs later. Formaldehyde (37%) was added (1-2mls/L) to prevent microbial growth. CNT samples (50 μg/ml) were incubated rotating in Gambles solution for 4 weeks at 37°C. Samples were diluted 1:200 and filtered onto PVC filter papers (0.1 μm pore size, 25 mm diameter, Skc Inc) pre-wetted with 10 ml of ddH_2O under vacuum using a membrane filter holder for vacuum filtration (Whatman, UK). The sample was washed three times with 10 ml of ddH_2O allowed to dry overnight and prepared for scanning electron microscopy. The size distributions of the functionalized CNT samples ($NT_{long-AL}$, $NT_{long-AR}$) were determined by SEM

Table 2.1: Composition of Gamble solution

NaCl	7.12g/L
$NaHCO_3$ (Sodium Bicarbonate)	1.95g/L
$CaCl_2.2H_2O$ (Calcium Chloride)	0.029g/L
Na_2HOP_4 (Sodium Phosphate)	0.148g/L
Na_2SO_4 (Sodium Sulfate)	0.079g/L
$MgCl_2.6H_2O$ (Magnesium Chloride)	0.212g/L
Glycine	0.118g/L
Na_3-citrate.$2H_2O$ (Sodium Citrate)	0.152g/L
Na_2-tartrate.$2H_2O$	0.18g/L
Na-pyruvate	0.172g/L
Lactic Acid	0.15g /L

2.1.13 Dispersion

A number of dispersion media were tested including dH_2O, foetal bovine serum (FBS), bovine serum albumin (BSA), Dipalmitoylphosphatidycholine (DPPC, semi-synthetic, 99% Purity, Sigma-Aldrich Company Ltd.) and triton-X. NT_{long2} (50 μg/ml) was dispersed in the different media by ultrasonication at 230V, 50Hz, 350W for 2 hours in an ultrasonic bath (FB11002, Fisherbrand, Thermo Fisher Scientific, Inc., MA, USA). Five hundred microlitres of the resulting suspension were filtered onto polycarbonate filters with 0.1 μm pore size (Millipore). Filters were washed thoroughly with dH_2O and allowed to dry overnight at room temperature. Filters were examined the following day and images captured by digital camera (Olympus).

2.1.14 Particle Suspensions

Particles were suspended in Roswell Park Memorial Institute-1640 (RPMI-1640) media (PAA Laboratories Ltd., UK) containing 0.5% bovine serum albumin (BSA; Sigma-Aldrich, Poole, UK) for in vitro treatments or sterile 0.9% saline (PAA Laboratories Ltd., UK) for in vivo experiments at a

stock concentration of 500 μg/ml and dispersed by sonication. Suspensions were prepared freshly each day and used immediately upon removal from the ultrasonic bath. For light microscopy images all samples from the particle panel were dispersed by ultrasonication in 0.5% BSA/saline solution at a concentration of 50 μg/ml. Ten microlitres of the resulting particle suspensions were mixed with 10 μl glycerol, mounted onto glass slides and examined at 40x magnification (Zeiss). Images were captured using Q capture Pro software (Media Cyberbernetics Inc., MD, USA).

2.1.15 Electron paramagnetic resonance

The free radical generating ability of the CNT panel was measured by EPR using the spin traps; Tempone-H and DMPO (+H_2O_2). The positive control; pyrogallol was used for superoxide generation and a Fenton Chemistry mix (iron ions plus H_2O_2) was a positive control for hydroxyl radical. Particles were diluted to a concentration of 0.01 mg/ml in saline and sonicated. To measure superoxide radicals Tempone-H (Alexis Biochemicals) was added to samples to give a final concentration of 1mM. Hanks buffer with Tempone-H and pyrogallol (1mM) diluted in Hanks buffer were used as negative and positive controls, respectively. EPR spectra were measured after 60 minutes incubation at 37°C using the following instrumental conditions: Microwave frequency: 9.39GHz, Magnetic field: 3355 G, sweep width: 55 G, sweep time: 30 seconds, gain 1E1. To measure hydroxyl radicals DMPO (Sigma) was added to particles to give a final concentration of 50mM. H_2O_2 was also added at a final concentration of 100μM to start the reaction. Saline with DMPO and Fe(II)SO_4 (100μM) with H_2O_2 (100μM) were used as negative and positive control, respectively. EPR spectra were measured immediately at room temperature using the following instrumental conditions: Microwave frequency: 9.39GHz, Magnetic field: 3360 G, sweep width: 75 G, sweep time: 30 seconds, gain: 7E1. Intensity values of the highest spectra peak were recorded and graphed against each other (arbitrary values).

2.2 In vitro

2.2.1 Met5A mesothelial cell line

The human mesothelial cell line (Met5A) was purchased from the American Type Culture Collection (ATCC, No. CRL-9444). The mesothelial cells were originally isolated from the pleural effusions caused by medical indications of thoracentesis (such as congestive heart failure) of a noncancerous patient (Ke et al., 1989; Lechner et al., 1985). To immortalise the cells, they were transfected with the pRSV-T plasmid (an SV40 ori- construct containing the SV40 early region and the Rous sarcoma virus long terminal repeat) and cloned. The Met5A cell line was fully adherent and maintained at sub-culture in RPMI-1640 with 10% heat inactivated foetal calf serum (PAA Laboratories Ltd., UK) supplemented with 2mM L-Glutamine and 100U/ml (1%) Penicillin/ Streptomycin (PAA

Laboratories Ltd., UK). The cells displayed a cobblestone-like appearance in culture. The cells were maintained at 37°C in 5% CO_2 and used between passages 6-25 from stocks maintained under air-phase liquid nitrogen in DMSO supplemented freezing media.

2.2.2 THP-1monocyte cell line

The THP-1 cell line was obtained from ATCC (Product: TIB-202). The THP-1 human monocyte cell line was originally derived from the blood of a boy with acute monocytic leukaemia. The monocytic nature of the cell line was characterized by lysozyme production and phagocytosis of latex particles and sensitized sheep erythrocytes (Tsuchiya et al., 1980). Cells were maintained in continuous culture in supplemented with 10 % FCS RPMI-1640 at 37 °C in a humidified atmosphere containing 5 % CO_2. Differentiation of the THP-1 monocytes into macrophages was by 48 hour incubation with phorbol myristate (PMA) (Sigma, Cat No p-8139) at a concentration of 10 ng/ml. Differentiated cells adhered to the flask, whereas undifferentiated monocytic cells remained in suspension and were removed by washing with PBS.

2.2.3 Cell Culture and Treatment

Prior to experimentation Met5A cells were seeded in 24-well plates (Corning, Amsterdam, The Netherlands) at a concentration of $2.5x10^5$ cells/well and allowed to adhere for 24 hours. THP-1 monocytic cells were differentiated into macrophages with 10 ng/ml PMA at a concentration of $2.5x10^5$ cells/well in 24-well plates for 48 hours. Prior to the treatment of both cell types the media was replaced with RPMI-1640 media containing 0% FCS, 1% penicillin/streptomycin and 1% L-Glutamate for 3 hours. Particle treatments were carried out with particle suspensed in RPMI media containing 0.5% BSA/saline, 1% penicillin/streptomycin and 1% L-Glutamate. Cells were treated with the CNT panel for 24 hours using a range of doses to determine cell viability, 5 $\mu g/cm^2$ was chosen as a sub-lethal dose for subsequent activation studies. Lipopolysaccharide (LPS) treatment was given at 10 ng/ml. Cytochalasin D (Enzo Life Science), potassium chloride (KCl) or diphenylene iodonium (DPI) was used to co-treat THP-1 cells along with NT_{long1}, NT_{long2}, or LPS. Light microscopy images of THP-1 cells treated with the panel of CNT were captured at x40 magnification using QCapture Pro software (Media Cybernetics, MD, USA).

2.2.4 Scanning electron microscopy

THP-1 cells were grown on Thermonox coverslips (Nunc, Roskilde, Denmark) and treated with NPCB, NT_{short} or NT_{long2} (5 $\mu g/cm^2$) for 24 hours. Cells were fixed with 10% Formalin and were stained with osmium tetroxide prior to critical point drying, mounted and gold sputter coated before examination by scanning electron microscopy (SEM) using an Hitachi S-2600N digital scanning electron microscope (Oxford Instruments, Oxfordshire, UK).

2.2.5 Trypan Blue Exclusion Assay

Met5A cells were plated as above before treatment with the particle panel for 24 hours at doses ranging from 5-50 μg/cm^2. The cell supernatant was removed and kept for lactate dehydrogenase (LDH) measurements, cells were washed once with PBS and incubated with 0.4% trypan blue (Sigma-Aldrich, Poole, UK) for 5 minutes. Excess trypan blue was removed and cells washed with PBS. Dead cells, as indicated by incorporation of the trypan blue dye, were counted and calculated as a percentage of total cells (500 total cells counted per treatment group).

2.2.6 Lactate dehydrogenase Assay

Cell supernatant from Met5A and THP-1 cells exposed to the CNT panel at doses ranging from 5-50 μg/cm^2 or LPS (1 μg/ml) was diluted 1:3 and 100 μl was added in triplicate to a 96 well plate (Corning, Amsterdam, The Netherlands). One hundred microlitres of the LDH test reagent (diaphorase/NAD+ mixed with iodotetrazolium chloride and sodium lactate at a ratio of 1:45) added to each well. Cells treated with 0.1% Triton-X were used as a positive control for 100% cell lysis. Following a 30 minute incubation period the absorbance of each well at 490 nm wavelength was established using a Synergy HT microplate reader (BioTek Instruments, Inc. VT, USA).

2.2.7 Cytokine Bead Array

The media levels of IL-1β, IL-6, IL-8 and TNFα cytokines were measured after direct exposure of the mesothelial cells and macrophages to the CNT panel (5 μg/cm^2) and exposure of the mesothelial cells to the conditioned media from CNT-treated macrophages by cytokine bead array (BD CBA Flex Set, BD Biosciences, San Jose, CA). Briefly, 25 μl of the mixed capture antibodies were added along with 50 μl of the supernatant samples and standards to each well of a 96-well plate and incubated at room temperature for one hour. Twenty-five microlitres of the mixed PE detection reagent was added to each well and incubated at room temperature for two hours. The plate was centrifuged at 1500 g force for 5 minutes and the supernatant completely removed. One hundred and fifty microlitres of the wash buffer was added to each well. The plate was agitated for 5 minutes to resuspend the beads before the samples were analyzed using the BD FACSArray Bioanalyzer (BD Biosciences, San Jose, CA). Results were analysed using FCAP array software and sample concentrations of each cytokine were established via extrapolation from the appropriate recombinant protein standard curve.

2.2.8 ELISA

The media levels of IL-1β and IL-6 after macrophage inhibition studies was established using ELISA DuoSet kits (R&D systems, Abingdon, UK) specific to each analyte of interest. Ninety-six well microtitre plates were incubated overnight at 4°C with 100 μl of coating antibody raised against IL-1β

or IL-6. The plates were washed 3 times with 0.05% Tween-20 in phosphate buffered saline (PBS; pH 7.2) and blocked using reagent diluent (1% BSA in PBS; R&D systems, Abingdon, UK) for 1 hour (room temperature) prior to further washing and addition of test samples/ standards in triplicate. After 2 hrs the plates were washed and a biotinylated detection antibody added to each well followed by a 2 hr incubation. The plates were then washed and 100 µl Streptavidin conjugated with horseradish peroxidise was added. The plates were washed and developed using a TMB substrate solution (Sigma-Aldrich, Poole, UK). The subsequent reaction was stopped with 0.5 M H_2SO_4, resulting in a yellow colour, and read at 450 nm. Sample concentrations of IL-1β, IL-6 were established via extrapolation from the appropriate recombinant protein standard curve.

2.3 In vivo

2.3.1 Experimental Animals

Eight to twelve week old (20-25 g) female C57BL/6 strain mice (Harlan, UK) were group- housed in standard caging with sawdust bedding, environmental enrichment with free access to sterile water and food within a pathogen-free Home Office approved facility. Animals were maintained on a normal 12 hr light and dark cycle and were allowed 7 days to acclimatise prior to study commencement. Post exposure animals were subject to daily checks for signs of distress or welfare issues. All *in vivo* work was carried out by staff holding a valid UK Home Office personal licence under a Home Office approved project license.

2.3.2 Intrapleural injection

A 27 gauge needle was fitted with a sleeve covering the needle shaft as far as the base of the bevelled edge of the needle tip (Figure 2.1). Animals were humanely restrained without anaesthetic via 'scruffing' to expose the chest prior to injection into the upper right thoracic cavity with a total volume of 100 µl. Animals were immediately placed back into their cage and monitored to ensure resumption of normal behaviour.

Figure 2.1: Modified needle for intrapleural injection.

2.3.3 Pharyngeal aspiration

Animals were anaesthetised using Isoflurane (2-chloro-2-(difluoromethoxy)-1,1,1 trifluoroethane) and the tongue was gently held at full extension while a 50 µl bolus of test sample pipetted to the base of the tongue. The animals were stimulated to inhale via covering of the nasal cavities to induce a gasp reflex and held until several breaths had occurred (Rao et al., 2003). The animals were further observed until full recovery and group housed for the duration of the experiment.

2.3.4 Lavage

At each time point the mice were killed by CO_2 asphyxiation. An incision was made into the skin of the animal at the base of the abdomen and the skin was then carefully removed to expose the underlying tissue. The abdominal wall was cut away. The animal was held by the xiphoid process at the base of the sternum and the falciform ligament connecting the diaphragm and liver was severed. A small incision was made in the diaphragm directly inferior to the xiphoid process through which a Pasteur pipette was used to lavage the cavity (Figure 2.2). The pleural cavity was lavaged with 3 washes of 1 ml of ice-cold saline which dispersed throughout both the left and right sides of the pleural cavity. The first lavage was retained in a separate tube for biochemical analysis.

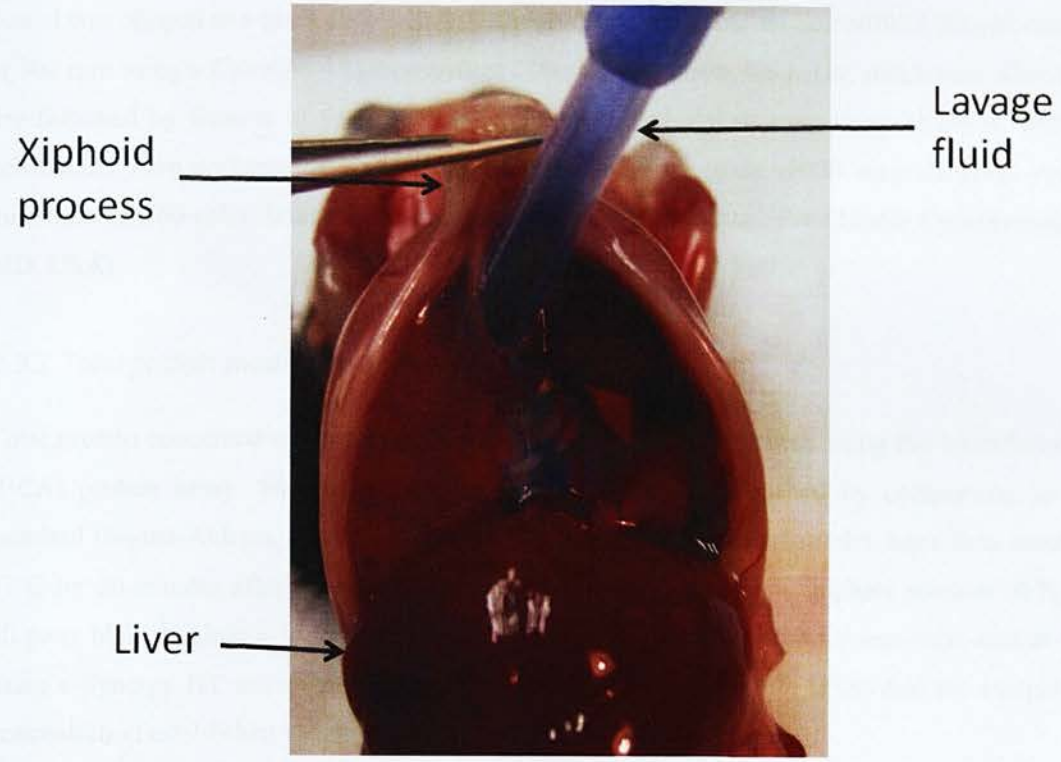

Figure 2.2: Technique for pleural lavage

2.3.5 Bronchoalveolar Lavage

At each time point, the mice were killed by terminal anaesthesia using an intraperitoneal injection with 0.5 ml of pentobarbitone (200 mg/ml) followed by exsanguination via the abdominal aorta. The thoracic cavity was exposed via removal of the diaphragm and cutting of the right portion of the rib cage and through the clavicle to expose the trachea. An incision was made in the trachea with a scalpel blade and cannulated using a 21 gauge needle and legated with suture. The lungs gently inflated using 0.8 ml of ice-cold sterile saline and agitated. The lavage was then gentle withdrawn to avoid rupture of blood vessels and placed on ice. The lungs were lavaged a total of three times using 0.8 ml washes, with the first wash kept separately on ice and the subsequent washes pooled. All lavages were placed on ice for the entire duration of the processing.

2.3.6 Differential cell count

The lavage fluid (both pleural and lung) was then centrifuged at 123g for 5 minutes at 4°C in a Mistral 3000i centrifuge (Thermo Fisher Scientific, Inc., MA, USA) and aliquots of the supernatant retained for total protein and cytokine measurements. The remaining cell pellet was re-suspended in 0.5 ml of 0.1 % BSA/ sterile saline solution. A total cell count was performed using a NucleoCounter (ChemoMetec, A/S, Allerod, Denmark). Cytocentrifugation preparations were made by placing ~40,000 cells into a cytology funnel with 300 µl of 0.5 ml of 0.1 % BSA/ sterile saline solution. The

funnel was clipped to a glass slide with a Shandon filter card (Thermo Scientific, UK) and centrifuged at 300 rpm using a Cytospin 4 cytocentrifuge (Thermo Scientific, UK). The slides were allowed to air dry followed by fixation of the cells with 100% methanol and staining using Diffquik. Differential cell counts were performed on cyto-centrifugation preparations at x1000 magnification, counting a minimum of 300 cells. Images of cells were taken using QCapture Pro (Media Cyberbernetics Inc., MD, USA).

2.3.7 Total protein measurements

Total protein concentration of the peritoneal lavage fluid was measured using the bicinchoninic acid (BCA) protein assay. Sample protein concentrations were established by comparison to a BSA standard (Sigma-Aldrich, Poole, UK) curve (0 – 1000 µg/ml). The samples were then incubated at 37°C for 30 minutes after the addition of the test reagent (1 part Cu^{2+} Sulphate solution (4 % w/v) to 50 parts bicinchoninic acid (Sigma-Aldrich, Poole, UK)). The absorbance was then read at 570 nm using a Synergy HT microplate reader (BioTek Instruments, Inc. VT, USA) and the sample protein concentration established via extrapolation from the BSA standard curve.

2.3.8.Dissection

2.3.9 Diaphragm

The veterebral column was severed below the diaphragm. The diaphragm was then carefully removed by cutting through the ribs and chest wall with care taken not to puncture the diaphragm. The free diaphragm was, at this stage, still attached to the excised portion of the rib cage as shown in Figure 2.3 to prevent the diaphragm tissue contracting under elastic tension. The diaphragm was washed in ice-cold saline and placed in 10% formalin fixative for 4 hours. Once removed from fixative the tissue was washed with 70% ethanol. The diaphragm was then removed from the ribs and the same full width section of the upper quadrant of the diaphragm was removed from each animal sampled (Figure 2.3 I). The diaphragm section was dehydrated through graded alcohol (ethanol) and imbedded on-edge in paraffin, with 4 µm sections of the diaphragm made. Sections were stained with H&E stain to show gross pathology, Pico-Sirius Red (PSR) red to show collagen deposition (red stain) and anti-Ki-67 proliferation marker (rabbit polyclonal anti-Ki-67, ab15580, Abcam, Cambridge, UK).

2.3.10 Chest wall

The two sides of the chest wall were separated by cutting along the sternum and spine. While the chest wall halves are still attached at the upper thoracic cavity the mediastinal lymph nodes, as described by van den Broeck (Van Den Broeck et al., 2006), were identified. The chest wall halves and lymph nodes are removed together and rinsed in ice-cold saline (Figure 2.3 II). The chest wall

tissue and lymph nodes are then carefully separated and placed into individual containers of 10% formalin fixative. After 4 hours fixation the posterior portion of the chest wall adjacent to the spine was isolated for further examination. For histology the tissue was dehydrated through graded alcohol (ethanol) and imbedded on-edge in paraffin, with 4 μm sections of the chest wall made. Sections were stained with H&E and PSR. For scanning electron microscopy the chest wall was stained with osmium tetraoxide before critical point dying, mounted, and gold sputter coated before examination by SEM using a Hitachi S-2600N digital SEM (Oxford Instruments, Oxfordshire, UK).

2.3.11 Backscatter SEM

Chest wall samples fixed for backscatter SEM were dehydrated in 50%, 70%, 90% and 100% normal grade acetones for 10 minutes each, then for a further two 10-minute changes in analar acetone. Dehydrated samples were critical point dried and mounted on SEM aliminium stubs and rotary-coated with about 8nm of carbon in an Edwards 306A vacuum coating system (Edwards High Vacuum, Crawley, UK).

BS-SEM of carbon-coated specimens was carried out using a Hitachi 4700 II field emission SEM (Hitachi High-Tech, Maidenhead, UK) at a beam accelerating voltage of 10kV and a working distance of about 8mm. Secondary electron (SE) and BSE images were taken simultaneously using an annular YAG crystal BSE detector and the upper SE detector to produce perfectly-synchronised image pairs.

3.2.12 Lymph nodes

After 4 hours fixation the excess fatty tissue surrounding the lymph nodes was removed. The lymph nodes were paraffin embedded whole, 4 μm sections were made and stained with H&E and PSR. For lymph node NiNW burden quantification six sequential sections were taken from each lymph node, giving 18 sections per treatment group. Images were taken at x10 magnification for tissue area measurement and x40 magnification for fibre counting using QCapture Pro software (Media Cybernetics Inc.).

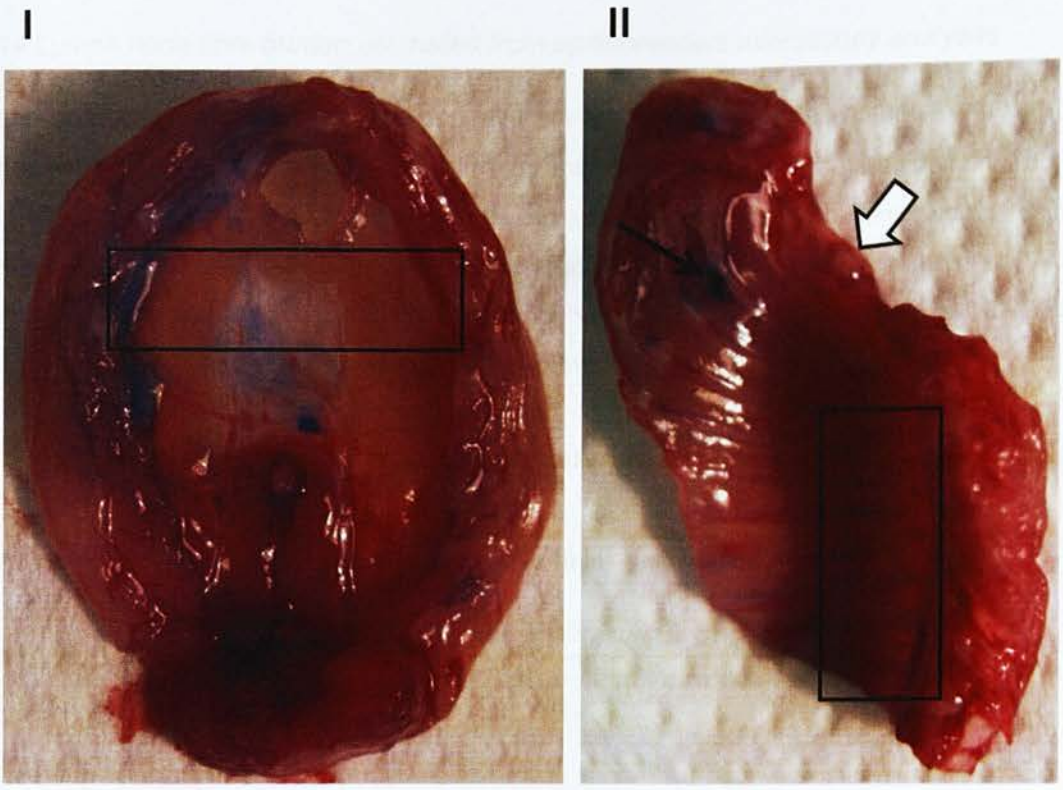

Figure 2.3: Excised tissue. (I) Pleural aspect of the mouse diaphragm. Black box indicates the area sampled and examined for lesion formation. (II) Chest wall tissue. Black box outlines area sampled for examination of the parietal pleura responses. Black arrow indicates accumulation of injectate surrounding the point of injection. White arrow indicates mediastinal lymph node attached to the chest wall.

2.3.13 Quantification of lesion formation

Serial images along the chest wall and diaphragm length were taken at x100 magnification using a Zeiss Axioskop microscope fitted with a Micropublisher 3.3 RTV camera using QCapture Pro software (Media Cyberbernetics Inc., MD, USA) and seamlessly realigned using Adobe Photoshop CS3 Version: 10.0.1 (Adobe systems Inc.) to show the entire section. Using calibrated software (Image-Pro Plus, Media Cybernetics Inc., MD, USA) the total length of each chest wall or diaphragm along the basement membrane was measured in order to adjust for any differences in size. Any areas of lesion, identified by histology as lymphocytic aggregates adhering to the mesothelial surface (excluding areas of liver, connective tissue or lymphatic tissue), were measured using the same software. Lesion area on each chest wall and diaphragm was calculated in mm^2 per unit length of chest wall or diaphragm (in mm) to yield lesion area per unit length (mm^2/mm). The collagen content was measured using Image-Pro Plus software by quantifying the red pixels in each section and expressed as area of positive collagen staining per unit length of chest wall or diaphragm (mm^2/mm).

2.3.14 Lymph node fibre burden estimated from epifluorescent microscopy analyses

Epifluorescent microscopy analyses were carried out by Dr. Adriele Prina-Mello (Trinity College Dublin). Five fields (with an average area of 40 μm^2) were analysed for each tissue section. The total area of the tissue sections was measured with the Image J software. For each tissue section analysed the NiNW present in each field were counted, the total number of NWs present in the tissue section calculated (Eq. 1), and the average concentration of NWs in the section (expressed as NiNW/μm^2) estimated (Eq. 2). Calculations were carried out as follows:

$$Total\ NWs/tissue\ section = Total\ NWs\ counted \times \frac{Tissue\ section\ area}{Area\ analysed} \qquad \textbf{Eq. 1}$$

where the area analysed is equal to 200 μm^2, *i.e.* five fields each with an area of 40 μm^2

$$NWs\ Concentration\ (NWs/\mu m^2) = \frac{Total\ NWs/tissue\ section}{Tissue\ section\ area} \qquad \textbf{Eq. 2}$$

2.3.15 Lung

The thoracic cavity was exposed, and the trachea cannulated using a 21 gauge needle and legated with clinical suture. The trachea was severed above the cannula and the lungs carefully dissected away from thoracic cavity with both the heart and lungs removed on-block. The lungs were then attached via the cannula to a 10 ml syringe and 10% formalin fixative added at a hydrostatic pressure of 20 cm H_2O. The trachea was then fully ligated and the cannula removed prior to full submersion of the lungs and heart in 10% formalin fixative for a period of 24 hrs. After fixation, the heart was removed and discarded whilst the individual lobes of the lung were dissected free and placed flat in a tissue cassette. As before, the lung tissue was dehydrated through graded alcohol (ethanol) and imbedded in paraffin with 4 µm sections cut so as to encompass all lobes of the lung. Sections were stained with H&E and PSR and serial images taken at x100 magnification using QCapture Pro software. The images were seamlessly re-aligned as before to show an entire section of the lung.

2.13.16 Whole body imaging of NT_{short}-DTPA [^{111}In] injected animals by Nano-SPECT/CT

Imaging of radiolabelled NT_{short} by Nano-SPECT/CT was carried out by Dr. Khuloud Al-Jamal and Mr. Antonio Nunes (School of Pharmacy, University of London) at the Department of Nuclear Medicine, St. Bartholomew's Hospital, London. Balb/C mice were anaesthetised by isofluorane inhalation. Each animal was injected directly into the pleural space with 100 µl containing 5 µg of NT_{short}-DTPA [^{111}In] containing approximately 3-5MBq. [^{111}In] DTPA of the same activity was injected for comparison. Immediately after injection (t=0-1 h) and at t=23-24 h, mice were imaged

using the Nano-SPECT/CT scanner (Bioscan, USA). SPECT images were obtained in 16 projections over 40-60 min using a 4-head scanner with 1.4 mm pinhole collimators. CT scans were taken at the end of each SPECT acquisition and all images were reconstructed with MEDISO software (Medical Imaging Systems). Fusion of SPECT and CT images was carried out using the PMOD software.

2.4 Statistics

All data was analysed using GraphPad Prism 5 (Version 5.03; GraphPad Software Inc. USA). Results were expressed as the mean + s.e.m. and multiple comparisons were analysed using one-way analysis of variance (ANOVA) with a Tukey-HSD method post-test and two sample comparisons were made using the Student's t-test. In all cases, values of $p < 0.05$ were considered significant.

Chapter 3: The pleural pathogenicity of carbon nanotubes

3.1 Acknowledgements

The carbon nanotube sample NT_{long2} was synthesised by Dr Ian Kinloch of the University of Manchester during his tenure at the University of Cambridge. The NT_{long1} sample was graciously gifted by Mitsui & Co and the nanoparticulate carbon black sample Printex 90 was gifted by Evonik Degussa GmbH, Düsseldorf, Germany. The fibre sizing for a sub-panel of the CNT samples was previously carried out by Dr. Craig A. Poland in the ELEGI laboratory (University of Edinburgh).

3.2 Aims and Hypothesis

As described in Chapter 1 the pathogenicity of a fibre is governed by the physical attributes of length, diameter and biopersistence which together form the basis of the fibre pathogenicity paradigm. The potential of certain CNT samples to adhere to the FPP raises concern that they may pose an asbestos-like inhalation hazard, leading to the development of diseases in the pleural cavity, including mesothelioma. The asbestos-like pathogenicity of long, but not short CNT has been previously demonstrated in a study carried out in the ELEGI laboratory which used the peritoneal cavity as a surrogate for pleural exposure (Poland et al., 2008). Although the peritoneal cavity serves as a convenient model to study mesothelial impacts of fibres and peritoneal mesothelioma do arise in asbestos–exposed individuals, the primary mesothelial target for inhaled fibres is the pleural mesothelium. Therefore the aim of this study was to compare the pathogenic potential of a panel of short, tangled and long CNT with long and short asbestos after direct injection into the pleural cavity of mice. Based on the importance of length/width of a fibrous particle in its toxicity, we hypothesised that, like asbestos, only CNT composed of long (>15-20 μm), thin (<3 μm) fibres will generate inflammation.

3.3 Results

3.3.1 Morphology of the CNT panel

To assess the role of length in the pleural response to CNT we assembled a panel of long, short and short/tangled CNT along with long and short amosite asbestos controls and a particulate carbon control; nanoparticle carbon black (NPCB). The physical characteristics of the CNT samples in dry powder form are described in Table 3.1.

Table 3.1: Gross morphology of fibre panel.

Sample	Macroscopic characteristics
LFA	Grey fibrous material aggregated into wool-like bundles
SFA	Grey powder aggregated into coarse granules
NPCB	Dense black powder of very fine material
NT_{short}	Dense black powder of fine, non-fibrous material
NT_{tang1}	Dense black powder of fine, non-fibrous material
NT_{tang2}	Dense black powder containing coarse aggregates of non-fibrous material
NT_{long1}	Fibrous black material forming loose, dusty bundles
NT_{long2}	Black, fibrous, non-dusty material forming bundles and dense flakes.

Figure 3.1 displays representative images of the fibre panel captured by TEM. The particles were dispersed using the solvent; isopropanol, prior to imaging to enable visualisation of individual fibres. The long fibre amosite asbesotos sample (herein referred to as LFA) was observed to consist of singlet fibres ranging from in length from several microns to over 100 μm, whereas the short fibre amosite asbesotos sample (SFA) consisted of short, rod-like fibres that were predominantely shorter than 5 μm in length. The NPCB sample consisted of small aggregates of spherical particles. The NT_{short} sample contained CNT that were straight but extremely short whereas both the NT_{tang1} and NT_{tang2} samples, although longer than the NT_{short} sample appeared curled and formed spherical aggregates due to the presence of a high proprtional of structural defects. Both NT_{long1} and NT_{long2} consisted of longer straight CNT. Of the 5 different CNT samples, only the samples designated NT_{long1} and NT_{long2} were seen to contain fibres as defined by the WHO definition of a fibre i.e. length greater than 5 μm, width less than 3 μm and an aspect ratio of 3:1 (WHO, 1997).

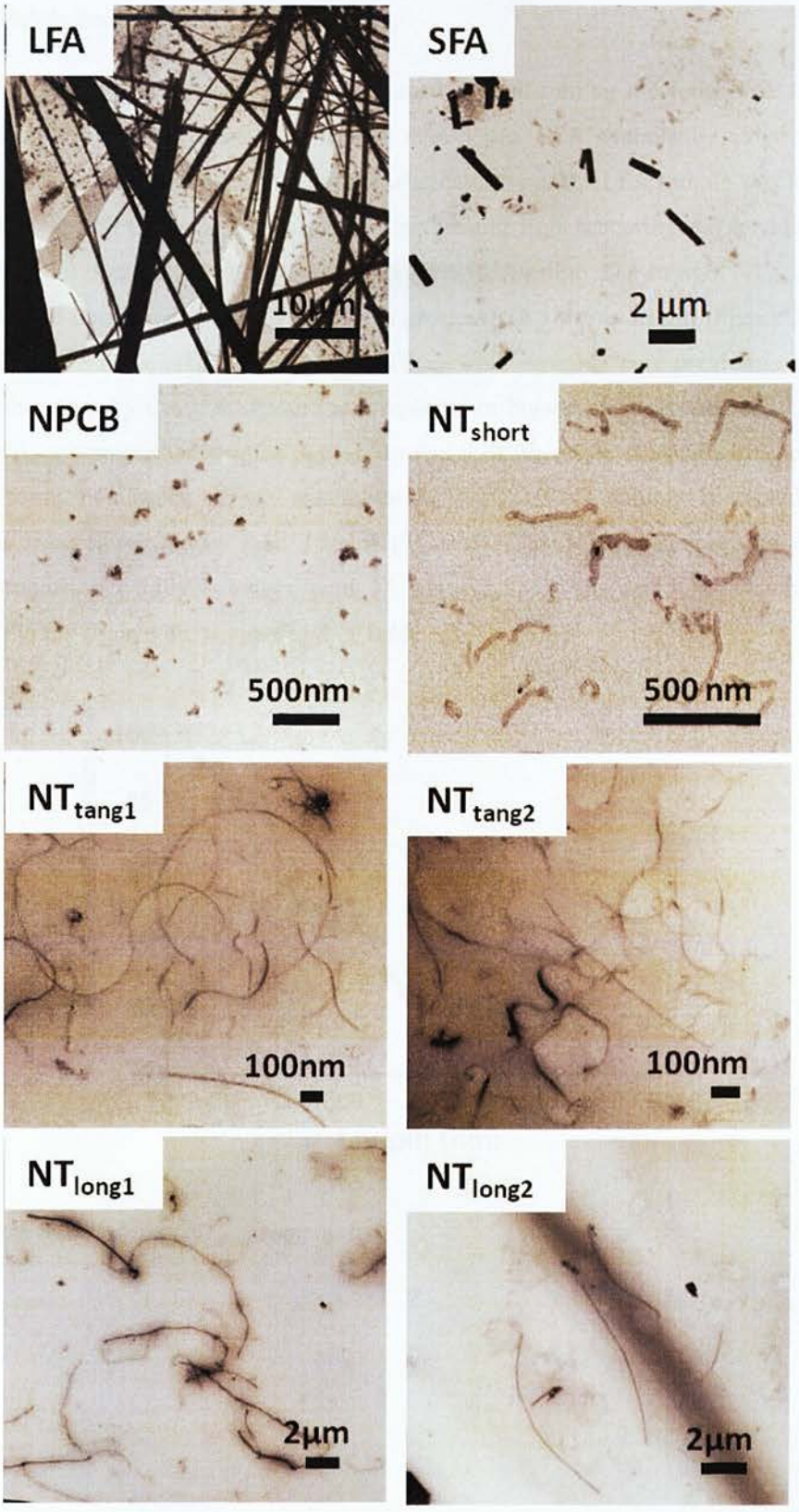

Figure 3.1: Microscopic morphology of the particle panel. Transmission electron microscopy was used to assess the differences in the morphology of the particle panel. Particle samples were dispersed in propan-2-ol. Note different scale bars for each particle type.

3.3.2 Size Distributions

The short fibre asbestos sample (SFA) was obtained by ball-milling the long fibre sample which produced a sample of fibres consistently shorter than 5 μm. SFA contained approximately 5% of fibres which could be considered long (> 15 μm) whereas 50% of the LFA sample was longer than 15 μm (Figure 3.3). The NPCB sample was assessed by dynamic light scattering and found to form small aggregates 85±7 nm in diameter when dispersed in 0.5% BSA/saline. The straight NT_{short} sample were sized by TEM and obsereved to contain no fibres greater than 3 μm in length (Figure 3.2). The size distribution for the NT_{tang1}, NT_{tang2}, NT_{long1} and NT_{long2} CNT samples were previously carried out in the ELEGI laboratory by Craig A. Poland and reported in Poland et al (Poland et al., 2008). Both NT_{tang1} and NT_{tang2} consisted of tangled aggregates and were therefore considered to be non-fibrous. Of the two forms of fibrous carbon nanotubes the NT_{long1} CNT sample contained a moderate proportion of long fibres longer than 15 μm (21.01%). The NT_{long2} sample contained a more substantial proportion of fibres longer than 15 μm (75.21%) (Figure 3.3). The morphological properties of the CNT panel are summarised in Table 3.2.

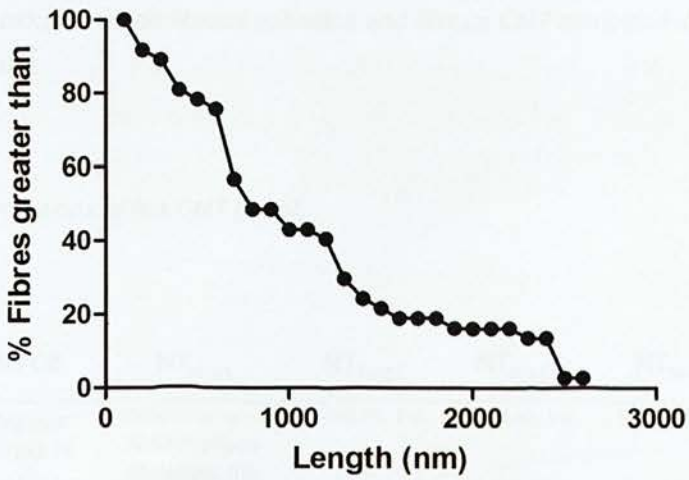

Figure 3.2: Size distribution of NT_{short} sample.

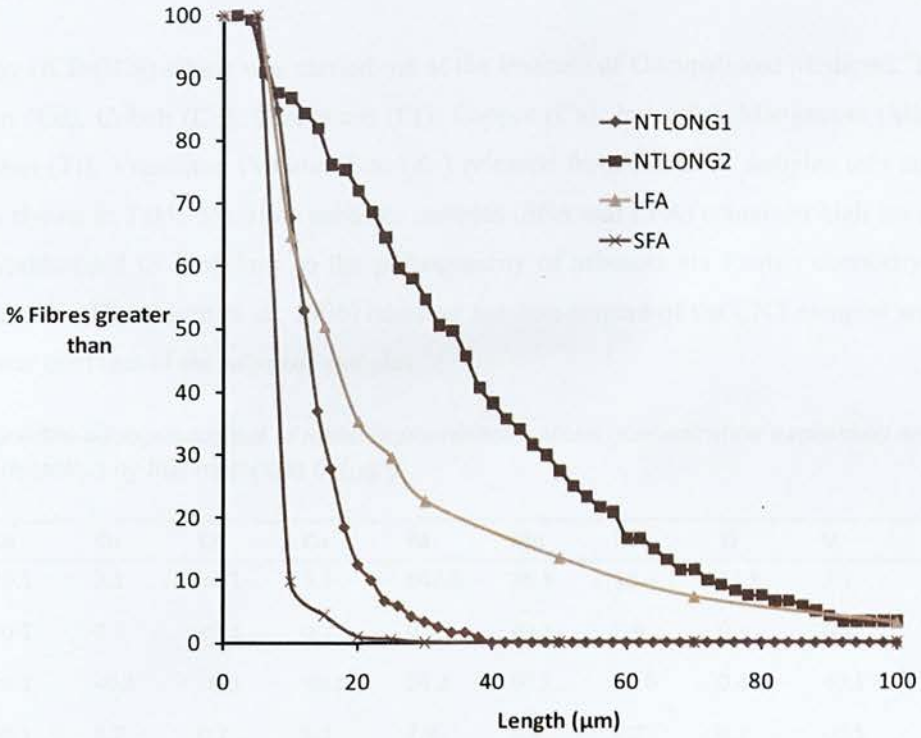

Figure 3.3: Size distribution of the fibrous asbestos and fibrous CNT samples.Fibre sizing carried out by Dr. Craig A. Poland.

Table 3.2: Fibre dimensions of the CNT panel.

	NPCB	NT_{short}	NT_{tang1}	NT_{tang2}	NT_{long1}	NT_{long2}
Source	Degussa Printex 90	Nanostructured & Amorphous Materials, Inc.	NanoLab, Inc.	NanoLab, Inc.	Mitsui & Co.	University of Manchester [Dr. I. Kinloch]
Diameter (nm)	14	25.7± 1.6	14.84 ± 0.05	10.4 0 ± 0.32	84.89 ± 1.9	165.02 ± 4.68
Length (µm)	-	1-2	1-5	5-20	Mean 13	Mean 36
% fibre greater than 15 µm	‡	‡	‡	‡	24.04	84.26

3.3.3 Metal contamination

The presence of contaiminating transition metals in the CNT samples is recognised as a potential driver of inflammation. Therefore the bioavailable metal contaminants released into an aqueous extract of the CNT panel were analysised using Inductively Coupled Plasma-Optical Emission

Spectroscopy (ICP-OES) which was carried out at the Institute of Occupational Medicine. The levels of Cadmium (Cd), Cobalt (Co), Chromium (Cr), Copper (Cu), Iron (Fe), Manganese (Mn), Nickel (Ni), Titanium (Ti), Vanadium (V) and Zinc (Zn) released from the CNT samples into an aqueous solution are shown in Table 3.3. Both asbestos samples (SFA and LFA) contained high levels of iron which is hypothesised to contribute to the pathogenicity of asbesots via Fenton chemistry and free radical generation (Donaldson et al., 1996) however the iron content of the CNT samples was at least 15 times lower than that of the asbestos samples.

Table 3.3: Soluble aqueous extract of metal contaminants. Metal concentration expressed as µg/g. The limit of detection by this method is 0.1µg/g.

Sample	Cd	Co	Cr	Cu	Fe	Mn	Ni	Ti	V	Zn
SFA	<0.1	2.1	<0.1	3.1	547.0	36.3	18.4	31.5	3.1	10.5
NPCB	<0.1	0.3	<0.1	0.2	0.1	<0.1	2.6	0.2	0.1	0.1
NT_{short}	<0.1	<0.1	<0.1	<0.1	24.2	50.3	21.6	0.4	<0.1	5.3
NT_{tang1}	<0.1	3.7	0.2	5.1	7.9	0.4	9.7	0.7	<0.1	5.5
NT_{tang2}	<0.1	<0.1	<0.1	1.0	13.4	<0.1	5.0	0.7	<0.1	7.5
LFA	<0.1	1.4	3.4	5.2	853.7	104.8	5.1	2.0	<0.1	27.3
NT_{long1}	<0.1	1.9	0.1	1.2	<0.1	<0.1	6.2	0.4	0.8	0.7
NT_{long2}	<0.1	3.4	<0.1	1.2	37.3	3.6	6.2	0.3	<0.1	<0.1

3.3.4 Electron Paramagnetic Resonance

In order to establish the level of intrinsic free-radical activity, each member of the particle panel was analysed using Electron Paramagnetic Resonance. The spin traps; Tempone-H and DMPO (± H_2O_2) were employed to detect superoxide radical generation and hydroxyl radical generation respectively (Figure 3.4). The EPR spectra obtained with the Tempone-H spin trap show a significant signal for the positive control; pyrogallol. SFA, NT_{tang1}, NT_{tang2} and LFA also generated a signal significantly greater than that of the vehicle control and their superoxide generating ability could be ranked as follows: SFA > NT_{tang1} > NT_{tang2}, LFA > NPCB, NT_{short}, NT_{long1}, NT_{long2}.

The DMPO spin trap was employed both with and without the addition of H_2O_2 to stimulate Fenton chemistry by the samples however only the positive control ($FeSO_4$ + H_2O_2) generated a EPR signal under either set of experimental conditions.

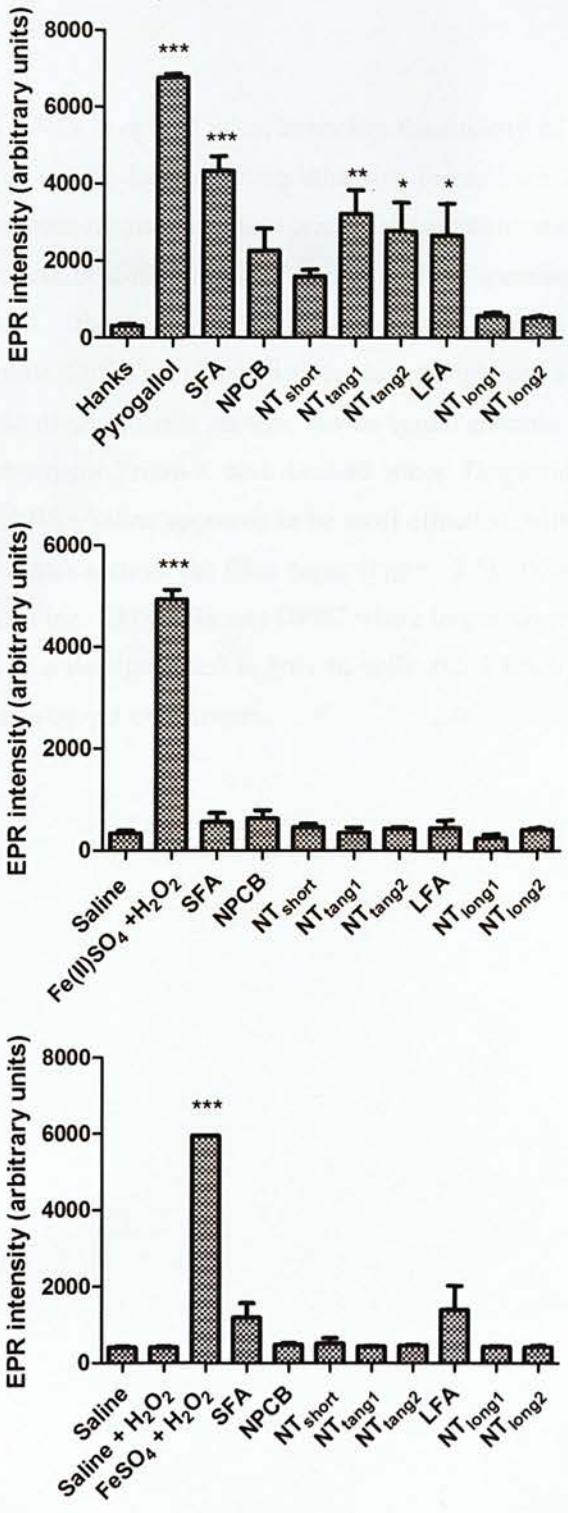

*Figure 3.4: Intrinsic free radical generation. Electron paramagnetic resonance was employed with the spin traps- Tempone-H and DMPO, to measure the intrinsic free radical generating potential of each of the particle panel. Significance vs. vehicle control indicated by * P<0.05, ** P<0.001, *** P<0.0001.*

3.3.5 Dispersion

The state of dispersion of CNTs is critical when assessing the toxicity of the CNT types based on physical parameters such as length. Due to strong attractive forces such as Van der Waals forces, CNT resist dispersion in aqueous media. Therefore prior to the administration of CNT into the mouse pleural cavity the effectiveness of different media in aiding the dispersion of CNT aggregates was examined. We compared the effectiveness of foetal bovine serum (FBS) with dipalmitoylphosphatidycholine (DPPC), a biocompatible phospholipid and a major component of lung surfactant, and with the ubiquitous globular protein, bovine serum albumin (BSA). These dispersants were compared with the detergent Triton-X and distilled water. Dispersion of NT_{long2} in solutions containing triton-X or 0.5% BSA/saline appeared to be most effective, with a uniform layer of CNT containing only small aggregates seen on the filter paper (Figure 3.5). Poorer quality dispersion was seen with dH_2O, 50% FBS/saline, 100% FBS and DPPC where larger aggregates of NT_{long2} remained (Figure 3.5). As triton-X is a detergent and is lytic to cells, 0.5% BSA/saline was chosen as the dispersion medium for all subsequent experiments.

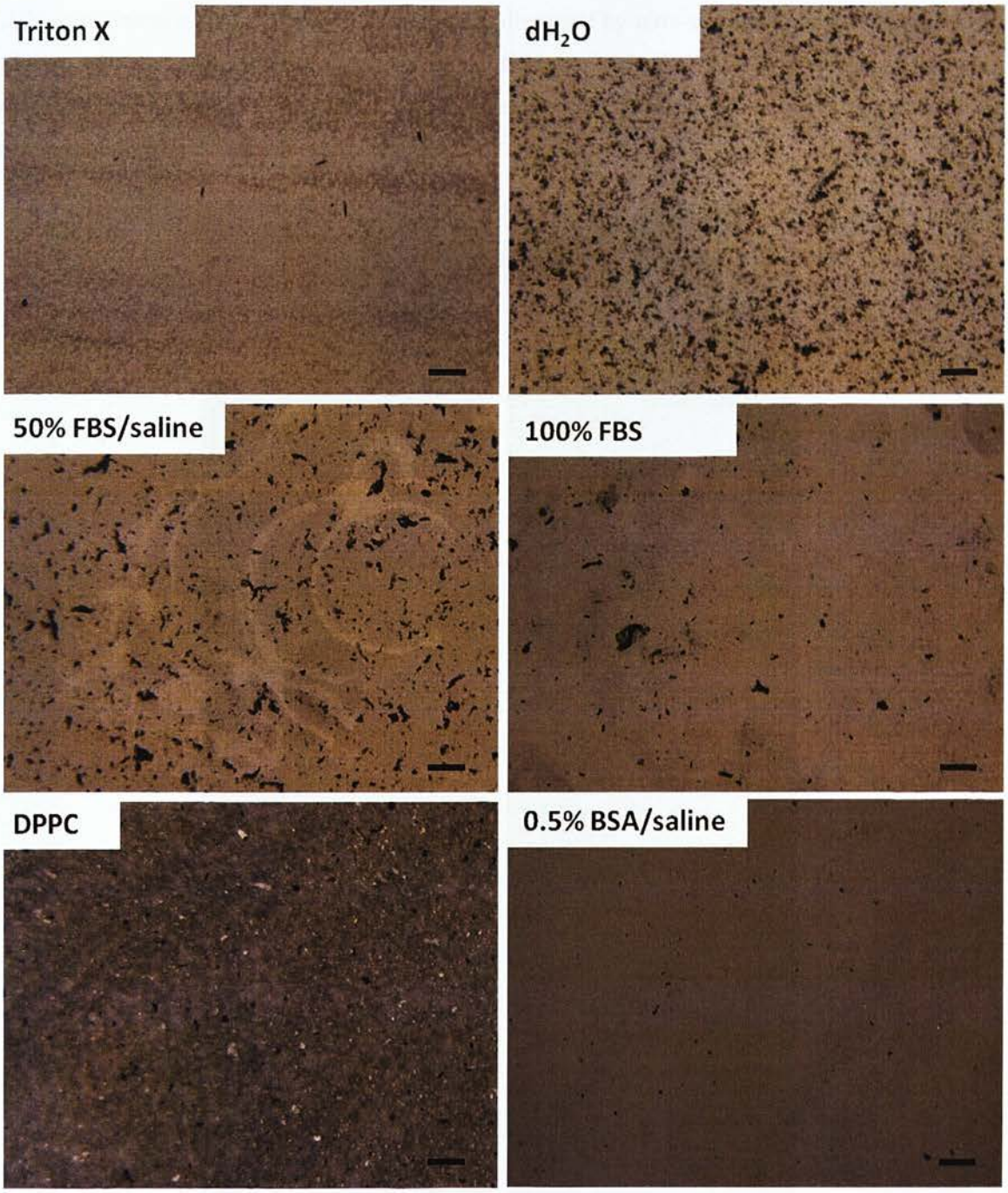

Figure 3.5: Comparison of dispersants. NTI_{ong2} (50 µg/ml) was dispersed by sonication in different dispersion media and filtered. The quality of dispersion was judged by the number of large aggregates left on the filter paper. Dispersion by Triton-X or 0.5% BSA/saline appeared to have the fewest visible aggregates. Scale bar indicates 10 mm.

Light microscopy of the CNT panel and controls, dispersed by ultra-sonication in 0.5% BSA/saline, prior to administration showed the presence of fibres in the LFA, NT_{long1} and NT_{long2} samples, whereas the SFA, NT_{short}, NT_{tang1} and NT_{tang2} samples were composed of small aggregates which were all considered to be of respirable size (Figure 3.6).

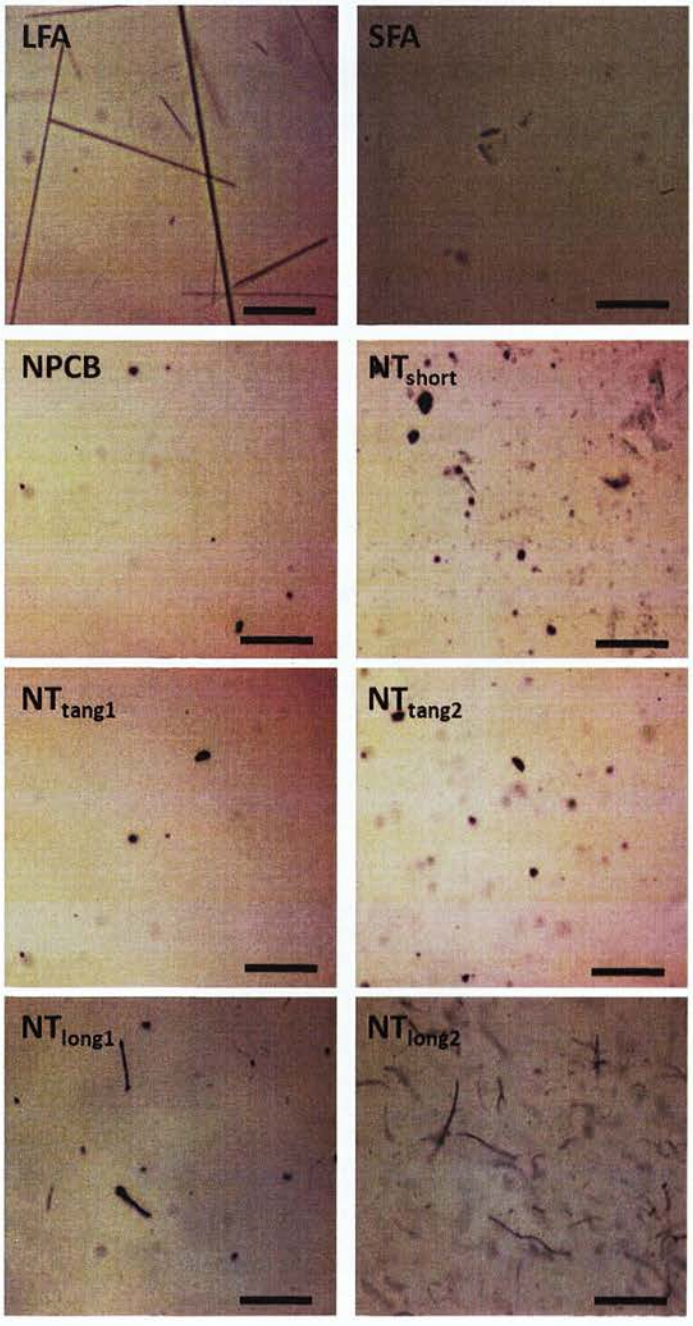

Figure 3.6: Representative light microscope images of CNT preparations dispersed in 0.5% BSA/saline. For light micrographs, CNTs and fibres were dispersed by ultrasonication in 0.5% BSA/saline at a concentration of 50 µg/ml to the standard degree of dispersion used for intrapleural injection. Scale bar indicates 20 µm.

3.3.6 Intrapleural injection

The aim of this study was to assess the hazard posed by CNT of diffferent morphology to the pleural mesothelium. A method of injection directly into the pleural cavity of mice using a modified needle was therefore developed and initially tested using trypan blue ink (Figure 3.7). Figure 3.7 (II) shows the pleural cavity as viewed through the diaphragm directly after injection with trypan blue. Blue dye can be seen dispersed throughout the pleural space as indicated by the white arrow indicating that the dose of CNT will be successfully delivered into and dispersed throughout the pleural cavity by this method.

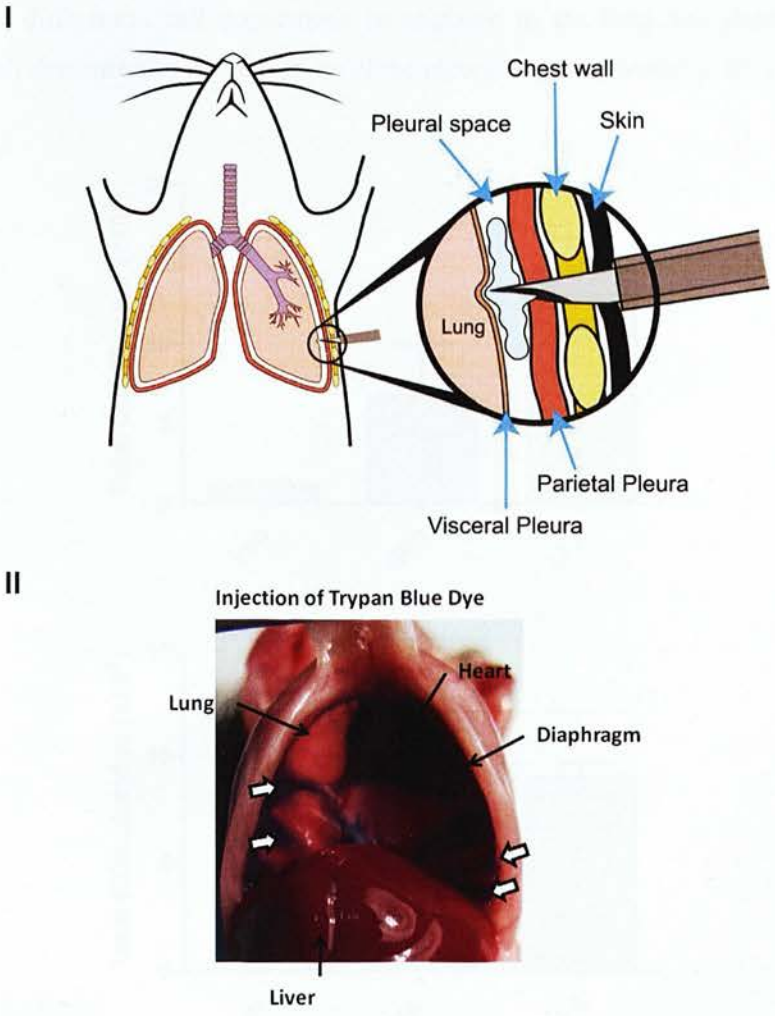

Figure 3.7: Intrapleural injection. (I) Schematic diagram of the injection method. A modified needle with a sleeve over the needle shaft which exposed only the very tip is used. The needle can pass through the chest wall but the sleeve prevents entry of the needle into the lung. (II) The injection

method was tested with trypan blue dye. Immediately after injection blue dye can be seen dispersed throughout the pleural cavity, as indicated by white arrows.

3.3.7 Acute inflammatory response to asbestos fibres

The pleural response was first examined after administration of the long and short amosite asbestos samples. Twenty-four hours after 5µg of LFA or SFA were injected into the pleural cavity the acute inflammatory response was measured by counting the total number of cells in the pleural lavage fluid and determining the number of granulocytes which were recruited to the pleural cavity. Injection of LFA resulted in an increase in both the total number of cells and the number of granulocytes in the pleural lavage fluid that was significantly greater than the vehicle control treated mice or the mice treated with the short SFA sample (Figure 3.8). Figure 3.9 shows cytospins of the pleural lavage fluid demonstrating the differential cell populations in response to the long and short asbestos fibre samples. This result demonstrates the sensitivity of the pleural exposure model to fibre length.

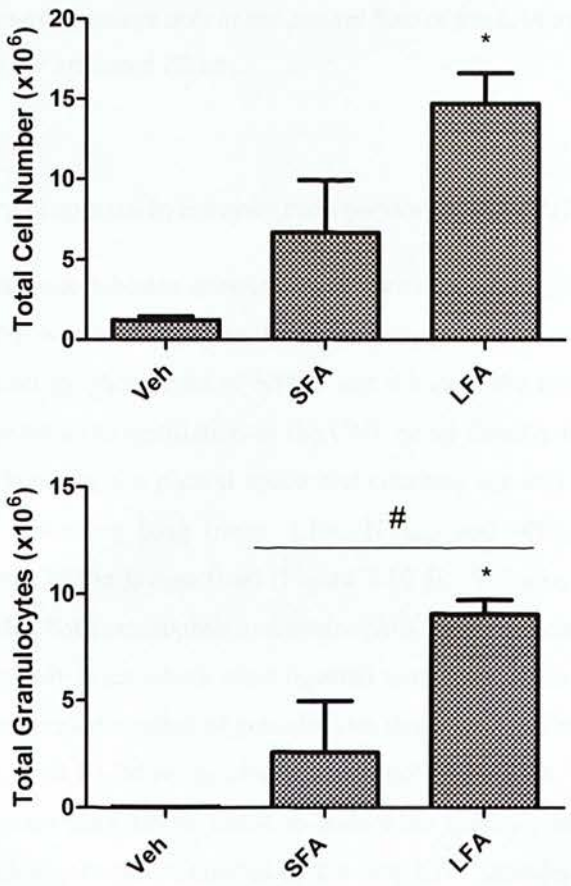

Figure 3.8: Acute pleural response to long and short asbestos fibres. Total cell number (I) and total granulocytes (II) were measured in the lavage fluid of mice injected with 5 µg of SFA or LFA and

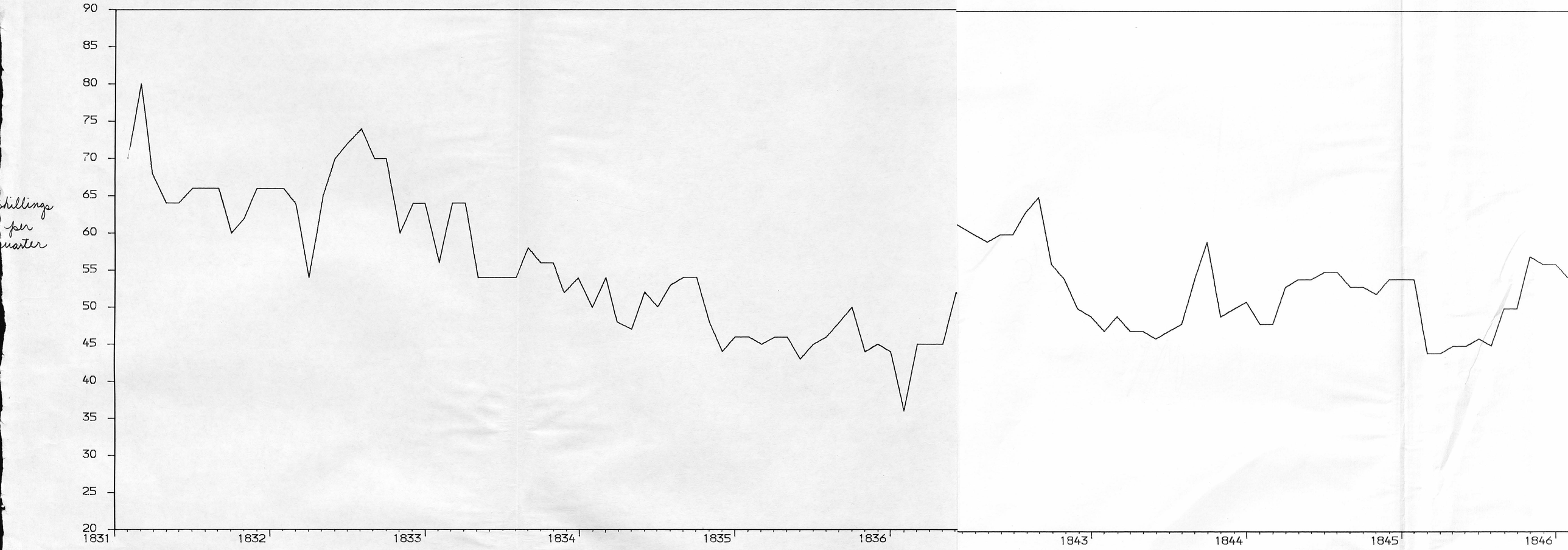

Price of Wheat in Dundee 1830-1850

*controls at 24 hours after injection. Significance versus vehicle control * indicates p<0.05, ** indicates p<0.001, significance between LFA and SFA # indicates p<0.05. Data expressed as mean ± sem, n=3*

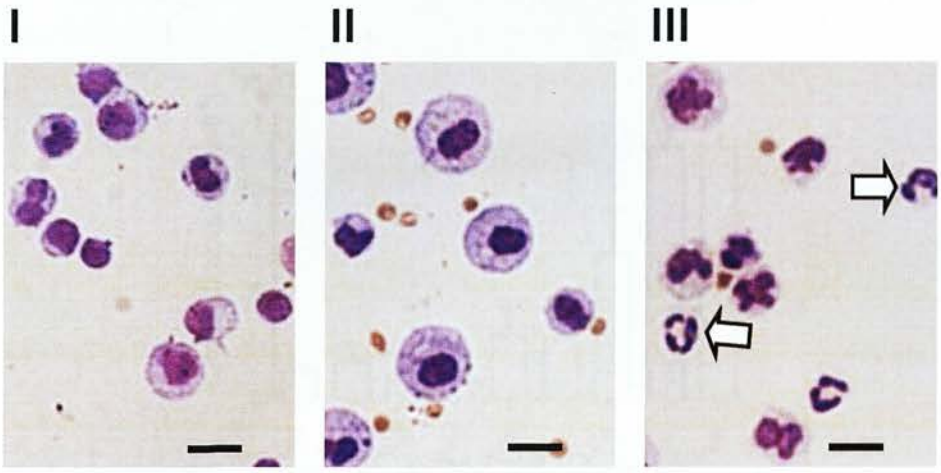

Figure 3.9: Cytospins of the pleural lavage fluid 24 post injection of vehicle control (I), SFA (II) or LFA (III). Inflammatory granulocytes, present only in the pleural fluid of the LFA treated mice are indicated by the white arrows. Scale bar indicates 20 µm.

3.3.8 Acute Inflammatory response to intrapleural injection of the CNT panel

Using the long and short amosite asbestos samples we confirmed that the pleural model was sensitive to long fibres. Our next step was to investigate the acute inflammogenic effects of CNT of different morphology and the compact graphene control NPCB and compare the responses to LFA and SFA. The acute inflammatory response to instillation of the CNT panel directly into the pleural space was measured at 24 hours by lavaging the pleural space and counting the cell types. Only intrapleural injection of the samples containing long fibres- LFA, NT_{long1} and NT_{long2}- showed a significant increase in total cell number in the lavage fluid (Figure 3.10 I). We also measured the number of granulocytes, which included both neutrophils and eosinophils, as an indicator of acute inflammation in the lavage fluid. Again only mice which were injected with long fibres elicited an inflammatory response as shown by the increased number of granulocytes that was significantly greater compared to the vehicle control (Figure 3.10 II). Mice injected intrapleurally with SFA, NPCB, NT_{short}, NT_{tang1} or NT_{tang2} which did not contain long fibres failed to induce an increase in the numbers of pleural granulocytes. The inflammatory response elicited by the long CNT samples was significantly greater than the vehicle control treated mice but also significantly greater than any increase in pleural granulocytes induced by the short CNT samples highlighting the sensitivity of this model to fibre length (Table 4). Protein levels in the lavage fluid, which are indicative of the fluid exudate of

inflammation, reflected the pattern seen with granulocyte influx, although SFA and NT_{tang1} samples did reach significance compared to the vehicle control (Figure 3.10 III).

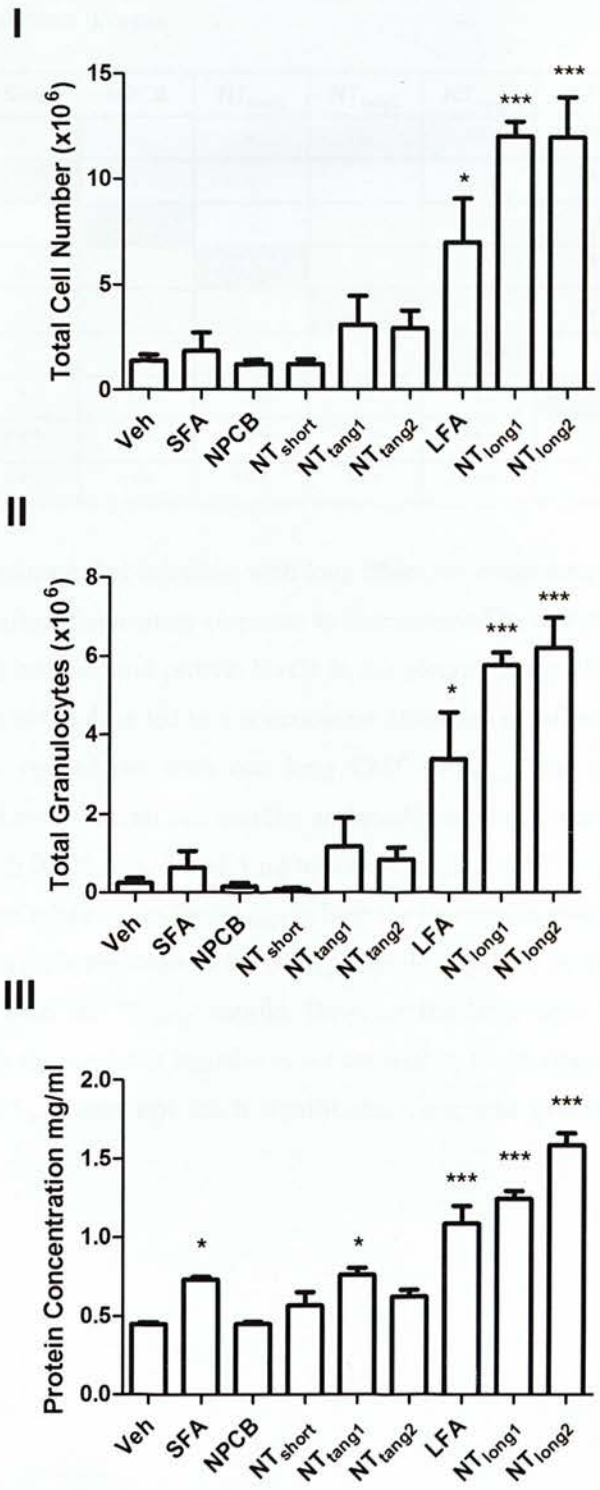

Figure 3.10: Acute inflammatory response to intrapleural injection of fibre panel. Total cell number (I), total granulocytes (II), and total protein (III) were measured in the lavage fluid of mice injected with 5

*µg of the particle panel and controls at 24 hours after injection. *p <0.05; **p < 0.01; ***p <0.001 versus vehicle control. Data represent mean ±SEM (n = 5 mice per treatment group).*

Table 3.4: Significance of differences in inflammatory responses as measured by granulocyte recruitment between treatment groups.

	VC	SFA	NPCB	NT_{short}	NT_{tang1}	NT_{tang2}	LFA	NT_{long1}	NT_{long2}
VC		-	-	-	-	-	**	***	***
SFA	-		-	-	-	-	*	***	***
NPCB	-	-		-	-	-	**	***	***
NT_{short}	-	-	-		-	-	*	***	***
NT_{tang1}	-	-	-	-		-	-	***	***
NT_{tang2}	-	-	-	-	-		-	***	***
LFA	**	*	**	*	-	-		-	*
NT_{long1}	***	***	***	***	***	***	-		-
NT_{long2}	***	***	***	***	***	***	*	-	

The results above demonstrate that injection with long fibres, of either amosite asbestos or MWCNT generate a significant acute inflammatory response as characterised by a dramatic increase in total cell number, total neutrophil number and protein levels in the pleural lavage fluid. The next step was to establish if an alteration of the dose led to a concomitant alteration in inflammatory response. A dose response was therefore carried out with one long CNT (NT_{long2}) and one short CNT (NT_{tang1}) exemplar. Figure 3.11 shows the total cell number and total granulocyte number in the pleural lavage fluid of mice treated with 0.125, 0.5, 2 and 5 µg/mouse of NT_{tang1} and NT_{long2}. The results indicate a clear linear dose-response relationship for NT_{long2} in both the increase in total cells and granulocytes. The number of granulocytes in response to the NT_{tang1} sample appear to be increasing with dose albeit to a much lower level than the NT_{long2} sample. However the large error bars associated with the highest dose suggest that this apparent increase is not consistent. Furthermore the level of granulocyte influx in response to NT_{tang1} does not reach significance compared to vehicle control at any dose tested.

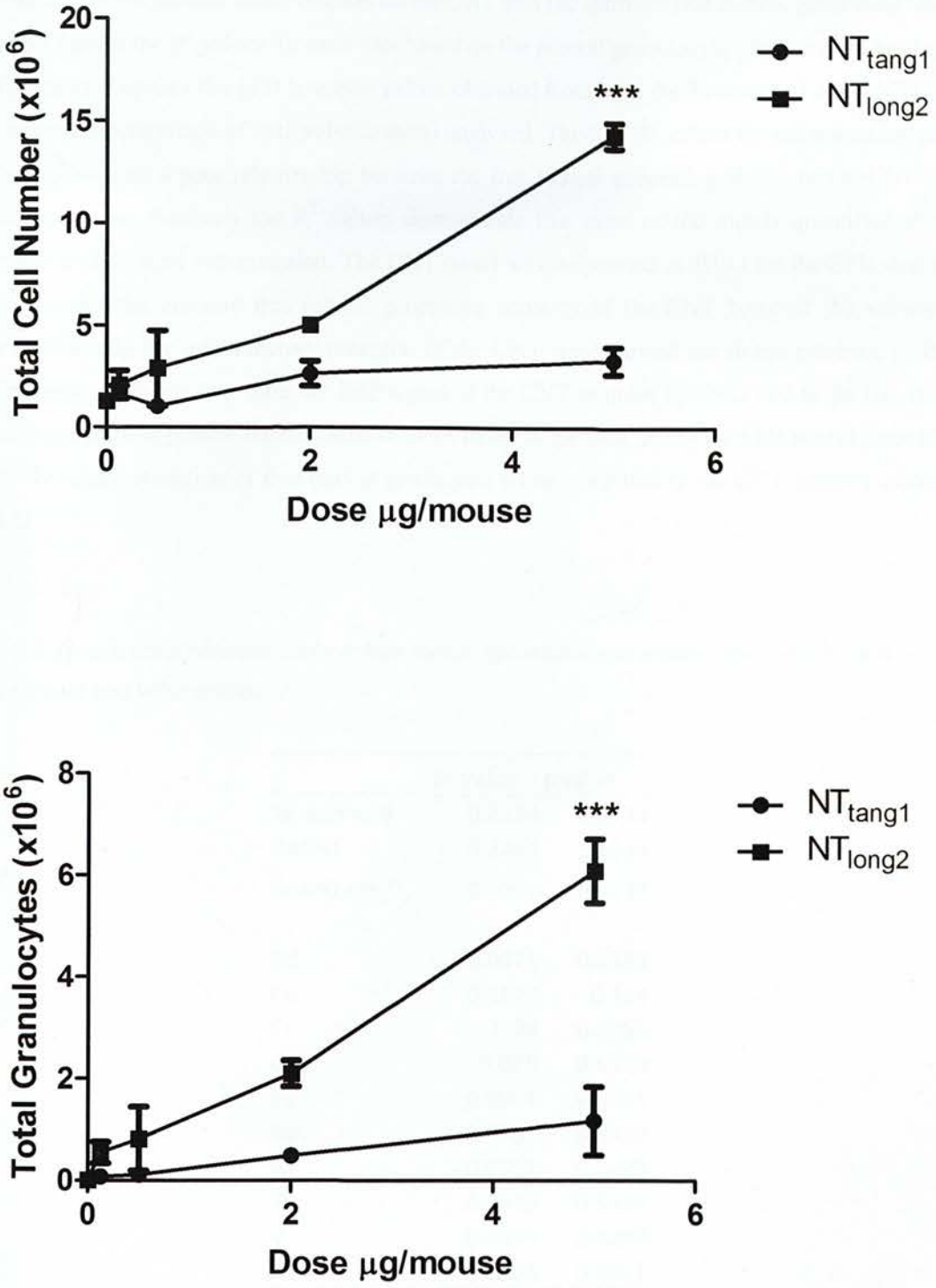

*Figure 3.11: Dose reponse post injection to short and long CNT. (I) Total cell number and (II) total granulocyte numbers were measured 24 hours post injection of a range of doses of NT_{tang1} and NT_{long2} CNT samples. ***p <0.001 versus vehicle control. Data represent mean ±SEM (n = 3 mice per treatment group).*

The neo-vascularisation of the lesions is necessary for the continued growth of the lesions over time and suggests that the lesions are permanent pathogenic changes in the pleural cavity which are unlikely to be resolved. Based on observations that common cellular and molecular mechanisms activated during wound healing are also often active in cancer tissue it has been postulated that tumours may be considered 'wounds that do not heal' (Dvorak, 1986). Chronic stimulation of macrophages by long fibres may lead to a persistent release of mitogenic signals essential for wound repair leading to aberrant proliferation of the mesothelial cells thereby promoting malignant transformation.

Lesion formation along the chest wall and diaphragm in response to the same mass dose of asbestos fibres was also examined at 6 months post injection and compared to mice treated with the NT_{long2} sample. Although the initial acute inflammatory response to long asbestos fibres was similar in magnitude to the response elicited by long CNT the extent of lesion development along the parietal pleural of both the chest wall and diaphragm was significantly less in mice exposed to the long asbestos fibre sample. This suggests that if performing a direct comparison on a mass basis, NT_{long2} is more potent at producing a pleural response than LFA. However considering the heterogeneity of the asbestos and long CNT samples in terms of fibre length and the relative difference in fibre densities mass may not be an appropriate metric to use to compare the potencies of different fibre types in the pleural space. The biologically effective dose is most likely to be comprised of the number of fibres above a threshold length. Due to the difficulties in performing accurate fibre counts and size distribution analysis of CNT because of their inherent structural propensity to aggregate, it was not possible to obtain 'potency per fibre' for LFA and CNT.

Here we have focussed on length as the important fibre dimension for the development of pleural pathogenicity. A recent study by Nagai et al, using the peritoneal model of mesothelial exposure, has proposed that CNT diameter rather than length is the critical factor in CNT-mediated fibrotic inflammation and carcinogenesis (Nagai et al., 2011). The authors demonstrated in vitro that mesothelial cytotoxicity was inversely correlated with the mean diameter of dispersed CNT. Furthermore only the thin CNT sample (diameter 50nm) caused fibrotic inflammation and tumour development after injection into the peritoneal cavity whereas rats treated with the thicker CNT (diameter 145nm) showed negligible fibrosis (Nagai et al., 2011). Although the mean diameter of the NT_{long2} sample used here is similar in value to the non-pathogenic sample in the Nagai study (165nm and 145nm respectively) the pleural responses to NT_{long2} reflected the fibrotic inflammation induced in the Nagai study by the NT with the smallest average diameter (50nm). Therefore the pathogenic potential of CNT at the mesothelium may not be restricted by diameter as the Nagai study suggests.

In summary, injection of long, straight carbon nanotubes into the pleural cavity of mice leads to the formation of a potent acute inflammatory response similar to the response elicited by long fibre

We attempted to correlate the level of acute inflammation generated by each member of the CNT panel with both the soluble metal fraction of the CNT and the intrinsic free radical generating ability. Figure 3.12 gives the R^2 values for each plot based on the pleural granulocyte number at 24 hours post injection plotted against the EPR intensity values obtained from both the Tempone-H and DMPO spin traps or the concentrations of each soluble metal analysed. The low R^2 values for inflammation versus EPR values suggest a poor relationship between the free radical generating ability of the CNT panel and inflammation. Similarly the R^2 values demonstrate that none of the metals quantified show a linear relationship with inflammation. The CNT panel was suspended in dH_2O for the EPR studies in order to assess the intrinsic free radical generating capacity of the CNT however the subsequent studies examining the inflammatory potential of the CNT were carried out in the presence of BSA. The difference in media may alter the ERP signal of the CNT samples however due to the free radical scavenging ability of protein the inclusion of BSA in the dispersion media for EPR would more likely lead to the underestimation of free radical production when compared to the CNT samples dispersed in dH_2O.

Table 3.5: Relationship between intrinsic free radical generation and inflammation and particle soluble metal content and inflammation.

	R^2 Value	p value
Tempone-H	0.2114	0.2131
DMPO	0.2264	0.1954
DMPO + H_2O_2	0.0001	0.9743
Cd	0.0071	0.8293
Co	0.3177	0.114
Cr	0.04	0.6055
Cu	0.025	0.6838
Fe	0.0051	0.8531
Mn	0.0001	0.9919
Ni	0.0552	0.5429
Ti	0.0439	0.5916
V	0.0075	0.8299
Zn	0.0003	0.9961

In order to examine the kinetics of the inflammatory response to the CNT samples the cellular inflammatory response in the pleural space was examined again at 7 days, 4, 12 and 24 weeks post-intrapleural injection, for representative long (NT_{long2}) and short (NT_{tang1}) CNT samples (Figure 3.12). The increase in total cells and granulocytes seen in the pleural lavage of mice injected with NT_{long2}

amosite asbestos. Injection of short or tangled CNT, forming small spherical aggregates does not cause inflammation showing that length is the primary cause of inflammation in this model. Retention of long fibres within the peritoneal cavity leads to the formation of large areas of fibrosis which again are not demonstrated with short spherical particles. This suggests that the fibre dimensions, in particular length of the CNT are critical drivers in CNT *in vivo* pathogenicity.

was maintained up to 7 days, with no reduction in the extent of the observed inflammation until 4 weeks post injection. The number of granulocytes in NT_{tang1} treated mice had waned to control levels by 7 days.

I

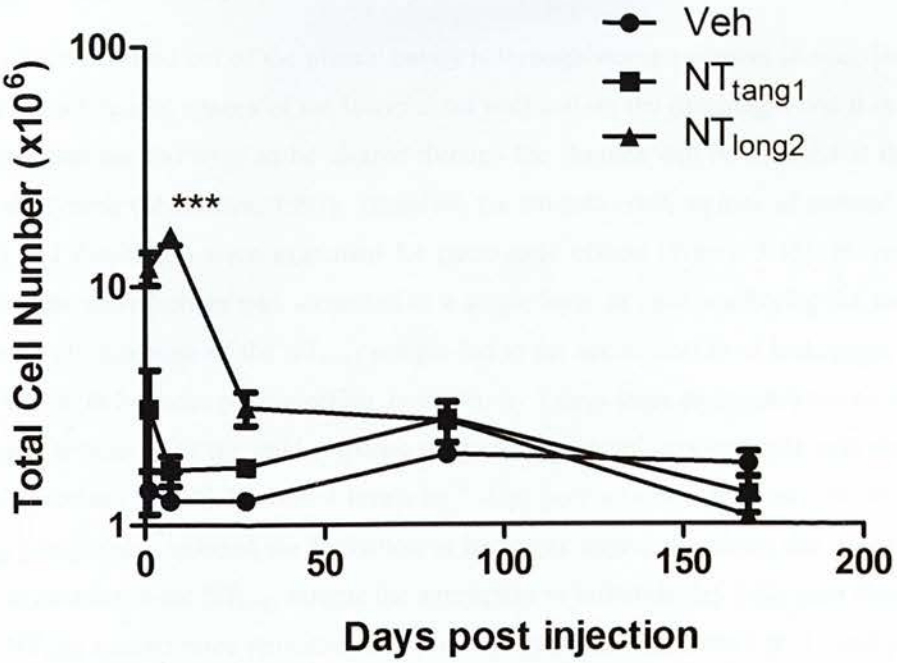

II

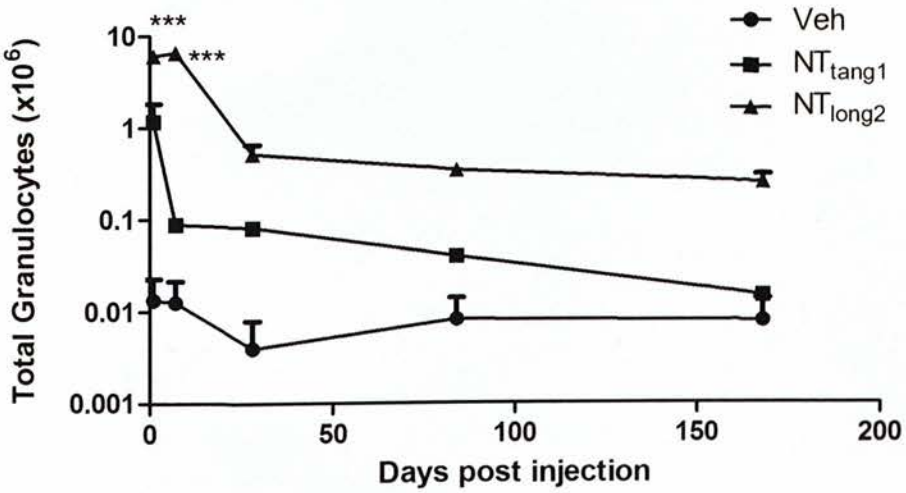

Chapter 4: Mechanism for the length-dependent inflammatory response to carbon nanotubes in the pleural space

4.1 Acknowledgements

Radio-labelling the short CNT sample (NT_{short}) and SPECT/CT imaging was carried out by Dr. Khuloud Al-Jamal and Mr. Antonio Nunes with input in the experimental design from Prof. Kostas Kostarelos (School of Pharmacy, University of London). Nickel nanowire synthesis was performed by Dr. Adriele Prina-Mello and Dr. Fiona Byrne at the Centre for Research on Adaptive Nanostructures and Nanodevices (CRANN), Trinity College Dublin. The size distribution of all the nickel nanowires was also performed by Dr. Fiona Byrne. Epifluorescent microscopy analysis of the lymph node tissue was performed by Dr. Adriele Prina-Mello.

4.2 Aims and Hypothesis

Particles deposited in the pleural space are cleared via passive removal in the flow of pleural fluid through stomata in the parietal pleura. The stomata which drain to the lymphatic system are 3-10 μm in diameter and are most densely situated in the caudal and posterior intercostals spaces of the chest wall and on the diaphragm (Chapter 1).

Failure to clear the long CNT from the pleural space, as suggested by the presence of CNT aggregates in the lesions of long CNT treated mice (Chapter 3, Figure 3.15), forms the basis of a proposed mechanism of long fibre pathogenicity in the pleural space, i.e. the inflammatory effects of long CNT and long fibres in general, arises as a consequence of retention at stomata. The rationale for this hypothesis is that the retention of long fibres facilitates the prolonged interaction of fibres with mesothelial cells and pleural macrophages at these points of egress of the lymph, whereas efficient clearance of short fibres will effectively remove the dose from the target tissue. The aim of this study is therefore to examine the role of stomatal size on the inflammatory potential of particles and fibres in the pleural space. The differential clearance of long and short fibres from the pleural cavity is also assessed using both CNT samples and an alternative high aspect ratio nanomaterial; nickel nanowires (NiNW).

4.3 Results

4.3.1 Pleural response to compact particles

We hypothesised that the inflammatory effects of long CNT and long fibres in general, arises as a consequence of a size-restricted clearance pathway from the pleural space, where the limiting factor is

*Figure 3.12: Progression of pleura inflammatory response over time. Total cell number (I) and total granulocytes (II) measured in lavage fluid of mice treated with either NT_{tang1} and NT_{long2} (5 µ/mouse) up to 168 days (24 weeks) post injection. Significance versus Vehicle control, * indicates p<0.05, ** indicates p<0.01, *** indicates p<0.001. Data respresents mean +s.e.m. of n=3 mice per treatment group.*

3.3.9 Acute response along the parietal pleura

The flow of pleural fluid out of the pleural cavity is through stomata present in abundance in certain regions in the intercostal spaces of the lower chest wall and on the diaphragm and it is hypothesised that particles that are too large to be cleared through the stomata will be retained at these points of egress of the lymph (Shinohara, 1997). Therefore the stomata- rich regions of parietal pleura of the chest wall and diaphragm were examined for pathogenic effects (Figure 3.13). In vehicle control-treated mice the mesothelium was identified as a single layer of cells overlaying the muscular tissue of the chest wall. Injection of the NT_{tang1} sample led to the accumulation of leukocytes over areas of the mesothelium at 24 hours post injection, however, by 7 days these aggregates are no longer visible. The complete resolution of the mild response to the NT_{tang1} sample corresponds with the reduction in pleural cell numbers to vehicle control levels by 7 days post injection as shown above. Injection of the NT_{long2} sample also induced the formation of leukocyte aggregates along the mesothelium by 24 hours but in contrast to the NT_{tang1} sample the aggregates of inflammatory cells seen along the parietal pleura of NT_{long2} treated mice remained and even increased in size from 1 to 7 days post-injection. Long nanotubes could also be seen in association with these inflammatory cell aggregates demonstrating their retention at this site.

the calibre of the pleural stomata whose maximum diameter is 10 μm (Figure 3.1 I). In order to test this hypothesis we examined the pleural response to a panel of compact particles of varying size and reactivity which included two well known pro-inflammatory particles that are small enough to exit through the stomata; quartz and coal mine dust, and polystyrene beads in two sizes – 3 μm and 10 μm (see Figure 3.1 II for size distributions).

I

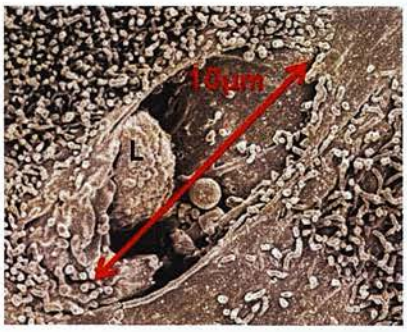

II

Particle	Size (μm)
Quartz	2.4 ± 0.8
Coal mine dust	2.1 ± 0.2
3μm beads	3 ± 0.1
10μm beads	10.3 ± 0.4

Figure 4.1: Size-restricted clearance from the pleural space. (I) SEM image of a lymphatic stoma (diameter 10 μm) found on the parietal pleura of the chest wall of a mouse. L indicates a leukocyte passing through the stoma. (II) Mean size of particles as measured by dynamic light scattering. Data represented as a mean ± sem.

The propensity of the particle samples to lyse erythrocytes, a simple assay to assess the reactivity of particles with biological membranes and a good indicator of the inflammatory potential of particles in vivo (Lu et al., 2009), was measured (Figure 4.2). Only the DQ12 quartz dust samples and the coal mine dust sample were shown to cause dose dependent haemolysis of red blood cells in vitro.

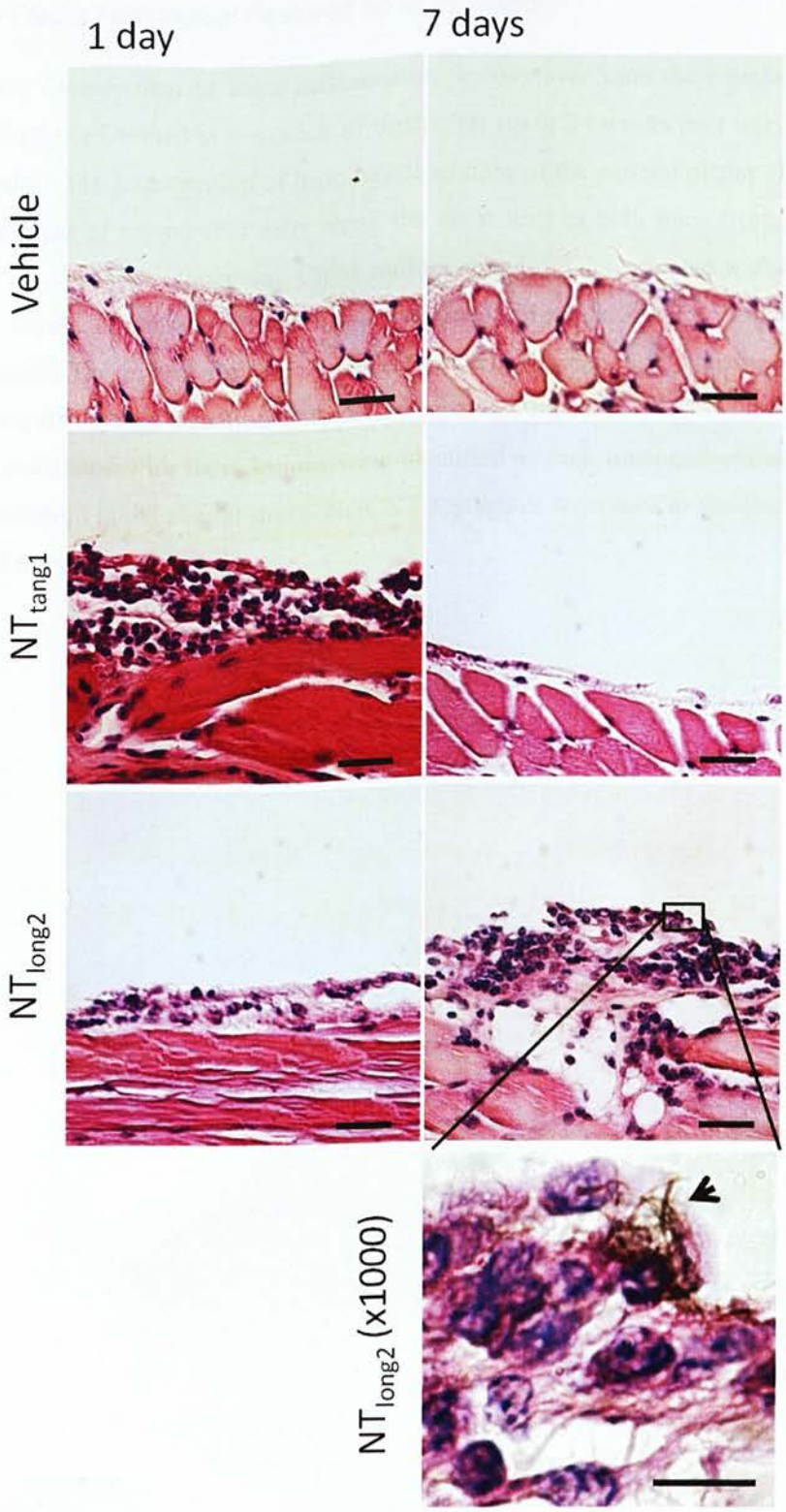

Figure 3.13: Histological examination of chest wall samples from mice injected with NT_{tang1} and NT_{long2} (5 µg/mouse) at 1 day and 7 days post injection. Aggregates of inflammatory cells are present in both NT_{tang1} and NT_{long2} samples at 1 day, but only in NT_{long2} samples at 7 days. Black arrow head indicates long CNT aggregates in x100 magnification of NT_{long2}, 7 day sample. Scale bar = 20µm.

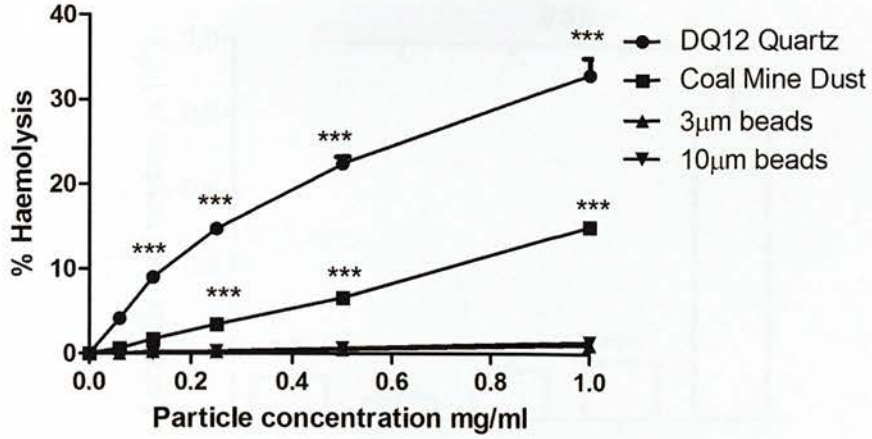

Figure 4.2: Haemolytic potential of the compact particle panel. Particle samples were dispersed in saline by sonication and incubated with washed red blood cells (RBC) for 30 minutes. Haeomoglobin release was measured by measureing the absorbance of haemoglobin (550 nm) in the supernatant. Haemolytic potential was calculated as % haemoglobin release compared to triton-x lysed RBC. Data represented as a mean ± sem (n=3).

Despite the reactivity of the quartz and coal mine dust samples within the haemolysis assay we hypothesised that only the 10 μm beads should be retained and would therefore elicit inflammation in the pleural space. As expected when instilled into the pleural space at the same mass dose as the CNT, no response was seen with the quartz, the coalmine dust or the 3 μm beads. In contrast the 10 μm beads which are too big to exit through the stomata elicited a significant influx of granulocytes into the pleural space at 24 hours (Figure 4.3).

3.3.10 Parietal Pleura Histological Features up to 24 weeks

To investigate the development of these inflammatory lesions over time the parietal pleura of the chest wall was further examined at a number of timepoints up to 24 weeks post injection of NT_{tangl} and NT_{long2} (Figure 3.14). Examination of histological sections of the parietal pleura of the chest wall showed a single layer of mesothelial cells along the chest wall in both mice treated with vehicle control or with NT_{tangl} at every timepoint. Chest wall sections from mice treated with NT_{long2} showed the presence of fibrotic lesions which continued to increase in size over time from 4 weeks to 24 weeks post-injection. The lesions had high collagen content, determined by staining with Picosirius Red (PSR), which displayed a stratified morphology separated by cellular aggregates. Aggregates of long nanotubes associated with these lesions were identified at each timepoint which demonstrated their sustained retention in the pleural space. No CNT aggregates were seen in the chest wall sections of NT_{tangl} treated mice.

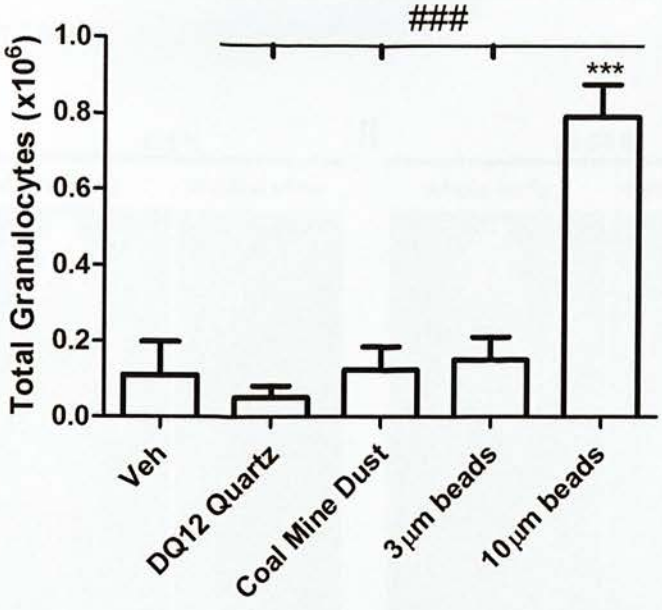

*Figure 4.3: Size-dependent inflammatory response to compact particles in the pleural space. Total granulocytes measured in the pleural lavage fluid of mice 24 hours after injection of particles (5 μg/mouse). Only the 10 μm beads caused a significant increase in granulocytes. Data represented as a mean ± sem. ***p<0.001 versus vehicle control.*

4.3.2 Length-dependent retention of fibres

We used two indirect approaches to assess the hypothesis that, similar to the large polystyrene beads, long CNT were retained in the pleural space whilst short fibres were cleared through the stomata.

4.3.3 SPECT/CT imaging of radiolabelled short CNT fibres

The first approach was to use dynamic SPECT/CT imaging to visualise the fate of radiolabelled short CNT (NT_{short}-DTPA [^{111}In]) after direct injection into the pleural space. We could only utilise short CNT since the process of radioactive labelling is destructive to the graphene structure and causes defects leading to fibre shortening. We were therefore unable to visualise, by this method, the fate of long CNT. Imaging during the first hour following administration of the radiolabelled CNT indicated widespread diffusion of the signal largely confined to, and throughout, the pleural cavity (Figure 4.4 I). Within 1 hour and increasingly thereafter, the short CNT were seen to accumulate in defined regions in the upper thoracic cavity. These areas were identified as the cranial mediastinal lymph nodes; two bilateral lymph nodes located lateral to the thymus. At 24 hours post-administration the signal from NT_{short} was localised almost exclusively within these lymph nodes (Figure 4.4 II). The control [^{111}In] DTPA label alone showed rapid translocation to the bladder with almost the entire dose cleared within the 1st hour after intrapleural administration (Figure 4.4 III). This demonstrated the

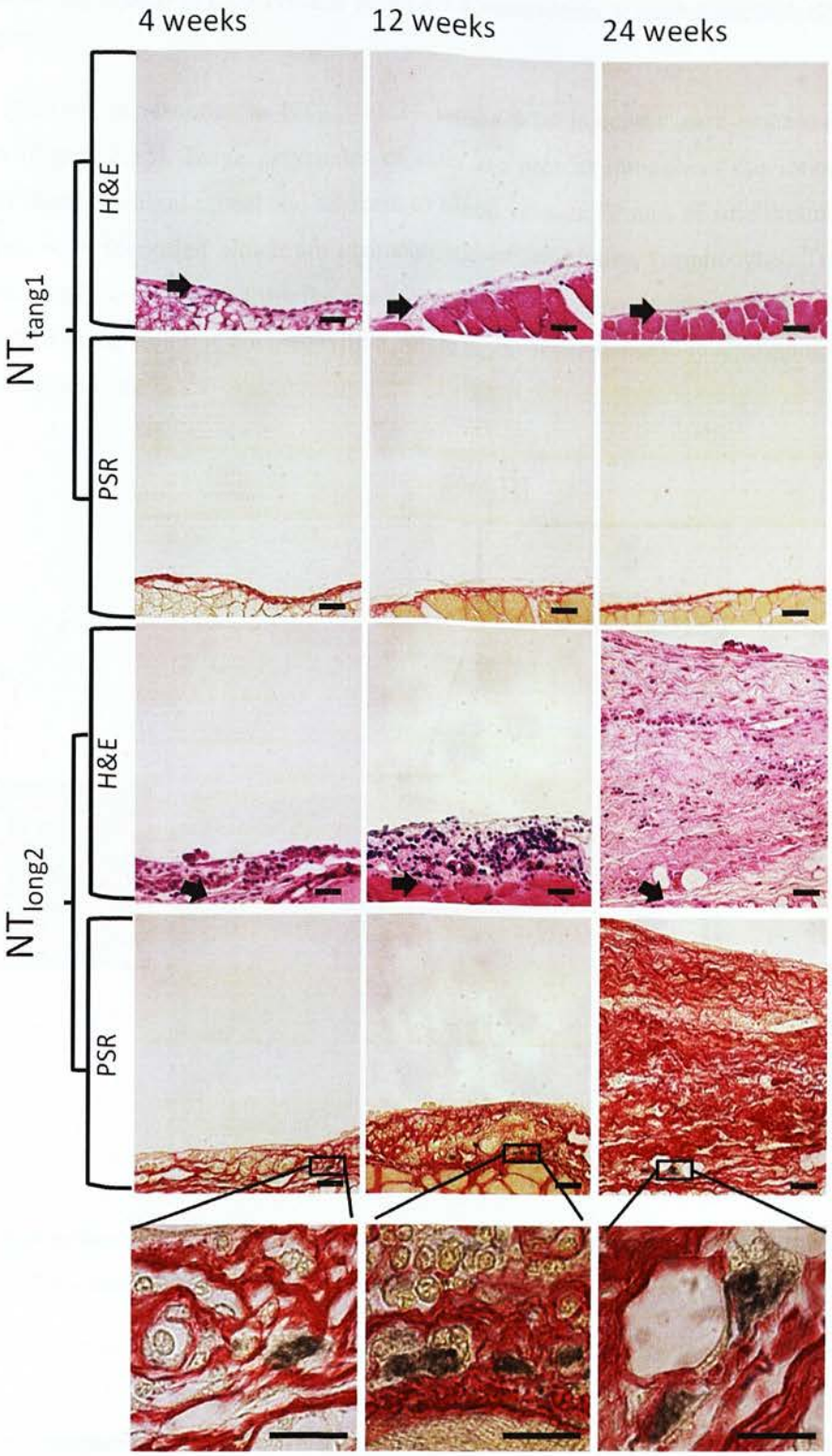

Figure 3.14: Lesion development up to 24 weeks. Parietal pleura of the chest wall of mice treated with NT_{tang1} and NT_{long2} (5 µg/mouse) were examined histologically at 4, 12 and 24 weeks post injection. Sections were stained with both Haematoxylin & Eosin (H&E) for gross morphology and Picosirius Red (PSR) to stain collagen. Black arrows indicate level of original mesothelium. Call-outs to high

stability of *in vivo* radiolabelling of short nanotubes and their clearance from the pleural cavity to the specific mediastinal lymph nodes.

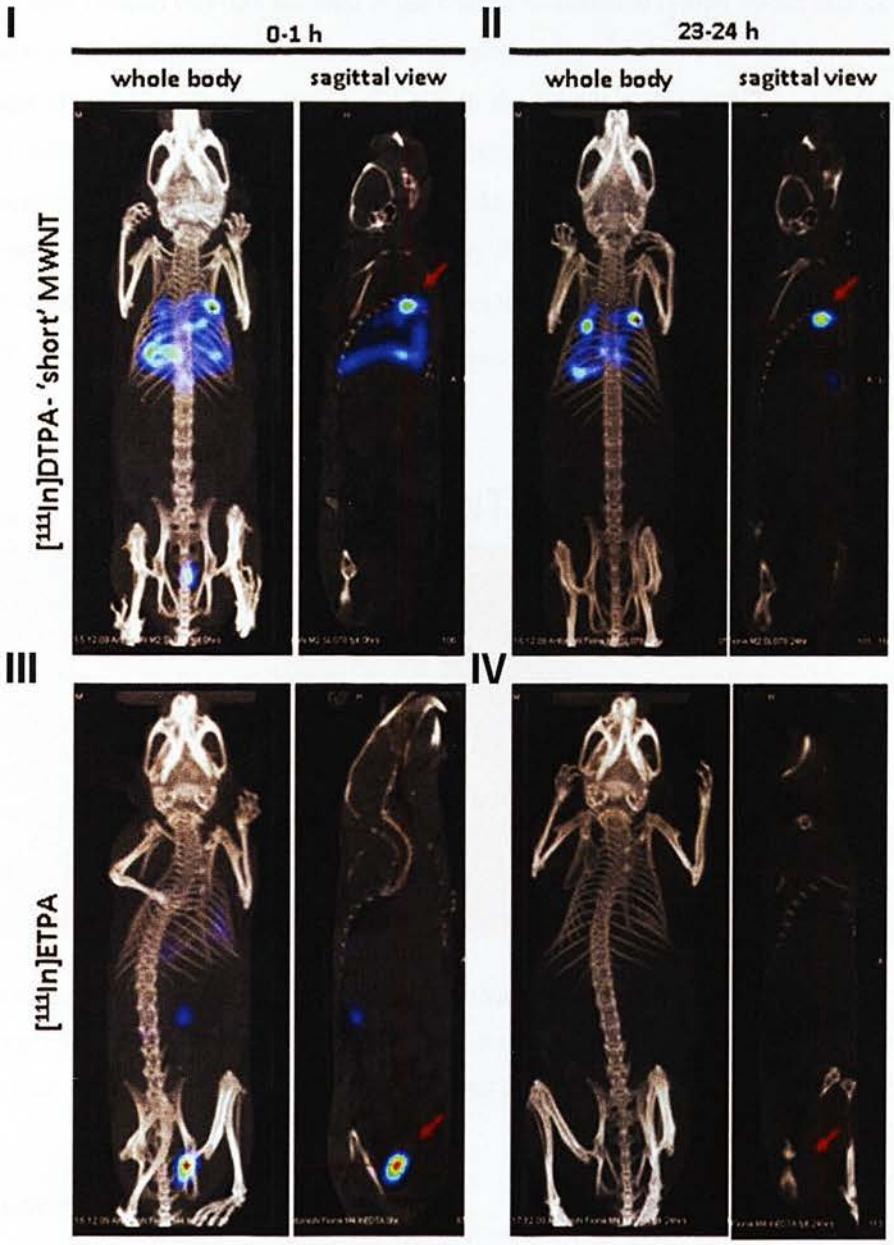

Figure 4.4: Clearance of CNT from the pleural space. Whole-body SPECT/CT imaging of NTshort-DTPA [^{111}In]. Imaging was preformed immediately (0 to 1 hour) and 1 day (23 to 24 hours) after intrapleural administration of 5 µg NTshort-DTPA [^{111}In] (I, II) or [^{111}In] DTPA (III, IV). SPECT/CT-fused images of the whole body (anterior view) and sagittal planes are shown. Arrows indicate the cranial mediastinal lymph nodes (I, II) and bladder (III, IV) in the case of NTshort-DTPA [^{111}In] and [^{111}In] DTPA, respectively.

power view show aggregates of CNT present within the fibrous lesion at each timepoint. Scale bar indicates 20 μm.

The lesions observed in response to NT_{long2} at 24 weeks post injection were examined at higher magnification (Figure 3.15). Large aggregates of cells are present throughout the lesion but more predominantly along the basal aspect and adjacent to blood vessels. Groups of small round cells with little cytoplasm were identified which are characteristic of infiltrating lymphocytes. This suggests cells are infiltrating into the lesion from the vascular system indicating a chronic inflammatory state. The upper surface of the lesion is covered with a single layer of predominately squamous cells which resemble mesothelial cells.

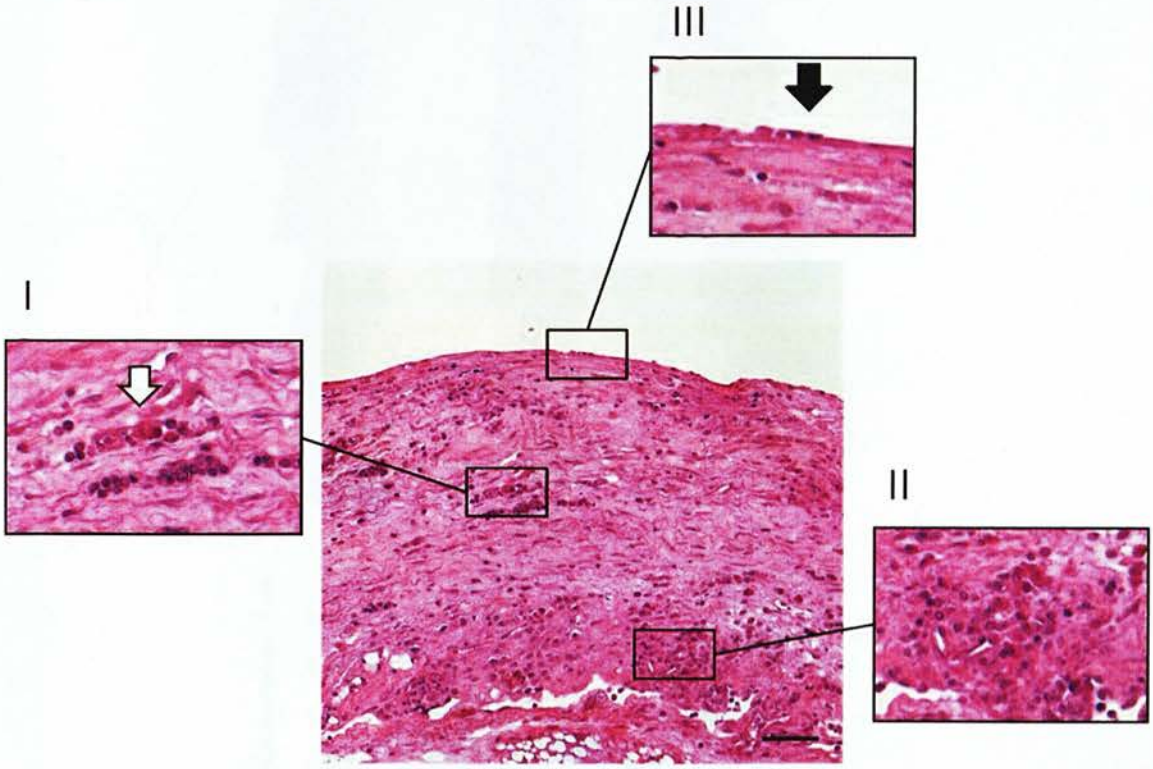

Figure 3.15: High power views NT_{long2}-induced lesion 24 weeks post injection. White arrow indicates lymphocytic infiltrate, black arrow indicates mesothelial cells overlaying the lesions. Scale bar= 20μm.

To determine the full extent of lesion development sequential low magnification microscopic images of chest wall sections were taken and digitally aligned (Figure 3.16). Using calibrated software the lesion area was measured. The area of lesion in a section was expressed in mm^2 and this value was divided by the total length of the chest wall section to account for differences in section length to give a lesion area volume (mm^2) per mm of chest wall. The rate of lesion growth from 4 to 12 weeks was calculated to be $0.0025mm^2$/week but increased to $0.0116mm^2$/week between 12 and 24 weeks post injection. The collagen content of the lesions was measured and shown to increase in percentage of

4.3.4 Clearance of long and short fibre to cranial mediastinal lymph nodes

We took advantage of the knowledge gained from the clearance of the radiolabelled CNT that the destination of fibres cleared through stomata is the cranial mediastinal lymph nodes and examined the fibre burden in these lymph nodes 24 hours after intrapleural injection of short and long CNT (Figure 4.5). The results showed a greater amount of CNT in the lymph nodes in NT_{short} treated mice than NT_{long2} treated mice. The accumulations of CNT observed in the mice treated with the long CNT sample were confined to the periphery of the lymph node whereas short CNT aggregates could also be seen in the centre of the lymph node tissue. However these results were qualitative because of the difficulties of counting the very small CNT in lymphoid tissue and interpretation was further confounded by the presence of short fibres in the NT_{long2} samples (approximately 15% fibres shorter than 15 μm).

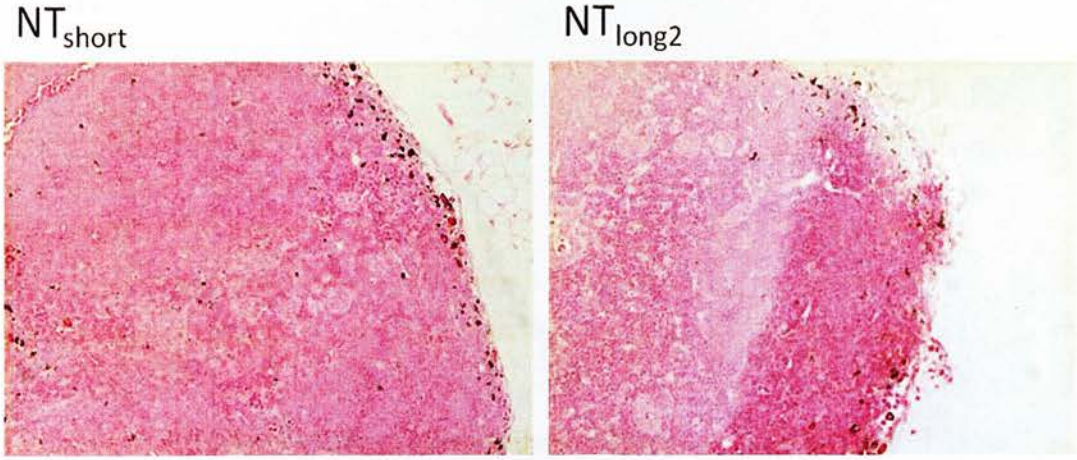

Figure 4.5: Mediastinal lymph node burden. Cranial mediastinal LNs removed from mice intrapleurally injected with non-radiolabelled long and short CNTs (5 μg/mouse) were sectioned and stained with H&E 24 hours post injection. Black nanotubes are visible especially around the periphery of the nodes.

4.3.5 Nickel oxide Nanowires

Alternative high aspect ratio nanofibres composed of nickel, so called nickel nanowires (NiNW), were employed to further explore the length-dependent retention of fibres in the pleural space. The benefit of using the NiNW samples to address this hypothesis is that they are synthesised in tight size categories with very few short fibres in the long sample ($NiNW_{long}$) and no long fibres in the short sample ($NiNW_{short}$) (Figure 4.6). The mean fibre length for the long and short NiNW samples was determined to be 24 μm and 4 μm respectively. Additionally the NiNW are more readily visualised as individual fibres than the CNT sample in tissue sections.

the total lesion from 23% at 4 weeks to 57% at 12 weeks. The proportion of collagen in the lesion then remained at approximately 50% at 24 weeks post injection. This suggests that the increase in lesion area is due to both cell accumulation or proliferation and collagen deposition.

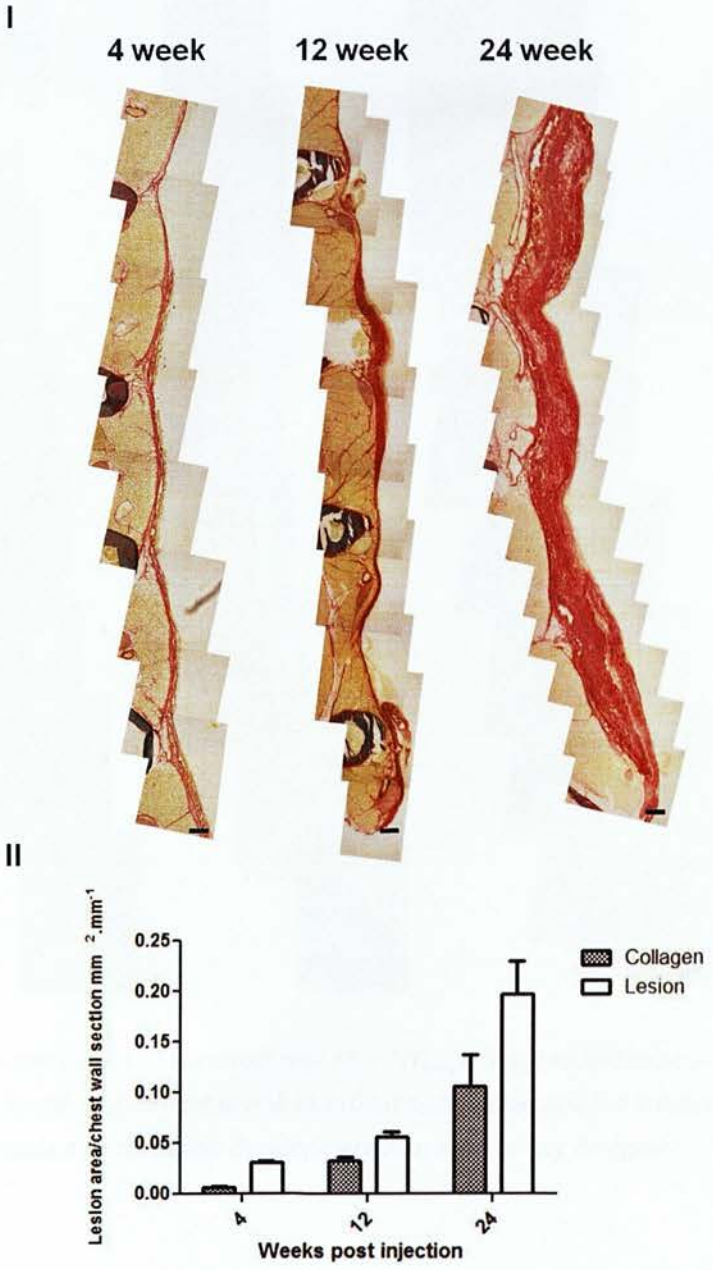

Figure 3.16: Lesion development along the parietal pleura in response to NT_{long2} (5 µg/mouse) over time. (I) Serial images were taken along the length of each chest wall at x100 magnification and the images re-aligned using Photoshop elements 4.0. (II) Lesion size and collagen content was quantified for the NT_{long2} samples and expressed as area per length of chest wall section ($mm^2.mm^{-1}$) (n=3, data represented as mean +s.e.m.).

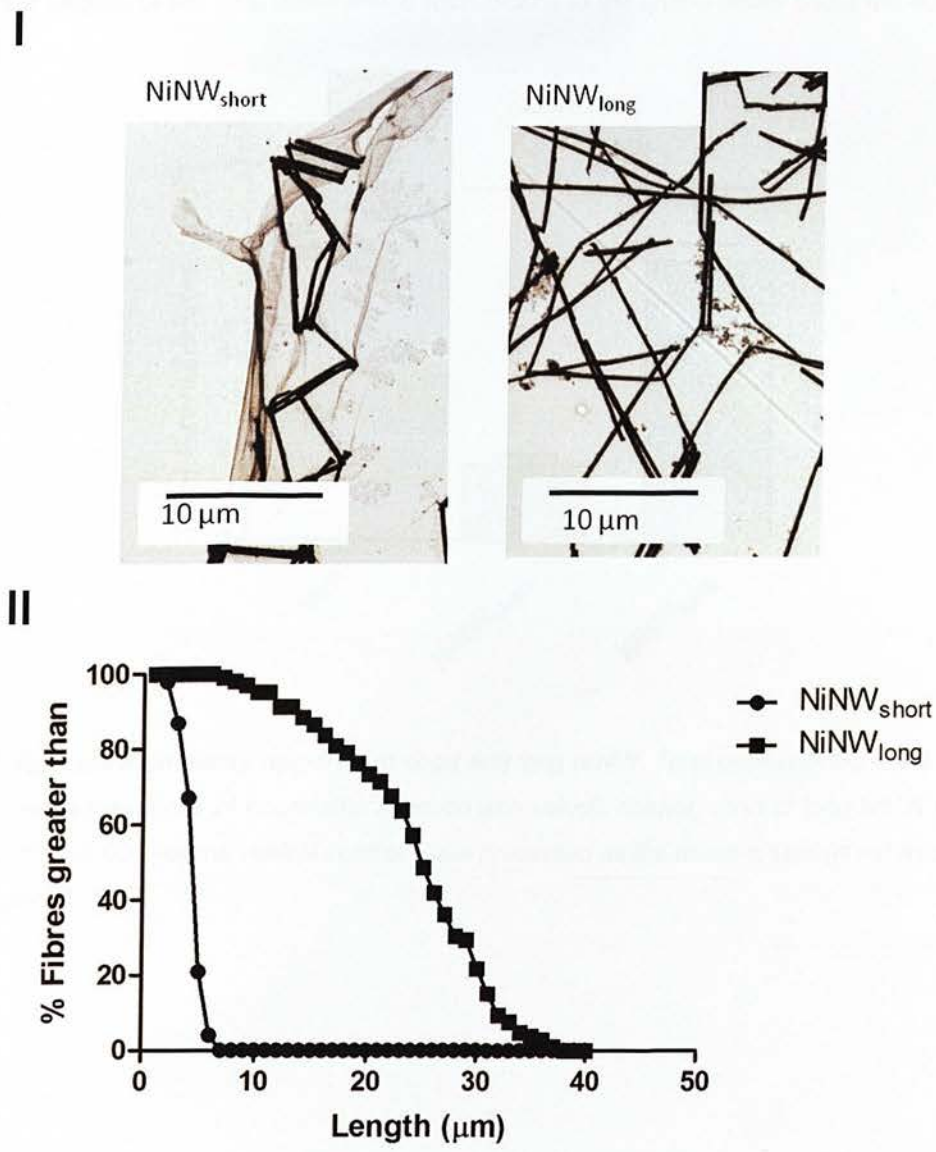

Figure 4.6: Nickel nanowires. (I) TEM images of short and long NiNW. (II) Size distribution of the short and long NiNW.

Similar to the CNT and asbestos samples injection of these NiNW samples into the pleural space resulted in a length-dependent acute inflammatory response (Figure 4.7). Therefore following injection into the pleural space we hypothesised that only short NiNW would appear in the lymph nodes on clearance from the pleural space. In contrast the predominately long NiNW would be retained in the pleural space and would not accumulate in the draining lymph nodes. Quantification of the number of NiNW in histological sections of excised mediastinal lymph tissue showed that a significantly greater number of fibres have migrated from the pleural space to the lymph nodes in mice treated with $NiNW_{short}$ compared to $NiNW_{long}$ (Figure 4.8 I, II). The length of the fibres in the $NiNW_{long}$ sample did not allow for the visualisation of a whole fibre in a single plane of view

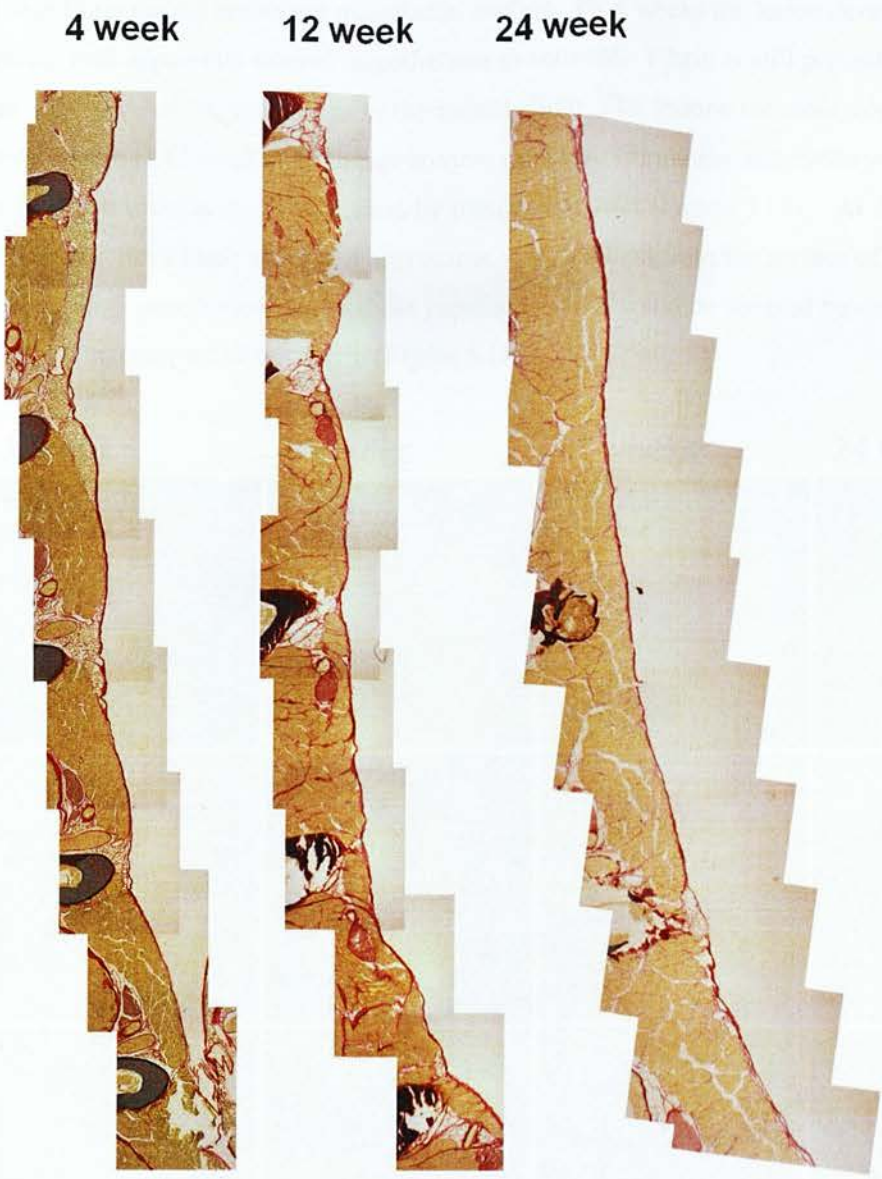

Figure 3.16: Parietal pleura of the chest wall after NT_{tang1} (5 µg/mouse) exposure. Serial images were taken along the length of each chest wall at x100 magnification and the images re-aligned using Photoshop elements 4.0. No lesion development was seen at any timepoint.

SEM images of comparable areas of the parietal pleura of the chest wall show the surface detail of the lesions as they develop over time from 1 week to 24 weeks post-injection (Figure 3.17). As in the histology sections, the vehicle control samples display continuous normal mesothelium at every timepoint. NT_{tang1} treated mice show a mild response at 1 week, with a small area of leukocyte aggregates on the mesothelial surface, a response which appears to resolve by 4 weeks with only a normal mesothelium seen at each subsequent timepoint. Conversely we see the development of a much more extensive lesion in NT_{long2} treated mice. At 1 week we see a large mat of leukocytes,

therefore the lengths of the long fibres which translocated to the lymph nodes could not be accurately measured.

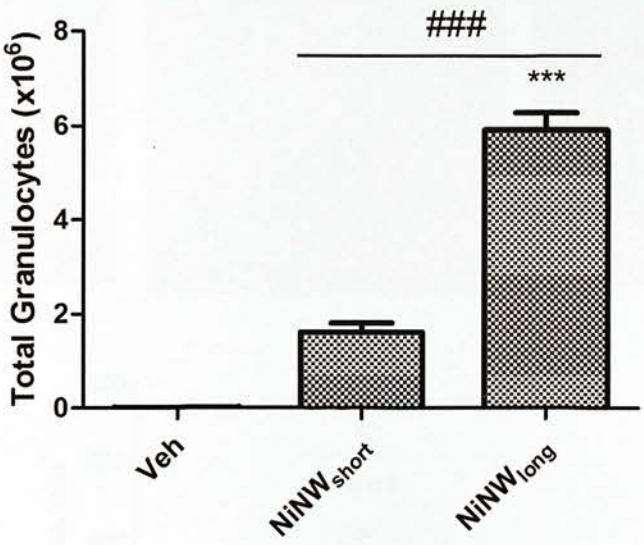

*Figure 4.7: Pleural inflammatory response to short and long NiNW. Total granulocytes in the pleural lavage fluid were measured 24 hours after injection with vehicle control, short or long NiNW (5 µg/mouse). ***p<0.001 versus vehicle control. Data presented as the mean ± sem (n = 3 mice per treatment group).*

bound with fibrin spread across the mesothelial surface. By 4 weeks the lesion develops more defined boundaries, with apparently normal mesothelium in between. Fibrin is still present which appears to assist in adherence of the aggregates to the mesothelium. The lesions are more contained within the intercostal spaces at 12 weeks. High-power view shows no fibrin now associated with the leukocytes and the apparent resurfacing of the lesion by mesothelial cells (Figure 3.18). At 24 weeks papillae; tongue-like structures made up of cell aggregates, which extend from the surface of the mesothelium-can be seen. High-power view shows these papillae to contain and be covered by mesothelial cells, as identified by the presence of microvilli (Figure 3.18).

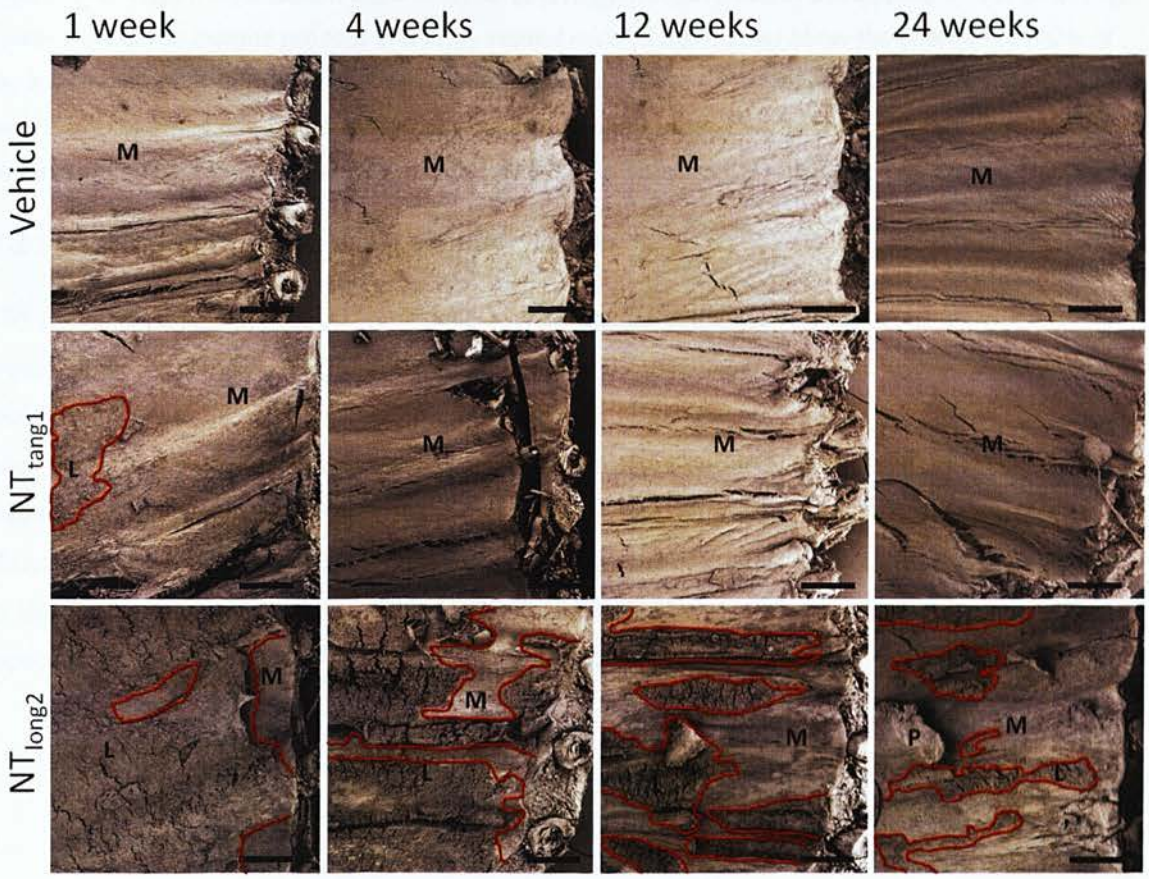

Figure 3.17: SEM analysis of lesion development over time. Mice were injected with Vehicle control (0.5% BSA/saline), NT_{tang1} or NT_{long2} (5 µg/mouse). Surface of the chest wall parietal pleura was examined by SEM at 1, 4, 12 and 24 weeks post-injection. Low magnification images (x30) show continuous, normal mesothelium (M) in vehicle control treated mice. (L) indicates the inflammatory lesions also outlined in red, which are mild and resolves quickly in NT_{tang1} treated mice or extensive and persistent in NT_{long2} treated mice. (P) indicates papillae; tongue-like extensions from the mesothelium, in NT_{long2} treated samples. Scale bar indicates 500 µm.

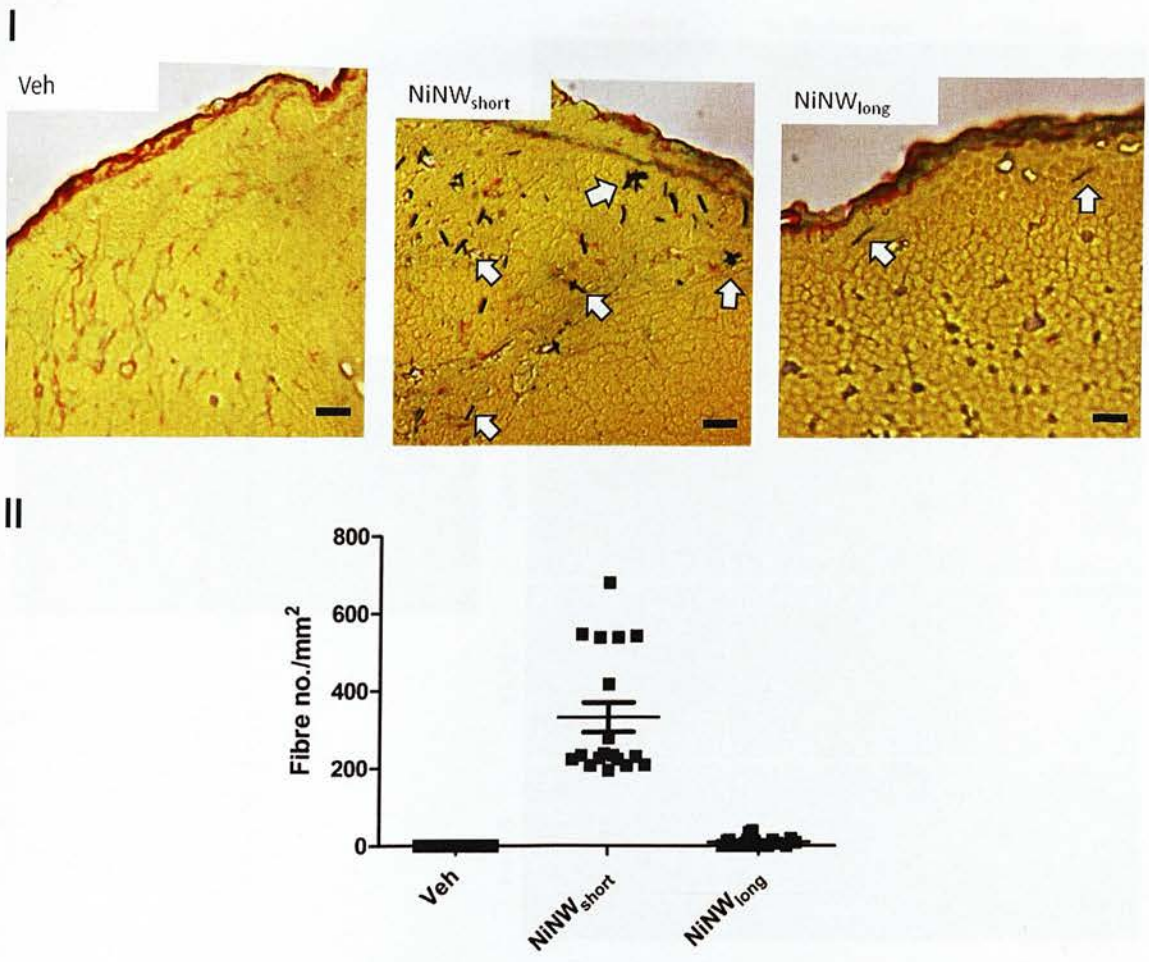

Figure 4.8: Mediastinal lymph node burden. Cranial mediastinal lymph nodes were removed from mice injected with vehicle control, short or long NiNW (5 µg/mouse) 24 hours post intrapleural injection and sectioned and stained with Sirius Red (I). White arrows indicate NiNW. Fibre number per square millimetre of lymph node tissue was determined by counting the total number of fibres from six sequential sections of each lymph node and measuring the area of tissue in each section. Scale bar indicates 10 µm.

Epifluorescence analysis of the tissues sections was used as a highly sensitive method for detection of the metallic NiNW in the lymph nodes of animals exposed to vehicle control (Figure 4.9) short NiNW (Figure 4.10) or long NiNW (Figure 4.11). NiNW were visible under epifluorescent microscopy as lighter areas (highlighted by red arrows in the images) thanks to localized surface plasmon resonance effects activated by their irradiation with an epifluorescent light source. Quantification of the numbers of NiNW which translocated to the lymph nodes is described in Table 4.1. As expected, a greater number of NiNW were identified in mice treated with $NiNW_{short}$ than with $NiNW_{long}$. No NiNW were identified in mice treated with vehicle control. This wholly supports the hypothesis that long fibres reaching the pleural space are selectively retained, never reaching the mediastinal lymph nodes, whilst short fibres are small enough to be cleared through the parietal stomata to the mediastinal nodes.

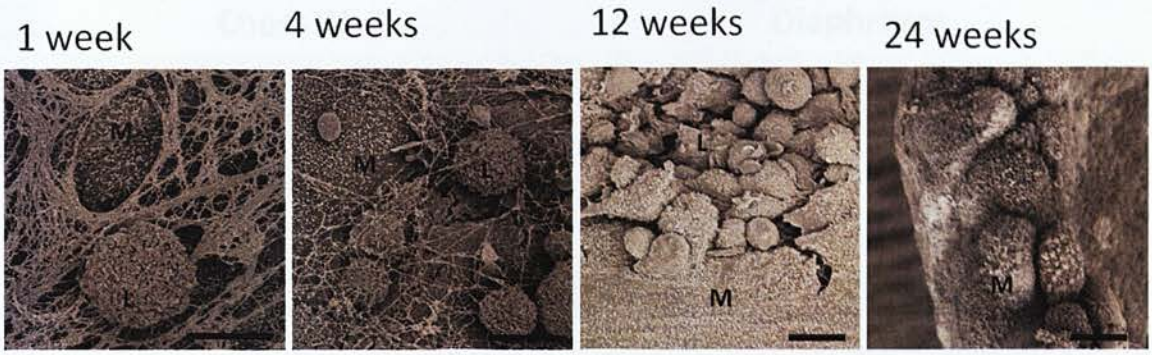

Figure 3.18: High magnification SEM analysis of NT_{long2}-mediated lesion development over time. High power view of the lesions present in NT_{long2} treated mice (5 µg/mouse) show the changing nature of the lesion over time from fibrinous leukocyte aggregates (L) at early timepoints to the progressive resurfacing of the lesion by mesothelial cells. The papillae present at 24 weeks appear to contain and be covered by mesothelial cells (M), as identified by the presence of microvilli. Scale bar = 10 µm.

3.3.11 Cellular proliferation along the mesothelium

The progressive resurfacing of the lesions by mesothelial cells as observed from the SEM analysis would suggest extensive proliferation of cells along the parietal pleura. To examine the extent of proliferation sections of chest wall and diaphragm from vehicle control, NT_{tang1} and NT_{long2} treated mice 24 weeks post injection were stained with anti-Ki67 antibody (Figure 3.19). Positive Ki67 staining, which identifies cells actively proliferating, was only observed along the surface of the parietal pleural lesion of NT_{long2} treated mice. Although the cell types are not differentially identified in the heterogeneous lesions the positive signal appears to be mostly concentrated along the pleural aspect of the lesion and therefore is likely that some of the positive cells will be mesothelial cells.

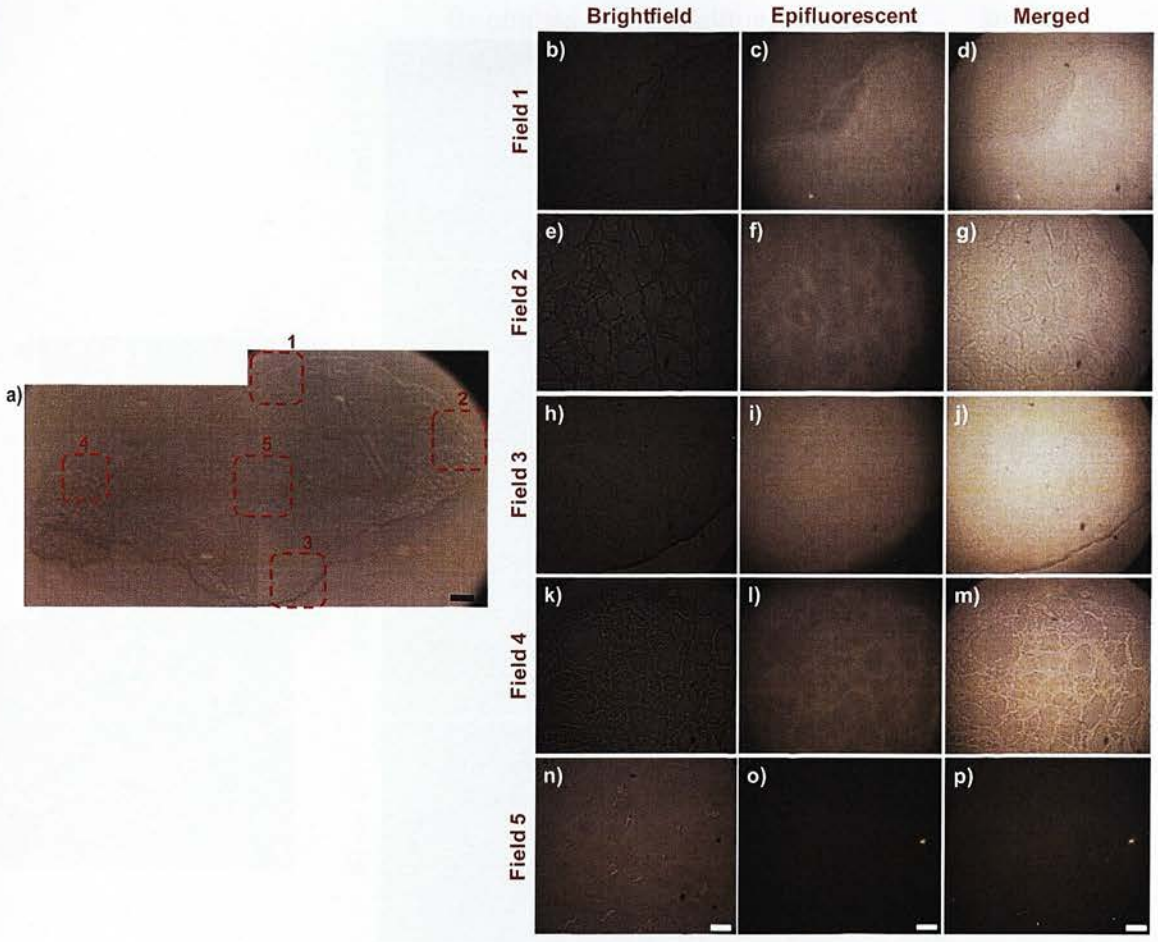

Figure 4.9: (a) Brightfield image of a lymph node sectionof an animal exposed to the vehicle control. (b-p) Enlargements of the tissue section showed in image a. (b, e, h, k n) Brightfield, (c, f, i, l, o) epifluorescence and (d, g, j, m, p) merged images showing the areas analysed in detail and highlighted with red boxes in image a. No NiNW are visible. (c, f, l) Epifluorescence background was generated by staining dyes previously added to the tissue section. The images are representative of all the tissue sections analysed. Scale bars: (a) 20 µm (20× magnification); (b-p) 10 µm (100x magnification).

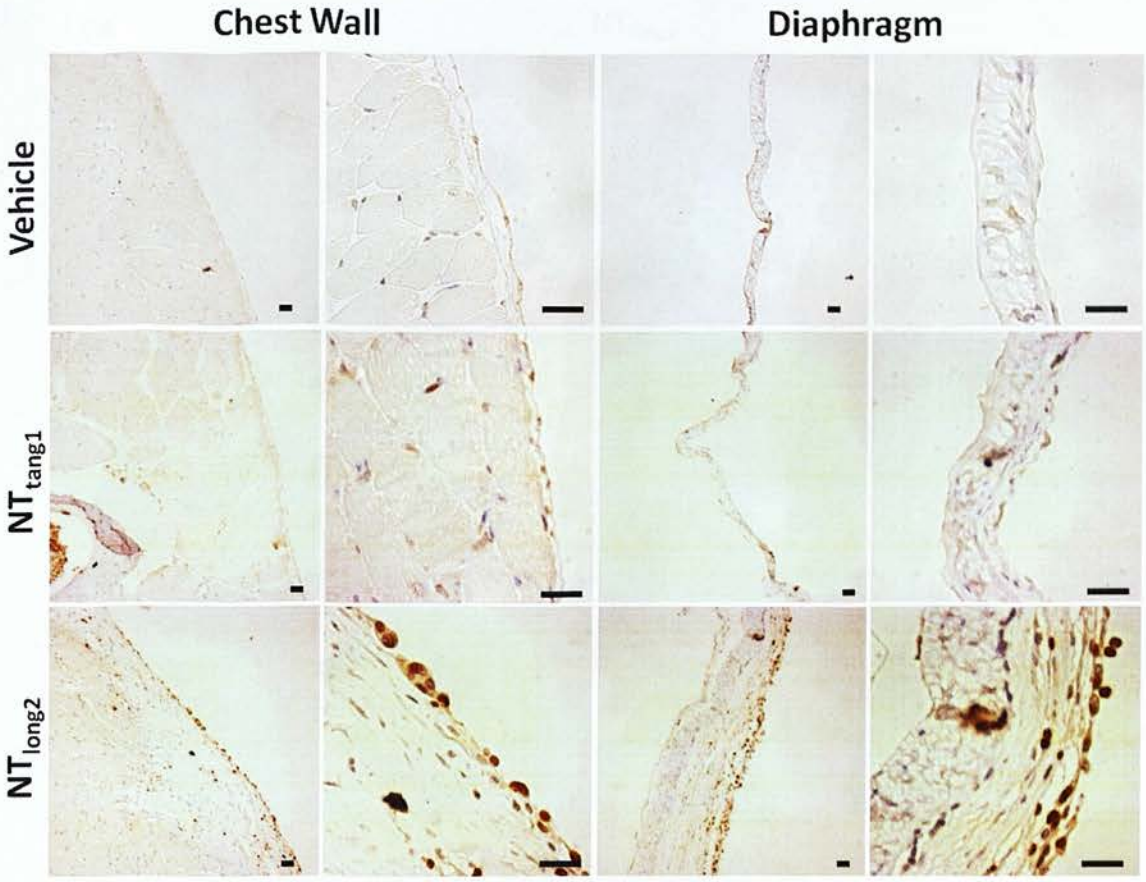

Figure 3.19: Cellular proliferation along the mesothelium of CNT treated mice. Cellular proliferation along the parietal pleural of the chest wall and diaphragm was examined in mice treated with vehicle control, NT_{tang1} and NT_{long2} (5 µg/mouse) at 24 weeks post injection. Sections were stained with anti-Ki67 antibody, a marker for actively proliferating cells. Ki67 positive staining was only detected along the mesothelium in mice treated with NT_{long2}. Scale bar = 20µm.

3.3.12 Comparison between long asbestos- and long CNT-induced lesion development

The extent of lesion development along the parietal pleura of the chest wall and diaphragm was also examined 24 weeks post injection of the LFA asbestos sample and compared to that of the long CNT sample (Figure 3.20, Figure 3.21). The extent of lesion development appeared to be much greater in response to the long CNT fibres than the long asbestos fibres administered at the same mass dose. Quantification of lesion area along the chest wall and diaphragm showed that the area of the lesions along the parietal pleura of mice treated with the NT_{long2} sample was significantly greater.

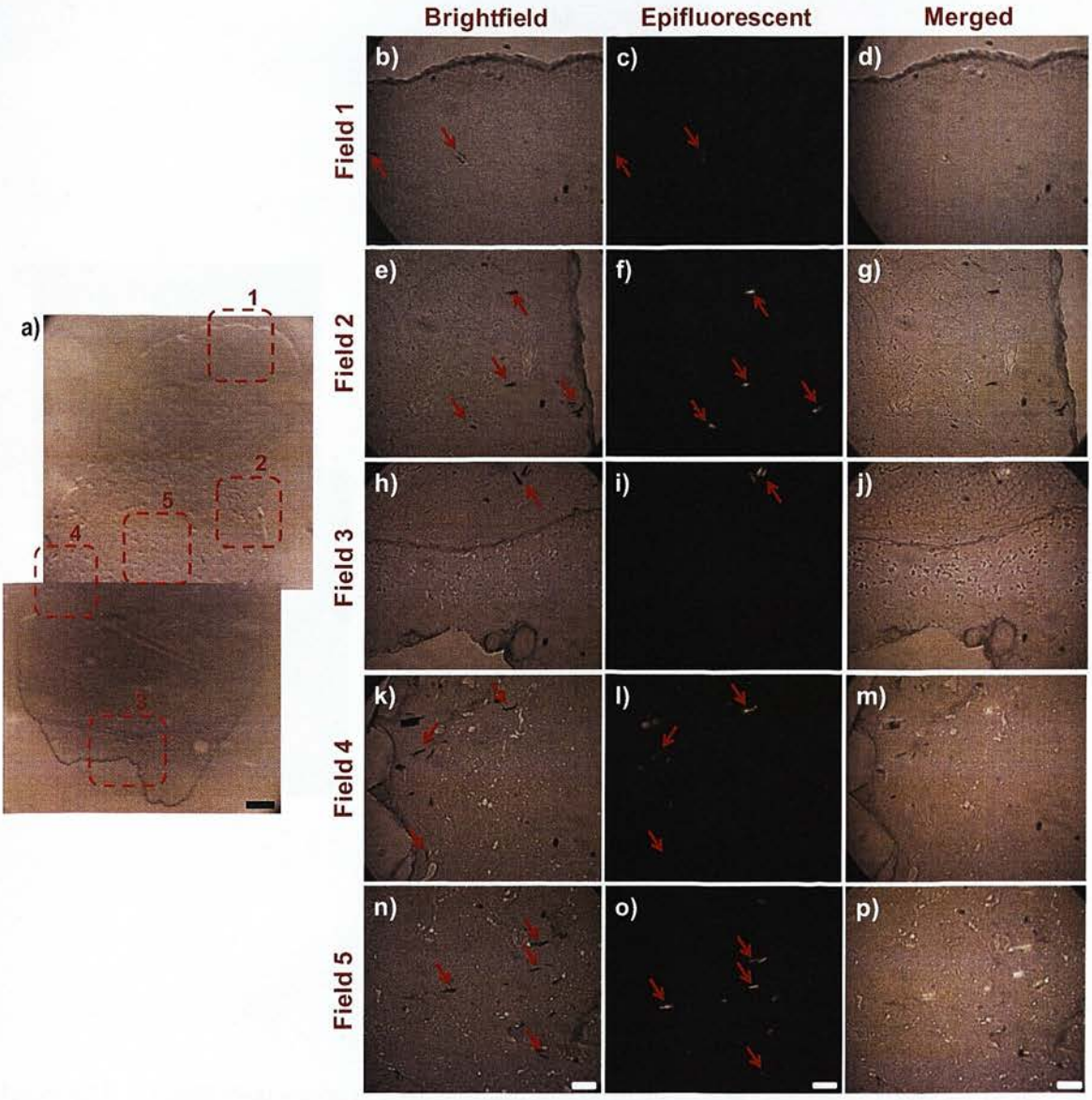

Figure 4.10: (a) Brightfield image of a lymph node section of an animal exposed to $NiNW_{short}$. (b-p) Enlargements of the tissue section showed in image a: red boxes highlight the areas analysed in detail. (b, e, h, k n) Brightfield, (c, f, i, l, o) epifluorescence and (d, g, j, m, p) merged images showing examples of single or multiple Ni NWs, visible as darker areas in brightfield and lighter areas in the epifluorescence images, are highlighted by arrows. The images are representative of all the tissue sections analysed. Scale bars: (a) 20 µm (20× magnification); (b-p) 10 µm (100x magnification).

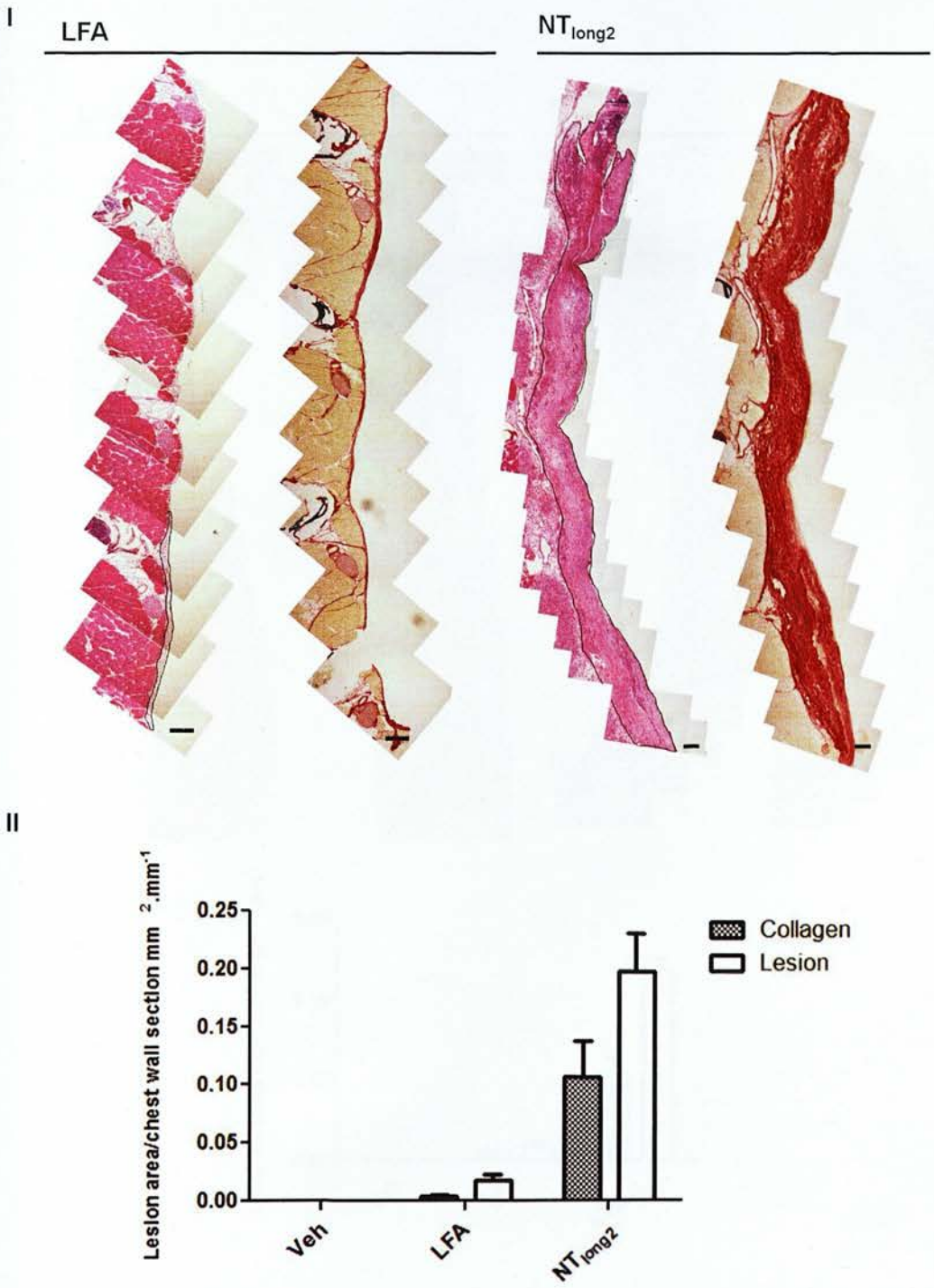

Figure 3.20: Comparison between the extent of lesion development along the chest wall in response to the same mass dose of LFA and NT_{long2} (5 µg/mouse) at 24 weeks post injection. (I) Serial images were taken along the length of each chest wall at x100 magnification and the images re-aligned using Photoshop elements 4.0. The areas of lesion are outlined in black for clarity. (II) Lesion size and collagen content was quantified and expressed as area per length of chest wall section ($mm^2.mm^{-1}$) (n=3, data represented as mean +s.e.m.).

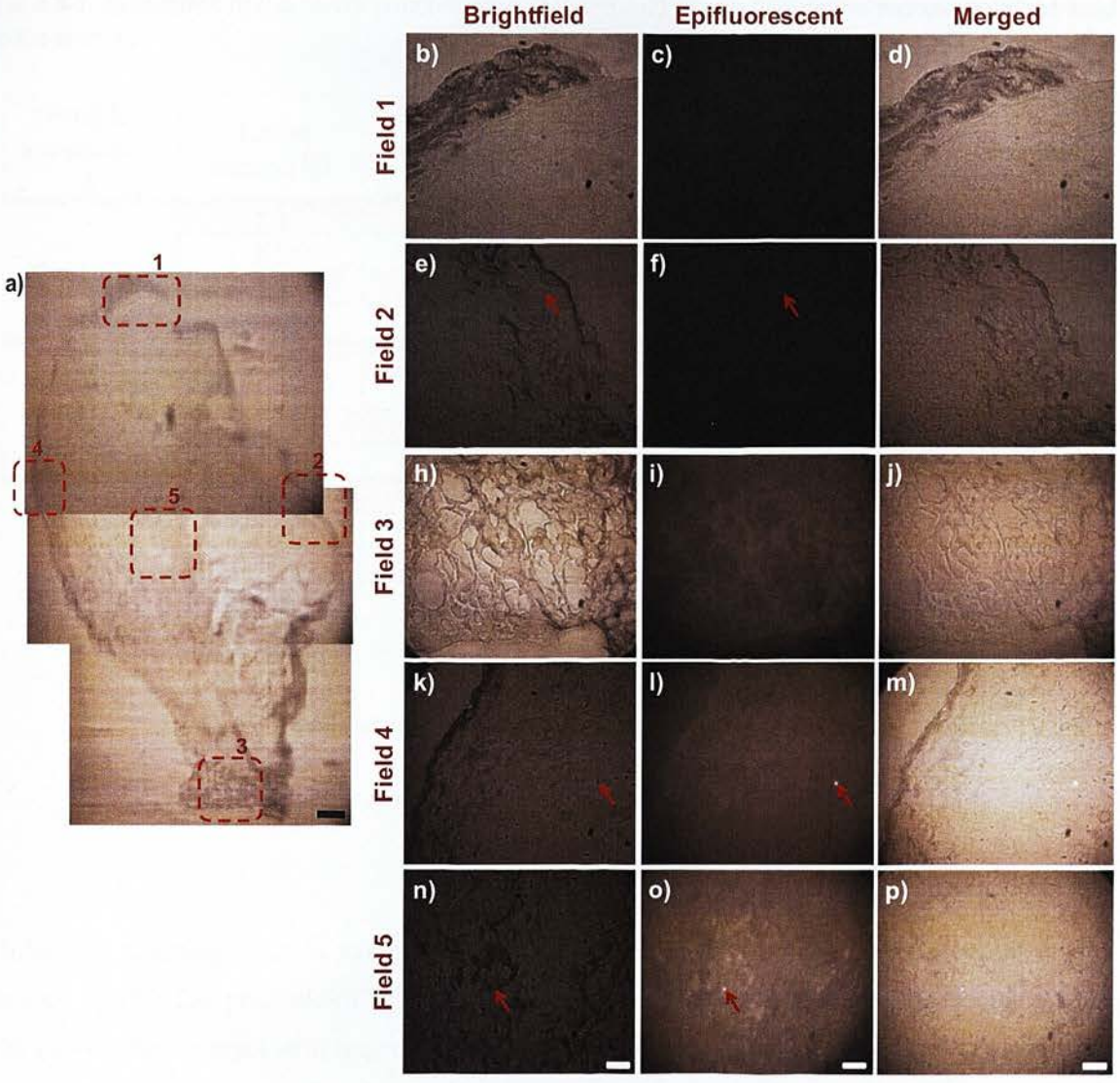

Figure 4.11: (a) Brightfield image of a lymph node section of an animal exposed to $NiNW_{long}$. (b-p) Enlargements of the tissue section showed in image a: red boxes highlight the areas analysed in detail. (b, e, h, k n) Brightfield, (c, f, i, l, o) epifluorescence and (d, g, j, m, p) merged images showing examples of single or multiple Ni NWs, visible as darker areas in brightfield and lighter areas in the epifluorescence images, are highlighted by arrows. The images are representative of all the tissue sections analysed. Scale bars: (a) 20 µm (20× magnification); (b-p) 10 µm (100x magnification).

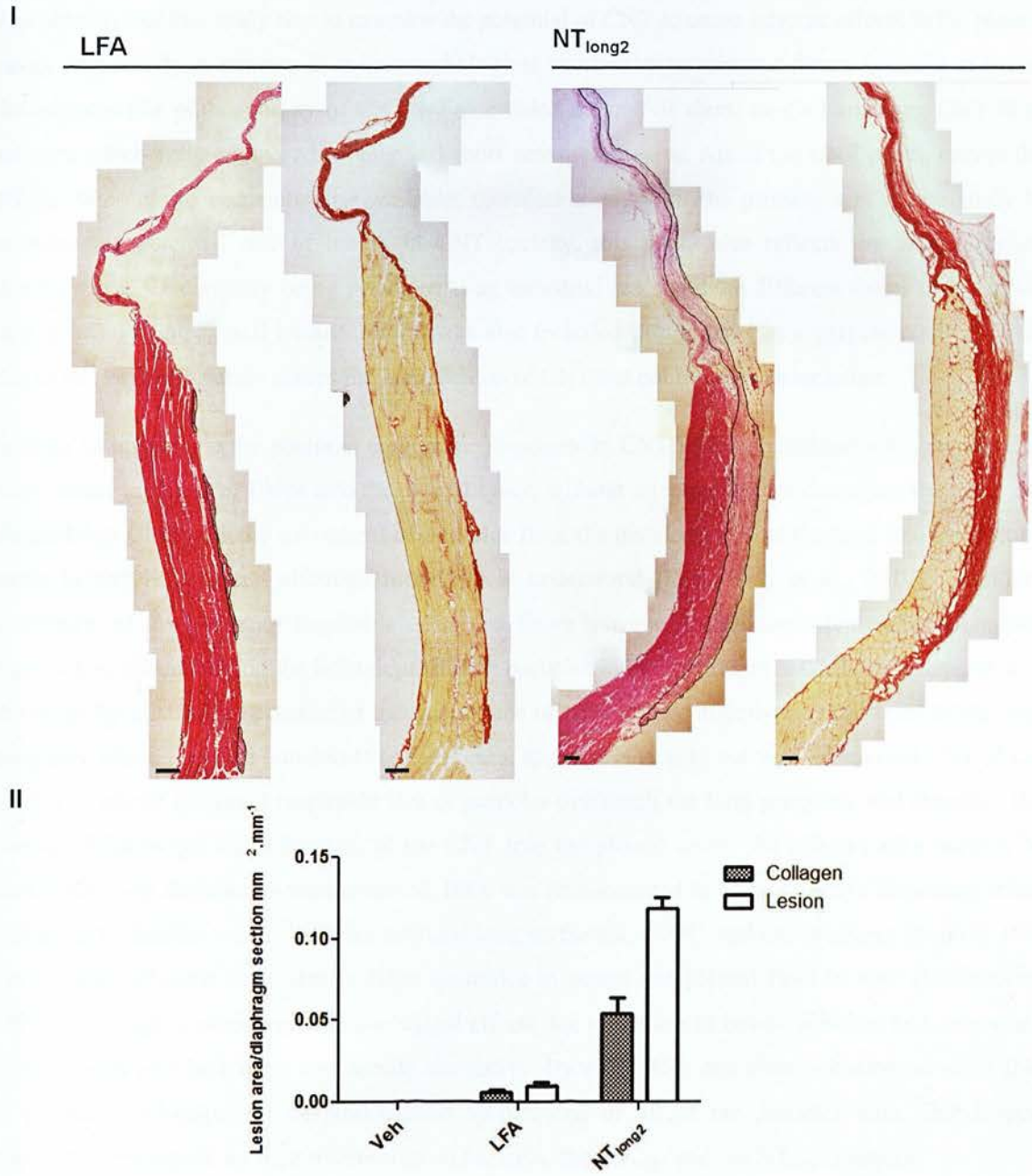

Figure 3.21: Comparison between the extent of lesion development along the diaphragm in response to the same mass dose of LFA and NT_{long2} (5 µg/mouse) at 24 weeks post injection. (I) Serial images were taken along the length of each diaphragm at x100 magnification and the images re-aligned using Photoshop elements 4.0. The areas of lesion are outlined in black for clarity. (II) Lesion size and collagen content was quantified and expressed as area per length of diaphragm section ($mm^2.mm^{-1}$) (n=3, data represented as mean +s.e.m.).

Table 4.1. Evaluation of the NiNW concentration (NiNW/µm2) depending on the sample administrated to the animals

Sample administrated	Tissue section ID	Tissue section area (µm²)	Total NWs counted†	Total NWs/section*	NWs concentration * (NWs/µm²)
Short NWs	1.1	811	48	195	0.25
	2.2	1184	23	136	0.12
	3.3	698	7	24	0.03
	Average	*898*	*26*	*118*	*0.13*
Long NWs	2.1	803	3	12	0.02
	1.3	369	3	6	0.02
	3.1	936	5	23	0.03
	Average	*703*	*4*	*14*	*0.02*
Vehicle	2.1	799	0	0	0
	3.1	940	0	0	0
	3.3	933	0	0	0
	Average	*891*	*0*	*0*	*0*

† NWs were counted on five fields (each with a mean area of 40 µm^2, for a total of 200 µm^2).

* Information estimated from experimental data reported in the table.

Backscatter scanning electron microscopy (BS-SEM) was used to examine the parietal pleura for retained NiNW. The principle of BS-SEM is based on the differential scattering of incoming beam electrons as they interact with target molecules of different atomic number (Z). Elements with high atomic number such as nickel reflect or back-scatter electrons more strongly than the lower *Z* light elements of which cells are composed (predominantly H, C, N, O, and P). BS-SEM therefore allows clear discrimination between the nanofibres and other cellular features provided they are at shallow depth within the cell. BS-SEM is widely used for detection of colloidal gold markers in immunocytochemistry (Hermann et al., 1996).

Analysis of the parietal pleura using BS-SEM further supports the hypothesis that the pleural inflammatory response is due to length-dependent retention as long fibres were identified associated with accumulations of leukocytes on the parietal pleura (Figure 4.12), whereas no short NiNW were detected on the mesothelium.

3.4 Discussion

The objective of this study was to examine the potential of CNT to cause adverse effects in the pleural cavity particularly in relation to their morphological similarities to asbestos fibres. In order to assess the asbestos-like pathogenicity of CNT we assembled a panel of short, tangled and long CNT fibre samples which were compared to long and short amosite asbestos. All of the CNT panel, except the NT_{long2} sample, are commercially available; therefore along with the primary aim of the study to examine the potential role of length in CNT toxicity, this panel also reflects the morphological diversity of CNT currently being produced at an industrial scale and the different forms of CNT that may pose an occupational hazard. NPCB was also included in the panel as a particle control which due to its graphenic nature shares the composition of CNT but not the fibrous structure.

In order to investigate the potential pathogenic responses to CNT *in vivo,* a method was developed to allow direct injection of fibres into the pleural space, without injecting into or damaging the lung. As discussed in Chapter 1 the movement of particles from the distal regions of the lung into the pleural space is widely accepted although incompletely understood (Donaldson et al., 2010). Therefore instillation of low doses of respirable dusts and fibres into the pleural space represents a credible approach to understanding the behaviour of such particles in the pleura, were CNT to be deposited in the lungs by inhalation. Because of the importance of respirability in delivering particles to the lung periphery where they can translocate to the pleural space, it is vital to use well –dispersed CNT in our studies to mimic the small respirable size of particles that reach the lung periphery and therefore the pleura. Prior to the administration of the CNT into the pleural cavity the efficacy of a number of commonly used dispersants were assessed. BSA was demonstrated to be an effective dispersant when compared to distilled water, FBS, the artificial lung surfactant, DPPC, and the detergent Triton-X 100. Furthermore albumin is present in large quantities in serum and pleural fluid in vivo (Miserocchi, 1997). Although to avoid any immunological effects due to the use of bovine albumin as a dispersant mouse serum may be a more appropriate alternative. By using BSA and ultrasonication we were able to produce well-dispersed, respirable-sized suspensions of all of the particles with fibre-shaped particles being visible by light microscopy in the LFA, the NT_{long1} and the NT_{long2} samples.

Administration of a bolus dose may cause normal physiology, homeostasis and detoxification or repair mechanisms to become overwhelmed and pathogenic responses which otherwise might not have occurred are induced or promoted.

Exposure to long CNT first caused an acute inflammatory response, characterised by granulocyte influx and increased protein concentration in the pleural fluid, followed by the progressive development of fibrotic lesions along the parietal pleura, and proliferation in the mesothelial layers. Short CNT did not elicit a significant inflammatory reaction at any timepoint examined and indeed the

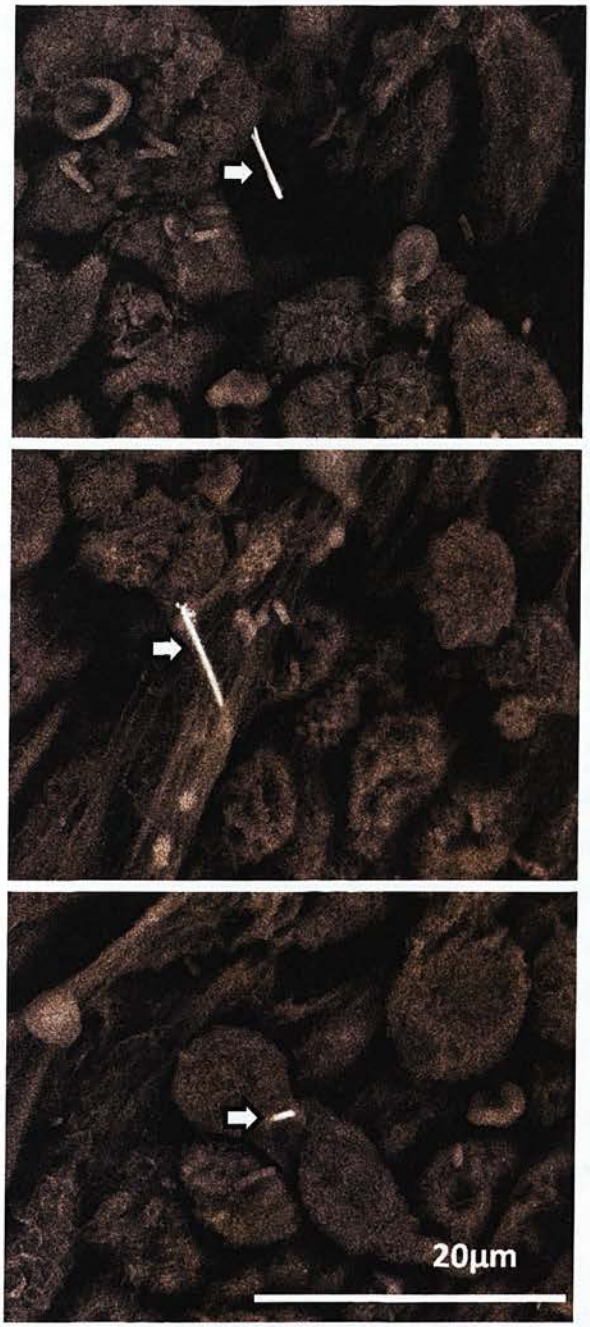

Figure 4.12: Back-scatter SEM of the chest wall 24 hours after intrapleural injection of $NiNW_{long}$ (5 µg/mouse). Long NiNW fibres (white arrows) were identified along the parietal pleural of the chest wall in association with inflammatory leukocyte aggregates by back-scatter SEM.

4.4 Discussion

The objective of this study was to address the hypothesis that the pathogenicity of long fibres in the pleural cavity is due to size-restricted clearance mechanisms. This hypothesis was first put forward by Kane et al, who noted the accumulation of long fibres injected into the peritoneal cavity around the

results obtained from short CNT- treated mice mirrored those of the vehicle controls. These results suggest that, like asbestos, the toxicity of CNT for the pleura adheres to the fibre pathogenicity paradigm as regards the role of length in this model of direct pleural exposure (Donaldson et al., 2010).

The presence of reactive transition metals introduced during the CNT synthetic process has been proposed as a possible factor contributing to the pathogenicity of CNT (Lindberg et al., 2009). For example, dose and time -dependent increases in intracellular reactive oxygen species and a decrease of the mitochondrial membrane potential induced in rat NR8383 macrophages and human A549 lung epithelial cells in response to CNT exposure in vitro was abolished after incubation with purified, low metal content CNT (Pulskamp et al., 2007). Similarly Kagan *et al* showed that Fe-containing SWCNT induced greater oxidative stress and glutathione depletion in mouse macrophages than purified SWCNT (Kagan et al., 2006). However no relationship was observed between the inflammatory potential of this panel of CNT in the pleural cavity and the soluble metal fraction or the intrinsic free radical generating ability of the CNT thereby strengthening the hypothesis that the pathogenic response to CNT in the pleural cavity is dependent on length. The methology employed in the measurement of endotoxin contamination of the CNT panel only takes into account soluble endotoxin. Therefore any endotoxin bound to the CNT that does not dissociate in aqueous solution may contribute to the inflammatory respone.

The generation and development of an inflammatory response to asbestos fibres injected into the peritoneal cavity has been described in detail by Moalli et al who examined the effects of mesothelial exposure to long and short asbestos fibres up to 6 months post injection (Moalli et al., 1987). Focal haemorrhage on the peritoneal surface of the diaphragm was initially observed at 3 to 6 hours post injection of the long asbestos only, followed by an influx of granulocytes and macrophages into the peritoneal cavity, and an increase in albumin (Moalli et al., 1987). A similar acute influx of inflammatory granulocytes into the pleural space was observed here after the injection of both long asbestos and long CNT fibres. As discussed in Chapter 1, mesothelial cells can effect significant inflammatory responses to bacteria, toxins and fibres in the pleural space via the apical secretion of chemokines such as IL-8 and the upregulation of cell adhesion molecules thereby stimulating the transmigration of inflammatory cells into the pleural cavity (Mutsaers, 2002). The propensity of this panel of long and short CNT to directly stimulate mesothelial cells to produce such pro-inflammatory and chemotactic factors was addressed in an in vitro study discussed in Chapter 5.

The acute length-dependent inflammatory response reported here reflects the inflammatory response observed after direct injection of long CNT into the peritoneal cavity (Poland et al., 2008). We found however that the inflammation produced by long CNT was sustained and was similar on day 7 to that seen on day 1. This is in contrast to the kinetics of inflammation seen in the peritoneal space to the

stomata on the diaphragm which lead them to propose that retention of long fibres at the diaphragmatic mesothelial surface was responsible for the subsequent inflammation, proliferation and granuloma formation (Moalli et al., 1987). Here we investigated the validity of this hypothesis as regards long fibre effects in the pleural cavity which has similar clearance mechanisms as the peritoneal cavity.

We initially investigated the retention-dependent inflammation hypothesis by using compact particles and examining their clearance and inflammatory potential in the pleural space. Quartz and coal mine dust are small particles, less than 3 μm in diameter, which due to their surface reactivity are known to play a causative role in the pathogenesis of silicosis and pneumoconiosis respectively (Mossman and Churg, 1998; Lapp and Castranova, 1993). The reactivity of these particles was confirmed here using the simple haemolysis assay which has been demonstrated to be predictive of the inflammatory potential of particles in the lung (Lu et al., 2009). The lack of response to these highly inflammogenic particles in the pleural exposure model can be explained by their small size whereby they are rapidly cleared from the pleural space in the flow of pleural fluid, eliminating the particle dose. To further investigate the single parameter of particle size in the pleural space we used two monodispersed samples of polystyrene beads which were identical in composition but different in diameter. As expected the larger, 10 μm beads, which are around the maximum stomatal diameter, initiated an acute inflammatory response where the smaller, 3 μm beads did not. Although a 10 μm bead is too large to ever reach the distal lung and pleural space upon inhalation, the inflammatory response to the 10 μm beads injected directly into the pleural space demonstrates the role of size-restricted clearance from the pleural space plays in the initiation of an inflammatory response to particles or fibres.

The elutriating effects of the lung serve to allow only particles with a diameter smaller than approximately 5 μm and therefore smaller than the diameter of the pleural stomata to reach the distal lung and translocate to the pleural space. Fibres however pose a unique problem. As discussed in Chapter 1.2 fibre respirability is a function of aerodynamic diameter which is dictated mostly by actual diameter as airborne fibres align themselves parallel to the airflow in the lungs (Morgan, 1995). Therefore it is the diameter and not length of fibres that affects transit through the lungs allowing high aspect ratio particles like CNT, which may have a diameter in the nano range but a length extending to tens of microns, to deposit in the very distal regions of the lung (Donaldson et al., 2010). Indeed the distal deposition of CNT was shown by Ryman-Rasmussen *et al.* who reported the presence of CNT in the sub-pleural tissue of the lung after a single inhalation exposure in mice (Ryman-Rasmussen et al., 2009). This suggests that long CNT fibres with a small enough diameter to reach the distal lung may translocate into the pleural space where their length may pose a problem for clearance.

same long CNT sample, where the inflammation waned considerably over one week following exposure to long CNT and long asbestos fibres (Poland et al., 2008). The persistence of inflammation in the pleural space may be a consequence of the conditions there, where movements of the chest wall and the close apposition of the parietal and visceral pleurae enhance the interactions between long CNT and the mesothelium.

Examination of the parietal pleura of the chest wall and diaphragm revealed the development of inflammatory lesions along the mesothelium of long CNT exposed mice. Analogous lesions have been reported on the mesothelium of the peritoneal cavity after instillation of long asbestos fibres into the peritoneal cavity (Moalli et al., 1987) and more recently along the diaphragm after inhalation of amosite asbestos (Bernstein et al., 2010b). The authors of the peritoneal exposure study suggest that, akin to the accumulation of alveolar macrophages in response to long fibres deposited at alveolar bifurcations, the development of lesions along the mesothelium is due to the selective retention of long fibres at points of egress of the pleural fluid (Moalli et al., 1987); a mechanism that is further addressed and discussed in Chapter 4. The retention of fibres in the pleural space will allow for prolonged interactions between the fibres and the resident pleura cells which may subsequently lead to macrophage activation and mesothelial cell damage stimulating a pathogenic response.

The lesions that form in response to the long CNT develop over time from fibrin-bound aggregates of activated leukocytes to dense fibrotic lesions with high collagen content. Both SWCNT and MWCNT have previously been shown to induce collagen deposition and fibrosis in the lung (Shvedova et al., 2005; Mercer et al., 2011). The rate of lesion growth observed along the parietal pleura cannot be accounted for solely by an increase in collagen deposition however, as the proportion of lesion area determined to be collagen remains at approximately 50% from 12 to 24 weeks post injection. This suggests there is also an increase in the size of cellular aggregates within the lesions which is supported by evidence for cellular proliferation within the lesions.

Leukocytic lesions and foci of mesothelial proliferation similar to those seen with the long CNT were also documented on the face of the parietal pleura in response to asbestos fibres. In a study carried out by Vasilieva et al multiple instillations of asbestos into the rat pleural space were used to examine the changes at the pleural mesothelium observed by scanning electron microscopy over 24 months leading up to mesothelioma development (Vasilieva et al., 1998). Similar hyperplastic areas of mesothelium were evident in our study highlighted by the Ki-67 antibody staining which showed dramatic increases in proliferation in the mesothelial and sub-mesothelial tissues only in mice exposed to long CNT. Mesothelial regeneration may occur by proliferation of uninjured cells at the periphery of the wound via attachment and proliferation of freely floating mesothelial cells (Foley-Comer et al., 2002). The normal processes of mesothelial healing and regeneration are aided by the presence of macrophages which produce factors that stimulate mesothelial proliferation (Mutsaers et al., 2002).

The use of radio-labelled short CNT and SPECT/CT imaging allowed us to identify the cranial mediastinal lymph nodes as the draining nodes of the pleural space in mice and the primary nodes where particles removed from the pleural space will deposit. This is consistent with a study carried out by Parungo et al who injected quantum dots into the pleural cavity with the aim of indentifying the first group of lymph nodes, the so called sentinel lymph nodes, draining the pleural space which they proposed could aid in the staging and treatment of mesothelioma (Parungo et al., 2005). Using both rat and pig models this study identified the mediastinal lymph nodes as the primary lymph nodes to which the pleural cavity drains. Due to the similarities between the lung lymphatic system of the pig and in humans (Riquet et al., 2000) it is reasonable to predict from the evidence presented by Parungo et al that pleural fluid in humans will similarly initially drain to the mediastinal lymph nodes. When we examined the fibre burden in the mediastinal lymph nodes after intrapleural injection of long and short CNT it was clear from the lymph node sections that the long CNT sample was not completely retained in the pleural space due to short fibres present in that sample that can translocate to the lymph node. However there was obviously more material in the 'short CNT' lymph node than in the 'long CNT' lymph node. Whilst qualitative, this argues for retention of the longer fibres in the NT_{long2} sample and translocation of the short fibres.

As the size-restricted clearance of fibres from the pleural space could not be clearly demonstrated using the heterogeneous CNT samples alternative high aspect ratio nanofibre samples, nickel nanowires (NiNW), which are manufactured in tight size categories, were employed. The use of NiNW demonstrated more convincingly that there was size-dependent retention as we saw only traces of nanowires in the lymph nodes from animals exposed to long NiNW but abundant NiNW in the lymph nodes from animals that received intrapleural short NiNW. This was further quantified by epifluorescent microscopy analysis of the lymph node tissue which was employed as a highly sensitive method of to detect NiNW in the tissue sections. Backscatter SEM (BS-SEM) was used in an attempt to demonstrate the selective retention of long NiNW fibres on the parietal pleural to complement the indirect evidence of length-dependent retention obtained by the examination of the lymph node burdens. The limitation of the BS-SEM method is that it can only penetrate a short distance into the tissue (Hermann et al., 1996). The aggregation of inflammatory leukocytes over the mesothelium in mice treated with the long NiNW samples would therefore obscure any fibres underneath. Nonetheless a number of long fibres were identified protruding from the surface of such aggregates. Conversely neither aggregates of inflammatory cells nor short NiNW themselves were identified which simultaneously demonstrates their effective clearance from the pleural cavity and lack of pathogenicity.

If the retention of long fibres along the parietal pleura is the initiating mechanism of mesothelioma development one would expect an abundance of long fibres to be evident in the pleural fibre burden of mesothelioma patients. Studies investigating the link between asbestos exposure and the development

of pleural pathologies have indeed detected asbestos fibres retained along the parietal pleura however the size and type of asbestos fibres associated with pleural disease remains controversial. Dodson *et al.* reported that short (<5 μm) chrysotile fibres were predominantly present in the pleura of ex-shipyard workers exposed to both chrysotile and amphibole asbestos fibre types (Dodson et al., 1990). Suzuki and Kohyama also reported an apparent predilection for short fibre movement into the pleural space after finding large amounts of short chrysotile fibres in pleural tissue even though the fibre burden in the lung contained a greater percentage of amosite fibres (Suzuki and Kohyama, 1991). A study by Boutin *et al.* however, which compared the fibre burden in areas containing black spots to normal areas of parietal pleura, found a high number of long fibres particularly associated with the black spots, with 22% of all fibres found in these areas greater than 5 μm in length (Boutin et al., 1996). They also showed a clear-cut concordance between the long amphibole asbestos fibre burden in the lung and the black spots of the parietal pleura, but not the areas of normal pleura. Heterogeneity of distribution of fibres within the pleural space can most likely account for the conflicting results from previous studies, which reported a preponderance of short chrysotile fibres in the pleura. Furthermore the identification of long fibres specifically associated with areas of the parietal pleura with high stomata content supports the model of length-dependent retention described here.

The determination of the threshold length for pleural pathology is crucial for the hazard assessment of CNT and other new forms of high aspect ratio nanomaterials as it will further illuminate the structure-activity relationship governing fibre pathogenicity in the pleural space. Although the heterogeneity of the CNT fibre samples precluded the determination of such a threshold here, it was a major aim of a study carried out within the ELEGI laboratory by Anja Schinwald who utilised silver nanowires (AgNW) of defined length-classes. Injection of the tightly size-controlled AgNW samples into the pleural cavity by the method described in Chapter 3 allowed the correlation between fibre length and pleural pathogenicity. Results showed a significant increase in pleura granulocyte numbers induced by injection of AgNW that were 5 μm in length compared to the 3 μm nanowires, however no significant increase in the severity of the inflammatory response was detected between the 5μm length nanowires and longer fibre samples (10 μm and 14 μm) (Schinwald et al., 2012a). These results suggest that nanofibres at or beyond 5 μm in length are pathogenic to the pleura and that nanofibres can be made benign-by-design for pleural effects if they are restricted to lengths of 4 μm or less. In Chapter 3, the size distribution for the SFA fibre sample indicates that a proportion of this sample contains fibres at or greater than the 5 μm cut-off, yet this sample is not inflammogenic in the pleural cavity. This may be due to differences in fibre number per mass dose, as per mass basis the number of SFA fibres would be less than the number of AgNW (both studies used a 5 μg/mouse dose), therefore the proportion of fibres above the threshold of 5μm may be insufficient to elicit an inflammatory response.

The length-dependent inflammatory response to the NiNW samples in the pleural cavity and also previously reported in the peritoneal cavity reflects the response to both asbestos fibres and CNT and further strengthens the hypothesis that the pathogenicity of fibres in the pleural space is dependent on length rather than fibre composition. Recently a paper by Tomatis *et al.* reported the greater toxicity of long asbestos fibres when compared to short asbestos fibres could be attributed to a number of factors other than length including greater free radical production and reactive surface (Tomatis et al., 2010). Whilst these factors may give added toxicity to any fibre we contend that the properties defined by the fibre pathogenicity paradigm; length, thinness and biopersistence remain the primary attributes a fibre must possess to elicit a pathogenic response. In particular length will retain the harmful dose, e.g. fibre-derived free radicals - in the pleural space whilst a short fibre will not remain in the pleural space to deliver its dose regardless of its other potential pathogenic properties as illustrated by the quartz and coal mine dust study (Figure 4.6).

Size-restricted clearance from the pleural cavity may also have implications for the hazard potential of other non-fibrous, high aspect ratio nanomaterials. One such material recently assessed by the ELEGI group is a graphene platelet, composed of stacked sheets of graphene. Due to their nanoscale dimensions graphene platelets up to 25 μm in diameter were calculated to be respirable and potentially deposit in the distal regions of the lung. Furthermore it was shown that the large diameter of the platelets lead to retention in the pleura and subsequent inflammation (Schinwald et al., 2012b). Therefore analogous to pathogenic fibres, a high aspect ratio nanomaterial that has an aerodynamic diameter small enough to allow distal deposition in the lung and two dimensions large enough to prevent efficient clearance from the pleural space may pose a novel hazard to the pleural mesothelium. This highlights the need to widen the FPP to include different forms of high aspect ratio materials that are being developed by the nanotechnology industry.

Chapter 5: Cellular mechanisms for length-dependent inflammatory response to carbon nanotubes in the pleural cavity.

5.1 Aims and hypothesis

We have shown that CNT elicit a length-dependent, asbestos-like inflammatory response in the pleural cavity of mice, where long fibres caused inflammation but short fibres did not. However the cellular mechanisms governing this response have yet to be elucidated. Here, we aim to use *in vitro* methods to elucidate the relative roles of the macrophages and mesothelial cells in driving the inflammatory response to long fibres. Using the same panel of CNT we examined the ability of long and short CNT to elicit pro-inflammatory responses in both a human non-transformed mesothelial cell line (Met5A), and macrophages derived from the human monocyte cell line (THP-1) as a surrogate for pleural macrophages, by direct exposure to CNT. The release of acute phase pro-inflammatory cytokines and chemokines were measured as an indicator of the pro-inflammatory potential of the members of the CNT panel. In addition to the potential for a direct CNT-mediated inflammatory response we hypothesized that the inflammatory response could be driven by cross-talk between the macrophages and mesothelial cells and so we also examined the effect of conditioned media from CNT-treated macrophages on the mesothelial pro-inflammatory response.

5.2 Results

5.2.1 Effect of direct exposure to CNT panel on mesothelial cell and macrophage viability.

The non-transformed human pleural mesothelial cell line, Met5A was used in this study. These cells were originally established by transfecting normal human mesothelial cells with a plasmid containing Simian virus (SV40) early region DNA, and they express SV40 large T antigen (Ke et al., 1989).

Mesothelial cell viability, as measured by trypan blue exclusion assay, was examined after 24 hour exposure to the CNT panel over a dose range from 5 to 50 $\mu g/cm^2$. A significant loss of cell viability was seen only in response to NT_{long1} (20 $\mu g/cm^2$) and NT_{long2} (50 $\mu g/cm^2$) (Figure 5.1 I). This loss of cell viability coincided with an increase in supernatant LDH levels in Met5A cultures treated with NT_{long1} and NT_{long2} at the higher doses only (Figure 5.1 II).

The THP-1 monocytes were differentiated into macrophages by exposure to 10 ng/ml phorbol 12-myristate 13-acetate (PMA) for 48 hours. This concentration of PMA has been shown to be optimal for THP-1 differentiation whilst minimising pro-inflammatory gene upregulation (Park et al., 2007). Exposure of macrophages (THP-1) to all the members of the CNT panel only caused a significant

increase in supernatant LDH levels at higher doses indicating a loss of membrane integrity (Figure 5.1 III). For both the NT_{tang1} and NT_{tang2} CNT samples there was a reduction in % LDH release from macrophages treated with the highest dose (50 $\mu g/cm^2$) compared to the 20 $\mu g/cm^2$ which may be as a results of CNT interference in the assay. In order to rule out CNT interference in the LDH assay, the CNT at the highest dose of 50 $\mu g/cm^2$ were incubated in media from cells ($5x10^5$), which were lysed with Triton-X, for 24 hours. The CNT were subsequently removed by centrifugation and the LDH assay was carried out on the media and the subsequent absorbance compared to a media control. No difference in the LDH absorbance reading was detected after incubation with any member of the CNT panel (Figure 5.2). However the use of Trition-X to lyse the cells may have affected the potential interaction between the CNT and LDH substrate. Furthermore the extremely high LDH absorbance readings recorded may mask more sublte differences between the treatment groups.

Based on the data from the cytotoxicity assays a sub-lethal dose of 5 $\mu g/cm^2$ was selected for treatments of both Met5A and THP-1 cells for the subsequent activation studies.

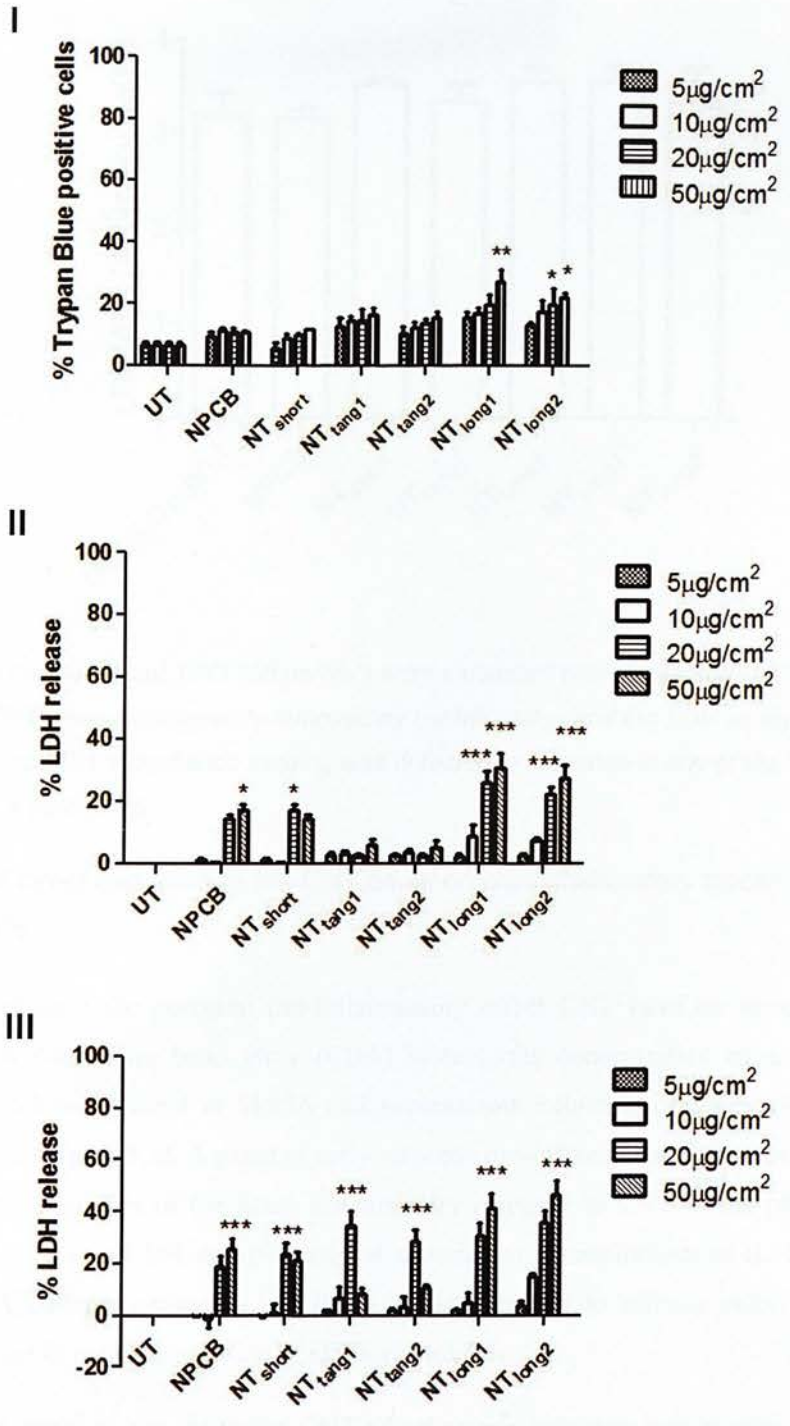

*Figure 5.1: The effect of the CNT panel on cell viability. The viability of mesothelial cells was measured by trypan blue exclusion (I) and LDH release (II) after a 24 hour exposure to the CNT panel at a range of doses from 5-50 μg/cm^2. LDH release was also used as an indicator of cell viability of macrophages at 24 hours after CNT treatment (III). Data expressed as a mean ± sem, n=3. Significance versus vehicle control *** indicates p<0.001.*

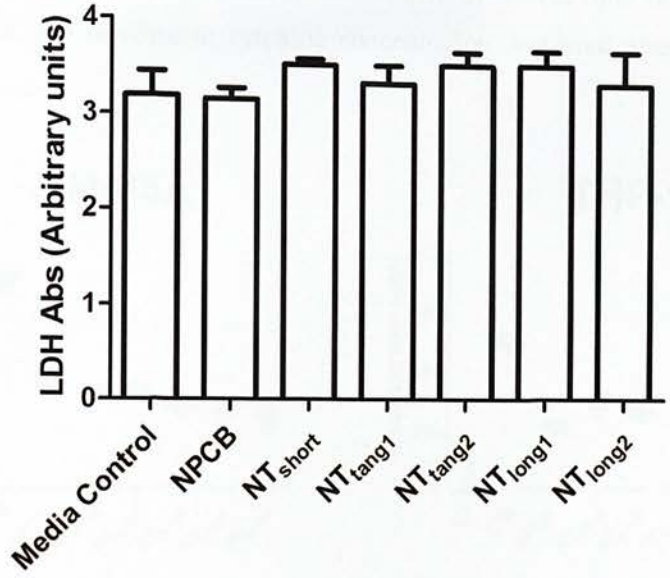

Figure 5.2: LDH control assay. CNT (50 µg/cm^2) were incubated with media from 100% lysed cells for 24 hours. The CNT were subsequently removed by centrifugation and the LDH assay was carried out. No reduction in the LDH absorbance reading was detected in response to any of the CNT panel. Data represent mean ± sem (n=3).

5.2.2 Effects of direct exposure to the CNT panel on pro-inflammatory cytokine release from mesothelial cells.

In order to investigate the potential pro-inflammatory effect CNT have on mesothelial cells we assayed, using a cytometric bead array (CBA) system, the concentration of a number of pro-inflammatory cytokines present in Met5A cell supernatants following direct exposure to the CNT panel for 24 hours (Figure 5.3). A panel of early response pro-inflammatory cytokines were chosen as likely candidates as drivers of the acute inflammatory response to CNT in the pleural cavity. No member of the CNT panel had an effect on the supernatant concentrations of IL-1β, IL-6, IL-8 or TNFα in Met5A cultures compared to LPS, a positive control to activate cells, which caused a significant increase in the concentration of all four cytokines.

5.2.3 Effects of direct exposure to the CNT panel on pro-inflammatory cytokine release from macrophages.

In order to investigate the impact of CNT phagocytosis on macrophage activation, we measured the concentration of IL-1β, IL-6, IL-8 and TNFα present in the THP-1 cells supernatants following exposure to the CNT panel (Figure 5.3). Only the CNT samples containing long fibres- NT_{long1} and NT_{long2} caused a significant increase in IL-1β and IL-6 concentrations compared to untreated cells. NT_{long1} also induced a significant increase in IL-8 concentration; however no increase was seen with

NT_{long2}. NT_{long2} did appear to elevate the concentration of TNFα, but this elevation was not statistically significant. No increase in cytokine concentration was seen after exposure to NPCB, NT_{short}, NT_{tang1} or NT_{tang2}.

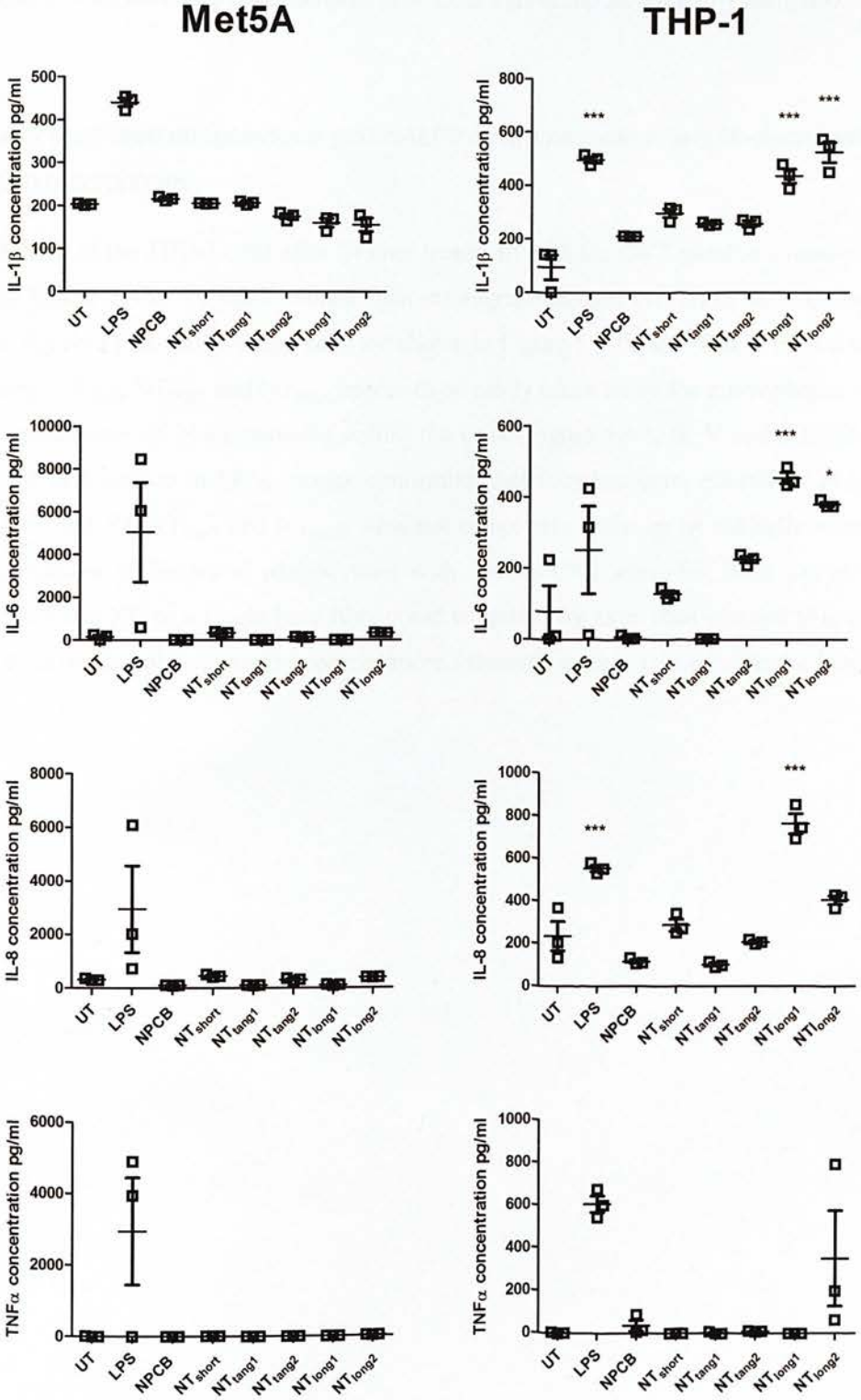

Figure 5.3: The effect of the direct exposure to the CNT panel on cytokine release from mesothelial cells and macrophages. Cells were treated with the particle panel (5 μg/cm^2)or LPS (10ng/ml) for 24 hours. No increase in the levels of IL-1β, IL-6, IL-8 or TNFα was detected after mesothelial cells were exposed to the CNT panel. However significant increases in IL-1β and IL-6 were seen in macrophages treated with long CNT samples only. Data expressed as a mean ± sem, n=3.

5.2.4 Role of frustrated phagocytosis and NALP3 inflammasome in length-dependent IL-1β release from macrophage.

The morphology of the THP-1 cells after 24 hour treatment with the CNT panel at a dose of 5 μg/cm^2 is shown in Figure 5.4 as Diffquik stained light micrograph images (I-VII) or as scanning electron micrograph figures (VIII-XI). Normal cells are shown in Figure 5.4 IV and VIII. NPCB and the short CNT samples; NT_{short}, NT_{tang1} and NT_{tang2} appear to be easily taken up by the macrophages as they are seen as accumulations of black particles within the cells (Figure 5.4 I, II, V and VI) but were not visible on the cell surface in SEM images confirming that they had been effectively phagocytosed (Figure 5.4 IX and X). NT_{long1} and NT_{long2} were not completely taken up by the cells which showed the classic features of frustrated phagocytosis with fibrous CNT extended from the cell surfaces (Figure 5.4 VII and XI) or a single long fibre could be shared by more than one cell (Figure 5.4 III). This state of frustrated phagocytosis appeared more extensive in cells treated with the longer NT_{long2} sample.

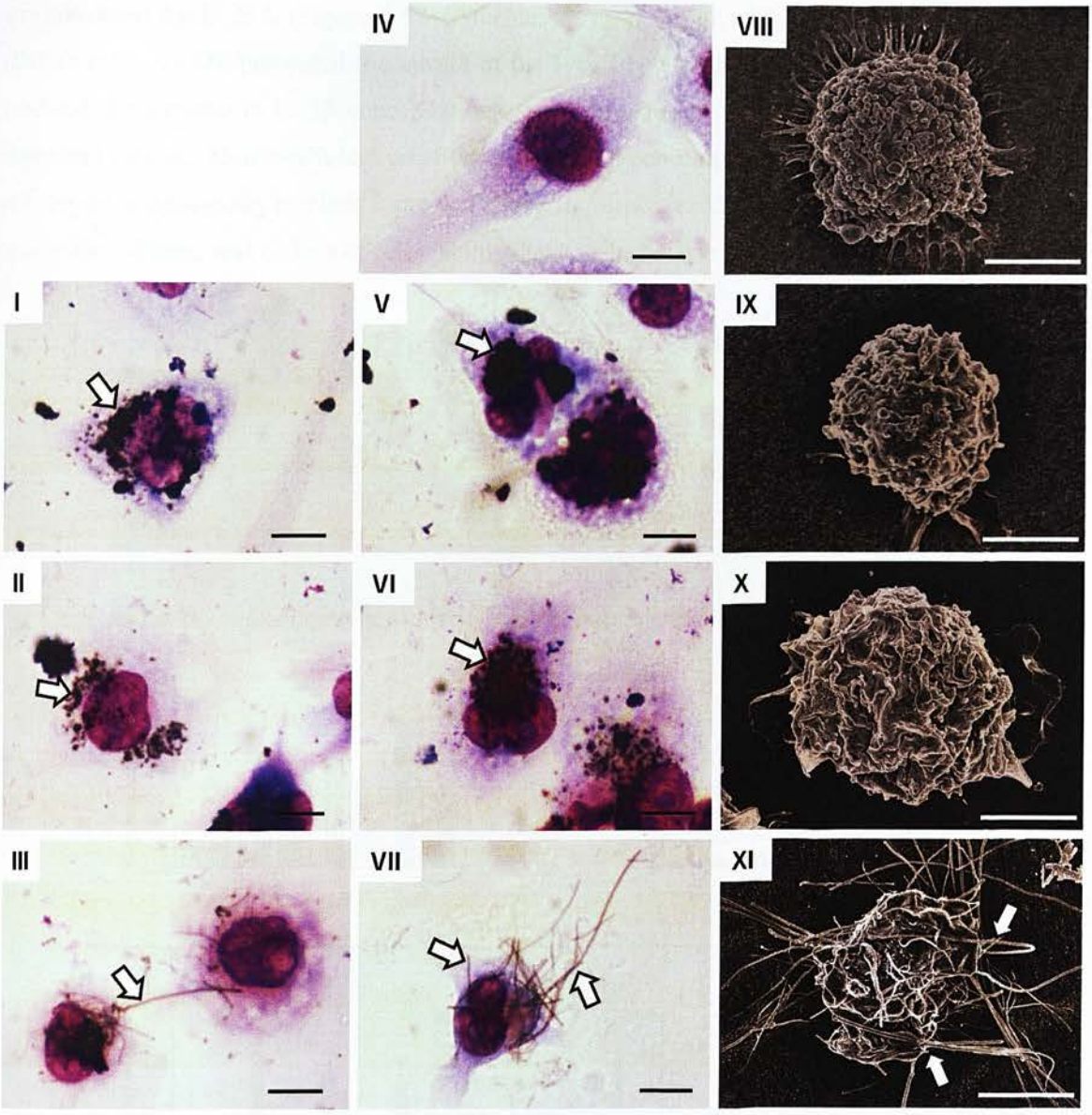

Figure 5.4: Uptake of CNT by macrophages. Light micrographs (I-VII) of THP-1 cells untreated (IV) or treated with the CNT panel (5 µg/cm^2). NPCB (I), NT_{short} (V), NT_{tang1} (II) and NT_{tang2} (VI) appear as aggregates within the cells (white arrows). However NT_{long1} (III) and NT_{long2} (VII) appear to be protruding from the cells (white arrows). Scale bar indicates 20µm. SEM images (VIII-XI) show an untreated THP-1 cell (VIII) and THP-1 cells treated with NPCB (IX), NT_{short} (X) and NT_{long2} (XI) (5 µg/cm^2). No particles can be seen associated with the cell surface or protruding from the cells in (IX) or (X) however the fibre from the NT_{long2} (XI) sample appear on the surface of the cells and also protruding from the cell. Scale bar indicates 10µm.

We selected one cytokine, IL-1β, to test the hypothesis that the length-dependent pro-inflammatory effects were due to frustrated phagocytosis of long fibres. THP-1 cells were co-incubated with the NT_{long1} and NT_{long2} samples and an inhibitor of phagocytosis (cytochalasin D) and the release of IL-1β

was measured by ELISA (Figure 5.5). Cytochalasin D, a potent inhibitor of actin polymerisation (DeFife et al., 1999), prevented the uptake of the long CNT by the THP-1 cells (Figure 5.5 I) and inhibited the increase in IL-1β concentration caused by exposure to NT_{long1} and NT_{long2} in a dose-dependent pattern. However it had no effect on the IL-1β concentrations caused by LPS, which does not require phagocytosis to elicit a pro-inflammatory response. Measurements of supernatant LDH levels showed there was no loss of cell viability due to cytochalasin D treatments (Figure 5.5 II).

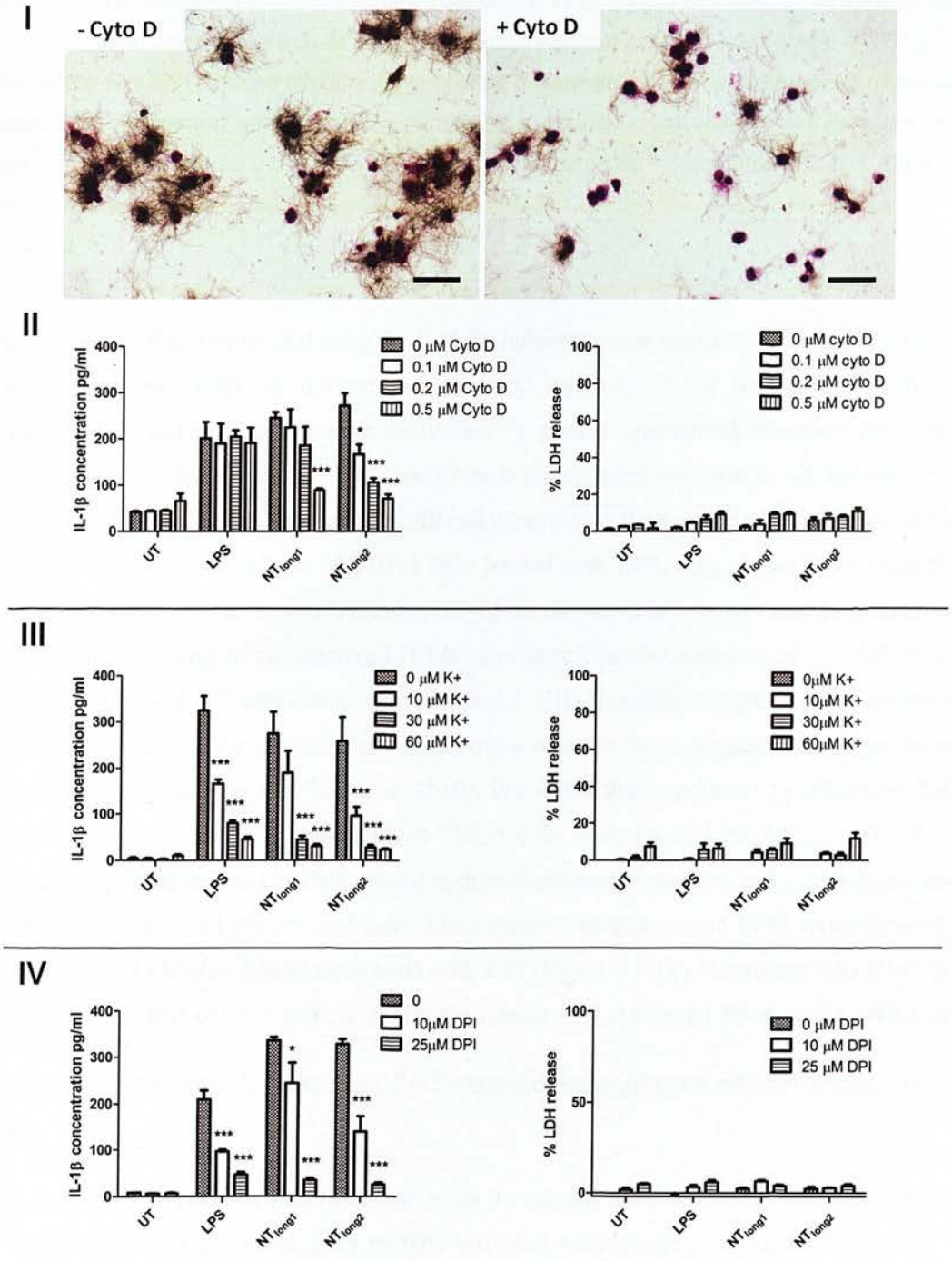

*Figure 5.5: Inhibition of IL-1β release from long CNT-treated macrophages. (I) Exemplar images of macrophages treated with NT_{long2} with or without cytochalasin D (0.5 μM). Cytochalasin D inhibits the attempted uptake of long fibres by the macrophages. (II) Cytochalasin D caused a dose-dependent inhibition of IL-1β release from macrophages treated with NT_{long1} and NT_{long2} (5 μg/cm^2) but not LPS (10 ng/ml). Significance versus 0 μM cytochalasin D within each treatment group *** indicates p<0.001. A loss of cell viability in the presence of cytochalasin D was not detected by LDH release. (III) Addition of potassium chloride (KCl) to the macrophage media caused a dose-dependent inhibition of IL-1β release from macrophages treated with LPS, NT_{long1} and NT_{long2}, without the loss of cell viability. Significance versus 0 μM KCl within each treatment group *** indicates p<0.001 (IV) Addition of the NADPH oxidase inhibitor, DPI, caused a dose-dependent inhibition of IL-1β release from macrophages treated with LPS, NT_{long1} and NT_{long2}. No loss in cell viability was detected by LDH release. Significance versus 0 μM DPI within each treatment group *** indicates p<0.001. Data expressed as mean ± sem, n=3.*

The release of IL-1β can be mediated by the NALP3 inflammasome therefore we examined the role of the NALP3 inflammasome in the pro-inflammatory response to the long CNT samples. The mechanism of NALP3 inflammasome activation is poorly understood however the efflux of potassium ions (K^+) from the cell is known to be a requirement common to all known activators (Petrilli et al., 2007b). We inhibited the K^+ efflux by increasing the extracellular K^+ concentration by adding KCl to the culture medium of THP-1 cells treated with LPS, NT_{long1} and NT_{long2} and found a significant reduction in the concentration of IL-1β in the supernatants of cells from each of the treatments. Measurements of supernatant LDH levels showed there was no loss of cell viability due to increased extracellular K^+ concentrations (Figure 5.5 III). Reactive oxygen species generated by NADPH oxidase during the phagocytosis of particles has also been suggested as a mechanism of NALP3 activation (Tschopp and Schroder, 2010). We tested this hypothesis by inhibiting NADPH oxidase using diphenylene iodonium (DPI) in THP-1 cells treated with LPS, NT_{long1} and NT_{long2} and measuring the release of IL-1β. DPI caused a dose-dependent reduction in IL-1β release into the supernatant of CNT- and LPS-exposed cells. Measurements of supernatant LDH levels showed there was no loss of cell viability due to treatments with DPI (Figure 5.5 IV). Therefore NALP3 activation and functional NADPH oxidase were related to the release of IL-1β from LPS-exposed THP-1 cells.

5.2.5 Effect of conditioned media from CNT-exposed macrophages on mesothelial cell viability.

In order to test the hypothesis that CNT that reach the pleural space indirectly stimulate mesothelial cells via the release of cytokines from particle-activated macrophages, we used conditioned media from CNT-exposed THP-1 cells to treat Met5A cells and measured the concentrations of pro-inflammatory cytokines in the Met5A supernatant (Figure 5.6 I).

No increase in LDH release from the Met5A cells treated with the conditioned media confirm the treatments did not caused a loss of membrane integrity and therefore cell viability (Figure 5.6 II).

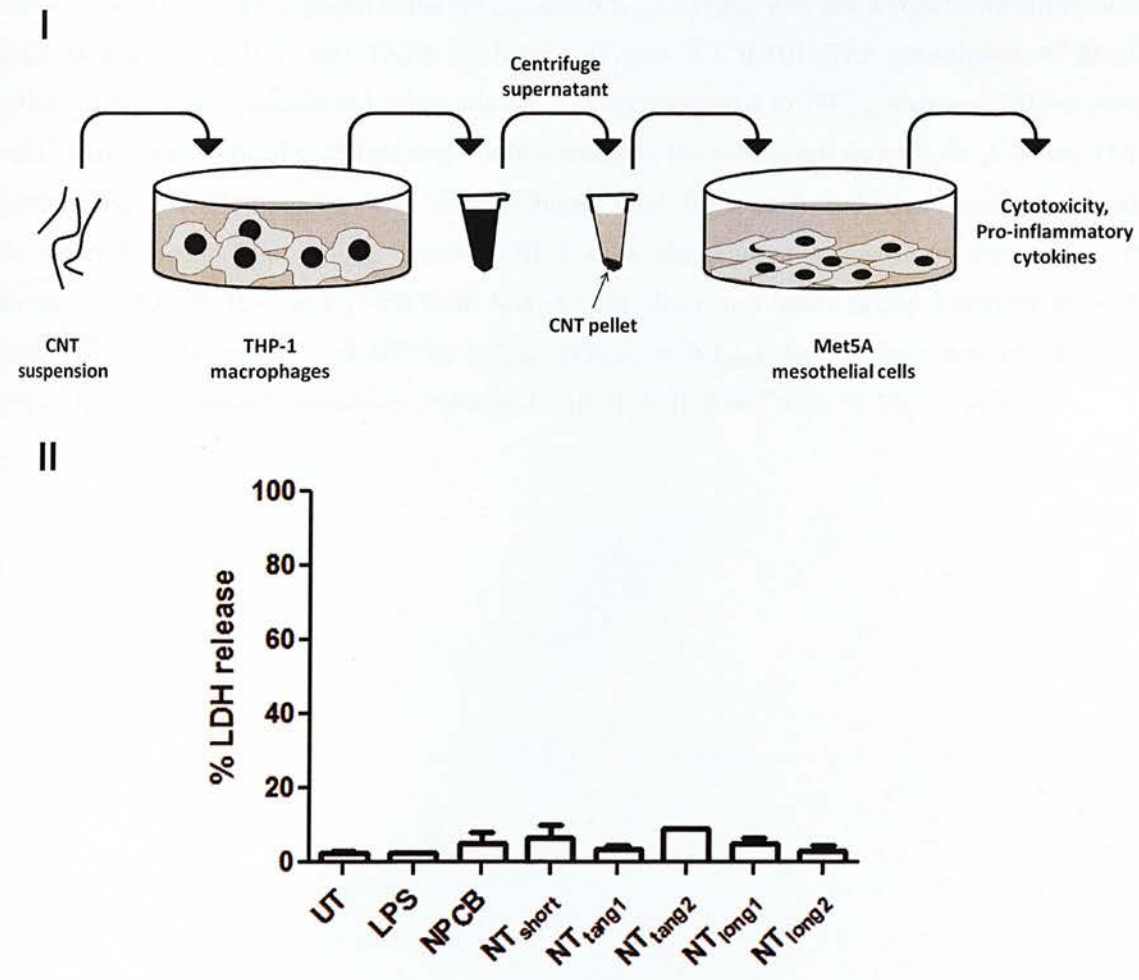

Figure 5.6: The effect of conditioned media from CNT-exposed macrophages on mesothelial cell viability. (I) Schematic diagram representing the conditioned media experimental procedure. THP-1 cells were treated with CNT suspensions for 24 hours (5 μg/cm^2), supernatant was removed and centrifuged to remove any suspended CNT, conditioned media was added to the Met5A cells for 24 hours after which cell viability and production of cytokines was measured. Cell viability of mesothelial cells was measured by LDH release (II) but no cell death was detected.

5.2.6 Effect of conditioned media from CNT-exposed macrophages on mesothelial cell production of pro-inflammatory cytokines.

Whilst direct exposure of Met5A cells to the CNT panel had not caused any increases in IL-1β, treatment with conditioned media from THP-1 cells exposed to LPS, NT_{long1} or NT_{long2} resulted in

approximately two-fold increase in IL-1β concentration compared with the combined total from both cell types exposed directly as shown by the horizontal lines on the bars (Figure 5.7 I).

Media from THP-1 cells exposed to the NT_{long1} and NT_{long2} samples also had a significant effect on the production of IL-6, IL-8 and TNFα by Met5A (Figure 5.7 II-IV). The potentiation of Met5A activation was most pronounced when Met5A had been exposed to NT_{long2}-exposed THP-1 media which resulted in a 20-fold, 30-fold and 6-fold increase in the concentrations of IL-6, IL-8 and TNFα respectively, when compared with the combined total from each cell type exposed directly. Conditioned media from NT_{long1} treated THP-1 cells also caused a significant increase in the production of IL-6, IL-8 and TNFα from Met5A cells albeit to a lesser extent. Exposure to media from THP-1 cells treated with NPCB, NT_{short}, NT_{tang1} or NT_{tang2} did not have any effect on the production of the pro-inflammatory cytokines; IL-1β, IL-6, IL-8 or TNFα, by Met5A cells.

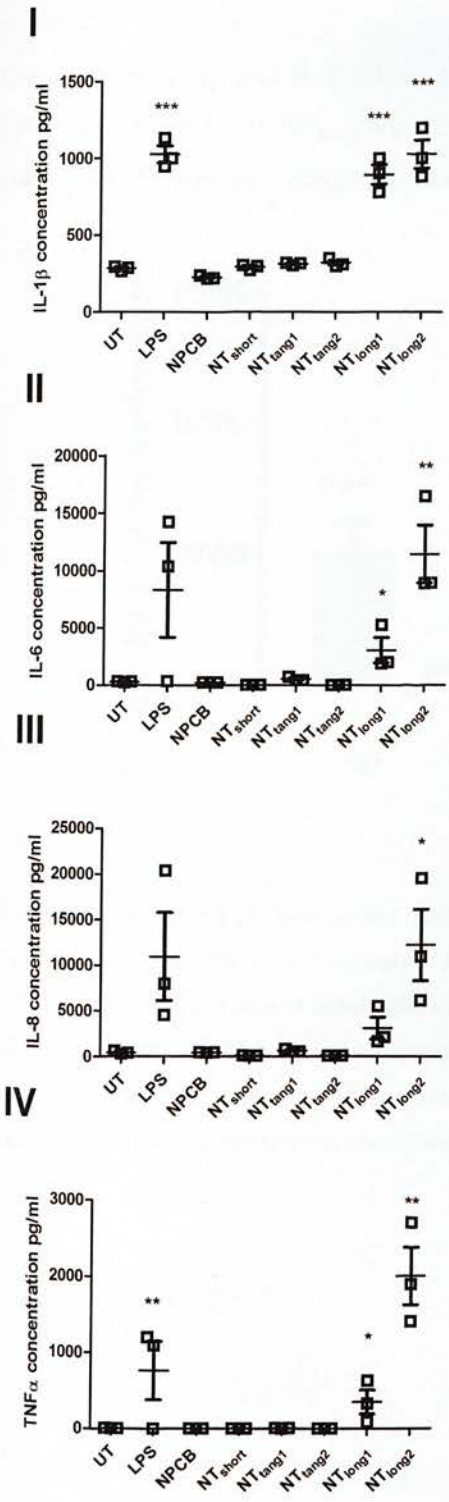

*Figure 5.7: The effect of conditioned media on cytokine release from cells. IL-1β (I), IL-6 (II), IL-8 (III) and TNFα (IV) supernatant levels were measured 24 hours after mesothelial cells were exposed to media from CNT-treated macrophages (5 μg/cm^2 for 24 hours). A length-dependent increase in concentration was observed for each of the cytokines. Data expressed as mean ± sem, n=3. Significance versus vehicle control *** indicates p<0.001.*

The levels of IL-1β and IL-6 released from Met5A cells treated with the conditioned media from THP-1 cells treated with NT_{long2} was attenuated when the THP-1 cells were co-exposed to NT_{long2} and cytochalasin D to prevent phagocytosis (Figure 5.8).

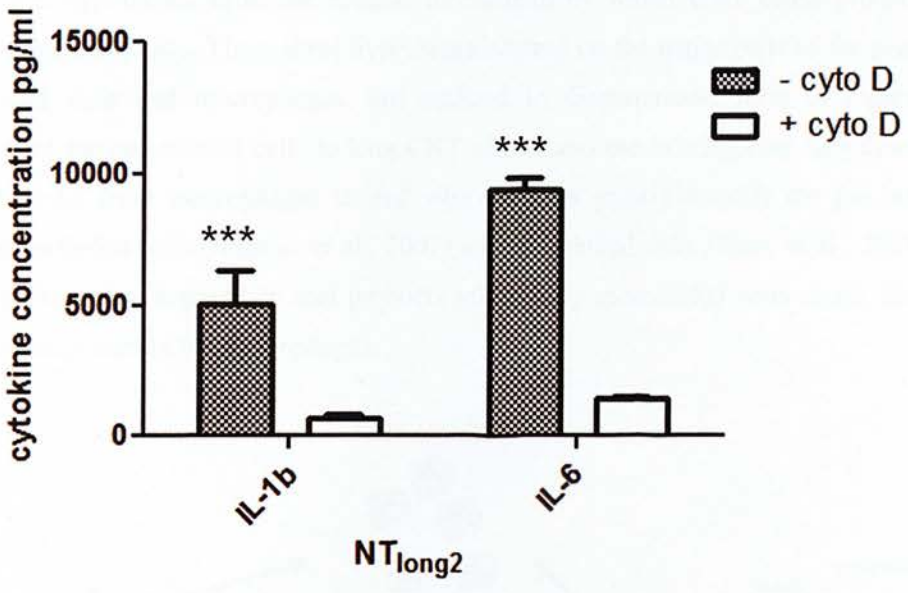

*Figure 5.8: The effect of conditioned media from macrophages co-exposed to NT_{long2} and cytochalasin D (0.5 μM) on mesothelial production of IL-1β and IL-6. A significant reduction in the levels of IL-1β and IL-6 release from mesothelial cells exposed to conditioned media from macrophages treated with NT_{long2} (5 μg/cm^2 for 24 hours) and cytochalasin D (0.5 μM) was observed compared to mesothelial cells treated with conditioned media from macrophages treated with NT_{long2} alone. Data expressed as mean ± sem, n=3. Significance versus vehicle control *** indicates p<0.001.*

5.4 Discussion

The objective of this study was to examine the cellular interactions that are driving the inflammatory response to CNT in the pleural cavity. Long and short CNT samples were examined since the inflammatory response to the CNT in the pleural space is length-dependent. The present study addressed three hypotheses as to the cellular mechanism by which CNT cause pro-inflammatory effects in the pleural cavity. These three hypotheses centred on the major cells of the pleural cavity, the mesothelial cells and macrophages, are outlined in diagrammatic form in Figure 5.9. The refractoriness of the mesothelial cells to long CNT effects and the existing literature describing how conditioned media from macrophages treated with particles greatly amplify the pro-inflammatory responses of epithelial cells (Jimenez et al., 2002) and endothelial cells (Shaw et al., 2011) led us to discount the alternative hypothesis, that products released by mesothelial cells could stimulate pro-inflammatory responses in the macrophages.

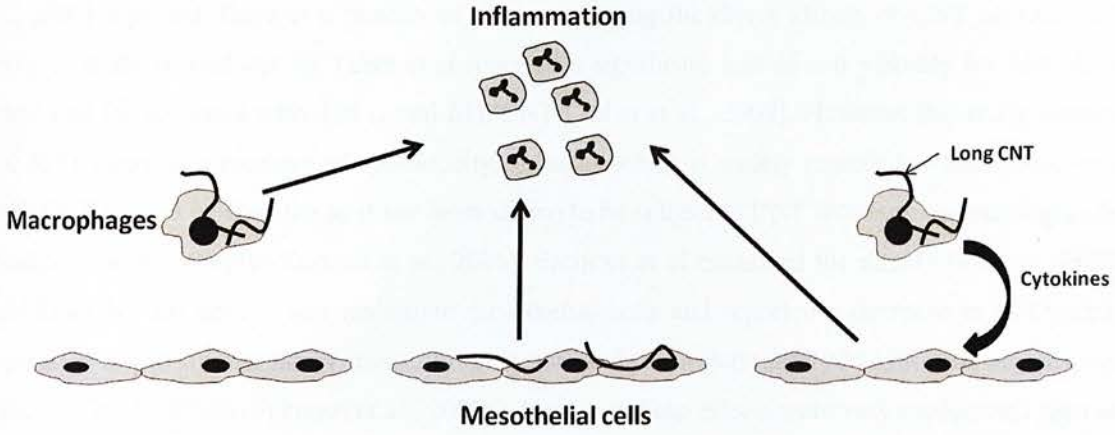

Figure 5.9: Potential mechanisms of the long fibre-mediated inflammatory response. Three potential mechanisms by which CNT cause inflammation in the pleural space were explored in this study. (I) Long fibres interact with the pleural macrophages producing cytokines that directly elicit an inflammatory response. (II) Long fibres interact directly with mesothelial cells with the subsequent factors released leading to granulocyte influx. (III) Long fibres interact with macrophages inducing the release of cytokines which stimulate the mesothelial cells, amplifying the inflammatory response. As initial results showed no response from the mesothelial cells to direct exposure to CNT, the effect of factors released from CNT-exposed mesothelial cells on macrophages was not examined.

The cytotoxicity of the CNT panel to both mesothelial and macrophage cell lines was initially assessed and determined to occur only at doses above 20 $\mu g/cm^2$. Recent concerns have been expressed in the literature as to the ability of CNT to interfere with common cytotoxicity assays (Kroll et al., 2009; Monteiro-Riviere and Inman, 2006). In particular the large surface area of CNT has been

shown to adsorb critical components of the assays thereby altering the output measured. Here we validated the use of the LDH assay as an accurate measure of cell membrane integrity by demonstrating the lack of effect of the CNT in measurement of the end product of the assay (Worle-Knirsch et al., 2006). The trypan blue exclusion assay was also used to measure cell death in the mesothelial cell line, where the results supported that of the LDH assay. However the trypan blue exclusion assay could not be carried out on THP-1 cells exposed to CNT as macrophages clumped together during the treatments making accurate assessment of the cellular viability by this method impossible.

Mesothelial cells are reported to be uniquely sensitive to asbestos fibres with direct exposure *in vitro* inducing death (Yang et al., 2010; Broaddus et al., 1996), inflammatory mediator production (Yang et al., 2010), oxidative stress (Swain WA and Faux SP, 2002) and genotoxicity (Xu et al., 1999; Lechner et al., 1985). Although the potential pathogenicity of CNT has been tested in a variety of lung-derived cell types with responses including inflammation (Ye et al., 2010) and oxidative stress (Pulskamp et al., 2007) reported, there is a paucity of data concerning the direct effects of CNT on mesothelial cells. A study carried out by Tabet et al reported a significant loss of cell viability for Met5A cells incubated for 48 hours with 100 μg/ml MWCNT (Tabet et al., 2009). However this study employed the MTT assay as a measure of cytotoxicity, an assay which is widely regarded as unsuitable for use with CNT treated cells as the as it has been shown to be subject to CNT interference resulting in false positive readings (Worle-Knirsch et al., 2006). Pacurari *et al* examined the direct effects of SWCNT and MWCNT on normal and malignant mesothelial cells and reported a decrease in cell viability, activation of pro-inflammatory transcription factors and pro-inflammatory MAPK pathway activation (Pacurari et al., 2008b; Pacurari et al., 2008a). However these effects were very modest and seen at 5-10 times the dose used in the present paper. There was also ongoing PARP activation suggesting that the cells were also undergoing apoptosis, making this data difficult to interpret as to the true role of direct pro-inflammatory effects of CNT on mesothelial cells at plausible doses. In contrast, within the present study we found mesothelial cell cytotoxicity only at the highest exposures used in preliminary studies but no evidence of pro-inflammatory responses after exposure of mesothelial cells to a low sub-lethal dose (5μg/cm^2) of the panel of CNT. Nagai et al demonstrated that different types of MWCNT induced different levels of cytotoxicity in mesothelial cells and reported that the degree of cytotoxicity was inversely correlated with the mean diameter of dispersed MWCNT possibly due to the ability of the thinnest MWCNT to pierce the mesothelial cells membrane (Nagai et al., 2011). Interestingly Nagai et al showed that although all the MWCNT samples induced a pro-inflammatory response from macrophages in vitro, only the thin MWCNT induced a fibrotic inflammatory response and tumour development in the peritoneal cavity (Nagai et al., 2011). This suggests a role for CNT-mediated direct damage of the mesothelial cells in the pathogenesis of disease.

In contrast to the findings with mesothelial cells, exposure of macrophages to the CNT panel resulted in the induction of modest length-dependent pro-inflammatory responses. This was evident when only the long fibre-containing samples (NT_{long1} and NT_{long2}) induced the production of the acute phase cytokines, IL-1β and IL-6. The lack of response to the short CNT samples and particulate graphene in the form of NPCB suggest that the pro-inflammatory response to CNT in the pleural space is solely dependent on length. Firstly, length is a controlling factor in the clearance of fibres from the pleura where only long fibres are selectively retained for sufficient time to interact with macrophages at stomatal openings. Furthermore exceeding a maximum length for macrophage uptake will lead to frustrated phagocytosis, a state where the macrophages are unable to fully engulf long fibres resulting in the release of oxidants and pro-inflammatory signals (Donaldson et al., 2010). Frustrated phagocytosis has long been known to play an important role in asbestos effects (Mossman and Churg, 1998; Donaldson et al., 2010) and has also been implicated more recently in the inflammatory responses to long CNT elicited from macrophages *in vitro* (Brown et al., 2007) and *in vivo* (Poland et al., 2008). Brown *et al* reported an increase in the production of TNFα and a concurrent increase of ROS by macrophages in response to CNT and showed that this response was specifically related to the length of the CNT fibres (Brown et al., 2007). The presence of macrophages undergoing frustrated phagocytosis in the peritoneal lavage fluid of mice exposed to long CNT was noted by Poland *et al* who suggested that this macrophage-mediated response may be playing a role in the inflammation (Poland et al., 2008). Here, using a panel of CNT similarly defined by length we showed the length-dependent release of a number of pro-inflammatory cytokines from macrophages exposed to the long fibre CNT samples only. We related the pro-inflammatory effects of the long CNT to frustrated phagocytosis by inhibiting the uptake of CNT fibres by the macrophages using a known inhibitor of phagocytosis (DeFife et al., 1999). Treatment of macrophages with cytochalasin D, which impairs phagocytosis by inhibiting actin filament assembly (DeFife et al., 1999), concomitantly with either of the two long CNT samples resulted in the abrogation of IL-1β release seen after treatment with the CNT samples alone. The macrophage response to LPS, which does not require active uptake into cells by phagocytosis, was not attenuated by the addition of cytochalasin D highlighting the necessity of particle uptake and the role of frustrated phagocytosis in the pro-inflammatory reaction produced in response to CNT exposure.

We briefly examined the activation of the NALP3 inflammasome which has been recently demonstrated in a comprehensive study carried out by Palomaki et al to be induced by long needle-like CNT fibres (Palomaki et al., 2011). The activation of the NALP3 inflammasome has been shown to play a key role in the initiation of an inflammatory response during the phagocytosis of a variety of large or toxic particles and long fibres, including asbestos (Dostert et al., 2008), silica (Dostert et al., 2008; Hornung et al., 2008), monosodium urate crystals (MSU) (Hornung et al., 2008) and nanofibre titanium dioxide (Hamilton et al., 2009). The NALP3 inflammasome controls the maturation and

release of IL-1β from activated cells by binding caspase-1 via an associated protein linker known as ASC (apoptosis-associated speck-like protein containing a carboxy-terminal CARD) which subsequently cleaves pro-IL-1β to produce the mature form which is then secreted (Tschopp and Schroder, 2010). The activation of the NALP3 inflammasome is reported to be a 2-hit process where an initial stimulation of the macrophages causes an up-regulation of pro-IL-1β production in the cells and a subsequent stimulus leads to activation of the inflammasome pathway and release of the mature form of IL-1β. This is often mimicked in vitro in freshly isolated macrophages by priming the cells with low doses of LPS (25 pg/ml) prior to treatment. This step was omitted here however as differentiation of the THP-1 monocytes into mature macrophages is reported to cause sufficient priming and pro-IL-1β accumulation (Hornung et al., 2008). Higher doses of LPS treatment alone have also been shown to cause full activation of the inflammasome and release of mature IL-1β (Yamamoto et al., 2004) which supports the use of LPS as a control in the experiments carried out here, however a more appropriate control may have been to use a particle known to cause NALP3 activation, for example quartz. Additionaly examiniation of the cell supernantant by Western Blotting using antibodies specific to both the pro- and mature forms of IL-1β could conclusively identify whether the increase in IL-1β measured by ELISA was indeed an increase in the mature cleaved form.

The activity of all known NALP3 activators, regardless of their structure or composition is blocked by inhibiting efflux of potassium ions (K^+) from the cell (Petrilli et al., 2007b). The exact role of potassium efflux in the induction of the inflammasome is unknown, however it has been hypothesized that the various stresses lead to a change in the intracellular ionic milieu which induces a conformational change in one or more of the inflammasome components (Petrilli et al., 2007a). Indeed it has been shown by Petrilli *et al* that intracellular concentrations of K^+ below 70mM promote the recruitment of caspase-1 to ASC (Petrilli et al., 2007b). By stimulating macrophages with long fibre CNT in the presence of high extracellular potassium we prevented the efflux of potassium from the cells and saw a subsequent reduction in the levels of IL-1β release supporting the contention that the activation of the NALP3 inflammasome is the pathway by which long CNT cause IL-1β release.

The generation of ROS has also been proposed to play a role in the activation of the NALP3 inflammasome (Tschopp and Schroder, 2010). An increase in cellular ROS concentrations has been shown to cause thioredoxin-interacting protein to dissociate from thioredoxin, to which it is constitutively bound in the phagocyte resting state, and bind to NALP3 leading to activation (Zhou et al., 2010). NADPH oxidases have been shown to be a source of ROS in macrophage cells exposed to CNT (Ye et al., 2011). In the resting phagocyte, components of the NADPH oxidase are spatially segregated with components in the membrane and cytosol. Upon stimulation, the cytosolic components translocate to the membrane and assemble into a functioning enzyme complex, generating extracellular or phagosomal superoxide anion (Nauseef, 2004). Frustrated phagocytosis is likely to ultimately result in chronic activation of NADPH oxidase and excessive ROS production. IL-

1β production in response to long CNT was attenuated in the presence of the NADPH oxidase inhibitor, DPI. The impairment of the long CNT-induced production of IL-1β by both inhibition of particle uptake and also inhibition of two key effectors of NALP3 activation (K^+ efflux and NADPH oxidase), suggests that attempted uptake of long CNT by macrophages and subsequent frustrated phagocytosis activate the NALP3 inflammasome leading to the production of IL-1β. To conclusively demonstrate that the NALP3 inflammasome plays a crucial role in the pro-inflammatory responses of the THP-1 macrophages to the long CNT examined here the activation or stimulation of specific molecular components of the pathway (e.g. Caspase-1) need to be further studied. However the induction of NALP3 via frustrated phagocytosis of long CNT is in keeping with studies examining the inflammatory response to asbestos and other fibrous particles which have demonstrated the importance of the NALP3-mediated inflammatory response to particles and fibres *in vivo*. Inhibition or knock-out studies of key components of the NALP3 inflammasome prior to administration of asbestos fibres (Dostert et al., 2008), silica (Dostert et al., 2008; Hornung et al., 2008; Cassel et al., 2008) or MSU (Hornung et al., 2008) crystals into the lungs of mice have all shown an attenuated inflammatory response compared to wild-type controls. The essential role for NALP3 in the activation of an inflammatory response suggests that direct interaction between macrophages and long fibres is the initiating mechanism for the development of fibre-related inflammation and subsequent disease arising from chronic inflammation.

Mesothelial cells are well equipped to participate in the initiation and resolution of inflammation. Secretion of chemokines by stimulated mesothelial cells promotes directed migration of granulocytes which can lead to influx of inflammatory cells from the vasculature into the serosal space (Visser et al., 1995b). Mesothelial cells have been shown to be directly stimulated to produce a range of pro-inflammatory mediators including cytokines, chemokines, growth factors and oxidants in response to bacterial endotoxin and asbestos but have also been shown to be highly responsive to factors secreted by macrophages (Mutsaers, 2002). Previous studies with PM10 and diesel soot have also shown that fixed cells– epithelial cells and endothelial cells respectively, show much greater responses to particle-free conditioned media from macrophages treated with particles than to direct treatment with the particles (Jimenez et al., 2002; Shaw et al., 2011). Similarly, in the present study a greatly amplified mesothelial pro-inflammatory response was conferred by the particle-free conditioned medium of long CNT-exposed macrophages. The role of cross-talk between macrophages and mesothelial cells in amplifying inflammation has been demonstrated previously by Betjes *et al* when peritoneal mesothelial cells were shown to produce high levels of IL-8 in response to conditioned media from macrophages treated with the bacteria *Staphylococcus epidermidis*, but not to the bacteria themselves (Betjes et al., 1993). IL-1β and TNFα also mimicked induction of the mesothelial IL-8 response and the response to the conditioned media was blocked by the addition of anti-IL-1β and anti-TNFα antibodies (Betjes et al., 1993). The pro-inflammatory effect of the supernatant from

macrophages exposed to the long CNT samples described here was similarly attenuated by inhibiting release of IL-1β and other unknown factors by blocking phagocytosis with cytochalasin D highlighting the importance of phagocytosis in eliciting secretion of cytokines that drive the pro-inflammatory effects on the mesothelial cells.

The cross-talk between macrophages and mesothelial cells is known to be important in the normal inflammatory processes in the serosal cavities but, if disregulated, may also help to promote the development of mesothelioma. The precise mechanism that leads to mesothelioma development in the presence of fibres is unknown but a role for chronic inflammation in response to retained biopersistent fibres has been postulated (Okada and Fujii, 2006). Exposure of normal human mesothelial cells to asbestos fibres *in vitro* has not been shown to lead to cell transformation even though phenotypic changes such as chromosomal changes and extended lifespan were observed (Lechner et al., 1985; Xu et al., 1999). However Wang *et al* (Wang et al., 2004) carried out a study examining the effect on mesothelial cells of erionite, a naturally occurring long biopersistent fibre which causes mesothelioma in man and rodents following inhalation (Wagner et al., 1985; Maltoni et al., 1982; Dikensoy, 2008). In this study, treatment of mesothelial cells with erionite in combination with pro-inflammatory cytokines highlighted a potential role for an inflammatory environment in the transformation of mesothelial cells (Wang et al., 2004). While erionite alone had no effect on cell transformation, both IL-1β and TNFα could stimulate formation of transformed cells as identified by their anchorage-independent growth in soft agar. While the cytokines could induce the formation of tumorigenic colonies alone the effect was more potent in the presence of the erionite fibres (Wang et al., 2004). TNFα has also been shown by Yang *et al* to inhibit asbestos-induced cell death by activating the NF-κB signalling pathway in mesothelial cells (Yang et al., 2006). The TNFα-mediated resistance to the cytotoxicity may promote tumour formation by increasing the pool of mesothelial cells with fibre-mediated genetic damage in the inflammogenic environment which evade normal cell death. This suggests that inflammation and inflammatory cytokines may play an important role in mesothelioma. Here we showed that mesothelial cells exposed to a cocktail of cytokines and other mediators produced by macrophages treated with long CNT amplify and stimulate the inflammatory response thereby likely contributing to disease development in the pleural space.

In summary, the data presented in this study describe a mechanism for the initiation of a long fibre mediated inflammatory response in the pleural space via frustrated phagocytosis. A stepwise model for the initiation of fibre-mediated inflammation in the pleural cavity can be put forward where first the fibres are retained due to size-restricted stomatal clearance (Chapter 3) which is followed by attempted uptake and frustrated phagocytosis of the pleural macrophages. This model is supportred by the lack of response to small pro-inflammatory particles (quartz and coal mine dust) demonstrated in Chapter 3 as although a proportion of the instilled dose of small particles would be taken up by the

pleural macrophages there was no inflammatory response. This suggests that retention in pleural space is a key step faciliatating the development of fibre-mediated pleural inflammation.

We also demonstrated that the supernatant from macrophages exposed to long fibres produces a much-amplified pro-inflammatory response in mesothelial cells. The amplified mesothelial cell response to macrophage products was attenuated by inhibition of macrophage phagocytosis, confirming a role for frustrated phagocytosis. Inhibiting the activation of the NALP3 inflammasome during macrophage/CNT interaction also prevented the macrophages from releasing the pro-inflammatory factors into the supernatant, demonstrating the involvement of the NALP3 inflammasome. This study furthers our understanding of the role of macrophage/mesothelial cross-talk as a mechanism underlying the generation of a length-dependent inflammatory response to CNT in the pleural space. In addition, this *in vitro* model may prove useful for *in vitro* toxicity screening of the large number of new high aspect ratio nanofibres currently being developed, thereby reducing the need for animal testing. The fact that long fibres pose a problem to drainage from the pleural space and also macrophage uptake posing two mechanisms by which the length will affect fibre clearance from this sensitive tissue suggests that determining the structure alone may suffice when considering the potential hazard of a fibre.

Chapter 6: Surface functionalisation of carbon nanotubes

6.1 Acknowledgements

A long MWCNT sample was produced at The Nanoscience Centre, University of Cambridge by Matthew Boyles (Edinburgh Napier University, Edinburgh, UK) and has been labelled NT_{long}. This sample was created using the same equipment and methodology as that used to create the NT_{long2} sample. The NT_{long} sample was functionalised in two separate ways by Amanda Higginbotham and Ashley Leonard in the laboratory of Prof. James Tour at Rice University, Houston, Texas.

6.2 Aims and Hypothesis

The mechanical properties and high aspect ratio of CNT has stimulated interest in the use of CNT as reinforcing fillers in nanocomposites where stiffness, strength and light weight are important considerations (Vaia and Wagner, 2004). For the optimal exploitation of the properties of CNT in the manufacture of high tensile strength composites the CNT must be present as individual fibres dispersed throughout the material rather than large aggregates (Vaia and Wagner, 2004). However, due to van der Waals forces, CNT are difficult to disperse homogeneously. Solutions to this problem may lie in altering the CNT surface chemistry which can be achieved by a number of methods including sidewall functionalisation, oxidative treatment and polymer wrapping (Tasis et al., 2006). The benefit of surface modification in the exploitation of the properties of CNT suggests that the use of functionalised CNT could become widespread and therefore pose a real risk of occupational exposure. Utilising two forms of long CNT functionalised by non-destructive radical addition we aim to examine whether the inflammatory response elicited by long CNT in the pleural cavity can be affected by alteration of the CNT surface. We hypothesise that unless the surface functionalisation affects the critical requirements for a fibre to be pathogenic as set out in the fibre pathogenicity paradigm (fibre dimensions and biopersistence), we will see no difference in the pathogenic response to these fibres compared to the pristine form.

6.3 Results

6.3.1 CNT Functionalisation

The surface of the CNT was functionalised using the Billups reaction protocol which involved the covalent linkage of either aryl iodide or alkyl iodide groups onto the sidewall of the CNT under reducing conditions (Stephenson et al., 2006). Figure 6.1 is a schematic diagram showing the reaction procedure where the CNT are functionalised after an electron transfer from the lithium to the sidewall of the nanotube. This reaction causes the CNT to disperse in the liquid ammonia solution, allowing a

high degree of coverage of functional groups through radical addition. Incubation of the pristine nanotubes with aryl iodide isophthalic acid under these conditions produced CNT bound with isophthalic acid side side groups ($C_6H_4(COOH)_2$, herein referred to $NT_{long\text{-}AR}$) whereas incubation with alkyl iodide produced an alkylated NT sample bound with long chains of carbon atoms (herein referred to as $NT_{long\text{-}AL}$) (Stephenson et al., 2006). The CNT functionalised by this method showed high disorder bands in Raman spectra compared to the pristine material which indicates a high degree of functionalisation (Stephenson et al., 2006). The addition of aryl groups onto the side wall of the CNT will affect the physical properties of the CNT including hydrophobicity. CNT in their pristine form are non-polar and hydrophobic, however the covalent attachment of polar aryl groups allows the $NT_{long\text{-}AR}$ sample to become more hydrophilic. The $NT_{long\text{-}AL}$ sample has no reduction in hydrophobicity as no polar head groups have been attached to the non-polar pristine NT.

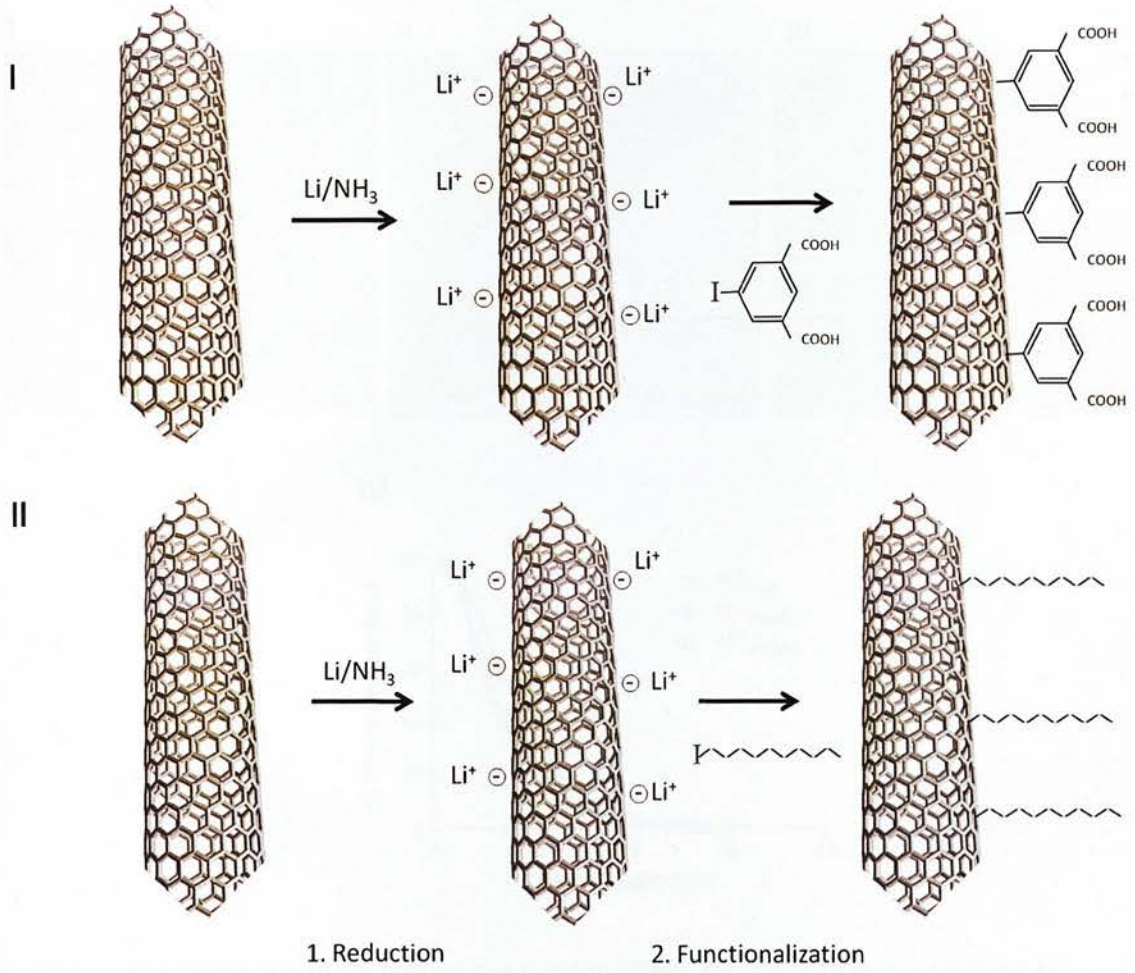

Figure 6.1: A schematic diagram of the functionalisation of CNT. Reduction of the CNT allows the dispersion of the CNT in ammonia and the covalent linkage of aryl groups (I) or alkyl chains (II) to the sidewall of the CNT.

6.3.2 CNT lengths

The size distribution of the pristine NT_{long} sample was measured and compared to that of the two functionalised samples. Light micrographs show the pristine NT_{long} and the functionalised $NT_{long\text{-}AR}$ and $NT_{long\text{-}AL}$ were heterogeneous samples containing fibres ranging from 1-30 microns in length (Figure 6.2 I-III). The size distributions were similar for each on the NT samples; regardless of functionalisation, for example the percentage of fibres greater than 10 μm (chosen as an arbitrary cut-off) for NT_{long}, $NT_{long\text{-}AR}$ and $NT_{long\text{-}AL}$ were 35%, 35% and 40%, respectively (Figure 6.2 IV). This demonstrates that this method of functionalisation was non-destructive and did not cause significant shortening of the CNT.

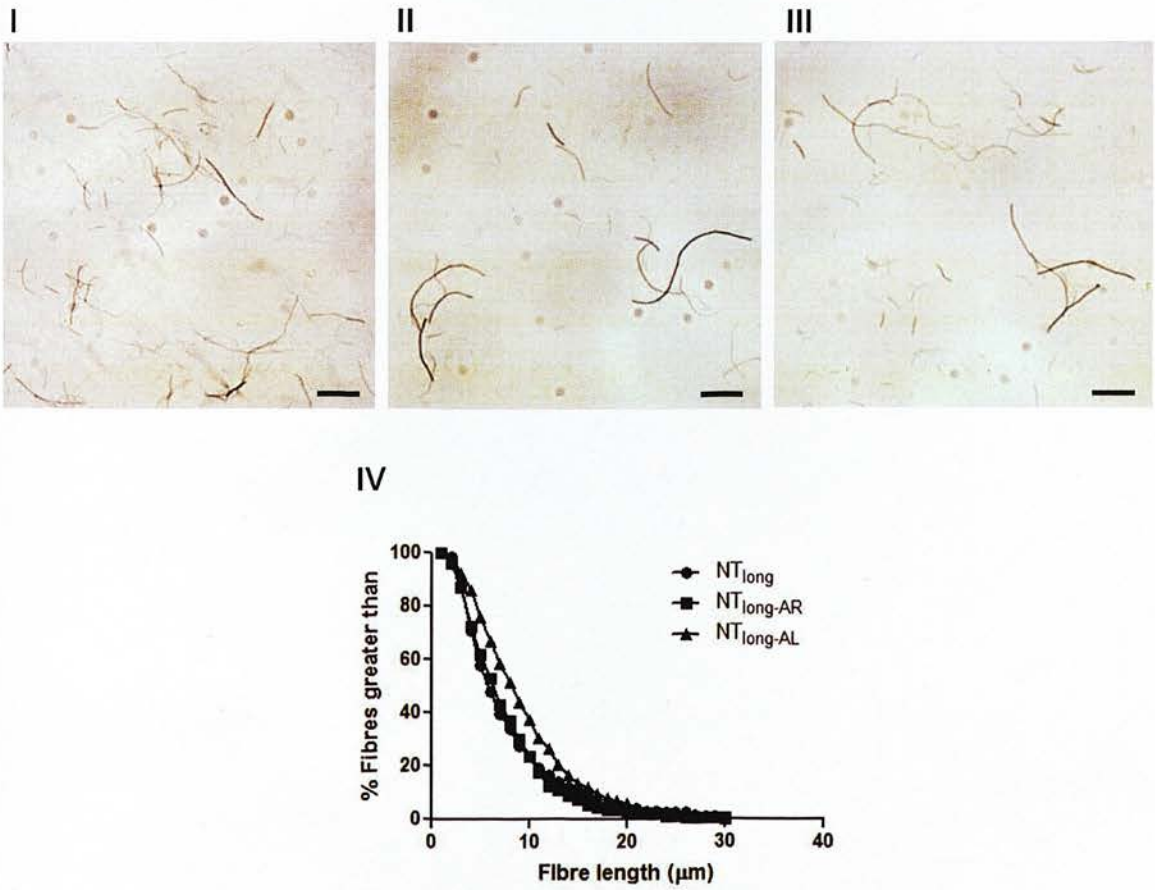

Figure 6.2: Size distribution of the pristine and functionalised CNT. Light micrographs of the NT_{long} (I), $NT_{long\text{-}AR}$ (II) and the $NT_{long\text{-}AL}$ (III) CNT samples. Scale bar= 10 μm. (IV) Size distributions of the CNT samples expressed as % fibre greater than (n=300 fibres measured). Fibre lengths and diameters were measured from high magnification SEM images of CNT samples deposited on filter paper. Only fibres where both ends were visible were included.

6.3.3 Pleural inflammatory response

The inflammatory response in the pleural cavity to the functionalised CNT was assessed 24 hours after direct injection into the pleural space and compared with the response to the NT_{long} sample. As expected the NT_{long} sample elicited a significant inflammatory response in the pleural space, as measured by a significant increase in total cell number and a significant increase in the number of granulocytes in the pleural lavage fluid over the vehicle control treated mice. Both functionalised CNT samples also elicited an increase in total cells and influx of granulocytes into the pleural cavity as was seen in response to NT_{long} (Figure 6.3 I, II), indicating the acute inflammatory response to the long fibres had not been modulated by the surface functionalisation.

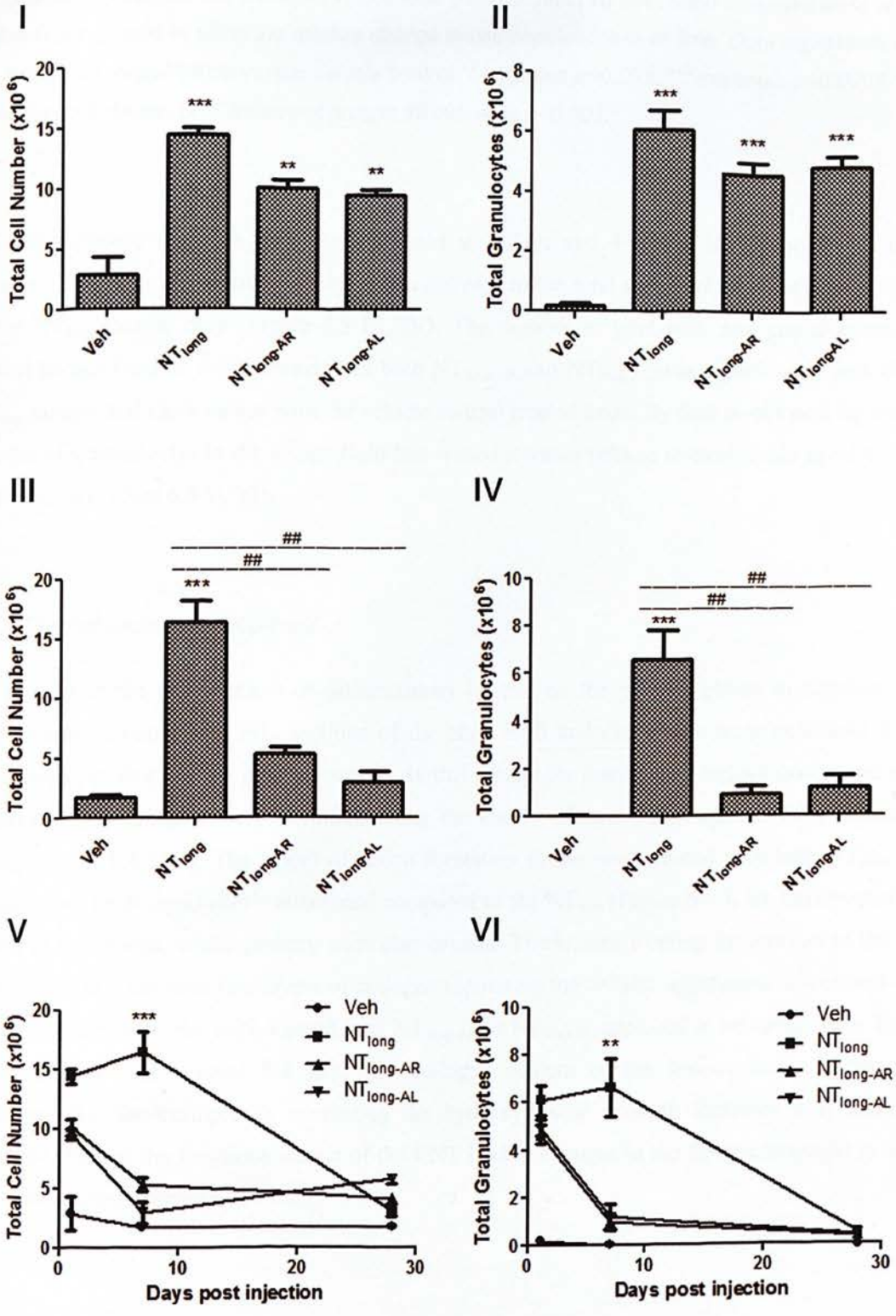

Figure 6.3: Acute inflammogenicity of the pristine and functionalised CNT samples. Inflammatory potential of the pristine and functionalised CNT in the pleural space was examined by measuring the total number of cells and the number of granulocytes in the pleural lavage fluid at 24 hours (I, II), 1 week (III, IV) and up to 4 weeks (V, VI) after direct injection of the CNT samples into the pleural cavity

*(5 µg/mouse). The total cell number (V) and total granulocytes (VI) from each timepoint were plotted on the single graphs to show the relative change in cell populations over time. Data represents mean ± s.e.m. (n=3). Significance versus vehicle control ** indicates p<0.001, *** indicates p<0.0001, significance between CNT treatment groups ## indicates p<0.001.*

The inflammatory response was also measured at 7 days and 4 weeks after exposure to the NT samples. At 7 days we measured a significant increase in the total cells and granulocytes in response to the NT_{long} sample only (Figure 6.3 III, IV). The number of total cells and granulocytes in the pleural lavage fluid of mice treated with both $NT_{long\text{-}AR}$ and $NT_{long\text{-}AL}$ was significantly less than the NT_{long} sample and more on par with the vehicle control treated mice. By four weeks post injection the number of granulocytes in the lavage fluid had waned towards vehicle control levels in all three NT-treated mice (Figure 6.3 V, VI).

6.3.4 Pleural lesion development

To investigate the development of inflammatory lesions on the parietal pleura in response to the pristine and functionalised NT, sections of the chest wall and diaphragm were examined by light microscopy at four weeks post injection. At this timepoint contiguous lesions composed of cell aggregates and collagen were identified along the chest wall and diaphragm of mice treated with NT_{long} (Figure 6.4 I, II). The extent of lesion formation in the mice treated with both $NT_{long\text{-}AR}$ and $NT_{long\text{-}AL}$ had been significantly attenuated compared to the NT_{long} (Figure 6.4 I, II). Differences in the nature of the lesions, where present, were also evident. The lesions forming in response to the NT_{long} were highly cellular with fine layers of collagen separating the cellular aggregates. In contrast to this the lesions present in the mice treated with $NT_{long\text{-}AR}$ or $NT_{long\text{-}AL}$ appeared to be collagenous but with fewer cells present (Figure 6.4 III). The collagen content of the lesions was not determined biochemically, for example by measuring the hydroxyproline content; therefore it is difficult to conclude whether the functionalisation of the CNT lead to changes in the fibrotic response as well as the inflammatory response.

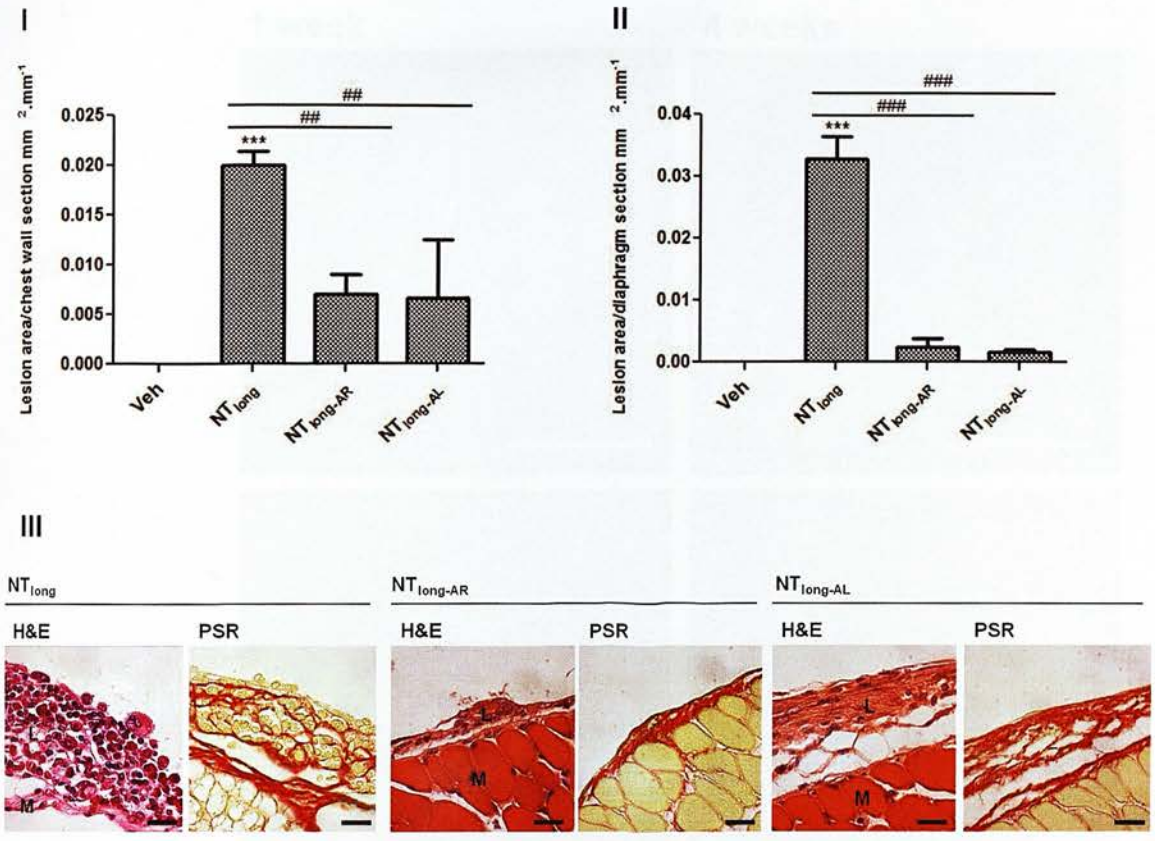

*Figure 6.4: Lesion development along the parietal pleura. Parietal pleura along the chest wall (I) and diaphragm (II) of mice treated with the CNT samples (5 µg/mouse) were examined 4 weeks after injection (n=3). Lesion area was quantified and expressed as area per length of chest wall section (mm^2/mm) (I) and area per length of diaphragm section (mm^2/mm), respectively. Data represents mean ± s.e.m. (n=3). Significance versus vehicle control *** indicates p<0.0001, significance between CNT treatment groups ## indicates p<0.001, ### indicates p<0.0001. Representative images of the chest wall sections stained with H&E for gross morphology and Picosirius red for collagen content are shown in (III), M indicates the underlying muscle of the chest wall, L indicates inflammatory lesions. Scale bar= 50 µm.*

Scanning electron microscopy was also used to examine the surface of the chest wall at 1 week and 4 weeks post injection (Figure 6.5). Extensive lesions overlaying the surface of the chest wall were evident at both 1 week and 4 weeks post exposure of the NT_{long} sample. Small areas of inflammatory lesion were identified in mice treated with $NT_{long\text{-}AR}$ and $NT_{long\text{-}AL}$ at 1 week post injection however the inflammatory response appeared all but completely resolved by 4 weeks in response to both functionalised NT samples.

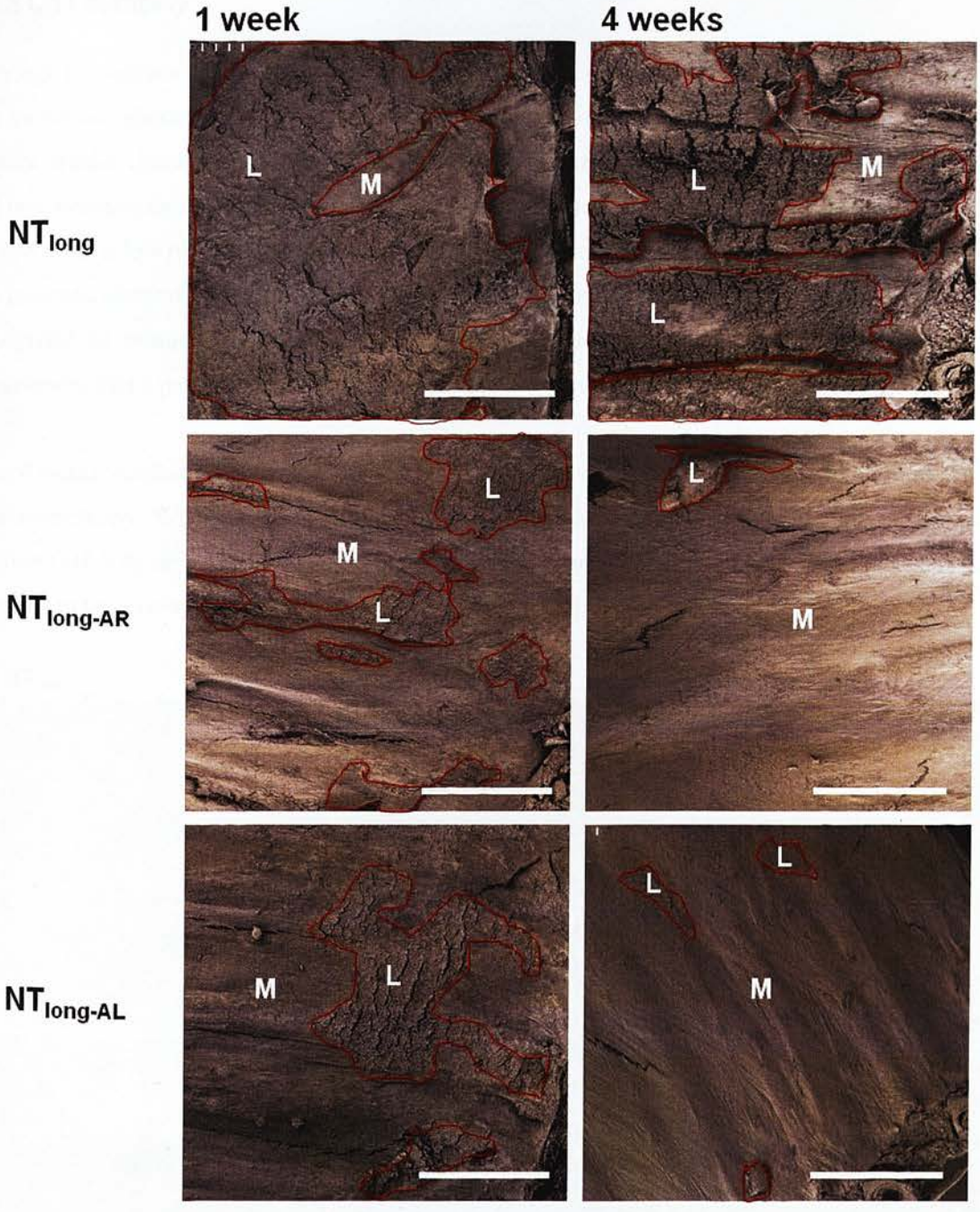

Figure 6.5: Scanning electron microscopy of the chest wall. The surface of the parietal pleural of the chest wall was examined by scanning electron microscopy at 1 and 4 weeks after direct injection of NT_{long}, $NT_{long\text{-}AR}$ and $NT_{long\text{-}AL}$ (5 µg/mouse) into the pleural space. M indicates areas of normal mesothelium, L indicates the inflammatory lesions (also outlined in red). Scale bar= 1 mm.

6.3.5 CNT durability

Although the surface functionalisation method employed here was non-destructive and did not cause any immediate shortening of the NT sample, the potential effect on the biopersistence of the fibres; another crucial characteristic of fibre pathogenicity, is unknown. As an alternative to an expensive and time-consuming *in vivo* biopersistence study we examined the durability of the functionalised NT *in vitro* using a low pH solution (pH 4.5) to mimic the conditions inside a lysosome. Gambles solution is a balanced electrolyte solution similar to the electrolyte environment of biological systems. Its pH is adjusted to mimic that inside macrophage phagolysosomes, potentially the most degradative environment that a particle should encounter following lung deposition and macrophage uptake.

After 4 weeks incubation in the low pH solution the pristine and functionalised NT were visualised by light microscopy. When compared to samples incubated for the same length of time in a neutral solution (pH 7.4) of 0.5% BSA/saline both the $NT_{long\text{-}AR}$ and $NT_{long\text{-}AL}$ samples, but not the NT_{long}, appeared to have been shortened to some degree (Figure 6.6).

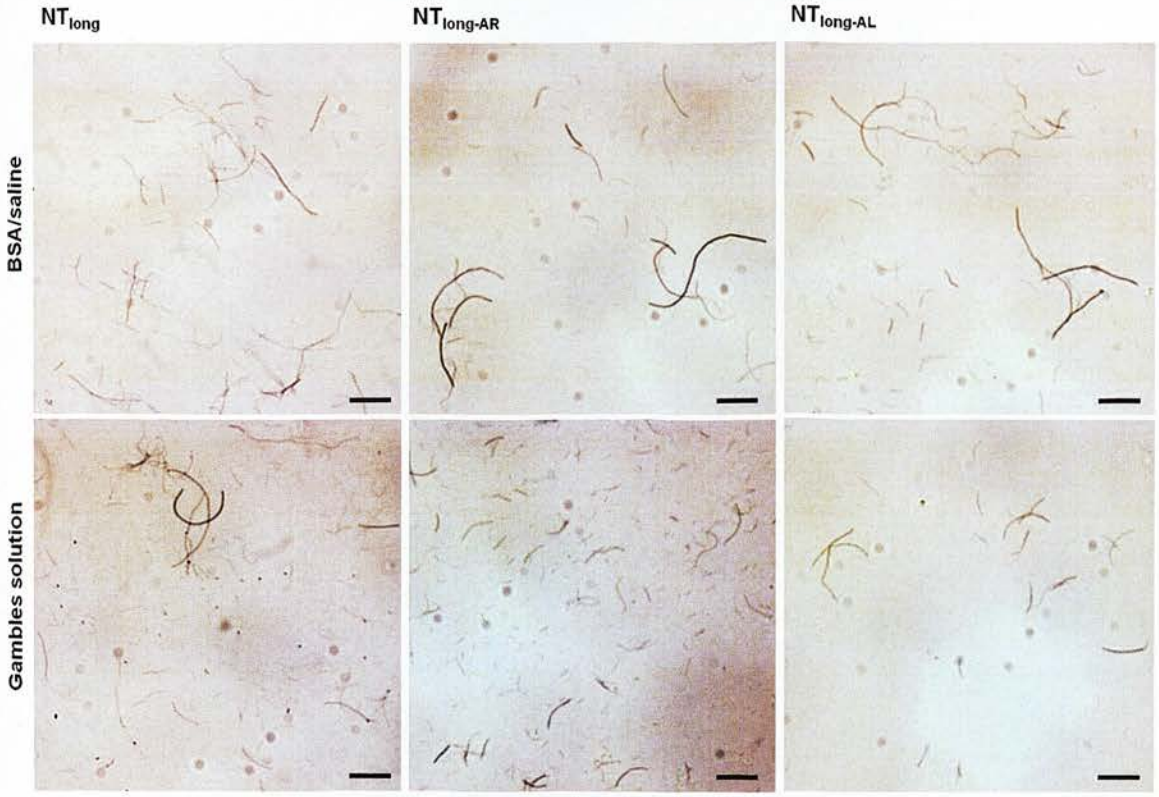

Figure 6.6: CNT samples after incubation in neutral pH BSA/saline or low pH Gamble's solutions. Light micrographs of the NT_{long}, $NT_{long\text{-}AR}$ and $NT_{long\text{-}AL}$ samples after 4 weeks incubation in the neutral pH BSA/saline solution (pH 7.4) or the low pH Gambles solution (pH 4.5). Scale bar= 10 µm.

In order to more accurately measure the size distribution of the functionalised NT samples after incubation in the Gambles the NT samples were visualised by scanning electron microscope. There

was no discernible difference in the size distribution of the NT_{long} samples incubated in the neutral pH BSA/saline solution compared to samples incubated in the low pH Gambles solution, however a reduction in the area under the curve of both the functionalised NT samples incubated in the Gambles compared to BSA/saline was evident when the size distribution is plotted as the percent fibres greater than length (Figure 6.7). The percent fibre greater than 10 μm for $NT_{long\text{-}AR}$ was reduced from 35% to 7% after incubation with the Gambles, similarly the percent fibres greater than 10 μm in the $NT_{long\text{-}AL}$ sample was reduced from 40% to 10%. A reduction in the area under the curve (Table 1) also indicates that the fibres have been shortened by their incubation in the low pH solution. Measurements of the fibre diameters showed no reduction between incubation in Gambles or BSA/saline for the three CNT samples.

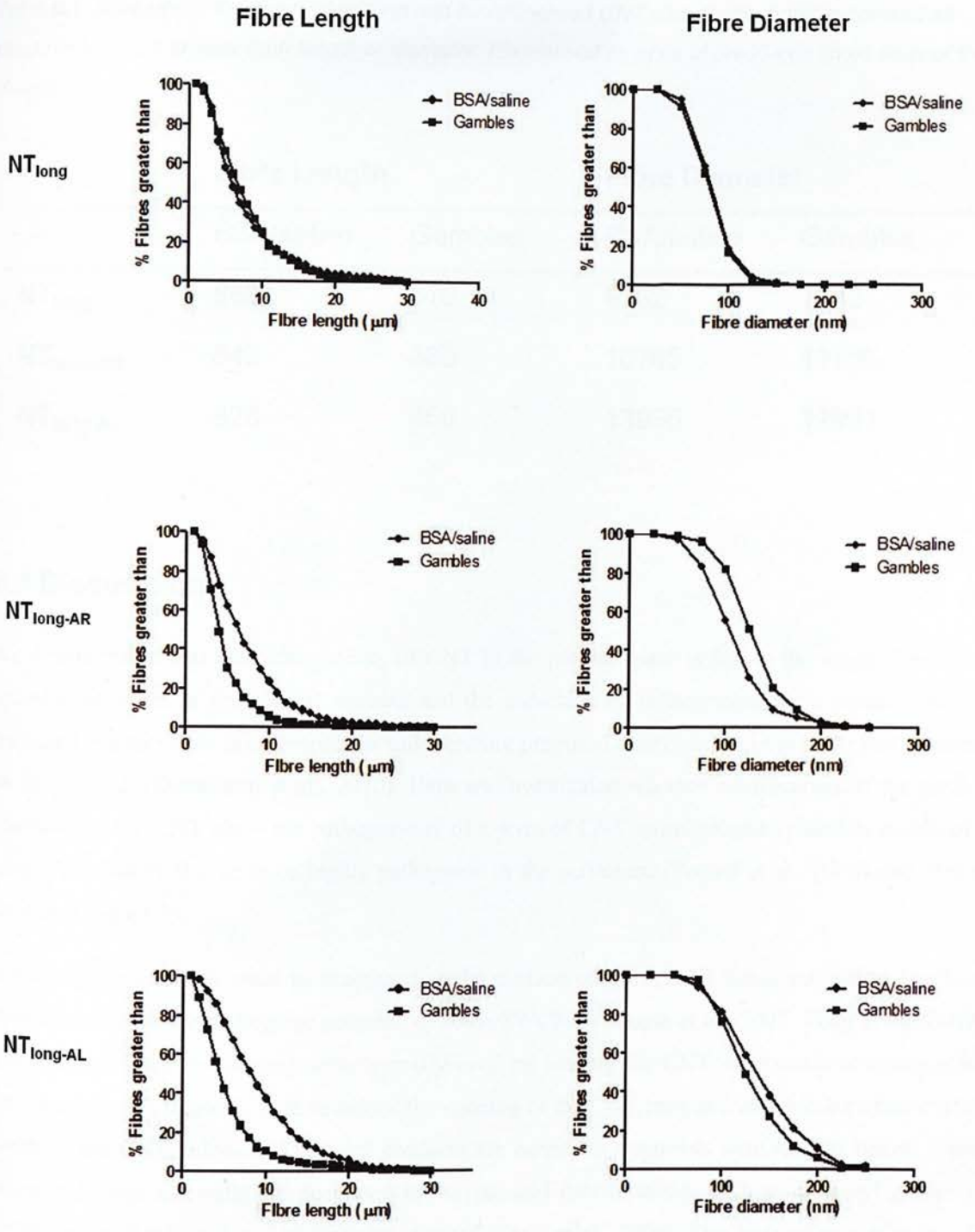

Figure 6.7: Size distributions of pristine CNT and functionalised CNT after incubation in BSA/saline or Gambles solutions. Fibre lengths and diameters were measured from high magnification SEM images of CNT samples deposited on filter paper and expressed as percentage fibres greater than (n=300 fibres measured). Only fibres where both ends were visible were included.

Table 6.1: Area under the curve of pristine and functionalised CNT size distributions expressed as percentage fibres greater than length or diameter. (Expressed as units of the X-axis times units of the Y-axis).

	Fibre Length		Fibre Diameter	
	BSA/saline	Gambles	BSA/saline	Gambles
NT_{long}	662	670	8262	7942
$NT_{long-AR}$	642	380	10785	12755
$NT_{long-AL}$	828	456	13950	12991

6.4 Discussion

We demonstrated that the pathogenicity of CNT in the pleural space is due to the length-dependent retention of fibres at the pleural stomata and the induction of inflammation as a consequence of frustrated phagocytosis in macrophages and therefore proposed a mechanism of toxicity that is reliant on fibre length (Donaldson et al., 2010). Here we investigated whether modification of the surface chemistry of the CNT alters the pathogenicity of a form of CNT morphologically similar to that of a sample previously shown to be highly pathogenic in the peritoneal (Poland et al., 2008) and pleural cavities (Chapter 3).

A technique commonly used to functionalise the surface of CNT, acid functionalisation has been shown to increase the pathogenic potential of some SWCNT (Saxena et al., 2007; Tong et al., 2009). The process of acid functionalisation typically involves heating the CNT in mixtures of strong acids such as nitric and sulphuric acid to induce the opening of the CNT ends and also break carbon-carbon bonds in the CNT sidewall. The final products are nanotube fragments with lengths below 1 μm, whose ends and sidewalls are decorated by oxygenated functionalities such as carboxyl groups to which various functional moieties can be attached (Tasis et al., 2006). The destructive nature of acid functionalisation which invariably shortens the CNT suggests that CNT functionalised in this manner would not be pathogenic in our model of mesothelial exposure regardless of their surface reactivity as they would not be retained to elicit a response. The aim of this study was to functionalise the surface of CNT using non-destructive methods that maintain the length of the CNT to allow a critical evaluation of the role of surface in the toxicity of a fibre in the pleural cavity. The method we employed was to attach aryl or alkyl groups to the sidewall of the CNT by radical addition which according to our size distribution measurements did not lead to an alteration in fibre length.

The inflammatory response to the functionalised CNT was initially assessed at 24 hours post - injection where our results showed a minor decrease in the total number of cells retrieved from the pleural space of mice treated with both functionalised CNT samples but no difference in the number of inflammatory granulocytes. The acute inflammatory response to the long functionalised CNT samples suggests the altered surface properties of the CNT do not affect the acute inflammatory response to long CNT in the pleural cavity. However it is feasible that subtle differences in the acute toxicity of the functionalised CNT may be initially obscured due to the administration of a bolus dose into the pleural space. This is supported by the striking difference between the pleural responses to the different forms of long CNT samples evident as early as 7 days post injection. A significant attenuation of the number of pleural granulocytes was detected in response to both functionalised CNT samples compared to the pristine CNT at 7 days post injection, which was accompanied by significantly reduced lesion development along the parietal pleura by 4 weeks.

The pathogenicity of the functionalised CNT samples examined here is consistent with the fibre pathogenicity paradigm with regard to their length and ability to induce an acute inflammatory response at 24 hours post injection, however due to the lack of sustained inflammatory response we hypothesised that these functionalised CNT diverge from the FPP because of their lack of biopersistence. CNT belong to the family of graphenic carbon materials composed primarily of carbon in sp^2-hybridised bonding states which are generally considered stable. Indeed a number of studies have observed SWCNT and MWCNT in the tissue of animals, months after the initial exposure (Muller et al., 2005; Ma-Hock et al., 2009; Murphy et al., 2011) although there is a lack of studies specifically designed to assess the biopersistence of CNT. To fully examine the biopersistence of a fibre requires lengthy in vivo experiments however fibre durability, the chemical mimicking of fibre dissolution is more readily determined. Searl et al assessed the relative biopersistence of nine mineral fibre types in the lung up to one year after intratracheal instillation and also measured the ability of the test materials to resist dissolution in a parallel series of simple in vitro acellular experiments (Searl et al., 1999). Comparison between the in vivo and in vitro results showed that differences in persistence of long fibres in the lung were correlated with measured rates of dissolution in vitro (Searl et al., 1999). Here we carried out a short term durability study to assess whether incubation of the CNT in a low pH salt solution, mimicking the phagolysosome environment, could affect the durability of the pristine and functionalised CNT. After 4 weeks incubation in the low pH Gamble's solution both functionalised CNT samples showed some degree of fibre shortening compared to samples that had been incubated in a neutral pH solution. In light of the apparent lack of durability of the functionalised CNT, Figure 6.8 depicts a potential mechanism proposed to explain the unusual attenuated pleural response to the long functionalised CNT samples characterised by an acute inflammatory response followed by loss of pathogenicity. CNT may be pathogenic in their pristine form but if they have defects as a consequence of their functionalisation they are vulnerable to

degradation in the acid lysosomal milieu over time and may shorten and are cleared and so do not cause a sustained response.

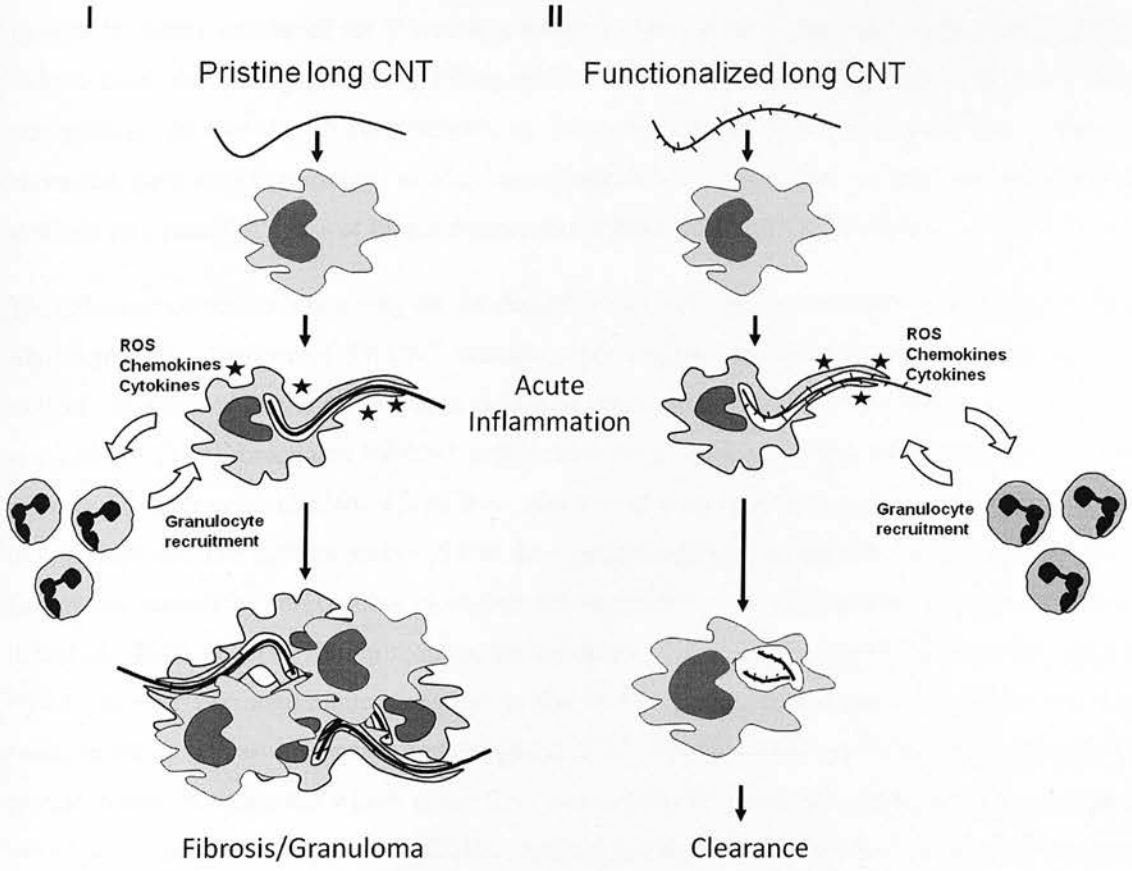

Figure 6.8: Diagrammatic representation of the importance of biopersistence in the sustained inflammatory response to long fibres. (I) Pristine, long CNT fibres in the pleural space are taken up by macrophages but due to their length stimulate a state of frustrated phagocytosis which leads to acute inflammation (Inflammatory mediators indicated by stars). The biopersistent nature of the pristine CNT means the CNT will not be broken down and cleared but will lead to continued recruitment of macrophages and a sustained response culminating in granuloma formation and fibrosis. (II) Non-biopersistent fibres, as we suppose the functionalised CNT to be, may elicit an acute inflammatory response due to their length but as the macrophages break down the long fibres they can be fully engulfed and successfully cleared.

A comprehensive study assessing the durability of a number of pristine CNT samples was carried out by our group in collaboration with the CSIRO, Australia (Osmond-McLeod et al., 2011). Following the incubation of the panel of CNT samples in Gamble's solution we assessed both the loss of mass and fibre shortening as a measure of durability and also assessed the impact of durability on CNT fibre-induced pathogenicity by examining the inflammatory response in the peritoneal cavity of a subset of the CNT panel after incubation in the Gamble's solution. The results showed that among this

panel only one CNT sample displayed a modest loss of mass over time. The percentage of long fibres in this sample also progressively decreased from the 0 to 3 to 10 weeks incubation. These changes in morphology were accompanied by a mitigation of the strong inflammatory and fibrotic response induced by fibres incubated for 0 weeks, consistent with the now shortened fibres being efficiently cleared from the peritoneal cavity (Osmond-McLeod et al., 2011). This demonstrates a loss of pathogenicity *in vivo* due to susceptibility to shortening caused by the acid treatment *in vitro*. The attenuated pathogenic response to the functionalised CNT described in the present study may similarly be a result of a loss of biopersistence in the functionalised CNT samples.

The influence of surface chemistry on the durability of CNT has recently been examined by Liu et al who incubated a number of SWCNT samples, with surfaces modified by various functionalisation methods, in a low pH solution to which H_2O_2 was added to create a mild oxidising environment (Liu et al., 2010). The carboxylated SWCNT sample underwent extensive degradation and fibre shortening whereas the other types of SWCNT; pristine, ozone treated and aryl-sulfonated, did not degrade under these conditions. The authors proposed that the 'collateral damage to the tubular graphenic backbone' i.e. defects, caused by the process of carboxylation promotes the degradation of carboxylated CNT (Liu et al., 2010). Carboxylation requires the breakage of two backbone C-C bonds in the graphene crystal leaving two active sites adjacent to the COOH group, which can be the sites for further oxidative attack (Balasubramanian and Burghard, 2005). Indeed carboxylation has also been shown to provide points of weakness which make CNT susceptible to enzymatic degradation *in vitro* and *in vivo* (Allen et al., 2008; Kagan et al., 2010). Radical addition, the process of functionalisation carried out here, is non-destructive as although it forms one bond attached to a backbone carbon atom, which disrupts the pi-conjugation at that site, the three bonds to the neighbouring carbon atoms in the backbone remain intact (Balasubramanian and Burghard, 2005). Therefore the mechanism by which this method of functionalisation results in increased vulnerability of the CNT samples to biodegradation remains unknown. Failure to explain the potential mechanism by which this method of functionalisation leads to a loss of CNT biopersistence suggests that a more robust examination of the durability of these functionalised CNT samples is required. The improved dispersibility of the functionalised CNT itself may have lead to systematic flaws in the fibre sizing method as measurements could potentially be skewed by an increase in shorter fibres released from CNT ropes, bundles or aggregates that would not have been dispersed in the pristine sample. If this was a significant problem, however differences in the fibre sizing of the three NT groups before incubation in the low pH solution would also be expected, which was not the case (Figure 6.2 IV). Raman microscopy would be a useful tool to specifically detect disruption of the carbon bonds of the CNT backbone which may lead to fibre shortening (Kagan et al., 2010).

Differences in the proteins and biomolecules that associate with the CNT surface, the so called corona, may provide an alternative explanation for the loss of a sustained pathogenic response to the

functionalised CNT sample. The interaction between particles and cells is influenced by the biomolecules which associate with the particle surface and the adsorption of these biomolecules is in turn influenced by the physiochemical properties of the material (Nel et al., 2009). The arylation and alkylation of the CNT alters the hydrophobicity of pristine CNT samples which affect how biomolecules, and subsequently cells, interact with particles. Hydrophilic surfaces present a substantial energy barrier to protein adsorption due to the requirement to displace water molecules and therefore have a repulsive effect compared to hydrophobic surfaces to which proteins will more readily associate (Wilson et al., 2005). The attenuation of the sustained inflammation and lesion formation in response to both hydrophilic and hydrophobic functionalised CNT samples however suggests that alterations in the protein corona are not specific to changes in hydrophobicity. Alternatively the addition of aryl groups or alkyl side-chains may prevent certain protein binding via steric hindrance. Gasser et al compared the protein binding profiles of pristine MWCNT with negatively and positively charged MWCNT and reported more pronounced differences between pristine and functionalised MWCNT whereas among functionalised MWCNT less variability was found (Gasser et al., 2010). The authors hypothesized that the surface charge played only a minor role in protein binding in contrast to steric hindrance which prevented the binding of larger proteins to either of the functionalised CNT (Gasser et al., 2010). The differences in protein binding and their potential role in CNT pathogenicity was not addressed here, but would be an interesting subject for future studies.

Our overall conclusion from this study is that the pathogenicity of CNT in the pleural cavity is attenuated by the radical addition of aryl and alkyl groups to the sidewall of long CNT however the mechanism for the loss of pathogenicity has not been elucidated. A loss of CNT durability leading to the breakdown and clearance of long fibres from the pleural space provides an explanation for the mitigation of the pathogenic response to the long functionalised CNT seen here, that falls within the current understanding of fibre pathogenicity. The alternative explanation discussed above suggesting that it is the alteration of the surface that prevents the development of a sustained response would require a re-evaluation of the FPP which presently does not take into account the chemical composition or surface properties of a fibre. Although the reasons for the loss of pathogenicity are unclear non-destructive functionalisation of CNT by radical addition may represent a desirable method of manufacturing CNT that have the required characteristics for optimal use, e.g. length and dispersibility but also a lower hazard to exposed workers. It is therefore important to establish the cause of the reduction in toxicity so that this may be fully understood and perhaps applied in the manufacture of CNT with the aim of producing CNT that are safe by design.

Chapter 7: Pulmonary and pleural response to CNT administered into the lungs.

7.1 Acknowledgements

Determination of a human equivalent dose was carried out with the assistance of Dr. Craig A. Poland, Institute of Occupational Medicine, Edinburgh.

7.2 Aims and Hypothesis

Despite the well characterised role of fibre length in asbestos-related diseases of the lung, including asbestosis and the development of lung tumours, only a small number of studies to date have questioned the role fibre length in the potential pulmonary toxicity of CNT. The aim of this study was to address the role of fibre length in the adverse effects of CNT in the lung by comparing the inflammatory responses to three structurally diverse CNT samples after aspiration exposure. Based on the propensity of the long CNT sample only to induce frustrated phagocytosis in macrophages, as described in Chapter 5, we hypothesise that the CNT-mediated effects in the lungs are similarly length-dependent.

The data presented in Chapter 3 strongly supports the contention that long CNT can cause asbestos-like pathogenic effects in the pleural space, however exposure to CNT by intrapleural injection is not physiologically relevant as it by-passes the clearance mechanisms of the lung. As such, our aim here is to ascertain whether CNT, previously shown to be inflammogenic in the pleural cavity after direct exposure, would elicit a similar pleural response after administration via the lung.

7.3 Results

7.3.1 Length-dependent inflammatory response of CNT in the lung at 1 and 6 weeks

The inflammatory response produced by aspiration of the 3 CNT samples (NT_{short}, NT_{tangl}, NT_{long2}) into the lungs at a dose of 50 μg/mouse was measured at 1 week post exposure by lavaging the lungs and measuring the cell types present. A significant increase in the number of inflammatory granulocytes in the BAL fluid was measured in response to the NT_{long2} sample only (Figure 7.1 I, II). CNT-induced lung damage was assessed by measuring acellular BAL fluid LDH activities as a measure of cytotoxicity, and protein concentrations as a measure of the integrity of the alveolar–blood barrier. This length-dependent pattern was reflected in the LDH measurements with a significant increase in LDH activity detected in mice treated with NT_{long2} at 1 week. No change was seen in the

protein concentration of the lavage fluid (Figure 7.1 III, IV). By 6 weeks the inflammatory response to NT_{long2} as measured by differential cell count and LDH levels had returned to vehicle control levels. No inflammatory response to NT_{short} or NT_{tangl} was detected at either 1 or 6 weeks in any of the assays.

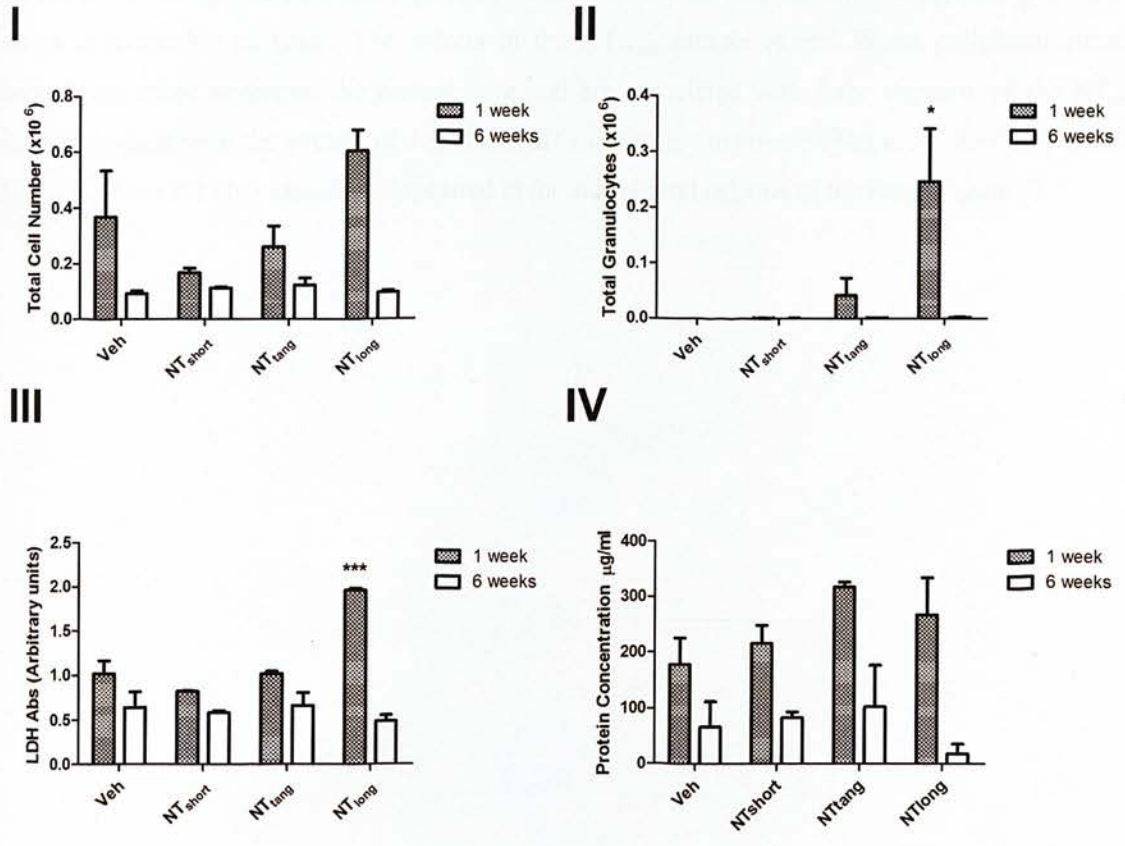

*Figure 7.1: Inflammatory response to CNT in the lungs at 1 week and 6 weeks. C57/Bl6 mice were exposed to the 3 CNT samples (NT_{short}, NT_{tang1}, NT_{long2}) by pharyngeal aspiration (50 µg/mouse). At 1 and 6 weeks post exposure the lungs were lavaged and total cell number (I), total granulocyte number (II), LDH levels (III) and protein concentration (IV) were measured. Significance indicated compares treatment groups to vehicle control from the same timepoint, * indicates p<0.05, ** indicates p<0.001, *** indicates p<0.0001.*

7.3.2 Fibrotic response to CNT in lung at 6 weeks

The pathology of the lungs exposed to the CNT panel was examined at 6 weeks after aspiration. Overall the lungs exposed to NT_{short} and NT_{tangl} appeared similar to vehicle control (Figure 7.2 7.3, 7.4). NT_{tangl} caused small, localised granuloma and minor lymphocyte infiltration but the majority of

the lung appeared normal (Figure 7.4). Individual macrophages could also be identified containing aggregates of the tangled CNT sample although these were few in number. Responses were minor and more likely due to the effect of instilling a bolus dose of particles into the lung rather than specific CNT effects. The NT_{long2} sample however produced a strong response characterised by extensive interstitial thickening and remodelling of the alveolar spaces (Figure 7.5). Within the interstitum there is evidence of collagen deposition. Lymphocyte infiltrates were also identified surrounding the blood vessels in a number of cases. The effects of the NT_{long2} sample extend to the peripheral airways although are more severe in the central lung and are associated with large deposits of the NT_{long2} fibres, consistent with the pattern of deposition after aspiration exposure (Rao et al., 2003). A number of NT_{long2} fibres are also identified deposited in the sub-pleural regions of the lung (Figure 5).

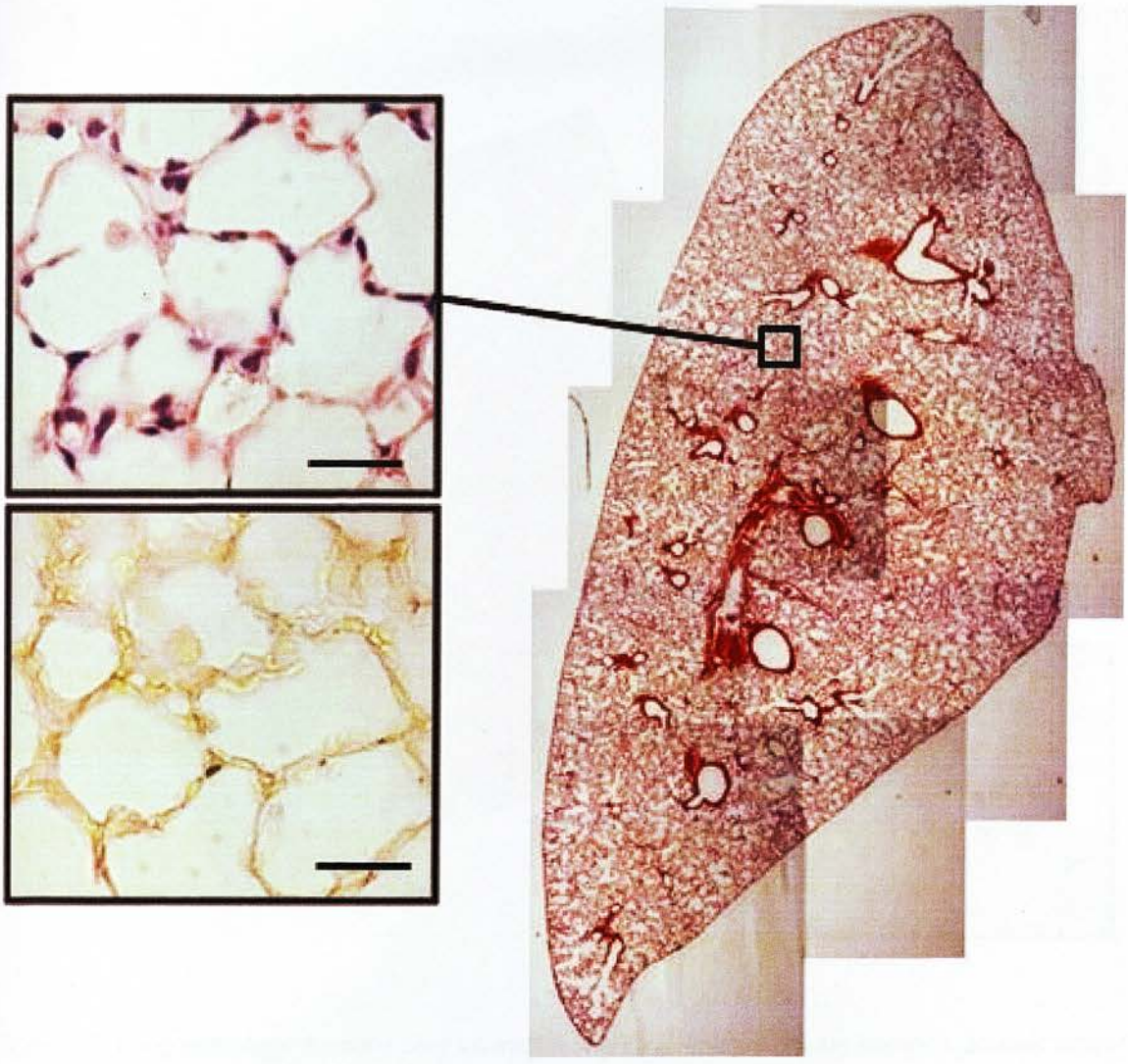

Figure 7.2: Lung pathology 6 weeks post aspiration of vehicle control. Images of lung sections, stained with H & E were realigned to show the gross morphology of the lungs 6 weeks post aspiration with vehicle control (0.5% BSA/saline). Call-outs stained with H & E and Pico Sirius Red (PSR), for collagen, show the normal delicate structure of the alveolar septa. Scale bar indicated 50 µm.

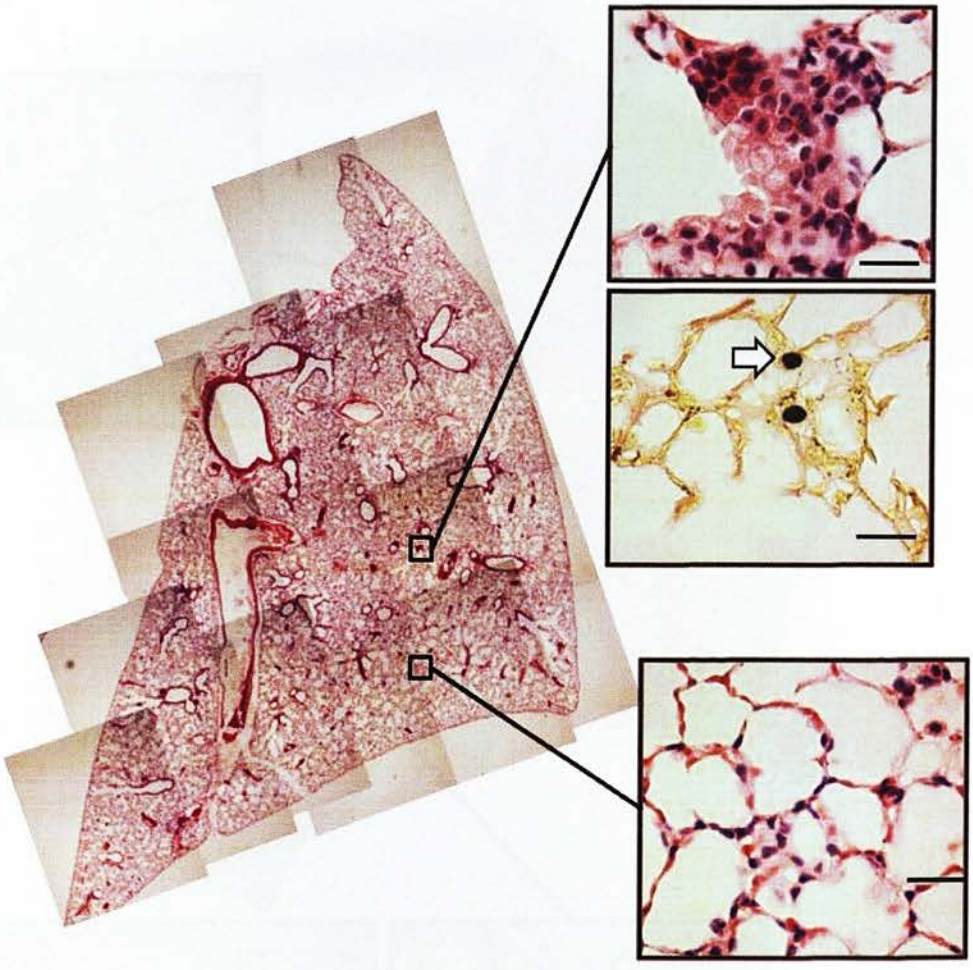

Figure 7.3: Lung pathology 6 weeks post aspiration of NT_{short}. Images of lung sections, stained with H & E were realigned to show the gross morphology of the lungs 6 weeks post aspiration with NT_{short} (50 µg/mouse). Small accumulations of cells and CNT aggregates (white arrows) are indentified in mice treated with NT_{short} but for the most part the lung resembled the vehicle control treated lungs. Scale bar indicated 50 µm.

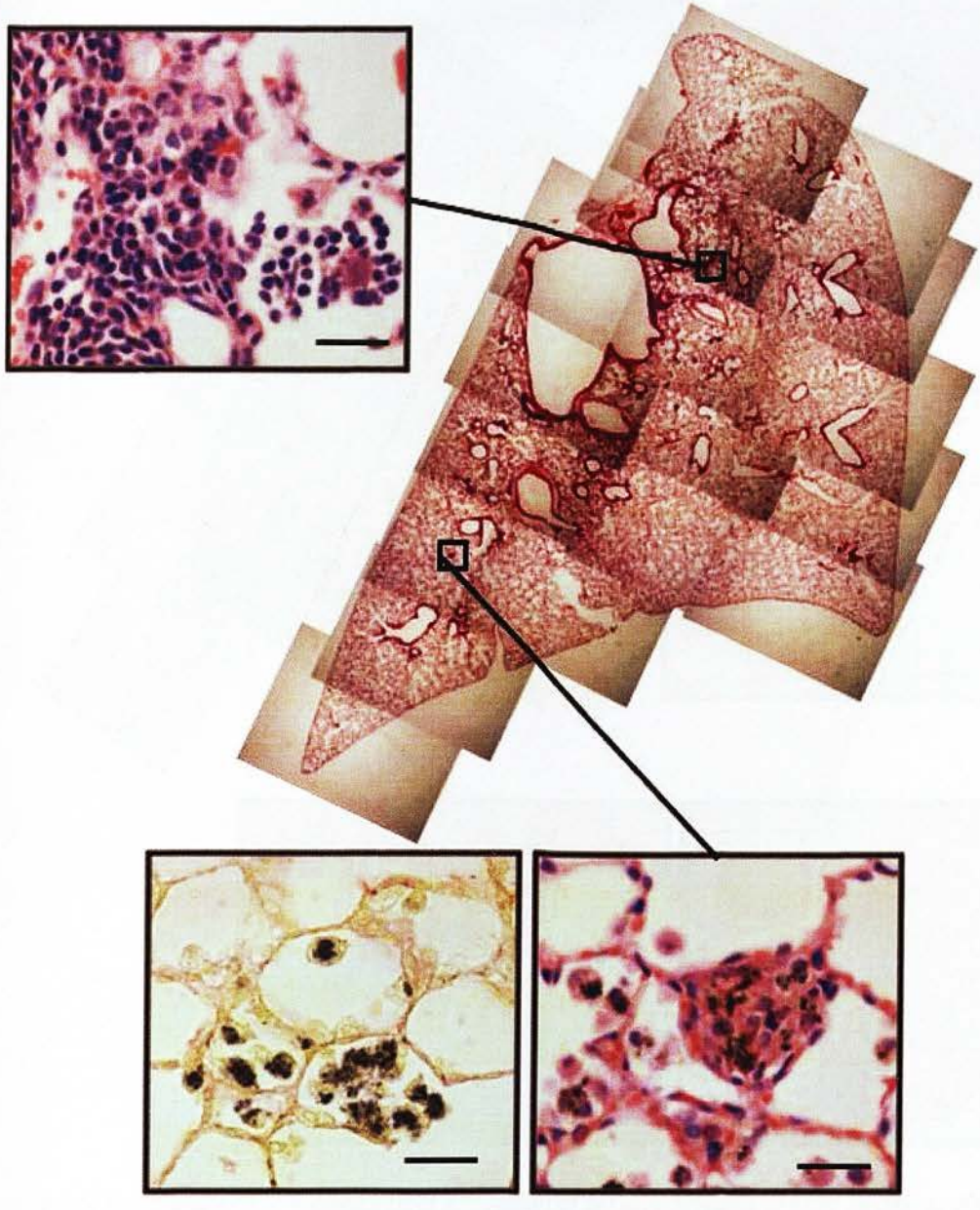

Figure 7.4: Lung pathology 6 weeks post aspiration of NT_{tang1}. Images of lung sections, stained with H & E were realigned to show the gross morphology of the lungs 6 weeks post aspiration with NT_{tang1} (50 µg/mouse). Small accumulations of cells and CNT aggregates are indentified in mice treated with NT_{tang1} but for the most part the lung resembled the vehicle control treated lungs. No deposition of collagen is evident in the PSR stained sections. Scale bar indicated 50 µm.

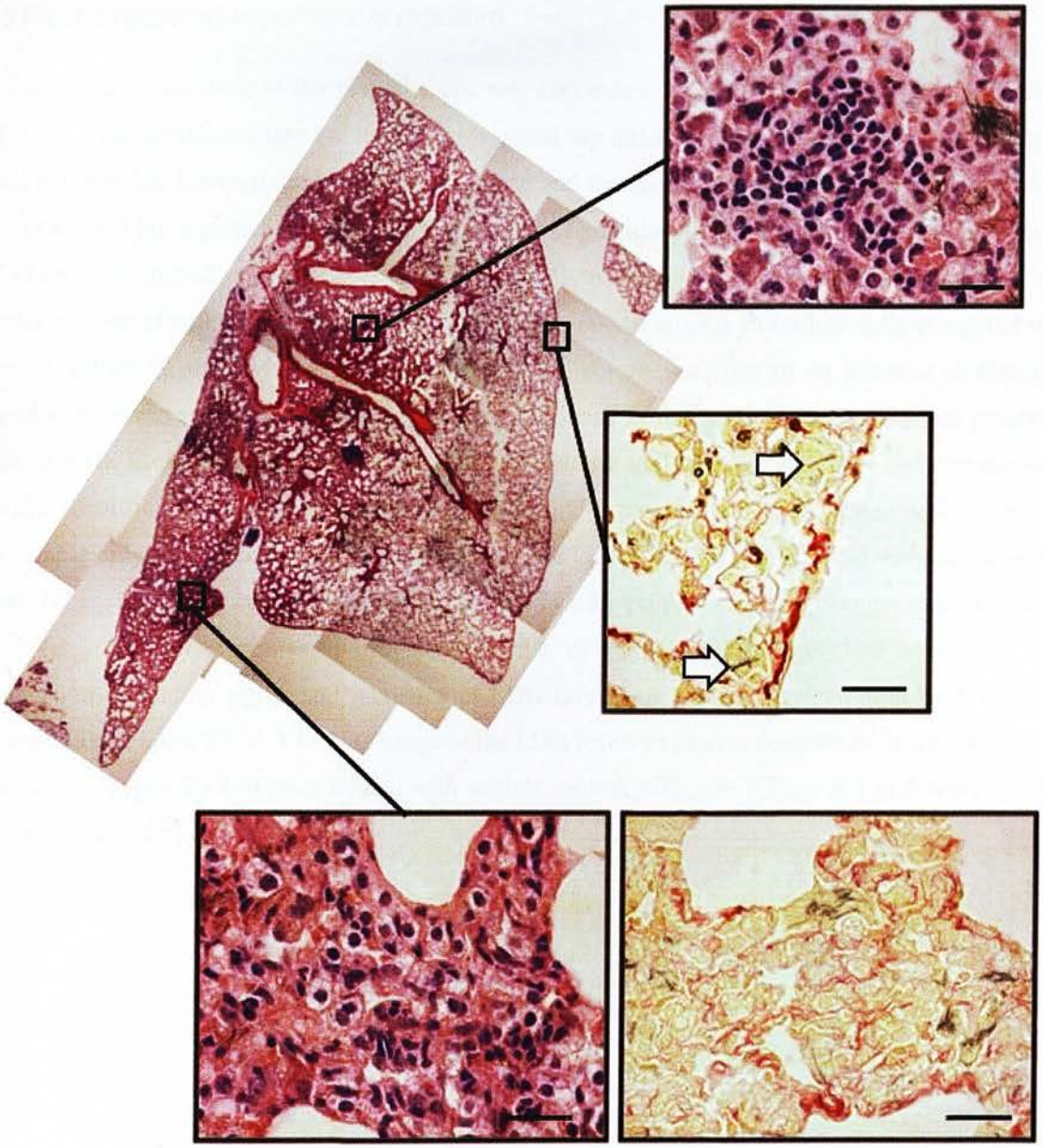

Figure 7.5: Lung pathology 6 weeks post aspiration of NT_{long2}. Images of lung sections, stained with H & E were realigned to show the gross morphology of the lungs 6 weeks post aspiration with NT_{long2} (50 µg/mouse). Callouts show lymphocyte infiltrates, extreme interstitial thickening and collagen deposition associated with interdispersed long CNT. Long CNT are indentified in the sub-pleural regions white arrows. Scale bar indicated 50 µm.

7.3.3 Pleural response to pulmonary exposure

The inflammatory response in the pleural space was also examined at 1 week and 6 weeks after the CNT panel were introduced into the lung by pharyngeal aspiration. At one week there was no change in total cell number between the vehicle control mice and the three CNT treatment groups; there was however a small but significant increase in the number of granulocytes identified in the pleural lavage fluid of the mice treated with NT_{long2} (Figure 7.6 I, II). By 6 weeks there was a significant increase in the total number of cells in the mice treated with NT_{long2} only – around 10 million cells compared to around 2 million in the controls. The majority of this increase was due to an increase in pleural macrophages however, there was also a significant increase in the number of granulocytes present (Figure 7.6 II). Foreign body giant cells (FBGC), which are indicative of a foreign body response, were also identified at the 6 week timepoint in the pleural lavage fluid of mice treated with the long CNT sample only. No FBGC cells were identified in the lavage fluid of mice treated with the vehicle control, NT_{short} or NT_{tangl} samples (Figure 7.6 III, IV). In addition to cytological changes, mice treated with NT_{long2} had alterations in biochemical profile of the pleural lavage fluid indicative of inflammation, including significant increases in LDH levels and protein concentration by 6 weeks post aspiration (Figure 7.6 V, VI). No change in the LDH levels or protein concentration was detected in the pleural lavage fluid of mice treated with vehicle control, NT_{short} or NT_{tangl} at 1 or 6 weeks post exposure (Figure 7.6).

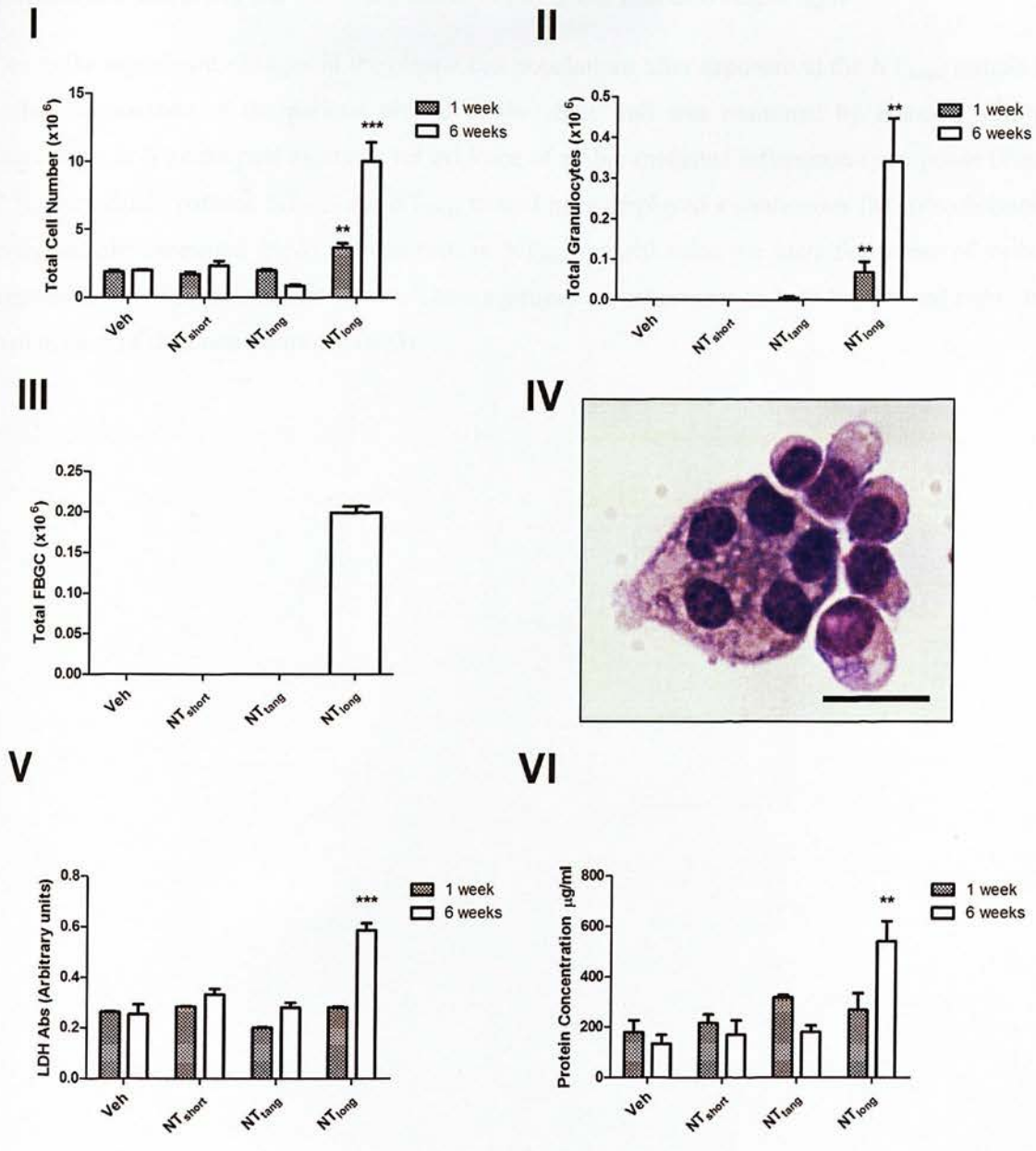

*Figure 7.6: Inflammatory response in the pleural cavity after pulmonary exposure to CNT. The inflammatory response in the pleural cavity after the CNT were delivered by pharyngeal aspiration (50 µg/mouse) was examined. At 1 and 6 weeks post exposure the pleural cavity was lavaged and total cell number (I), total granulocyte number (II), LDH levels (V) and protein concentration (VI) were measured. Foreign body giant cells (III, IV) were quantified at 6 weeks post exposure. Scale bar indicates 20 µm. Significance indicated compares treatment groups to vehicle control from the same timepoint, * indicates $p<0.05$, ** indicates $p<0.001$, *** indicates $p<0.0001$.*

7.3.4 Response along the parietal pleural of the chest wall and diaphragm

Due to the significant changes in the pleural cell populations after exposure to the NT_{long2} sample the surface appearance of the parietal pleural of the chest wall was examined by scanning electron microscopy at 6 weeks post exposure for evidence of a fibre-mediated inflammatory response (Figure 7.7). The vehicle control, NT_{short} and NT_{tangl} treated mice displayed a continuous flat mesothelium in every sample examined (n=3). In contrast, in NT_{long2}-treated mice we identified areas of cellular aggregates overlaying the mesothelium. These aggregates were present on both the left and right chest wall of each of the mice examined (n=3).

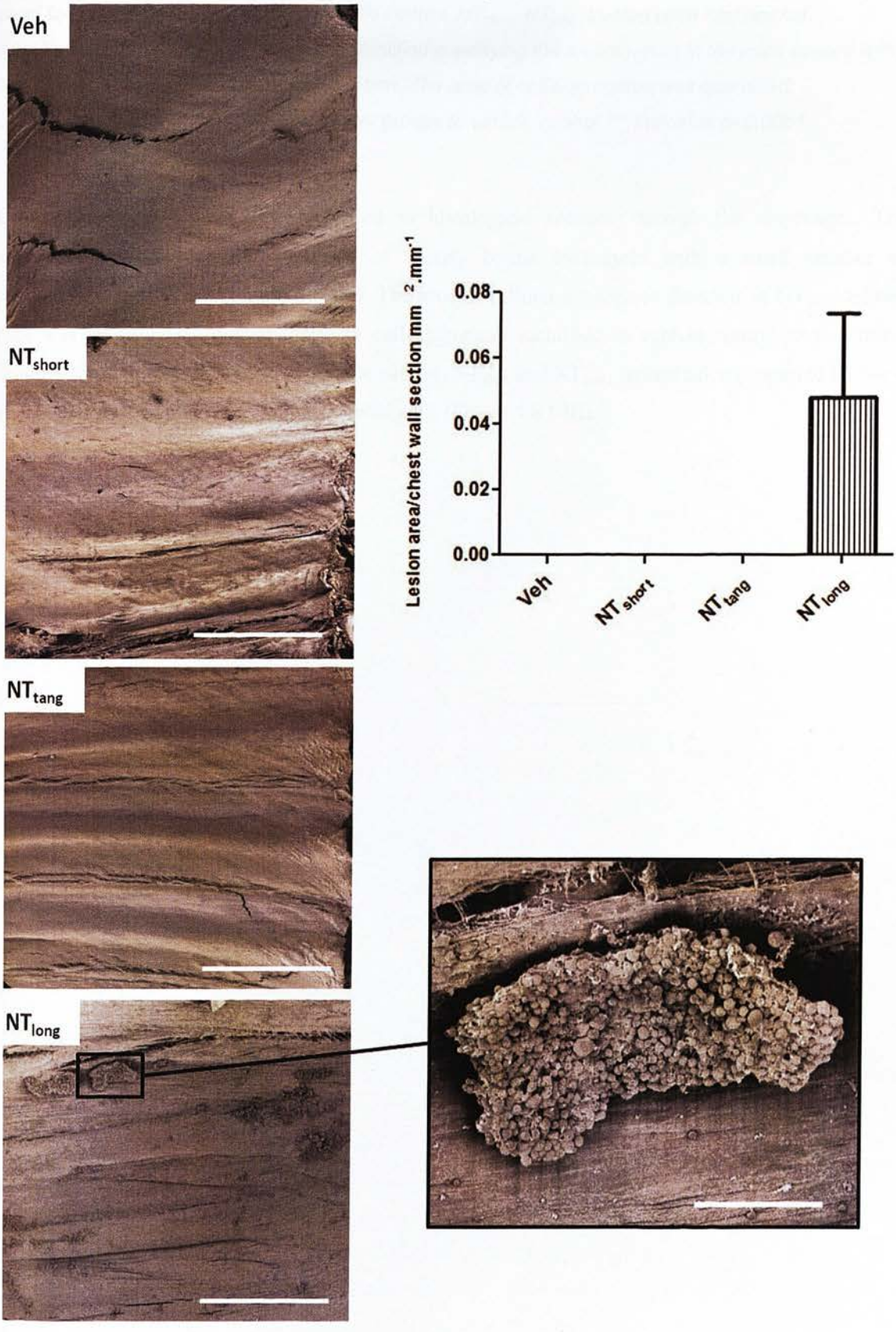

Figure 7.7: Lesion formation along the chest wall after pulmonary exposure to CNT. The chest wall was examined by scanning electron microscopy 6 weeks after the mice were exposed to the CNT

*panel by aspiration (50 µg/mouse). Vehicle control, NT_{short}, NT_{tang1} treated mice had normal mesothelium. Aggregates of cells were identified overlaying the mesothelium in the mice treated with the NT_{long2} sample. Scale bar indicates 1 mm. The area of cell aggregates was quantified. Significance indicated compares treatment groups to vehicle control *** indicates p<0.0001.*

Cellular aggregates were also identified in histological sections through the diaphragm. The aggregates appeared to be composed of loosely bound leukocytes with a small number of granulocytes and FBGC (Figure 7.8 IV). The area of cellular aggregates detected in NT_{long2} treated mice was significantly greater than any cell aggregates identified in vehicle control treated mice. Sections through the diaphragm of vehicle control, NT_{short} and NT_{tang1} treated mice supported the view seen by SEM of a single layer of mesothelial cells (Figure 7.8 I-III).

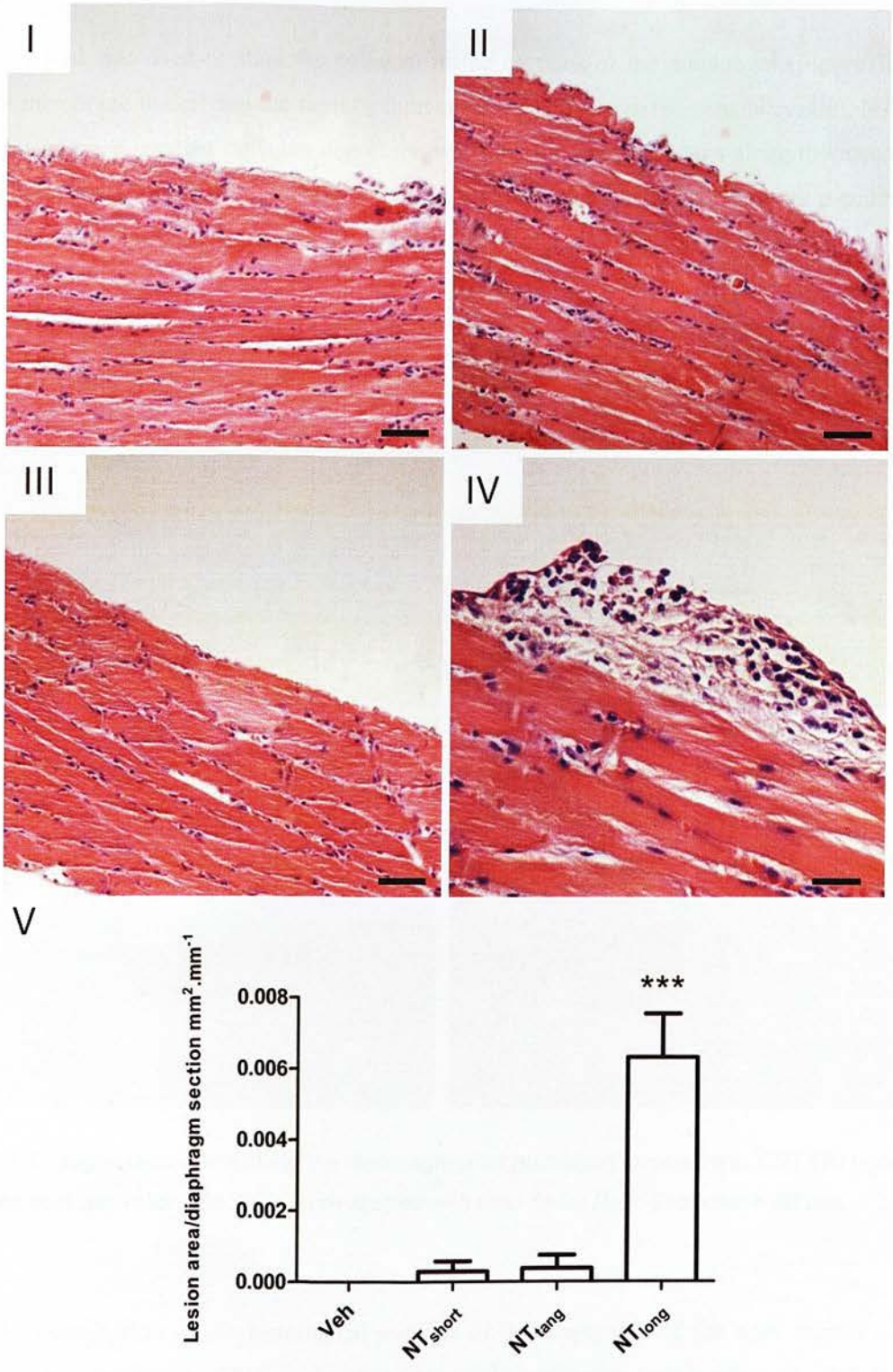

*Figure 7.8: Lesion formation along the diaphragm after pulmonary exposure to CNT (50 µg/mouse) at 6 weeks post aspiration. Histological sections through the diaphragm show the aggregation of inflammatory cells along the mesothelium in the mice treated with the NT_{long2} sample only. This lesion development was quantified. Scale bar indicates 50 µm. Significance indicated compares treatment groups to vehicle control *** indicates p<0.0001.*

Pico Sirius Red was used to stain the collagen in the sections of the diaphragm (Figure 7.9). The basement membrane underlying the mesothelium stained positively in the vehicle control, NT_{short} and NT_{tangl} treated mice. Further collagen deposition was identified in the lesions along the mesothelium of the mice treated with the NT_{long2} sample. The collagen extended from the basement membrane and formed a fine reticulated mesh between the aggregates of cells.

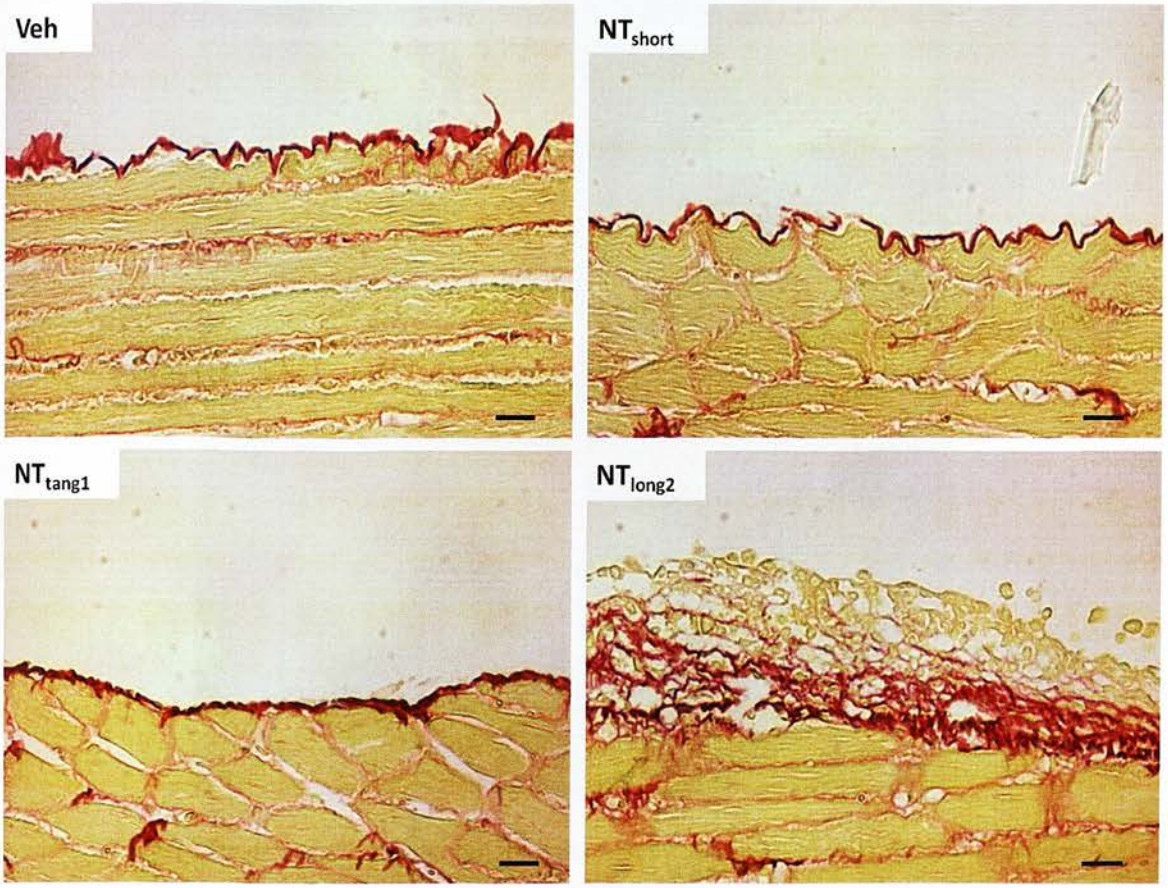

Figure 7.9: Collagen deposition along the diaphragm after pulmonary exposure to CNT (50 µg/mouse) at 6 weeks post aspiration. Sections were stained with Pico Sirius Red. Scale bar = 50 µm.

During the examination of the histological sections of the diaphragm of the mice treated with the NT_{long2} sample a number of CNT fibres were identified, confirming translocation of CNT from the lung into the pleural space (Figure 7.10). The CNT were most often associated with leukocytes or protruding from the mesothelial surface. No CNT were identified along the diaphragm in the mice treated with the NT_{short} or NT_{tangl} treated mice.

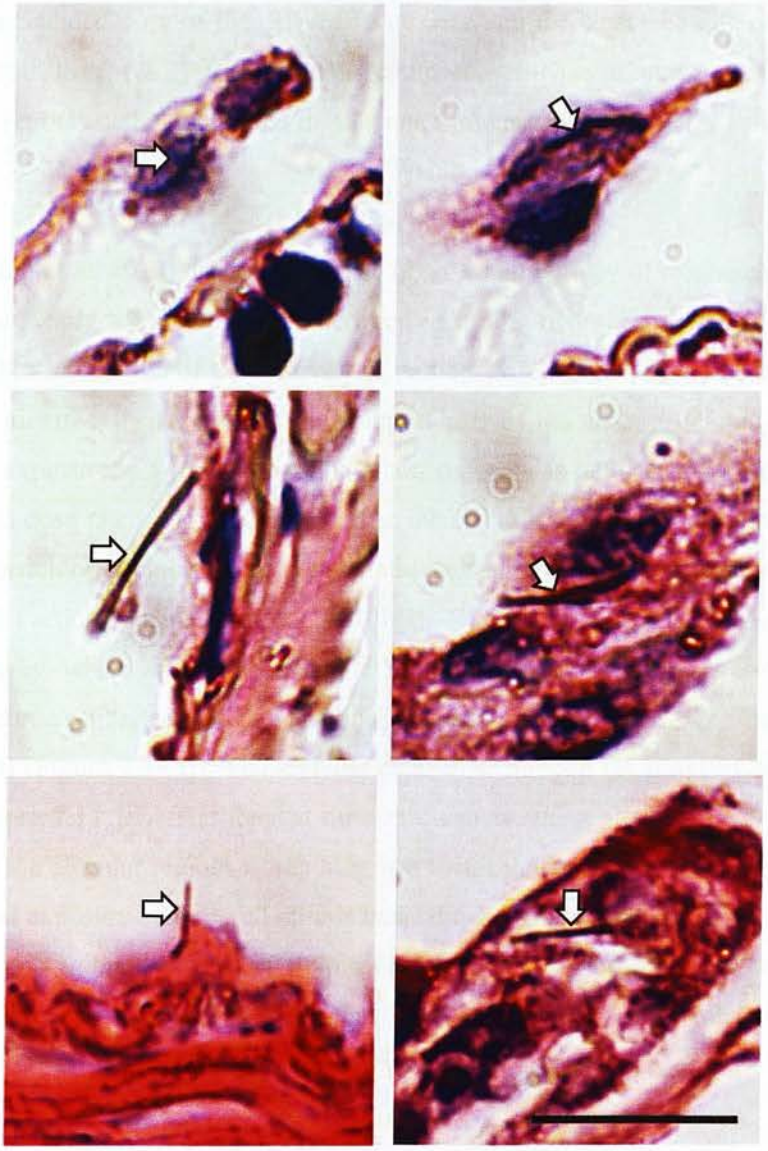

Figure 7.10: CNT retained at the diaphragm after pulmonary exposure to CNT (50 µg/mouse) at 6 weeks post aspiration. Long CNT were identified along the diaphragm of the mice treated with the NT_{long2} sample. Scale bar = 20 µm.

7.3.5 Derivation of a human equivalent dose

In order to extend the relevance of these findings to human exposure a human equivalent dose to the aspirated dose used in mice was calculated for the NT_{long} sample (Figure 7.11 I). Assuming a mouse alveolar surface area of 0.05 m^2 (Stone, 1992), the 50 µg dose used here would result in a normalised dose of 1000 µg/m^2. This would be an equivalent retained dose of 102,200 µg in a human taking into consideration the increase in alveolar surface area (102.2 m^2, Stone, 1992). The external dose which would generate the calculated retained dose was derived by first calculating the deposited dose which

would result in a retained dose of the derived value based on the clearance rate of a typical human. The clearance half time (t1/2) for insoluble compact particles in humans is suggested to be approximately 1 year (Pauluhn, 2010) and the clearance rate is calculated by the following equation:

$$k=\ln(2)/t1/2$$

$$k=\ln(2)/365= 0.0019$$

This equation (Tran et al. 2012) describes the rate (k) constant per day of clearance from the alveolar region during the steady state equilibrium between incoming deposited dose and outgoing cleared dose and allows the calculation of the reservoir of particle dose in the lung termed the retained dose. In terms of rate kinetics, this represents the simplest part of the dose curve and only occurs with chronic repeated exposure to a particulate. The retained dose was multiplied by the clearance rate to give the deposited dose rate of 194.08 μg/day. The inhaled dose rate was then calculated taking into account the proportion of the inhaled dose that would deposit in the alveolar regions of the lung using the Multiple-Path Particle Dosimetry Model (MPPD). The particle physical attributes- aerodynamic diameter and density, which are required for the MPPD calculation were not known for the NT_{long2} sample and therefore estimated based on published data of morphologically similar fibrous CNT (McKinney, 2009) (Figure 7.11 II). The alveolar deposition fraction for fibrous CNT was calculated to be 12.9% (Figure 7.11 III). The inhaled dose rate that would result in a deposited dose rate of 194.08 μg/day in the alveolar regions of the lung was then calculated to be 1505 μg/day. The human equivalent external exposure level based on this inhaled dose rate was derived by taking into account the respiration minute volume (RMV) of a typical human (0.01534 m^3/min, Bide et al 2000) and the exposure duration over a period of a working day (480 minutes) and was calculated to be 0.2 mg/m^3 (Figure 7.11 I).

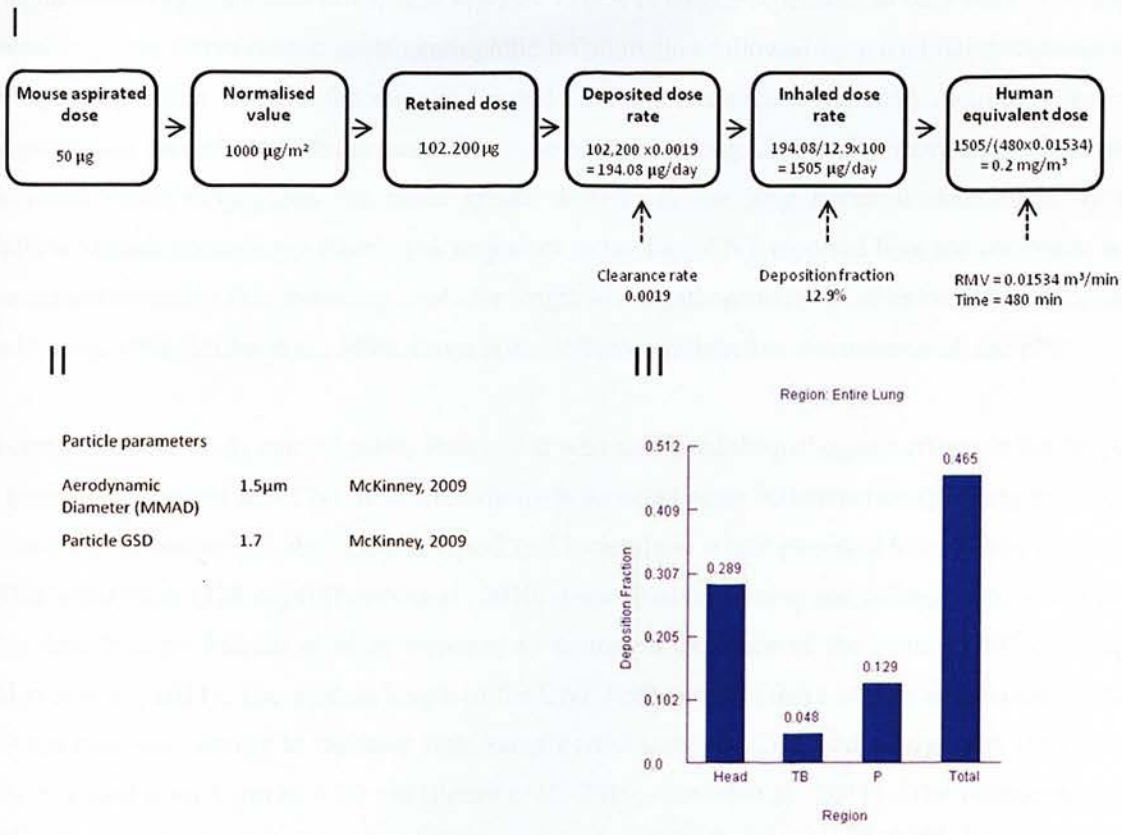

Figure 7.11: Determination of a human equivalent dose. Schematic diagram of the process for deriving a human equivalent exposure for the NT_{long} sample based on the aspirated mouse dose of 50 µg (I). (II) The particle properties required for the Multiple-Path Particle Dosimetry Model (MPPD) taken from McKinney et al (28) measurements of a morphologically-similar, fibrous CNT sample. (III) Results from the MPPD computational model describing the predicted deposition fraction for the entire lung. TB= trachobronchial, P= pulmonary.

7.4 Discussion

Our objectives within this study were to examine the role of fibre length in the inflammatory response to CNT in the lung and also to ascertain whether CNT, previously shown to be inflammogenic in the pleural cavity after direct exposure (Chapter 3), would elicit a similar pleural response after administration via the lung. Three CNT samples, representing short (NT_{short}), tangled (NT_{tangl}) and long (NT_{long2}) CNT were selected from the panel and administered to mice via pharyngeal aspiration.

The inflammatory responses in the lung reported here was length-dependent as only the CNT sample containing long fibres caused acute neutrophilic inflammation followed by interstitial thickening and collagen deposition whereas the short or tangled CNT did not elicit a response. Aspiration into the airspaces was carried out with the same mass dose of short or long CNT and so more short fibres were delivered which emphasises the much greater activity of the long fibres as determined by the 'inflammogenic potency per fibre'. The responses to the long CNT reported here are consistent with experimental studies demonstrating a role for length in the pathogenicity of asbestos fibres (Mossman and Churg, 1998; Miller et al., 1999; Davis et al., 1986b) and therefore consistent with the FPP.

A comprehensive study carried out by Porter *et al* who examined the pathogenic effects in the lungs to a number of doses of MWCNT over time similarly reported acute inflammation (peaking at 7 days), granuloma formation and also alveolar type-2 cell hyperplasia which persisted from 7 days to the end of the experiment (128 days) (Porter et al., 2010). Interstitial thickening and collagen deposition were also described by Mercer *et al* in response to aspiration exposure of the same MWCNT sample (Mercer et al., 2011). The median length of the CNT fibres used in these studies was reported to the 3.9 μm however, similar to the long fibre sample used here, the CNT had a large size distribution which ranged from 1 μm to > 20 μm (Porter et al., 2010; Mercer et al., 2011). The heterogeneity of CNT fibre lengths may obfuscate the effects of fibre length in the response to CNT; however a clear length-dependent pathogenicity in the lungs has been demonstrated in response to alternative high aspect ratio nanomaterials. Nickel nanowires (NiNW), which are manufactured in tight size categories have shown a similar length-dependent pathogenicity in the lungs with the long NiNW (20 μm in length) eliciting an acute inflammatory response at 24 hours followed by interstitial thickening of the alveolar septa where the shorter 4 μm NiNW did not (Poland et al., 2011). The association of long CNT with areas of granuloma formation and collagen deposition observed here suggests that the inability of the alveolar macrophages to remove the fibres is leading to chronic activation and persistent inflammation. Therefore the length-dependent mode of action in initiating an inflammatory response is believed to be mediated via frustrated phagocytosis of the alveolar macrophages attempting to engulf the long CNT.

A recent collaborative study involving the members of the ELEGI lab, University of Edinburgh and researchers at the University of Bern examined the acute inflammatory response and the development of pathological lesions in the gas-exchange regions of the lung after aspiration exposure of a long straight CNT sample (NT_{long1}, from the panel described in Chapter 3) or a tangled CNT sample (NT_{tang1}) (Muhlfeld et al., 2011). To minimise the effects of a bolus dose and to elucidate more subtle CNT-mediated effects the dose employed in this study (10 μg/mouse) was 5 times less than the dose employed here. Surprisingly results showed a greater acute inflammatory response to the short/tangled fibres 24 hours post aspiration and a significant increase in the thickness of the interstitial connective

tissue by 28 days post-exposure. Conversely 28 days after aspiration exposure to the long CNT sample resulted in positive immunostaining of TNFα in alveolar macrophages and significant hypertrophy of type-II epithelial cells (Muhlfeld et al., 2011). The differences in responses reported indicate that long and short CNT may mediate effects on the lung via distinct mechanisms. The authors proposed that the long MWCNT were less easily interstitialised than the short ones because of their bulk, whereas the short MWCNT readily enter the interstitium as previously described by Shvedova *et al* (Shvedova et al., 2005) and by Ryman-Rasmussen *et al* (Ryman-Rasmussen et al., 2009) thus evading clearance by alveolar macrophages. The positive staining of alveolar macrophages for TNFα in response to the long CNT sample only suggest that, as we see in the study presented here, the long fibre effects are mediated by stimulation of the alveolar macrophages. Examination of the ultrastructure of the interstitial connective tissue, which may have illuminated more subtle effects of the short CNT samples as described by Muhlfeld *et al* (Muhlfeld et al., 2011), was not carried out here. Additionally, the problems of sampling for electron microscopy studies should not be underestimated. Given the very focal nature of particle deposition and subsequent response, there is real potential for tissue samples to be taken from regions away from the responding foci resulting in misleading data.

Here for the first time we demonstrate a length-dependent hazard of CNT to both the lungs and the pleural space following the introduction of long, but not short, CNT into the airspaces of the lungs. The deposition of CNT in the distal regions of the lungs and the concomitant development of a pathogenic response in both the subpleural region of the lungs and the visceral pleural covering the surface of the lungs have previously been reported. In the study of Ryman-Rasmussen *et al* (Ryman-Rasmussen et al., 2009) mononuclear cell aggregates were identified on the surface of the visceral pleural which increased in size and number over time in response to inhalation exposure of CNT but not carbon black nanoparticles (Ryman-Rasmussen et al., 2009). Asbestos fibres deposited in the lungs have also been shown to stimulate proliferation of mesothelial cells along the visceral pleura as early as one week post exposure (Adamson et al., 1993). However the initiation of mesothelioma along the parietal pleural suggest the key fibre effects leading to mesothelioma development will take place at this site rather than the visceral pleural surrounding the lungs which only becomes involved on progression of the disease. Subsequently the relevance of assessing fibre-mediated inflammation or mesothelial cell proliferation in the sub-pleural regions of the lungs or along the visceral pleura when addressing early responses related to the potential mesothelioma hazard of a fibre is questionable. Therefore we examined the parietal pleural response to CNT focussing on lesion development along the parietal pleura and the inflammatory response in pleural space itself.

The pleural cellular changes in response to aspiration exposure of the long CNT were characterised by an increase in the number of macrophages and granulocytes in the pleural cavity with concomitant

increases in LDH and protein levels in the pleural fluid. This response is consistent with the increase in inflammatory leukocytes observed in the pleural space in rats after pulmonary exposure to long asbestos fibres by both intratracheal instillation (Oberdoerster et al., 1983) and inhalation (Choe et al., 1997). However in light of the paracrine responses of mesothelial cells to macrophage conditioned media described in Chapter 5 we considered whether the pleural inflammatory response is a reaction to inflammatory mediators originating in the lungs. Li *et al* have previously demonstrated the development of a reactive inflammatory response in the pleural cavity to the instillation of the bacterium, *Corynebacterium parvum*, into the airspaces of the lungs (Li et al., 1993). Intratracheal instillation of *C. parvum* was shown to cause a transient appearance of neutrophils in the pleural space and an increase in the number of pleural macrophages up to 5 days post pulmonary exposure. The similar pattern of inflammatory cell influx into both the alveolar and pleural spaces, with no detectable translocation of the bacterium to the pleural space, suggested that there may be some communication of diffusible factors between the lungs and the pleural space which stimulates an inflammatory response (Li et al., 1993). However the likelihood that the pleural response reported here was solely due to inflammation in the lungs was discounted as the tempo of inflammation differs in the two compartments. The inflammatory response in the pleural cavity is not evident until 6 weeks after the CNT have been introduced into the lungs by which time the acute inflammatory response in the lungs has substantially diminished. This suggests the influx of macrophages and granulocytes into the pleural space 6 weeks post exposure is not mediated by chemotactic factors released from the lungs but is specific to the pleural cavity itself.

Examination of the parietal pleura identified cellular aggregates along the chest wall and diaphragm of the mice exposed to the long fibre- containing CNT sample only. Similar to the early stage lesions identified after direct injection of long CNT into the pleural space (Chapter 3) the lesions identified here appear to be primarily composed of mononuclear leukocytes with a small number of granulocytes and FBGC, and collagenous. Long CNT were also identified associated with macrophages or protruding from the mesothelium in histological sections of the diaphragm. Recently, inhalation of amosite asbestos fibres was shown to produce similar inflammatory lesions along the parietal pleura with the presence of amosite asbestos fibres on the diaphragm 7 days after the end of inhalation exposure (Bernstein et al., 2010a).

To our knowledge this is the first time a pleural response has been described following deposition of CNT into the lungs. The evidence of fibre translocation supports our contention that the inflammatory response detected in the pleural space was a foreign body response. Furthermore the identification of fibres in the mice treated with the long CNT sample only and the apparent length of these fibres (5-20 μm) supports the mechanistic hypothesis proposed in Chapter 4 stating that long fibres which

translocate to the pleural space will deposit on the parietal pleura and be retained due to the small calibre of the stomatal openings. Once retained, the fibres may generate an inflammatory and fibrotic response which could lead eventually to the formation of mesothelioma (Donaldson et al., 2010). As the identification of retained CNT in this study was qualitative it is not possible to determine the dose of long CNT required to elicit an inflammatory response in the pleural cavity. Indeed the kinetics of CNT fibre translocation from the lungs into the pleural space remains largely unknown and most likely will depend on a myriad of factors including physicochemical attributes of the fibres themselves and the biological responses in the lungs. Inflammation within the lung and a subsequent increase in permeability has been proposed to alter the kinetics of particle translocation. Studies by Davis and colleagues showed that co-exposure of rats to amosite asbestos and to quartz increased the incidence of pleural mesothelioma, which the authors purported was due to increased transport through the visceral pleural and therefore an elevation in parietal pleura fibre dosimetry (Davis et al., 1991). Therefore the inflammatory response in the lungs of the mice exposed to the long CNT sample may have similarly increased the rate of CNT translocation into the pleural space which in itself may account for the presence of CNT at the parietal pleural in the long CNT-treated mice only. The clearance mechanisms of the pleural cavity will however preclude the quantification of short CNT which have translocated from the lungs as they will not be retained. Particle clearance from the distal regions of the lung is dependent on uptake by alveolar macrophages. Failure to clear long CNT which will not be efficiently phagocytosed, as a consequence of frustrated phagocytosis, from the distal regions of the lung may provide greater opportunity for long CNT to translocate to the pleural space.

In order to assess whether the dose of NT_{long} that caused pathogenic effects in the mouse lung and pleural cavity were relevant for potential human exposures a human equivalent dose was established for the NT_{long} sample. An exposure level of 0.2 mg/m^3 was determined to result in the equivalent retained dose in the human lungs to the 50 μg dose mice were exposed to by aspiration in this study. Such a retained dose occurs as a result of the equilibrium between the incoming deposited dose rate and the outgoing clearance rate and therefore the external exposure level expressed here reflects a chronic exposure where workers may be exposed to a particle-rich environment over a number of years. Han et al measured the airborne dust levels in a research laboratory and reported a peak CNT-containing airborne dust level of approximately 0.4 mg/m^3. Thus the estimates for a human equivalent dose reported here suggest that the CNT dose tested in mice in this study approximate reasonable, realistic human occupational exposures.

The calculated human equivalent exposure concentration shown here is purely indicative as to reach this results several assumptions have been made. Firstly extrapolation from a mouse study where the fibres were administered in a bolus dose by aspiration assumes that the initial concentration given is equal to the actual dose within the alveolar region of the mice. The aspiration technique has been

validated for the administration of particles by Rao et al who using fluorescent beads and beryllium oxide particles demonstrated the similarities between deposition pattern of particles administered by aspiration and inhalation where the beads were widely disseminated into the distal regions of the lung with a bronchiolocentric pattern. Although Rao et al reported a linear correlation between the dose administered and the amount deposited in the lung, the amount retrieved after aspiration was reported to be between 77 and 88% of the dose administered. This suggests a proportion of particles administered by aspiration may be lost, presumably in the upper airways/ nasopharynx. Secondly, it is also worth considering that the rate of clearance from the human lungs cited is based upon an insoluble, compact (roughly spherical) particle (Pauluhn, 2010a). Fibre length has been shown to affect the rate of clearance from the lung with the clearance of long fibres demonstrated to be much slower than for compact particles most likely due to hindrance of alveolar macrophages (Holmes and Morgan, 1980; Morgan et al., 1982). The net result of slower clearance is that lower levels of exposure are required to culminate in the same retained dose. Finally for the extrapolation of a dose that will lead to similar pathological changes in the pleural space the anatomical differences between mice and humans such as in visceral pleural thickness (Tyler, 1983) may need to be taken into account when comparing across animal species and when extrapolating from animals to humans.

In conclusion we have shown that CNT elicit a length-dependent inflammatory response in the lungs after pharyngeal aspiration which is in accordance with the FPP. The length-dependent pathogenicity of CNT and other forms of HARN in the lungs highlights the relevance of the FPP when considering the hazard of new fibre-like nanomaterials and suggests that the role of fibre dimensions should be assessed when considering the inhalation toxicity of any new HARN. Furthermore the translocation and selective retention of long fibres in the pleural cavity leading to an inflammatory response suggests that CNT may also pose an asbestos-like mesothelioma hazard. The results of this small-scale, mouse-model study are not sufficient to extrapolate the potential risks of CNT exposures in the workplace which would require long-term inhalation studies utilizing realistic CNT exposures. This study does however contribute greatly to the burgeoning evidence that certain types of CNT can pose an asbestos-like hazard and therefore require appropriate risk assessment.

Chapter 8: Concluding remarks

The purpose of this study was to examine the pathogenicity of CNT in relation to the fibre pathogenicity paradigm (FPP) by examining the effect of CNT in the pleural space, a target tissue for asbestos-related disease. Direct instillation of long and short CNT into the pleural cavity produced length-dependent inflammatory responses in which both the size-restricted clearance mechanisms from the pleural cavity and frustrated phagocytosis of pleural macrophages played a critical role. The pathogenic response to the long CNT sample was persistent and resulted in the development of fibrotic lesions along the parietal pleura that steadily increased in size over time. Aspiration of the CNT into the lung resulted in pathogenic responses in both the lung and pleural cavity that were similarly dependent on length. Figure 8.1 summarises the results obtained in this study incorporated into a model which suggests the potential sequence of pathobiological events that may take place in response to pulmonary exposure to short or long CNT.

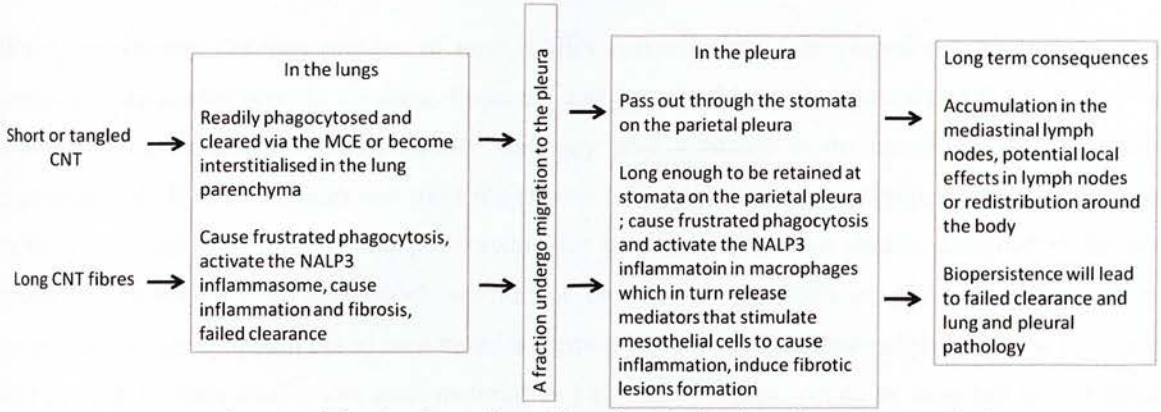

Figure 8.1: Sequence of events following deposition of short/tangled or long fibrous CNT in the lungs. MCE = mucociliary escalator.

The direct role for fibre length and biopersistence in the adverse pleural responses to the CNT samples demonstrate that CNT adhere to the FPP. Therefore long CNT samples may pose an asbestos-like inhalation hazard. Further testing using more physiologically relevant routes of exposure (e.g. inhalation) must be carried out to confirm or refute the findings of a length-dependent mesothelial hazard presented here and to allow for appropriate risk assessment. These should ideally be whole of life in nature to ascertain the potential carcinogenicity of the CNT in the animal model and also use a panel of CNT to critically test the paradigms of toxicology rather than focus on the analysis of single material type as has been the approach of inhalation studies on CNT to date (Ma-Hock et al., 2009; Pauluhn, 2010b).

Compliance with the FPP suggests that the biologically effective dose (BED) for CNT is the proportion of a CNT sample composed of long biopersistent fibres. Hazard assessment based on SAR, such as the study described here, can be integrated with exposure data to allow for appropriate risk assessment based on the biologically active component of an exposure dose. Full characterisation of the physiochemical properties of the CNT that become airborne during the manufacture and processing of CNT and CNT containing products is therefore critical for the risk assessment based on the BED. Of course, other studies have demonstrated alternative properties of CNT distinct from their fibrous structure which imbue the samples with pathogenicity, for example surface defects (Muller et al., 2008) which must also be taken into account when determining the BED of a CNT sample and the subsequent regulatory approach to be employed.

The length-dependent inflammatory response to an alternative HARN, NiNW, as reported in Chapter 4 suggests that the FPP will be applicable to the wide variety of new high aspect ratio nanomaterials currently being developed. Therefore a cautionary approach should be taken to safe working practices with all forms of nanofibres that meet the criteria for a pathogenic fibre as set out in the FPP.

When considering the vast number of new HARN currently being developed the advantages of a tiered toxicity testing process are clear. From the data presented here we contend that the FPP may be a useful initial screen to identify HARN that may pose a hazard to the mesothelium. Using this approach, only HARN samples that meet the criteria of length, thinness and biopersistence, as set out in the FPP, could be subsequently put forward for in vitro and in vivo studies designed to further assess the mesothelial hazard which would not be relevant for short or non-biopersistent fibre samples. Such an approach based on a tiered screening system could dramatically reduce the time and cost needed to individually test each material and also allay ethical concerns over the use of large numbers of animals for in vivo testing. Further work to fine tune the criteria that make up the FPP, for example the identification of cut-off lengths below which a fibre sample will not be retained (Schinwald et al., 2012a), will allow for more precise *in silico* hazard characterisation and again reduce the numbers of test samples requiring further in vitro or in vivo testing.

Understanding the properties that contribute to toxicity leads to the potential for engineering solutions to reduce the inherent toxicity of a fibre, therefore identification of the link between the FPP and toxicity of HARN can be exploited to design HARN that are safe. The safe design of HARN from the point of view of the paradigm is relatively straightforward as making HARN short, thick or non-biopersistent will reduce their hazard. If this were achieved UK industry could avoid the consequences of tight regulation of workplace hygiene that may be costly and even terminal for some aspects of the nanotechnology industry. There may however be a contradiction in the production of safe HARN if safety stipulates short, biodegradable fibres which conflict with the technical

requirements of those new materials in which case management of the risks from these materials by safe handling to minimise exposure needs to be mandatory.

Although here inflammation in the pleural cavity was primarily used as a short-term endpoint to determine hazard we contend that, due to the links between asbestos-mediated chronic inflammation and carcinogenesis as discussed in Chapter 1, this model may be useful for illuminating the events leading to pleural mesothelioma. Further examination of the signalling pathways chronically activated in the progressively developing inflammatory lesion in vivo may provide an insight into fibre-mediated carcinogenesis and may lead to the identification of potential therapeutic targets. Furthermore our demonstration of length –sensitive in vitro tests using macrophages and mesothelial cells suggest combined culture system could be used as a means of looking at mechanism without the use of animals, another key policy point in UK government approach to nanotoxicology.

Chapter 9: Bibliography

Adamson,I.Y., Bakowska,J., and Bowden,D.H. (1993). Mesothelial cell proliferation after instillation of long or short asbestos fibers into mouse lung. Am. J. Pathol. *142*, 1209-1216.

Adamson,I.Y.R., Bakowska,J., and Prieditis,H. (2000). Proliferation of Rat Pleural Mesothelial Cells in Response to Hepatocyte and Keratinocyte Growth Factors. American Journal Of Respiratory Cell And Molecular Biology *23*, 345-349.

Agostoni,E. and Zocchi,L. (2007). Pleural liquid and its exchanges. Respiratory Physiology & Neurobiology *159*, 311-323.

Allen,B.L., Kichambare,P.D., Gou,P., Vlasova,I.I., Kapralov,A.A., Konduru,N., Kagan,V.E., and Star,A. (2008). Biodegradation of Single-Walled Carbon Nanotubes through Enzymatic Catalysis. Nano Letters *8*, 3899-3903.

Arai,H., Endo,M., Sasai,Y., Yokosawa,A., Sato,H., Motomiya,M., and Konno,K. (1975). Histochemical demonstration of hyaluronic acid in a case of pleural mesothelioma. Am. Rev. Respir. Dis. *111*, 699-702.

Armstrong,J.A. and Hart,P.D. (1971). RESPONSE OF CULTURED MACROPHAGES TO MYCOBACTERIUM TUBERCULOSIS, WITH OBSERVATIONS ON FUSION OF LYSOSOMES WITH PHAGOSOMES. The Journal of Experimental Medicine *134*, 713-740.

Aschberger,K., Johnston,H.J., Stone,V., Aitken,R.J., Hankin,S.M., Peters,S.A., Tran,C.L., and Christensen,F.M. (2010). Review of carbon nanotubes toxicity and exposure--appraisal of human health risk assessment based on open literature. Crit Rev. Toxicol. *40*, 759-790.

Awasthi,K., Srivastava,A., and Srivastava,O.N. (2005). Synthesis of carbon nanotubes. J. Nanosci. Nanotechnol. *5*, 1616-1636.

Balasubramanian,K. and Burghard,M. (2005). Chemically functionalized carbon nanotubes. Small. *1*, 180-192.

Bartrip,P.W. (2004). History of asbestos related disease. Postgrad. Med. J. *80*, 72-76.

Bergstrand,H. (1990). The generation of reactive oxygen-derived species by phagocytes. Agents Actions Suppl. *30:199-211.*, 199-211.

Bernstein,D.M. and Hoskins,J.A. (2006). The health effects of chrysotile: current perspective based upon recent data. Regul. Toxicol. Pharmacol. *45*, 252-264.

Bernstein,D.M., Rogers,R.A., Sepulveda,R., Donaldson,K., Schuler,D., Gaering,S., Kunzendorf,P., Chevalier,J., and Holm,S.E. (2010a). The pathological response and fate in the lung and pleura of chrysotile in combination with fine particles compared to amosite asbestos following short-term inhalation exposure: interim results. Inhal. Toxicol. *22*, 937-962.

Bernstein,D.M., Rogers,R.A., Sepulveda,R., Donaldson,K., Schuler,D., Gaering,S., Kunzendorf,P., Chevalier,J., and Holm,S.E. (2010b). The pathological response and fate in the lung and pleura of

chrysotile in combination with fine particles compared to amosite asbestos following short-term inhalation exposure: interim results. Inhalation Toxicology *22*, 937-962.

Bernstein,D.M., Rogers,R.A., Sepulveda,R., Donaldson,K., Schuler,D., Gaering,S., Kunzendorf,P., Chevalier,J., and Holm,S.E. (2011). Quantification of the pathological response and fate in the lung and pleura of chrysotile in combination with fine particles compared to amosite-asbestos following short-term inhalation exposure. Inhalation Toxicology *23*, 372-391.

Berthiaume,Y., Voisin,G., and Dagenais,A. (2006). The alveolar type I cells: the new knight of the alveolus? J. Physiol. *572*, 609-610.

Betjes,M.G.H., Tuk,C.W., Struijk,D.G., Krediet,R.T., Arisz,L., Hart,M., and Beelen,R.H.J. (1993). Interleukin-8 Production by Human Peritoneal Mesothelial Cells in Response to Tumor-Necrosis-Factor-Alpha, Interleukin-1, and Medium Conditioned by Macrophages Cocultured with Staphylococcus-Epidermidis. Journal Of Infectious Diseases *168*, 1202-1210.

Bocchetta,M. and Carbone,M. (2008). SV40 Tag/p53 complexes actively promote malignant cell growth of human mesothelial cells. Cell Oncol. *30*, 455.

Bocchetta,M., Eliasz,S., De Marco,M.A., Rudzinski,J., Zhang,L., and Carbone,M. (2008). The SV40 large T antigen-p53 complexes bind and activate the insulin-like growth factor-I promoter stimulating cell growth. Cancer Res. *68*, 1022-1029.

Bonner,J.C., Osornio-Vargas,A.R., Badgett,A., and Brody,A.R. (1991). Differential proliferation of rat lung fibroblasts induced by the platelet-derived growth factor-AA, -AB, and -BB isoforms secreted by rat alveolar macrophages 10. Am. J. Respir. Cell Mol. Biol. *5*, 539-547.

Bouros.D. Pleural Disease. 2004. New York, NY, Marcel Decker, Inc.

Boutin,C., Dumortier,P., Rey,F., Viallat,J.R., and De Vuyst,P. (1996). Black spots concentrate oncogenic asbestos fibers in the parietal pleura. Thoracoscopic and mineralogic study. Am. J. Respir. Crit Care Med. *153*, 444-449.

Boutin,C., Rey,F., Gouvernet,J., Viallat,J.R., Astoul,P., and Ledoray,V. (1993). Thoracoscopy in pleural malignant mesothelioma: a prospective study of 188 consecutive patients. Part 2: Prognosis and staging. Cancer *72*, 394-404.

Broaddus,V.C., Yang,L., Scavo,L.M., Ernst,J.D., and Boylan,A.M. (1996). Asbestos induces apoptosis of human and rabbit pleural mesothelial cells via reactive oxygen species. Journal of Clinical Investigation *98*, 2050-2059.

Brown,D.M., Kinloch,I.A., Bangert,U., Windle,A.H., Walter,D.M., Walker,G.S., Scotchford,C.A., Donaldson,K., and Stone,V. (2007). An in vitro study of the potential of carbon nanotubes and nanofibres to induce inflammatory mediators and frustrated phagocytosis. Carbon *45*, 1743-1756.

Butler,J.P., Huang,J., Loring,S.H., Lai-Fook,S.J., Wang,P.M., and Wilson,T.A. (1995). Model for a pump that drives circulation of pleural fluid. J. Appl. Physiol. *78*, 23-29.

Byrne,F., Prina-Mello,A., Whelan,A., Mohamed,B.M., Davies,A., Gun'ko,Y.K., Coey,J.M.D., and Volkov,Y. (2009). High content analysis of the biocompatibility of nickel nanowires. Journal of Magnetism and Magnetic Materials *321*, 1341-1345.

Carbone,M., Emri,S., Dogan,A.U., Steele,I., Tuncer,M., Pass,H.I., and Baris,Y.I. (2007). A mesothelioma epidemic in Cappadocia: scientific developments and unexpected social outcomes. Nature Reviews Cancer *7*, 147-154.

Carbone,M., Kratzke,R.A., and Testa,J.R. (2002). The pathogenesis of mesothelioma. Semin. Oncol. *29*, 2-17.

Cassel,S.L., Eisenbarth,S.C., Iyer,S.S., Sadler,J.J., Colegio,O.R., Tephly,L.A., Carter,A.B., Rothman,P.B., Flavell,R.A., and Sutterwala,F.S. (2008). The Nalp3 inflammasome is essential for the development of silicosis. Proceedings Of The National Academy Of Sciences Of The United States Of America *105*, 9035-9040.

Chapman,S.J., Cookson,W.O., Musk,A.W., and Lee,Y.C. (2003). Benign asbestos pleural diseases. Curr. Opin. Pulm. Med. *9*, 266-271.

Chatgilialoglu,C. and O'Neill,P. (2001). Free radicals associated with DNA damage. Exp. Gerontol. *36*, 1459-1471.

Chattopadhyay,J., Sadana,A.K., Liang,F., Beach,J.M., Xiao,Y., Hauge,R.H., and Billups,W.E. (2005). Carbon nanotube salts. Arylation of single-wall carbon nanotubes. Org. Lett. *7*, 4067-4069.

Choe,N., Tanaka,S., Xia,W.J., Hemenway,D.R., Roggli,V.L., and Kagan,E. (1997). Pleural macrophage recruitment and activation in asbestos-induced pleural injury. Environmental Health Perspectives *105*, 1257-1260.

Churg,A. and Vedal,S. (1994). Fiber burden and patterns of asbestos-related disease in workers with heavy mixed amosite and chrysotile exposure. Am. J. Respir. Crit Care Med. *150*, 663-669.

Cooke,W.E. (1924). FIBROSIS OF THE LUNGS DUE TO THE INHALATION OF ASBESTOS DUST. Br. Med. J. *2*, 147-140.

Crapo,J.D., Barry,B.E., Gehr,P., Bachofen,M., and Weibel,E.R. (1982). Cell number and cell characteristics of the normal human lung. Am. Rev. Respir. Dis. *126*, 332-337.

Darnton,A.J., McElvenny,D.M., and Hodgson,J.T. (2006). Estimating the number of asbestos-related lung cancer deaths in Great Britain from 1980 to 2000 Ann Occup Hyg *50*, 29-38.

Davis,J.M., Addison,J., Bolton,R.E., Donaldson,K., Jones,A.D., and Smith,T. (1986a). The pathogenicity of long versus short fibre samples of amosite asbestos administered to rats by inhalation and intraperitoneal injection Br. J Exp. Pathol. *67*, 415-430.

Davis,J.M. and Cowie,H.A. (1990). The relationship between fibrosis and cancer in experimental animals exposed to asbestos and other fibers. Environ. Health Perspect. *88:305-9.*, 305-309.

Davis,J.M., Jones,A.D., and Miller,B.G. (1991). Experimental studies in rats on the effects of asbestos inhalation coupled with the inhalation of titanium dioxide or quartz. Int. J. Exp. Pathol. *72*, 501-525.

Davis,J.G., Addison,J., Bolton,R.E., Donaldson,K., Jones,A.D., and Smith,T. (1986b). The pathogenicity of long versus short fiber samples of amosite asbestos administered to rats by inhalation and intraperitoneal injection. British Journal Of Experimental Pathology *67*, 415-430.

DeFife,K.M., Jenney,C.R., Colton,E., and Anderson,J.M. (1999). Disruption of filamentous actin inhibits human macrophage fusion. Faseb Journal *13*, 823-832.

Dikensoy,O. (2008). Mesothelioma due to environmental exposure to erionite in Turkey. Current Opinion in Pulmonary Medicine *14*, 322-325.

Dodson,R.F., Williams,M.G., Corn,C.J., Brollo,A., and Bianchi,C. (1990). Asbestos Content of Lung-Tissue, Lymph-Nodes, and Pleural Plaques from Former Shipyard Workers. American Review Of Respiratory Disease *142*, 843-847.

Dogan,A.U., Dogan,M., and Hoskins,J.A. (2008). Erionite series minerals: mineralogical and carcinogenic properties. Environmental Geochemistry and Health *30*, 367-381.

Doll,R. (1993). Mortality from lung cancer in asbestos workers 1955. Br. J. Ind. Med. *50*, 485-490.

Donaldson,K. (2009). The inhalation toxicology of p-aramid fibrils. Crit Rev. Toxicol. *39*, 487-500.

Donaldson,K., Aitken,R., Tran,L., Stone,V., Duffin,R., Forrest,G., and Alexander,A. (2006). Carbon nanotubes: a review of their properties in relation to pulmonary toxicology and workplace safety. Toxicol. Sci. *92*, 5-22.

Donaldson,K., Beswick,P.H., and Gilmour,P.S. (1996). Free radical activity associated with the surface of particles: a unifying factor in determining biological activity? Toxicology Letters *88*, 293-298.

Donaldson,K., Brown,G.M., Brown,D.M., Bolton,R.E., and Davis,J.G. (1989). Inflammation generating potential of long and short fiber amosite asbestos samples. British Journal Of Industrial Medicine *46*, 271-276.

Donaldson,K., Murphy,F., Schinwald,A., Duffin,R., and Poland,C.A. (2011). Identifying the pulmonary hazard of high aspect ratio nanoparticles to enable their safety-by-design. Nanomedicine *6*, 143-156.

Donaldson,K., Murphy,F.A., Duffin,R., and Poland,C.A. (2010). Asbestos, carbon nanotubes and the pleural mesothelium: a review of the hypothesis regarding the role of long fibre retention in the parietal pleura, inflammation and mesothelioma. Part Fibre Toxicol. *7*, 5.

Donaldson,K. and Seaton,A. (2012). A short history of the toxicology of inhaled particles. Part Fibre Toxicol. *9*, 13.

Dostert,C., Petrilli,V., Van Bruggen,R., Steele,C., Mossman,B.T., and Tschopp,J. (2008). Innate immune activation through Nalp3 inflammasome sensing of asbestos and silica. Science *320*, 674-677.

Duffin,R., Gilmour,P.S., Schins,R.P., Clouter,A., Guy,K., Brown,D.M., MacNee,W., Borm,P.J., Donaldson,K., and Stone,V. (2001). Aluminium lactate treatment of dq12 quartz inhibits its ability to cause inflammation, chemokine expression, and nuclear factor-kappab activation. Toxicol. Appl. Pharmacol. *176*, 10-17.

Dvorak,H.F. (1986). Tumors: wounds that do not heal. Similarities between tumor stroma generation and wound healing. N. Engl. J. Med. *315*, 1650-1659.

Emilio Agostoni. Mechanics of the Pleural Space. Compr Physiol 2011, Supplement 12: Handbook of Physiology, The Respiratory System, Mechanics of Breathing , 531-559. 1986.

Falk,P., Ma,C., Chegini,N., and Holmdahl,L. (2000). Differential regulation of mesothelial cell fibrinolysis by transforming growth factor beta 1. Scand. J. Clin. Lab Invest. *60*, 439-447.

Foley-Comer,A.J., Herrick,S.E., Al Mishlab,T., Prele,C.M., Laurent,G.J., and Mutsaers,S.E. (2002). Evidence for incorporation of free-floating mesothelial cells as a mechanism of serosal healing. Journal of Cell Science *115*, 1383-1389.

Fraire,A.E., Greenberg,S.D., Spjut,H.J., Dodson,R.F., Williams,G., Lach-Pasko,E., and Roggli,V.L. (1997). Effect of erionite on the pleural mesothelium of the Fischer 344 rat. Chest. *111*, 1375-1380.

GAMBLE,J.L. (1952). Chemical Anatomy, Physiology, and Pathology of Extracellular Fluid. Fifth Edition. Soil Science *74*.

Gasser,M., Rothen-Rutishauser,B., Krug,H.F., Gehr,P., Nelle,M., Yan,B., and Wick,P. (2010). The adsorption of biomolecules to multi-walled carbon nanotubes is influenced by both pulmonary surfactant lipids and surface chemistry. Journal of Nanobiotechnology *8*.

Gehr, P., Brand, P., and Heyder, J. Particle deposition in the repiratory tract. Particle Lung Cell Interactions.Ed Gehr P.and Heyder J.Vol 143 in 'Lung Biology in Health and Disease' Executive Editor C.Lenfant.Marcel Dekker New York. 229-322. 2000.

Gevenois,P.A., de,M., V, Madani,A., Winant,C., Sergent,G., and De Vuyst,P. (1998). Asbestosis, pleural plaques and diffuse pleural thickening: three distinct benign responses to asbestos exposure. Eur. Respir. J. *11*, 1021-1027.

Goerke,J. (1998). Pulmonary surfactant: functions and molecular composition. Biochim. Biophys. Acta. *%19;1408*, 79-89.

Halle,A., Hornung,V., Petzold,G.C., Stewart,C.R., Monks,B.G., Reinheckel,T., Fitzgerald,K.A., Latz,E., Moore,K.J., and Golenbock,D.T. (2008). The NALP3 inflammasome is involved in the innate immune response to amyloid-beta. Nat. Immunol. *9*, 857-865.

Hamilton,R.F., Wu,N.Q., Porter,D., Buford,M., Wolfarth,M., and Holian,A. (2009). Particle length-dependent titanium dioxide nanomaterials toxicity and bioactivity. Particle and Fibre Toxicology *6*.

Han,J.H., Lee,E.J., Lee,J.H., So,K.P., Lee,Y.H., Bae,G.N., Lee,S.B., Ji,J.H., Cho,M.H., and Yu,I.J. (2008). Monitoring multiwalled carbon nanotube exposure in carbon nanotube research facility. Inhal. Toxicol. *20*, 741-749.

Hansell,A. (2008). Airborne environmental exposure to asbestos. Am. J. Respir. Crit Care Med. *178*, 556-557.

Helland,A., Wick,P., Koehler,A., Schmid,K., and Som,C. (2007). Reviewing the environmental and human health knowledge base of carbon nanotubes. Environ Health Perspect. *115*, 1125-1131.

Hermann,R., Walther,P., and Muller,M. (1996). Immunogold labeling in scanning electron microscopy. Histochem. Cell Biol. *106*, 31-39.

Heyder,J. (2004). Deposition of inhaled particles in the human respiratory tract and consequences for regional targeting in respiratory drug delivery. Proc. Am. Thorac. Soc. *1*, 315-320.

Hillerdal,G. (1999). Mesothelioma: cases associated with non-occupational and low dose exposures. Occup. Environ. Med. *56*, 505-513.

Hirao,T., Bueno,R., Chen,C.J., Gordon,G.J., Heilig,E., and Kelsey,K.T. (2002). Alterations of the p16INK4 locus in human malignant mesothelial tumors. Carcinogenesis *23*, 1127-1130.

Holmes,A. and Morgan,A. (1980). Clearance of anthophyllite fibers from the rat lung and the formation of asbestos bodies. Environ. Res. *22*, 13-21.

Hornung,V., Bauernfeind,F., Halle,A., Samstad,E.O., Kono,H., Rock,K.L., Fitzgerald,K.A., and Latz,E. (2008). Silica crystals and aluminum salts activate the NALP3 inflammasome through phagosomal destabilization. Nature Immunology *9*, 847-856.

Houtmeyers,E., Gosselink,R., Gayan-Ramirez,G., and Decramer,M. (1999). Regulation of mucociliary clearance in health and disease [see comments]. [Review] [98 refs]. Eur Respir J *13*, 1177-1188.

Hughes,J.M. and Weill,H. (1991). Asbestosis as a precursor of asbestos related lung cancer: results of a prospective mortality study. Br. J. Ind. Med. *48*, 229-233.

Iijima, S. *Helical microtubules of graphite carbon*. Nature 354, 56. 1991.

Jagirdar,J., Begin,R., Dufresne,A., Goswami,S., Lee,T.C., and Rom,W.N. (1996). Transforming growth factor-beta (TGF-beta) in silicosis. Am. J. Respir. Crit. Care Med. *154*, 1076-1081.

Jaklitsch,M.T., Grondin,S.C., and Sugarbaker,D.J. (2001). Treatment of malignant mesothelioma. World J. Surg. *25*, 210-217.

Janssen-Heininger,Y.M., Poynter,M.E., and Baeuerle,P.A. (2000). Recent advances towards understanding redox mechanisms in the activation of nuclear factor kappaB. Free Radic. Biol. Med. *28*, 1317-1327.

Jantz,M.A. and Antony,V.B. (2008). Pathophysiology of the pleura. Respiration *75*, 121-133.

Jimenez,L.A., Drost,E.M., Gilmour,P.S., Rahman,I., Antonicelli,F., Ritchie,H., MacNee,W., and Donaldson,K. (2002). PM(10)-exposed macrophages stimulate a proinflammatory response in lung epithelial cells via TNF-alpha. Am. J Physiol Lung Cell Mol. Physiol *282*, L237-L248.

Jimenez,L.A., Zanella,C., Fung,H., Janssen,Y.M., Vacek,P., Charland,C., Goldberg,J., and Mossman,B.T. (1997). Role of extracellular signal-regulated protein kinases in apoptosis by asbestos and H2O2. Am. J. Physiol. *273*, L1029-L1035.

Johnson,N.F. (1980). Release of lamellar bodies from alveolar type 2 cells. Thorax. *35*, 192-197.

Johnston,H.J., Hutchison,G.R., Christensen,F.M., Peters,S., Hankin,S., Aschberger,K., and Stone,V. (2010). A critical review of the biological mechanisms underlying the in vivo and in vitro toxicity of carbon nanotubes: The contribution of physico-chemical characteristics. Nanotoxicology. *4*, 207-246.

Jones,A.D. (1993). Respirable industrial fibres: deposition, clearance and dissolution in animal models. Ann Occup. Hyg *37*, 211-226.

Kagan,V.E., Konduru,N.V., Feng,W.H., Allen,B.L., Conroy,J., Volkov,Y., Vlasova,I.I., Belikova,N.A., Yanamala,N., Kapralov,A., Tyurina,Y.Y., Shi,J.W., Kisin,E.R., Murray,A.R., Franks,J., Stolz,D., Gou,P.P., Klein-Seetharaman,J., Fadeel,B., Star,A., and Shvedova,A.A. (2010). Carbon nanotubes degraded by neutrophil myeloperoxidase induce less pulmonary inflammation. Nature Nanotechnology *5*, 354-359.

Kagan,V.E., Tyurina,Y.Y., Tyurin,V.A., Konduru,N.V., Potapovich,A.I., Osipov,A.N., Kisin,E.R., Schwegler-Berry,D., Mercer,R., Castranova,V., and Shvedova,A.A. (2006). Direct and indirect effects of single walled carbon nanotubes on RAW 264.7 macrophages: role of iron Toxicol. Lett. *165*, 88-100.

Kalomenidis,I. and Light,R.W. (2004). Pathogenesis of the eosinophilic pleural effusions. Curr. Opin. Pulm. Med. *10*, 289-293.

Kamp,D.W., Graceffa,P., Pryor,W.A., and Weitzman,S.A. (1992). The role of free radicals in asbestos-induced diseases. [Review] [212 refs]. Free Radical Biology & Medicine *12*, 293-315.

Kamp,D.W., Israbian,V.A., Yeldandi,A.V., Panos,R.J., Graceffa,P., and Weitzman,S.A. (1995). Phytic acid, an iron chelator, attenuates pulmonary inflammation and fibrosis in rats after intratracheal instillation of asbestos. Toxicol. Pathol. *23*, 689-695.

Kamp,D.W. and Weitzman,S.A. (1999). The molecular basis of asbestos induced lung injury. Thorax. *54*, 638-652.

Ke,Y., Reddel,R.R., Gerwin,B.I., Reddel,H.K., Somers,A.N.A., Mcmenamin,M.G., Laveck,M.A., Stahel,R.A., Lechner,J.F., and Harris,C.C. (1989). Establishment of A Human Invitro Mesothelial Cell Model System for Investigating Mechanisms of Asbestos-Induced Mesothelioma. American Journal Of Pathology *134*, 979-991.

Kilburn,K.H. and Warshaw,R.H. (1991). Abnormal lung function associated with asbestos disease of the pleura, the lung, and both: a comparative analysis. Thorax. *46*, 33-38.

Kroczynska,B., Cutrone,R., Bocchetta,M., Yang,H., Elmishad,A.G., Vacek,P., Ramos-Nino,M., Mossman,B.T., Pass,H.I., and Carbone,M. (2006). Crocidolite asbestos and SV40 are cocarcinogens in human mesothelial cells and in causing mesothelioma in hamsters. Proc. Natl. Acad. Sci. U. S A. *%19;103*, 14128-14133.

Kroll,A., Pillukat,M.H., Hahn,D., and Schnekenburger,J.+. (2009). Current in vitro methods in nanoparticle risk assessment: Limitations and challenges. European Journal of Pharmaceutics and Biopharmaceutics *72*, 370-377.

Lai-Fook,S.J. (2004). Pleural mechanics and fluid exchange. Physiological Reviews *84*, 385-410.
Lai-Fook,S.J. and Houtz,P.K. (2007). Protein concentration of pleural liquid, peritoneal liquid and plasma measured in mice. Faseb Journal *21*, A554-A555.

Lam,C.W., James,J.T., McCluskey,R., and Hunter,R.L. (2004). Pulmonary toxicity of single-wall carbon nanotubes in mice 7 and 90 days after intratracheal instillation. Toxicol. Sci. *77*, 126-134.

Lapp,N.L. and Castranova,V. (1993). How silicosis and coal workers' pneumoconiosis develop--a cellular assessment. Occup. Med. *8*, 35-56.

Larocca,P.J. and Rheinwald,J.G. (1984). Coexpression of simple epithelial keratins and vimentin by human mesothelium and mesothelioma in vivo and in culture. Cancer Res. *44*, 2991-2999.

Lechner,J.F., Tokiwa,T., LaVeck,M., Benedict,W.F., Banks-Schlegel,S., Yeager,H., Jr., Banerjee,A., and Harris,C.C. (1985). Asbestos-associated chromosomal changes in human mesothelial cells. Proc. Natl. Acad. Sci. U. S. A *82*, 3884-3888.

Lehnert, B. E. Pulmonary and thoracic macrophage populations and clearance of particles from the lungs. Environ Health Perspect. 97, 17-46. 1992.

Li,F.K., Davenport,A., Robson,R.L., Loetscher,P., Rothlein,R., Williams,J.D., and Topley,N. (1998). Leukocyte migration across human peritoneal mesothelial cells is dependent on directed chemokine secretion and ICAM-1 expression. Kidney Int. *54*, 2170-2183.

Li,J. (1993). Ultrastructural study on the pleural stomata in human. Funct. Dev. Morphol. *3*, 277-280.

Li,S., Wu,W., Campidelli,S., Sarnatskaïa,V., Prato,M., Tridon,A., Nikolaev,A., Bianco,A., and Snezhkova,E. (2008). Adsorption of carbon nanotubes on active carbon microparticles. Carbon *46*, 1091-1095.

Li,X.Y., Brown,G.M., Lamb,D., and Donaldson,K. (1993). Reactive pleural inflammation caused by intratracheal instillation of killed microbes. Eur Respir J *6*, 27-34.

Lindberg,H.K., Falck,G.C., Suhonen,S., Vippola,M., Vanhala,E., Catalan,J., Savolainen,K., and Norppa,H. (2009). Genotoxicity of nanomaterials: DNA damage and micronuclei induced by carbon nanotubes and graphite nanofibres in human bronchial epithelial cells in vitro. Toxicol. Lett. *186*, 166-173.

Liu,J.Y., Morris,G.F., Lei,W.H., Hart,C.E., Lasky,J.A., and Brody,A.R. (1997). Rapid activation of PDGF-A and -B expression at sites of lung injury in asbestos-exposed rats. American Journal Of Respiratory Cell And Molecular Biology *17*.

Liu,W., Ernst,J.D., and Broaddus,V.C. (2000). Phagocytosis of crocidolite asbestos induces oxidative stress, DNA damage, and apoptosis in mesothelial cells. Am. J. Respir. Cell Mol. Biol. *23*, 371-378.

Liu,X.Y., Hurt,R.H., and Kane,A.B. (2010). Biodurability of single-walled carbon nanotubes depends on surface functionalization. Carbon *48*, 1961-1969.

Liu,Z. and Klominek,J. (2004). Chemotaxis and chemokinesis of malignant mesothelioma cells to multiple growth factors. Anticancer Res. *24*, 1625-1630.

Lu,S., Duffin,R., Poland,C., Daly,P., Murphy,F., Drost,E., MacNee,W., Stone,V., and Donaldson,K. (2009). Efficacy of simple short-term in vitro assays for predicting the potential of metal oxide nanoparticles to cause pulmonary inflammation. Environ Health Perspect. *117*, 241-247.

Ma-Hock,L., Treumann,S., Strauss,V., Brill,S., Luizi,F., Mertler,M., Wiench,K., Gamer,A.O., van Ravenzwaay,B., and Landsiedel,R. (2009). INHALATION TOXICITY OF MULTI-WALL CARBON NANOTUBES IN RATS EXPOSED FOR 3 MONTHS. Toxicol. Sci.

Maltoni,C., Minardi,F., and Morisi,L. (1982). Pleural mesotheliomas in Sprague-Dawley rats by erionite: first experimental evidence. ENVIRONMENTAL RESEARCH *29*, 238-244.

Maynard,A.D., Baron,P.A., Foley,M., Shvedova,A.A., Kisin,E.R., and Castranova,V. (2004). Exposure to carbon nanotube material: aerosol release during the handling of unrefined single-walled carbon nanotube material. J. Toxicol. Environ. Health A *67*, 87-107.

McDonald,A.D., Case,B.W., Churg,A., Dufresne,A., Gibbs,G.W., Sebastien,P., and McDonald,J.C. (1997). Mesothelioma in Quebec chrysotile miners and millers: epidemiology and aetiology. Ann. Occup. Hyg. *41*, 707-719.

McKinney,J.D., Richard,A., Waller,C., Newman,M.C., and Gerberick,F. (2000). The practice of structure activity relationships (SAR) in toxicology. Toxicol. Sci. *56*, 8-17.

Mercer,R.R., Hubbs,A.F., Scabilloni,J.F., Wang,L.Y., Battelli,L.A., Friend,S., Castranova,V., and Porter,D.W. (2011). Pulmonary fibrotic response to aspiration of multi-walled carbon nanotubes. Particle and Fibre Toxicology *8*.

Mercer,R.R., Hubbs,A.F., Scabilloni,J.F., Wang,L.Y., Battelli,L.A., Schwegler-Berry,D., Castranova,V., and Porter,D.W. (2010). Distribution and persistence of pleural penetrations by multi-walled carbon nanotubes. Particle and Fibre Toxicology *7*.

Methner,M., Hodson,L., Dames,A., and Geraci,C. (2010). Nanoparticle Emission Assessment Technique (NEAT) for the identification and measurement of potential inhalation exposure to engineered nanomaterials--Part B: Results from 12 field studies. J. Occup. Environ. Hyg. *7*, 163-176.

Miller,B.G., Searl,A., Davis,J.M., Donaldson,K., Cullen,R.T., Bolton,R.E., Buchanan,D., and Soutar,C.A. (1999). Influence of fibre length, dissolution and biopersistence on the production of mesothelioma in the rat peritoneal cavity. Ann Occup Hyg *43*, 155-166.

Miserocchi,G. (1997). Physiology and pathophysiology of pleural fluid turnover. Eur. Respir. J. *10*, 219-225.

Miserocchi,G. (2009). Mechanisms controlling the volume of pleural fluid and extravascular lung water. Eur. Respir. Rev. *18*, 244-252.

Miserocchi,G., Sancini,G., Mantegazza,F., and Chiappino,G. (2008). Translocation pathways for inhaled asbestos fibers. Environmental Health *7*.

Mitchev,K., Dumortier,P., and De Vuyst,P. (2002). 'Black Spots' and hyaline pleural plaques on the parietal pleura of 150 urban necropsy cases. Am. J. Surg. Pathol. *26*, 1198-1206.

Miura,T., Shimada,T., Tanaka,K., Chujo,M., and Uchida,Y. (2000). Lymphatic drainage of carbon particles injected into the pleural cavity of the monkey, as studied by video-assisted thoracoscopy and electron microscopy. Journal of Thoracic and Cardiovascular Surgery *120*, 437-447.

Moalli,P.A., Macdonald,J.L., Goodglick,L.A., and Kane,A.B. (1987). Acute injury and regeneration of the mesothelium in response to asbestos fibers. American Journal Of Pathology *128*, 426-445.

Monteiro-Riviere,N.A. and Inman,A.O. (2006). Challenges for assessing carbon nanomaterial toxicity to the skin. Carbon *44*, 1070-1078.

Morgan,A. (1995). Deposition of inhaled asbestos and man-made mineral fibres in the respiratory tract. Ann. Occup. Hyg. *39*, 747-758.

Morgan,A., Holmes,A., and Davison,W. (1982). Clearance of sized glass fibres from the rat lung and their solubility in vivo. Ann. Occup. Hyg. *25*, 317-331.

Mossman,B.T. and Churg,A. (1998). Mechanisms in the pathogenesis of asbestosis and silicosis. Am. J. Respir. Crit Care Med. *157*, 1666-1680.

Muhlfeld,C., Poland,C.A., Duffin,R., Brandenberger,C., Murphy,F.A., Rothen-Rutishauser,B., Gehr,P., and Donaldson,K. (2011). Differential effects of long and short carbon nanotubes on the gas-exchange region of the mouse lung. Nanotoxicology.

Muller,J., Huaux,F., Fonseca,A., Nagy,J.B., Moreau,N., Delos,M., Raymundo-Pinero,E., Beguin,F., Kirsch-Volders,M., Fenoglio,I., Fubini,B., and Lison,D. (2008). Structural defects play a major role in the acute lung toxicity of multiwall carbon nanotubes: toxicological aspects. Chem. Res. Toxicol. *21*, 1698-1705.

Muller,J., Huaux,F., Moreau,N., Misson,P., Heilier,J.F., Delos,M., Arras,M., Fonseca,A., Nagy,J.B., and Lison,D. (2005). Respiratory toxicity of multi-wall carbon nanotubes
1. Toxicol. Appl. Pharmacol. *207*, 221-231.

Muller,K.M., Schmitz,I., and Konstantinidis,K. (2002). Black spots of the parietal pleura: morphology and formal pathogenesis. Respiration *69*, 261-267.

Murphy,F.A., Poland,C.A., Duffin,R., Al Jamal,K.T., Ali-Boucetta,H., Nunes,A., Byrne,F., Prina-Mello,A., Volkov,Y., Li,S., Mather,S.J., Bianco,A., Prato,M., MacNee,W., Wallace,W.A., Kostarelos,K., and Donaldson,K. (2011). Length-dependent retention of carbon nanotubes in the pleural space of mice initiates sustained inflammation and progressive fibrosis on the parietal pleura. Am. J. Pathol. *178*, 2587-2600.

Murthy,S.S. and Testa,J.R. (1999). Asbestos, chromosomal deletions, and tumor suppressor gene alterations in human malignant mesothelioma. J. Cell Physiol. *180*, 150-157.

Mutsaers,S.E. (2002). Mesothelial cells: Their structure, function and role in serosal repair. Respirology *7*, 171-191.

Mutsaers,S.E. (2004). The mesothelial cell. International Journal of Biochemistry & Cell Biology *36*, 9-16.

Mutsaers,S.E., Prele,C.M., Brody,A.R., and Idell,S. (2004). Pathogenesis of pleural fibrosis. Respirology. *9*, 428-440.

Mutsaers,S.E., Whitaker,D., and Papadimitriou,J.M. (2002). Stimulation of mesothelial cell proliferation by exudate macrophages enhances serosal wound healing in a murine model. American Journal Of Pathology *160*, 681-692.

Nagai,H., Okazaki,Y., Chew,S.H., Misawa,N., Yamashita,Y., Akatsuka,S., Ishihara,T., Yamashita,K., Yoshikawa,Y., Yasui,H., Jiang,L., Ohara,H., Takahashi,T., Ichihara,G., Kostarelos,K., Miyata,Y., Shinohara,H., and Toyokuni,S. (2011). Diameter and rigidity of multiwalled carbon nanotubes are

critical factors in mesothelial injury and carcinogenesis. Proc. Natl. Acad. Sci. U. S A. *108*, E1330-E1338.

Nauseef,W.M. (2004). Assembly of the phagocyte NADPH oxidase. Histochemistry and Cell Biology *122*, 277-291.

Nel,A.E., Madler,L., Velegol,D., Xia,T., Hoek,E.M.V., Somasundaran,P., Klaessig,F., Castranova,V., and Thompson,M. (2009). Understanding biophysicochemical interactions at the nano-bio interface. Nature Materials *8*, 543-557.

Noppen,M., de Waele,M., Li,R., Vander Gucht,K., D'Haese,J., Gerlo,E., and Vincken,W. (2000). Volume and cellular content of normal pleural fluid in humans examined by pleural lavage. Am. J. Respir. Crit. Care Med. *162*, 1023-1026.

Nurminen,M. and Tossavainen,A. (1994). Is there an association between pleural plaques and lung cancer without asbestosis? Scand. J. Work Environ. Health. *20*, 62-64.

Nygren,J., Suhonen,S., Norppa,H., and Linnainmaa,K. (2004). DNA damage in bronchial epithelial and mesothelial cells with and without associated crocidolite asbestos fibers. Environ. Mol. Mutagen. *44*, 477-482.

Oberdoerster,G., Ferin,J., Marcello,N.L., and Meinhold,S.H. (1983). Effect of intrabronchially instilled amosite on lavagable lung and pleural cells. Environ. Health Perspect. *51:41-7.*, 41-47.

Okada,F. and Fujii,J. (2006). Molecular mechanisms of inflammation-induced carcinogenesis. Journal of Clinical Biochemistry and Nutrition *39*, 103-111.

Osmond-McLeod,M.J., Poland,C.A., Murphy,F., Waddington,L., Morris,H., Hawkins,S.C., Clark,S., Aitken,R., McCall,M.J., and Donaldson,K. (2011). Durability and inflammogenic impact of carbon nanotubes compared with asbestos fibres. Part Fibre Toxicol. *8*, 15.

Owens,M.W. and Milligan,S.A. (1995). Pleuritis and pleural effusions. Curr. Opin. Pulm. Med. *1*, 318-323.

Pache,J.C., Janssen,Y.M., Walsh,E.S., Quinlan,T.R., Zanella,C.L., Low,R.B., Taatjes,D.J., and Mossman,B.T. (1998). Increased epidermal growth factor-receptor protein in a human mesothelial cell line in response to long asbestos fibers. Am J Pathol. *152*, 333-340.

Pacurari,M., Yin,X.J., Ding,M., Leonard,S.S., Schwegler-Berry,D., Ducatman,B.S., Chirila,M., Endo,M., Castranova,V., and Vallyathan,V. (2008a). Oxidative and molecular interactions of multi-wall carbon nanotubes (MWCNT) in normal and malignant human mesothelial cells. Nanotoxicology *2*, 155-170.

Pacurari,M., Yin,X.J., Zhao,J., Ding,M., Leonard,S.S., Schwegler-Berry,D., Ducatman,B.S., Sbarra,D., Hoover,M.D., Castranova,V., and Vallyathan,V. (2008b). Raw single-wall carbon nanotubes induce oxidative stress and activate MAPKs, AP-1, NF-kappaB, and Akt in normal and malignant human mesothelial cells. Environ Health Perspect. *116*, 1211-1217.

Palomaki,J., Valimaki,E., Sund,J., Vippola,M., Clausen,P.A., Jensen,K.A., Savolainen,K., Matikainen,S., and Alenius,H. (2011). Long, Needle-like Carbon Nanotubes and Asbestos Activate the NLRP3 Inflammasome through a Similar Mechanism. ACS Nano.

Park,E.K., Jung,H.S., Yang,H.I., Yoo,M.C., Kim,C., and Kim,K.S. (2007). Optimized THP-1 differentiation is required for the detection of responses to weak stimuli. Inflammation Research *56*, 45-50.

Parungo,C.P., Colson,Y.L., Kim,S.W., Kim,S., Cohn,L.H., Bawendi,M.G., and Frangioni,J.V. (2005). Sentinel lymph node mapping of the pleural space. Chest *127*, 1799-1804.

Pauluhn,J. (2010a). Multi-walled carbon nanotubes (Baytubes): approach for derivation of occupational exposure limit. Regul. Toxicol. Pharmacol. *57*, 78-89.

Pauluhn,J. (2010b). Subchronic 13-Week Inhalation Exposure of Rats to Multiwalled Carbon Nanotubes: Toxic Effects Are Determined by Density of Agglomerate Structures, Not Fibrillar Structures. Toxicol. Sci. *113*, 226-242.

Peacock,C., Copley,S.J., and Hansell,D.M. (2000). Asbestos-related benign pleural disease. Clin. Radiol. *55*, 422-432.

Perdue,T.D. and Brody,A.R. (1994). Distribution of transforming growth-factor-beta-1, fibronectin, and smooth-muscle actin in asbestos-induced pulmonary fibrosis in rats. Journal Of Histochemistry & Cytochemistry *42*.

Peto,J., Hodgson,J.T., Matthews,F.E., and Jones,J.R. (1995). Continuing increase in mesothelioma mortality in Britain Lancet *345*, 535-539.

Petrilli,V., Dostert,C., Muruve,D.A., and Tschopp,J. (2007a). The inflammasome: a danger sensing complex triggering innate immunity. Current Opinion in Immunology *19*, 615-622.

Petrilli,V., Papin,S., Dostert,C., Mayor,A., Martinon,F., and Tschopp,J. (2007b). Activation of the NALP3 inflammasome is triggered by low intracellular potassium concentration. Cell Death and Differentiation *14*, 1583-1589.

Pison,U., Herold,R., and Sch++rch,S. (1996). The pulmonary surfactant system: biological functions, components, physicochemical properties and alterations during lung disease. Colloids and Surfaces A: Physicochemical and Engineering Aspects *114*, 165-184.

Pociask,D.A., Sime,P.J., and Brody,A.R. (2004). Asbestos-derived reactive oxygen species activate TGF-beta1. Lab Invest. *84*, 1013-1023.

Poland,C.A., Byrne,F., Cho,W.S., Prina-Mello,A., Murphy,F.A., Davies,G.L., Coey,J.M., Gounko,Y., Duffin,R., Volkov,Y., and Donaldson,K. (2011). Length-dependent pathogenic effects of nickel nanowires in the lungs and the peritoneal cavity. Nanotoxicology.

Poland,C.A., Duffin,R., Kinloch,I., Maynard,A., Wallace,W.A., Seaton,A., Stone,V., Brown,S., MacNee,W., and Donaldson,K. (2008). Carbon nanotubes introduced into the abdominal cavity of mice show asbestos-like pathogenicity in a pilot study. Nat. Nanotechnol. *3*, 423-428.

Porter,D.W., Hubbs,A.F., Mercer,R.R., Wu,N.Q., Wolfarth,M.G., Sriram,K., Leonard,S., Battelli,L., Schwegler-Berry,D., Friend,S., Andrew,M., Chen,B.T., Tsuruoka,S., Endo,M., and Castranova,V. (2010). Mouse pulmonary dose- and time course-responses induced by exposure to multi-walled carbon nanotubes. Toxicology *269*, 136-147.

Prina-Mello,A., Diao,Z., and Coey,J. (2006). Internalization of ferromagnetic nanowires by different living cells. Journal of Nanobiotechnology *4*, 9.

Puhakka,A., Ollikainen,T., Soini,Y., Kahlos,K., Saily,M., Koistinen,P., Paakko,P., Linnainmaa,K., and Kinnula,V.L. (2002). Modulation of DNA single-strand breaks by intracellular glutathione in human lung cells exposed to asbestos fibers. Mutat. Res. *514*, 7-17.

Pulskamp,K., Diabate,S., and Krug,H.F. (2007). Carbon nanotubes show no sign of acute toxicity but induce intracellular reactive oxygen species in dependence on contaminants. Toxicology Letters *168*, 58-74.

Ramos-Nino,M.E., Timblin,C.R., and Mossman,B.T. (2002a). Mesothelial cell transformation requires increased AP-1 binding activity and ERK-dependent Fra-1 expression. Cancer Res. *62*, 6065-6069.
Ramos-Nino,M.E., Haegens,A., Shukla,A., and Mossman,B.T. (2002b). Role of mitogen-activated protein kinases (MAPK) in cell injury and proliferation by environmental particulates. Molecular And Cellular Biochemistry *234-235*, 111-118.

Rao,G.V., Tinkle,S., Weissman,D.N., Antonini,J.M., Kashon,M.L., Salmen,R., Battelli,L.A., Willard,P.A., Hoover,M.D., and Hubbs,A.F. (2003). Efficacy of a technique for exposing the mouse lung to particles aspirated from the pharynx. J. Toxicol. Environ. Health A *66*, 1441-1452.

Riquet,M., Souilamas,R., Hubsch,J.P., Briere,J., Colomer,S., and Hidden,G. (2000). Lymphatic drainage of heart and lungs: comparison between pig and man. Surg. Radiol. Anat. *22*, 47-50.

Roberts,G.H. (1971). The pathology of parietal pleural plaques. J. Clin. Pathol. *24*, 348-353.

Royal Society and Royal Academy of Engineering (2004). Nanoscience and nanotechnologies: opportunities and uncertainties. The Royal Society.

Rusch,V.W. (1996). A proposed new international TNM staging system for malignant pleural mesothelioma from the international mesothelioma interest group. Lung Cancer *14*, 1-12.

Ryman-Rasmussen,J.P., Cesta,M.F., Brody,A.R., Shipley-Phillips,J.K., Everitt,J.I., Tewksbury,E.W., Moss,O.R., Wong,B.A., Dodd,D.E., Andersen,M.E., and Bonner,J.C. (2009). Inhaled carbon nanotubes reach the subpleural tissue in mice. Nature Nanotechnology *4*, 747-751.

Sakamoto,Y., Nakae,D., Fukumori,N., Tayama,K., Maekawa,A., Imai,K., Hirose,A., Nishimura,T., Ohashi,N., and Ogata,A. (2009). Induction of mesothelioma by a single intrascrotal administration of multi-wall carbon nanotube in intact male Fischer 344 rats. Journal of Toxicological Sciences *34*, 65-76.

Saxena,R.K., Williams,W., Mcgee,J.K., Daniels,M.J., Boykin,E., and Gilmour,M.I. (2007). Enhanced in vitro and in vivo toxicity of poly-dispersed acid-functionalized single-wall carbon nanotubes. Nanotoxicology *1*, 291-300.

Schinwald,A., Murphy,F., Prina-Mello,A., Poland,C., Byrne,F., Glass,J., Dickerson,J., Schultz,D., Movia,D., Jeffree,C., MacNee,W., and Donaldson,K. (2012a). The threshold length for fibre-induced acute pleural inflammation: shedding light on the early events in asbestos-induced mesothelioma. Toxicol. Sci.

Schinwald,A., Murphy,F.A., Jones,A., MacNee,W., and Donaldson,K. (2012b). Graphene-based nanoplatelets: a new risk to the respiratory system as a consequence of their unusual aerodynamic properties. ACS Nano. *6*, 736-746.

Searl,A., Buchanan,D., Cullen,R.T., Jones,A.D., Miller,B.G., and Soutar,C.A. (1999). Biopersistence and durability of nine mineral fibre types in rat lungs over 12 months. Ann. Occup. Hyg. *43*, 143-153.

Shaw,C.A., Robertson,S., Miller,M.R., Duffin,R., Tabor,C.M., Donaldson,K., Newby,D.E., and Hadoke,P.W. (2011). Diesel exhaust particulate--exposed macrophages cause marked endothelial cell activation. Am. J. Respir. Cell Mol. Biol. *44*, 840-851.

Shinohara,H. (1997). Distribution of lymphatic stomata on the pleural surface of the thoracic cavity and the surface topography of the pleural mesothelium in the golden hamster. Anatomical Record *249*, 16-23.

Shukla,A., Gulumian,M., Hei,T.K., Kamp,D., Rahman,Q., and Mossman,B.T. (2003a). Multiple roles of oxidants in the pathogenesis of asbestos-induced diseases. Free Radic. Biol. Med *34*, 1117-1129.

Shukla,A., Ramos-Nino,M., and Mossman,B. (2003b). Cell signaling and transcription factor activation by asbestos in lung injury and disease. Int. J. Biochem. Cell Biol. *35*, 1198-1209.

Shvedova,A.A., Kisin,E.R., Mercer,R., Murray,A.R., Johnson,V.J., Potapovich,A.I., Tyurina,Y.Y., Gorelik,O., Arepalli,S., Schwegler-Berry,D., Hubbs,A.F., Antonini,J., Evans,D.E., Ku,B.K., Ramsey,D., Maynard,A., Kagan,V.E., Castranova,V., and Baron,P. (2005). Unusual inflammatory and fibrogenic pulmonary responses to single-walled carbon nanotubes in mice
1. Am J Physiol Lung Cell Mol. Physiol *289*, L698-L708.

Shvedova,A.A., Kisin,E.R., Murray,A.R., Johnson,V.J., Gorelik,O., Arepalli,S., Hubbs,A.F., Mercer,R.R., Keohavong,P., Sussman,N., Jin,J., Yin,J., Stone,S., Chen,B.T., Deye,G., Maynard,A., Castranova,V., Baron,P.A., and Kagan,V.E. (2008). Inhalalation versus aspiration of single walled carbon nanotubes in C57/Bl6 mice: Inflammation, fibrosis, oxidative stress and mutagenesis. Am. J. Physiol Lung Cell Mol. Physiol ***295***, L552-L565.

Stanton,M.F., Layard,M., Tegeris,A., Miller,E., May,M., Morgan,E., and Smith,A. (1981). Relation of particle dimension to carcinogenicity in amphibole asbestoses and other fibrous minerals. Journal Of The National Cancer Institute *67*, 965-975.

Stephenson,J.J., Sadana,A.K., Higginbotham,A.L., and Tour,J.M. (2006). Highly functionalized and soluble multiwalled carbon nanotubes by reductive alkylation and arylation: The billups reaction. Chemistry of Materials *18*, 4658-4661.

Stone,K.C., Mercer,R.R., Gehr,P., Stockstill,B., and Crapo,J.D. (1992). Allometric relationships of cell numbers and size in the mammalian lung. Am. J. Respir. Cell Mol. Biol. *6*, 235-243.

Sturm,R. and Hofmann,W. (2009). Theoretical calculations of the deposition of non-spherical particles in the upper airways of the human lung. Zeitschrift fur Medizinische Physik *19*, 38-46.

Suzuki,Y. and Kohyama,N. (1991). Translocation of Inhaled Asbestos Fibers from the Lung to Other Tissues. American Journal Of Industrial Medicine *19*, 701-704.

Swain WA and Faux SP. Activation of p38 MAP Kinase by Crocidolite in Mesothelial Cells is Dependent upon Oxidative Stress. Ann.Occup.Hyg. 46 Suppl 1, 136-139. 2002.

Tabet,L., Bussy,C., Amara,N., Setyan,A., Grodet,A., Rossi,M.J., Pairon,J.C., Boczkowski,J., and Lanone,S. (2009). Adverse effects of industrial multiwalled carbon nanotubes on human pulmonary cells. J. Toxicol. Environ. Health A. *72*, 60-73.

Takagi,A., Hirose,A., Nishimura,T., Fukumori,N., Ogata,A., Ohashi,N., Kitajima,S., and Kanno,J. (2008). Induction of mesothelioma in p53+/- mouse by intraperitoneal application of multi-wall carbon nanotube. J. Toxicol. Sci. *33*, 105-116.

Tasis,D., Tagmatarchis,N., Bianco,A., and Prato,M. (2006). Chemistry of Carbon Nanotubes. Chem. Rev. *106*, 1105-1136.

Tomatis,M., Turci,F., Ceschino,R., Riganti,C., Gazzano,E., Martra,G., Ghigo,D., and Fubini,B. (2010). High aspect ratio materials: role of surface chemistry vs. length in the historical "long and short amosite asbestos fibers". Inhalation Toxicology *22*, 984-998.

Tong,H.Y., Mcgee,J.K., Saxena,R.K., Kodavanti,U.P., Devlin,R.B., and Gilmour,M.I. (2009). Influence of acid functionalization on the cardiopulmonary toxicity of carbon nanotubes and carbon black particles in mice. Toxicology And Applied Pharmacology *239*, 224-232.

Tsao,A.S., Wistuba,I., Roth,J.A., and Kindler,H.L. (2009). Malignant pleural mesothelioma. J. Clin. Oncol. *%20;27*, 2081-2090.

Tschopp,J. and Schroder,K. (2010). NLRP3 inflammasome activation: the convergence of multiple signalling pathways on ROS production? Nature Reviews Immunology *10*, 210-215.

Tweedale,G. (2002). Asbestos and its lethal legacy. Nat. Rev. Cancer *2*, 311-315.

Tyler,W.S. (1983). Comparative subgross anatomy of lungs. Pleuras, interlobular septa, and distal airways. Am. Rev. Respir. Dis. *128*, S32-S36.

Vaia,R.A. and Wagner,H.D. (2004). Framework for nanocomposites. Materials today *7*, 32-37.

Van Den Broeck,W., Derore,A., and Simoens,P. (2006). Anatomy and nomenclature of murine lymph nodes: Descriptive study and nomenclatory standardization in BALB/cAnNCr1 mice. Journal of Immunological Methods *312*, 12-19.

van der,B.S., Koffijberg,H., Burgers,J.A., Baas,P., van de Vijver,M.J., de Mol,B.A., and Moons,K.G. (2012). Prognosis and prognostic factors of patients with mesothelioma: a population-based study. Br. J. Cancer. 10.

Van Gelder,T., Damhuis,R.A., and Hoogsteden,H.C. (1994). Prognostic factors and survival in malignant pleural mesothelioma. Eur. Respir. J. *7*, 1035-1038.

van,d.V., V, Verheggen,M.M., Bernasconi,S., Sozzani,S., Naber,B.A., van der Linden-van Beurden CA, Hoogsteden,H.C., Mantovani,A., and Versnel,M. (1998). Interleukin-1beta and interferon-gamma differentially regulate release of monocyte chemotactic protein-1 and interleukin-8 by human bronchial epithelial cells. Eur. Cytokine Netw. *9*, 269-277.

Vasilieva,L.A., Pylev,L.N., and Rovensky,Y.A. (1998). Pathogenesis of experimentally induced asbestos mesothelioma in rats. Cancer Letters *134*, 209-216.

Virta, R. L. Geological Survey US. Asbestos geology, minerology, mining and uses. 2002. U.S. Dept. of the Interior, U.S. Geological Survey, Reston, VA.

Visser,C.E., Steenbergen,J.J.E., Betjes,M.G.H., Meijer,S., Arisz,L., Hoefsmit,E.C.M., Krediet,R.T., and Beelen,R.H.J. (1995a). Interleukin-8 Production by Human Mesothelial Cells After Direct Stimulation with Staphylococci. Infection and Immunity *63*, 4206-4209.

Visser,C.E., Steenbergen,J.J.E., Betjes,M.G.H., Meijer,S., Arisz,L., Hoefsmit,E.C.M., Krediet,R.T., and Beelen,R.H.J. (1995b). Interleukin-8 Production by Human Mesothelial Cells After Direct Stimulation with Staphylococci. Infection and Immunity *63*, 4206-4209.

Wagner,J.C., Skidmore,J.W., Hill,R.J., and Griffiths,D.M. (1985). Erionite exposure and mesotheliomas in rats. Br. J. Cancer *51*, 727-730.

Wagner,J.C., SLEGGS,C.A., and MARCHAND,P. (1960). Diffuse pleural mesothelioma and asbestos exposure in the North Western Cape Province. Br. J. Ind. Med. *17:260-71.*, 260-271.

Wang,N.S. (1975). The preformed stomas connecting the pleural cavity and the lymphatics in the parietal pleura. Am. Rev. Respir. Dis. *111*, 12-20.

Wang,P.M. and Lai-Fook,S.J. (1993). Effect of ventilation frequency and tidal volume on pleural space thickness in rabbits. J. Appl. Physiol. *75*, 1836-1841.

Wang,Y.H., Faux,S.P., Hallden,G., Kirn,D.H., Houghton,C.E., Lemoine,N.R., and Patrick,G. (2004). Interleukin-1 beta and tumour necrosis factor-alpha promote the transformation of human immortalised mesothelial cells by erionite. International Journal of Oncology *25*, 173-178.

Warheit,D.B. and Hartsky,M.A. (1990). Species comparisons of proximal alveolar deposition patterns of inhaled particulates. Experimental Lung Research *16*, 83-99.

Warheit,D.B., Laurence,B.R., Reed,K.L., Roach,D.H., Reynolds,G.A., and Webb,T.R. (2004). Comparative Pulmonary Toxicity Assessment of Single-wall Carbon Nanotubes in Rats. Toxicol. Sci. *77*, 117-125.

Whawell,S.A. and Thompson,J.N. (1995). Cytokine-induced release of plasminogen activator inhibitor-1 by human mesothelial cells. Eur. J. Surg. *161*, 315-318.

WHO (1997). Determination of airborne fibre number concentrations: a recommended method by phase constrast optical microscopy. World Health Organisation Geneva.

Wilson,C.J., Clegg,R.E., Leavesley,D.I., and Pearcy,M.J. (2005). Mediation of biomaterial-cell interactions by adsorbed proteins: A review. Tissue Engineering *11*, 1-18.

Worle-Knirsch,J.M., Pulskamp,K., and Krug,H.F. (2006). Oops they did it again! Carbon nanotubes hoax scientists in viability assays. Nano Lett. *6*, 1261-1268.

Xiao,G.H., Gallagher,R., Shetler,J., Skele,K., Altomare,D.A., Pestell,R.G., Jhanwar,S., and Testa,J.R. (2005). The NF2 tumor suppressor gene product, merlin, inhibits cell proliferation and cell cycle progression by repressing cyclin D1 expression. Mol. Cell Biol. *25*, 2384-2394.

Xu,L.X., Flynn,B.J., Ungar,S., Pass,H.I., Linnainmaa,K., Mattson,K., and Gerwin,B.I. (1999). Asbestos induction of extended lifespan in normal human mesothelial cells: interindividual susceptibility and SV40 T antigen. Carcinogenesis *20*, 773-783.

Yamamoto,M., Yaginuma,K., Tsutsui,H., Sagara,J., Guan,X., Seki,E., Yasuda,K., Yamamoto,M., Akira,S., Nakanishi,K., Noda,T., and Taniguchi,S. (2004). ASC is essential for LPS-induced activation of procaspase-1 independently of TLR-associated signal adaptor molecules. Genes Cells. *9*, 1055-1067.

Yang,H., Rivera,Z., Jube,S., Nasu,M., Bertino,P., Goparaju,C., Franzoso,G., Lotze,M.T., Krausz,T., Pass,H.I., Bianchi,M.E., and Carbone,M. (2010). Programmed necrosis induced by asbestos in human mesothelial cells causes high-mobility group box 1 protein release and resultant inflammation. Proc. Natl. Acad. Sci. U. S A *107*, 12611-12616.

Yang,H.N., Bocchetta,M., Kroczynska,B., Elmishad,A.G., Chen,Y.B., Liu,Z.M., Bubici,C., Mossman,B.T., Pass,H.I., Testa,J.R., Franzoso,G., and Carbone,M. (2006). TNF-alpha inhibits asbestos-induced cytotoxicity via a NF-kappa B-dependent pathway, a possible mechanism for asbestos-induced oncogenesis. Proceedings Of The National Academy Of Sciences Of The United States Of America *103*, 10397-10402.

Yang,H.N., Testa,J.R., and Carbone,M. (2008). Mesothelioma Epidemiology, Carcinogenesis, and Pathogenesis. Current Treatment Options in Oncology *9*, 147-157.

Ye,S.F., Wang,Y.W., Jiao,F., Zhang,H.G., Lin,C.L., Wu,Y.H., and Zhang,Q.Q. (2011). The Role of NADPH Oxidase in Multi-Walled Carbon Nanotubes-Induced Oxidative Stress and Cytotoxicity in Human Macrophages. Journal of Nanoscience and Nanotechnology *11*, 3773-3781.

Ye,S.F., Wen,W., Wang,Y.F., Lin,C.L., Wu,Y.H., and Zhang,Q.Q. (2010). Multi-walled Carbon Nanotubes Induces Nuclear Factor-kappa B Activation in A549 Cells. Chemical Journal of Chinese Universities-Chinese *31*, 497-501.

Yeates,D., Gerrity,T., and Garrard,C. (1981). Particle deposition and clearance in the bronchial tree. Annals of Biomedical Engineering *9*, 577-592.

Yeganeh,B., Kull,C.M., Hull,M.S., and Marr,L.C. (2008). Characterization of airborne particles during production of carbonaceous nanomaterials. Environmental Science & Technology *42*, 4600-4606.

Yu,M.F., Lourie,O., Dyer,M.J., Moloni,K., Kelly,T.F., and Ruoff,R.S. (2000). Strength and breaking mechanism of multiwalled carbon nanotubes under tensile load. Science. *287*, 637-640.

Zanella,C.L., Posada,J., Tritton,T.R., and Mossman,B.T. (1996). Asbestos causes stimulation of the extracellular signal-regulated kinase-1 mitogen-activated protein-kinase cascade after phosphorylation of the epidermal growth-factor receptor. Cancer Research *56*, 5334-5338.

Zhou,R.B., Tardivel,A., Thorens,B., Choi,I., and Tschopp,J. (2010). Thioredoxin-interacting protein links oxidative stress to inflammasome activation. Nature Immunology *11*, 136-U51.

Appendix 1: Publications

1. **Asbestos, carbon nanotubes and the pleural mesothelium: a review of the hypothesis regarding the role of long fibre retention in the parietal pleura, inflammation and mesothelioma.** Donaldson,K., Murphy,F.A., Duffin,R., and Poland,C.A. (2010). Part Fibre Toxicol. *7*, 5.

2. **Identifying the pulmonary hazard of high aspect ratio nanoparticles to enable their safety-by-design.**Donaldson,K., Murphy,F., Schinwald,A., Duffin,R., and Poland,C.A. (2011). Nanomedicine *6*, 143-156.

3. **Length-dependent retention of carbon nanotubes in the pleural space of mice initiates sustained inflammation and progressive fibrosis on the parietal pleura**.Murphy,F.A., Poland,C.A., Duffin,R., Al Jamal,K.T., Ali-Boucetta,H., Nunes,A., Byrne,F., Prina-Mello,A., Volkov,Y., Li,S., Mather,S.J., Bianco,A., Prato,M., MacNee,W., Wallace,W.A., Kostarelos,K., and Donaldson,K. (2011). Am. J. Pathol. *178*, 2587-2600.

4. **The mechanism of pleural inflammation by long carbon nanotubes: interaction of long fibres with macrophages stimulates them to amplify pro-inflammatory responses in mesothelial cells.**Murphy,F.A., Schinwald,A., Poland,C.A., and Donaldson,K. (2012). Part Fibre Toxicol. *9:8.*, 8.

5. **Length-dependent pleural inflammation and parietal pleural responses after deposition of carbon nanotubes in the pulmonary airspaces of mice.** Murphy, F.A., Poland, C.A., Duffin, R., and Donaldson, K. (2012). Nanotoxicology early online.

Donaldson et al. Particle and Fibre Toxicology 2010, 7:5
http://www.particleandfibretoxicology.com/content/7/1/5

PARTICLE AND FIBRE TOXICOLOGY

REVIEW Open Access

Asbestos, carbon nanotubes and the pleural mesothelium: a review of the hypothesis regarding the role of long fibre retention in the parietal pleura, inflammation and mesothelioma

Ken Donaldson*, Fiona A Murphy, Rodger Duffin, Craig A Poland

Abstract

The unique hazard posed to the pleural mesothelium by asbestos has engendered concern in potential for a similar risk from high aspect ratio nanoparticles (HARN) such as carbon nanotubes. In the course of studying the potential impact of HARN on the pleura we have utilised the existing hypothesis regarding the role of the parietal pleura in the response to long fibres. This review seeks to synthesise our new data with multi-walled carbon nanotubes (CNT) with that hypothesis for the behaviour of long fibres in the lung and their retention in the parietal pleura leading to the initiation of inflammation and pleural pathology such as mesothelioma. We describe evidence that a fraction of all deposited particles reach the pleura and that a mechanism of particle clearance from the pleura exits, through stomata in the parietal pleura. We suggest that these stomata are the site of retention of long fibres which cannot negotiate them leading to inflammation and pleural pathology including mesothelioma. We cite thoracoscopic data to support the contention, as would be anticipated from the preceding, that the parietal pleura is the site of origin of pleural mesothelioma. This mechanism, if it finds support, has important implications for future research into the mesothelioma hazard from HARN and also for our current view of the origins of asbestos-initiated pleural mesothelioma and the common use of lung parenchymal asbestos fibre burden as a correlate of this tumour, which actually arises in the parietal pleura.

Background

The experience with asbestos highlighted that high aspect ratio particles (fibres) pose an additional hazard to the lung beyond that produced by conventional compact particles and gave rise to the discipline of fibre toxicology. Over several decades up to the present, fibre toxicology has evolved a structure activity paradigm that explains the pathogenicity of fibres that is the most robust in particle toxicology. Whilst this paradigm explains the relationship between fibre characteristics and their pathogenicity, the exact sequence of events, following fibre deposition leading to a fibre-type hazard to the pleura and pleural mesothelium has not been clarified. In particular we poorly understand the mechanism whereby fibres seem to selectively deliver their dose to the parietal pleura, whilst the visceral pleura is not initially affected [1]. There has been no unifying hypothesis as to exactly how, within the normal understanding of particle clearance of particles out of the lungs, sustained fibre 'dose' is delivered to the parietal pleura sufficient to produce the distinctive profile of pleural effects associated with fibre exposure in man and animals. In this paper we advance a plausible hypothetical mechanism that emphasises translocation of a fraction of all deposited particles and fibres to the pleural space but the retention of only long fibres in the parietal pleura. This retention of fibre dose at the parietal pleura then serves as the driver that initiates mesothelial injury and inflammation that over time leads to pleural pathology, including mesothelioma. This mechanism is, we contend, generalisable to carbon nanotubes and potentially to other high aspect ratio nanoparticles (HARN) that are currently a cause for

* Correspondence: ken.donaldson@ed.ac.uk
University of Edinburgh, Centre for Inflammation Research, Queens Medical Research Institute, 47 Little France Crescent, Edinburgh, EH16 4TJ, UK

concern due to their asbestos-like morphology and which represent the driving stimulus for this work.

The application of this hypothesis to nanotubes arises from our initial work regarding the similarities in length-dependent mesothelial inflammogenicity of asbestos and carbon nanotubes in the peritoneal cavity [2]. The role of failed peritoneal and pleural cavity clearance of long fibres in their pathogenicity was advanced in its essential form by Kane and co-workers [3,4]. Boutin and co-workers [5-7] have also made essentially the same suggestion as regards asbestos and clearance from the parietal pleura in relation to human asbestos-related mesothelioma. We therefore fully recognise these intellectual precedents in our restatement and elaboration of the hypothesis here in relation to our work with long and short nanotubes in the pleural cavity [2]. This new work, which is mentioned to a small extent in this review, is being submitted for full peer-review elsewhere (Murphy, F., Poland, C.A., Ali-Boucetta, H., Al-Jamal K. T., Duffin, R., Nunes, A., Herrero, M-A., Mather, S. J., Bianco, A., Prato, M., Kostarelos, Donaldson, K. Long but not short nanotubes are retained in the pleural space initiating sustained mesothelial inflammation. Submitted for publication)This present review sets out the anatomical and pathophysiological background concerning the behaviour of particles and fibres in the pleural space and elaborates the evolving hypothesis that might explain how long fibres and long nanotubes might deliver 'dose' to the parietal pleura.

Fibres and the pleural mesothelium

Particles tend to deliver their effects to the lung itself in the form of fibrosis or lung cancer. PM_{10} particles also affect susceptible populations, exacerbating existing airways disease and cardiovascular disease, probably via pro-inflammatory effects emanating from the lungs. The additional hazard posed by fibres relates to the mesothelial lining of the pleural cavity and to some extent the peritoneal cavity. Individuals exposed to asbestos demonstrate a wide range of pleural pathologies including pleural effusion (a build up of fluid within the pleural space), pleural fibrosis and pleural mesothelioma [8]. A variable, usually small, proportion of mesotheliomas developing in individuals exposed to asbestos arise in the peritoneal cavity, likely as a result of fibre translocation from the pleural cavity to the peritoneal cavity [9]. The mechanism of production of pleural mesothelioma is not well understood although various mechanisms have been advanced [10]. However some contact between fibres and mesothelial cells is a reasonable supposition (see below) and numerous studies have demonstrated effects such as genotoxicity [11] and pro-inflammatory effects [10] following exposure of mesothelial cells to asbestos and other fibres *in vitro*.

The classical fibre pathogenicity structure:activity paradigm

Several decades of fibre toxicology have lead to an overarching fibre toxicology structure:activity paradigm involving length, diameter and biopersistence (reviewed in [12] Figure 1).

The fibre paradigm identifies the geometry of fibres as their most important toxicological characteristic and not the chemical make-up, except in so far as the composition makes a contribution to biopersistence (see later). This independence from composition is evident in the fact that the paradigm embraces fibres composed of diverse materials including amphibole and serpentine asbestos minerals, vitreous and ceramic fibres and an organic fibre (reviewed in [12]). Diameter is important

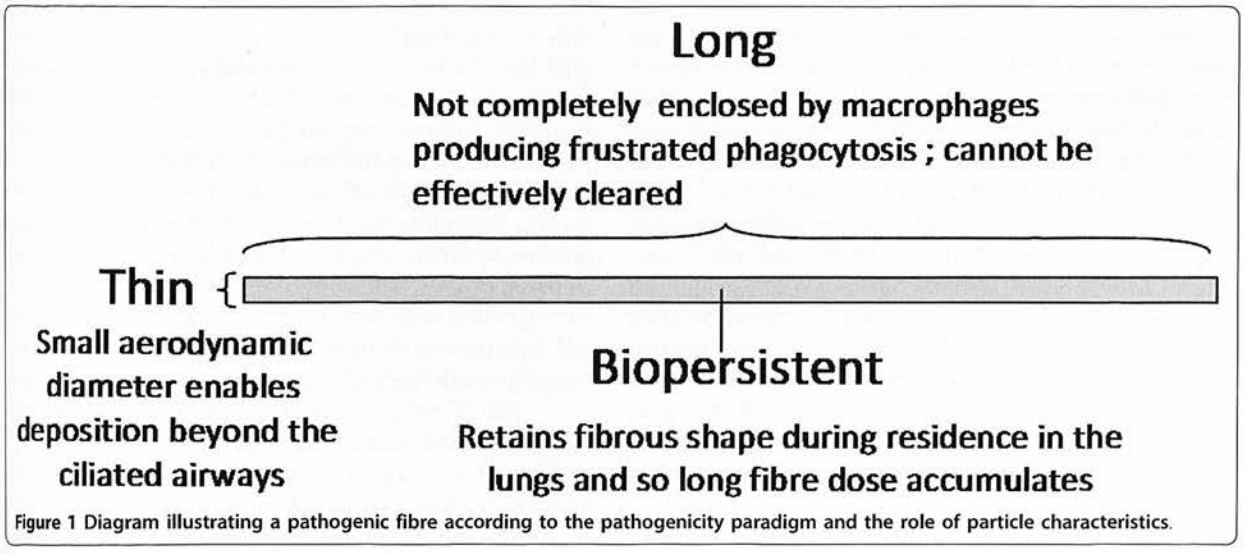

Figure 1 Diagram illustrating a pathogenic fibre according to the pathogenicity paradigm and the role of particle characteristics.

because of the central role that fibre diameter plays in defining aerodynamic diameter (D_{ae}) and the dependence of pulmonary deposition on D_{ae} [13]. Clearance from beyond the ciliated airways is dominated by slow, macrophage-mediated clearance [14] and so fibres which deposit there have the potential to contribute most to build-up of dose. Length impacts little on D_{ae} for thin fibres [15] except when length is sufficient to cause interception, a mechanism of particle deposition that is confined to fibres, involving the centre of gravity of the fibre following the airstream at a bifurcation whilst the tip of the fibre makes contact with the wall, resulting in deposition. The penetration of long fibres (>50 μm) beyond the ciliated airways is explicable on the basis that the aerodynamic diameter of a straight fibre is around 3 times its actual diameter [15]. This results from its alignment with the airflow as the fibres move aerodynamically through these tubes, aligned along the axis of the bronchial tree.

The evidence demonstrating that length is a key factor in pathogenicity of fibres comes from a number of sources but the best data are from experimental toxicological studies where it is possible to isolate length categories and assess their effects, unlike the mixed nature of human exposures. In the seventies Stanton carried out a large number of studies aimed at understanding the role of fibre characteristics in mesothelioma using implantation of fibres in gelatin, directly onto the pleural mesothelial surface. Although this is a highly artificial exposure, in a summary of these studies [16] Stanton identified that carcinogenicity was related to 'durable' fibres longer than 10 μm. In the study by Davis *et al.* [17] rats were exposed in a chamber to clouds with equal airborne mass concentration of either long amosite asbestos fibre or a short fibre amosite sample obtained from it by ball-milling. After lifetime exposure there was substantial tumour and fibrosis response in those rats exposed to the long amosite and but virtually no response in rats exposed to the short amosite. Adamson *et al.* used long and short crocidolite and following deposition in mouse lungs reported fibrosis [18] and proliferative responses [19] at the pleura with the long, but not the short samples. The mouse peritoneal cavity has been used as a model of direct mesothelial exposure and much greater toxic [20], inflammatory [21] and granuloma-generating [4] responses were evident in mice that were exposed to high doses of long fibres than was seen with shorter fibres. *In vitro* systems have also demonstrated the greater potency of long compared to short fibres in assays of pro-inflammatory and genotoxic activity [22-27].

Biopersistence and length interact in determining the clearance of long fibres from the lungs since long fibres may undergo dissolution which could result in complete dissolution, or most likely weakening of the fibre such that it undergoes breakage into shorter fibres, which can be more rapidly cleared than long fibres. The retention half-time ($T_{1/2}$) of a compact, inert, respirable, tracer particle, or a short fibre, in the respiratory tract of a rat is commonly ~60 days [28]. However long fibres (> 20 μm) are more slowly cleared as they cannot be easily enclosed by macrophages [29] leading to frustrated phagocytosis (see below). Thus long fibres are more likely to accumulate in the lungs allowing the long fibre dose to build up. Long fibres that are composed of bio-soluble (non-biopersistent) structural components can undergo weakening and breakage in the lungs [30]. The knowledge described above lead to the evolution of the fibre pathogenicity paradigm show in Figure 1 highlighting that a pathogenic fibre is one that is long, thin and biopersistent.

Carbon nanotubes and the classical fibre pathogenicity paradigm

Carbon nanotubes (CNT) are one of the most important products of nanotechnology, representing significant investment and are already incorporated into a large number of products and this is likely to increase. However, the essentially fibrous structure of CNT has lead to concern that they might cause asbestos-like pathology in the lung and mesothelium [2,31]. Carbon nanotubes can exist as compact tangles of nanotubes that are essentially particles, or as longer, straighter 'fibres' and we would anticipate that the hazard from these two different forms of carbon nanotube would differ. Particle effects would be confined to the lungs as fibrosis and cancer whilst fibres, exemplified by asbestos, are known have the same types of pulmonary effect but to also affect the pleura. We previously carried out a study where we exposed the peritoneal mesothelium, as a convenient model for the pleural mesothelium, to carbon nanotubes to determine whether they showed an asbestos-like, length-dependent toxicity [2]. These studies revealed that carbon nanotubes in the form of long fibres showed a similar, or greater, propensity to produce inflammation and fibrosis in the peritoneal cavity, to that produced by long asbestos. In contrast neither short asbestos fibres nor short, tangled CNT caused any significant inflammation. One important underlying process in the toxicity of long fibres is the failure of the macrophage to completely enclose them- termed incomplete or 'frustrated' phagocytosis, which is a pro-inflammatory condition. Long carbon nanotubes very likely cause inflammation via this process when long enough, i.e. longer than about 15 μm [2]. Frustrated phagocytosis of long fibres as it likely applies to asbestos and carbon nanotubes is illustrated in Figures 2 and 3.

In terms of the fibre pathogenicity paradigm, it is possible for carbon nanotubes to be pathogenic by being

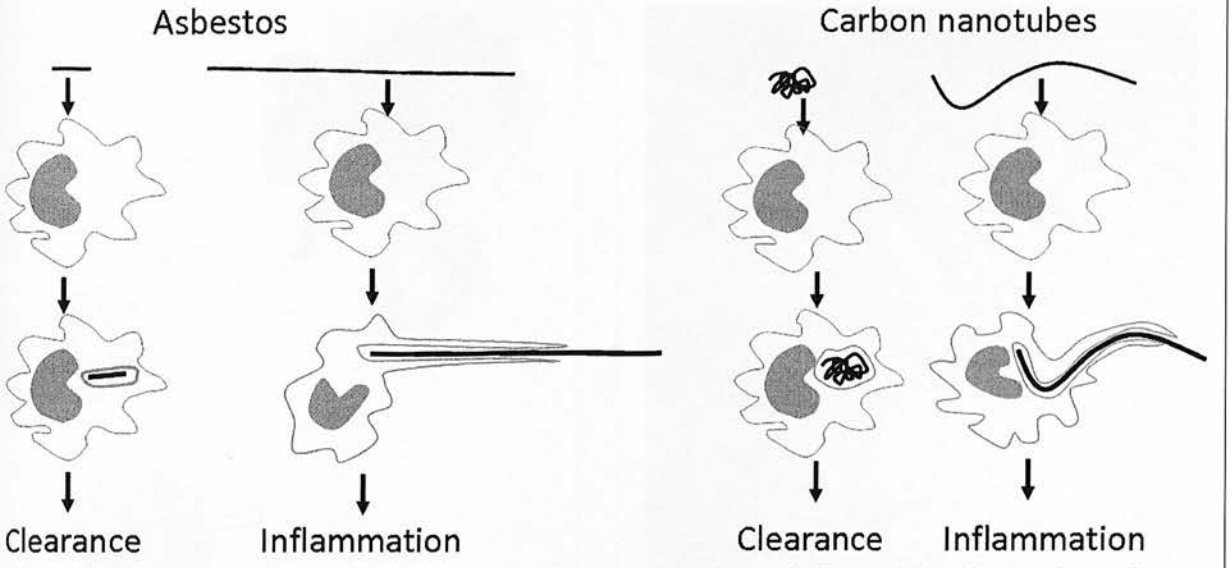

Figure 2 The frustrated phagocytosis paradigm as it relates to long and short fibres of asbestos (left) and various forms of carbon nanotubes (right). When confronted by short asbestos fibres or tangled, compact carbon nanotube 'particles' the macrophage can enclose them and clear them. However the macrophage cannot extend itself sufficiently to enclose long asbestos or long nanotubes, resulting in incomplete or frustrated phagocytosis, which leads to inflammation.

thin, long and biopersistent but unlike other fibres it is also possible for CNT to exist in forms that do not comply with the paradigm for a pathogenic fibre. For example CNT can exist as short forms, and longer but tangled forms (see right side of Figure 2), neither of which would pose a problem to macrophages in terms of phagocytosis or clearance. Whilst singlet nanotubes are always thin they form tangles, ropes and wires of intertwined tubes and these can be thicker, although still likely to be thin enough to be respirable. However, in larger tangles and bundles the aerodynamic diameter may well increase beyond respirability. Graphene, the basic structural component of CNT is an exceedingly strong material [31] and so is likely to be biopersistent when the graphene is pristine, with few defects and underivatised, and that is suggested by our own data (in preparation). However CNT derivatised by some chemistries, with increased amounts of defects in the graphene structure, may be less biopersistent.

Injection of fibres into the peritoneal cavity as a surrogate for fibre effects in the pleural cavity: the role of retention of long fibres in the peritoneal cavity in long fibre-induced inflammogenicity and fibrogenicity

The peritoneal cavity and its viscera are covered by a mesothelium and this was recognised as a convenient surrogate for the pleural cavity mesothelium in fibre studies over 30 years ago. Subsequently asbestos fibres were found to produce inflammation [21] and mesotheliomas [32] in the peritoneal cavity following injection. Although the peritoneal cavity would not be expected to have evolved the efficient clearance mechanisms shown by the lungs, in fact it does have a system for removing particles. Instilled particles are rapidly drawn cranially in the lymph flow through the diaphragm to the parathymic lymph nodes [33]. This involves transit through the diaphragm via stomata which are pore like structures less than 10 μm in diameter (Figure 4) linking the peritoneal cavity to the underlying lymphatic capillaries and which were implicated in fibre effects by Kane and co-workers in 1987 [4].

Kane and co-workers [3] noted that long asbestos fibres accumulated preferentially at the peritoneal face of the diaphragm around the stomata since they could not be cleared through them due to their length. Kane *et al.* contended that retention of long fibres at the diaphragmatic mesothelial surface initiated inflammation, proliferation and granuloma formation. Short fibres did not cause this effect, easily exiting through the stomata. However, if short fibre were injected at such high dose that their sheer volume blocked the stomata this prevented clearance allowing retention, resulting in inflammation [3]. We confirmed that low dose exposure of the mouse peritoneal cavity to long multi walled carbon nanotubes (MWCNT) [34] resulted in accumulation of the long CNT at the diaphragm, suggesting that they are also too long or bulky to exit through the stomata. Retention of the long CNT in the peritoneal cavity

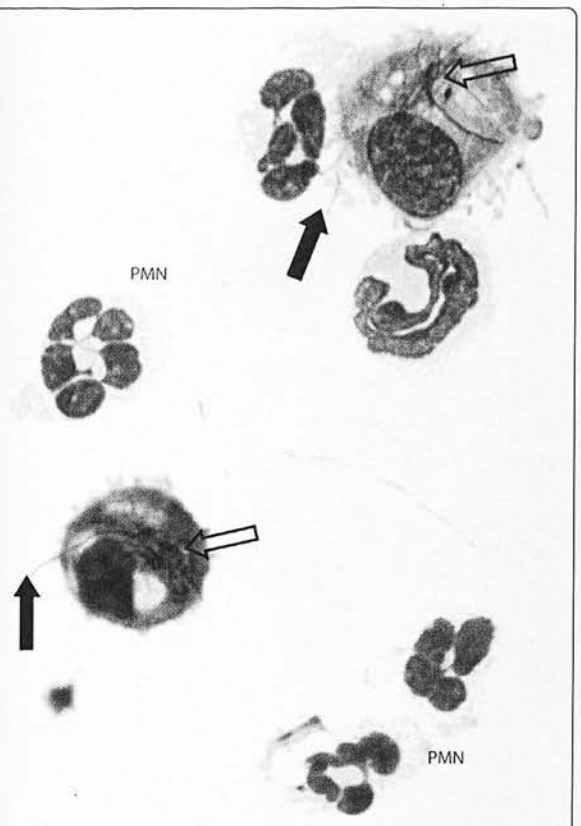

Figure 3 Frustrated phagocytosis (arrows) and the associated acute inflammatory reaction in the bronchoalveolar lavage of mice whose lungs have been instilled with long nanotubes. Aspiration of 50 μg of long fibrous multi-walled carbon nanotubes (CNT) into the lungs of C57BL/6 mice caused an acute inflammatory reaction at 24 hrs typified by a large influx of inflammatory neutrophils (PMN) into the bronchoalveolar lavage. CNT bundles and singlet fibres were seen both within macrophages (hollow arrow) and extending outside the macrophage in the process of incomplete or frustrated phagocytosis (black arrows). All images at taken at ×1000 magnification.

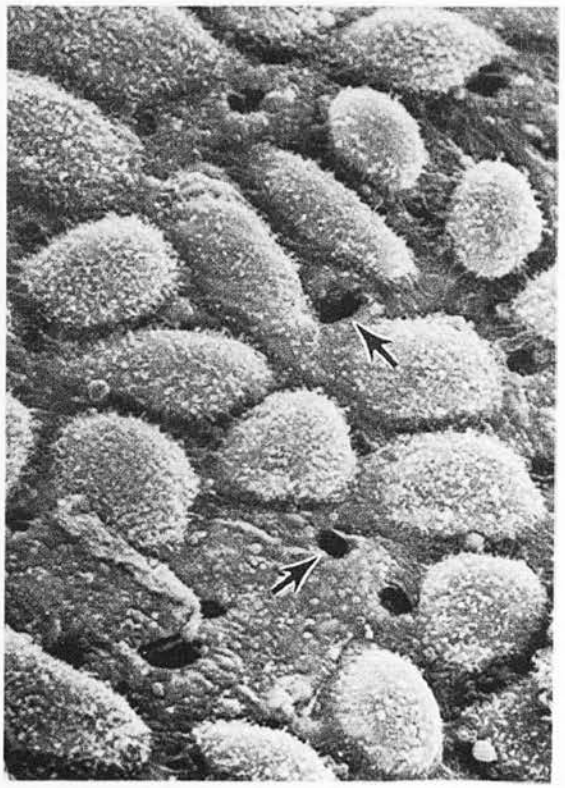

Figure 4 SEM of the surface of the peritoneal face of the diaphragm of a mouse showing the stomata (arrows) reproduced with permission from Moalli et al [4].

initiated granulomas with classical foreign body giant cells in the peritoneal lavage (Figure 5) and in the granulomas (Figure 6) [2]. Short, tangled CNT were not retained and were never seen at the diaphragm or viscera and did not induce inflammation or granuloma formation, their absence from sections strongly suggesting that were cleared through the stomata.

Therefore, we would postulate that there are two important parts to the mechanism of the pro-inflammatory effects of long fibres in the peritoneal cavity, shared by both asbestos and long MWCNT

i) failure of long fibres to negotiate the diaphragmatic stomata with subsequent retention of the long fibre dose at the diaphragm; this contrasts with smaller particles which easily leave the peritoneal cavity through the diaphragmatic stomata to accumulate in the parathymic nodes [33],

ii) at the point where the long fibre dose accumulates at the peritoneal face of the diaphragm macrophages attempt to phagocytose the long fibres; they then undergo frustrated phagocytosis stimulating inflammation and mesothelial cell damage, leading to chronic inflammation and granuloma development [2].

The consequences of pro-inflammatory and fibrogenic effect of long fibre retention at the diaphragm were most evident in the extent of the granuloma/fibrosis response seen 6 months following instillation of 10 μg of long or short nanotubes (see [2] for a full description of the NT tang 2 and NT long 1 nanotubes used in this study). As Figure 6 shows, the presence of quite a large aggregate of short/tangled nanotubes produced very little tissue reaction (Figure 6A and 6B). In contrast, loose aggregates and singlet fibres of long nanotubes caused a florid granuloma response (Figure 6C and 6D). The multi-layered basketwork -like arrangement of largely acellular collagen in the granuloma is strongly reminiscent of the structure of an asbestos-induced pleural plaque (see later).

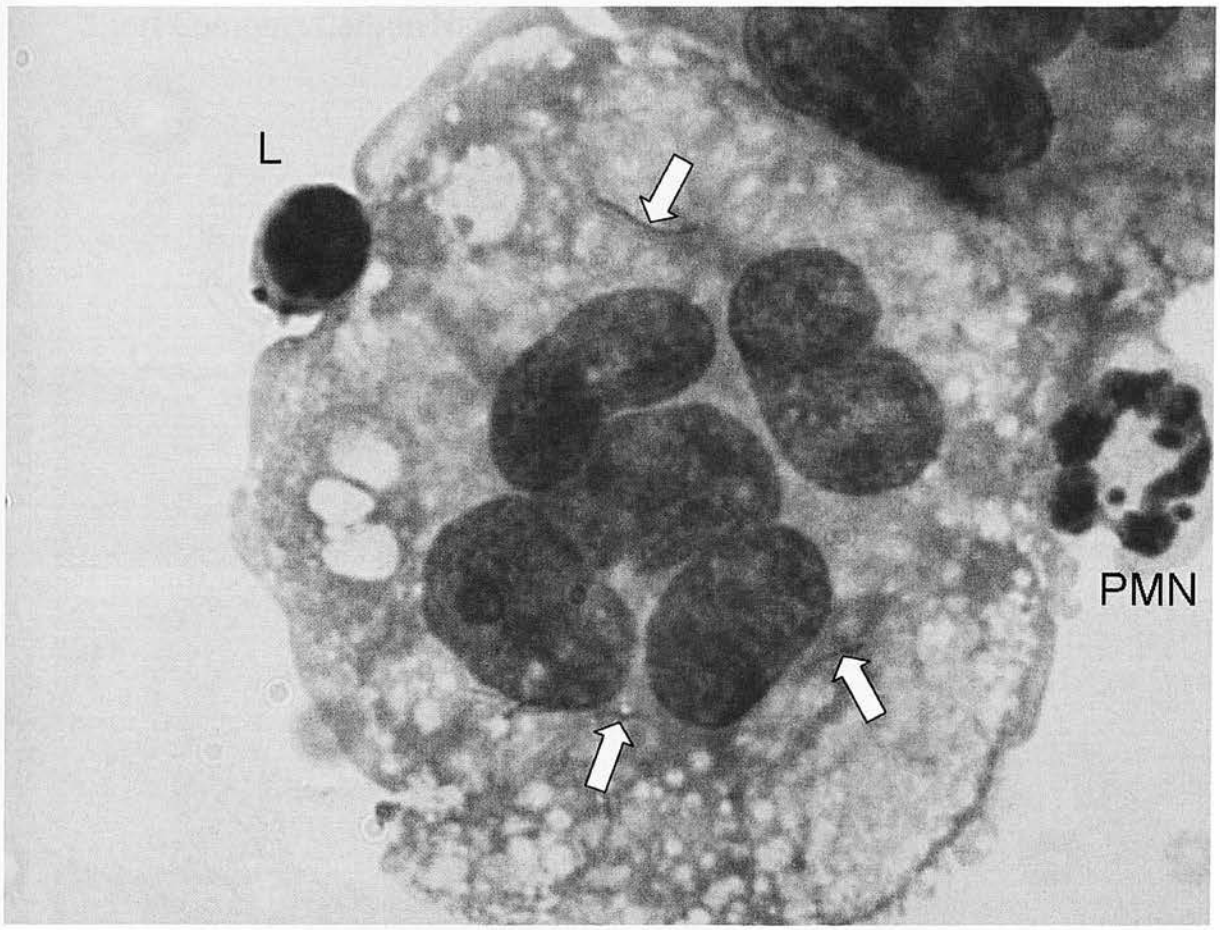

Figure 5 Multinucleate giant cell lavaged from the peritoneal cavity of a mouse instilled with long carbon nanotubes. CNT are visible in the cytoplasm (arrows); PMN = Poymorphonuclear Neutrophilic Leukocyte; L = lymphocyte (Magnification ×100).

The issue of peritoneal mesothelioma arises and begs the question as to the extent of translocation of fibres from the pleural space to the peritoneal cavity. Little is known about this and it has never been quantified in man. The mere fact that far-and-away most mesotheliomas arise in the pleural cavity suggests that long fibres are retained there, so short fibres can reach the peritoneal cavity but, by virtue of their low pathogenicity, generally do not cause much harm there.

Pleural structure and function

Although the peritoneal cavity serves as a convenient model to study mesothelial impacts of fibres, the primary mesothelial target for inhaled fibres is the pleural mesothelium. The chest cavity, or pleural cavity is the cavity that surrounds the lungs and heart, comprising the ribs and associated muscles and connective tissue. This cavity is covered by the parietal pleura, which is attached to the chest wall and is covered by a continuous 'parietal' mesothelial cell layer. The lungs themselves are enclosed by the visceral pleura which is integral to the lung surface and which has a surface 'visceral' mesothelial layer. The tight fit of the lungs to the inside of the chest wall means that the two mesothelial layers are closely apposed and there is a thin space between them that contains the pleural fluid (Figure 7) and also a population of pleural macrophages.

The visceral and parietal mesothelium are both composed of a single layer of mesothelial cells, a basal lamina of connective tissue and a loose connective tissue layer with blood and lymph vessels. Mesothelial cells have several functions in normal pleural action [35]. Pleural fluid is constantly produced by hydrostatic pressure from the sub-pleural capillaries [35], supplemented by glycoproteins secreted by the mesothelial cells [36]. The pleural fluid and its constant outflow (see below) maintains tight coupling of the lungs to the chest wall, allowing diaphragmatic muscle contraction and relaxation to expand and passively relax the lungs during breathing movements. The pleural space is a narrow,

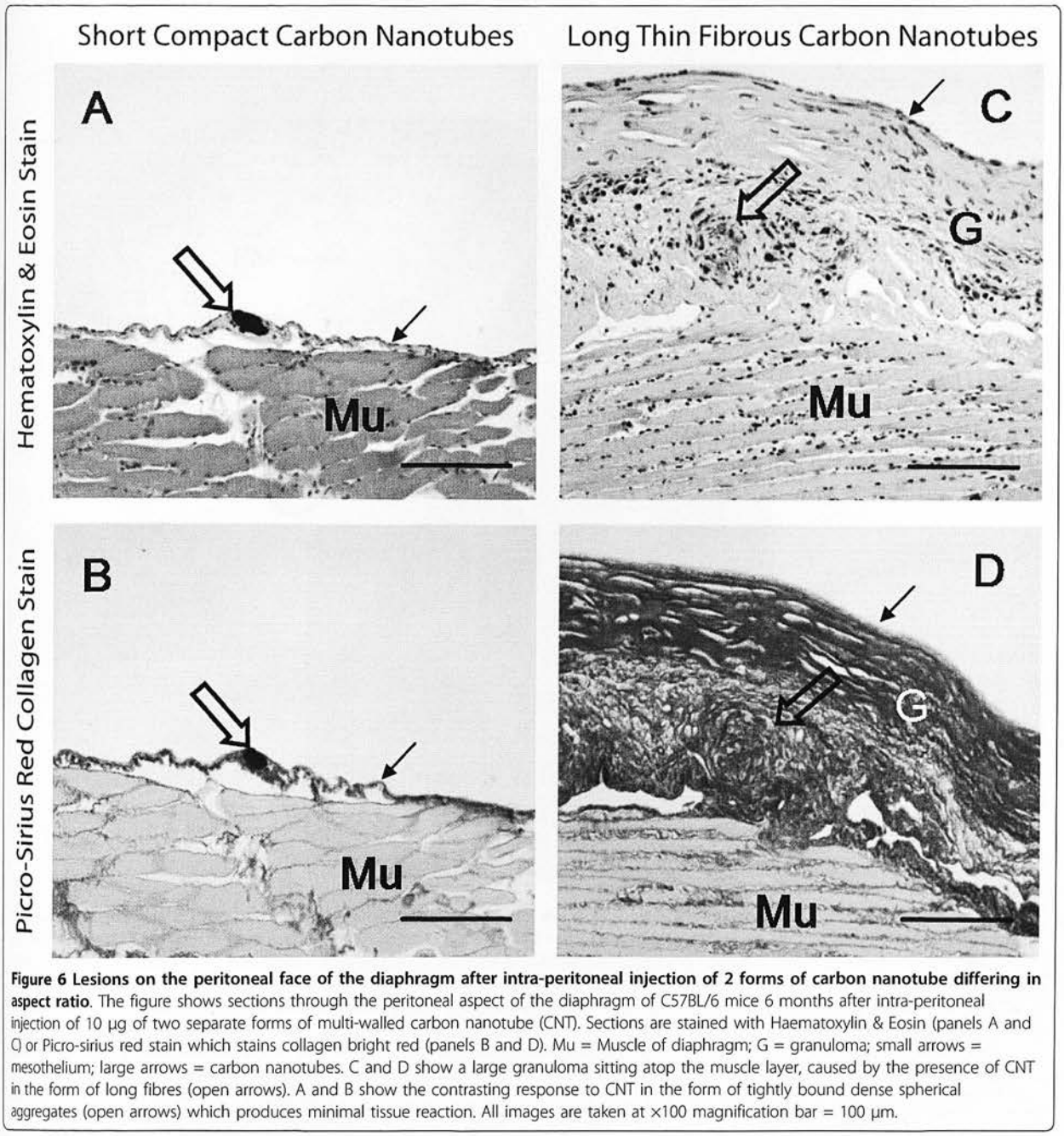

Figure 6 Lesions on the peritoneal face of the diaphragm after intra-peritoneal injection of 2 forms of carbon nanotube differing in aspect ratio. The figure shows sections through the peritoneal aspect of the diaphragm of C57BL/6 mice 6 months after intra-peritoneal injection of 10 μg of two separate forms of multi-walled carbon nanotube (CNT). Sections are stained with Haematoxylin & Eosin (panels A and C) or Picro-sirius red stain which stains collagen bright red (panels B and D). Mu = Muscle of diaphragm; G = granuloma; small arrows = mesothelium; large arrows = carbon nanotubes. C and D show a large granuloma sitting atop the muscle layer, caused by the presence of CNT in the form of long fibres (open arrows). A and B show the contrasting response to CNT in the form of tightly bound dense spherical aggregates (open arrows) which produces minimal tissue reaction. All images are taken at ×100 magnification bar = 100 μm.

variable space, that is up to 20 μm or so in sheep rapidly fixed at death and presumed to be similar in size in humans [35]. The pleural fluid turns over rapidly [37], continuously exiting through stomata in the parietal (not the visceral) pleura via lymphatic capillaries; these stomatal openings on the parietal pleural surface are between 3 and 10 μm in diameter (Figure 8). They are often found in association with 'milky spots', large accumulations of leukocytes present on the parietal pleura [38] and presumed to be involved in immune activity in the pleural space. The pleural fluid outflow through these stomata drains to the lung lymph nodes in the region of the mediastinum and this pathway is important in the clearance of particles and fibres that reach the pleural space (see below). The drainage of fluid from the pleural space carries particles in the lymph to the hilar lymph nodes, mediastinal lymph nodes, parasternal lymph nodes and posterior mediastinal lymphoid tissue [39]. The stomata are most densely situated in the most caudal and posterior intercostal

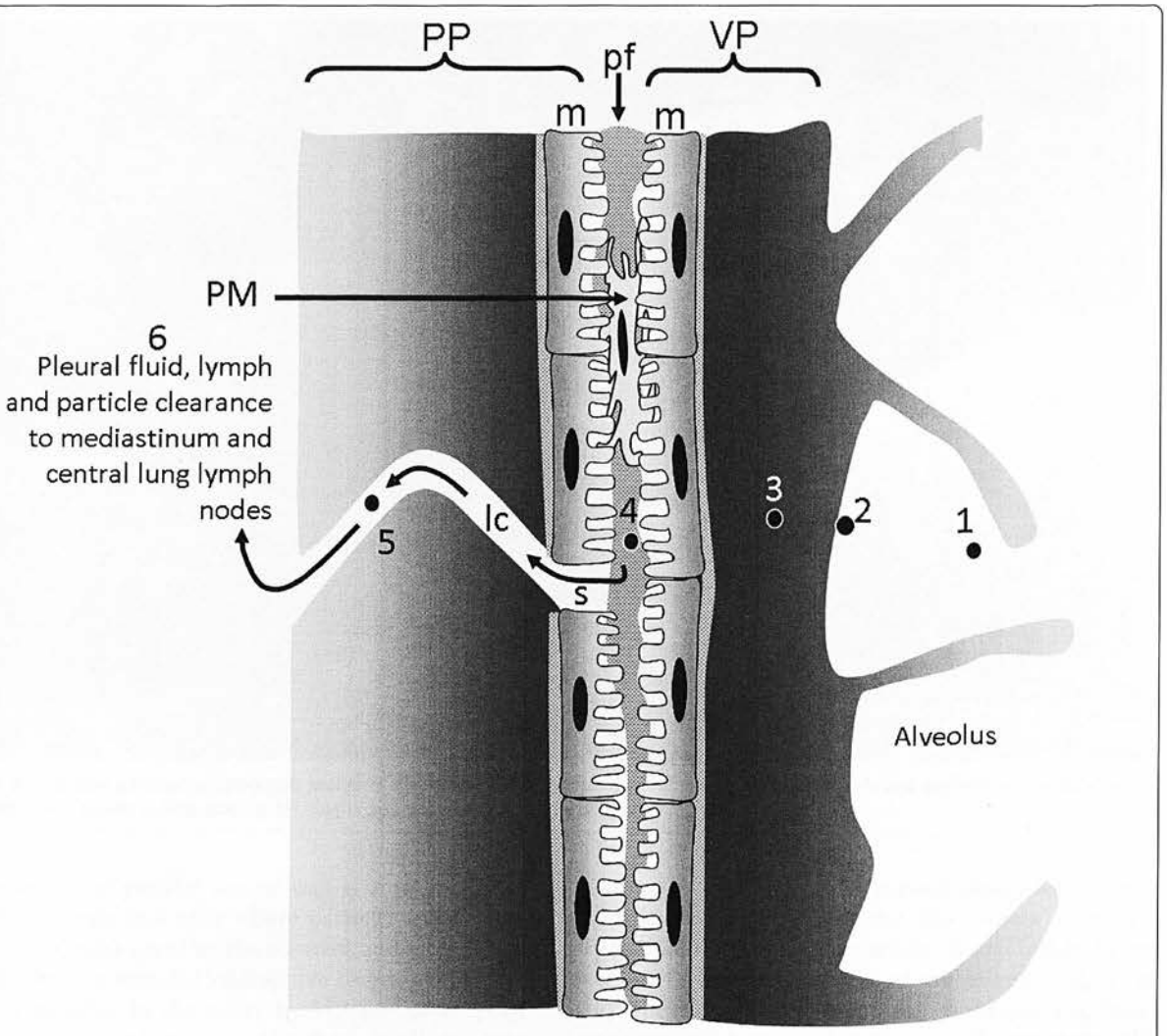

Figure 7 Diagrammatic representation of the relationship between the visceral and parietal pleurae. The visceral pleura (VP) and the parietal pleura (PP) are seen in close apposition separated by a pleural space that contains a small volume of pleural fluid (pf). Contact between the 2 pleurae is made via the mesothelial cell layers (m) on the surface of the parietal and visceral pleurae. Pleural macrophages (PM) are present in the pleural space. The rigid chest wall is tightly locked to the lungs by the adherence of the visceral pleura to the parietal pleura allowing movements of the chest wall caused by the action of the diaphragmatic muscle and intercostal muscle (IM) to expand and relax the lungs, allowing pulmonary inspiration and expiration. The pathway for particles to reach the pleural space is unknown but the path for an airborne particle (1) that deposits in the distal alveoli (2) is shown as it passes into the interstitium (3) enters the pleural space (4) and exits through a stoma in the parietal pleura (s) into a lymphatic capillary (lc, 5) to enter the lymph flow to the lymph nodes in the mediastinum and central lung.

spaces although and are more lightly scattered in more cranial and anterior intercostal regions [40].

A fraction of all deposited particles transit through the pleura, exit via the stomata and form 'black spots' around the stomata

Applying the classical dose/response toxicology paradigm to the unique pleural pathology seen with asbestos and other fibre exposures, it may be assumed that since the response occurs at the pleura, the dose must be applied at the pleura. It might be argued therefore that since fibres produce pleural pathology whilst particles do not, fibres must reach the pleura and particles must not. However, a body of literature exists to the effect that in fact a proportion of **all** deposited particles reach the pleura, pass through the pleural space and exit through the stomata. In the process of this they elicit range of low to higher grade responses there in the form of parietal pleural 'black spots'.

Evidence that all particles pass through the pleura comes from a substantial literature concerning the almost universal existence of these "black spots",

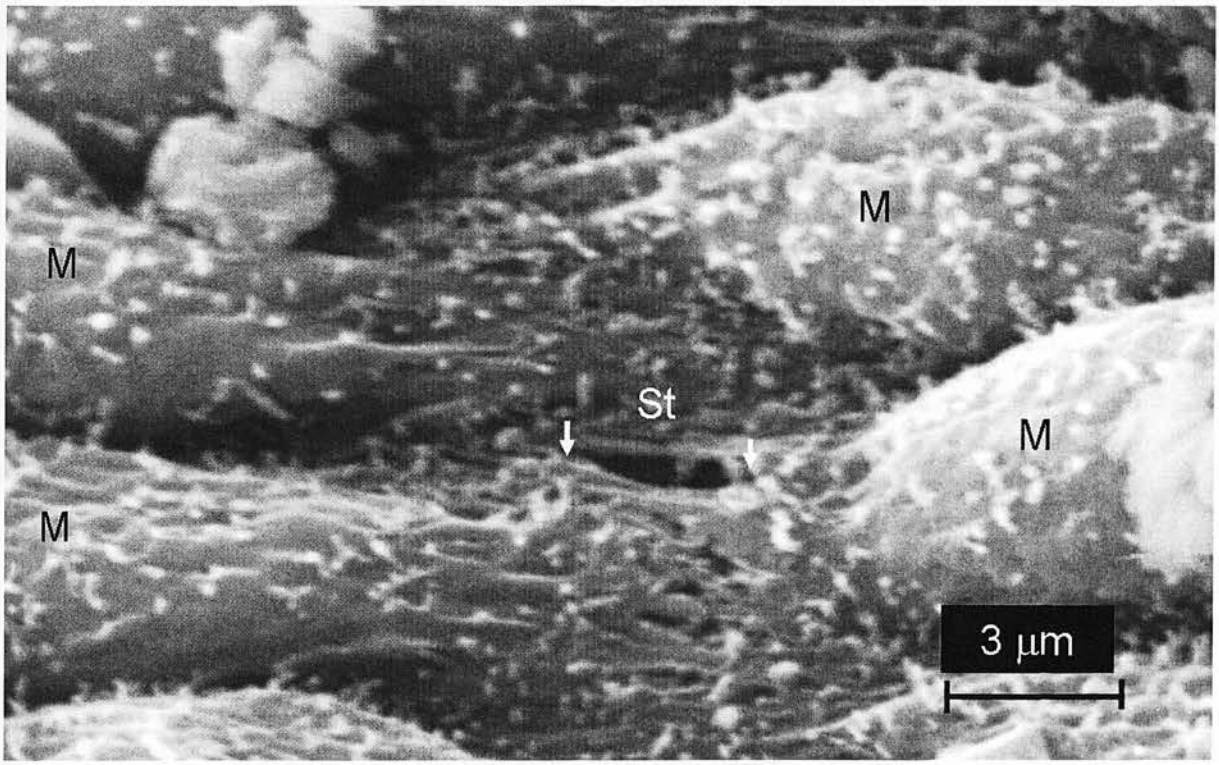

Figure 8 Scanning electron micrograph image of chest wall from a normal rat showing the parietal pleural surface with mesothelial cells (M) and a stoma (white arrows, St) that is approximately 3 μm in diameter.

observable on the parietal pleural wall at autopsy. These mark the stomata and arise where particles must focus to exit the pleural space at the stomata and where they enter the sub-mesothelial connective tissue around the stomatal mouths. In the study by Mitchev *et al.* [41], 150 consecutive necropsies of urban dwellers were examined in Belgium. Of the 96 male and 54 female necropsies, whose age ranged from 22-93 years, black spots were almost invariably seen (>90% of autopsies) on the parietal pleura. The authors noted that their location appeared to be related to the structures responsible for the lymphatic drainage of the pleural cavity and they considered these to mark the points of pleural fluid resorption. Black spots were also present on the pleural face of the diaphragm, suggesting that there is pleural fluid outflow in a caudal direction. The black spots in the Mitchev study of normal individuals at autopsy clearly reflects that deposited soot particles normally pass through the pleura some of them accumulating in the parietal pleural wall forming black spots. The black spots contain particles and elicit a tissue response which is a low grade in city dwellers, where there is accumulation of dust-laden macrophages and lymphocytes. In coal miners, however, with their large exposures to particles, the mixed dust particles trigger a higher-grade inflammatory reaction of the parietal pleura with concomitant low grade fibrosis in the 'black spots' which are very pronounced [42]. Occasionally pleural inflammatory reactions to interstitialisation of the mixed dust at the black spots are more pronounced, producing more severe granulomatous structures with concentrically arranged collagen fibres [42]. In one study [42], 12 patients with black spots (8 at autopsy and 4 surgically) who were largely miners, had their black spots removed and sectioned for histological purposes. As might be expected with such high dust exposure, the black spots were extremely well-demarcated and followed the lines of lymph flow across and through the parietal pleura.

The most severe and frequently-documented example of pleural response to dust is asbestos pleural plaques. Pleural plaques are commonly seen in asbestos-exposed individuals occurring only on the parietal pleura and diaphragm as discrete, raised, irregularly shaped areas a few millimetres to 10 centimetres in size, having a greyish to ivory white colour depending on their thickness [43]. It is important to note that pleural plaques occur in greatest profusion in exactly the sites where the stomata are in greatest profusion i.e. pleural plaques are '...most commonly found on the posterior wall of the lower half of the pleural spaces, those in the intercostal

space tended to have an elliptical shape and ran parallel to the ribs above and below...'. On histological section plaques can be seen to be composed of dense bands or weaves of avascular and largely acellular collagen, with only the occasional fibroblast nucleus to be seen; they are sometimes calcified [44]. These collagenous plaques, whilst commonly seen in association with asbestos exposure are not unique to it, being found following pleural infection or trauma and so can be presumed to be the way that the pleura reacts to injury [44].

Thus there is clear evidence that a proportion of all deposited particles, most commonly urban particulate matter, reach the parietal pleura where they may interstitialise around the stomata and elicit responses. The severity of the response is dependent on the intrinsic toxicity of the dust, with increasing levels of inflammatory/fibrotic response as follows:- soot < mixed mineral dust < short asbestos. The benign nature of asbestos pleural plaque-type responses is evident in the lack of reports of mesothelioma in city dwellers or coalminers despite the prevalence of black spots in these populations and the notable lack of asbestos pleural plaque progression to malignancy [45]. Since normal asbestos pleural plaques are benign and not pre-cancerous, we hypothesise that pleural plaques are a special case of a 'black' spot caused by short asbestos fibres which elicit an unusually florid collagenous response, or as a result of a very high dose of short fibres reaching the peri-stomatal wall. The emphasis on shortness here is important since the key feature of black spots, we contend, is that the particles and short fibres are small enough to negotiate the stomatal openings where they mostly clear to the lymph nodes whilst some interstitialise into the sub-mesothelial interstitium through the proximal lymphatic capillary walls. As described below, this contrasts with events that may occur with long fibres; these cannot negotiate the stomata leading to retention at the stomatal openings, initiating a very different pathobiological sequence of events culminating in a different pathological outcome.

Our knowledge regarding the pathway by which particles reach the pleura from the lung parenchyma is well summed up in a recent review '... How asbestos fibres that have impacted the airway wall migrate to the pleural surface ..... is quite obscure. ..' [1]. Lymphatic flow from the parenchyma to the pleural space is one obvious possibility [46] but such a pathway, if it exists, is not well-documented [1]. A fluid dynamics model of fibre translocation highlights two possible pathways [47], the first of these being by normal lymph flow centrally to the mediastinum and then into the blood via the thoracic duct followed by extra-vasation in the pleural capillaries during the formation of pleural fluid. This rather tortuous route disregards the filtering role of the lymph nodes and seems to us to be intuitively unlikely. The second route requires inflammation in the parenchyma, caused by the fibres, to reverse both the normal flow of lymph and the normal trans-pleural pressure, resulting in a net flow of fluid and fibres directly into the pleural space from the underlying parenchyma [47]. This latter process cannot be the explanation for normal transit of particles to the pleura that gives rise to black spots (see above) in normal people, who have no pulmonary inflammation. Therefore, even if such an inflammation-dependent pathway exists, a pathway that is independent of inflammation clearly operates for compact particles in normal people. Further research is needed to establish the mechanism of transport of fibres to the pleural space.

Long fibre retention at the stomata of the parietal pleura

So from the above there is good evidence to support the contention that a fraction of all deposited particles reach the pleura by an obscure pathway and that short fibres and compact particles leave the pleura through the stomatal openings. Most of the particles are transported to lymph nodes and some enter the interstitium at the mouth of the stoma to form a 'black spot' or equivalent. Long fibres that reach the pleural space, however are an exception to this, since they have the potential to physically block the stomata due to their difficulty in negotiating the bend into the stoma which would result in interception of the ends of the fibre with the walls of the stomatal openings and with the lymph vessels walls themselves. This is likely to lead to mesothelial and endothelial cell damage at this site, inflammation and the accumulation of pleural macrophages attempting to phagocytose these retained fibres. The macrophages are likely to undergo frustrated phagocytosis in attempting to enclose the long fibres and so release cytokines and oxidants. This would lead to further inflammation, fibrosis and genotoxicity in the bystander mesothelial cells in these areas of congestion around the stomatal entrances. Direct interaction between retained long fibres and mesothelial cells around the stomata could also result in direct genotoxicity. Eventually some stomata are likely to be entirely blocked by cells and fibres. Figure 9 demonstrates diagrammatically the difference between formation of black spots and pleural plaques with particles and short fibres (A), compared to the response to long fibre retention at parietal stomata (B).

This means that that the primary lesion caused by long fibres must form at the parietal pleura, the site of retention of long fibre dose and therefore the site of response. Mesothelioma would therefore originate not at the visceral pleura but at the parietal pleura. There is

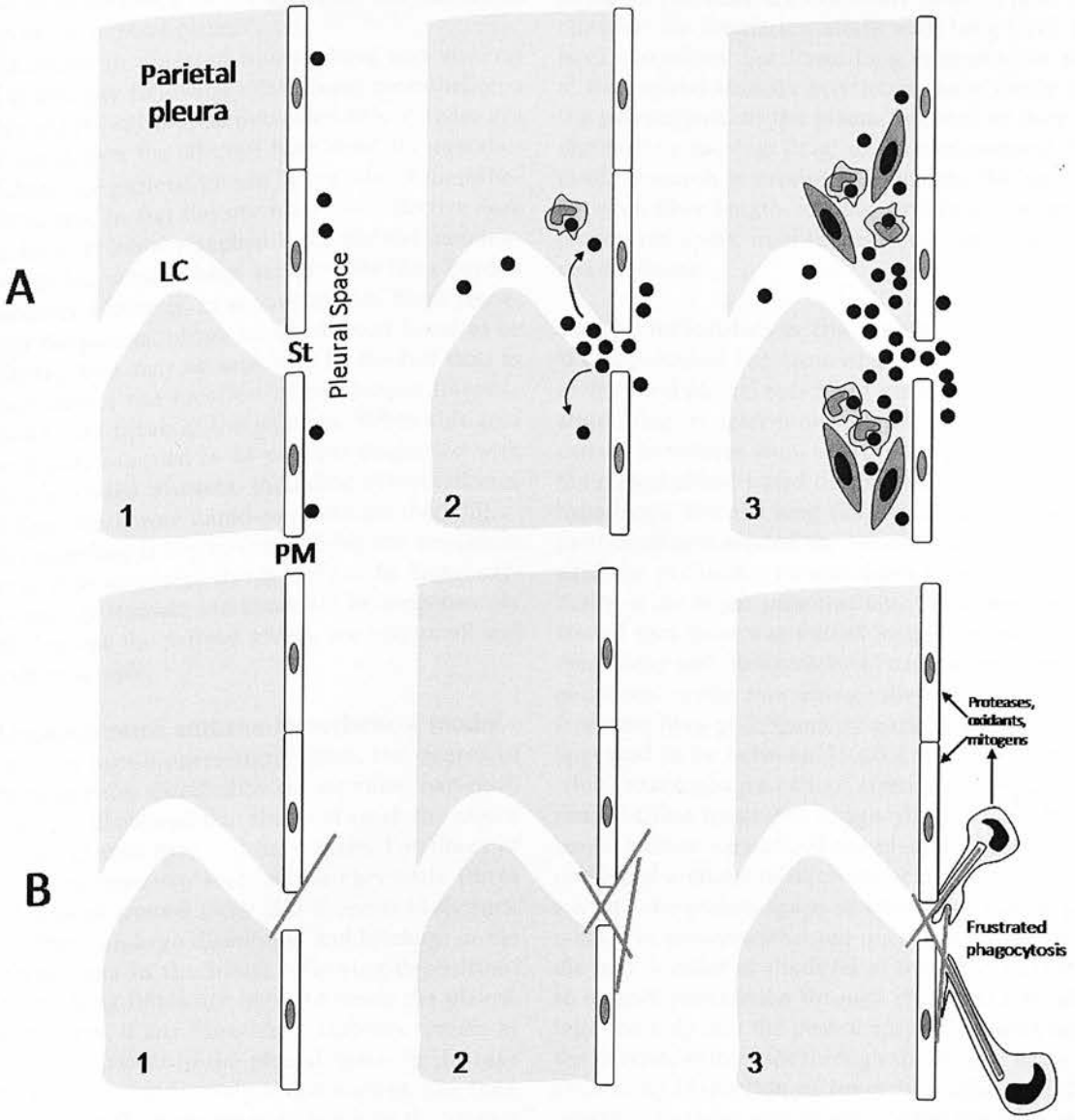

Figure 9 A) diagram showing the events leading up to formation of black spots. A1) particles enter the pleural space; A2) in focusing to exit via the stoma (St) some particles interstitialise through the loose lymphatic capillary endothelium and macrophages begin to accumulate in response; A3) macrophages and particles form a mature 'black spot' with mesenchymal cell activation and proliferation depending on the toxicity and dose of the particle. B) In B1 a single long fibre is intercepted as it attempts to negotiate the stomatal opening and is retained; 2) other fibres are caught up and there is an accumulation of retained long fibres; 3) macrophages attempt to phagocytose the fibres and undergo frustrated phagocytosis releasing a range of pro-inflammatory, genotoxic and mitogenic mediators close to the pleural mesothelial cells. PM = pleural mesothelium; St = stoma; LC = lymph capillary.

good evidence to suggest that this is indeed the case, and numerous studies using thoracoscopy have confirmed that the origin of mesothelioma is the parietal pleura [6]. This is reflected in the staging of mesothelioma which recognises that early mesothelioma is confined to the parietal pleura, while more advanced mesothelioma involves the visceral pleura [48]. Indeed, the prognosis for mesothelioma when it only involves the parietal pleura is much better by around 30 months, than the prognosis arising when mesothelioma involves visceral pleura [6]. This reflects the earliness of the disease stage when it is still confined to the parietal pleura. From a toxicological viewpoint this means that the focus of attention in trying to determine whether any fibre is likely to cause mesothelioma should not be focussed on the question 'Do fibres reach the pleura?'

but should be focussed on the question 'Are the fibres retained in the parietal pleura?'.

Fibres found in digested human lung and visceral pleura at autopsy following death from mesothelioma are often short [49] but, as described below, these are not the site to seek the effective fibre 'dose' for mesothelioma, since the parietal pleura is the site of mesothelioma initiation. In fact the site where the effective dose for long fibres is initially applied is the parietal mesothelium, which has seldom been sampled for fibre burden or dimensions. However, in several studies, fibres recovered from the parietal pleura have also been found to be short [50,51]. This may be explained by the fact that, as described above, the location of the longer fibres is likely to be very focal, at the stomata. When this area was specifically sampled in 14 patients diagnosed with asbestos-associated diseases, including mesothelioma, much longer fibres were found concentrated there [5].

Correct sampling is key to determining the important measure of dose and since this is likely to be found only in 'hot-spots' at stomata but these are heterogeneously distributed across the parietal pleura, are very small and so difficult to sample.

Fibre biopersistence and the hypothetical model

In the case of non-biopersistent fibres, the degree of their biopersistence, specified by the retention half-time, will dictate the likelihood that they will reach the pleura and the impact that they will have there. For fibres of very low biopersistence such as the chrysotile fibres with half-lives of around 1 day [52] it seems likely such chrysotile fibres undergo dissolution and breakage in the lung parenchyma in the hours following deposition, such that no long fibres are likely to reach the pleura; only short fibres, if any fibre-like structures remain at all, are likely to transit to the pleural space. In the case of fibres that are moderately biopersistent, the long fibres may retain their structure en route to the pleural space, all the while undergoing dissolution/breakage. If long fibres are sufficiently biopersistent to retain their fibrous structure long enough to enter the pleural space they may be retained at the parietal stomata, initiating frustrated phagocytosis and granuloma formation. Depending on the extent of their biopersistence, however, fibres could still dissolve and break within the macrophages as a result of the high pH within the phagolysosomes, allowing the granuloma to resolve. The exact tempo of translocation of particles and fibres to the pleural space is unknown, but in less than 1 day following inhalation of short, essentially particulate, CNT in mice, the CNT were evident in the sub-pleural extracellular matrix [53]. This suggests that compact particles or very short HARN may reach the pleural space rapidly following deposition; however such short HARN and compact particles are not likely to be retained at the stomata. No inhalation study with long CNT has yet been carried out but fibres long enough to be retained at the parietal stomata may move more slowly through the parenchyma, to the pleura, because of their greater dimensions causing 'drag' to their movement through fluid. Research is needed to elucidate the relationship between fibre length and biopersistence in leading to pleural transport, mesothelial injury, inflammation and mesothelioma.

Carbon nanotubes in the pleura

We approached the issue of the potential mesothelial toxicity and pleural toxicity of carbon nanotubes by first attempting to determine whether, similar to asbestos, carbon nanotubes showed length-dependent toxicity to the mesothelium. Based on the above argument we also hypothesise that the long CNT would be retained at the parietal pleural around the stomata. In early studies we used the peritoneal mesothelium lining the peritoneal cavity as the target mesothelium. These studies demonstrated that there was indeed length-dependent inflammogenicity and fibrogenicity of carbon nanotubes in the peritoneal cavity, mimicking asbestos [2]. As predicted from the fibre pathogenicity paradigm, the key length appeared to be between 15-20 μm, the length beyond which macrophages cannot stretch and enclose fibres, thus eliciting frustrated phagocytosis. In the follow up to the studies we utilised the pleural mesothelium and developed a model of injection of nanotubes and asbestos into the pleural space of mice. This can be affected quickly in non-anaesthetised mice using a very fine needle with a collar at the level of the bevel in the needle to restrict penetration through the chest wall allowing injection only into the pleural space. Following injection, the injectate distributes through the pleural space as was evident by inspection of lungs immediately following injection. In these studies we injected the same panel of fibres used in the peritoneal cavity in the Poland studies, i.e. long and short amosite asbestos samples, two long nanotubes samples and two short/tangled nanotubes samples and nanoparticulate carbon black as a graphene control. Following injection the pleural cavity was lavaged to determine the inflammatory response. We found clear evidence of length-related inflammation in the pleural space with both the long amosite and the two long nanotubes samples causing inflammation while all the other short samples failed to elicit significant inflammation (Figure 10).

In a time course, the long nanotubes caused a sustained high level of inflammation at 7 days, which was the same as was present at 1 day. This is in contrast to the events in the peritoneal space where there is a decline in inflammatory response over 7 days to levels

of about one-fifth present on day 1 by day 7. Based on our hypothesis that long fibres were retained at the parietal pleural and that short fibres were not, we used paraffin wax histology to examine the parietal pleural surfaces. In keeping with the hypothesis, long fibres which were visible on day 1 following injection were still visible in granulomas at the surface of the parietal pleura on day 7 (Figure 11). No short fibres were visible in sections of parietal pleura at 1 or 7 days, however the activated, thickened mesothelium seen at day 1 had returned to normal by day 7 suggesting that the short fibres had been cleared (Murphy, F., Poland, C. A., Ali-Boucetta, H., Al-Jamal K.T., Duffin, R., Nunes, A., Herrero, M-A., Mather, S. J., Bianco, A., Prato, M., Kostarelos, Donaldson, K. Long but not short nanotubes are retained in the pleural space initiating sustained mesothelial inflammation. Submitted for publication).

We therefore hypothesise that the retention of long fires at the stomatal openings on the parietal pleura, coupled with frustrated phagocytosis of pleural leukocytes that attempt to ingest them, produce a chronic pleural mesothelial inflammatory response. Chronic inflammation is known to be a driver for proliferation, genotoxicity, growth factor synthesis and release that are likely to culminate in pathology such as fibrosis, pleural effusion and mesothelioma (Figure 12).

Implications for testing of high aspect ratio nanoparticles (HARN)

The foregoing discussion has highlighted the importance of the parietal pleura as the target for the long fibre hazard following pulmonary deposition and the site of initiation of mesothelioma. In addition to carbon nanotubes, there are a whole new generation of high aspect ratio nanoparticles (HARN), such as nanorods and nanowires. These are made of a wide range of materials, including silica, silver, nickel and various forms of carbon. There is a need to test these materials and understand their potential for causing mesothelioma. Mesothelioma has a very long latent period and in rats, following inhalation of asbestos, mesothelioma commonly does not develop until near the end of life in a small proportion of animals. The peritoneal cavity has been used as a more efficient model for mesothelioma induction but has been criticised because of its non-physiological nature and irrelevance for risk assessment. However, the peritoneal cavity does show size-restricted clearance and subsequent sensitivity to retained long fibres. An appreciation of the role of the parietal pleura as the site where fibres are retained leading to pleural pathology of various sorts which accompany exposure to fibres, means that a rational testing strategy could attempt to identify early changes in this tissue following fibre exposure. New techniques that allow investigators to home in on specific areas, eg laser capture, would enable the areas of the parietal pleura where the stomatal openings occur to be identified and studied in detail for the presence of fibres and their molecular consequences. Thus there is the prospect of studying oxidative stress, inflammation and genotoxicity at an early stage in the very target tissue where mesothelioma is likely to arise. This should revolutionise the ability to screen for pathogenic fibres amongst emerging HARN and allow us to look anew at the effects of asbestos and more conventional fibres that affect the pleural mesothelium and we look forward to future studies that utilise this knowledge.

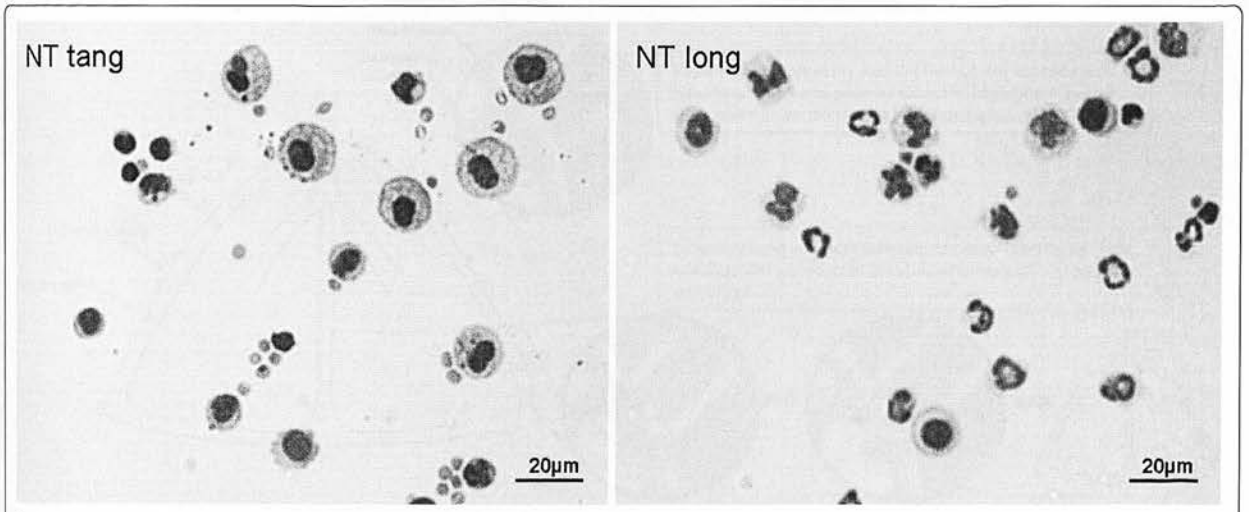

Figure 10 Cytospin preparations of pleural lavage cells from mice treated with short/tangled CNT (left) and long CNT (right). Arrows indicate granulocytes. Note PMN and eosinophils (arrows) indicative of inflammation in pleural leukocytes from rats exposed to the long NT only.

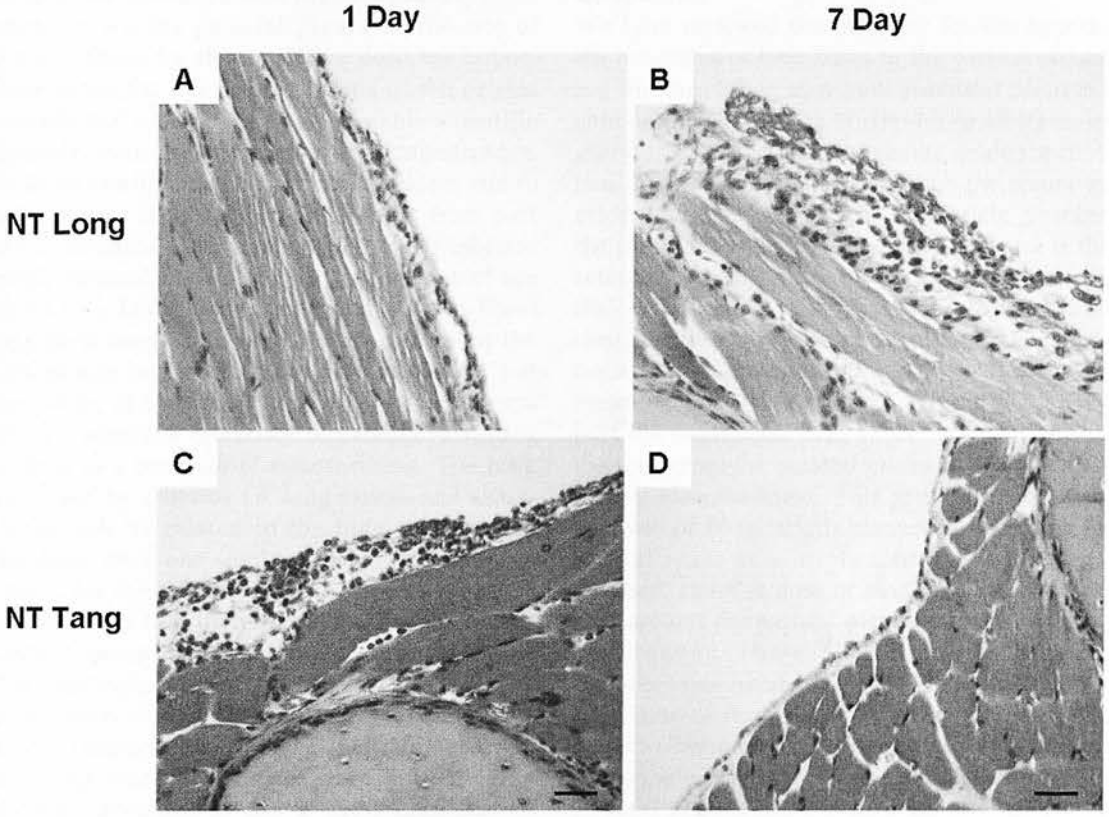

Figure 11 Histological sections through the chest wall of mice treated with long straight nanotubes (A, B) or short, tangled nanotubes (C, D) for 1 or 7 days. Note the progressive thickening of the mesothelium in A and B in response to long straight nanotubes; this contrasts with the acute thickening of the pleural layer with short/tangled CNT which shows resolution to normal mesothelium by 7 days (D). Scale bars represent 20 μm.

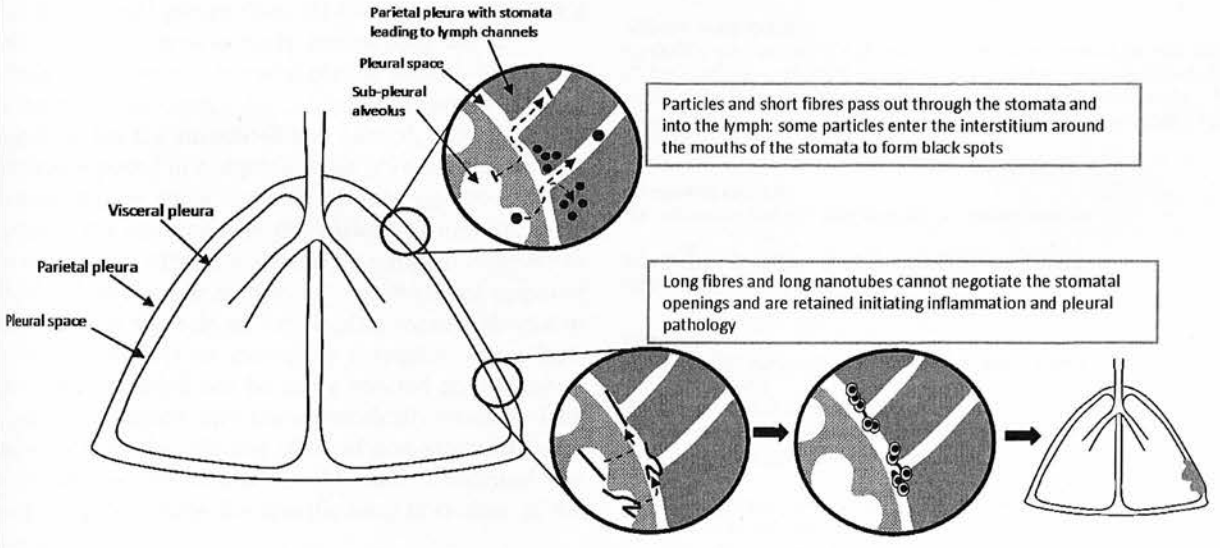

Figure 12 Hypothesised sequence of events leading to pleural responses as a consequence of long fibre retention at the parietal pleural stomatal openings.

Implications for asbestos and mesothelioma

The emphasis on the parietal pleura as the site of retention and focus for the long fibre dose has important implications for our understanding of the origins of mesothelioma, a subject of considerable scientific and, arguably, even greater medico-legal significance. Mesothelioma continues to be a global problem due to ongoing exposure to fibres and as a legacy from past exposure to asbestos, even in countries where asbestos is currently banned or has been regulated out of use for decades [54]. Lung tissue burdens of asbestos fibres have long been used as an index of exposure, but the above discussion highlighting the parietal pleura, not the lung tissue, as the site of origin of mesothelioma calls into question the relevance of parenchymal lung fibre burdens as a correlate of mesothelioma. The **lung** diseases caused by asbestos i.e. lung cancer and asbestosis - may well be related to the lung parenchyma tissue burdens, since one would reasonably look in the target tissue for the effective dose. However the same logic would dictate that the effective dose for mesothelioma, which arises in the parietal pleura, should be sought in that tissue. In fact the parietal pleura fibre burden has been studied, but only very occasionally; for example Dodson and Atkinson [55] cite Sebastien [56] as stating that, for asbestos fibre burden "lung parenchymal retention is not a good indicator of pleural retention: indeed, there was no relationship between parenchymal and pleural concentrations". This would be predicted from the arguments presented in this paper. Therefore, whilst the lung parenchyma is a site of fibre accumulation that is likely related to exposure, the lung parenchyma is not expected to focus the effective dose for mesothelioma in the way that the parietal pleura does [5] through its action as a kind of 'sieve' that selectively retains long fibres.

Even supposing the parietal pleura were to be chosen as the tissue of choice for assessing effective dose of long fibre for the mesothelioma hazard, a considerable problem is posed in sampling it for fibre-burden analysis because of their small size and the heterogeneous distribution of the stomata over the parietal pleura. Yet these are exactly the sites that should be sampled in order to find the dose responsible for the mesothelioma response or to sample the site of developing mesothelioma in order to determine its molecular ontogeny. These 'hotspots' of dose could not be easily selected at autopsy by a pathologist unless they knew specifically where to look and even then the diluting effect of non-stomatal tissue in the immediate vicinity could easily confound any attempt to determine the specific long fibre dose at the stomata.

Conclusion

We have reviewed the evidence for the hypothesis for the behaviour of long fibres in the parietal pleura, focusing on nanotubes as a new potential pleural hazard, although the discussion is relevant to all fibres including asbestos. We argue from existing evidence that a fraction of all deposited particles reach the pleura and from evidence on the mechanism of particle clearance from the pleura, to argue that the parietal pleura is the site of retention of long fibres (Figure 10). We suggest that their retention there, a consequence of length-restricted clearance through the normal stomatal clearance system, initiates inflammation and pleural pathology including mesothelioma. We cite data from thoracoscopy to support the contention that, as would be anticipated from the foregoing, the parietal pleura is the site of origin of pleural mesothelioma. This general hypothesis on the key role of fibre length-restricted clearance from the pleural space as a mechanism for delivering a high, focussed, effective dose of long fibres to the mesothelial cells around the parietal pleural stomata, has important implications. These lie in future research into the mesothelioma hazard from HARN but also for our current view of the origins of asbestos-initiated pleural mesothelioma and the use of lung parenchymal fibre burden as a correlate of this tumour, which arises in the parietal pleura, not the lung parenchyma or visceral pleura.

Acknowledgements

We gratefully acknowledge the financial support of the Colt Foundation (KD, CAP, RD) and the UK Department of Health (FM)

Authors' contributions

KD Drafted the manuscript and provided background material for inclusion. CP Provided important input on the hypothesis and the data described. RD Provided key input in the review of literature and its interpretation. FM Provide important data and background and developed the hypothesis. All authors read and approved the final manuscript.

Competing interests

The authors declare that they have no competing interests.

Received: 18 December 2009 Accepted: 22 March 2010
Published: 22 March 2010

References

1. Cugell DW, Kamp DW: **Asbestos and the pleura: a review.** *Chest* 2004, 125:1103-1117.
2. Poland CA, Duffin R, Kinloch I, Maynard A, Wallace WA, Seaton A, *et al*: **Carbon nanotubes introduced into the abdominal cavity of mice show asbestos-like pathogenicity in a pilot study.** *Nat Nanotechnol* 2008, 3:423-428.
3. Kane AB, Macdonald JL, Moalli PA: **Acute injury and regeneration of mesothelial cells produced by crocidolite asbestos fibers.** *American Review Of Respiratory Disease* 1986, 133:A198.

4. Moalli PA, Macdonald JL, Goodglick LA, Kane AB: **Acute injury and regeneration of the mesothelium in response to asbestos fibers.** *American Journal Of Pathology* 1987, **128**:426-445.
5. Boutin C, Dumortier P, Rey F, Viallat JR, De Vuyst P: **Black spots concentrate oncogenic asbestos fibers in the parietal pleura. Thoracoscopic and mineralogic study.** *Am J Respir Crit Care Med* 1996, **153**:444-449.
6. Boutin C, Rey F, Gouvernet J, Viallat JR, Astoul P, Ledoray V: **Thoracoscopy in pleural malignant mesothelioma: a prospective study of 188 consecutive patients. Part 2: Prognosis and staging.** *Cancer* 1993, **72**:394-404.
7. Viallat JR, Raybuad F, Passarel M, Boutin C: **Pleural migration of chrysotile fibers after intratracheal injection in rats.** *Arch Environ Health* 1986, **41**:282-286.
8. Kane AB: **Epidemiology and pathology of asbestos-related diseases.** *Reviews In Mineralogy* 1993, **28**:347-359.
9. Donaldson K, Borm PJ, Castranova V, Gulumian M: **The limits of testing particle-mediated oxidative stress in vitro in predicting diverse pathologies; relevance for testing of nanoparticles.** *Part Fibre Toxicol* 2009, **6**:13.
10. Yang H, Testa JR, Carbone M: **Mesothelioma epidemiology, carcinogenesis, and pathogenesis.** *Curr Treat Options Oncol* 2008, **9**:147-157.
11. Puhakka A, Ollikainen T, Soini Y, Kahlos K, Saily M, Koistinen P, *et al*: **Modulation of DNA single-strand breaks by intracellular glutathione in human lung cells exposed to asbestos fibers.** *Mutat Res* 2002, **514**:7-17.
12. Donaldson K: **The inhalation toxicology of p-aramid fibrils.** *Critical Reviews In Toxicology* 2009.
13. Kreyling WG, Moller W, Semmler-Behnke M, Oberdorster G: **Particle dosimetry: Deposition and clearance from the respiratory tract and translocaton to extra-pulmonary sites.** *Particle Toxicology* CRC Press, Boca Raton USADonaldson K, Borm P 2007, **Chapter 3**:47-74.
14. Schlesinger RB, Ben-Jebria A, Dahl AR, Snipes MB, Ultman J: **Disposition of inhaled toxicicants.** *Handbook of Human Toxicology* CRC Press Boca RatonMassaro EJ 1997, 493-550.
15. Walton WH: **Chapter 5. Airborne dusts.** *Mineral Fibers and Health* Boca Raton, FL:CRC PressLiddell D, Miller K 1991, 55-77.
16. Stanton MF: **Some etiological considerations of fibre carcinogenesis.** *'Biological effects of asbestos'* WHO IARC LyonBogovski P, Gilson JC, Timbrell V, Wagner JC 1973, 289-294.
17. Davis JM, Addison J, Bolton RE, Donaldson K, Jones AD, Smith T: **The pathogenicity of long versus short fibre samples of amosite asbestos administered to rats by inhalation and intraperitoneal injection.** *Br J Exp Pathol* 1986, **67**:415-430.
18. Adamson IY, Bakowska J, Bowden DH: **Mesothelial cell proliferation after instillation of long or short asbestos fibers into mouse lung.** *Am J Pathol* 1993, **142**:1209-1216.
19. Adamson IY, Bakowska J, Bowden DH: **Mesothelial cell proliferation: a nonspecific response to lung injury associated with fibrosis.** *Am J Respir Cell Mol Biol* 1994, **10**:253-258.
20. Goodglick LA, Kane AB: **Cytotoxicity of long and short crocidolite asbestos fibers invitro and invivo.** *Cancer Research* 1990, **50**:5153-5163.
21. Donaldson K, Brown GM, Brown DM, Bolton RE, Davis JG: **Inflammation generating potential of long and short fiber amosite asbestos samples.** *British Journal Of Industrial Medicine* 1989, **46**:271-276.
22. Donaldson K, Li XY, Dogra S, Miller BG, Brown GM: **Asbestos-stimulated tumor-necrosis-factor release from alveolar macrophages depends on fiber length and opsonization.** *Journal Of Pathology* 1992, **168**:243-248.
23. Hill IM, Beswick PH, Donaldson K: **Differential release of superoxide anions by macrophages treated with long and short fibre amosite asbestos is a consequence of differential affinity for opsonin.** *Occupational & Environmental Medicine* 1995, **52**:92-96.
24. Ye J, Shi X, Jones W, Rojanasakul Y, Cheng N, Schwegler-Berry D, *et al*: **Critical role of glass fiber length in TNF-alpha production and transcription factor activation in macrophages.** *American Journal Of Physiology* 1999, **276**:L426-L434.
25. Hesterberg TW, Tsutsui T, Barrett JC: **Neoplastic transformation of syrian-hamster embryo (She) Cells by asbestos and fiberglass - the importance of fiber dimension.** *Proceedings Of The American Association Of Cancer Research* 1983, **24**:96.
26. Donaldson K, Golyasnya N: **Cytogenetic and pathogenic effects of long and short amosite asbestos.** *Journal Of Pathology* 1995, **177**:303-307.
27. Jensen CG, Watson M: **Inhibition of cytokinesis by asbestos and synthetic fibres.** *Cell Biol Int* 1999, **23**:829-840.
28. Muhle H, Bellmann B, Creutzenberg O: **Toxicokinetics of solid paticles in chronic rat studies using diesel soot, carbon black, toner, titanium dioxide and quartz.** *Toxic and Carcinogenic effects of solid particles in the respiratory tract* ILSI Press Washington DCMohr U, Dungworth D, Oberdorster G 1994, 29-41.
29. Searl A, Buchanan D, Cullen RT, Jones AD, Miller BG, Soutar CA: **Biopersistence and durability of nine mineral fibre types in rat lungs over 12 months.** *Ann Occup Hyg* 1999, **43**:143-153.
30. Hesterberg TW, Miiller WC, Musselman RP, Kamstrup O, Hamilton RD, Thevenaz P: **Biopersistence of man-made vitreous fibers and crocidolite asbestos in the rat lung following inhalation.** *Fundamental And Applied Toxicology* 1996, **29**:267-279.
31. Donaldson K, Aitken R, Tran L, Stone V, Duffin R, Forrest G, *et al*: **Carbon nanotubes: a review of their properties in relation to pulmonary toxicology and workplace safety.** *Toxicol Sci* 2006, **92**:5-22.
32. Davis JM: **Structural variations between pleural and peritoneal mesotheliomas produced in rats by the injection of crocidolite asbestos.** *Ann Anat Pathol (Paris)* 1976, **21**:199-210.
33. Abu-Hijleh MF, Habbal OA, Moqattash ST: **The role of the diaphragm in lymphatic absorption from the peritoneal cavity.** *J Anat* 1995, **186(Pt 3)**:453-467.
34. Donaldson K, Addison J, Miller BG, Cullen RT, Davis JG: **Use of the short-term inflammatory response in the mouse peritoneal-cavity to assess the biological-activity of leached vitreous fibers.** *Environmental Health Perspectives* 1994, **102**:159-162.
35. Agostoni E, Zocchi L: **Pleural liquid and its exchanges.** *Respir Physiol Neurobiol* 2007, **159**:311-323.
36. Baumann MH, Strange C, Sahn SA, Kinasewitz GT: **Pleural macrophages differentially alter pleural mesothelial cell glycosaminoglycan production.** *Exp Lung Res* 1996, **22**:101-111.
37. Lai-Fook SJ: **Pleural mechanics and fluid exchange.** *Physiol Rev* 2004, **84**:385-410.
38. Li YY, Li JC: **Ultrastructure and three-dimensional study of the lymphatic stomata in the costal pleura of the rabbit.** *Microsc Res Tech* 2003, **62**:240-246.
39. Liu J, Wong HL, Moselhy J, Bowen B, Wu XY, Johnston MR: **Targeting colloidal particulates to thoracic lymph nodes.** *Lung Cancer* 2006, **51**:377-386.
40. Shinohara H: **Distribution of lymphatic stomata on the pleural surface of the thoracic cavity and the surface topography of the pleural mesothelium in the golden hamster.** *Anat Rec* 1997, **249**:16-23.
41. Mitchev K, Dumortier P, De Vuyst P: **'Black Spots' and hyaline pleural plaques on the parietal pleura of 150 urban necropsy cases.** *Am J Surg Pathol* 2002, **26**:1198-1206.
42. Muller KM, Schmitz I, Konstantinidis K: **Black spots of the parietal pleura: morphology and formal pathogenesis.** *Respiration* 2002, **69**:261-267.
43. Roberts GH: **The pathology of parietal pleural plaques.** *J Clin Pathol* 1971, **24**:348-353.
44. Churg A: **Non-neoplastic disease caused by asbestos.** *Pathology of Occupational Lung Disease* Williams and Wilkins, BaltimoreChurg A, Green FHY , Second 1998, **Chapter 9**:277-338.
45. Churg A, Green F: **Pathology of Occupational Lung Disease.** Williams and Wilkins, Baltimore, 2 1999.
46. Mutsaers SE, Prele CM, Brody AR, Idell S: **Pathogenesis of pleural fibrosis.** *Respirology* 2004, **9**:428-440.
47. Miserocchi G: **Physiology and pathophysiology of pleural fluid turnover.** *Eur Respir J* 1997, **10**:219-225.
48. Boutin C, Schlesser M, Frenay C, Astoul P: **Malignant pleural mesothelioma.** *Eur Respir J* 1998, **12**:972-981.
49. Churg A, Wiggs B, Depaoli L, Kampe B, Stevens B: **Lung asbestos content in chrysotile workers with mesothelioma.** *Am Rev Respir Dis* 1984, **130**:1042-1045.
50. Dodson RF, Williams MG Jr, Corn CJ, Brollo A, Bianchi C: **Asbestos content of lung tissue, lymph nodes, and pleural plaques from former shipyard workers.** *Am Rev Respir Dis* 1990, **142**:843-847.

51. Kohyama N, Suzuki Y: **Analysis of asbestos fibers in lung parenchyma, pleural plaques, and mesothelioma tissues of North American insulation workers.** *Ann N Y Acad Sci* 1991, **643**:27-52.
52. Bernstein DM, Rogers R, Smith P: **The biopersistence of brazilian chrysotile asbestos following inhalation.** *Inhal Toxicol* 2004, **16**:745-761.
53. Ryman-Rasmussen JP, Tewksbury EW, Moss OR, Cesta MF, Wong BA, Bonner JC: **Inhaled Multi-walled Carbon Nanotubes Potentiate Airway Fibrosis in Murine Allergic Asthma.** *American Journal Of Respiratory Cell And Molecular Biology* 2008, 2008-0276OC.
54. McElvenny DM, Darnton AJ, Price MJ, Hodgson JT: **Mesothelioma mortality in Great Britain from 1968 to 2001.** *Occup Med (Lond)* 2005, **55**:79-87.
55. Dodson RF, Atkinson MA: **Measurements of asbestos burden in tissues.** *Ann N Y Acad Sci* 2006, **1076**:281-291.
56. Sebastien P, Janson X, Gaudichet A, Hirsch A, Bignon J: **Asbestos retention in human respiratory tissues: comparative measurements in lung parenchyma and in parietal pleura.** IARC Sci Publ 1980, 237-246.

doi:10.1186/1743-8977-7-5
Cite this article as: Donaldson *et al.*: **Asbestos, carbon nanotubes and the pleural mesothelium: a review of the hypothesis regarding the role of long fibre retention in the parietal pleura, inflammation and mesothelioma.** *Particle and Fibre Toxicology* 2010 **7**:5.

Identifying the pulmonary hazard of high aspect ratio nanoparticles to enable their safety-by-design

High aspect ratio, or fiber-shaped, nanoparticles (HARNs) represent a growth area in nanotechnology as their useful properties become more apparent. Carbon nanotubes, the best known and studied of the HARNs are handled on an increasingly large scale, with subsequent potential for human inhalation exposure. Their resemblance to asbestos fibers precipitated fears that they might show the same type of pathology as that caused by asbestos and there is emerging evidence to support this possibility. The large number of other HARNs, including nanorods, nanowires and other nanofibers, require similar toxicological scrutiny. In this article we describe the unusual hazard associated with fibers, with special reference to asbestos, and address the features of fibers that dictate their pathogenicity as developed in the fiber pathogenicity paradigm. This paradigm is a robust structure:toxicity model that identifies thin, long, biopersistent fibers as the effective dose for fiber-type pathogenic effects. It is likely that HARNs will in general conform to the paradigm and such an understanding of the features that make fibers pathogenic should enable us to design safer HARNs.

KEYWORDS: carbon nanotubes fibers high aspect ratio mesothelioma nanotoxicology

Ken Donaldson[†1,2], Fiona Murphy[1], Anja Schinwald[1], Rodger Duffin[1] & Craig A Poland[2]

[1]MRC/University of Edinburgh Centre for Inflammation Research, ELEGI Colt Laboratory, Queen's Medical Research Institute, 47 Little France Crescent, Edinburgh, EH16 4TJ, UK
[2]Institute of Occupational Medicine, Research Avenue, North Riccarton, Edinburgh, UK
[†]Author for correspondence: Tel.: +44 131 242 6580 ken.donaldson@ed.ac.uk

High aspect ratio nanoparticles: definitions & volume of production

Owing to the unique properties of matter in the nanosize scale, nanomaterials are being incorporated into a wide variety of consumer products, and research in developing new nanomaterials is proceeding remarkably fast. A material is defined as a nano-object (used here to define a nanoparticle as nano-object) as having one, two or three external dimensions in the nanoscale [1], (i.e., a nanoparticle is a particle with at least one dimension less than 100 nm). According to the structure and nanoscale dimension of the material it can be further split into three different categories. 1D nanoscale materials are referred to as nano-layers, -films or -surfaces, whereas 2D nanoscale materials are categorized as nanotubes, nanowires and nanorods; the third category consists of nanoparticles, which are nanoscale in all three dimensions.

This article focuses on nanomaterials, which are nanoscale in 2D, particularly high aspect ratio (aspect ratio [AR] = length:width ratio) nanomaterials for which the acronym HARNs, signifying high aspect ratio nanoparticles, has been used [2]. The reason for focusing on HARNs in this article are:

- Their useful and novel electrophysical properties and their increasing production compared with other nanoscale materials, as a consequence of which there is increasing potential for inhalation exposure;
- Concern that, if HARNs are inhaled into the lungs they may behave similar to asbestos, some of which can be classified as HARNs, albeit natural in origin;
- Exposure to asbestos fibers caused a worldwide epidemic of disease, although not all fibers that can be breathed into the lungs are as pathogenic as asbestos and the different forms of asbestos are not equally pathogenic. Therefore, if we can fully understand what features render a fiber pathogenic then we have the potential to develop HARNs that are safe by design.

As the name implies, HARNs have a high ratio of length-to-diameter, with a high surface area and can be composed of a variety of elements and compounds; at present, HARNs include nanotubes, nanowires and nanorods (Figure 1). The terms nanowire and nanorod are used interchangeably in literature and the definition of these terms is still somewhat vague. The distinguishing feature between nanowires and nanorods is their length. Nanowires can be up to millimeters in length whereas each dimension of nanorods is within 100 nm. Therefore, the standard AR of nanorods is 3–5 in comparison with the AR of nanowires, which can

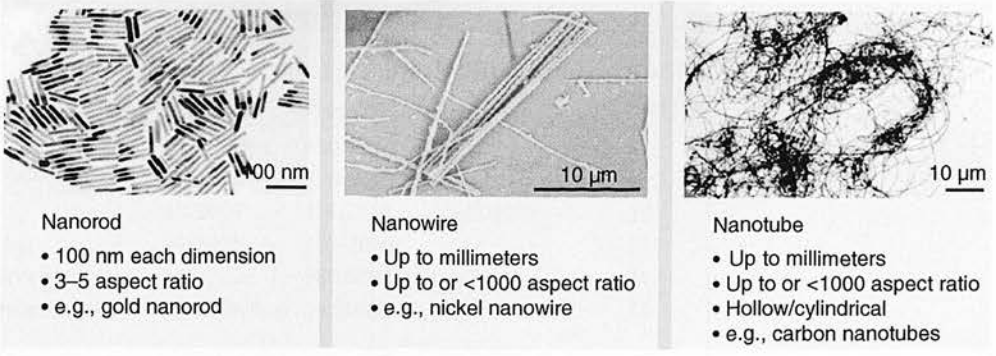

Figure 1. Images and characteristics of the different types of high aspect ratio nanoparticles. Gold nanorod image used with permission from [11].

be greater than 1000. Another term used in the literature for HARNs is nanofibers, which are occasionally used as an umbrella term for nanowires and nanotubes. According to the WHO a fiber is a particle that has a maximum diameter of 3 µm, a minimum length of 5 µm and an AR greater than 3:1 [3]. Best known of all HARNs are carbon nanotubes (CNTs), which are long, thin cylindrical structures comprising single or multiple layers of concentric graphene sheets. CNTs have been optimized for a huge range of applications by derivatization of the surface with a range of chemical moieties. Carbon, packed in the graphenic structure of CNTs exhibits exceptional properties from electrical and thermal conductivity to tensile strength and rigidity. The development and optimization of CNTs for a huge range of applications, from use in electronics to structural engineering, has been a feature of the developing nanotechnologies industry [4].

The advantages in the production of nanowires, nonCNTs and nanorods over CNTs could include controllability of length, diameter, geometry, surface functionality and purity during the production process. Various techniques have been developed to synthesize nanowires and nanorods based on different methods (e.g., evaporation–condensation, dissolution–condensation and vapor–liquid–solid), but the template-based approaches have proved the most versatile. Dependent on the material under use, different template-based synthesis methods can be utilized [5]. For electrically conductive materials, the electrochemical deposition method is used and various nanowires and nanorods have been synthesized using this method, including metals such as Au, Ni, Co, Fe and Pb, as well as semiconductors, conductive polymers and oxides. Their applications range from electronic devices to tools for biology and medicine [6]. With regard to nanomedicine applications, CNTs in particular have been identified for a number of potential uses, including imaging, enhancement of bone growth and targeting and delivery of drugs [7–9]. Prina-Mello *et al.* produced ferromagnetic nickel nanowires with various ARs for manipulating, identification and counting of living cells [10]. Sharma *et al.* studied the neuroprotective efficacy of compounds attached to nanowires in comparison with normal compound delivery and reported an enhanced beneficial effect of the nanowire–drug delivered compound [11]. Other template-based synthesis methods are electrophoretic deposition from colloidal dispersion and template filling. A wide range of HARNs has been produced using the electrophoretic deposition method including polycrystalline oxides such as ZnO, TiO_2 and SiO_2 [5]. Amongst these, ceramic nanoparticles have drawn special attention in the fields of drug delivery, imaging, sensing and thermotherapy due to their biocompatibility, simple preparation and ease of surface modification. In addition, silica nanotubes combined with iron oxide seem to be a promising tool for image-guided drug delivery. The tubular shape permits loading of large amounts of the desired molecule, whereas the outer surface can be modified using, for example, polyethylenglycol or targeting moieties [12].

Year by year there is a near exponential increase in publications based on nanomaterials as well as a considerable expansion in market potential (Table 1) [13]. According to the data summarized in a recent report by the Federal Ministry of Education and Science in Germany, the compound annual growth rate of HARNs (excluding CNTs) is 30%. Even more outstanding is the annual growth rate of single-walled CNTs, which is 200% [101]. These figures correlate with the number of HARN-related publications, which rose from 86 in the year 2000 to 1822 in the year 2009 (Figure 2).

Table 1. Estimated market for nanoparticles.

Market segment	World market volume [M$]/base year			CAGR (%)
	Past	*Present*	*Future*	
MWCNT	290/2006	650/2010		80
SWCNT	78/2006	5000/2010		200
Nanofibers (excluding CNTs)	48/2007	176/2012	825/2017	30
Metallic nanopowders (e.g., Ag)	89/2005	770/2010		53
Ceramic nanopowder (US market)	220/2006	580/2011		21
Nanotechnology in the healthcare market (US market)	23,000/2006	53,000/2011		18
Nanomedicine	18,000/2006	39,000/2011		17

Market growth trends and forecasts are based on information derived from relevant financial and market information, amongst others.
CAGR: Compound annual growth rate; CNT: Carbon nanotube; MWCNT: Multiwalled carbon nanotube; SWCNT: Single-walled carbon nanotube.
Data from [13,101].

Comparing this number with the amount of publications on nanoparticles, which was 3231 in the year 2009, the increasing importance of HARNs in nanotechnology industry becomes obvious. The increasing growth of the HARN industry suggests considerable potential for human exposure to airborne HARNs as these materials are handled in the workplace during industrial preparation and use. However, despite rapid growth in the publications reporting the development, optimization and potential applications of various HARNs, the number of publications based on toxicity studies of HARNs makes up only 6% of all publications, whereas the proportion of toxicity studies on nanoparticles is 19% out of all nanoparticle publications. These data illustrate quite clearly the worrying mismatch between the increases in research focused on the development and use of HARNs versus research concerned with potential health effects of exposure to HARNs.

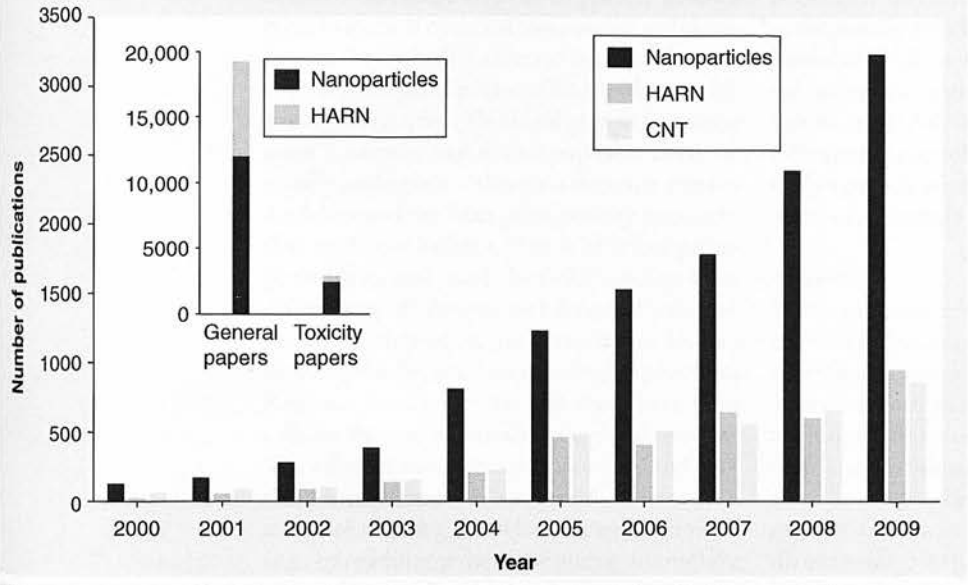

Figure 2. Number of publications on the topics of nanoparticles, high aspect ratio nanoparticles, excluding carbon nanotubes, and carbon nanotubes. Shows the increase in the number of publications on the main three categories of nanomaterials from 2000 to 2009. HARN in this graph include nanofibers, nanowires, nanorods and nanotubes made of materials other than carbon. These data are based on publications in the PubMed database. The search in the database was performed using the 'advanced search option' and 'limits' to specify the date range of publications in each field. Number of publication was revealed using the search terms 'carbon nanotubes' and 'nanoparticles'. HARN data was obtain by summing the number of hits from 'nanofibers', 'nanowires', 'nanorods' and 'nanotubes' using the 'Search Builder option NOT' to exclude CNTs.
CNT: Carbon nanotube; HARN: High aspect ratio nanoparticle.

Asbestos

Consideration of the likely adverse health effects arising from inhalation exposure associated with the use of HARNs is inevitably viewed in the context of the asbestos experience. Asbestos comprises a number of crystalline silicate minerals found ubiquitously in the earth's crust, which was discovered to be industrially useful in the late nineteenth century. The subsequent mining, working and incorporation of asbestos fibers into a vast range of consumer products gave rise to exposure of workers and end-users. Asbestos occurs as six minerals – one of the serpentine class (chrysotile) and five of the amphibole class (amosite, crocidolite, tremolite, anthophyllite and actinolite). Of these, only chrysotile, amosite and crocidolite have proved to be of significant industrial importance, with concomitant human exposure, although tremolite exposure occurs as a contaminant of chrysotile.

Annual world production of asbestos is currently approximately 2,000,000 tons worldwide with Russia as the leading producer, followed by China, Kazakhstan, Brazil, Canada, Zimbabwe, and Colombia, which together accounted for 96% of the world production of asbestos in 2007.

There is an important distinction to be made between chrysotile and the amphibole asbestos types in terms of chemical composition and chemical stability, which is reflected in the differences in their pathogenic potency (discussed in the following paragraphs). This highlights an important point – namely, that not all respirable fibers are equally pathogenic – there is a structure:toxicity model termed the 'fiber pathogenicity paradigm' that predicts whether a fiber is or is not pathogenic (described later). Notwithstanding these differences, all commercial forms of asbestos, including chrysotile, are classified as human carcinogens by the International Agency for Research on Cancer [14] and there have been calls for them to be banned on a global scale [15]. The asbestos minerals are crystalline, and contain fracture planes, or weaknesses, in the crystal structure meaning that when the rock is stressed (e.g., by crushing of the ore or during mining) the crystal fractures into long thin fibers that can be released into the air. These high AR fibers, which can be, in the case of chrysotile fibrils, less than 100 nm in diameter but very long, are normally termed fibers, but they can be seen as naturally occurring HARNs. Owing to their lightness and shape, asbestos fibers can readily become airborne and remain there for a protracted time. If they are inhaled and are thin enough, they can deposit in various parts of the respiratory tree, depending on their aerodynamic size. Once deposited in the lungs the accumulation of fibers can lead to a number of diseases principal amongst which are fibrosis or scarring of the lung parenchyma and bronchogenic carcinoma. In addition, asbestos exposure also causes a number of diseases in the pleura, including mesothelioma, pleural effusion and pleural fibrosis.

The fiber pathogenicity paradigm

Most important for the HARN issue is the question – what are the properties of fibers that imbue them with pathogenicity? If we understand the properties that render fibers pathogenic or not then we can use this information to test or benchmark HARNs as to their likelihood of showing asbestos-like pathogenic behavior. We can also potentially utilize the paradigm to design safe HARNs.

Several decades of fiber toxicology studies, on both asbestos and synthetic vitreous fibers (SVF) have resulted in the fiber pathogenicity paradigm, which highlighted the fiber parameters that dictate whether or not a fiber will be pathogenic when inhaled from an airborne respirable cloud (Figure 3).

These factors are width, length and biopersistence (Figure 3). It should be noted that the pathogenicity paradigm pertains only to the fiber hazard of HARNs. It does not describe the potential hazard that might occur from inhalation exposure to any HARNs that is not long enough (see following paragraphs), in which case it is effectively a particle whose toxicology is understood in terms of an entirely different paradigm.

Width

Width or diameter is the main factor that determines aerodynamic diameter, which is the property that controls whether, or where, in the respiratory tract any particle deposits. Deposition in the lungs is complex, resulting from the size and aerodynamic behavior of the fibers as they negotiate the complex branching structure of the pulmonary airways in the airstream. Aerodynamic diameter (D_{ae}) is the measure that defines where in the respiratory tree any fiber deposits with the extra role of interception, which is a mode of deposition specific to fibers that results from the center of gravity of a fiber following the airstream at a bifurcation while the tip makes contact with the surface of the lung causing immediate deposition. D_{ae} is determined predominantly by the width of the fiber, the aerodynamic diameter of any conventional fiber, composed of material of around unit density, being approximately

three-times its width [16]. The lung has fast and effective clearance in the larger airways, where the mucociliary escalator traps the particles in mucus, which is then swept up to the mouth for swallowing to the gut. Beyond the ciliated airways in the gas exchange regions, clearance is by macrophages that move around on the lung surface and phagocytose or engulf the particles. The particle or short fiber-loaded macrophages then move upwards onto the mucociliary escalator for upward clearance to the mouth and the gut leading to effective clearance of particles [17] and short fibers [18]. This more fragile and slow clearing alveolar and terminal bronchiolar compartment beyond the ciliated airways where blood is very close to the body surface for gas exchange is considered to be much more sensitive to particle effects. This region is termed the respiratory zone and the aerodynamic size fraction of fibers that reaches this zone is termed the respirable fraction, and is generally considered to be the fraction of greatest health concern. Alveolar macrophage clearance from this region is highly effective for micron-sized particles, which are sconfined to the air space and can be collected by the alveolar macrophages [17]. However, Semmler Behnke *et al.* have shown very different clearance/retention kinetics for nanoparticles [19]. These show 80% interstitialization of Ir nanoparticles, which are re-entrained over 6 months back on to the epithelial surface where they are cleared, probably in macrophages, resulting in only 10% retention after 6 months.

Length

Once deposited, length is the factor that determines whether a fiber can be effectively cleared from beyond the ciliated airways by macrophages and whether the attempt of macrophages to phagocytose the fibers leads to inflammation [20,21]. Long fibers (>~15 µm) cannot be engulfed and effectively phagocytosed by macrophages while short fibers are effectively cleared [18]. For some HARNs, the rigidity or ability to coil up into a bundle could be an important factor in modifying the length. In the process of attempting phagocytosis, the macrophage extends along the fiber, but cannot close the phagosome owing to the length of the fiber. This situation of frustrated phagocytosis (FIGURE 4) leads to lysosomal instability, activation of the NALP inflammasome; a multiprotein complex that modulates innate immune function, and chronic stimulation of the cell resulting in the macrophage releasing a range of proinflammatory molecules [22].

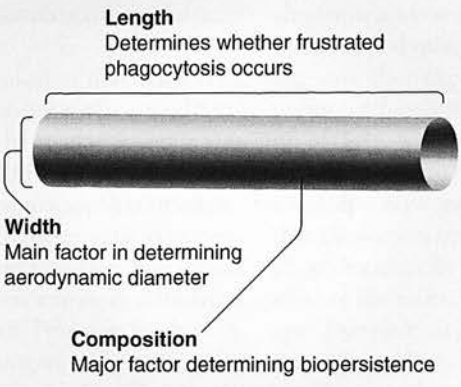

Figure 3. Important parameters governing the pathogenicity of any respirable fiber.

Biopersistence

The property of retaining structural integrity during residence in lung tissue is known a biopersistence. The concept of biopersistence arises from the observation that different natural and man-made fibers with the same length distribution had very different lung retention times following deposition in the lungs and those which were most biopersistent in the lungs had the highest fibrogenic and carcinogenic potential [23]. Within the lung, the less biopersistent components of the fiber may wholly, or partially, dissolve causing them to split longitudinally, as seen with fibrils of chrysotile asbestos, or break transversely as in the case of glass fibers. This arises as a result of the fluid milieu of the lung leaching certain structural components or to the acidic environment of

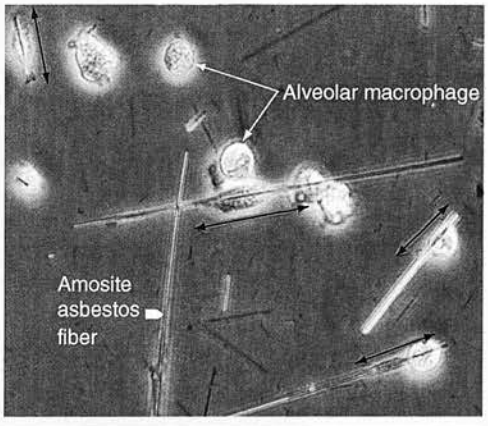

Figure 4. Frustrated phagocytosis in alveolar macrophages by amosite asbestos fibers. Image of macrophages of the NR8383 cell line; white arrow, attempting to phagocytose long amosite asbestos fibers (white chevron). The resultant elongation of the cells along the fibers as they attempt, but fail, to completely enclose the long fiber (black arrows) is termed frustrated phagocytosis.

macrophage phagolysosomes acting in the same way to weaken the fiber.

The effect that dissolution may have on a fiber can be varied, causing surface modification or weakening of the structure leading to breaks with subsequent formation of short fibers, more easily cleared by macrophages (Figure 5). The influence of characteristics, such as susceptibility to dissolution and breakage, was shown by Miller *et al.* using rat exposure data from the Colt Fiber Research Program in the UK and studies from the program of the Thermal Insulation Manufacturers Association in Switzerland and the USA [24]. The role of biopersistence was more directly shown by Searl *et al.* by comparing the length fraction of biopersistent amosite asbestos against nonbiopersistent man-made vitreous fiber (MMVF)-10 between 3 days and 12 months postinhalation in rats. In the case of the MMVF-10 sample, the number of short fibers increased after 12 months indicating breakage of the long fibers supplementing the population of short fibers [18]. Even within the asbestos family of minerals there are differences in biopersistence. Chrysotile asbestos has been shown to be less biopersistent than the amphibole forms of asbestos, such as crocidolite and tremolite. This has been attributed to the layer of a magnesium hydroxide or brucite between the silicate sheets of chrysotile, which is more prone to dissolution causing the layers to unravel and break. The importance of this was shown by McDonald and colleagues who analyzed post-mortem lung tissue from Quebec chrysotile miners by electron microscopy for levels of different forms of asbestos. They found that despite the main exposure being to chrysotile asbestos with only tremolite as a minor contaminant, chrysotile and tremolite were found in approximately equal quantities in the lungs [25]. This suggests that exposure to low levels of biopersistent tremolite lead to a cumulative build up of dose, while the dissolution of chrysotile led to a reduction in retained dose over time. As a concept, exposure to a fiber with a dimension that allows penetration of the lung but does not allow clearance by macrophages leaves only one route of clearance, namely dissolution or breakage. Therefore, exposure to a biopersistent fiber that will not dissolve or break means that it shall persist in the lung environment where it may trigger pathological effects.

Biopersistence studies with HARNs

The only HARN that has been investigated from the point of view of biopersistence is the CNT. It would be anticipated that single-walled CNTs (SWCNTs) are more amenable to degradation than multiwalled CNTs (MWCNTs) and that treatments that disrupted the graphene structure of SWCNTs introducing defects, would also render the CNTs more easily degradable. This has been confirmed in recent studies by Kane and colleagues, who concluded that greater biosolubility would be seen in any SWCNTs following any treatment 'that causes collateral damage to the tubular graphenic backbone in the form of neighboring active sites that provide points of attack for further oxidative degradation' [26]. Similar results were found when SWCNTs that have been highly oxidized by acid treatment and then exposed to neutrophil peroxidase underwent dissolution [27]. It seems unlikely that unoxidized/unmodified SWCNTs or MWCNTs that have undergone mild oxidation would be rendered soluble by the general

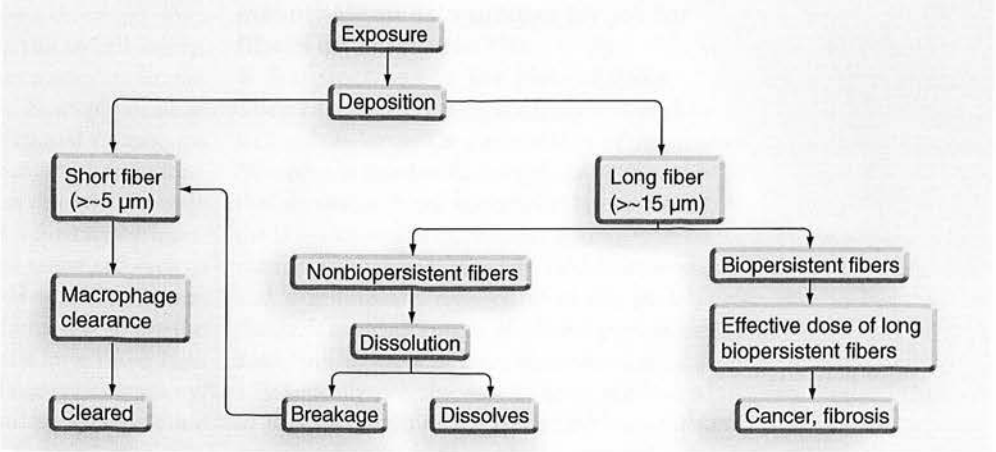

Figure 5. The relationship between biopersistence, clearance and the biologically effective dose of long fibers.

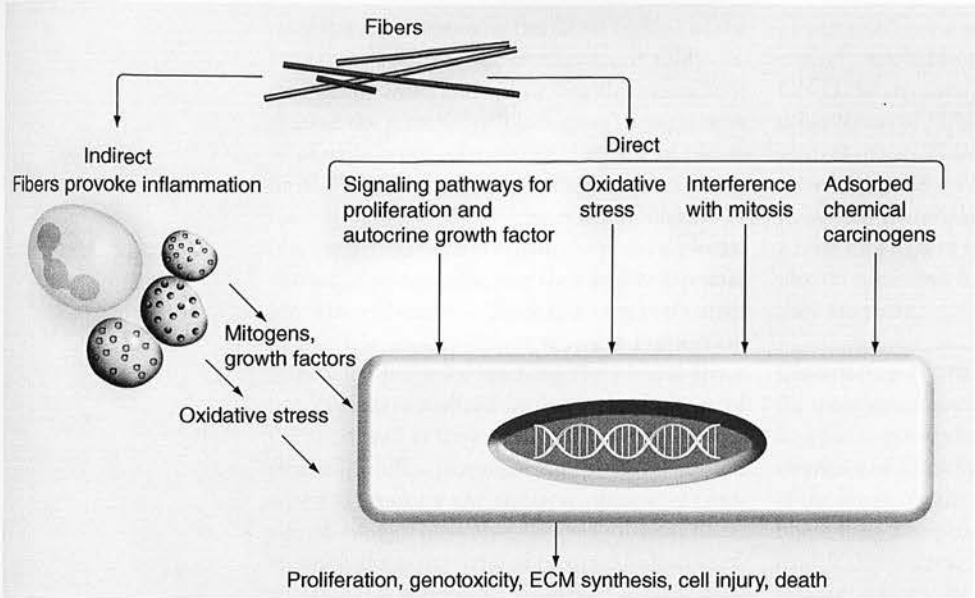

Figure 6. The target cell shown could be an epithelial cell in the lining of the bronchial tree (bronchogenic carcinoma) or a mesothelial cell in the parietal pleura (pleural mesothelioma) and the diagram illustrates the direct and indirect pathways by which fibers may cause procarcinogenic effects.
Adapted from [57].

oxidizing environment of the lungs. This is borne out by numerous studies where CNTs have been introduced into the lungs and have been readily visible in sections months later.

The general issue of CNT biopersistence should be addressed using conventional durability (measuring solubility *in vitro*) or biopersistence (measuring change in lung burden over time) protocols that are available [28,29].

Mechanism of lung disease caused by long fibers

The process of inflammation is the initial cellular response to cell death and oxidative stress arising as a direct result of the accumulation of long fibers in tissue above a threshold dose. Inflammation in turn gives rise to cell injury, gene expression of proinflammatory molecules and further oxidative stress, as amply demonstrated in cells and lungs exposed to asbestos and other fibers (FIGURE 6). Thus, there are at least two ways that oxidative stress can arise in tissue where fibers have deposited – directly by interaction between the fibers and target cell such as epithelial cells, and indirectly when inflammatory leukocytes release oxidants that affect the target cells. The milieu in the lung tissue containing long fibers, with cell injury genotoxicity, oxidative stress and proliferation, is a fertile one for genetic injury, mutation, fibrosis and cancer. A proportion of the fibers that deposit peripherally in the lungs translocate to the pleural tissues [2] (see following sections) where they cause a similar sequence of events leading to a number of unusual fiber-specific pleural diseases, including fibrosis, pleural effusion and mesothelioma. Mesothelioma is a tumor arising on the parietal pleura of the chest wall, which is almost exclusively linked to asbestos exposure, although there are other agents that may occasionally cause this effect. Mesothelioma has become a major concern from exposure to respirable fibers since it occurs at low exposure when the other effects are not apparent and because of its insidious and uniformly fatal course.

Mesothelioma & the pleural mesothelium as a unique target for fibers including HARNs

Translocation to the pleural space

The pleural space is the space between the chest wall and the lungs. The entire surface of the pleural cavity is lined with a single layer of mesothelial cells, with the mesothelial layer covering the lungs known as the visceral pleural, whereas the mesothelial layer attached to the chest wall and diaphragm is referred to as the parietal pleura. The development of pleural pathologies due to inhalation of asbestos fibers would suggest a biologically effective dose of fibers is delivered to this extrapulmonary tissue. Although the exact mechanism of fiber translocation from the lungs to the pleural space is unknown, there is a body of literature that suggests a proportion of all

particles that deposit in the distal regions of the lung translocate to the pleural space. A study carried out by Mitchev *et al.* on healthy individuals showed the presence of 'black spots', benign areas of particle accumulation, on the parietal pleura in 92.7% of a cohort of 150 urban dwellers examined at autopsy [30]. A greater accumulation of black spots has been noted on the parietal pleural surface of miners reflecting their higher exposure levels to coal dust [31]. Black spots represent areas of particle accumulation where a proportion of inhaled particles reaching the pleural space become interstitialized in the parietal pleura of the chest wall as they are in the process of being cleared. Studies investigating the link between asbestos exposure and the development of pleural pathologies have also detected asbestos fibers retained along the parietal pleura. Dodson *et al.* reported that short (<5 µm) chrysotile fibers were predominantly translocated into the pleura in the lungs of ex-shipyard workers exposed to both chrysotile and amphibole asbestos fiber types [32]. Kohyama and Suzuki also reported an apparent predilection for short fiber movement into the pleural space after finding large amounts of short chrysotile fibers in pleural tissue even though the fiber burden in the lung contained a greater percentage of amosite fibers [33]. A study by Boutin *et al.* [34], however, which compared the fiber burden in areas containing black spots to normal areas of parietal pleura, found a high number of long fibers particularly associated with the black spots, with 22% of all fibers found in these areas greater than 5 µm in length. They also showed a clear-cut concordance between the long amphibole asbestos fiber burden in the lung and the black spots of the parietal pleura, but not the areas of normal pleura. Heterogeneity of distribution of fibers within the pleural space can most likely account for the conflicting results from previous studies, which reported a preponderance of short chrysotile fibers in the pleura. These studies suggest that both short and long fibers deposited in the distal alveolar regions of the lung follow an incompletely elucidated route of particle clearance from the lung to the pleural space.

No published study has as yet reported the translocation of HARN fibers to the pleural space after administration into the lung; however, recently a study by Ryman-Rasmussen *et al.* [35] reported the deposition of inhaled short CNTs throughout the lungs and directly adjacent to the visceral pleura, wholly consistent with the notion that CNTs can reach the distal lung and the pleura. From the current understanding of particle/fiber movement from the lungs it is entirely probable that subpleurally deposited CNTs, as reported by Ryman-Rasmussen, and other forms of HARNs will translocate into the pleural space. This suggests the more pertinent question to be asked regarding the toxicity of these new materials and their potential to cause a fiber-like hazard is not whether they reach the pleural space but how they are dealt with once they are there.

Clearance from the pleural space

As mentioned previously, length is a controlling factor governing the macrophage-mediated clearance of fibers from the distal alveolar regions of the lungs. Similarly, clearance of particles and fibers from the pleural space appears to also be length dependent. The primary mechanism of clearance from the pleural space is to remove the particles passively in the flow of pleural fluid out of the pleural space where it joins the lymphatic system [36]. Stomata or pores, approximately 3–10 µm in diameter, act as a sieve for drainage from the pleural space and are found in highest abundance in the most caudal, posterior intercostal spaces and to a lesser extent in the ventral, parasternal region [36,37]. Normally, the elutriating effects of the lungs serve to allow only particles smaller than approximately 5 µm, and therefore smaller than the diameter of the stomata, to reach the distal lung and pleural space. These particles are easily cleared in the flow of pleural fluid where they drain to the mediastinal, parasternal and hilar lymph nodes [38]. However, this clearance mechanism appears to fail when high AR fibers are encountered (Figure 7). In contrast to the movement of fibers in the lung, where it is the diameter of the fibers rather than the length that is the ruling factor in fiber deposition, in the pleural space when the length of a fiber is greater than the diameter of the stomata, interception of the fiber ends with the mesothelial cells surrounding the stomata will occur [2]. This results in blockage of the stomata, accumulation of fibers at these drainage points and potential damage to the mesothelial cells. The presence of fibers in the pleural space will attract resident pleural macrophages, which will accumulate at these areas of deposition. Similar to the attempts of alveolar macrophages to clear long fibers from the lung, pleural macrophages may be unable to fully engulf the fibers leading to a state of frustrated phagocytosis causing further inflammation, fibrosis and genotoxicity in the adjacent mesothelial cells in the areas of congestion around the stomatal entrances.

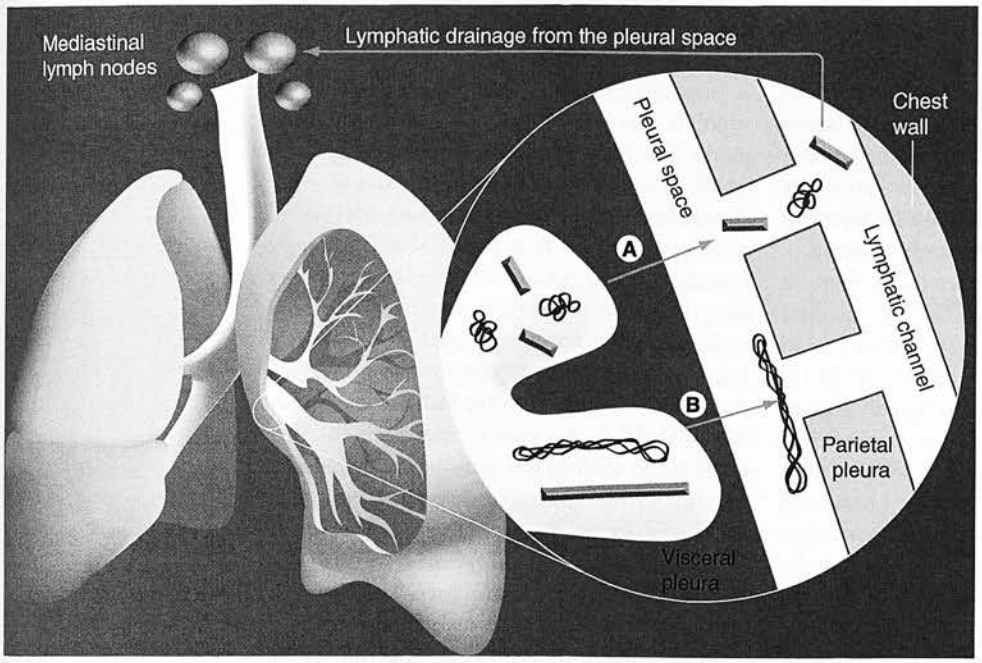

Figure 7. Size-dependent clearance from the pleural space. (A) Short fibers and small carbon nanotube tangles that deposit subpleurally migrate to the pleural space and exit in the flow of pleural fluid through the stomata where they follow the lymphatic drainage to the mediastinal lymph nodes. **(B)** Long fibers and long carbon nanotubes also reach the pleural space but cannot negotiate the stomata and so they are retained where they cause inflammation and potentially long-term disease.

HARNs in the pleural space

The role of length-dependent retention in the pleural space in the pathogenesis of disease needs to be considered when testing the potential of new types of HARNs to cause pleural disease. A study carried out recently in our laboratory investigated the potential adverse reaction to fiber-like MWCNTs in the pleural space, focusing on the response at the parietal pleura of the chest wall and diaphragm [MURPHY *ET AL.*, MANUSCRIPT IN PREPARATION]. A method of injection into the pleural space was developed to ensure that the dose of particles was delivered into the pleural cavity without injection into the lung. A panel of both long and short MWCNTs were injected directly into the pleural cavity and the inflammatory response in the pleural space and at the parietal pleura was examined at a number of time points up to 6 months postinjection. Acute inflammation followed by progressive fibrosis and granuloma development was found only in response to the long MWCNT samples and the long amosite asbestos control with long MWCNTs visible in association with the granulomas at each time point. Short MWCNTs failed to cause a sustained response with only a mild thickening of the mesothelium visible at day one, which had completely resolved by day 7.

The sustained response to the long but not short MWCNTs fully supports the hypothesis that length-dependent retention is the driving force behind the pathogenesis of long fibers in the pleural space. In particular, the retention of long fibers at the parietal pleura provides an explanation of the enhanced ability of long asbestos fibers to cause mesothelioma after inhalation compared with short fibers [39,40]. The operation of a similar length-dependent mechanism of clearance from the peritoneal cavity (see following sections) also explains the markedly greater potential of long fibers instilled into the peritoneal cavity to cause mesothelioma at that site compared with short fibers [39].

Diameter of fibers determines whether a fiber will reach the distal regions of the lung and therefore translocate to the pleural space, whereas length of the fiber is the limiting factor controlling clearance from the pleural space. This suggests that any HARNs with sufficiently small diameter and long length could pose a mesothelioma hazard.

Using the peritoneal cavity as a model of direct mesothelial exposure

When assessing the biological activity of various forms of fibers, the peritoneal cavity of rodents has often been used as a surrogate for the thoracic mesothelium due to the similarity of the

two cavities in terms of the mesothelial lining and the ease of access to the peritoneal cavity [41–44]. The peritoneal or abdominal cavity is the largest body cavity and contains the abdominal organs covered with a mesothelium, which is easily accessible for the introduction of fibers. In surface area, the peritoneal mesothelium is equal to that of the skin [45] and in many ways the peritoneal cavity is analogous to the pleural cavity, which is not surprising considering its shared origin, in the primitive mesoderm during embryonic development. The pleural and peritoneal cavities differ in that the two main roles of the pleural cavity are to lubricate the movement of the lungs and provide a fluid-filled tight coupling between the lung surface and thoracic cage. There is no such coupling role for the peritoneal cavity, instead its primary role is to lubricate the motion of the organs contained within the abdomen and as such whilst the cavity is lubricated, it is not fluid filled. The peritoneal cavity is lined with a mesothelium with a structure identical to that of the pleural, and indeed all mesothelial layers [46]. It also contains stomata that overlie lymphatic lacunae (similar to those seen in the pleural cavity) linking the cavity to the underlying diaphragmatic lymphatics. The diaphragm is considered the principle route of drainage from the peritoneal cavity [47–49] via the parasternal lymph trunks to the parasternal and mediastinal lymph nodes [48]. The physiological nature of the peritoneal cavity means that particles which enter the cavity can be rapidly removed in the liquid flow from the cavity through the diaphragm, or taken up by resident phagocytic cells. Particles that cannot negotiate the narrow (3–12 µm) stomatal openings [50] are retained causing an inflammatory and fibrotic response as demonstrated with asbestos and CNTs [51].

Despite the fact that the peritoneal cavity is a dynamic environment, with size-dependent routes of clearance via the stomata to outlying lymph nodes [52] and lined with a highly responsive mesothelium capable of mediating an inflammatory response [50], the rodent peritoneal assay is not without its critics. The main criticism relates to the lack of physiological relevance as a route of exposure. Indeed, the peritoneal model is not a model of inhalation exposure, it is simply a surrogate for the thoracic mesothelium, as a specific cellular target for asbestos carcinogenicity. Fiber length-dependent retention occurs in both the pleural space and the peritoneal cavity, making the latter an appropriate model for clearance/retention of particulates in the mesothelial space. It is notable that a proportion of the mesotheliomas that arise in asbestos-exposed individuals occur in the peritoneal cavity and so there is exposure of the peritoneal mesothelium to fibers following inhalation and translocation, and a response that mimics mesothelioma formation in the pleural space [53].

Recently, there have been several studies using the peritoneal assay to investigate the *in vivo* response to CNTs. One of the first was a study by our own group in which the role of length in inflammogenicity and fibrosis was examined using a 50 µg intraperitoneal injection of CNTs of differing length and appropriate asbestos controls [51]. We found that long, fiber-like CNTs generated a strong and persistent inflammatory response similar to that seen with long amosite asbestos fibers. Short CNTs, compact carbon particles and short lengths (<5 µm) of amosite asbestos generated no such inflammation and there was no evidence of retention in the peritoneal space suggesting rapid clearance [54]. Over an extended period, the long CNT and asbestos samples generated substantial fibrosis and the presence of foreign body giant cells typical of a foreign body reaction, again not seen with the compact particle controls. This led us to the conclusion that the length of the CNT and asbestos, in line with the structure:toxicity relationship, was causing length-dependent retention in the peritoneal cavity and subsequent response. This work has more recently been supported by a study by Yamashita and colleagues. They found that MWCNTs injected into the peritoneal cavity of mice generated inflammation and genetic damage, which was related to the length and thickness of the CNTs, although interestingly they did not find this the case for SWCNTs [55]. Again, it was this key length of approximately 15 µm that they found to be most inflammogenic in this fiber-sensitive model. The importance of fiber length in a model based on clearance and retention was demonstrated in a paper by Muller and colleagues [56]. They utilized the peritoneal model to investigate the potential carcinogenicity of MWCNTs, using crocidolite as a positive control particle. Over a period of 2 years they were unable to demonstrate a carcinogenic response to the CNTs for which, among other reasons, they cited the length of the CNTs as a contributing factor behind their negative findings. This was because the CNTs used were all less than 0.7 µm and so if singlet fibers were present then they very likely were rapidly cleared leaving only large, nonfibrous agglomerates.

Conclusion: future research and designing safe HARNs

The fiber pathogenicity paradigm is independent of specific chemical composition and therefore embraces asbestos, glass fibers and one organic fiber [16]. Our studies with CNTs [51] and as yet unpublished studies with NiO nanowires point towards the likelihood that all HARNs will conform to the general fiber pathogenicity paradigm, although further research is needed. This future research should address the general utility of the paradigm for a range of HARNs, including nanorods, nanowires and nanotubes of various compositions. Such studies would entail examining a wide range of HARNs for ability to cause length-dependent proinflammatory effects *in vitro* and studies on length-dependent retention at the parietal pleural stomata. Another major aim would be to provide quantitative data on biopersistence, the key attribute of the paradigm, for each HARN and to be able to relate the biopersistence data to pathogenic potential. Nanotechnology methodology could be used to address the key question regarding the true cut-off of length for a 'long' fiber, which is not answerable using naturally occurring fibers that always exist in a broad length distribution. The types of methodologies used to make HARNs are such that the HARNs can be manufactured in tight length distributions. By making HARNs in 3-µm length categories (e.g., -9, -12, -15, -18 and -20 µm long) these could be used to answer the big question – what is the length beyond which long fiber effects occur? This may amount to more than one value since the length beyond which frustrated phagocytosis occurs leading to effect in the lungs might be different from the length beyond which retention in the pleural space occurs, leading to pleural effects, since the length-dependent processes involved are quite different.

The three properties identified by the fiber pathogenicity paradigm as those that determine the likelihood that any fiber sample will pose a fiber-type (asbestos-type) hazard – long, thin and biopersistent – form the biologically effective dose for fiber-type effects. Therefore, the safe design of HARNs from the point of view of the paradigm is relatively straightforward and making HARNs short, thick or nonbiopersistent will reduce their hazard. In particular, designing in time-dependent programmed biodegradeability would be a very desirable approach to safe HARN design. TABLE 2 shows the best current assessment of the quantiative values that would be used to attain safe HARNs. Of course, the advantages of HARNs in any industrial setting may well rely upon properties that accompany length, thinness or biopersistence, and the intrinsic properties of the material may also dictate fiber dimensions and biopersistence. There may well be a contradiction in the production of safe HARNs, if safety stipulates short, low AR particles or biodegradable ones, which will conflict with the technical requirements of these new materials. Therefore, management of the risks from these materials, by safe handling to minimize exposure, needs to be mandatory. Where HARNs cannot be made safe-by-design, as in any industrial setting, due regard must therefore be paid to the size distribution and quantity of the airborne fibers in the workplace air.

Hygiene precautions to reduce inhalation exposure should be set in motion concomitant with the extent of the hazard identified by these size data and knowledge of the biopersistence derived empirically from biopersistence/durability studies or from knowledge of the inherent properties of the material of which the fibers are composed. Many workplaces handle hazardous materials, they simply handle them in safe ways that minimize exposure and HARNs are no different. However, it is difficult at the moment to measure dimensions of very thin fibers in the air and there needs to be more research in this direction so that real-time monitoring of airborne nanofibers can occur in workplaces.

Table 2. Safe values for the three factors in the fiber pathogenicity paradigm.

Characteristic of the FPP	'Safe' value	Rationale/comment
Width	>3 µm	Too thick to be respirable/cut-off for respirability in humans is 5 µm aerodynamic diameter; for fibers, the aerodynamics is approximately three-times the actual diameter
Length	<5 µm	Too short to cause frustrated phagocytosis/the actual value is unknown, but is somewhere between 10 and 20 µm
Biopersistent	Undergoes rapid dissolution in the lungs	Long fibers dissolve and break so are shortened and long fiber dose does not build-up/the actual soluble components lost will depend on the composition of the HARN

HARN: High aspect ratio nanoparticle; FPP: Fiber pathogenicity paradigm.

Financial & competing interests disclosure

The authors acknowledge financial assitance from The Colt Foundation and the UK Department of Health. The authors have no other relevant affiliations or financial involvement with any organization or entity with a financial interest in or financial conflict with the subject matter or materials discussed in the manuscript apart from those disclosed.

No writing assistance was utilized in the production of this manuscript.

Executive summary

High aspect ratio nanomaterials: definitions & volume of production

- High aspect ratio nanomaterials (HARNs) are a new class of material that are nanoscale and have a high length-to-width ratio (e.g., nanotubes, nanowires and nanorods).
- HARNs are increasingly being incorporated into a wide variety of products with a consequent increase in potential for inhalation exposure.
- There is a need to match the increases in research into the development and applications of HARNs versus HARN-related safety research.

Asbestos & the fiber pathogenicity paradigm

- Inhalation exposure to asbestos and naturally occurring high aspect ratio fibers can lead to a number of diseases that affect the lungs (e.g., fibrosis and bronchogenic carcinoma) or the pleura (e.g., mesothelioma, pleural effusion and pleural fibrosis).
- The fiber pathogenicity paradigm is a structure/toxicity model for fibers that highlights width, length and biopersistence in dictating whether or not a fiber will be pathogenic upon inhalation.

Mechanism of lung disease caused by long fibers

- Long fibers can interact directly with target cells (e.g., epithelial or mesothelial cells) causing cell death and oxidative stress or by provoking an inflammatory response recruiting leukocytes that will then release oxidants, cytokines and growth factors, creating a fertile environment for genetic injury, mutation, fibrosis and cancer.

Clearance from the pleural space

- The development of pleural pathologies is a particle response unique to fibrous particles.
- A proportion of all particles deposited in the distal lung will translocate to the pleural space but subsequent clearance from the pleural space is size dependent.
- Small particles and short fibers are easily cleared in fluid flow through stomata in the parietal pleural into the lymphatic system; however, fibers longer than the calibre of the stomatal openings cannot pass through and are retained where they may cause inflammation, fibrosis and genotoxicity in the adjacent mesothelial cells. This suggests that any biopersistent HARN with sufficiently small diameter and long length could pose a mesothelioma hazard.
- The peritoneal cavity is often used as a surrogate for the thoracic cavity when investigating the pathogenicity of fibers owing to the similarity of the mesothelial lining of the two cavities and the greater ease of access to the peritoneal cavity. Clearance from the peritoneal cavity, similar to the pleural cavity is via stomata in the diaphragm, which drain to the lymphatics.

Conclusion: future research & designing safe high aspect ratio nanomaterials

- HARNs have the potential to conform to the fiber pathogenicity paradigm and, therefore, may pose an occupational inhalation hazard.
- Identification of the link between structure and toxicity of HARNs can be exploited to design HARNs that are safer (i.e., short, thick and nonbiopersistent fibers). However, if these properties conflict with the technical requirements of the HARN, sufficient management of the risks to exposure needs to be mandatory.

Bibliography

Papers of special note have been highlighted as:
• of interest
•• of considerable interest

1 Nanotechnologies – terminology and definitions for nano-objects – nanoparticle, nanofibre and nanoplate. ISO/TS 27687 (2008).

2 Donaldson K, Murphy F, Duffin R, Poland C: Asbestos, carbon nanotubes and the pleural mesothelium: a review of the hypothesis regarding the role of long fiber retention in the parietal pleura, inflammation and mesothelioma. *Part. Fiber Toxicol.* 7, 5 (2010).

•• **A comprehensive review detailing the hypothesis that selective retention of long fibers in the pleural space leads to inflammation and disease.**

3 WHO: Determination of airborne fiber number concentrations: a recommended method by phase constrast optical microscopy. WHO, Geneva, Switzerland, ISBN: 924 1544961 (1997).

4 Aitken RJ, Chaudhry MQ, Boxall AB, Hull M: Manufacture and use of nanomaterials: current status in the UK and global trends. *Occup. Med. (Lond.)* 56(5), 300–306 (2006).

5 Cao G, Liu D: Template-based synthesis of nanorod, nanowire, and nanotube arrays. *Adv. Colloid Interface Sci.* 136(1–2), 45–64 (2008).

6 Corr SA, O'Byrne A, Gun'ko YK *et al.*: Magnetic-fluorescent nanocomposites for biomedical multitasking. *Chem. Commun. (Camb.)* (43), 4474–4476 (2006).

7 Pascu SI, Arrowsmith RL, Bayly SR, Brayshaw S, Hu Z: Towards nanomedicines: design protocols to assemble, visualize and test carbon nanotube probes for multi-modality biomedical imaging. *Philos. Transact. A Math. Phys. Eng. Sci.* 368(1924), 3683–3712 (2010).

8 Sahithi K, Swetha M, Ramasamy K, Srinivasan N, Selvamurugan N: Polymeric composites containing carbon nanotubes for bone tissue engineering. *Int. J. Biol. Macromol.* 46(3), 281–283 (2010).

9 Liang F, Chen B: A review on biomedical applications of single-walled carbon nanotubes. *Curr. Med. Chem.* 17(1), 10–24 (2010).

10 Prina-Mello A, Diao Z, Coey JM: Internalization of ferromagnetic nanowires by different living cells. *J. Nanobiotechnology* 4, 9 (2006).

11 Sharma HS, Ali SF, Tian ZR *et al.*: Nanowired-drug delivery enhances neuroprotective efficacy of compounds and reduces spinal cord edema formation and improves functional outcome following spinal cord injury in the rat. *Acta Neurochir. Suppl.* 106, 343–350 (2010).

12 Son SJ, Bai X, Nan A, Ghandehari H, Lee SB: Template synthesis of multifunctional nanotubes for controlled release. *J. Control. Release* 114(2), 143–152 (2006).

13 nano.DE-Report 2009. Status quo der Nanotechnologie in Deutschland. Bundesministerium für Bildung und Forschung, Bonn, Berlin, Germany, 2009.

14 IARC: *Asbestos: IARC Monographs. Supplement 7.* IARC France, World Health Organization, France (1987).

15 LaDou J: The asbestos cancer epidemic. *Environ. Health Perspect.* 112(3), 285–290 (2004).

16 Donaldson K: The inhalation toxicology of p-aramid fibrils. *Crit. Rev. Toxicol.* 39(6), 487–500 (2009).

17 Langenback EG, Bergofsky EH, Halpern JG, Foster WM: Supramicron-sized particle clearance from alveoli: route and kinetics. *J. Appl. Physiol.* 69(4), 1302–1308 (1990).

18 Searl A, Buchanan D, Cullen RT, Jones AD, Miller BG, Soutar CA: Biopersistence and durability of nine mineral fiber types in rat lungs over 12 months. *Ann. Occup. Hyg.* 43(3), 143–153 (1999).

19 Semmler-Behnke M, Takenaka S, Fertsch S *et al.*: Efficient elimination of inhaled nanoparticles from the alveolar region: evidence for interstitial uptake and subsequent reentrainment onto airways epithelium. *Environ. Health Perspect.* 115(5), 728–733 (2007).

20 Ye J, Shi X, Jones W *et al.*: Critical role of glass fiber length in TNF-α production and transcription factor activation in macrophages. *Am. J. Physiol.* 276(3 Pt 1), L426–L434 (1999).

21 Donaldson K, Li XY, Dogra S, Miller BG, Brown GM: Asbestos-stimulated tumor-necrosis-factor release from alveolar macrophages depends on fiber length and opsonization. *J. Pathol.* 168, 243–248 (1992).

22 Hamilton RF, Wu N, Porter D, Buford M, Wolfarth M, Holian A: Particle length-dependent titanium dioxide nanomaterials toxicity and bioactivity. *Part. Fiber Toxicol.* 6, 35 (2009).

* **Demonstrates that alteration of anatase TiO_2 nanomaterial into a long fiber structure creates a highly toxic particle that initiates an inflammatory response in alveolar macrophages.**

23 Bignon J, Saracci R, Touray JC: Introduction: INSERM-IARC-CNRS workshop on biopersistence of respirable synthetic fibers and minerals. *Environ. Health Perspect.* 102(Suppl. 5) 3–5 (1994).

24 Miller BG, Jones AD, Searl A *et al.*: Influence of characteristics of inhaled fibers on development of tumours in the rat lung. *Ann. Occup. Hyg.* 43(3), 167–179 (1999).

25 McDonald JC: Mineral fiber persistence and carcinogenicity. *Ind. Health* 36(4), 372–375 (1998).

26 Liu X, Hurt RH, Kane AB: Biodurability of single-walled carbon nanotubes depends on surface functionalization. *Carbon NY.* 48(7), 1961–1969 (2010).

27 Kagan VE, Konduru NV, Feng W *et al.*: Carbon nanotubes degraded by neutrophil myeloperoxidase induce less pulmonary inflammation. *Nat. Nanotechnol.* 5(5), 354–359 (2010).

28 Bernstein DM and Riego Sintes JM: Methods for the determination of the hazardous properties for human health of man made mineral fibers (MMMF). European Commission Joint Research Centre. Institute for Health and Consumer Protection, Unit: Toxicology and Chemical Substances. European Chemicals Bureau April 1999. ECB/TM/26 rev 7 ISPRA Italy (1999).

29 Maxim LD, Hadley JG, Potter RM, Niebo R: The role of fiber durability/biopersistence of silica-based synthetic vitreous fibers and their influence on toxicology. *Regul. Toxicol. Pharmacol.* 46(1), 42–62 (2006).

30 Mitchev K, Dumortier P, De Vuyst P: 'Black spots' and hyaline pleural plaques on the parietal pleura of 150 urban necropsy cases. *Am. J. Surg. Pathol.* 26(9), 1198–1206 (2002).

31 Muller KM, Schmitz I, Konstantinidis K: Black spots of the parietal pleura: morphology and formal pathogenesis. *Respiration* 69(3), 261–267 (2002).

32 Dodson RF, Williams MG, Jr, Corn CJ, Brollo A, Bianchi C: Asbestos content of lung tissue, lymph nodes, and pleural plaques from former shipyard workers. *Am. Rev. Respir. Dis.* 142(4), 843–847 (1990).

33 Kohyama N, Suzuki Y: Analysis of asbestos fibers in lung parenchyma, pleural plaques, and mesothelioma tissues of North American insulation workers. *Ann N Y Acad. Sci.* 643, 27–52 (1991).

34 Boutin C, Dumortier P, Rey F, Viallat JR, De Vuyst P: Black spots concentrate oncogenic asbestos fibers in the parietal pleura. Thoracoscopic and mineralogic study. *Am. J. Respir. Crit. Care Med.* 153(1), 444–449 (1996).

35 Ryman-Rasmussen JP, Cesta MF, Brody AR *et al.*: Inhaled carbon nanotubes reach the subpleural tissue in mice. *Nat. Nanotechnol.* 4(11), 747–751 (2009).

* **Reports the distal and subpleural deposition of carbon nanotubes in the lungs of mice after a single inhalation exposure; suggests the ability of carbon nanotubes to migrate to the pleural space.**

36 Ryman-Rasmussen JP, Cesta MF, Brody AR *et al.*: Inhaled carbon nanotubes reach the subpleural tissue in mice. *Nat. Nanotech.* 4, 747–751 (2009).

37 Shinohara H: Distribution of lymphatic stomata on the pleural surface of the thoracic cavity and the surface topography of the pleural mesothelium in the golden hamster. *Anat. Rec.* 249(1), 16–23 (1997).

38 Parungo CP, Colson YL, Kim SW *et al.*: Sentinel lymph node mapping of the pleural space. *Chest* 127(5), 1799–1804 (2005).

39 Davis JG, Addison J, Bolton RE, Donaldson K, Jones AD, Smith T: The pathogenicity of long versus short fiber samples of amosite asbestos administered to rats by inhalation and intraperitoneal injection. *Br. J. Exp. Pathol.* 67, 415–430 (1986).

* **Landmark study comparing the pathogenicity of long and short asbestos using two routes of exposure – inhalation and intraperitoneal injection – and demonstrating the markedly greater potential of long fibers to cause fibrosis, pulmonary tumors and mesothelioma.**

40 Berman DW, Crump KS, Chatfield EJ, Davis JM, Jones AD: The sizes, shapes, and mineralogy of asbestos structures that induce lung tumors or mesothelioma in AF/HAN rats following inhalation. *Risk Anal.* 15(2), 181–195 (1995).

41 Cullen RT, Searl A, Miller BG, Davis JM, Jones AD: Pulmonary and intraperitoneal inflammation induced by cellulose fibers. *J. Appl. Toxicol.* 20(1), 49–60 (2000).

42 Kane AB, Macdonald JL, Moalli PA: Acute injury and regeneration of mesothelial cells produced by crocidolite asbestos fibers. *Am. Rev. Respir. Dis.* 133, A198–A198 (1986).

43 Moalli PA, Macdonald JL, Goodglick LA, Kane AB: Acute injury and regeneration of the mesothelium in response to asbestos fibers. *Am. J. Pathol.* 128, 426–445 (1987).

** **Examined the mesothelial response to intraperitoneal injection of asbestos fibers and advanced the hypothesis that it is the size of the lymphatic stomata on the peritoneal surface of the diaphragm that accounts for the selective accumulation of long fibers and the subsequent inflammatory response.**

Donaldson K, Addison J, Miller BG, Cullen RT, Davis JG: Use of the short-term inflammatory response in the mouse peritoneal- cavity to assess the biological-activity of leached vitreous fibers. *Environ. Health Perspect.* 102, 159–162 (1994).

Wegner G: Chirurgische Bemerkungen uber die Peritonealhohle, mit besonderer Berucksichtigung der Ovariotomie. *Arch Klin Chir* 20, 51–145 (1877)

Whitaker D, Papadimitriou JM, Walters MN: The mesothelium: a histochemical study of resting mesothelial cells. *J. Pathol.* 132(3), 273–284 (1980).

Tsilibary EC, Wissig SL: Absorption from the peritoneal cavity: SEM study of the mesothelium covering the peritoneal surface of the muscular portion of the diaphragm. *Am. J. Anat.* 149(1), 127–133 (1977).

Abu-Hijleh MF, Habbal OA, Moqattash ST: The role of the diaphragm in lymphatic absorption from the peritoneal cavity. *J. Anat.* 186(Pt 3), 453–467 (1995).

Ertarh RR, Carr KE: Ultrastructural observations on the peritoneum in the mouse. *J. Anat.* 188(Pt 1), 211–215 (1996).

50 Mutsaers SE, Prele CM, Brody AR, Idell S: Pathogenesis of pleural fibrosis. *Respirology* 9(4), 428–440 (2004).

51 Poland CA, Duffin R, Kinloch I *et al.*: Carbon nanotubes introduced into the abdominal cavity of mice show asbestos-like pathogenicity in a pilot study. *Nat. Nanotechnol.* 3(7), 423–428 (2008).

▪▪ **Used the peritoneal model of mesothelium exposure and showed for the first time that multiwalled carbon nanotubes can produce asbestos-like, length-dependent inflammogenic and fibrotic responses.**

52 Sureshkumar V, Paul B, Uthirappan M *et al.*: Proinflammatory and anti-inflammatory cytokine balance in gasoline exhaust induced pulmonary injury in mice. *Inhal. Toxicol.* 17(3), 161–168 (2005).

53 Donaldson K, Borm PJ, Castranova V, Gulumian M: The limits of testing particle-mediated oxidative stress *in vitro* in predicting diverse pathologies; relevance for testing of nanoparticles. *Part. Fiber Toxicol.* 6(1), 13 (2009).

54 Donaldson K, Stone V, Seaton A, Tran L, Aitken R, Poland C: Induction of mesothelioma in $p53^{+/-}$ mouse by intraperitoneal application of multi-wall carbon nanotube. *J. Toxicol. Sci.* 33(3), 385–388 (2008).

55 Yamashita K, Yoshioka Y, Higashisaka K *et al.*: Carbon nanotubes elicit DNA damage and inflammatory response relative to their size and shape. *Inflammation* 33(4), 276–280 (2010).

56 Muller J, Delos M, Panin N, Rabolli V, Huaux F, Lison D: Absence of carcinogenic response to multiwall carbon nanotubes in a 2-year bioassay in the peritoneal cavity of the rat. *Toxicol. Sci.* 110(2), 442–448 (2009).

57 Kane AB: Mechanisms of mineral fiber carcinogenesis. *IARC Sci. Publ.* (140), 11–34 (1996).

Website

101 Nanotechnology: Nanofibers: Technologies and Developing Markets www.bccresearch.com/report/NAN043A.html

The American Journal of Pathology, Vol. 178, No. 6, June 2011

DOI: 10.1016/j.ajpath.2011.02.040

Cardiovascular, Pulmonary, and Renal Pathology

Length-Dependent Retention of Carbon Nanotubes in the Pleural Space of Mice Initiates Sustained Inflammation and Progressive Fibrosis on the Parietal Pleura

Fiona A. Murphy,* Craig A. Poland,*† Rodger Duffin,* Khuloud T. Al-Jamal,‡§ Hanene Ali-Boucetta,‡ Antonio Nunes,‡ Fiona Byrne,¶‖ Adriele Prina-Mello,¶‖ Yuri Volkov,¶‖ Shouping Li,** Stephen J. Mather,†† Alberto Bianco,‡‡ Maurizio Prato,** William MacNee,* William A. Wallace,§§¶¶ Kostas Kostarelos,‡ and Ken Donaldson*

From the University of Edinburgh/Medical Research Council, the Centre for Inflammation Research, Queen's Medical Research Institute, Edinburgh, United Kingdom; Safenano,† Institute of Occupational Medicine, Edinburgh, United Kingdom; the Nanomedicine Laboratory,‡ Centre for Drug Delivery Research, the School of Pharmacy, University of London, London, United Kingdom; the Department of Pharmacy,§ the Institute of Pharmaceutical Science, King's College London, London, United Kingdom; the School of Physics,¶ the Centre for Research on Adaptive Nanostructures and Nanodevices, and the School of Medicine,‖ Trinity College, Dublin, Ireland; the Department of Pharmaceutical Sciences,** Center of Excellence for Nanostructured Materials, University of Trieste, Trieste, Italy; the Department of Nuclear Medicine,†† St. Bartholomew's Hospital, London, United Kingdom; CNRS,‡‡ Institut de Biologie Moléculaire et Cellulaire, Immunologie et Chimie Thérapeutiques, Strasbourg, France; and the Department of Pathology,§§ Royal Infirmary of Edinburgh, and the Division of Pathology,¶¶ College of Medicine and Veterinary Medicine, University of Edinburgh, Edinburgh, United Kingdom*

The fibrous shape of carbon nanotubes (CNTs) raises concern that they may pose an asbestos-like inhalation hazard, leading to the development of diseases, especially mesothelioma. Direct instillation of long and short CNTs into the pleural cavity, the site of mesothelioma development, produced asbestos-like length-dependent responses. The response to long CNTs and long asbestos was characterized by acute inflammation, leading to progressive fibrosis on the parietal pleura, where stomata of strictly defined size limit the egress of long, but not short, fibers. This was confirmed by demonstrating clearance of short, but not long, CNT and nickel nanowires and by visualizing the migration of short CNTs from the pleural space by single-photon emission computed tomographic imaging. Our data confirm the hypothesis that, although a proportion of all deposited particles passes through the pleura, the pathogenicity of long CNTs and other fibers arises as a result of length-dependent retention at the stomata on the parietal pleura. ***(Am J Pathol 2011, 178:2587–2600; DOI: 10.1016/j.ajpath.2011.02.040)***

Carbon nanotubes (CNTs) are high-aspect ratio nanoparticles formed from a single graphene cylinder (single-walled CNTs) or several graphene cylinders stacked inside each other [multiwalled CNTs (MWCNTs)]. They are typically up to tens of nanometers in diameter but can

Supported in part by the Department of Health (F.A.M.); The Colt Foundation (C.A.P. and K.D.); the EC FP7 NAMDIATREAM (NMP-2009-246479) research project (F.B. and A.P.-M.) and Science Foundation Ireland, as part of the CRANN CSET-funded facilities; and the European Commission FP7 ANTICARB (HEALTH-2008-20157) research project (K.T.A.-J., A.B., M.P., and K.K.).

Accepted for publication February 9, 2011.

Author Contributions: F.A.M., C.A.P., R.D., and K.D. initiated, designed, and directed all experiments and took responsibility for planning and writing the manuscript; F.A.M., K.T.A.-J., A.N., and S.L. performed the SPECT/CT imaging experiment and analyzed the data; H.A.-B. performed transmission electron microscopy on the CNT panel; F.B., A.P.-M., and Y.V. manufactured and provided the NiNW samples and contributed to writing the manuscript; S.J.M. provided reagents and facilities for radiolabeling and SPECT/CT imaging; A.B., and M.P. prepared the short CNTs for labelling and analyzed the data; and S.L., A.B., W.M., and K.K. provided intellectual input and contributed to the writing of the manuscript.

This is an independent report commissioned and funded by the Policy Research Programme in the Department of Health. The views expressed are not necessarily those of the Department.

Address reprint request to Ken Donaldson, Ph.D., Centre for Inflammation Research, Queen's Medical Research Institute, 47 Little France Crescent, Edinburgh EH16 4TJ, United Kingdom. E-mail: ken.donaldson@ed.ac.uk.

Table 1. Characteristics of the carbon nanotube panel

Variable	NT_{short}	NT_{tang1}	NT_{tang2}	NT_{long1}	NT_{long2}	$NiNW_{short}$	$NiNW_{long}$
Source	Nanostructured & Amorphous Materials, Inc.	NanoLab, Inc.	NanoLab, Inc.	Mitsui & Co.	University of Manchester (Dr I. Kinloch)	CRANN–Trinity College Dublin (Drs F. Byrne and A. Prina-Mello)	CRANN–Trinity College Dublin (Drs F. Byrne and A. Prina-Mello)
Diameter (nm)							
Supplied by the manufacturer	20–30	15 ± 5	15 ± 5	40–50	20–100	4.3 ± 1.0	24.0 ± 7.0
Determined by the authors		14.84 ± 0.05	10.40 ± 0.32	84.89 ± 1.9	165.02 ± 4.68	200 ± 10	200 ± 10
Length as supplied by the manufacturer (μm)	0.5–2	1–5	5–20	13 (mean)	56 (maximum)	1–5	24 (median)
% of fibers							
>15 μm	ND	ND	ND	24.04	84.26	ND	85
>20 μm	ND	ND	ND	11.54	76.85	ND	73

Data are given as mean ± SEM.
CRANN, Centre for Research on Adaptive Nanostructures and Nanodevices; NiNW, nickel nanowires; ND, not detected.

extend to millimeters in length.[1] The structural and electrical properties of CNTs are advantageous for a range of industrial applications,[2] leading to CNTs becoming one of the major products of the nanoscale technologies in production volume terms. Their high-aspect ratio makes CNTs a useful industrial material and is also the basis for their similarity to asbestos, raising concern that the special pathogenic properties of asbestos may be mimicked.[1,3–5]

Exposure arising from the mining, milling, and industrial use of asbestos in the 20th century led to a global epidemic of cancer (eg, lung cancer and mesothelioma) and noncancerous diseases (eg, asbestosis, pleural effusions, and pleural plaques).[6] A large body of toxicological research produced a fiber pathogenicity paradigm that describes the characteristics of asbestos and other fibers that render them hazardous or nonhazardous. To be hazardous, a fiber must be thinner than 3 μm, longer than 10 to 20 μm, and biopersistent in the lungs and pleura, not dissolving or breaking into shorter fibers.[7] Sufficient exposure needs to be experienced for the number of long, thin, biopersistent fibers to reach a threshold dose at the target tissue for disease to be initiated. When these criteria are met and the threshold dose is exceeded, there can be a cascade of pathobiological processes, including recruitment of inflammatory cells, genotoxicity, mutation, and fibrosis in the target tissue,[6,8–10] leading to the spectrum of disease previously described.

Mesothelioma is almost exclusively found after asbestos exposure and is a particle response unique to fibrous particles.[8] Therefore, the potential effect that a new fiber-shaped particle like CNT may have on the mesothelium is a major concern in particle toxicology and occupational medicine. Previously, CNTs showed length-dependent inflammogenicity to the peritoneal mesothelium, similar to asbestos. After direct i.p. injection of long CNTs, an inflammatory response with granuloma formation and fibrosis occurred, whereas there was a negligible response to short and tangled CNTs.[11] As suggested in studies by Kane et al,[12] we concluded that long fibers are retained in the peritoneal cavity as a consequence of their inability to exit through stomata in the diaphragm, through which short fibers can egress. Herein, we developed a method to deliver CNTs into the more relevant pleural space to expose both the pleural mesothelial layers and assessed the inflammatory responses and the likely mechanism by which length-dependent pathogenicity might occur at this key site. The injection of long asbestos into the pleural space causes mesothelioma in rodents during a protracted period,[13] thus validating the intrapleural instillation model for studying premesothelioma processes.

Key to the acceptance of this model of direct exposure of the pleural mesothelium is the recognition that a proportion of all particles that deposit in the peripheral lung transit through to the pleura and normally exit through the stomata in the parietal pleura to the underlying lymphatic system and thereby to the mediastinal lymph nodes (LNs).[14] The recognition of this process is based on the presence of black spots (anthracotic areas) around stomata on the parietal pleura of almost all urban dwellers at autopsy,[15] with similar more severe lesions seen in miners,[16] reflecting their higher dust exposure. We hypothesized that particles and short CNTs that reach the pleural space would be readily cleared from the pleural space in the lymphatic flow through the stomata to the mediastinal LNs but that long fibers cannot negotiate the stomata and are, therefore, retained at the parietal pleura, initiating inflammation and pleural pathological conditions, including mesothelioma.[17] Therefore, the instillation of low doses of respirable dusts and fibers into the pleural space represents a credible approach to understanding the behavior of such particles in the pleura, where they are deposited in the lungs by inhalation.

Materials and Methods

Particle Panel

The panel of particles investigated consisted of five different samples of MWCNTs and three control particles that consisted of mixed-length amosite asbestos enriched for long fibers (50.36% fibers >15 μm and 35.25% fibers >20 μm), hereafter referred to as long-fiber asbestos (LFA); shortened amosite asbestos (SFA; 4.46% fibers >15 μm and 0.99% fibers >20 μm); and nanoparticle carbon black. The MWCNT panel comprised four commercially available CNTs and one sample produced in an academic research laboratory (University of Manchester, Manchester, UK) (Table 1). The MWCNT samples were categorized as long (NT_{long1} and NT_{long2}), short and tangled (NT_{tang1} and NT_{tang2}), or short and straight (NT_{short}), based on the manufacturer's description and physical characteristics observed using scanning electron microscopy (SEM), transmission electron microscopy, and light microscopy, as previously described by Poland et al.[11] The NT_{long1} sample (Mitsui & Co Ltd, Tokyo, Japan) was produced by catalytic chemical vapor synthesis using the floating reaction method. The NT_{long2} sample was produced in an academic research laboratory (University of Manchester, Manchester, UK) using a catalytic vapor discharge method with a ferrocene-toluene feedstock to grow nanotubes from iron catalysts held on a silica plate. These nanotubes grew aligned as mats, meaning they were straight and unentangled. The nanotubes were harvested from the mats using a razor blade, with some residual iron remaining within the nanotubes. We also included one commercially available NT_{short} and two curled and tangled nanotubes of different lengths (NT_{tang1}, which was cut to form predominantly short NT fibers; and NT_{tang2}, the original-length NT sample; NanoLab, Inc., Waltham, MA). These nanotubes were produced by catalytic vapor discharge with an iron and ceramic oxide (aluminosilicate) catalyst support that was removed using HCl and hydrofluoric acid treatment. Trace metals and endotoxin levels previously tested and reported by Poland et al were low and, thus, not considered to play a role in these studies. Quartz particles (DQ12), coal mine dust particles, and two samples of commercially available polystyrene beads (10- and 3-μm beads; Polysciences, Warrington, PA) were also used in this study. The mean particle diameters of DQ12 quartz and coal mine dust were measured by dynamic light scattering using a 90 plus Particle Size Analyzer (Brookhaven Instruments Corp., Holtsville, NY). Nickel nanowires (NiNWs) were fabricated by electrochemical template synthesis using alumina membranes (Anodisc 25; Whatman, Maidstone, UK), with an average pore diameter of 200 nm.[18,19] Short and long NiNWs with average lengths of 4.3 ± 1.0 μm and 24.0 ± 7.0 μm (values are ± SEM) respectively, were then examined by SEM (Carl Zeiss Ultra Plus, Hertfordshire, UK).

Transmission Electron Microscopy

A drop of SFA, LFA, or CNT sample (0.5 mg/mL in water) was placed on a grid with a support film of Formvar-carbon, excess material was blotted off with filter paper, and the material was examined under an FEI CM120 BioTwin Transmission Electron Microscope (Philips, Eindhoven, the Netherlands) using a Lab6 emitter. Images were captured using an AMT Digital Camera (AMT, Woburn, MA).

Light Microscopy

The particle panel was suspended in 0.5% bovine serum albumin (BSA; Sigma-Aldrich, Poole, UK) and saline at a concentration of 50 μg/mL and dispersed by sonication at 230 V, 50 Hz, and 350 W for 2 hours in an ultrasonic bath (FB11002; Fisherbrand, Thermo Fisher Scientific, Inc., Waltham, MA). The particle suspensions, 10 μL, were placed on glass slides. Glycerol, 10 μL (Sigma-Aldrich), was added to each slide and mixed with the particle suspension to reduce the flow of particles and enable a clear picture to be captured. A glass coverslip was placed over the suspensions and sealed. Images were captured at ×40 magnification using QCapture Pro software (Media Cybernetics Inc., Bethesda, MD).

Intrapleural Injection and Lavage

Samples were prepared for *in vivo* use by ultrasonication in a sterile 0.5% BSA-saline solution and were injected into the pleural cavity of female C57Bl/6 mice (aged 8 weeks) at a dose of 50 μg/mL (100 μL; total dose, 5 μg per mouse). Injection directly into the pleural space without perforating the lung was enabled by the addition of a sleeve over the tip of the 27-Gauge, which prevented the needle from passing through the pleural space into the lung. After 24 hours ($n = 5$), 7 days ($n = 4$), 4 weeks ($n = 4$), 12 weeks ($n = 4$), and 24 weeks ($n = 5$), the mice were euthanized by asphyxiation in 100% CO_2 and the pleural space was lavaged using three 1-mL washes of sterile saline kept on ice. The lavage fluid was centrifuged at 123 × *g* for 5 minutes at 4°C in a Mistral 3000i centrifuge (Thermo Fisher Scientific, Inc.) to separate the cellular fraction, and the supernatant protein content was established using the bicinchoninic acid protein assay (Sigma-Aldrich). The cell pellet was resuspended in PBS, and a total cell count was then performed using a Nucleo-Counter (ChemoMetec, A/S, Allerød, Denmark). Differential cell counts were performed on cytocentrifugation preparations and stained with a Diff-Quik stain set (Dade Behring Gmbh, Marburg, Germany).

Tissue Dissection

The lower right posterior portion of the chest wall was carefully removed from the mice after lavage of the pleural space. This region of the parietal pleura was identified by Shinohara[20] as a region rich in stomata. The tissue was washed in ice-cold saline and placed overnight in methacarn fixative (60% methanol, 30% chloroform, and

10% glacial acetic acid). Samples were embedded in paraffin, sectioned, and stained with H&E for gross pathology, picrosirius red to stain collagen, and Ki-67 proliferation marker (rabbit polyclonal anti–Ki-67, ab15580; Abcam, Cambridge, UK) ($n = 3$ per treatment). The same region of the chest wall removed from one mouse per treatment for surface analysis by SEM was fixed in 3% glutaraldehyde–0.1 mol/L sodium cacodylate (pH 7.2) buffer. After overnight incubation in fixative, the area of interest was excised from the surrounding tissue. The specific region of chest wall that was examined corresponded to an area 1 × 0.5 cm along the spine, which encompassed the lower six ribs and intercostal spaces.

Quantification of Lesions

The excised tissue was dehydrated through graded alcohol (ethanol) and embedded on edge in paraffin. Sections of the chest wall, 4 μm, were stained with H&E; and serial images were taken at ×10 magnification using QCapture Pro software (Media Cybernetics Inc., Bethesda, MD). The images were seamlessly realigned using Photoshop CS3 (Adobe Systems Inc., San Jose, CA) to provide a high-resolution image of the large sections of chest wall. By using calibrated Image-Pro Plus software (Media Cybernetics Inc.), the total length of each chest wall section along the mesothelium was measured to adjust for any differences in size between reconstructed sections. By using the same software, the area occupied by lesions was measured and expressed as lesion area per unit chest wall length ($\mu m^2/\mu m$). The collagen content was measured using Image-Pro Plus software by quantifying the red pixels in each section and expressed as area of positive collagen staining per unit length of chest wall (mm^2/mm) ($n = 3$).

Scanning Electron Microscopy

The excised diaphragm was stained with osmium tetroxide before critical point drying, mounted, and gold sputter coated before examination by SEM using a Hitachi S-2600N digital SEM (Oxford Instruments, Oxfordshire, UK).

Whole-Body Imaging of NT_{short}–DTPA [^{111}In]-Injected Animals by Single-Photon Emission Computed Tomography

NT_{short}-NH_3^+ samples were obtained following the procedure by Li et al[21] and incubated with diethylenetriaminepentaacetic acid (DTPA) for 48 hours at 50°C. The NT_{short}-DTPA was recovered by centrifugation and labeled with the radioactive tracer [^{111}In]Cl_3 (Amersham Pharmacia Biosciences, Buckinghamshire, UK). The [^{111}In]Cl_3 alone, used as a control, was also subjected to the same conditions of the labeling reaction. Balb/C mice were anesthetized by isoflurane inhalation. Each animal received an intrapleural injection of 100 μL containing 5 μg of NT_{short}-DTPA[^{111}In], with an activity of approximately 3 to 5 MBq. [^{111}In]DTPA with the same activity was injected for comparison. Within 1 hour of injection (t = 0 to 1 hour) and at t = 23 to 24 hours, mice were imaged using the Nano-SPECT/CT scanner (Bioscan, Washington, DC). Single-photon emission computed tomographic (SPECT) images were obtained in 16 projections over 40 to 60 minutes using a four-head scanner with 1.4-mm pinhole collimators. CT scans were taken at the end of each SPECT acquisition, and all images were reconstructed with MEDISO software (Medical Imaging Systems, London, UK). Fusion of SPECT and CT images was performed using PMOD software (PMOD, Zurich, Switzerland).

Quantification of LN NiNW Burden

NiNW samples were prepared and injected into the pleural cavity following the same protocol as was used for CNT samples. Mice ($n = 3$) were sacrificed 24 hours after injection, and the mediastinal LNs were carefully excised, fixed, sectioned, and stained with picrosirius red to allow for clear visualization of the NiNW. Six sequential sections were taken from each LN, giving 18 sections per treatment group. Images were taken at ×10 magnification for tissue area measurement and ×40 magnification for fiber counting using QCapture Pro software (Media Cybernetics Inc.).

Statistical Analysis

All data are shown as the mean ± SEM and were analyzed using one-way analysis of variance. Multiple comparisons were analyzed using the Tukey–honestly significant difference method, with values of $P < 0.05$ considered statistically significant (Instat; Graphpad Software Inc., San Diego, CA).

Results

CNT-Fiber Panel

To specifically assess the role of length in the pleural response to CNTs, we assembled a panel[11] that consisted of long, short, and short and tangled CNTs; control LFA and SFA; and nanoparticle carbon black as a particulate carbon control. The morphological features of the CNT samples were determined by transmission electron microscopy analysis (Figure 1). Light microscopy analysis of the CNT panel and control samples, dispersed by ultrasonication in 0.5% BSA-saline, before administration, showed the presence of fibers in the LFA, NT_{long1}, and NT_{long2} samples; the SFA, NT_{short}, NT_{tang1}, and NT_{tang2} samples were composed of small aggregates of respirable size (Figure 1). Members of the CNT panel were administered by injection directly into the pleural space through the chest wall in unanesthetized mice, using a modified fine-bore needle to prevent injection into the lung; both short- and longer-term responses were examined.

Acute Inflammatory Response to Intrapleural Injection of the CNT-Fiber Panel

The acute inflammatory response produced by instillation of the CNT-fiber panel directly into the pleural space was

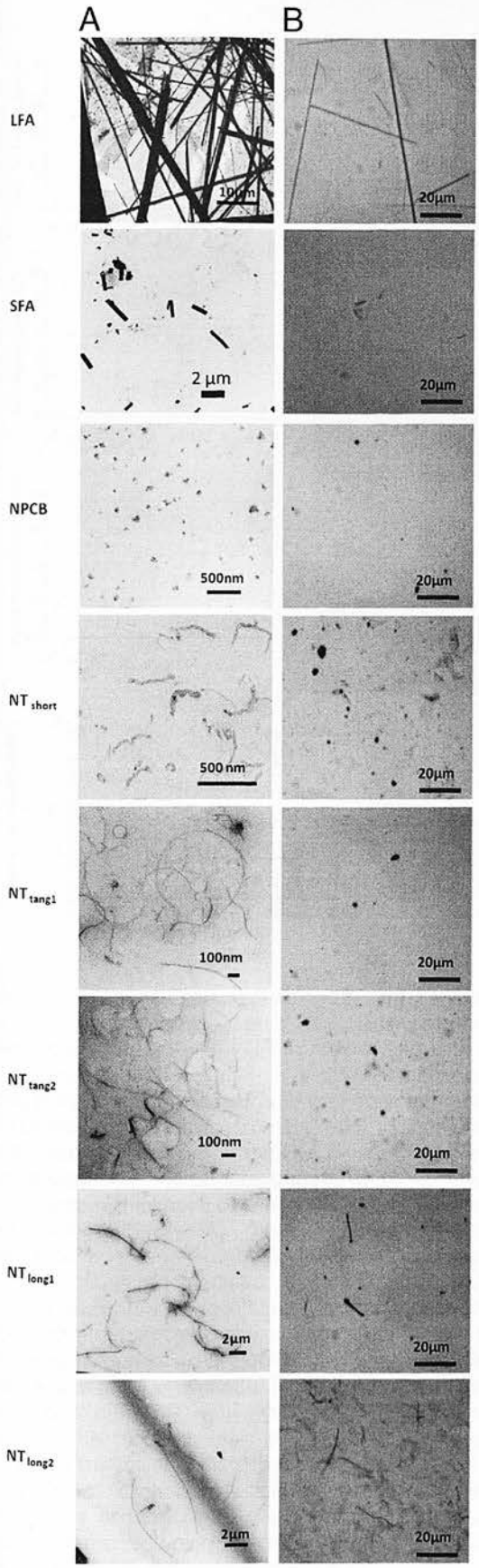

measured at 24 hours by lavaging the pleural space and counting the cell types. Only intrapleural injection of the samples containing long fibers (ie, LFA, NT_{long1}, and NT_{long2}) caused a significant increase in total cell number (Figure 2A) in the lavage fluid. We also determined the number of granulocytes, which included mainly neutrophils and a few eosinophils, as an indicator of acute inflammation in the lavage fluid. Only mice that were injected with long CNTs or asbestos showed significantly increased granulocytes in the pleural lavage compared with the vehicle control (Figure 2B). Mice injected intrapleurally with SFA, nanoparticle carbon black, NT_{short}, NT_{tang1}, or NT_{tang2}, which did not contain long fibers, failed to show any significant increase in the numbers of pleural granulocytes compared with controls (Figure 2B). Protein levels in the lavage fluid, which are indicative of the fluid exudate of inflammation, reflected the pattern seen with granulocyte influx (Figure 2C). The acute inflammatory response in the pleural space was examined up to 7 days after intrapleural injection, for representative long (NT_{long2}) and short (NT_{tang1}) CNT samples (Figure 2D). The increase in the number of granulocytes seen in the pleural lavage of mice injected with NT_{long2} was maintained up to 7 days, with no reduction in the extent of the inflammation, whereas the few granulocytes in NT_{tang1}-treated mice had waned to control levels by 7 days (Figure 2D). By 4 weeks, the number of granulocytes in the NT_{long2}-treated mice was greatly reduced but remained higher than the level of granulocytes in the vehicle control or NT_{tang1}-treated mice up to 24 weeks after injection.

Parietal Pleura Histological Features up to 7 Days

A histological examination was performed on parietal pleura samples from mice injected with short and long CNT exemplars (NT_{tang1} and NT_{long2}, respectively) at 1 and 7 days after intrapleural instillation to examine the development of the early inflammatory mesothelial response (Figure 2E). Aggregates of inflammatory cells were present on the pleural surface in both NT_{tang1} and NT_{long2} samples at 1 day, but by 7 days, the parietal pleura from mice instilled with NT_{tang1} looked completely normal. There was evidence of increasing inflammatory cell accumulation and long CNT retention only in NT_{long2} samples at 7 days (Figure 2E).

Parietal Pleura Histological Features up to 24 Weeks

To investigate the development of the inflammatory lesions on the parietal pleura over time, the parietal

Figure 1. CNT panel. **A:** Transmission electron microscopy (different magnifications used). **B:** Light micrographs of each member of the CNT panel. For light micrographs, CNTs and fibers were dispersed by ultrasonication in 0.5% BSA-saline at a concentration of 50 μg/mL to the standard degree of dispersion used for intrapleural injection. NPCB indicates nanoparticle carbon black.

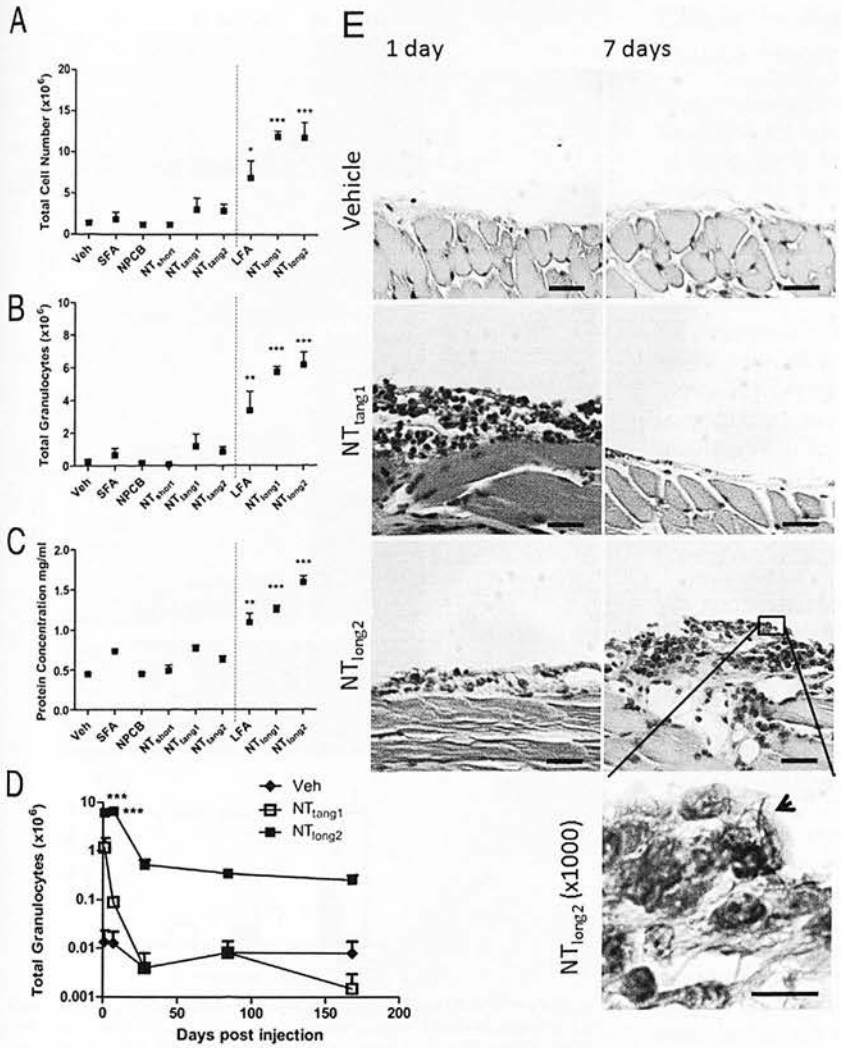

Figure 2. Acute inflammatory response to intrapleural injection of CNT. Total cell number (**A**), total granulocytes (**B**), and total protein (**C**) were measured in the lavage fluid of mice injected with 5 μg of CNT and controls at 24 hours after injection. Total granulocytes (**D**) were measured in lavage fluid of mice treated with either NT_{tang1} or NT_{long2} up to 168 days (24 weeks) after injection. $^{*}P < 0.05$; $^{**}P < 0.01$; $^{***}P < 0.001$ versus vehicle (Veh) control. Data represent mean ± SEM (n = 5 mice per treatment group). **E:** Histological examination of chest wall samples from mice injected with NT_{tang1} and NT_{long2} at 1 and 7 days after injection. Aggregates of inflammatory cells are present in both NT_{tang1} and NT_{long2} samples at 1 day but only in NT_{long2} samples at 7 days. The **arrowhead** indicates long CNT aggregates in ×100 magnification of NT_{long2} (7-day sample). Scale bar = 20 μm. NPCB indicates nanoparticle carbon black.

pleura was further examined at 4, 12, and 24 weeks after injection of NT_{tang1} and NT_{long2}. At all these points, mice treated with vehicle control and with the NT_{tang1} sample had a single layer of mesothelial cells along the parietal pleural surface with no inflammatory involvement. In contrast, parietal pleura sections from mice treated with NT_{long2} showed the presence of a fibrotic layer over the parietal pleura, which continued to increase in thickness over time from 4 to 24 weeks after injection (Figure 3A). The lesions had high collagen content, determined by staining with picrosirius red; and displayed stratified reticular morphological features separated by cellular aggregates. The area of lesion development and the collagen content of the lesions were quantified (Figure 3B). High-power views of the lesion at 24 weeks after injection show vascularization of the lesions, with lymphocyte infiltrates surrounding the blood vessels (Figure 3C). The upper surface of the lesion also appeared to be covered by plump, reactive, and proliferating mesothelial cells. Aggregates of long CNTs were seen in the deeper layers of the developing lesions, reflecting the site of CNT retention in the parietal pleura (Figure 3A). No CNT aggregates were seen in the parietal pleural sections of NT_{tang1}-treated mice. Similar lesion development was seen on examination of the pleural face of the diaphragm of the NT_{long2}- but not the NT_{tang1}- or vehicle control–treated mice (data not shown).

SEM Analysis of the Parietal Pleural Surface

The surface appearance of the parietal pleura was examined by SEM in areas known to have high stomatal density at 1, 4, 12, and 24 weeks in mice exposed to long and short CNTs. The vehicle control samples displayed a continuous normal mesothelium at every point (Figure 4, A–D), with no leukocyte aggregates. NT_{tang1}-treated mice showed a mild response at 1 week, characterized by small areas of leukocyte aggregation on the mesothelial surface (Figure 4E), a response that had resolved by 4 weeks; only a normal mesothelium was seen at subsequent points (Figure 4, F–H). In contrast, in NT_{long2}-treated mice, more extensive and persistent lesions developed (Figure 4, I–L). At 1 week, we observed a large mat of leukocytes forming an almost contiguous layer across the pleural

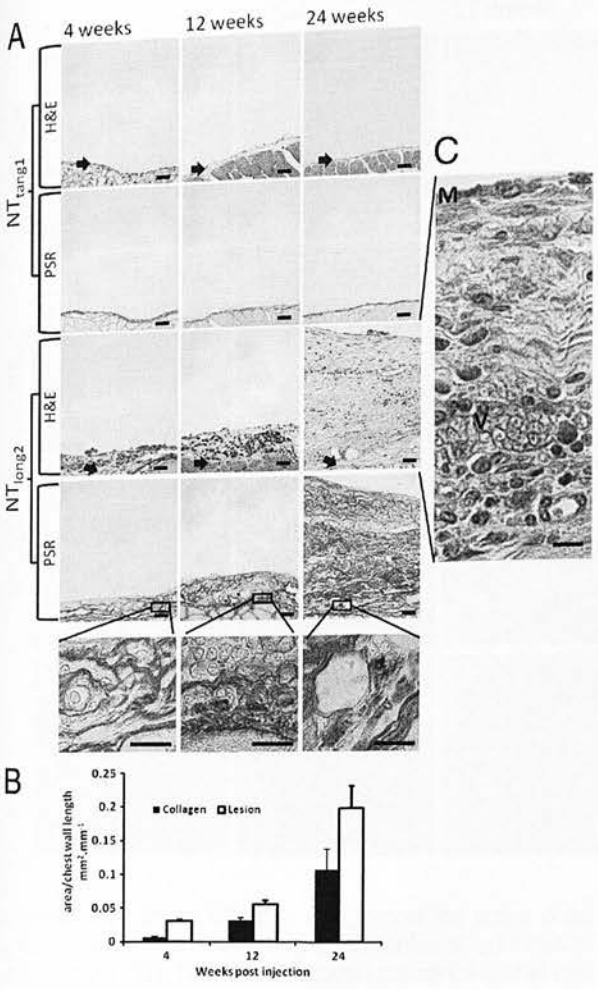

Figure 3. Fibrotic lesion development. **A:** Parietal pleura of the chest wall of mice treated with NT_{tang1} and NT_{long2} were examined histologically at 4, 12, and 24 weeks after injection. Sections were stained with both H&E for gross morphological features and picrosirius red for collagen. **Arrows** indicate level of original mesothelium. Call outs to a high-power view show aggregates of CNT present within the fibrous lesion at each point. Scale bar = 20 μm. **B:** Lesion size and collagen content were quantified for the NT_{long2} samples and expressed as area per length of chest wall section (mm^2/mm). Data are represented as the mean ± SEM ($n = 3$). **C:** High-power views of the lesion at 24 weeks show the lesion is vascularized (V) and covered with a layer of mesothelial cells (M). Scale bar = 20 μm.

surface, bound with fibrin (Figure 4M). By 4 weeks, the lesion had decreased in size and had developed well-defined boundaries, with apparently normal mesothelium in between. Fibrin was still present and appeared to be involved in the adherence of the aggregates to the mesothelium. By 12 weeks, the lesions were more contained within the intercostal depressions. High-power views (Figure 4, M–P) showed no fibrin in association with the leukocytes by 12 and 24 weeks and the apparent attempt by mesothelial cells to regrow over the surface of the lesions. At 24 weeks, papillae or tongue-like structures composed of cell aggregates, which extend from the surface of the mesothelium, can be seen. A high-power view shows these papillae to contain and be covered by mesothelial cells, as identified by the presence of microvilli on the cell surface.

Cellular Proliferation in the Mesothelium of the Parietal Pleura

The progressive covering of lesions by mesothelial cells, as observed from the SEM analysis, implies proliferation of cells along the parietal pleural surface. Sections of parietal pleura and diaphragm from vehicle control–, NT_{tang1}-, and NT_{long2}-treated mice 24 weeks after injection were stained with Ki-67 antibody (Figure 5). Positive Ki-67 staining, which identifies actively proliferating cells, was only observed along the mesothelial surface of the pleural mesothelium of NT_{long2}-treated mice and not in mice treated with short nanotubes (NT_{tang1}). The positive-staining cells were mostly concentrated along the mesothelial layer of the parietal pleura and on the pleural face of the diaphragm in association with the layer of fibrosis.

Size-Related Pleural Retention of Compact Particles

We hypothesized that the inflammatory effects of long CNTs and long fibers in general arise as a consequence of retention at stomata whose maximum diameter is 10 μm (Figure 6A). To test this hypothesis, we used two well-known proinflammatory particles that are small enough to exit through the stomata (ie, quartz and coal mine dust) and polystyrene beads in two sizes (3 and 10 μm, Figure 6B). All of these particles, except the 10-μm beads, were small enough to exit the stomata. We hypothesized that only the 10-μm beads should be retained and would, therefore, elicit inflammation in the pleural space. When instilled into the pleural space at the same mass dose as the CNTs, no response was seen with the quartz or coal mine dust, despite their reactivity within the lung, or the 3-μm beads. In contrast, the 10-μm beads that are too big to exit through the stomata elicited inflammation at 24 hours (Figure 6C).

Length-Dependent Retention of Fibers

We used two indirect approaches to assess the hypothesis that, similar to the large polystyrene beads, long CNTs were retained in the pleural space while short fibers were cleared through the stomata.

SPECT/CT Imaging of Radiolabeled Short CNT Fibers

Dynamic SPECT/CT imaging was used to visualize the fate of radiolabeled short CNTs (NT_{short}-DTPA[^{111}In]) after direct injection into the pleural space. Imaging during the first hour after administration of the radiolabeled CNTs indicated widespread diffusion of the signal, largely confined to, and throughout, the pleural cavity (Figure 7A). Even within 1 hour and increasingly thereafter, the short CNTs accumulated in the cranial mediastinal LNs (two bilateral LNs located lateral to the thymus). At 24 hours after administration, the signal from NT_{short} was localized almost exclusively within these LNs (Figure 7B). The control [^{111}In]DTPA label alone showed rapid

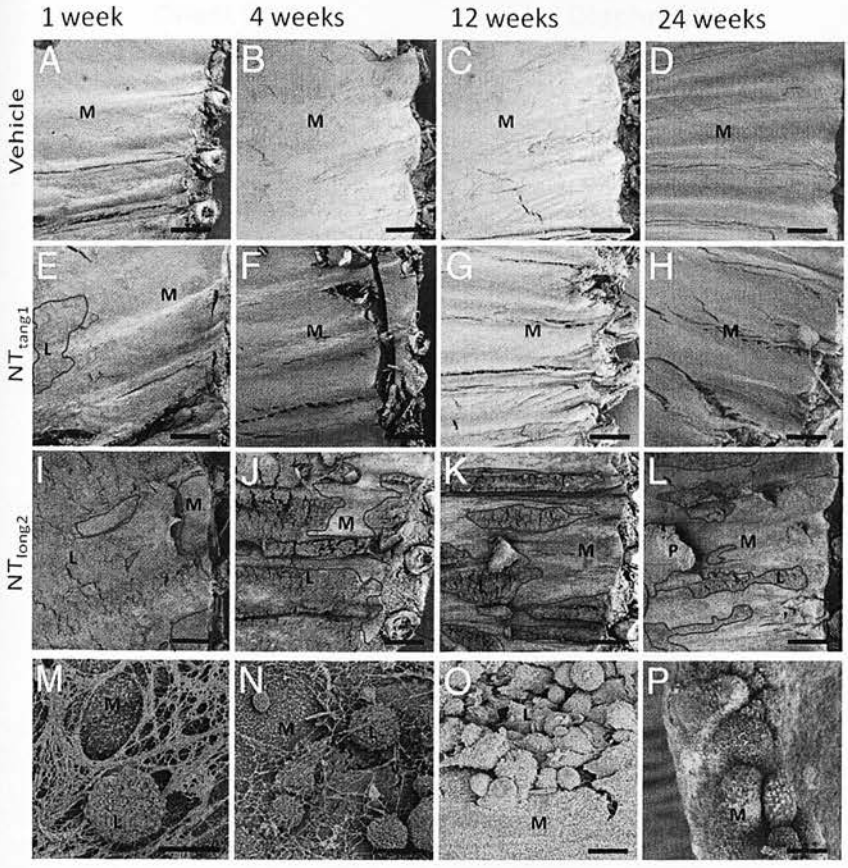

Figure 4. SEM analysis of lesion development over time. The surface of the chest wall parietal pleura was examined by SEM at 1, 4, 12, and 24 weeks after injection. **A–L:** Low-magnification images (×30) show continuous normal mesothelium (M) in vehicle control–treated mice. L indicates the inflammatory lesions (also outlined in red), which are mild and resolve quickly in NT_{long1}-treated mice or are extensive and persistent in NT_{long2}-treated mice. P indicates papillae, tonguelike extensions from the mesothelium, in NT_{long2}-treated samples. Scale bar = 500 μm. **M–P:** High-power view of the lesions present in NT_{long2}-treated mice shows the changing nature of the lesion over time from fibrinous leukocyte aggregates at early points to the progressive resurfacing of the lesion by mesothelial cells. The papillae present at 24 weeks appear to contain and be covered by mesothelial cells, as identified by the presence of microvilli. Scale bar = 10 μm.

translocation to the bladder, with almost the entire dose cleared within the first hour after intrapleural administration (Figure 7C). This demonstrated the stability of *in vivo* radiolabeling of short nanotubes and their clearance from the pleural cavity to the specific mediastinal LNs.

Visualization of Clearance of Long and Short Fibers in Cranial Mediastinal LNs

We took advantage of the knowledge gained from the SPECT/CT that the destination of fibers cleared through stomata is the cranial mediastinal LNs and examined the fiber burden in these LNs 24 hours after intrapleural injection of short and long CNTs (Figure 7E). The results showed apparently greater CNTs in the LNs in NT_{short}-treated mice than in NT_{long2}-treated mice. However, these results were qualitative because of the difficulties of counting the small CNTs in lymphoid tissue; interpretation was further confounded by the presence of short fibers in the NT_{long2} samples (approximately 15% of the fibers were <15 μm).

To gain further evidence, we examined clearance to the mediastinal LNs using short and long versions of alternative high-aspect ratio nanowires made of nickel. NiNWs are more readily visualized histologically than CNTs and have the additional benefit that they are synthesized in tight-size categories, with few short fibers in the long sample and no long fibers in the short sample (Figure 8A). This narrow size distribution range is mainly because of the controlled fabrication process used. The injection of these NiNW samples into the pleural space resulted in a similar length-dependent acute inflammatory response (Figure 8B). After injection into the pleural space, we hypothesized that, as was the case with CNTs, exclusively short NiNWs would appear in the LNs on clearance from the pleural space while the predominately long NiNWs would be retained in the pleural space and, therefore, would not accumulate in the draining LNs. Quantification of the number of NiNWs in histological sections of excised mediastinal lymph tissue showed that significantly more fibers have migrated from the pleural space to the LNs in mice treated with short compared with long NiNWs (Figure 8, C and D). This completely supports the hypothesis that long fibers reaching the pleural space are selectively retained, never reaching the mediastinal LNs, whereas short fibers are small enough to be cleared through the parietal stomata to the mediastinal nodes.

Discussion

To our knowledge, for the first time, we report a clear length-dependent inflammogenicity for CNTs when injected directly into the pleural space of mice. At the initial time of 24 hours, LFA and SFA were included as positive and negative controls, respectively; for the end points examined, the responses to the CNTs followed this length-dependent pattern. Exposure to long CNTs first

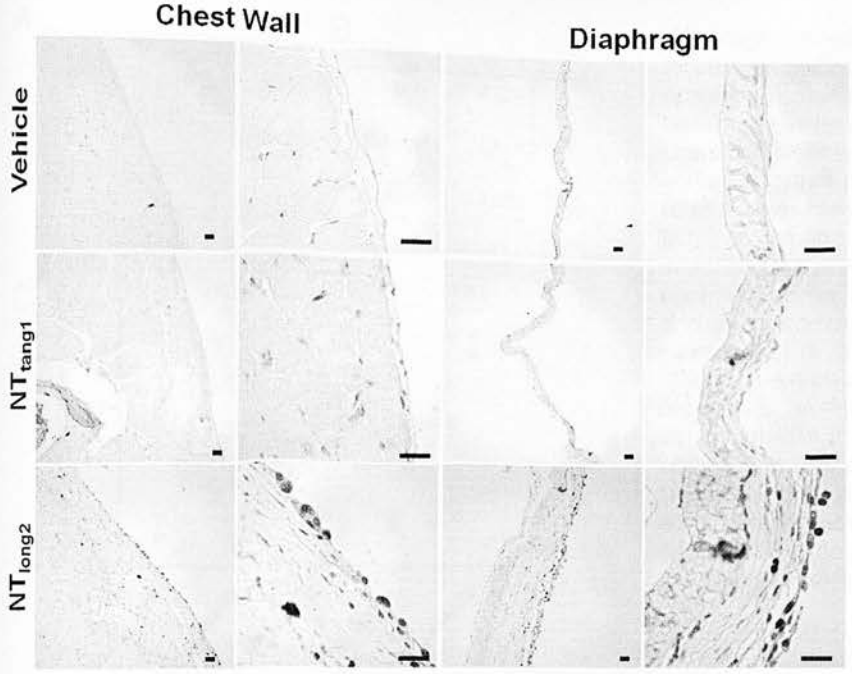

Figure 5. Cellular proliferation along the mesothelium of CNT-treated mice. Cellular proliferation along the parietal pleural of the chest wall and diaphragm was examined in mice treated with vehicle control, NT_{tangl}, and NT_{long2} at 24 weeks after injection. Sections were stained with anti–Ki-67 antibody, a marker for actively proliferating cells. Ki-67–positive staining was only detected along the mesothelium in mice treated with NT_{long2}. Scale bar = 20 μm.

caused an acute inflammatory response, characterized by granulocyte influx, mostly neutrophils, and increased protein concentration in the pleural fluid, followed by the progressive development of fibrotic lesions along the parietal pleura and proliferation in the mesothelial layers. Short CNTs did not elicit a significant inflammatory reaction at any point examined and, indeed, the results obtained from short CNT-treated mice mirrored those of the vehicle controls. These results suggest that, like asbestos, the toxicity of CNTs for the pleura adheres to the fiber pathogenicity paradigm[11] regarding the role of length in this model of direct pleural exposure.

Because of the importance of respirability in delivering particles to the lung periphery, where they can be translocated to the pleural space, it is vital to use well-dispersed particles in our studies that presuppose that the particles reach the lung periphery and the pleura. By using BSA and ultrasonication, we were able to produce well-dispersed respirable-sized suspensions of all of the particles, with fiber-shaped particles being visible by light microscopy in the LFA, NT_{long1}, and NT_{long2} samples. Given the resolution of the light microscope, we assume that the visible fibers in the CNT preparation are ropes of intertwined MWCNTs.[11] After injection into the pleural space, we detected an inflammatory response to the long, but not short, CNTs. Also, in a time course with one of the long CNT samples, we found the inflammation elicited was sustained over 1 week at the level seen at 1 day. Given the basic premise of toxicology that response follows dose, we presumed that the long CNTs were retained in the pleural space, where they are a stimulus to inflammation, whereas the short CNTs are cleared.

Length-dependent pathogenicity of asbestos and other fibers is one of the defining properties of the fiber pathogenicity paradigm[17] and has been documented in several models *in vivo*[9,22–25] and *in vitro*,[25–27] whereas frustrated or incomplete phagocytosis by macrophages has been implicated as a mechanism leading to inflammation with long fibers[26] and CNTs.[28] Length-related retention was first advanced by Kane et al[12] to explain length-dependent asbestos inflammation in the peritoneal cavity. In fact, the peritoneal and pleural cavities have similar mechanisms of clearance, involving fluid flow out of the respective cavities through stomata that are highly size selective.[17]

Clearance from the pleural space is via passive removal of the particles in the flow of pleural fluid out through stomata in the parietal pleura, into the lymphatic system.[14] Stomata (diameter, 3 to 10 μm) act as a "sieve" for drainage from the pleural space and are found along the parietal pleura of the chest wall and diaphragm, in highest abundance in the most caudal posterior intercostal spaces in rodents.[20] Failure to clear the long CNTs from the pleural space, as suggested by the presence of CNT aggregates in the lesions of long CNT-treated mice, forms the basis of a proposed mechanism of long-fiber pathogenicity in the pleural space (ie, retention of long fibers at these points of egress of the lymph), resulting in an inflammatory response. Mesothelioma arises on the parietal pleura,[29] the site of retention of the long-fiber dose. We found that the inflammation produced by long CNTs was sustained and was similar on day 7 to that seen on day 1. This is in contrast to the tempo of inflammation seen in the peritoneal space to the same long CNT sample, where the inflammation waned considerably over 1 week after long CNT and long asbestos.[11] The persistence of inflammation in the pleural space may be a consequence of the conditions there, where movements of the chest wall and close apposition of the parietal and visceral pleurae enhance the interactions between long CNTs and the mesothelium at their points of retention. Sustained inflammation arising from retained

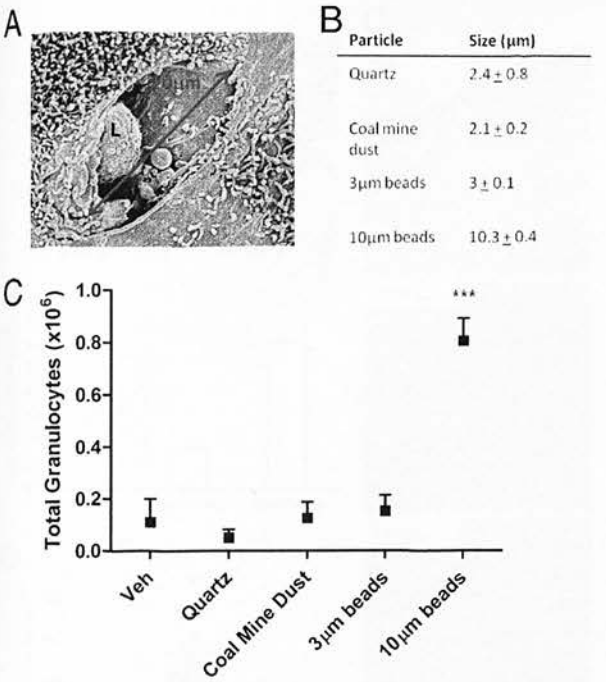

Figure 6. Size-dependent inflammatory response to compact particles in the pleural space. **A:** SEM image of a lymphatic stoma (diameter, 10 μm) found on the parietal pleura of the internal chest wall of a mouse. L indicates a leukocyte passing through the stoma. **B:** Mean size of particles as measured by dynamic light scattering. Data are represented as mean ± SEM. **C:** Total granulocytes measured in pleural lavage fluid of mice 24 hours after injection of "inflammatory" particles: quartz (DQ12) and coal mine dust or 3- and 10-μm beads. Only the 10-μm beads caused a significant increase in granulocytes. Data are represented by mean ± SEM. $^{***}P < 0.001$ versus vehicle (Veh) control.

long fibers produces an inflammatory response at the sites of retention. These foci of inflammation were most evident in the SEM images of the parietal pleura that showed leukocyte aggregates over a relatively large area of the face of the parietal pleura in regions documented to have large concentrations of stomata. The relatively high doses used in our studies produced these anticipated large areas of leukocyte accumulation, which lessened somewhat with time, but only remained substantial in the case of the long CNTs. Analogous lesions have been reported on the mesothelium of the peritoneal cavity after instillation of long asbestos fibers[30] and, similar to what we observed herein, showed a tendency for the lesions to be covered by mesothelial cells with time after instillation.[30] Multiple instillations of asbestos into the rat pleural space, known to cause mesothelioma, were used in one study[31] to examine the changes at the pleural mesothelium observed by SEM over 24 months, leading up to mesothelioma development. Leukocytic lesions and foci of mesothelial proliferation, similar to those seen with the long CNTs, were also documented on the face of the parietal pleura. Hyperplastic areas of mesothelium, reported by Vasilieva et al,[31] were evident in our study, highlighted by the Ki-67 antibody staining, which showed dramatic increases in proliferation in the mesothelial and submesothelial tissues only in mice exposed to long CNTs. Recently, inhalation of amphibole asbestos produced similar leukocytic lesions on the pleural face of the diaphragm, detected by electron microscopy.[32] This latter study is particularly important because it supports our contention[17] that a proportion of fibers that deposit in the distal lung enter the pleural space but that only long fibers are retained, causing a reaction. There are additional structures present along the pleural mesothelium referred to as *milky spots*, which contain accumulations of lymphocytes and macrophages that are reported to be important in the response to pleural injury. These milky spots are found in abundance along the mediastinum and in the vicinity of the pulmonary ligaments.[33] The examination of the parietal pleura reported herein focused on the caudal dorsal intercostal spaces, regions reported to be rich in stomata[14,20]; no milky spots were encountered in the tissue sections examined. However, considering their composition of macrophages and lymphocytes, it is likely that the cells resident in the milky spots contributed to the inflammatory responses reported herein. The accumulation of inflammatory leukocytes at the points of retention of long fibers at the stomata and

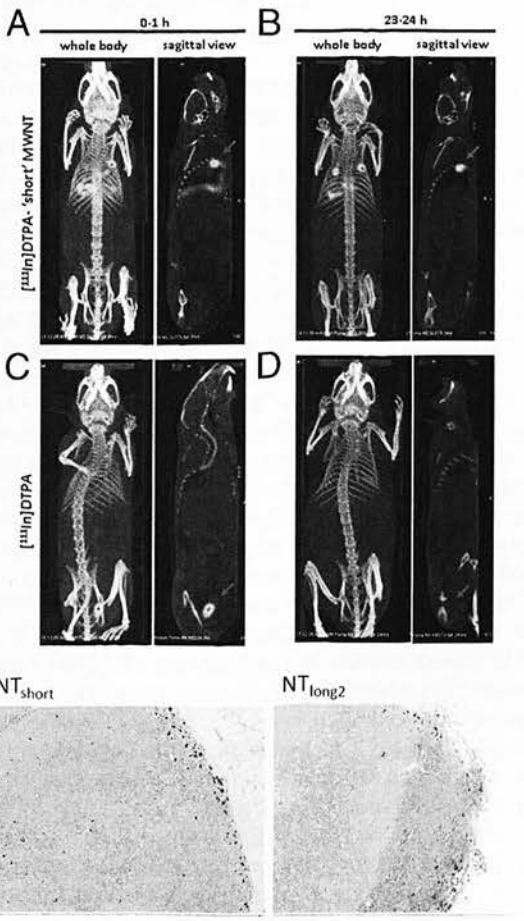

Figure 7. Clearance of CNTs from the pleural space. Whole-body Nano-SPECT/CT imaging of NT_{short}-DTPA[^{111}In]. Imaging was performed immediately (0 to 1 hour) and 1 day (23 to 24 hours) after intrapleural administration of 5 μg of NT_{short}-DTPA[^{111}In] (**A** and **B**) or [^{111}In]DTPA (**C** and **D**). The scanning duration was 60 minutes. SPECT/CT-fused images of the whole body (anterior view) and sagittal planes are shown. **Arrows** indicate the cranial mediastinal LNs (**A** and **B**) and bladder (**C** and **D**) in the case of NT_{short}-DTPA[^{111}In] and [^{111}In]DTPA, respectively. **E:** Cranial mediastinal LNs removed from mice intrapleurally injected with nonradiolabeled long and short CNTs sectioned and stained with H&E.

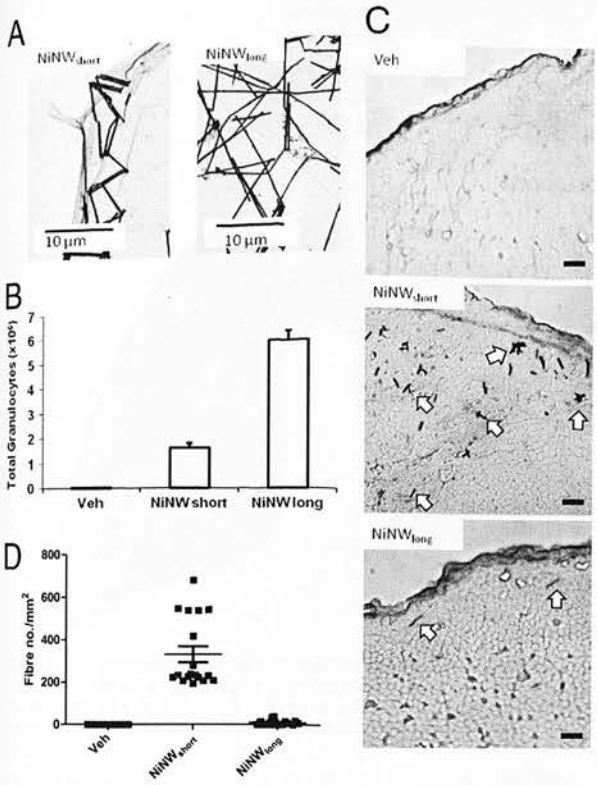

Figure 8. Clearance of short NiNWs to the cranial mediastinal LNs. **A:** Transmission electron microscopy images of short and long NiNWs. **B:** Total granulocytes in the pleural lavage fluid 24 hours after injection with vehicle (Veh) control or short or long NiNWs. ***$P < 0.001$ versus Veh control. **C:** Histological sections of cranial mediastinal LNs excised from mice 24 hours after intrapleural injection of short or long NiNWs ($n = 3$) and stained with picrosirius red to make the NiNWs more visible. **Arrows** indicate NiNWs. Scale bar = 10 μm. **D:** Fiber number per square millimeter of LN tissue was determined by counting the total number of fibers from six sequential sections of each cranial mediastinal LN and measuring the area of tissue in each section. Data are presented as the mean ± SEM ($n = 3$ mice per treatment group).

mesothelial proliferation at these foci are likely to result in an environment rich in cytokines, growth factors, and oxidants. This environment is fertile for producing further mesothelial injury, proliferation, remodeling, mutation, and, ultimately, transformation.

Some confirmation for this hypothesis was obtained in the form of a rapidly developing florid submesothelial fibrotic response that developed over the pleural surfaces only in animals treated with long fibers. This layer of fibrosis formed on the diaphragm and the parietal pleura, both regions rich in stomata, where long fibers would be expected to be retained. The fibrosis that formed was progressive, becoming approximately 20 times thicker and having more collagen between 1 and 24 weeks. These lesions were similar to those seen in the peritoneal cavity with long fibers[11,30] and have some similarities to pleural plaques[34] in the layered parallel reticular network of collagen that characterizes the lesions.

We investigated the validity of our model for retention-dependent inflammation by using compact particles and examining their clearance and inflammatory potential. Quartz and coal mine dust are small particles (<3 μm) that would reach the periphery of the lung and could enter the pleural space. They are known to be inflammogenic in the lungs after inhalation,[35,36] playing a causative role in the pathogenesis of silicosis and pneumoconiosis.[37] The lack of response to these highly inflammogenic particles in the pleural exposure model can be explained by their small size (ie, they are rapidly cleared from the pleural space in the flow of pleural fluid). Based on these studies, we undertook a simple proof-of-concept study to investigate the single parameter of particle size and its potential connection to inflammation in the pleural space using two monodispersed samples of polystyrene beads that were identical in composition but different in diameter. As expected at the same mass dose (meaning many more small beads), the larger 10-μm beads, which are approximately the maximum stomatal diameter, initiated an acute inflammatory response, whereas the smaller 3-μm beads did not initiate this response. Although a 10-μm bead is too large to ever reach the distal lung and pleural space on inhalation, the inflammatory response to the 10-μm beads injected directly into the pleural space demonstrates the role that size-restricted clearance from the pleural space plays in the initiation of an inflammatory response to particles or fibers.

Normally, the elutriating effects of the lung serve to allow only particles smaller than approximately 5 μm and, therefore, smaller than the diameter of the pleural stomata to reach the distal lung and translocate to the pleural space. Particles of this size will be easily cleared in the flow of pleural fluid, where they drain to the mediastinal, parasternal, and hilar LNs.[38] However, fiber respirability is a function of aerodynamic diameter, dictated mostly by actual diameter as air-borne fibers align themselves parallel to the airflow in the lungs. Therefore, it is the diameter (not the length) of fibers that affects transit through the lungs, allowing high-aspect ratio particles like CNTs, which may have a diameter in the nanometer range but a length extending to tens of micrometers, to deposit in the distal regions of the lung.[17] Indeed, the distal deposition of CNTs was shown by Ryman-Rasmussen et al,[39] who reported the presence of CNTs in the subpleural tissue of the lung after a single inhalation exposure in mice. Translocation of particles and fibers from the distal lung to the pleural space is not well understood. Mercer et al[40] showed MWCNTs penetrating the visceral pleura of the lung and extending into the pleural space over several points after a single pharyngeal aspiration exposure in mice, suggesting a direct route of translocation. An alternatively suggested mechanism of translocation is the primary translocation of fibers into the blood, from where they can potentially move to any area of the body, including the pleural space[41]; however, that mechanism was not investigated herein. The movement of distally deposited CNTs into the pleural space is in agreement with literature suggesting that a proportion of all particles deposited distally will pass into the pleural space, thus validating the use of a direct pleural exposure model that bypasses the lung to answer the more pertinent question of how the CNTs are dealt with once in the pleural space.

We examined the clearance of fibers from the pleural space by first showing the clearance of short radiola-

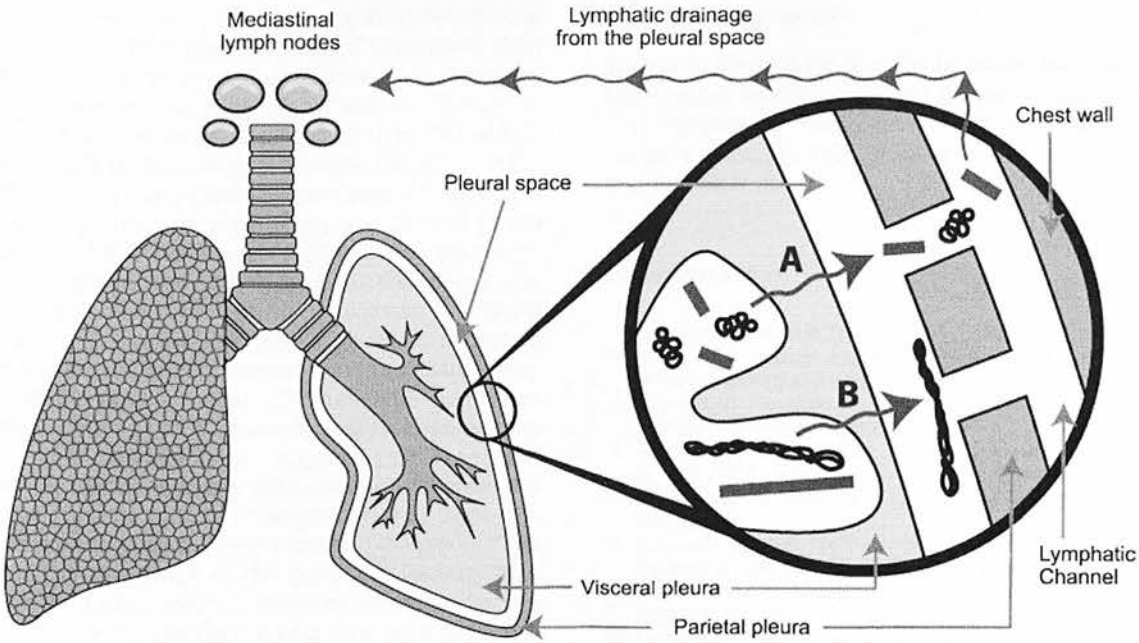

Figure 9. Diagrammatic representation of length-dependent clearance from the pleural space. **A:** Short fibers and small CNT tangles that deposit in alveoli that are situated subpleurally and migrate to the pleural space and exit in the flow of pleural fluid through the stomata, where they follow the lymphatic drainage to the mediastinal LNs. **B:** Long fibers and long CNTs also reach the pleural space from subpleural alveoli but they cannot negotiate the stomata and are retained, where they cause inflammation and potentially long-term disease.

beled CNTs instilled into the pleural space to the mediastinal LNs within 24 hours. Although a direct comparison of short and long CNTs would be ideal in this model, we could only use short CNTs because the process of radioactive labeling shortens long CNTs; therefore, we were unable to visualize, by this method, the retention of the long CNTs. However, this experiment allowed us to identify the cranial mediastinal LNs as the draining nodes for pleural drainage of particles. When we examined the fiber burden in these LNs after intrapleural injection of long and short CNTs, it was clear from the LN sections that the long CNT sample was not completely retained in the pleural space because of short fibers present in that sample that can translocate to the LNs. However, there was obviously more of the "short CNT" sample in the LNs than the "long CNT" sample. Although qualitative, this argues for retention of the longer fibers in the long CNT sample and translocation of the short fibers. We used the NiNWs that are present in tight-sized classes (ie, little short in the long and little long in the short) and demonstrated more convincingly that there was size-dependent retention because we saw only traces of nanowires in the LNs from animals exposed to long NiNWs but abundant nanowires in the LNs from animals that received intrapleural short NiNWs. The response in the LNs to the accumulations of short NiNWs was not closely examined; however, there were no changes in the gross morphological features or enlargement of the LNs of mice exposed to long or short CNTs or NiNWs when compared with vehicle control–treated mice.

We also saw a greater inflammatory response to the long NiNWs than the short NiNWs, strengthening the hypothesis that the pathogenicity of fibers in the pleural space is dependent on length rather than fiber composition. There have been suggestions that CNTs can undergo a degree of dissolution depending on their form[42,43]; thus, the retention/translocation kinetics of long CNTs from the pleural space could change over time if the CNTs undergo any biodissolution. Recently, Tomatis et al[44] reported that the greater toxicity of long asbestos fibers when compared with short asbestos fibers could be attributed to several factors other than length, including greater free radical production and reactive surface. Although these factors may give added toxicity to any fiber, we contend that the properties defined by the fiber pathogenicity paradigm (ie, length, thinness, and biopersistence) remain the primary attributes that a fiber must possess to elicit a pathogenic response. In particular, length will retain the harmful dose (eg, fiber-derived free radicals) in the pleural space; no matter how reactive any short fiber is, it will not remain in the pleural space to deliver its dose.[17] This theory was supported by the quartz and coal mine dust study (Figure 6). However, we are still not able to determine the size limit for retention in these studies. We believe that it should be possible to define a safe length below which there is no pleural retention, but we are unable to define this value based on the present experiments. It is a goal of future studies. However, for straight single fibers, such as NiNWs, our data show that the length beyond which there is parietal pleural retention is longer than approximately 4.3 μm, the length of the short NiNWs that were not retained; and $<\sim$24 μm, the length of the long NiNWs that were retained. Future studies will be aimed at refining this figure so that it more closely approaches the actual length limit.

In conclusion, we showed that injection of long nanofibers into the pleural space leads to persistent inflammation and eventually fibrosis at the parietal mesothe-

lium, where mesothelioma arises and other pleural pathological conditions may originate.[17] In contrast, short nanofibers cause no or modest resolving inflammation, with no parietal pleural pathological features (Figure 9). The data also support the contention that this length dependence is underlined by a dramatic difference in the retention of long fibers (versus short fibers) at stomata in the parietal pleura; the short fibers are cleared to the mediastinal LNs. These studies highlight the importance of fiber length in nanofiber toxicity to the pleura and illuminate the mechanism of the mesothelioma hazard from any long biopersistent fibers, such as asbestos, based on size-dependent retention and proinflammatory effects at the parietal pleura. This research illuminates our understanding of CNT toxicological features as they relate to fiber-type effects and suggests that any nanofiber that is aerodynamically small enough to enter the lungs satisfies the criteria of length and that biopersistence is likely to pose a similar hazard to the pleura. This is argued on the basis of the general relevance of a length-related mechanism of retention and the effect of biopersistence in enabling the long-fiber dose to be delivered to the mesothelium over a protracted time. The necessarily limited data on NiNW (a nanofiber of different composition from CNT) showed the predicted length-related inflammation in the pleural space. These and other data in preparation in our laboratory (not described herein), showing that silver nanowires also produce length-dependent inflammation in the pleural space, support the general relevance of the fiber pathogenicity paradigm for nanofibers. This has important public health implications for the likely risk that long biopersistent nanofibers might pose to the mesothelium if there is sufficient inhalation exposure and highlights the necessity for adequate risk assessment and management for people likely to be exposed to these fibers in workplace air.

Finally, although fiber length is clearly important for fiber effects in both the lung and pleural space, the understanding of the events in the pleural space described herein suggests that the critical length beyond which a long-fiber effect is induced might be different between the lungs and the pleura. In the lungs, the small aerodynamic diameter of fibers, provided that they are thin, means that long thin fibers easily reach the distal lung beyond the ciliated airways. In this position, the accumulation of the long-fiber dose is the result of frustrated phagocytosis and the failure of macrophages ingesting long fibers to make their way out of the lungs, with subsequent proinflammatory stimulation and genotoxicity in target cells. If fibers do reach the pleural space, the dominant feature dictating pathogenicity is retention at stomata because there is rapid clearance of all particles and fibers that are small enough to negotiate the parietal stomata. In the pleural space, much shorter fibers could be the source of problems than in the lungs because of the restricted anatomical "headroom" above the stomata caused by the close apposition of the visceral pleura. This would limit the ability of even short fibers to maneuver and negotiate the stomata and the convoluted subpleural lymphatic capillaries.

Acknowledgments

We thank Mitsui & Co and Dr. Ian Kinloch (University of Manchester, Manchester, UK) for the provision of MWCNT samples; and Stephen Mitchell (University of Edinburgh, Edinburgh, UK) for sample preparation for SEM and technical assistance.

References

1. Donaldson K, Aitken R, Tran L, Stone V, Duffin R, Forrest G, Alexander A: Carbon nanotubes: a review of their properties in relation to pulmonary toxicology and workplace safety. Toxicol Sci 2006, 92:5–22
2. Maynard AD: Nanotechnology: the next big thing, or much ado about nothing? Ann Occup Hyg 2007, 51:1–12
3. Maynard AD, Aitken RJ, Butz T, Colvin V, Donaldson K, Oberdorster G, Philbert MA, Ryan J, Seaton A, Stone V, Tinkle SS, Tran L, Walker NJ, Warheit DB: Safe handling of nanotechnology. Nature 2006, 444:267–269
4. Shvedova AA, Kisin ER, Porter D, Schulte P, Kagan VE, Fadeel B, Castranova V: Mechanisms of pulmonary toxicity and medical applications of carbon nanotubes: two faces of Janus? Pharmacol Ther 2009, 121:192–204
5. Kostarelos K: The long and short of carbon nanotube toxicity. Nature Biotechnol 2008, 26:774–776
6. Mossman BT, Churg A: Mechanisms in the pathogenesis of asbestosis and silicosis. Am J Respir Crit Care Med 1998, 157:1666–1680
7. Donaldson K, Tran CL: An introduction to the short-term toxicology of respirable industrial fibres. Mutat Res 2004, 553:5–9
8. Craighead JE, Abraham JL, Churg A, Green FH, Kleinerman J, Pratt PC, Seemayer TA, Vallyathan V, Weill H: The pathology of asbestos-associated diseases of the lungs and pleural cavities: diagnostic criteria and proposed grading schema: report of the Pneumoconiosis Committee of the College of American Pathologists and the National Institute for Occupational Safety and Health. Arch Pathol Lab Med 1982, 106:544–596
9. Davis JG, Addison J, Bolton RE, Donaldson K, Jones AD, Smith T: The pathogenicity of long versus short fiber samples of amosite asbestos administered to rats by inhalation and intraperitoneal injection. Br J Exp Pathol 1986, 67:415–430
10. Kane AB. Mechanisms of mineral fibre carcinogenesis. Mechanisms of Fibre Carcinogenesis. Edited by AB Kane, P Boffetta, R Saracci, JD Wilbourn. IARC Sci Pub 1996, pp 11–34
11. Poland CA, Duffin R, Kinloch I, Maynard A, Wallace WA, Seaton A, Stone V, Brown S, MacNee W, Donaldson K: Carbon nanotubes introduced into the abdominal cavity of mice show asbestos-like pathogenicity in a pilot study. Nat Nanotechnol 2008, 3:423–428
12. Kane AB, Macdonald JL, Moalli PA: Acute injury and regeneration of mesothelial cells produced by crocidolite asbestos fibers. Am Rev Respir Dis 1986, 133:A198
13. Wagner JC, Pooley FD: Mineral fibers and mesothelioma. Thorax 1986, 41:161–166
14. Wang NS: The preformed stomas connecting the pleural cavity and the lymphatics in the parietal pleura. Am Rev Respir Dis 1975, 111:12–20
15. Mitchev K, Dumortier P, De Vuyst P: "Black spots" and hyaline pleural plaques on the parietal pleura of 150 urban necropsy cases. Am J Surg Pathol 2002, 26:1198–1206
16. Muller KM, Schmitz I, Konstantinidis K: Black spots of the parietal pleura: morphology and formal pathogenesis. Respiration 2002, 69:261–267
17. Donaldson K, Murphy FA, Duffin R, Poland CA: Asbestos, carbon nanotubes and the pleural mesothelium: a review of the hypothesis regarding the role of long fibre retention in the parietal pleura, inflammation and mesothelioma. Part Fibre Toxicol 2010, 7:5
18. Byrne F, Prina-Mello A, Whelan A, Mohamed BM, Davies A, Gun'ko YK, Coey JMD, Volkov Y: High content analysis of the biocompatibility of nickel nanowires. J Magn Magn Mater 2009, 321:1341–1345
19. Prina-Mello A, Diao Z, Coey J: Internalization of ferromagnetic nanowires by different living cells. J Nanobiotechnol 2006, 4:9
20. Shinohara H: Distribution of lymphatic stomata on the pleural surface of the thoracic cavity and the surface topography of the pleural mesothelium in the golden hamster. Anat Rec 1997, 249:16–23

21. Li SP, Wu W, Campidelli S, Sarnatskaia V, Prato M, Tridon A, Nikolaev A, Nikolaev V, Bianco A, Snezhkova E: Adsorption of carbon nanotubes on active carbon microparticles. Carbon 2008, 46:1091–1095
22. Wright G, Kuschner M. The influence of varying lengths of glass and asbestos fibers on tissue responses in the guinea pigs. Inhaled Particles, vol 4. Edited by WH Walton. Oxford, Pergamon Press, 1977, pp 455–474
23. Drew RT, Kuschner M, Bernstein DM: The chronic effects of exposure of rats to sized glass fibres. Ann Occup Hyg 1987, 31:711–729
24. Donaldson K, Brown GM, Brown DM, Bolton RE, Davis JM: Inflammation generating potential of long and short fibre amosite asbestos samples. Br J Ind Med 1989, 46:271–276
25. Goodglick LA, Kane AB: Cytotoxicity of long and short crocidolite asbestos fibers in vitro and in vivo. Cancer Res 1990, 50:5153–5163
26. Ye J, Shi X, Jones W, Rojanasakul Y, Cheng N, Schwegler-Berry D, Baron P, Deye GJ, Li C, Castranova V: Critical role of glass fiber length in TNF-alpha production and transcription factor activation in macrophages. Am J Physiol 1999, 276(Pt 1):L426–L434
27. Dogra S, Donaldson K: Effect of long and short fibre amosite asbestos on in vitro TNF production by rat alveolar macrophages: the modifying effect of lipopolysaccharide. Ind Health 1995, 33:131–141
28. Brown DM, Kinloch IA, Bangert U, Windle AH, Walter DM, Walker GS, Scotchford CA, Donaldson K, Stone V: An in vitro study of the potential of carbon nanotubes and nanofibres to induce inflammatory mediators and frustrated phagocytosis. Carbon 2007, 45:1743–1756
29. Boutin C, Rey F, Gouvernet J, Viallat JR, Astoul P, Ledoray V: Thoracoscopy in pleural malignant mesothelioma: a prospective study of 188 consecutive patients: part 2: prognosis and staging. Cancer 1993, 72:394–404
30. Moalli PA, Macdonald JL, Goodglick LA, Kane AB: Acute injury and regeneration of the mesothelium in response to asbestos fibers. Am J Pathol 1987, 128:426–445
31. Vasilieva LA, Pylev LN, Rovensky YA: Pathogenesis of experimentally induced asbestos mesothelioma in rats. Cancer Lett 1998, 134:209–216
32. Bernstein DM, Rogers RA, Sepulveda R, Donaldson K, Schuler D, Gaering S, Kunzendorf P, Chevalier J, Holm SE: The pathological response and fate in the lung and pleura of chrysotile in combination with fine particles compared to amosite asbestos following short-term inhalation exposure: interim results. Inhal Toxicol 2010, 22:937–962
33. Kanazawa K, Roe FJ, Yamamoto T: Milky spots (Taches-laiteuses) as structures which trap asbestos in mesothelial layers and their significance in the pathogenesis of mesothelial neoplasia. Int J Cancer 1979, 23:858–865
34. Roberts GH: The pathology of parietal pleural plaques. J Clin Pathol 1971, 24:348–353
35. Brown GM, Donaldson K: Inflammatory responses in lungs of rats inhaling coal-mine dust: enhanced proteolysis of fibronectin by bronchoalveolar leukocytes. Br J Ind Med 1989, 46:866–872
36. Donaldson K, Brown GM, Brown DM, Robertson MD, Slight J, Cowie H, Jones AD, Bolton RE, Davis JM: Contrasting bronchoalveolar leukocyte responses in rats inhaling coal mine dust, quartz, or titanium dioxide: effects of coal rank, airborne mass concentration, and cessation of exposure. Environ Res 1990, 52:62–76
37. Lapp NL, Castranova V: How silicosis and coal workers' pneumoconiosis develop: a cellular assessment. Occup Med 1993, 8:35–56
38. Parungo CP, Colson YL, Kim SW, Kim S, Cohn LH, Bawendi MG, Frangioni JV: Sentinel lymph node mapping of the pleural space. Chest 2005, 127:1799–1804
39. Ryman-Rasmussen JP, Cesta MF, Brody AR, Shipley-Phillips JK, Everitt JI, Tewksbury EW, Moss OR, Wong BA, Dodd DE, Andersen ME, Bonner JC: Inhaled carbon nanotubes reach the subpleural tissue in mice. Nat Nanotechnol 2009, 4:747–751
40. Mercer RR, Hubbs AF, Scabilloni JF, Wang LY, Battelli LA, Schwegler-Berry D, Castranova V, Porter DW: Distribution and persistence of pleural penetrations by multi-walled carbon nanotubes. Part Fibre Toxicol 2010, 7:28
41. Miserocchi G, Sancini G, Mantegazza F, Chiappino G: Translocation pathways for inhaled asbestos fibers. Environ Health 2008, 7:4
42. Liu XY, Hurt RH, Kane AB: Biodurability of single-walled carbon nanotubes depends on surface functionalization. Carbon 2010, 48: 1961–1969
43. Kagan VE, Konduru NV, Feng W, Allen BL, Conroy J, Volkov Y, Vlasova II, Belikova NA, Yanamala N, Kapralov A, Tyurina YY, Shi J, Kisin ER, Murray AR, Franks J, Stolz D, Gou P, Klein-Seetharaman J, Fadeel B, Star A, Shvedova AA: Carbon nanotubes degraded by neutrophil myeloperoxidase induce less pulmonary inflammation. Nat Nanotechnol 2010, 5:354–359
44. Tomatis M, Turci F, Ceschino R, Riganti C, Gazzano E, Martra G, Ghigo D, Fubini B: High aspect ratio materials: role of surface chemistry vs length in the historical "long and short amosite asbestos fibers." Inhalation Toxicol 2010, 22:984–998

PARTICLE AND FIBRE TOXICOLOGY

RESEARCH Open Access

The mechanism of pleural inflammation by long carbon nanotubes: interaction of long fibres with macrophages stimulates them to amplify pro-inflammatory responses in mesothelial cells

Fiona A Murphy[1], Anja Schinwald[1], Craig A Poland[2] and Ken Donaldson[1*]

Abstract

Carbon nanotubes (CNT) are high aspect ratio nanoparticles with diameters in the nanometre range but lengths extending up to hundreds of microns. The structural similarities between CNT and asbestos have raised concern that they may pose a similar inhalation hazard. Recently CNT have been shown to elicit a length-dependent, asbestos-like inflammatory response in the pleural cavity of mice, where long fibres caused inflammation but short fibres did not. However the cellular mechanisms governing this response have yet to be elucidated. This study examined the in vitro effects of a range of CNT for their ability to stimulate the release of the acute phase cytokines; IL-1β, TNFα, IL-6 and the chemokine, IL-8 from both Met5a mesothelial cells and THP-1 macrophages. Results showed that direct exposure to CNT resulted in significant cytokine release from the macrophages but not mesothelial cells. This pro-inflammatory response was length dependent but modest and was shown to be a result of frustrated phagocytosis. Furthermore the indirect actions of the CNT were examined by treating the mesothelial cells with conditioned media from CNT-treated macrophages. This resulted in a dramatic amplification of the cytokine release from the mesothelial cells, a response which could be attenuated by inhibition of phagocytosis during the initial macrophage CNT treatments. We therefore hypothesise that long fibres elicit an inflammatory response in the pleural cavity via frustrated phagocytosis in pleural macrophages. The activated macrophages then stimulate an amplified pro-inflammatory cytokine response from the adjacent pleural mesothelial cells. This mechanism for producing a pro-inflammatory environment in the pleural space exposed to long CNT has implications for the general understanding of fibre-related pleural disease and design of safe nanofibres.

Keywords: Carbon nanotubes, Pleura, Mesothelioma, Asbestos, Inflammation

Background

Carbon nanotubes (CNT) are high aspect ratio nanoparticles comprising single (SWCNT) or concentrically stacked multiwalled (MWCNT) graphene sheets rolled seamlessly into a cylinder. Their high aspect-ratio and novel properties make CNT a useful industrial material and has led to their incorporation into a wide variety of consumer products. However, as the applications of CNT continue to grow, so too does the potential for occupational inhalation exposure with obvious potential hazards for worker health [1]. The structural similarities between CNT and asbestos have raised particular concern regarding the potential pathogenicity of CNT in the lung and serosal cavities, specifically the pleural and peritoneal spaces, which are key target tissues for asbestos-related disease [2].

Carbon nanotubes have been found to cause a range of pathogenic effects, oxidative stress [3] inflammation and NLRP3 inflammasome activation [4], fibrosis [5,6] and genotoxicity [7].

The mesothelial lining of the pleural cavity has long been known to be particularly sensitive to asbestos exposure producing pleural effusion, pleural plaques and

* Correspondence: ken.donaldson@ed.ac.uk
[1]MRC/University of Edinburgh Centre for Inflammation Research, ELEGI Colt Laboratory, Queen's Medical Research Institute, 47 Little France Crescent, Edinburgh EH16 4TJ, UK
Full list of author information is available at the end of the article

fibrosis [8]. Cancer arising in the mesothelial cells lining both the peritoneal and pleural cavities, mesothelioma, is a response almost unique to fibrous particles. The exact mechanisms leading to fibre-induced mesothelioma formation are unknown although fibre dimensions [9-11], biopersistence [12], the generation of reactive oxygen species (ROS) [13] and inflammation [14] have all been implicated. Due to its uniformly poor prognosis, mesothelioma is the disease of most concern when contemplating the potential toxicity of new high aspect ratio nanoparticles; pleural plaques and effusion are also a consequence of long fibre dose in the pleural space. The ability of fibres to induce an inflammatory response in the pleura has been considered to be a key mechanism in the production of mesothelioma and other pleural pathology[15,16]. A length dependent inflammatory response, similar to that seen with asbestos, has been reported for CNT and other high aspect ratio nanomaterials (HARN) in a number of studies using the peritoneal cavity as a model of mesothelium exposure [17,18] and more recently in a study conducted by the present authors investigating the response to CNT instilled into the pleural cavity [19]. The length-dependent response in the pleural cavity was characterised by an initial acute inflammatory reaction as indicated by an influx of granulocytes and an increase in protein concentration in the lavage fluid [19]. The length-dependent response to CNT in vivo was attributed to the fibre length-restricted clearance mechanisms from the pleural space through stomata in the parietal pleura leading to specific retention of long fibres while short fibres are efficiently cleared [19]. Nevertheless the detailed interactions between the CNT and pleural mesothelial cells and macrophages at these points of retention are unknown and are the focus of the present study.

Inhaled fibres that reach the pleural space will encounter mesothelial cells lining the pleural cavity and also resident pleural macrophages. Mesothelial cells, historically thought of as barrier cells that provide a lubricated surface that locks the parietal pleura to the visceral pleura allowing for lung movements, are now also known to play a prominent role in the initiation, perpetuation and resolution of inflammation in the pleural cavity [20]. During injury or infection, mesothelial cells can respond by producing a spectrum of pro- and anti-inflammatory cytokines and chemokines, growth factors, oxidants, extracellular matrix molecules and mediators of the complement cascade [20]. Macrophages are also present in the pleural space and can play a role in host defence and immuno-inflammatory responses [21]. The primary function of professional phagocytes such as pleural macrophages is to ingest foreign material that may pose a threat to the body and so pleural macrophages are likely to play a key role in the removal of inhaled particles and fibres that are retained in the pleural space. We therefore hypothesised that the response of the mesothelial cells and macrophages upon exposure to CNT or other fibres will be crucial in the pathogenesis of fibre-related pleural inflammation and therefore in subsequent pleural disease.

Here, we aim to use in vitro methods to elucidate the relative roles of the macrophages and mesothelial cells in driving the inflammatory response to long fibres. Long and short CNT samples were examined in an effort to infer whether the response to the CNT was length-dependent, as is the case in the inflammatory response in the pleural space in vivo [19]. Using the same panel of CNT as described by Murphy et al. [19] we examined the ability of long and short CNT to elicit pro-inflammatory responses in both a human non-transformed mesothelial cell line (Met5A), and macrophages derived from the human monocyte cell line (THP-1) as a surrogate for pleural macrophages, by direct exposure to CNT. The release of TNFα, IL-6, IL-8 and IL-1β; acute phase pro-inflammatory cytokines was measured as an indicator of the pro-inflammatory potential of the CNT panel. In addition we hypothesized that the inflammatory response could be driven by cross-talk between the macrophages and mesothelial cells and so we also examined the effect of conditioned media from CNT-treated macrophages on the mesothelial pro-inflammatory response.

Results

Effect of direct exposure to CNT panel on mesothelial cell and macrophage viability

Mesothelial cell viability, as measured by trypan blue exclusion assay, was examined after 24 hour exposure to the CNT panel over a dose range from 5 to 50 μg/cm^2. A significant loss of cell viability was seen only in response to NT_{long1} (20 μg/cm^2) and NT_{long2} (20 ug/cm^2, 50 μg/cm^2) (Figure 1A). This loss of cell viability coincided with an increase in supernatant LDH levels in Met5A cultures treated with NT_{long1} and NT_{long2} at the two highest doses only (Figure 1B). Exposure of macrophages (THP-1) to all the members of the CNT panel caused a significant increase in supernatant LDH only at the higher doses (Figure 1C). Trypan blue exclusion assay could not be carried out on THP-1 cells exposed to CNT as macrophages clumped together during the treatments making accurate assessment of the cellular viability by this method impossible. Based on these data a sub-lethal dose of 5 μg/cm^2 was selected for treatments of both Met5A and THP-1 cells for the subsequent activation studies.

Effects of direct exposure to the CNT panel on pro-inflammatory cytokine release from mesothelial cells

In order to investigate the effect CNT might have on mesothelial cell activation we assayed, using a cytometric bead array system, the concentration of a number of

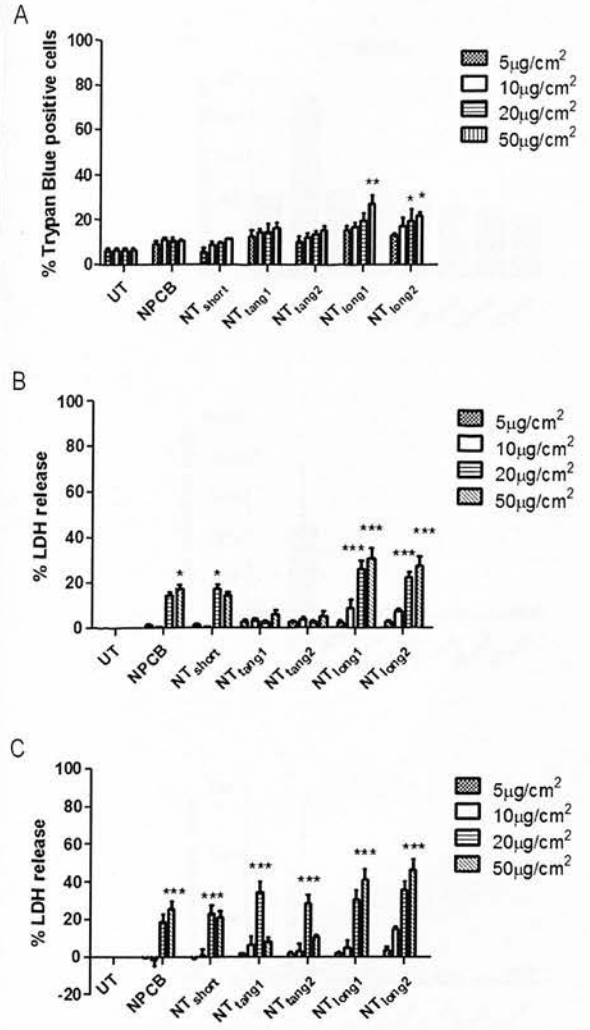

Figure 1 The effect of the CNT panel on cell viability. The viability of mesothelial cells was measured by trypan blue exclusion (A) and LDH release (B) after a 24 hour exposure to the CNT panel, UT indicates untreated control. LDH release was also used as an indicator of cell viability of macrophages at 24 hours after CNT treatment (C). Data expressed as a mean ± sem, n = 3. Significance versus vehicle control *** indicates $p < 0.001$.

pro-inflammatory cytokines present in Met5A cell supernatants following direct exposure to the CNT panel for 24 hours (Figure 2A). No member of the CNT panel had an effect on the supernatant concentrations of IL-1β, IL-6, IL-8 or TNFα in Met5A cultures compared to LPS, a positive control to activate cells, which caused a significant increase in the concentration of all four cytokines.

Effects of direct exposure to the CNT panel on pro-inflammatory cytokine release from macrophages

In order to investigate the impact of CNT phagocytosis on macrophage activation, we measured the concentration of IL-1β, IL-6, IL-8 and TNFα present in the THP-1 cells supernatants following exposure to the CNT panel (Figure 2B). Only the CNT samples containing long fibres- NT_{long1} and NT_{long2} caused a significant increase in IL-1β and IL-6 concentrations compared to untreated cells. NT_{long1} also induced a significant increase in IL-8 concentration; however no increase was seen with NT_{long2}. NT_{long2} did appear to elevate the concentration of TNFα, but this elevation was not statistically significant. No increase in cytokine concentration was seen after exposure to NPCB, NT_{short}, NT_{tang1} or NT_{tang2}.

Role of frustrated phagocytosis in length-dependent IL-1β release from macrophage

The appearance of the THP-1 cells after 24 hour treatment with the CNT panel at a dose of 5 $\mu g/cm^2$ is shown in Figure 3 as Diffquik stained light micrograph images (A-G) or as scanning electron micrograph figures (H - K). Normal cells are shown in Figure 3D and 3H. NPCB and the short CNT samples; NT_{short}, NT_{tang1} and NT_{tang2} appear to be easily taken up by the macrophages as they are seen as accumulations of black particles within the cells (Figure 3A, B, E and 3F) but were not visible on the cell surface in SEM images confirming that they had been effectively phagocytosed (Figure 3I and 3J). NT_{long1} and NT_{long2} were not completely taken up by the cells which showed the classic features of frustrated phagocytosis with fibrous CNT extended from the cell surfaces (Figure 3G and 3K) or a single long fibre could be shared by more than one cell (Figure C). This state of frustrated phagocytosis appeared more extensive in cells treated with the longer NT_{long2} sample. We selected one cytokine, IL-1β, to test the hypothesis that the length-dependent pro-inflammatory effects were due to frustrated phagocytosis of long fibres. THP-1 cells were co-incubated with the NT_{long1} and NT_{long2} samples and an inhibitor of phagocytosis (cytochalasin D) and the release of IL-1β was measured by ELISA (Figure 4). Cytochalasin D, a potent inhibitor of actin polymerisation, prevented the uptake of the long CNT by the THP-1 cells (Figure 4A) and inhibited the increase in IL-1β concentration caused by exposure to NT_{long1} and NT_{long2} in a dose-dependent pattern. However it had no effect on the IL-1β concentrations caused by LPS, which does not require phagocytosis to elicit a pro-inflammatory response. Measurements of supernatant LDH levels showed there was no loss of cell viability due to cytochalasin D treatments (Figure 4B).

Effect of conditioned media from CNT-exposed macrophages on mesothelial cell viability

In order to test the hypothesis that CNT that reach the pleural space stimulate mesothelial cells indirectly via the release of cytokines from particle-activated macrophages, we used conditioned media from CNT-exposed THP-1

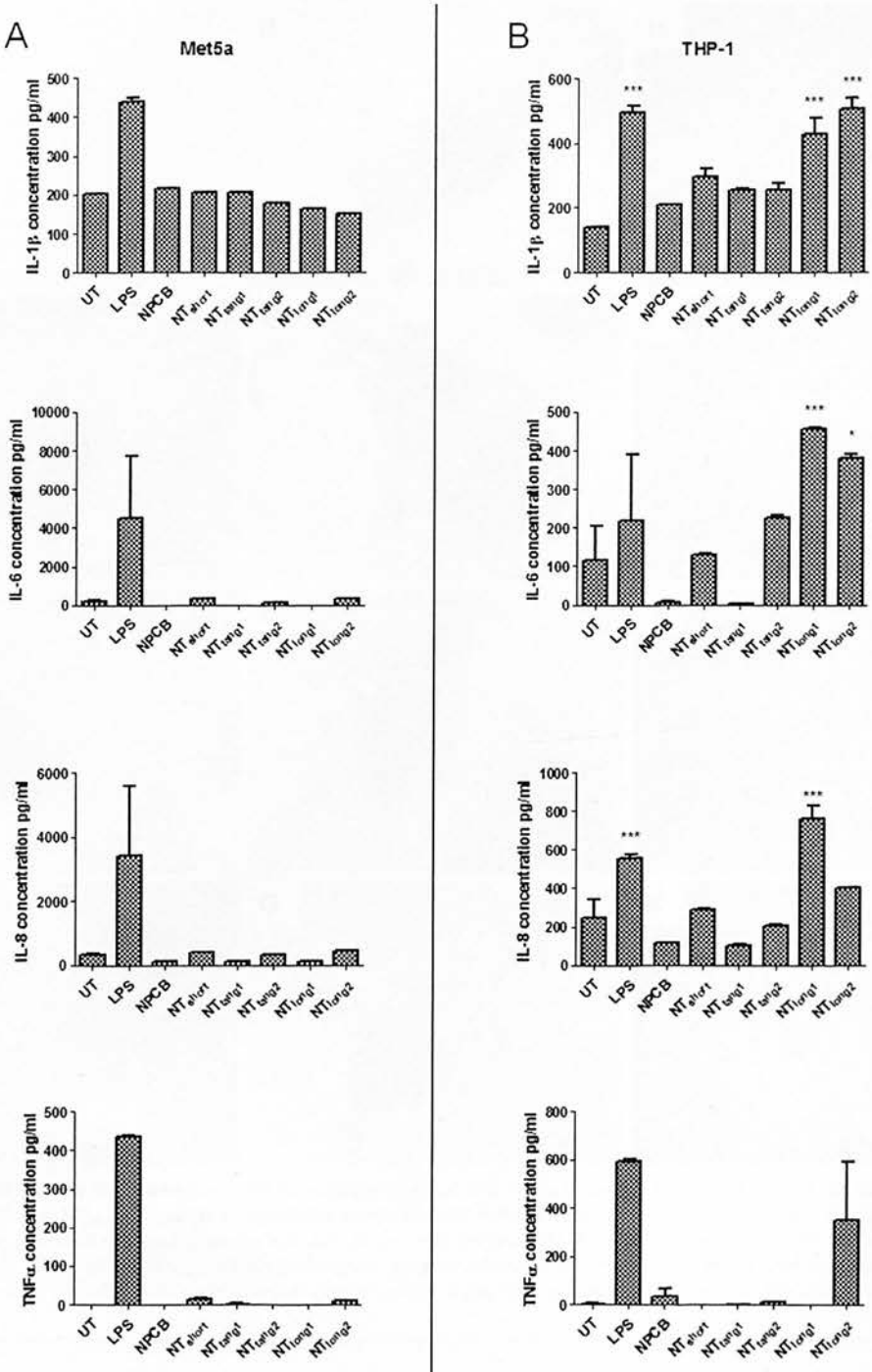

Figure 2 The effect of the direct exposure to the CNT panel on cytokine release from mesothelial cells and macrophages. No increase in the levels of IL-1β, IL-6, IL-8 or TNFα was detected after mesothelial cells were exposed to the CNT panel. However significant increases in IL-1β and IL-6 and IL-8 were seen in macrophages treated to long CNT samples only. UT indicates untreated control Data expressed as a mean ± sem, n = 3.

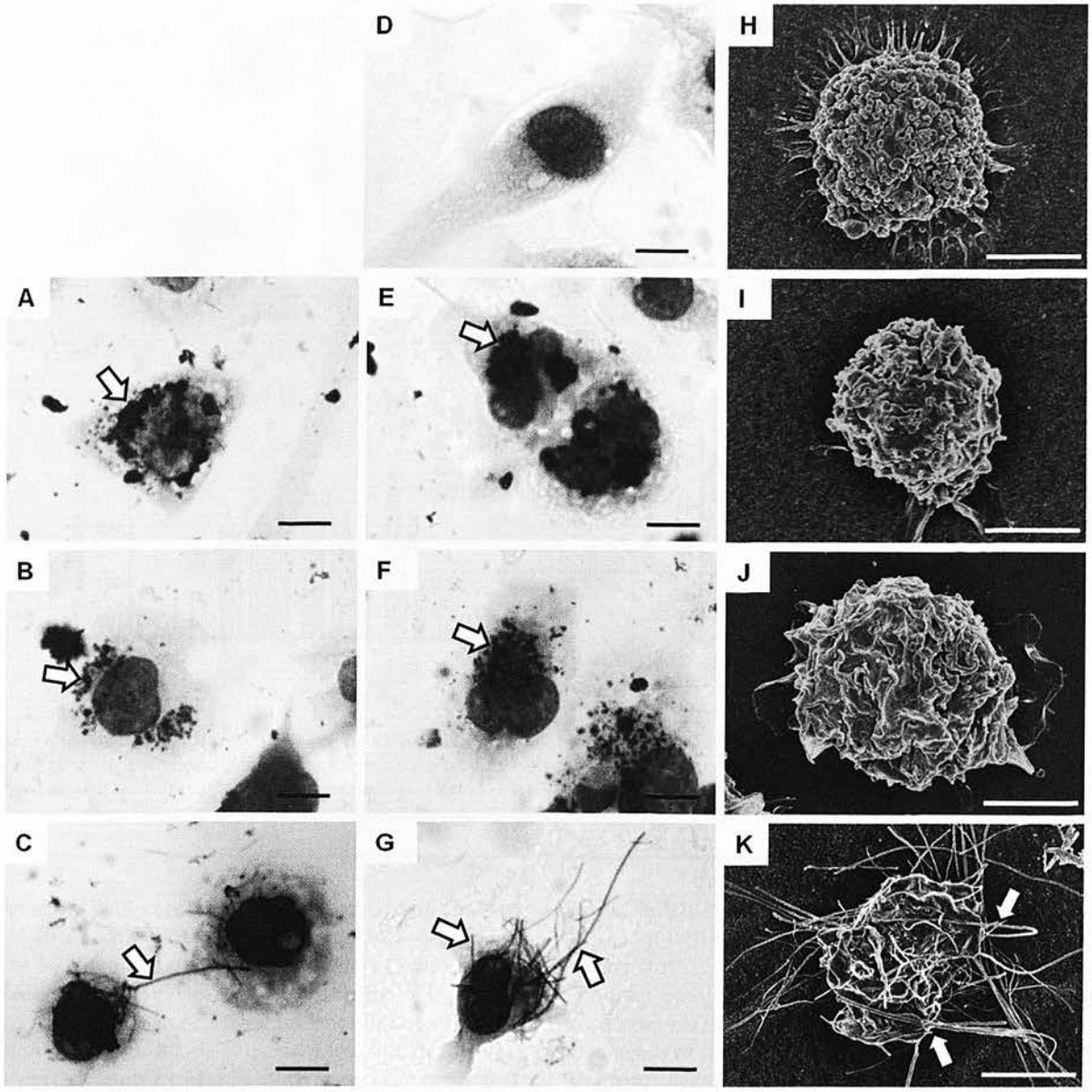

Figure 3 Uptake of CNT by macrophages. Light micrographs (A-G) of THP-1 cells untreated (D) or treated with the CNT panel. NPCB (A), NT_{short} (E), NT_{tang1} (B) and NT_{tang2} (F) appear as aggregates within the cells (white arrows). However NT_{long1} (C) and NT_{long2} (G) appear to be protruding from the cells (white arrows). Scale bar indicates 20 μm. SEM images (H-K) show an untreated THP-1 cell (H) and THP-1 cells treated with NPCB (I), NT_{short} (J) and NT_{long2} (K). No particles can be seen associated with the cell surface or protruding from the cells in I or J however the fibre from the NT_{long2} (K) sample appear on the surface of the cells and also protruding from the cell. Scale bar indicates 10 μm.

cells to treat Met5A cells and measured the concentrations of pro-inflammatory cytokines in the Met5A supernatant (Figure 5A).

No increase in LDH release from the Met5A cells treated with the conditioned media confirm the treatments did not caused a loss of membrane integrity and therefore cell viability (Figure 5B).

Effect of conditioned media from CNT-exposed macrophages on mesothelial cell production of pro-inflammatory cytokines

Whilst direct exposure of Met5A cells to the CNT panel had not caused any increases in IL-1β, treatment with conditioned media from THP-1 cells exposed to LPS, NT_{long1} or NT_{long2} resulted in approximately two-fold

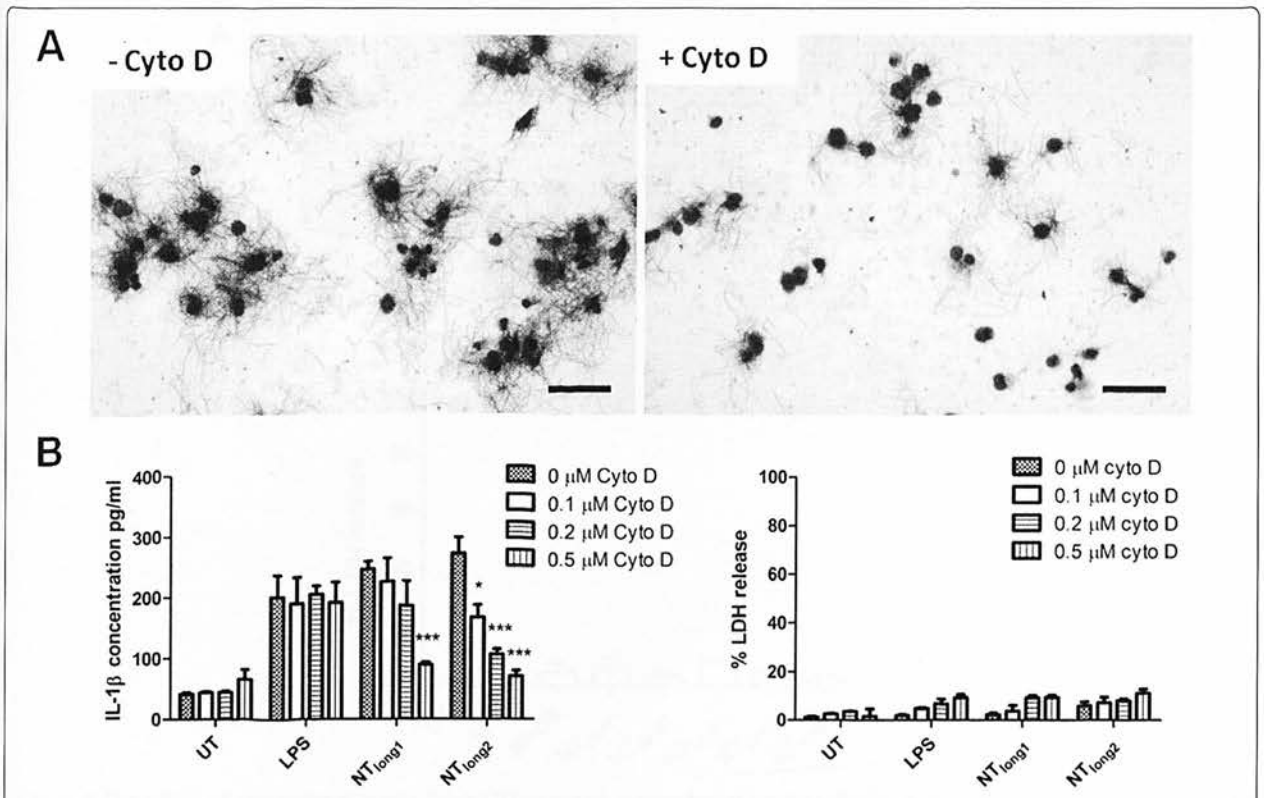

Figure 4 Inhibition of IL-1β release from long CNT-treated macrophages. (A) Example images of macrophages treated with NT_{long2} with or without cytochalasin D. Cytochalasin D inhibits the attempted uptake of long fibres by the macrophages. (B) Cytochalasin D caused a dose-dependent inhibition of IL-1β release from macrophages treated with NT_{long1} and NT_{long2} but not LPS. Significance versus 0 μM cytochalasin D within each treatment group *** indicates $p < 0.001$. A loss of cell viability in the presence of cytochalasin D was not detected by LDH release. Data expressed as mean ± sem, n = 3.

increase in IL-1β concentration compared with the combined total from both cell types exposed directly as shown by the horizontal lines on the bars (Figure 6A).

Media from THP-1 cells exposed to the NT_{long1} and NT_{long2} samples also had a significant effect on the production of IL-6, IL-8 and TNFα by Met5A (Figure 6B-D). The potentiation of Met5A activation was most pronounced when Met5A had been exposed to NT_{long2}-exposed THP-1 media which resulted in a 20-fold, 30-fold and 6-fold increase in the concentrations of IL-6, IL-8 and TNFα respectively, when compared with the combined total from each cell type exposed directly. Conditioned media from NT_{long1} treated THP-1 cells also caused a significant increase in the production of IL-6, IL-8 and TNFα from Met5A cells albeit to a lesser extent. Exposure to media from THP-1 cells treated with NPCB, NT_{short}, NT_{tang1} or NT_{tang2} did not have any effect on the production of the pro-inflammatory cytokines; IL-1β, IL-6, IL-8 or TNFα, by Met5A cells.

The levels of IL-1β and IL-6 released from Met5A cells treated with the conditioned media from THP-1 cells treated with NT_{long2} was attenuated when the THP-1 cells were co-exposed to NT_{long2} and cytochalasin D to prevent phagocytosis (Figure 7).

Iron content

The iron content of the CNT samples is given in the Additional file 1.

Interference of CNT in the assays

We precluded interference of CNT in the assays used here and the evidence is present in the Additional file 1.

Discussion

We previously reported that long CNT but not short CNT were capable of causing inflammation in the peritoneal [17] and pleural spaces [19]. Whilst retention of the long fibres at stomata represent the key initiating step the cellular mechanism, especially the interaction between macrophages and mesothelial cells, leading to inflammation was not elucidated. The present study addressed three hypotheses as to the mechanism by which CNT cause pro-inflammatory effects in the pleural cavity. These three hypotheses centred on the major cells of the pleural cavity, mesothelial cells and macrophages, are outlined in diagrammatic form in Figure 8. The refractoriness of the

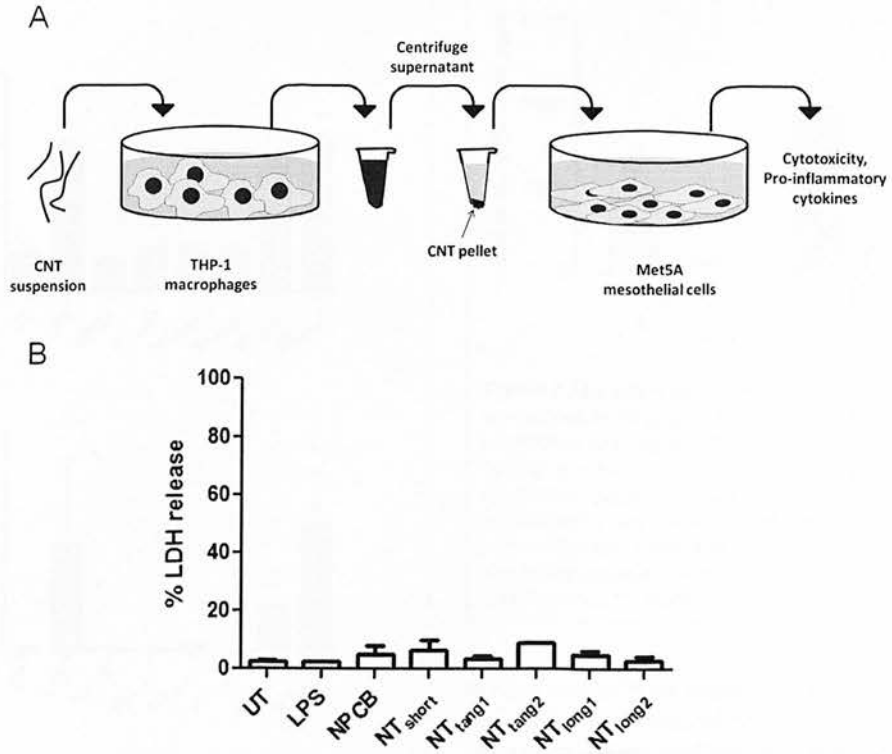

Figure 5 The effect of conditioned media from CNT-exposed macrophages on mesothelial cell viability. (A) Schematic diagram representing the conditioned media experimental procedure. THP-1 cells were treated with CNT suspensions for 24 hours, supernatant was removed and centrifuged to remove any suspended CNT, conditioned media was added to the Met5A cells for 24 hours after which cell viability and production of cytokines was measured. Cell viability of mesothelial cells was measured by LDH release (B) but no cell death was detected.

mesothelial cells to long CNT effects and the existing literature describing how conditioned media from macrophages treated with particles greatly amplify the pro-inflammatory responses of epithelial cells [22] and endothelial cells [23] led us to discount the alternative hypothesis, that products released by mesothelial cells could stimulate amplifying pro-inflammatory responses in the macrophages. Whilst mesothelial cells did prove refractory, in terms of cytokine release, to direct exposure to long and short CNT, macrophages exposed to long fibre CNT samples did release significant quantities of pro-inflammatory cytokines. When the supernatant from the long fibre-exposed macrophages was added to mesothelial cells it stimulated the mesothelial cells to release substantial quantities of cytokines that were much greater than those produced by the macrophages in response to long CNT or the mesothelial cells exposed to long CNT (Summarised in Table 1) or the sum of these two. Therefore the pro-inflammatory milieu generated by macrophages in response to long fibre CNT samples was a potent activator of mesothelial cells and caused a dramatic amplification of cytokine production by the mesothelial cells. Supernatants were centrifuged at 13,000 rpm for 5 minutes to remove any CNT and this procedure produced a black pellet and a clear supernatant. When the clear supernatant was added to the target mesothelial cells, in contrast to the direct treatment with CNT where black CNT were readily visible inside the cells, no particles were visible in or on the cells. It is not possible to preclude the presence of very small amounts of CNT but these would be trace amounts well below the threshold of effect.

The mechanism and outcome of phagocytosis of long CNT differs from that of short CNT or NPCB, in that phagocytosis proceeds initially but the macrophage cannot effectively enclose the extended structure of a long fibre culminating in the phenomenon of 'frustrated phagocytosis' [24]. The uptake of long fibres by macrophages and the subsequent pro-inflammatory response from the mesothelial cells exposed to their supernatant could be attenuated by inhibiting the phagocytosis of the long fibres by macrophages during the initial treatments using the microfilament poison Cytochalasin D; this confirms that the process of frustrated phagocytosis is is the key one that leads to inflammation in the case of the long fibre CNT. The macrophage response to LPS, which does not require microfilament-mediated

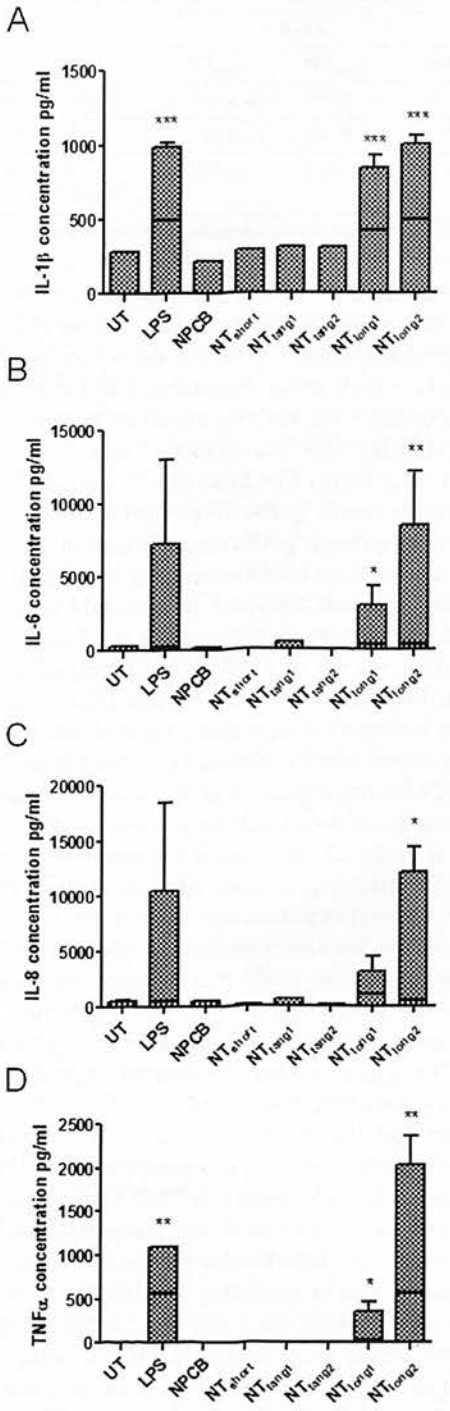

Figure 6 The effect of conditioned media on cytokine release from cells. IL-1β, IL-6, IL-8 and TNFα supernatant levels were measured 24 hours after mesothelial cells were exposed to media from CNT-treated macrophages. A length-dependent increase in concentration was observed for each of the cytokines. The black horizontal lines on the graph indicate the level of cytokine expressed by the THP-1 cells which is still present in the conditioned media. Data expressed as mean ± sem, n = 3. Significance versus vehicle control *** indicates $p < 0.001$.

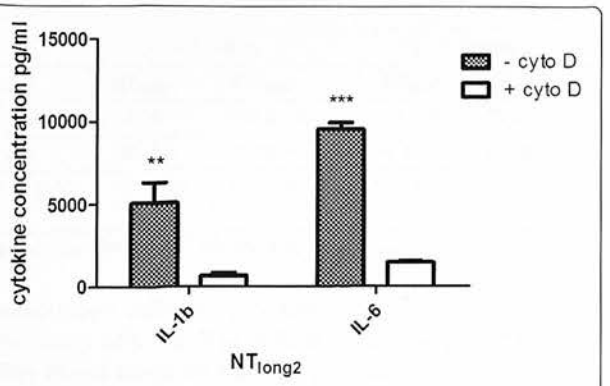

Figure 7 The effect of conditioned media from macrophages co-exposed to NT_{long2} and cytochalasin D on mesothelial production of IL-1β and IL-6. A significant reduction in the levels of IL-1β and IL-6 release from mesothelial cells exposed to conditioned media from macrophages treated with NT_{long2} and cytochalasin D was observed compared to mesothelial cells treated with conditioned media from macrophages treated with NT_{long2} alone. Data expressed as mean ± sem, n = 3. Significance versus vehicle control *** indicates $p < 0.001$.

uptake into cells by phagocytosis, was not attenuated by the addition of cytochalasin D highlighting the necessity of particle uptake and the role of frustrated phagocytosis in the pro-inflammatory reaction produced in response to CNT exposure. Our results suggest that indirect activation of mesothelial cells by pro-inflammatory cytokines elaborated from longCNT-exposed macrophages is a key initiating event in the development of pleural inflammation and disease.

Previous studies have described that long, needle-like CNT and asbestos activated the NLRP3 inflammasome

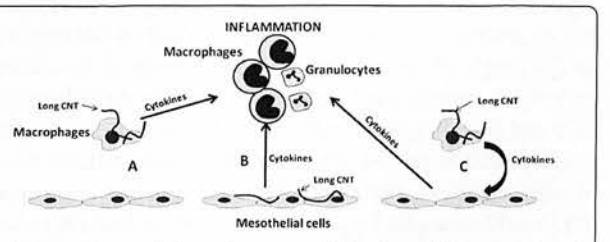

Figure 8 Potential mechanisms of the long fibre-mediated inflammatory response. The following three potential mechanisms by which CNT cause inflammation in the pleural space were explored in this study. (A) Long fibres interact with the pleural macrophages producing cytokines that directly elicit an inflammatory response. (B) Long fibres interact directly with mesothelial cells with the subsequent factors released leading to granulocyte influx. (C) Long fibres interact with macrophages inducing the release of cytokines which stimulate the mesothelial cells, amplifying the inflammatory response. As initial results showed no response from the mesothelial cells to direct exposure to CNT, the effect of factors released from CNT-exposed mesothelial cells on macrophages was not examined.

Table 1 Summary of cytokine release from cells

	IL-1β		IL-6		IL-8		TNFα	
	NT_{short}	NT_{long2}	NT_{short}	NT_{long2}	NT_{short}	NT_{long2}	NT_{short}	NT_{long2}
Mesothelial cells (pg/m)	205 ± 26	153 ± 17	340 ± 11	347 + 2	392 ± 15	458 ± 16	15 ± 2	10 ± 3
Macrophages (pg/ml)	296 ± 23	506 ± 34	128 ± 39	380 + 8	286 ± 8	403 ± 4	6 ± 2	350 ± 200
Mesothelial cells + conditioned media (pg/ml)	293 ± 2	1012 ± 59	214 ± 8	8479 + 3640	121 ± 29	12130 ± 2254	14 ± 4	2029 ± 328

The cytokine release for the three treatment groups are compared side by side using one short CNT (NT_{short}) and one long CNT (NT_{long2}) as exemplars

and secretion of IL-1β from LPS-primed human macrophages [25] whilst our macrophages were not primed with LPS. In our study the THP-1 cells had been differentiated with PMA [26]which gives then a phenotype similar to resting monocyte-derived macrophages.

A proportion of all particles and fibres that deposit in the distal regions of the lung will translocate into the pleural cavity thereby facilitating direct interactions between them and the patrolling macrophages of the pleural space and the mesothelial cells lining it [24]. According to Mercer et al. [34]CNT that reach the distal lung are likely to be predominantly present inside alveolar macrophages. However CNT in the immediate subpleural site, whilst a low proportion of all CNT, were all in tissue i.e. not in macrophages [27]. Therefore the CNT in the pleural space may be taken there inside alveolar macrophages, whilst the non-phagocytosed CNT that reach the pleural space from the sub-pleural tissue may be taken up by pleural macrophages. Research is needed to better understand the secretory profile of pleural macrophages or alveolar macrophages containing CNT in the pleural space. Mesothelial cells are reported to be uniquely sensitive to asbestos fibres with direct exposure in vitro inducing death [28,29], inflammatory mediator production [28], oxidative stress [30] and genotoxicity [39,40]. Although the potential pathogenicity of CNT has been tested in a variety of lung-derived cell types with responses including inflammation [33] and oxidative stress [34] reported, there is a paucity of data concerning the direct effects of CNT on mesothelial cells. Pacurari et al. examined the direct effects of SWCNT and MWCNT on normal and malignant mesothelial cells and reported a decrease in cell viability, activation of pro-inflammatory transcription factors and pro-inflammatory MAPK pathway activation [35,36]. However these effects were very modest and seen at 5-10 times the dose used in the present paper. There was also ongoing PARP activation suggesting that the cells were also undergoing apoptosis, making this data difficult to interpret as to the true role of direct pro-inflammatory effects of CNT on mesothelial cells at plausible doses. In contrast, within the present study we found mesothelial cell cytotoxicity only at the highest exposures used in preliminary studies but no evidence of pro-inflammatory responses after exposure of mesothelial cells to a low sub-lethal dose (5 $\mu g/cm^2$) of the panel of CNT. The inflammatory response to CNT after direct injection into the pleural space in vivo, characterised by an influx of inflammatory granulocytes [19], would undoubtedly require the actions of acute phase cytokines such as IL-1β, TNFα, IL-6 and IL-8. The inability of CNT to directly stimulate the production of such cytokines in mesothelial cells in vitro would suggest the interactions between CNT and mesothelial cells are not directly responsible for the initiation of inflammation.

In contrast to the findings with mesothelial cells, exposure of macrophages to the CNT panel resulted in the induction of modest length-dependent pro-inflammatory responses. This was evident when only the long fibre-containing samples (NT_{long1} and NT_{long2}) induced the production of the acute phase cytokines IL-1β and IL-6. The lack of response to the short CNT samples and particulate graphite in the form of NPCB suggest that the pro-inflammatory response to CNT in the pleural space is solely dependent on length. Length is a controlling factor in the clearance of fibres from the pleura where only long fibres are selectively retained for sufficient time to actually become involved in interactions with macrophages at stomatal openings [19]. Any fibre that exceeds a maximum length for macrophage uptake will result in frustrated phagocytosis, a state where the macrophages are unable to fully engulf long fibres resulting in the release of oxidants and pro-inflammatory signals [24]. Frustrated phagocytosis has long been known to play an important role in asbestos effects [24,37] and has also been implicated more recently in the inflammatory responses to long CNT elicited from macrophages in vitro [38] and in vivo [17] and long TiO_2 nanofibres [39]. Brown et al. reported an increase in the production of TNFα and a concurrent increase of ROS by macrophages in response to CNT and showed that this response was specifically related to the length of the CNT fibres [38]. The presence of macrophages undergoing frustrated phagocytosis in the peritoneal lavage fluid of mice exposed to long CNT was noted by Poland et al. who suggested that this macrophage-mediated response may be playing a role in the inflammation [17]. Here, using a panel of CNT similarly defined by length we showed the length-dependent release of a number of pro-inflammatory

cytokines from macrophages exposed to the long fibre CNT samples only. Frustrated phagocytosis of TiO_2 nanobelts longer than 15 μm was demonstrated by Hamilton et al. who also described the mechanism by which the inability of macrophages to completely enclose long fibres lead to pro-inflammatory responses via lysosomal destabilisation and NALP3 inflammasome activation [39]. The NALP3 inflammasome controls the maturation and release of IL-1β from activated cells [40] and activation of the NALP3 inflammasome via lysosomal destabilisation and the release of the lysosomal enzyme cathepsin B was reported in response to macrophage uptake of crystalline silica particles [41]. The activation of the NALP3 inflammasome by long CNT has also recently been demonstrated by Palomaki et al. in primary macrophages primed with LPS who, also reported a role for the $P2X_7$ receptor and its downstream tyrosine kinases, Src and Syk, in the activation of the NALP3 inflammasome in response to 'rigid, needle-like material' [42]. The induction of NALP3 via frustrated phagocytosis of long CNT is in keeping with studies examining the inflammatory response to asbestos and other fibrous particles which have also demonstrated the importance of the NALP3-mediated inflammatory response to particles and fibres in vivo. Inhibition or knock-out studies of key components of the NALP3 inflammasome prior to administration of asbestos fibres [43], silica [41,43,44] or MSU [41] crystals into the lungs of mice have all shown an attenuated inflammatory response compared to wild-type controls. The role for NALP3 in the activation of an inflammatory response suggests that direct interaction between macrophages and long fibres is the initiating mechanism for the development of long fibre-related inflammation and subsequent disease. Mesothelial cells are well equipped to participate in the initiation and resolution of inflammation. Secretion of chemokines by stimulated mesothelial cells promotes directed migration of granulocytes which can lead to influx of inflammatory cells from the vasculature into the serosal space [45]. Mesothelial cells have been shown to be directly stimulated to produce a range of pro-inflammatory mediators including cytokines, chemokines, growth factors and oxidants in response to bacterial endotoxin and asbestos but have also been shown to be highly responsive to factors secreted by macrophages [20]. Previous studies with PM10 and diesel soot have also shown that fixed cells-epithelial cells and endothelial cells respectively, show much greater responses to particle-free conditioned media from macrophages treated with particles than to direct treatment with the particles [22,23]. Similarly, in the present study a greatly amplified mesothelial pro-inflammatory response was conferred by the particle-free conditioned medium of long CNT-exposed macrophages. The role of cross-talk between macrophages and mesothelial cells in amplifying inflammation has been demonstrated previously by Betjes et al. when peritoneal mesothelial cells were shown to produce high levels of IL-8 in response to conditioned media from macrophages treated with the bacteria *Staphylococcus epidermidis*, but not to the bacteria themselves [46]. IL-1β and TNFα also mimicked induction of the mesothelial IL-8 response and the response to the conditioned media was blocked by the addition of anti-IL-1β and anti-TNFα antibodies [46]. The pro-inflammatory effect of the supernatant from macrophages exposed to the long CNT samples described here was similarly attenuated by inhibiting release of IL-1β by blocking phagocytosis with cytochalasin D highlighting the importance of phagocytosis in eliciting secretion of cytokines that drive the pro-inflammatory effects on the mesothelial cells. The acute inflammatory response seen in the pleural space after the injection of long CNT is characterised by the rapid influx of granulocytes into the pleural cavity [19]. The data suggest that it is a release of high levels of mesothelial IL-8 or KC, the mouse analogue of IL-8 in response to stimulatory factors released from macrophages attempting to phagocytose long CNT fibres that explains the inflammatory cell influx in vivo. Taking these 3 studies together [22,23,46] TNFα and IL-1β are the most likely candidate cytokines released by macrophages undergoing frustrated phagocytosis of long CNT that drive the pro-inflammatory effects in the mesothelial cells seen in our studies.

The mesothelial response to macrophage stimulation is also important in tissue repair. Macrophages were recruited in large numbers to the pleural space following long CNT deposition there [19]. Macrophages have been shown to stimulate mesothelial cell proliferation in response to injury in vivo with the rate of serosal healing dependent on the number of macrophages present [47] and also the macrophage-mediated release of cytokines such as TNFα [48]. Our data suggest that macrophages exposed to long CNT in the pleural space will have similar mitogenic effects on mesothelial cells which may lead to disregulated growth patterns.

The cross-talk between macrophages and mesothelial cells is known to be important in the normal inflammatory processes in the serosal cavities but, if disregulated, may also help to promote the development of mesothelioma. The precise mechanism that leads to mesothelioma development in the presence of fibres is unknown but a role for chronic inflammation in response to retained biopersistent fibres has been postulated [15]. Exposure of normal human mesothelial cells to asbestos fibres in vitro has not been shown to lead to cell transformation even though phenotypic changes such as chromosomal changes and extended lifespan were observed [31,32]. However Wang et al. [49] carried out a study examining the effect on mesothelial cells of erionite, a

naturally occurring long biopersistent fibre which causes mesothelioma in man and rodents following inhalation [50-52]. In this study, treatment of mesothelial cells with erionite in combination with pro-inflammatory cytokines highlighted a potential role for an inflammatory environment in the transformation of mesothelial cells [49]. While erionite alone had no effect on cell transformation, both IL-1β and TNFα could stimulate formation of transformed cells as identified by their anchorage-independent growth in soft agar. While the cytokines could induce the formation of tumorigenic colonies alone the effect was more potent in the presence of the erionite fibres [49]. TNFα has also been shown by Yang et al. to inhibit asbestos-induced cell death by activating the NF-κB signalling pathway in mesothelial cells [53]. The TNFα-mediated resistance to the cytotoxicity may promote tumour formation by increasing the pool of mesothelial cells with fibre-mediated genomic damage in the inflammogenic environment which evade normal cell death. This suggests that inflammation and inflammatory cytokines may play an important role in mesothelioma. Here we showed that mesothelial cells exposed to a cocktail of cytokines and other mediators produced by macrophages treated with long CNT amplify and propagate the inflammatory response thereby likely contributing to disease development in the pleural space.

A recent paper [54] has focused on the diameter of CNT and claimed that MWCNTs ~50 nm diameter showed mesothelial cell membrane piercing and cytotoxicity in vitro and subsequent inflammogenicity; in contrast CNT with a diameter of ~150 nm or ~2-20 nm were less inflammogenic. We found no support for this diameter hypothesis - the samples with least activity (short or tangled CNT) had diameters of 14.8, 10.4 and 84.9 nm respectively whilst the most active (the long CNT) was 165 nm diameter, quite close to the 150 nm diameter found to have no activity in the Nagai study [54].

Iron has been implicated in CNT activity via it's ability to cause oxidative stress [55,56]. However the levels of iron in our sample showed no relationship with activity in any of the assays; in particular the long CNT which had the most activity, had least iron.

Although we deal here solely with inflammation as a factor in fibre pathogenicity and mesothelioma production there are other effects of long fibres on mesothelial cells such as clastogenic and genotoxic ones that are important in themselves and possibly in concert with inflammation in leading to mesothelioma [54,57].

Conclusion

In summary, the data presented in this study describe a mechanism for the initiation of a long fibre mediated inflammatory response in the pleural space via frustrated phagocytosis. Only long fibres are retained in the pleural space and we have shown firstly that the incomplete phagocytosis of long CNT by macrophages, but not mesothelial cells, elicits a modest pro-inflammatory cytokine response. Secondly we show that the supernatant from macrophages exposed to long fibres produces a much-amplified pro-inflammatory response in target mesothelial cells. This amplified mesothelial cell response to macrophage products was attenuated by inhibition of macrophage phagocytosis, of long fibres confirming a role for frustrated phagocytosis. This study furthers our understanding of the role of macrophage/mesothelial cross-talk as a mechanism underlying the generation of a length-dependent inflammatory response to CNT in the pleural space. In addition, this in vitro model may prove useful for in vitro toxicity screening of the large number of new high aspect ratio nanofibres currently being developed, thereby reducing the need for animal testing.

Methods

CNT panel

The panel of particles investigated consisted of 5 different samples of multiwalled CNT and nano-particle carbon black (NPCB) as was used previously in Murphy et al. [19] (Table 2). The NT_{long1} sample (Mitsui & Co. Ltd., Japan) was produced by catalytic chemical vapour synthesis using the floating reaction method. The NT_{long2} sample was produced in an academic research laboratory (Dr Ian Kinloch, University of Manchester) using catalytic vapour discharge (CVD) method using a ferrocene-toluene feedstock to grow nanotubes from iron catalysts held on a silica plate. These nanotubes grew aligned as mats, meaning they were straight and un-entangled. The nanotubes were harvested from the mats using a razor blade, with some residual iron remaining within the nanotubes. We also included one commercially available short straight CNT ($NT_{short;}$ Nanoamor Inc., TX, USA) and two curled and tangled nanotubes of different lengths (NT_{tang1} which was cut to form predominantly short NT fibres and the original length NT sample (NT_{tang2}); NanoLab, Inc., MA, USA). These were produced by CVD with an iron and ceramic oxide (aluminosilicate) catalyst support which was removed using HCl and Hydrofluoric acid treatment. Trace metals and endotoxin levels previously tested and reported in Poland et al. [17] were low and thus not considered to play a role in these studies.

CNT suspensions

CNT were suspended in RPMI-1640 media (PAA Laboratories Ltd., UK) containing 0.5% bovine serum albumin (BSA; Sigma-Aldrich, Poole, UK) at a concentration of 500 μg/ml and dispersed by sonication at 230 V, 50 Hz, 350 W for 2 hours in an ultrasonic bath

Table 2 Characteristics of the particle panel

	NPCB	NT_{short}	NT_{tang1}	NT_{tang2}	NT_{long1}	NT_{long2}
Source	Degussa Printex 90	Nanostructured & Amorphous Materials, Inc.	NanoLab, Inc.	NanoLab, Inc.	Mitsui & Co.	University of Manchester [Dr. I. Kinloch]
Diameter (nm)	14	25.7 ± 1.6	14.84 ± 0.05	10.40 ± 0.32	84.89 ± 1.9	165.02 ± 4.68
Length (μm)	-	1-2	1-5	5-20	Mean 13	Mean 36
% fibre greater than 15 μm	‡	‡	‡	‡	24.04	84.26

(FB11002, Fisherbrand, Thermo Fisher Scientific, Inc., MA, USA). Suspensions were prepared freshly each day and used immediately upon removal from the ultrasonic bath.

Cell culture and treatment

The immortalised human mesothelial cell lineMet5A, and the monocytic cell line THP-1 were obtained from the American Type Culture Collection (ATCC) and maintained at sub-culture in RPMI-1640 supplemented with 10% foetal calf serum (PAA Laboratories Ltd., UK) at 37°C and 4% CO_2. Prior to experimentation Met5A cells were seeded in 24-well plates (Corning, Amsterdam, The Netherlands) at a concentration of 2.5×10^5 cells/well and allowed to adhere for 24 hours. THP-1 monocytic cells (2.5×10^5 cells/well) were differentiated into macrophages with 10 ng/ml phorbol 12-myristate 13-acetate (PMA; Sigma-Aldrich, Poole, UK) in 24-well plates for 48 hours. Prior to the treatment of both cell types the media was replaced with RPMI media containing 0% FCS, 1% penicillin/streptomycin and 1% L-Glutamate. Cells were treated with the CNT panel for 24 hours using a range of doses to determine cell viability, 5 μg/cm^2 was chosen as a sub-lethal dose for subsequent activation studies. Cytochalasin D (Enzo Life Science) was used to co-treat THP-1 cells along with NT_{long1}, NT_{long2}, or LPS. Light microscopy images of THP-1 cells treated with the panel of CNT were captured at ×40 magnification using QCapture Pro software (Media Cybernetics, MD, USA). For the conditioned media treatments THP-1 cells were treated with the CNT panel (5 μg/cm2) for 24 hours, supernatant was removed and centrifuged at 13,000 rpm for 5 minutes to remove any CNT. Conditioned media was added to the Met5A cells for 24 hours.

Scanning electron microscopy

THP-1 cells were grown on Thermonox coverslips (Nunc, Roskilde, Denmark) and treated with NPCB, NT_{short} or NT_{long2} for 24 hours. Cells were fixed with 10% Formalin and were stained with osmium tetroxide prior to critical point drying, mounted and gold sputter coated before examination by scanning electron microscopy (SEM) using an Hitachi S-2600 N digital scanning electron microscope (Oxford Instruments, Oxfordshire, UK).

Trypan blue exclusion assay

Met5A cells were plated as above before treatment with the particle panel for 24 hours at doses ranging from 5-50 μg/cm^2. The cell supernatant was removed and kept for LDH measurements, cells were washed once with PBS and incubated with 0.4% trypan blue (Sigma-Aldrich, Poole, UK) for 5 minutes. Excess trypan blue was removed and cells washed with PBS. Dead cells, as indicated by incorporation of the trypan blue dye, were counted and calculated as a percentage of total cells.

Lactate dehydrogenase assay

One hundred microlitres of cell supernatant from Met5A and THP-1 cells exposed to the CNT panel at doses ranging from 5-50 μg/cm^2 or LPS (1 μg/ml) was added in triplicate to a 96 well plate (Corning, Amsterdam, The Netherlands) and 100 μl of the LDH test reagent (diaphorase/NAD + mixed with iodotetrazolium chloride and sodium lactate at a ratio of 1:45) added to each well. Cells treated with 0.1% Triton-X were used as a positive control for 100% cell lysis. Following a 30 minute incubation period the absorbance of each well at 490 nm wavelength was established using a Synergy HT microplate reader (BioTek Instruments, Inc. VT, USA).

Cytokine bead array

The media levels of IL-1β, IL-6, IL-8 and TNFα were measured after direct exposure of the mesothelial cells and macrophages to the CNT panel and exposure of the mesothelial cells to the conditioned media from CNT-treated macrophages by cytokine bead array (BD CBA Flex Set, BD Biosciences, San Jose, CA). Briefly, 25 μl of the mixed capture antibodies were added along with 50 μl of the supernatant samples and standards to each well of a 96-well plate and incubated at room temperature for one hour. Twenty-five microlitres of the mixed PE detection reagent was added to each well and incubated at room temperature for two hours. The plate was centrifuged at 1500 rpm for 5 minutes and the supernatant completely

removed. One hundred and fifty microlitres of the wash buffer was added to each well. The plate was agitated for 5 minutes to resuspend the beads before the samples were analyzed using the BD FACSArray Bioanalyzer (BD Biosciences, San Jose, CA). Results were analysed using FCAP array software and sample concentrations of each cytokine were established via extrapolation from the appropriate recombinant protein standard curve.

ELISA

The media levels of IL-1β and IL-6 after macrophage inhibition studies was established using ELISA DuoSet kits (R&D systems, Abingdon, UK) specific to each analyte of interest. Ninety-six well microtitre plates were incubated overnight at 4°C with 100 μl of coating antibody raised against IL-1β or IL-6. The plates were washed 3 times with 0.05% Tween-20 in phosphate buffered saline (PBS; pH 7.2) and blocked using reagent diluent (1% BSA in PBS; R&D systems, Abingdon, UK) for 1 hour (room temperature) prior to further washing and addition of test samples/standards in triplicate. After 2 hrs the plates were washed and a biotinylated detection antibody added to each well followed by a further 2 hr incubation, followed by washing and the addition of HRP conjugated Streptavidin. The plates were washed and developed using a TMB substrate solution (Sigma-Aldrich, Poole, UK). The subsequent reaction was stopped with 0.5 M H_2SO_4, resulting in a yellow colour, and read at 450 nm. Sample concentrations of IL-1β, IL-6 were established via extrapolation from the appropriate recombinant protein standard curve.

Statistical analysis

All data are shown as the mean + s.e.m. and these were analysed using one-way analysis of variance (ANOVA). Multiple comparisons were analysed using the Tukey-HSD method, with values of $P < 0.05$ considered statistically significant (Instat, Graphpad Software Inc., CA, USA).

Additional material

Additional file 1: Supplementary information.

Abbreviations

CNT: carbon nanotubes; THP-1: macrophage cell line; Met5A: mesothelial cell line; NPCB: nanoparticulate carbon black; PARP: Poly (ADP-ribose) polymerase; TiO2: titanium dioxide; NALP3: NACHT: LRR and PYD domains-containing protein 3; P2X7: purinergic receptor; MSU: monosoium urate; IL-8: Interleukin 8; KC: keratinocyte -derived chemokine; TNFα: tumour necrosis factor α; NF-κB: Nuclear factor-κB; CVD: catalytic vapour discharge; ATCC: American Type Culture Collection; RPMI: Roswell Park Memorial Institute Medium; FCS: foetal calf serum; SEM: scanning electron microscopy; PBS: phosphate buffered saline; LDH: lactate dehydrogenase; FACS: fluorescence activated cell sorter.

Acknowledgements

We gratefully acknowledge Mitsui & Co. and Dr. Ian Kinloch (University of Manchester) for the provision of multiwalled carbon nanotube samples. We thank S. Mitchell (University of Edinburgh) for sample preparation for SEM and technical assistance. We thank the UK Department of Health (F.A.M.) and The Colt Foundation for the financial support (A. S., K.D.). This is an independent report commissioned and funded by the Policy Research Programme in the Department of Health and the views expressed are not necessarily those of the Department.

Author details

[1]MRC/University of Edinburgh Centre for Inflammation Research, ELEGI Colt Laboratory, Queen's Medical Research Institute, 47 Little France Crescent, Edinburgh EH16 4TJ, UK. [2]Institute of Occupational Medicine, Research Avenue North, Riccarton, Edinburgh EH14 4AP, UK.

Authors' contributions

All authors have made substantial contributions to conception and design and interpretation of data; FAM acquired the data with the assistance of AS. All authors were involved drafting or revising the manuscript and all authors have given final approval of the version to be published. All authors take public responsibility for the content. All authors read and approved the final manuscript.

Competing interests

KD has carried out consultancy for the nanotechnology industry not related to the scientific content of this manuscript.

Received: 20 December 2011 Accepted: 3 April 2012
Published: 3 April 2012

References

1. Donaldson K, Aitken R, Tran L, Stone V, Duffin R, Forrest G, *et al*: **Carbon nanotubes: a review of their properties in relation to pulmonary toxicology and workplace safety.** *Toxicol Sci* 2006, **92**:5-22.
2. Donaldson K, Murphy F, Schinwald A, Duffin R, Poland CA: **Identifying the pulmonary hazard of high aspect ratio nanoparticles to enable their safety-by-design.** *Nanomedicine* 2011, **6**:143-156.
3. Ye S, Wang Y, Jiao F, Zhang H, Lin C, Wu Y, *et al*: **The role of NADPH oxidase in multi-walled carbon nanotubes-induced oxidative stress and cytotoxicity in human macrophages.** *J Nanosci Nanotechnol* 2011, **11**:3773-3781.
4. Meunier E, Coste A, Olagnier D, Authier H, Lefevre L, Dardenne C, *et al*: **Double-walled carbon nanotubes trigger IL-1beta release in human monocytes through Nlrp3 inflammasome activation.** *Nanomedicine* 2011.
5. Shvedova AA, Kisin ER, Mercer R, Murray AR, Johnson VJ, Potapovich AI, *et al*: **Unusual inflammatory and fibrogenic pulmonary responses to single-walled carbon nanotubes in mice.** *Am J Physiol Lung Cell Mol Physiol* 2005, **289**:L698-L708.
6. He X, Young SH, Schwegler-Berry D, Chisholm WP, Fernback JE, Ma Q: **Multiwalled carbon nanotubes induce a fibrogenic response by stimulating reactive oxygen species production, activating NF-kappaB signaling, and promoting fibroblast-to-myofibroblast transformation.** *Chem Res Toxicol* 2011, **24**:2237-2248.
7. Donaldson K, Poland CA, Schins RP: **Possible genotoxic mechanisms of nanoparticles: criteria for improved test strategies.** *Nanotoxicology* 2010, **4**:414-420.
8. Donaldson K, Brown RC, Brown GM: **New perspectives on basic mechanisms in lung-disease .5. Respirable industrial fibers - mechanisms of pathogenicity.** *Thorax* 1993, **48**:390-395.
9. Stanton MF, Wrench C: **Mechanisms of mesothelioma induction with asbestos and fibrous glass.** *Journal of the National Cancer Institute* 1972, **48**:797-821.
10. Walker C, Everitt J, Barrett JC: **Possible cellular and molecular mechanisms for asbestos carcinogenicity.** *American Journal Of Industrial Medicine* 1992, **21**:253-273.
11. Miller BG, Searl A, Davis JM, Donaldson K, Cullen RT, Bolton RE, *et al*: **Influence of fibre length, dissolution and biopersistence on the production of mesothelioma in the rat peritoneal cavity.** *Ann Occup Hyg* 1999, **43**:155-166.

12. Barrett JC: **Cellular and Molecular Mechanisms of Asbestos Carcinogenicity - Implications for Biopersistence.** *Environmental Health Perspectives* 1994, **102**:19-23.
13. Okada F: **Beyond foreign-body-induced carcinogenesis: Impact of reactive oxygen species derived from inflammatory cells in tumorigenic conversion and tumor progression.** *International Journal Of Cancer* 2007, **121**:2364-2372.
14. Yang HN, Testa JR, Carbone M: **Mesothelioma Epidemiology, Carcinogenesis, and Pathogenesis.** *Current Treatment Options in Oncology* 2008, **9**:147-157.
15. Okada F, Fujii J: **Molecular mechanisms of inflammation-induced carcinogenesis.** *Journal of Clinical Biochemistry and Nutrition* 2006, **39**:103-111.
16. Nagai H, Toyokuni S: **Biopersistent fiber-induced inflammation and carcinogenesis: lessons learned from asbestos toward safety of fibrous nanomaterials.** *Arch Biochem Biophys* 2010, **502**:1-7.
17. Poland CA, Duffin R, Kinloch I, Maynard A, Wallace WA, Seaton A, *et al*: **Carbon nanotubes introduced into the abdominal cavity of mice show asbestos-like pathogenicity in a pilot study.** *Nat Nanotechnol* 2008, **3**:423-428.
18. Takagi A, Hirose A, Nishimura T, Fukumori N, Ogata A, Ohashi N, *et al*: **Induction of mesothelioma in p53+/- mouse by intraperitoneal application of multi-wall carbon nanotube.** *J Toxicol Sci* 2008, **33**:105-116.
19. Murphy FA, Poland CA, Duffin R, Al Jamal KT, Ali-Boucetta H, Nunes A, *et al*: **Length-dependent retention of carbon nanotubes in the pleural space of mice initiates sustained inflammation and progressive fibrosis on the parietal pleura.** *Am J Pathol* 2011, **178**:2587-2600.
20. Mutsaers SE: **Mesothelial cells: Their structure, function and role in serosal repair.** *Respirology* 2002, **7**:171-191.
21. Jantz MA, Antony VB: **Pathophysiology of the pleura.** *Respiration* 2008, **75**:121-133.
22. Jimenez LA, Drost EM, Gilmour PS, Rahman I, Antonicelli F, Ritchie H, *et al*: **PM(10)-exposed macrophages stimulate a proinflammatory response in lung epithelial cells via TNF-alpha.** *Am J Physiol Lung Cell Mol Physiol* 2002, **282**:L237-L248.
23. Shaw CA, Robertson S, Miller MR, Duffin R, Tabor CM, Donaldson K, *et al*: **Diesel exhaust particulate–exposed macrophages cause marked endothelial cell activation.** *Am J Respir Cell Mol Biol* 2011, **44**:840-851.
24. Donaldson K, Murphy FA, Duffin R, Poland CA: **Asbestos, carbon nanotubes and the pleural mesothelium: a review of the hypothesis regarding the role of long fibre retention in the parietal pleura, inflammation and mesothelioma.** *Part Fibre Toxicol* 2010, **7**:5.
25. Palomaki J, Valimaki E, Sund J, Vippola M, Clausen PA, Jensen KA, *et al*: **Long, needle-like carbon nanotubes and asbestos activate the NLRP3 inflammasome through a similar mechanism.** *ACS Nano* 2011, **5**:6861-6870.
26. Daigneault M, Preston JA, Marriott HM, Whyte MK, Dockrell DH: **The identification of markers of macrophage differentiation in PMA-stimulated THP-1 cells and monocyte-derived macrophages.** *PLoS One* 2010, **5**:e8668.
27. Mercer RR, Hubbs AF, Scabilloni JF, Wang L, Battelli LA, Schwegler-Berry D, *et al*: **Distribution and persistence of pleural penetrations by multi-walled carbon nanotubes.** *Part Fibre Toxicol* 2010, **7**:28.
28. Yang H, Rivera Z, Jube S, Nasu M, Bertino P, Goparaju C, *et al*: **Programmed necrosis induced by asbestos in human mesothelial cells causes high-mobility group box 1 protein release and resultant inflammation.** *Proc Natl Acad Sci USA* 2010, **107**:12611-12616.
29. Broaddus VC, Yang L, Scavo LM, Ernst JD, Boylan AM: **Asbestos induces apoptosis of human and rabbit pleural mesothelial cells via reactive oxygen species.** *Journal of Clinical Investigation* 1996, **98**:2050-2059.
30. Swain WA, Faux SP: **Activation of p38 MAP Kinase by Crocidolite in Mesothelial Cells is Dependent upon Oxidative Stress.** *Ann Occup Hyg* 2002, **46(Suppl 1)**:136-139.
31. Xu LX, Flynn BJ, Ungar S, Pass HI, Linnainmaa K, Mattson K, *et al*: **Asbestos induction of extended lifespan in normal human mesothelial cells: interindividual susceptibility and SV40 T antigen.** *Carcinogenesis* 1999, **20**:773-783.
32. Lechner JF, Tokiwa T, LaVeck M, Benedict WF, Banks-Schlegel S, Yeager H Jr, *et al*: **Asbestos-associated chromosomal changes in human mesothelial cells.** *Proc Natl Acad Sci USA* 1985, **82**:3884-3888.
33. Ye SF, Wen W, Wang YF, Lin CL, Wu YH, Zhang QQ: **Multi-walled Carbon Nanotubes Induces Nuclear Factor-kappa B Activation in A549 Cells.** *Chemical Journal of Chinese Universities-Chinese* 2010, **31**:497-501.
34. Pulskamp K, Diabate S, Krug HF: **Carbon nanotubes show no sign of acute toxicity but induce intracellular reactive oxygen species in dependence on contaminants.** *Toxicology Letters* 2007, **168**:58-74.
35. Pacurari M, Yin XJ, Zhao J, Ding M, Leonard SS, Schwegler-Berry D, *et al*: **Raw single-wall carbon nanotubes induce oxidative stress and activate MAPKs, AP-1, NF-kappaB, and Akt in normal and malignant human mesothelial cells.** *Environ Health Perspect* 2008, **116**:1211-1217.
36. Pacurari M, Yin XJ, Ding M, Leonard SS, Schwegler-Berry D, Ducatman BS, *et al*: **Oxidative and molecular interactions of multi-wall carbon nanotubes (MWCNT) in normal and malignant human mesothelial cells.** *Nanotoxicology* 2008, **2**:155-170.
37. Mossman BT, Churg A: **Mechanisms in the pathogenesis of asbestosis and silicosis.** *Am J Respir Crit Care Med* 1998, **157**:1666-1680.
38. Brown DM, Kinloch IA, Bangert U, Windle AH, Walter DM, Walker GS, *et al*: **An in vitro study of the potential of carbon nanotubes and nanofibres to induce inflammatory mediators and frustrated phagocytosis.** *Carbon* 2007, **45**:1743-1756.
39. Hamilton RF, Wu NQ, Porter D, Buford M, Wolfarth M, Holian A: **Particle length-dependent titanium dioxide nanomaterials toxicity and bioactivity.** *Particle and Fibre Toxicology* 2009, **6**:35.
40. Tschopp J, Schroder K: **NLRP3 inflammasome activation: the convergence of multiple signalling pathways on ROS production?** *Nature Reviews Immunology* 2010, **10**:210-215.
41. Hornung V, Bauernfeind F, Halle A, Samstad EO, Kono H, Rock KL, *et al*: **Silica crystals and aluminum salts activate the NALP3 inflammasome through phagosomal destabilization.** *Nature Immunology* 2008, **9**:847-856.
42. Palomaki J, Valimaki E, Sund J, Vippola M, Clausen PA, Jensen KA, *et al*: **Long, Needle-like Carbon Nanotubes and Asbestos Activate the NLRP3 Inflammasome through a Similar Mechanism.** *ACS Nano* 2011.
43. Dostert C, Petrilli V, Van Bruggen R, Steele C, Mossman BT, Tschopp J: **Innate immune activation through Nalp3 inflammasome sensing of asbestos and silica.** *Science* 2008, **320**:674-677.
44. Cassel SL, Eisenbarth SC, Iyer SS, Sadler JJ, Colegio OR, Tephly LA, *et al*: **The Nalp3 inflammasome is essential for the development of silicosis.** *Proceedings Of The National Academy Of Sciences Of The United States Of America* 2008, **105**:9035-9040.
45. Visser CE, Steenbergen JJE, Betjes MGH, Meijer S, Arisz L, Hoefsmit ECM, *et al*: **Interleukin-8 Production by Human Mesothelial Cells After Direct Stimulation with Staphylococci.** *Infection and Immunity* 1995, **63**:4206-4209.
46. Betjes MGH, Tuk CW, Struijk DG, Krediet RT, Arisz L, Hart M, *et al*: **Interleukin-8 Production by Human Peritoneal Mesothelial Cells in Response to Tumor-Necrosis-Factor-Alpha, Interleukin-1, and Medium Conditioned by Macrophages Cocultured with Staphylococcus-Epidermidis.** *Journal Of Infectious Diseases* 1993, **168**:1202-1210.
47. Mutsaers SE, Whitaker D, Papadimitriou JM: **Stimulation of mesothelial cell proliferation by exudate macrophages enhances serosal wound healing in a murine model.** *American Journal Of Pathology* 2002, **160**:681-692.
48. Mutsaers SE, McAnulty RJ, Laurent GJ, Versnel MA, Whitaker D, Papadimitriou JM: **Cytokine regulation of mesothelial cell proliferation in vitro and in vivo.** *European Journal of Cell Biology* 1997, **72**:24-29.
49. Wang YH, Faux SP, Hallden G, Kirn DH, Houghton CE, Lemoine NR, *et al*: **Interleukin-1 beta and tumour necrosis factor-alpha promote the transformation of human immortalised mesothelial cells by erionite.** *International Journal of Oncology* 2004, **25**:173-178.
50. Wagner JC, Skidmore JW, Hill RJ, Griffiths DM: **Erionite exposure and mesotheliomas in rats.** *Br J Cancer* 1985, **51**:727-730.
51. Maltoni C, Minardi F, Morisi L: **Pleural mesotheliomas in Sprague-Dawley rats by erionite: first experimental evidence.** *ENVIRONMENTAL RESEARCH* 1982, **29**:238-244.
52. Dikensoy O: **Mesothelioma due to environmental exposure to erionite in Turkey.** *Current Opinion in Pulmonary Medicine* 2008, **14**:322-325.
53. Yang HN, Bocchetta M, Kroczynska B, Elmishad AG, Chen YB, Liu ZM, *et al*: **TNF-alpha inhibits asbestos-induced cytotoxicity via a NF-kappa B-dependent pathway, a possible mechanism for asbestos-induced oncogenesis.** *Proceedings Of The National Academy Of Sciences Of The United States Of America* 2006, **103**:10397-10402.

54. Nagai H, Okazaki Y, Chew SH, Misawa N, Yamashita Y, Akatsuka S, *et al*: **Diameter and rigidity of multiwalled carbon nanotubes are critical factors in mesothelial injury and carcinogenesis.** *Proc Natl Acad Sci USA* 2011, **108**:E1330-E1338.
55. Kagan VE, Tyurina YY, Tyurin VA, Konduru NV, Potapovich AI, Osipov AN, *et al*: **Direct and indirect effects of single walled carbon nanotubes on RAW 264.7 macrophages: role of iron.** *Toxicol Lett* 2006, **165**:88-100.
56. Johnston HJ, Hutchison GR, Christensen FM, Peters S, Hankin S, Aschberger K, *et al*: **A critical review of the biological mechanisms underlying the in vivo and in vitro toxicity of carbon nanotubes: The contribution of physico-chemical characteristics.** *Nanotoxicology* 2010, **4**:207-246.
57. Kane AB: **Mechanisms of mineral fibre carcinogenesis.** In *Mechanisms of Fibre Carcinogenesis.* Edited by: Kane AB, Boffetta P, Saracci R, Wilbourn JD. IARC Publications, Lyon; 1996:11-34.

doi:10.1186/1743-8977-9-8
Cite this article as: Murphy *et al.*: **The mechanism of pleural inflammation by long carbon nanotubes: interaction of long fibres with macrophages stimulates them to amplify pro-inflammatory responses in mesothelial cells.** *Particle and Fibre Toxicology* 2012 **9**:8.

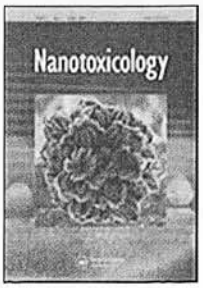

Length-dependent pleural inflammation and parietal pleural responses after deposition of carbon nanotubes in the pulmonary airspaces of mice.

Journal:	*Nanotoxicology*
Manuscript ID:	TNAN-2012-0077
Manuscript Type:	Original Article
Date Submitted by the Author:	20-Apr-2012
Complete List of Authors:	Murphy, Fiona; MRC Toxicology Unit, Poland, Craig; institute of Occupational Medicine, SafeNano Duffin, Rodger; CXR Biosciences, Donaldson, Ken; University of Edinburgh, ELEGI Colt Laboratory
Keywords:	Nanoparticles, Nanotoxicology, Fibre Toxicology, Mechanistic toxicology, Nanotubes

Length-dependent pleural inflammation and parietal pleural responses after deposition of carbon nanotubes in the pulmonary airspaces of mice.

Fiona A. Murphy[1], Craig A. Poland[2], Rodger Duffin[1], Ken Donaldson[1]

[1]MRC/University of Edinburgh Centre for Inflammation Research

ELEGI Colt Laboratory

Queen's Medical Research Institute

47 Little France Crescent

Edinburgh

EH16 4TJ

[2]Institute of Occupational Medicine

Research Avenue North

Riccarton

Edinburgh

EH14 4AP

*Corresponding author

Professor Ken Donaldson

MRC/University of Edinburgh Centre for Inflammation Research

ELEGI Colt Laboratory

Queen's Medical Research Institute

47 Little France Crescent

Edinburgh

EH16 4TJ

phone 0131 242 6580

email ken.donaldson@ed.ac.uk

Abstract

Background: Carbon nanotubes (CNT) are fibre-like nanomaterials whose structural similarity to asbestos has raised concerns that they may also pose a mesothelioma hazard. The objective of this study was to examine the inflammatory potential of three CNT samples of differing length on the lungs and pleural cavity following introduction into the airspaces of mice.

Results: Aspiration of the two short /tangled and one long CNT sample into the lungs of mice resulted in a length-dependent inflammatory response at 1 week, i.e. only the long CNT sample caused acute neutrophilic inflammation in bronchoalveolar lavage at one week and progressive thickening of the alveolar septa. We also report length-dependent inflammatory responses in the pleural lavage after exposure only to the long CNT. The inflammatory response in the pleural cavity to long fibres and the appearance of lesions along the chest wall and diaphragm, was not present at 1 week and only evident by 6 weeks post exposure.

Conclusion: Length-dependent pathogenicity is a feature of asbestos and the results presented here demonstrate similar length-dependent pathogenicity of CNT in the lungs and pleural space following airspace deposition. The data support the contention that long CNT reach the pleura from the airspaces, and that they are retained at the parietal pleura and cause inflammation and lesion development. The parietal pleura is the site of origin of mesothelioma and inflammation is

considered to be a process involved in asbestos carcinogenesis and so our data supports the contention that CNT may pose an asbestos-like mesothelioma hazard.

Introduction

Carbon nanotubes (CNT) are a new form of manufactured carbon comprising single (singled-walled, SWCNT) or concentrically stacked (multiwalled, MWCNT) graphene sheets rolled seamlessly to form a fibre. The physical properties of SWCNT and MWCNT, e.g. high tensile strength and conductivity, make CNT increasingly desirable for a variety of manufacturing and medical applications which typifies the exponential growth of the nanotechnology industries [1]. The continuing increase in production of CNT will concomitantly lead to a heightened risk of occupational exposure which raised concern that the exposure to CNT via inhalation, ingestion or dermal contact will lead to harmful effects [2].

As inhalation is a primary route of exposure a number of studies have been carried out in recent years to assess the potential pulmonary hazard of CNT. Various pathological responses including acute neutrophilic inflammation [3;4], cytokine production [4;5], granulomatous inflammation [4;6;7], interstitial thickening [7] and fibrosis [5;8] have been observed to varying degrees of severity in a number of rodent lung models exposed to both SWCNT and MWCNT. The structural similarity between some forms of CNT and asbestos fibres has raised concerns that the morphology of CNT may pose an asbestos-type hazard to the lung [9]. Fibre dimensions have long been recognised as an important characteristic in the pathogenicity of asbestos fibres as demonstrated in a study by

Davis *et al*, who exposed rats by inhalation to an equal airborne mass concentration of either long amosite asbestos fibre or a short fibre sample obtained by ball-milling the long sample [10]. After lifetime exposure widespread pulmonary fibrosis and tumour development was detected in those rats exposed to the long amosite and but virtually no pathological response seen in rats exposed to the short fibre sample [10]. The importance of fibre dimensions is such that, along with the ability to persist in the body, it forms the basis of the fibre pathogenicity paradigm (FPP) which states that for a fibre to be pathogenic it must be long, thin and biopersistent [11]. As CNT, by virtue of their nanoscale diameters and graphenic structure, can be considered thin and biopersistent [12] we demonstrated that long CNT conform to the FPP and display an asbestos-like pathogenicity in the peritoneal and pleural cavities[13;14]. Similarly, greater biological activity of long CNT compared to shorter CNT has been demonstrated in vitro [15;16]. One aim of this study was to address the role of fibre length in the adverse effects of CNT in the lung by comparing the inflammatory responses to 3 CNT samples of different length after aspiration exposure.

The pleural cavity is an additional target for asbestos-mediated pathogenic effects, since exposure to asbestos fibres has been shown to induce the development of pleural plaques, pleural effusion and, of most concern, mesothelioma [17]. The FPP was originally developed from work examining the pathogenicity of fibres in the lungs [10] , pleural [18] and peritoneal [10;19] cavities indeed the development of mesothelioma is clearly related to asbestos fibre dimensions in all 3 of these sites [10;20]. Recently we reported that the potential of CNT to induce asbestos-like inflammation and pathology in a mouse model of direct pleural exposure was length-dependent [13]. A general mechanism for fibre pathogenicity in the pleural cavity related to the size-restricted clearance mechanisms from the pleural space and subsequent selective retention of long fibres has been proposed [11]. This mechanism is independent of chemical composition, except in so far as the composition affects biopersistence, and has been validated by the fact that a number of diverse fibre types including asbestos, CNT and a number of nanowires all generate a length-dependent inflammatory responses after direct injection into the pleural or peritoneal cavities [13;14;21]. Our

hypothesis in the present paper is that long CNT, previously shown to be inflammogenic in the pleural cavity after intrapleural injection, elicit a similar pleural response after administration via the airspaces of the lungs.

Whilst we are studying the early inflammatory effects of long fibres at the parietal pleura, we contend that we are illuminating the events leading to mesothelioma in the long term. This is argued on the basis that :- 1)mesothelioma originates at the parietal pleura, as would be anticipated from this being the initial site of localisation of long fibre 'dose' [11] ; 2) inflammation is considered to be an important process in carcinogenesis caused by asbestos and CNT [22;23]; 3) the pathological responses at the parietal pleura after a single intrapleural administration of long CNT increase in severity over time [13].

Materials and Methods:

CNT panel

The panel of particles investigated consisted of 3 different samples of multiwalled CNT as used previously in Murphy *et al* [13] (Table 1 and Supplementary Material Figure 3). The short straight CNT (NT_{short}; Nanostructured & Amorphous Materials Inc.) and short tangled CNT (NT_{tang}; NanoLab, Inc., MA, USA) were both purchased commercially and produced by Chemical Vapour Deposition with an iron and ceramic oxide (alumino-silicate) catalyst support which was removed using HCl and Hydrofluoric acid treatment. The NT_{long} sample was produced in an academic research laboratory (Dr Ian Kinloch, University of Manchester) using catalytic vapour discharge (CVD) method using a ferrocene-toluene feedstock to grow nanotubes from iron catalysts held on a silica plate. These nanotubes grew aligned as mats, meaning they were straight and un-entangled. The nanotubes were harvested from the mats using a razor blade, with some residual iron remaining within the

nanotubes. Trace metals and endotoxin levels previously tested and reported in Poland *et al [14]* were low and thus not considered to play a role in these studies.

Experimental Animals

For description of the mice and their housing see supplementary material

Pharyngeal aspiration

Mice were anesthetised and a 0.5 ml bolus of saline containing particles was aspirated into the airspaces of the lungs using conventional methods (see Supplementary material).

Analysis of bronchoalveolar lavage

For details of the methodology of determiming the differential cell count, total protein and LDH measurement in the BAL see Supplemetary material

Tissue Dissection and fixation

Chest wall and diaphragm

Three separate mice per treatment group were used for tissue analysis.

Light microscopy The diaphragm was removed, rinsed three times by emersion in ice-cold sterile saline and placed into 10% formalin. After 4 hours incubation in fixative, the diaphragm was carefully excised from the surrounding ribs and the same full width section of the upper quadrant of the diaphragm removed was sampled from each animal. The diaphragm sections were dehydrated through graded alcohol (ethanol) and imbedded on-edge in paraffin, then 4 µm sections of the diaphragm were cut and stained with haematoxylin and eosin (H&E) stain. Serial images were taken at x100 magnification along the diaphragm length using QCapture Pro software (Media Cyberbernetics Inc., MD, USA) and seamlessly re-aligned using Adobe Photoshop CS3 Version: 10.0.1 (Adobe systems Inc.) to show the entire length of the diaphragm section. Using calibrated software

(Image-Pro Plus, Media Cybernetics Inc., MD, USA) the total basement membrane length of each diaphragm was measured in order to adjust for any differences in size between diaphragms. Any areas identified by histology as macrophage aggregates adhering to the diaphragm surface (excluding areas of Liver, connective tissue or lymphatic tissue), were defined as 'lesions' and the surface area measured using the same software. In practice only CNT_{long}-exposed mice showed these lesions but the control and $CNT_{short/tangled}$ exposed mice had occasional small aggregates of a few cells presumed to be normal pleural macrophages and these were quantified as 'lesions'. Lesion area on each diaphragm was calculated in mm^2 per unit length of diaphragm (in mm) to yield lesion area per unit diaphragm length (mm^2/mm).

Lung

The heart and lungs were removed 'en block' and fixed by instillation of 10% formalin. The entire lung was immersed in fixative for a period of 4 hrs prior to processing. After fixation, the heart was removed and discarded, whilst the individual lobes of the lung were dissected free and placed flat in a tissue cassette. As before, the lung tissue was dehydrated through graded alcohol (ethanol) and imbedded in paraffin with 4µm sections cut so as to encompass all lobes of the lung. Sections were stained with H&E stain to show gross pathology and Picro-Sirius Red (PSR) red to show collagen deposition (red stain) and serial images taken at x100 magnification using QCapture Pro software. The images were seamlessly re-aligned as before to show an entire section of the lung.

Scanning electron microscopy Both sides of the chest wall were removed and rinsed in ice-cold sterile saline and placed into 10% glutaraldehyde fixative. The excised chest wall was fixed with osmium tetroxide prior to critical point drying, mounted and gold sputter coated before examination by scanning electron microscopy (SEM) using a Hitachi S-2600N digital scanning electron microscope (Oxford Instruments, Oxfordshire, UK).

Statistics

All data are shown as the mean + s.e.m. and these were analysed using one-way analysis of variance (ANOVA). Multiple comparisons were analysed using the Tukey-HSD method, with values of $P < 0.05$ considered statistically significant (Instat, Graphpad Software Inc., CA, USA.

Results:

Length-dependent inflammatory response of CNT in the lung at 1 and 6 weeks

The inflammatory response produced by aspiration of the CNT panel into the lung was measured at 1 week and 6 weeks post -exposure by lavaging the lungs and quantifying the cell types present. At one week post aspiration there was a significant increase in the number of granulocytes in the BAL fluid in response to the NT_{long} sample only (Fig 1A, B). CNT-induced lung damage was assessed by measuring BAL LDH as a measure of cytotoxicity, and BAL protein as a measure of the integrity of the alveolar–blood barrier. A length-dependent pattern was reflected in the LDH measurements with a significant increase in LDH activity only detected in mice treated with NT_{long} at 1 week. No change was seen in the protein concentration of the lavage fluid (Fig 1C, D). By 6 weeks the inflammatory response to NT_{long} as measured by differential cell count and LDH levels had returned to vehicle control levels. No inflammatory response to NT_{short} or NT_{tang} was detected at either 1 or 6 weeks in any of the assays.

Fibrotic response to CNT in lung at 6 weeks

The pathology of the lungs exposed to the CNT panel was examined at 6 weeks after aspiration. Overall the lungs exposed to NT_{short} and NT_{tang} appeared similar to vehicle control (Fig 2A, B and C). NT_{tang} caused small, localised granuloma and minor lymphocyte infiltration but the majority of the lung appeared normal (Fig 2C). Responses were minor and consistent with the effect of instilling a bolus dose of particles into the lung rather than specific CNT effects. The NT_{long} sample however produced a strong response characterised by extensive interstitial thickening and remodelling of the alveolar spaces (Fig 2D). Within the interstitium there was evidence of collagen deposition and lymphocyte infiltrates were also identified surrounding the blood vessels. The effects of the NT_{long}

sample extended to the peripheral airspaces although they were more severe in the central lung associated with deposits of the NT_{long} fibres. A number of NT_{long} fibres are also identified deposited in the sub-pleural regions of the lung (Fig 2D).

Pleural response to pulmonary exposure

The inflammatory response in the pleural space was also examined at 1 week and 6 weeks after the CNT panel were introduced into the lung by pharyngeal aspiration. At one week there was no change in total cell number in pleural lavage between the vehicle control mice and the three CNT treatment groups; there was however a small but significant increase in the number of granulocytes identified in the pleural lavage fluid of the mice treated with NT_{long} (Fig 3A, B). By 6 weeks there was a striking and significant increase in the total number of pleural lavage cells in the mice treated with NT_{long} only – around 10 million cells compared to around 2 million in the controls and the $CNT_{short/tangled}$ - treated. The majority of this increase in the pleural lavage cell number was due to an increase in pleural macrophages but, there was also a significant increase in the number of granulocytes present (Fig 3B). Foreign body giant cells, which are indicative of a foreign body response, were also identified at the 6 week timepoint in the pleural lavage fluid of mice treated with the long CNT sample only. No FBGC cells were identified in the lavage fluid of mice treated with the vehicle control, NT_{short} or NT_{tang} samples (Fig 3C, D). In addition to cytological changes, mice treated with NT_{long} had alterations in the biochemical profile of the pleural lavage fluid indicative of inflammation, including significant increases in LDH levels and protein concentration by 6 weeks post aspiration (Fig 3E, F). No change in the LDH levels or protein concentration was detected in the pleural lavage fluid of mice treated with vehicle control, NT_{short} or NT_{tang} at 1 or 6 weeks post exposure (Fig 3).

Response along the parietal pleura and diaphragm

Based on our experience of lesions on the parietal pleura after intra-pleural injection of long fibres [13] the surface appearance of the parietal pleural was examined by scanning electron microscopy at 6 weeks post-exposure (Fig 4). The vehicle control, NT_{short} and NT_{tang} treated mice displayed a continuous flat mesothelium, with occasional adherent macrophages, in every sample examined (n=3, left and right chest). In contrast, in NT_{long}-treated mice we identified distinct cellular aggregates overlaying the mesothelium. These aggregates were present on both the left and right parietal pleurae of each of the mice examined (n=3). Similar cellular aggregates were also identified in histological sections at the pleural face of the diaphragm. The aggregates appeared to be composed of leukocytes with a small number of granulocytes and FBGC (Fig 5D) and showed collagen deposition as revealed by Sirius red staining (Figure 5F). The area of cellular aggregates detected in NT_{long} -treated mice was significantly greater than small occasional adherent macrophage identified on the parietal mesothelial surface of control and short/tangled CNT-treated mice (Figure 5E) . Sections through the diaphragm of vehicle control, NT_{short} and NT_{tang} treated mice supported the view seen by SEM of a single layer of mesothelial cells (Fig 6A-C).

A number of CNT were also identified in sections of the diaphragm of mice treated with the NT_{long} sample only, confirming translocation of CNT from the lung into the pleural space (Fig 6). The CNT were most often associated with leukocytes or protruding from the mesothelial surface.

Derivation of a human equivalent dose

The equivalent human exposure, over a protracted time (years) that would lead to a steady-state human lung mass dose equivalent to the 50μg dose instilled into the mice was found to be 200μg/m^3. For details of the calculation of this figure see the Supplementary material.l

Discussion

Our objectives in this study were to investigate the pathological effects of CNT in the context of their fibrous nature and so their similarities to asbestos. We are therefore especially interested in the pleural effects, of which mesothelioma raises the most concern.

The length-dependent inflammatory responses to CNT reported here is consistent with experimental studies demonstrating a role for length in the pathogenicity of asbestos fibres [10;24;25] and therefore consistent with the FPP. Length can act as a toxicity factor in a number of ways- firstly in macrophage-mediated clearance of asbestos fibres from the distal regions of the lungs, where long fibres a re cleared much more slowly than short fibres [26;27]. Secondly, whilst short fibres are efficiently taken up and removed from the lung by alveolar macrophages long fibres cannot be completely phagocytosed but rather stimulate a state of chronic activation or 'frustrated phagocytosis'. Frustrated phagocytosis is accompanied by the release of oxidants [28] and cytokines [15;29] as well as lysosomal destabilisation [30;31] which may directly stimulate cytokine release increasing recruitment of inflammatory cells to the lungs and activating the surrounding epithelial cells leading to an inflammatory response. Thirdly ,long but not short fibres which reach the pleural space are retained at the parietal pleura where they initiate inflammation and fibrotic lesion development [13]. The ability of long CNT to stimulate frustrated phagocytosis in macrophages *in vitro* has been described in studies which have shown specific length-dependent increases in the release of pro-inflammatory cytokines after macrophages were treated with long fibre-containing CNT samples [15;16]. The mechanism by which frustrated phagocytosis leads to pro-inflammatory effects has been linked to the activation of the NALP3 inflammasome [32].

The responses to the long CNT reported here are consistent with a study carried out by Porter *et al* who examined the pathogenic effects in the lungs to various aspirated doses of MWCNT over time. and reported acute inflammation (peaking at 7 days), granuloma formation and alveolar type-2 cell hyperplasia which persisted from 7 days to the end of the experiment (128 days) [7]. Interstitial thickening and collagen deposition were also described by Mercer *et al* in response to aspiration

exposure of the same MWCNT sample [33]. The median length of the CNT fibres used in these studies was reported to be 3.9μm but, similar to the long fibre sample used here, their CNT had a wide length distribution which ranged from 1μm to > 20μm [7;33]. The heterogeneity of CNT fibre lengths can obfuscate the effects of fibre length in the response to CNT; however a clear length-dependent pathogenicity in the lungs has been demonstrated in response to other high aspect ratio nanomaterials. Nickel nanowires (NiNW), which are manufactured in tight size categories have shown length-dependent pathogenicity in the lungs with the long NiNW (20μm in length) eliciting an acute inflammatory response at 24 hours followed by interstitial thickening of the alveolar septa, whilst the shorter 4μm NiNW did not [21]. Similarly nanobelts composed of anatase TiO_2 which were 15μm in length were shown to initiate a pro-inflammatory response from alveolar macrophages via the induction of the NALP3 inflammasome and release of inflammatory cytokines, whilst shorter 5μm nanobelts did not [30]. These studies, using nanofibre samples in well defined size categories, support the contention that fibre length is a key biologically effective dose as laid out in the fibre pathogenicity paradigm. The length-dependent responses in the lungs and pleural space to CNT reported here, suggests that this also holds true for CNT and highlights the general likely applicability of the FPP for the hazard assessment of new forms of HARN.

Here for the first time we demonstrate a length-dependent hazard of CNT to both the lungs and the pleural space following introduction of long CNT into the airspaces of the lungs; short CNT had no significant effects.. The deposition of CNT in the airspaces of the lungs and the concomitant development of a pathogenic response in both the subpleural region of the lungs and the visceral pleura have previously been reported. In the study of Ryman-Rasmussen *et al* [34] mononuclear cell aggregates were identified on the surface of the visceral pleural which increased in size and number over time in response to ongoing inhalation exposure to CNT but not carbon black nanoparticles [34]. Asbestos fibres deposited in the lungs have also been shown to stimulate proliferation of mesothelial cells along the visceral pleura as early as one week post exposure [35]. However

evidence is highly in favour of the parietal pleura as the site of retention of long fibres dose [11;36;37]. Subsequently the relevance of assessing fibre-mediated inflammation or mesothelial cell proliferation in the sub-pleural regions of the lungs or along the visceral pleura when addressing early responses related to the potential mesothelioma hazard of a fibre is questionable. For example the clinical staging of mesothelioma, as set out by the International Mesothelioma Interest Group, describe early stage tumour development (T1a) as involving only the parietal pleura and diaphragm with no involvement of the visceral pleura. T1b describes a slightly more advanced tumour that involves all pleural surfaces but only minimal involvement of the visceral pleura [36;38].

A plausible mechanistic model supports the above argument for the parietal pleura as the site of initiation of mesothelioma. In this model both long and short fibres reach the pleural space and are transported to the parietal pleura in the fluid flow but, whilst short fibres pass through the stomata, long fibres are too big to negotiate the stomata and are retained at the parietal pleura [11]. Therefore the key fibre effects leading to mesothelioma development will take place at these sites of long fibre retention, rather than the visceral pleura. Therefore we examined the parietal pleural response to CNT focussing on lesion development along the parietal pleura and the inflammatory response in pleural space itself.

The inflammatory response in the pleural space observed after aspiration into the lungs was seen only with the long CNT and was characterised by an increase in the number of macrophages and granulocytes in the pleural lavage with concomitant increases in LDH and protein levels. This response is consistent with the increase in inflammatory leukocytes observed in the pleural space in rats after pulmonary exposure to long asbestos fibres by both intratracheal instillation [39] and inhalation [40]. Similar to the length-dependent response to CNT in the lungs, the inflammatory reaction in the pleural space was confined to the CNT sample containing long fibres – NT_{long}. Li *et al* previously demonstrated the development of a reactive inflammatory response in the pleural cavity following the instillation of the bacterium, *Corynebacterium parvum*, into the airspaces of the lungs

[41]. *C. parvum* was shown to cause a transient neutrophilic inflammation in both the pleural space and in the lungs that had the same time-course. Since there was no detectable translocation of the bacteria to the pleural space it is interpreted as communication of diffusible factors between the lungs and the pleural space resulting in a 'reactive' pleural inflammation [41]. This was not the case in the lungs/pleural responses described here for long CNT since the tempo of inflammation differed dramatically in the two compartments. There was no inflammatory response in the pleural cavity when the lung inflammation was greatest, at the acute timepoint. In contrast,, pleural inflammation was present at 6 weeks after aspiration by which time the acute inflammatory response in the lungs had largely subsided. Furthermore FBGCs were detected in the pleural lavage and we have previously reported these only in close association with the lesions caused by instillation of long CNT only into the peritoneal [14] and pleural [13] spaces; this supports the contention that long CNT reached and were retained in the pleural space after deposition in the lungs.

To further support our contention that the inflammatory response detected in the pleural space was a foreign body response, we examined the parietal surface of the diaphragm by light microscopy and identified CNT which had translocated there across the pleural space from the lungs. The mechanism of fibre translocation out of the lungs into the pleural space and into the parietal pleura and diaphragm is not known but there is a wealth of literature to support the idea that a proportion of all particles and fibres deposited in the distal region of the lungs will translocate to the pleural space (reviewed in [11]). Indeed the penetration of CNT from the lung periphery through the visceral pleura into the pleural space after aspiration exposure has been quantified by Mercer *et al* who determined that 0.6% of the deposited fibre burden reached the visceral pleura [8].

In a recent review [11], we put forward a mechanistic hypothesis stating that if long CNT enter the pleural space, due to the flow of pleural fluid they will deposit on the parietal pleura and accumulate around stomata (i.e., outlets in the parietal pleura through which lymphatic drainage occurs) where they are retained. Once retained, the long fibres can generate an inflammatory/fibrotic response

and are in close contact with mesothelial cells for a protracted time so that genotoxic effects could occur. Both inflammation and genotoxicity are processes which are linked to the formation of mesothelioma [11]. Here, only long CNT fibres are identified along the diaphragm of mice treated with the NT_{long} sample, consistent with the hypothesis that short fibres are efficiently removed. Along with the retention of long fibres on the diaphragm we also show the development of inflammatory lesions on the parietal pleura 6 weeks after aspiration of the long CNT into the lungs. These lesions were primarily composed of mononuclear leukocytes but a small number of granulocytes and FBGC were also seen, along with collagen deposition. Recently, inhalation of amosite asbestos fibres was shown to produce similar inflammatory lesions along the parietal pleura with the presence of amosite asbestos fibres on the diaphragm 7 days after the end of inhalation exposure [42]. After the direct injection of long CNT into the pleural space the retention of biopersistent fibres at the parietal pleura was shown to lead to a state of chronic inflammation with progressive and extensive fibrotic lesion formation [13]. Chronic inflammation is considered a likely contributing factor in the development of mesothelioma with *in vitro* studies demonstrating the promotion of mesothelial cell transformation [43] and evasion of cell death [20] in the presence of pro-inflammatory cytokines. We therefore contend that the development of an inflammatory response in the pleural cavity after instillation of long CNT into the lungs implies that inhalation of long CNT is likely to pose a mesothelioma hazard.

In order to assess whether the dose of NT_{long} that caused pathogenic effects in the mouse lung and pleural cavity were plausible a human equivalent dose was established for the NT_{long} dose used in the study. A steady-state exposure level of 200μg/m^3 was determined to be the human exposure that would result in an allometrically equivalent retained dose in human lungs to the 50μg aspirated dose used in the mice here. This is the steady state dose that would arise as the result of the equilibrium between the deposited dose rate and the outgoing clearance rate during chronic ongoing exposure and so reflects the likely experience of a worker exposed to a CNT-rich

environment over a number of years. Han *et al* measured the airborne dust levels in a research laboratory and reported a peak CNT-containing airborne dust level of approximately 400μg/m^3[44]. Thus the long CNT dose tested in mice in this study approximated to a dose that could accumulate in human lungs after a plausible long term exposure.

The calculated human equivalent exposure concentration shown here is purely indicative as several assumptions have been made in terms of the actual dose within the alveolar region of the mice, the clearance rate of CNT from the lungs of humans, and the true aerodynamic diameter of the CNTs in question which would affect the deposition efficiency. It is worth considering that the clearance rate used is based upon an insoluble, compact (roughly spherical) particle that allows for normal clearance. Clearance of long fibres is much slower than for compact particles due to hindrance of alveolar macrophages and this is also likely to be true of long fibre CNT. The net result of slower clearance is that lower levels of exposure are required to culminate in the same retained dose. Understanding the true deposition efficiency, clearance and retention rates for the complex forms of CNT represents a significant challenge to understanding of CNT dose in the lung requiring further research.

In conclusion we have shown that CNT elicit a length-dependent inflammatory response in the lungs and pleura after pharyngeal aspiration, which is in accordance with the FPP. Our data suggests that the role of fibre dimensions should be assessed when considering the inhalation toxicity of any new HARN. Furthermore the data suggest that the translocation to -and selective retention of long fibres in -the parietal pleura, leads to an inflammatory response and fibrotic lesion development. The parietal pleura is the site of origin of mesothelioma and inflammation is considered to be a process involved in asbestos carcinogenesis and so our data supports the contention that long fibres of CNT may pose a mesothelioma risk . The results of this small-scale, mouse study are not sufficient to confidently extrapolate to the potential mesothelioma risks of CNT exposures in the workplace which would require long-term inhalation studies utilizing plausible CNT exposures. This study does

however contribute to the evidence that certain types of CNT and long HARN in general may pose an asbestos-like mesothelioma hazard and therefore require more research and, in the meantime, precautionary risk assessment and management.

Acknowledgements

We gratefully acknowledge Mitsui & Co. and Dr. Ian Kinloch (University of Manchester) for the provision of multiwalled carbon nanotube samples. We thank S. Mitchell (University of Edinburgh) for sample preparation for SEM and technical assistance. We thank the UK Department of Health (F.A.M.) and The Colt Foundation for the financial support (C.A.P, K.D.). This is an independent report commissioned and funded by the Policy Research Programme in the Department of Health and the views expressed are not necessarily those of the Department.

Table legend

Table 1: Characteristics of the CNT samples used in the study

Figure legends

Figure 1. Inflammatory response to CNT in the lungs at 1 week and 6 weeks. C57/Bl6 mice were exposed to the CNT panel by pharyngeal aspiration. At 1 and 6 weeks post exposure the lungs were lavaged and total cell number (A), total granulocyte number (B), LDH levels (C) and protein

concentration (D) were measured. Significance indicated compares treatment groups to vehicle control from the same timepoint, * indicates $p<0.05$, ** indicates $p<0.001$, *** indicates $p<0.0001$.

Figure 2. Lung pathology 6 weeks post aspiration with the CNT panel. The effect of the panel of CNT on the structure of the lungs is demonstrated 6 weeks after aspiration into the lungs. Each panel shows an entire lung section stained with H&E to demonstrate gross pathology. Higher magnification callouts show the normal alveolar structure in the vehicle control treated mice (A) or changes due to the CNT treatment (B, C, D). Small accumulations of cells and CNT aggregates are identified in mice treated with NT_{short} (B) and NT_{tang}(C) whereas mice treated with NT_{long}(D) show lymphocyte infiltrates, extreme interstitial thickening and collagen deposition associated with interspersed long CNT. Long CNT are identified in the sub-pleural regions.

Figure 3. Inflammatory response in the pleural cavity after pulmonary exposure to CNT. The inflammatory response in the pleural cavity after the CNT were delivered by pharyngeal aspiration was examined. At 1 and 6 weeks post exposure the pleural cavity was lavaged and total cell number (A), total granulocyte number (B), LDH levels (E) and protein concentration (F) were measured. Foreign body giant cells (C, D) were quantified at 6 weeks post exposure. Scale bar indicates 20μm. Significance indicated compares treatment groups to vehicle control from the same timepoint, * indicates $p<0.05$, ** indicates $p<0.001$, *** indicates $p<0.0001$.

Figure 4. Lesion formation along the chest wall after pulmonary exposure to CNT. The chest wall was examined by scanning electron microscopy 6 weeks after the mice were exposed to the CNT panel by aspiration. Vehicle control, NT_{short}, NT_{tang} treated mice (see labels on images) had normal mesothelium. Aggregates of cells were identified overlying the mesothelium in the mice treated with the NT_{long} sample (see image labelled NT_{long} and callout showing a higher magnification).

Figure 5. Lesion formation along the diaphragm after pulmonary exposure to CNT. Histological sections through the diaphragm showing normal parietal pleura in the case of the vehical control (A)and the short CNT (B) and tangled CNT (C). Only the mice treated with the long CNT showed occassional the aggregations of inflammatory cells along the mesothelium (D). On staining with Sirius Red reticular collagen fibres could be seen stained red (Figure F arrow). The extent of these lesions was quantified and this is shown in (E). Significance indicated compares treatment groups to vehicle control *** indicates $p<0.0001$.

Reference List

1. Maynard,A.D. (2007) Nanotechnology: the next big thing, or much ado about nothing? *Ann.Occup.Hyg.*, **51**, 1-12.

2. Donaldson,K., Aitken,R., Tran,L., Stone,V., Duffin,R., Forrest,G., and Alexander,A. (2006) Carbon nanotubes: a review of their properties in relation to pulmonary toxicology and workplace safety. *Toxicol.Sci.*, **92**, 5-22.

3. Muller,J., Huaux,F., Moreau,N., Misson,P., Heilier,J.F., Delos,M., Arras,M., Fonseca,A., Nagy,J.B., and Lison,D. (2005) Respiratory toxicity of multi-wall carbon nanotubes *Toxicol.Appl.Pharmacol.*, **207**, 221-231.

4. Shvedova,A.A., Kisin,E.R., Murray,A.R., Johnson,V.J., Gorelik,O., Arepalli,S., Hubbs,A.F., Mercer,R.R., Keohavong,P., Sussman,N., Jin,J., Yin,J., Stone,S., Chen,B.T., Deye,G., Maynard,A., Castranova,V., Baron,P.A., and Kagan,V.E. (2008) Inhalalation versus aspiration of single walled carbon nanotubes in C57/Bl6 mice: Inflammation, fibrosis, oxidative stress and mutagenesis. *Am.J.Physiol Lung Cell Mol.Physiol*, **295**, L552-L565.

5. Shvedova,A.A., Kisin,E.R., Mercer,R., Murray,A.R., Johnson,V.J., Potapovich,A.I., Tyurina,Y.Y., Gorelik,O., Arepalli,S., Schwegler-Berry,D., Hubbs,A.F., Antonini,J., Evans,D.E., Ku,B.K., Ramsey,D., Maynard,A., Kagan,V.E., Castranova,V., and Baron,P. (2005) Unusual inflammatory and fibrogenic pulmonary responses to single-walled carbon nanotubes in mice *Am J Physiol Lung Cell Mol.Physiol*, **289**, L698-L708.

6. Lam,C.W., James,J.T., McCluskey,R., and Hunter,R.L. (2004) Pulmonary toxicity of single-wall carbon nanotubes in mice 7 and 90 days after intratracheal instillation. *Toxicol.Sci.*, **77**, 126-134.

7. Porter,D.W., Hubbs,A.F., Mercer,R.R., Wu,N., Wolfarth,M.G., Sriram,K., Leonard,S., Battelli,L., Schwegler-Berry,D., Friend,S., Andrew,M., Chen,B.T., Tsuruoka,S., Endo,M., and Castranova,V. (2010) Mouse pulmonary dose- and time course-responses induced by exposure to multi-walled carbon nanotubes. *Toxicology*, **269**, 136-147.

8. Mercer,R.R., Hubbs,A.F., Scabilloni,J.F., Wang,L., Battelli,L.A., Schwegler-Berry,D., Castranova,V., and Porter,D.W. (2010) Distribution and persistence of pleural penetrations by multi-walled carbon nanotubes. *Part Fibre Toxicol.*, **7**, 28.

9. The Royal Society and the Royal Academy of Engineering (2004) Nanoscience and nanotechnologies: opportunities and uncertainties. *R.*

10. Davis,J.G., Addison,J., Bolton,R.E., Donaldson,K., Jones,A.D., and Smith,T. (1986) The pathogenicity of long versus short fiber samples of amosite asbestos administered to rats by inhalation and intraperitoneal injection. *British Journal Of Experimental Pathology*, **67**, 415-430.

11. Donaldson,K., Murphy,F.A., Duffin,R., and Poland,C.A. (2010) Asbestos, carbon nanotubes and the pleural mesothelium: a review of the hypothesis regarding the role of long fibre retention in the parietal pleura, inflammation and mesothelioma. *Part Fibre Toxicol.*, **7**, 5.

12. Osmond-McLeod,M.J., Poland,C.A., Murphy,F., Waddington,L., MOrris,H., Hawkins,S.C., Clark,S., Aitken,R., McCall,M.J., and Donaldson,K. (2011) Durability and inflammogenic impact of carbon nanotubes compared with asbestos fibres. *Part Fibre Toxicol.*, **8**, 15.

13. Murphy,F.A., Poland,C.A., Duffin,R., Al Jamal,K.T., Ali-Boucetta,H., Nunes,A., Byrne,F., Prina-Mello,A., Volkov,Y., Li,S., Mather,S.J., Bianco,A., Prato,M., MacNee,W., Wallace,W.A., Kostarelos,K., and Donaldson,K. (2011) Length-dependent retention of carbon nanotubes in the pleural space of mice initiates sustained inflammation and progressive fibrosis on the parietal pleura. *Am.J Pathol.*, **178**, 2587-2600.

14. Poland,C.A., Duffin,R., Kinloch,I., Maynard,A., Wallace,W.A., Seaton,A., Stone,V., Brown,S., MacNee,W., and Donaldson,K. (2008) Carbon nanotubes introduced into the abdominal cavity of mice show asbestos-like pathogenicity in a pilot study. *Nat.Nanotechnol.*, **3**, 423-428.

15. Brown, D. M., Kinloch, I., Bangert, U., Windle, A. H., Walter, D. M., Walker, G. S., Scotchford, C. A., Donaldson, K., and Stone, V. An in vitro study of the potential of carbon nanotubes and nanofibres to induce inflammatory mediators and frustrated phagocytosis. Carbon 45, 1743-1756. 2007.

16. Palomaki,J., Valimaki,E., Sund,J., Vippola,M., Clausen,P.A., Jensen,K.A., Savolainen,K., Matikainen,S., and Alenius,H. (2011) Long, needle-like carbon nanotubes and asbestos activate the NLRP3 inflammasome through a similar mechanism. *ACS Nano*, **5**, 6861-6870.

17. Donaldson,K., Brown,R.C., and Brown,G.M. (1993) New perspectives on basic mechanisms in lung-disease .5. Respirable industrial fibers - mechanisms of pathogenicity. *Thorax*, **48**, 390-395.

18. Stanton, M. F. and Wrench, C. Mechanisms of mesothelioma induction with asbestos and fibrous glass. Journal of theNational Cancer Institute 48, 797-821. 1972.

19. Donaldson,K., Brown,G.M., Brown,D.M., Bolton,R.E., and Davis,J.G. (1989) Inflammation generating potential of long and short fiber amosite asbestos samples. *British Journal Of Industrial Medicine*, **46**, 271-276.

20. Yang,H., Testa,J.R., and Carbone,M. (2008) Mesothelioma epidemiology, carcinogenesis, and pathogenesis. *Curr.Treat.Options.Oncol.*, **9**, 147-157.

21. Poland,C.A., Byrne,F., Cho,W.S., Prina-Mello,A., Murphy,F.A., Davies,G.L., Coey,J.M., Gounko,Y., Duffin,R., Volkov,Y., and Donaldson,K. (2011) Length-dependent pathogenic effects of nickel nanowires in the lungs and the peritoneal cavity. *Nanotoxicology*.

22. Kane,A.B. (1996) Mechanisms of mineral fibre carcinogenesis. *in Mechanisms of Fibre Carcinogenesis.Edited by Kane AB, Boffetta P, Saracci R and Wilbourn JD*,11-34.

23. Nagai,H. and Toyokuni,S. (2010) Biopersistent fiber-induced inflammation and carcinogenesis: lessons learned from asbestos toward safety of fibrous nanomaterials. *Arch Biochem.Biophys.*, **502**, 1-7.

24. Mossman,B.T. and Churg,A. (1998) Mechanisms in the pathogenesis of asbestosis and silicosis. *Am.J.Respir.Crit Care Med.*, **157**, 1666-1680.

25. Miller,B.G., Searl,A., Davis,J.M., Donaldson,K., Cullen,R.T., Bolton,R.E., Buchanan,D., and Soutar,C.A. (1999) Influence of fibre length, dissolution and biopersistence on the production of mesothelioma in the rat peritoneal cavity. *Ann Occup Hyg*, **43**, 155-166.

26. Coin,P.G., Roggli,V.L., and Brody,A.R. (1994) Persistence of long, thin chrysotile asbestos fibers in the lungs of rats. [Review] [24 refs]. *Environmental Health Perspectives*, **102 Suppl 5**, 197-199.

27. Searl,A., Buchanan,D., Cullen,R.T., Jones,A.D., Miller,B.G., and Soutar,C.A. (1999) Biopersistence and durability of nine mineral fibre types in rat lungs over 12 months. *Ann.Occup.Hyg.*, **43**, 143-153.

28. Hansen,K. and Mossman,B.T. (1987) Generation of superoxide (O2-.) from alveolar macrophages exposed to asbestiform and nonfibrous particles *Cancer Res.*, **47**, 1681-1686.

29. Ye,J., Shi,X., Jones,W., Rojanasakul,Y., Cheng,N., Schwegler-Berry,D., Baron, Deye,G.J., Li,C., and Castranova,V. (1999) Critical role of glass fiber length in TNF-alpha production and transcription factor activation in macrophages. *American Journal Of Physiology*, **276**, L426-L434.

30. Hamilton,R.F., Wu,N., Porter,D., Buford,M., Wolfarth,M., and Holian,A. (2009) Particle length-dependent titanium dioxide nanomaterials toxicity and bioactivity. *Part Fibre Toxicol.*, **6**, 35.

31. O'Neill,L.A. (2008) Immunology. How frustration leads to inflammation. *Science*, **320**, 619-620.

32. Schroder,K. and Tschopp,J. (2010) The inflammasomes. *Cell*, **140**, 821-832.

33. Mercer,R.R., Hubbs,A.F., Scabilloni,J.F., Wang,L., Battelli,L.A., Friend,S., Castranova,V., and Porter,D.W. (2011) Pulmonary fibrotic response to aspiration of multi-walled carbon nanotubes. *Part Fibre Toxicol.*, **8**, 21.

34. Ryman-Rasmussen,J.P., Cesta,M.F., Brody,A.R., Shipley-Phillips,J.K., Everitt,J.I., Tewksbury,E.W., Moss,O.R., Wong,B.A., Dodd,D.E., Andersen,M.E., and Bonner,J.C. (2009) Inhaled carbon nanotubes reach the subpleural tissue in mice. *Nat.Nanotechnol.*, **4**, 747-751.

35. Adamson,I.Y., Bakowska,J., and Bowden,D.H. (1993) Mesothelial cell proliferation after instillation of long or short asbestos fibers into mouse lung *Am.J.Pathol.*, **142**, 1209-1216.

36. Boutin,C., Rey,F., Gouvernet,J., Viallat,J.R., Astoul,P., and Ledoray,V. (1993) Thoracoscopy in pleural malignant mesothelioma: a prospective study of 188 consecutive patients. Part 2: Prognosis and staging. *Cancer*, **72**, 394-404.

37. Boutin,C., Dumortier,P., Rey,F., Viallat,J.R., and De Vuyst,P. (1996) Black spots concentrate oncogenic asbestos fibers in the parietal pleura. Thoracoscopic and mineralogic study. *Am.J.Respir.Crit.Care Med.*, **153**, 444-449.

38. Rusch,V.W. (1996) A proposed new international TNM staging system for malignant pleural mesothelioma from the International Mesothelioma Interest Group. *Lung Cancer*, **14**, 1-12.

39. Oberdoerster,G., Ferin,J., Marcello,N.L., and Meinhold,S.H. (1983) Effect of intrabronchially instilled amosite on lavagable lung and pleural cells. *Environ Health Perspect.*, **51**, 41-47.

40. Choe,N., Tanaka,S., Xia,W.J., Hemenway,D.R., Roggli,V.L., and Kagan,E. (1997) Pleural macrophage recruitment and activation in asbestos-induced pleural injury. *Environmental Health Perspectives*, **105**, 1257-1260.

41. Li,X.Y., Brown,G.M., Lamb,D., and Donaldson,K. (1993) Reactive pleural inflammation caused by intratracheal instillation of killed microbes. *Eur Respir J*, **6**, 27-34.

42. Bernstein,D.M., Rogers,R.A., Sepulveda,R., Donaldson,K., Schuler,D., Gaering,S., Kunzendorf,P., Chevalier,J., and Holm,S.E. (2010) The pathological response and fate in the lung and pleura of chrysotile in combination with fine particles compared to amosite asbestos following short-term inhalation exposure: interim results. *Inhal.Toxicol.*, **22**, 937-962.

43. Wang,Z.L. (2004) Functional oxide nanobelts: materials, properties and potential applications in nanosystems and biotechnology. *Annu.Rev.Phys.Chem.*, **55**, 159-196.

44. Han,J.H., Lee,E.J., Lee,J.H., So,K.P., Lee,Y.H., Bae,G.N., Lee,S.B., Ji,J.H., Cho,M.H., and Yu,I.J. (2008) Monitoring multiwalled carbon nanotube exposure in carbon nanotube research facility. *Inhal.Toxicol.*, **20**, 741-749.

	NT_{short}	NT_{tang}	NT_{long}
Source	Nanostructured & Amorphous Materials, Inc.	NanoLab, Inc.	University of Manchester [Dr. I. Kinloch]
Diameter (nm)	25.7± 1.6	14.84 ± 0.05	165.02 ± 4.68
Length (μm)	1-2	1-5	Mean 36
% fibre greater than 15 μm	‡	‡	84.26

Table 1: Characteristics of the CNT samples used in the study
140x92mm (150 x 150 DPI)

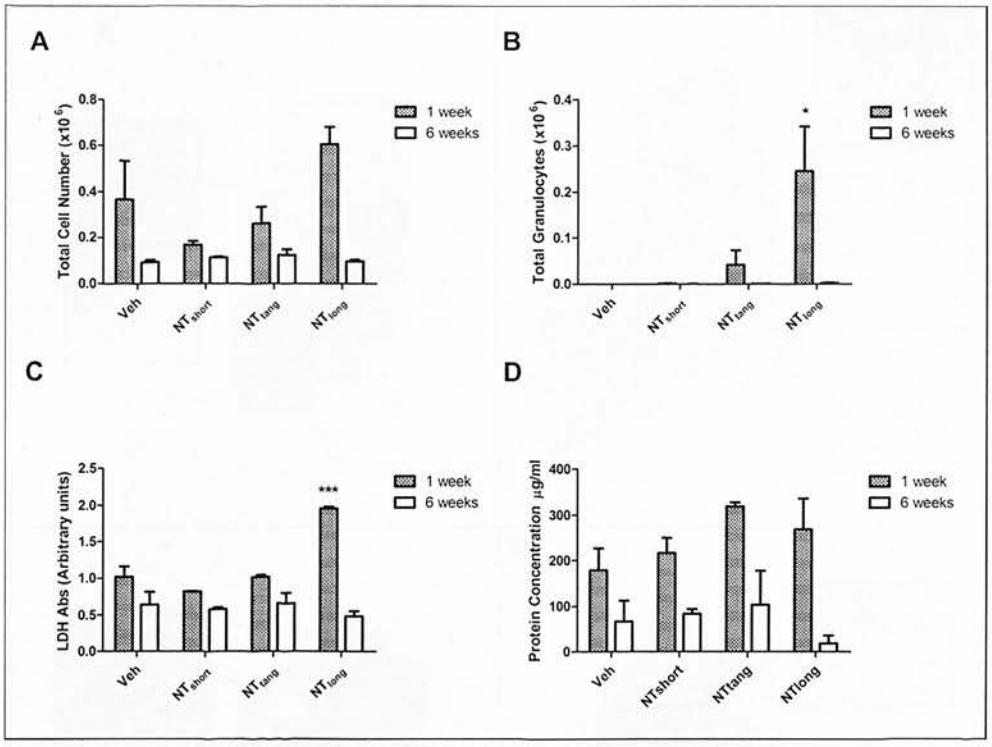

Inflammatory response to CNT in the lungs at 1 week and 6 weeks. C57/Bl6 mice were exposed to the CNT panel by pharyngeal aspiration. At 1 and 6 weeks post exposure the lungs were lavaged and total cell number (A), total granulocyte number (B), LDH levels (C) and protein concentration (D) were measured. Significance indicated compares treatment groups to vehicle control from the same timepoint, * indicates $p<0.05$, ** indicates $p<0.001$, *** indicates $p<0.0001$.
160x119mm (150 x 150 DPI)

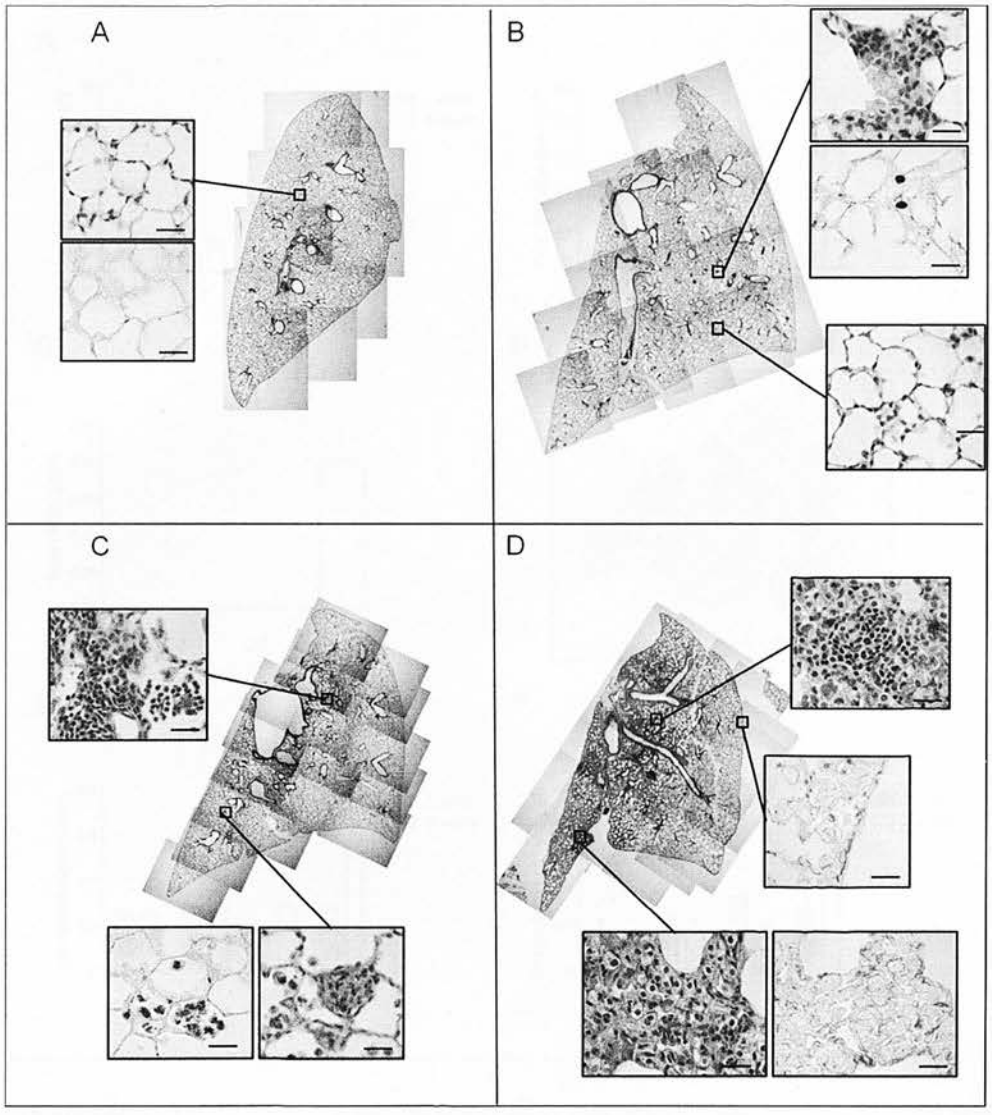

Figure 2. Lung pathology 6 weeks post aspiration with the CNT panel. The effect of the panel of CNT on the structure of the lungs is demonstrated 6 weeks after aspiration into the lungs. Each panel shows an entire lung section stained with H&E to demonstrate gross pathology. Higher magnification callouts show the normal alveolar structure in the vehicle control treated mice (A) or changes due to the CNT treatment (B, C, D). Small accumulations of cells and CNT aggregates are identified in mice treated with NTshort (B) and NTtang(C) whereas mice treated with NTlong(D) show lymphocyte infiltrates, extreme interstitial thickening and collagen deposition associated with interspersed long CNT. Long CNT are identified in the sub-pleural regions.
159x179mm (150 x 150 DPI)

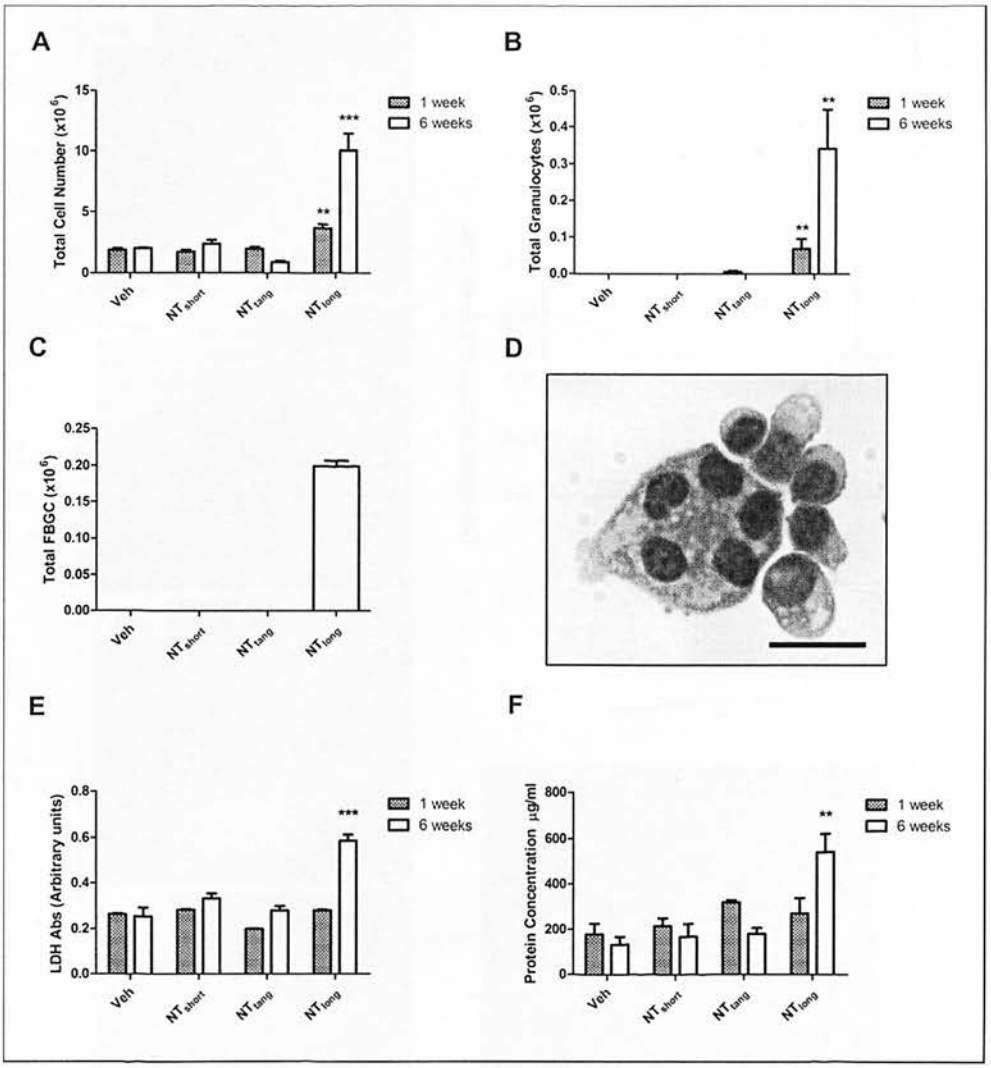

Figure 3. Inflammatory response in the pleural cavity after pulmonary exposure to CNT. The inflammatory response in the pleural cavity after the CNT were delivered by pharyngeal aspiration was examined. At 1 and 6 weeks post exposure the pleural cavity was lavaged and total cell number (A), total granulocyte number (B), LDH levels (E) and protein concentration (F) were measured. Foreign body giant cells (C, D) were quantified at 6 weeks post exposure. Scale bar indicates 20µm. Significance indicated compares treatment groups to vehicle control from the same timepoint, * indicates $p<0.05$, ** indicates $p<0.001$, *** indicates $p<0.0001$.
159x171mm (150 x 150 DPI)

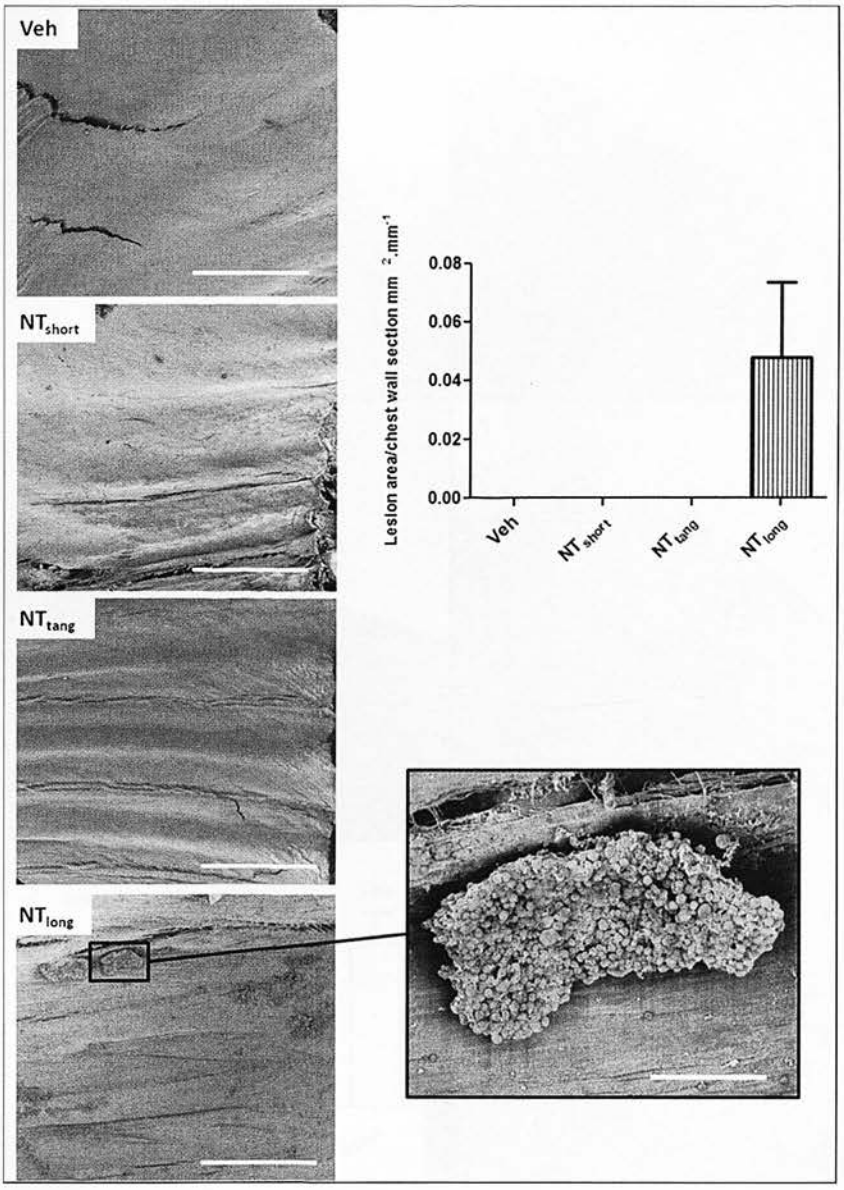

Figure 4. Lesion formation along the chest wall after pulmonary exposure to CNT. The chest wall was examined by scanning electron microscopy 6 weeks after the mice were exposed to the CNT panel by aspiration. Vehicle control, NTshort, NTtang treated mice (see labels on images) had normal mesothelium. Aggregates of cells were identified overlying the mesothelium in the mice treated with the NTlong sample (see image labelled NTlong and callout showing a higher magnification).
128x181mm (150 x 150 DPI)

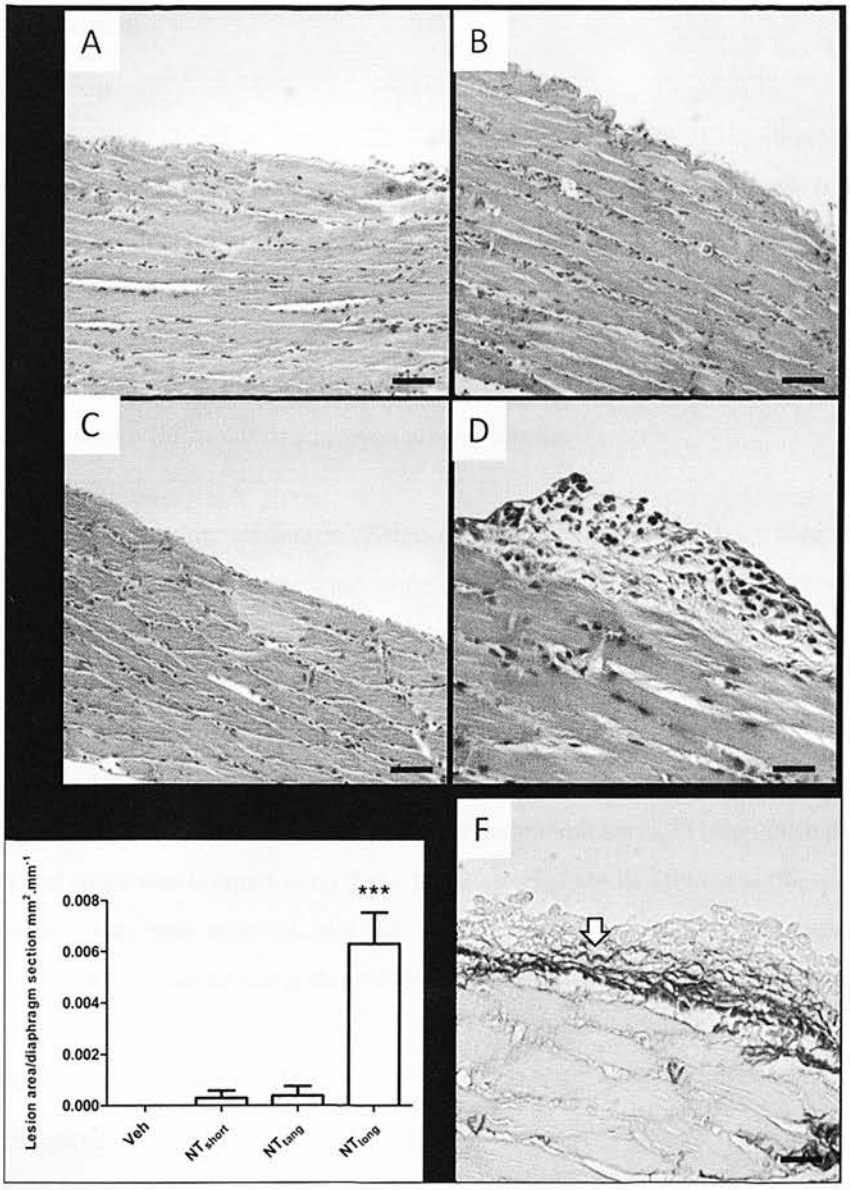

Figure 5. Lesion formation along the diaphragm after pulmonary exposure to CNT. Histological sections through the diaphragm showing normal parietal pleura in the case of the vehical control (A)and the short CNT (B) and tangled CNT (C). Only the mice treated with the long CNT showed occassional the aggregations of inflammatory cells along the mesothelium (D). On staining with Sirius Red reticular collagen fibres could be seen stained red (Figure F arrow). The extent of these lesions was quantified and this is shown in (E). Significance indicated compares treatment groups to vehicle control *** indicates $p<0.0001$.
124x175mm (150 x 150 DPI)

Murphy et al Length-dependent pleural inflammation and parietal pleural responses after deposition of carbon nanotubes in the pulmonary airspaces of mice.

Supplementary material

Experimental Animals

Eight to twelve week old (20-25 g) female C57BL/6 strain mice (Harlan, UK) were group- housed in standard caging with sawdust bedding, environmental enrichment with free access to sterile water and food within a pathogen-free Home Office approved facility. Animals were maintained on a normal 12 hr light and dark cycle and were allowed 7 days to acclimatise prior to study commencement. Post exposure animals were subject to daily checks for signs of distress or welfare issues (none identified). All *in vivo* work was carried out by staff holding a valid UK Home Office personal licence under a Home Office approved project licence.

Pharyngeal aspiration

Mice were anesthetised using isoflurane (2-chloro-2-(difluoromethoxy)-1,1,1 trifluoroethane) and the tongue was gently held at full extension while a 50 µl bolus of test sample pipetted to the base of the tongue. The animals were stimulated to inhale via covering of the nasal cavities to induce a gasp reflex and held until several breaths had occurred [1]. The animals were further observed until a full recovery and group housed for the duration of the experiment. At each time point the mice were sacrificed by terminal anaesthesia using an intraperitoneal injection with 0.5 ml of 2, 2, 2-tribromomethanol followed by exsanguination via the abdominal aorta. In three mice per treatment group the pleural space was lavaged using three 1ml washes of sterile saline and the lavages kept on ice. The thoracic cavity was exposed, and the trachea cannulated using a 21 gauge needle and legated. The lungs were lavaged using three 0.8ml washes of ice-cold sterile saline and the lavages kept on ice.

Analysis of the bronchoalveolar lavage

Differential cell count

The lavage fluid (both lung and peritoneal) was then centrifuged at 123g for 5 minutes at 4°C in a Mistral 3000i centrifuge (Thermo Fisher Scientific, Inc., MA, USA) and aliquot of the supernatant retained for total protein and cytokine measurements. The remaining cell pellet was re-suspended in 0.5 ml of 0.1 % BSA/ sterile saline solution. A total cell count was then performed using a NucleoCounter (ChemoMetec, A/S, Allerod, Denmark). Differential cell counts were performed on cyto-centrifugation preparations, stained with Diff Quik. Images of cells were taken using QCapture Pro (Media Cyberbernetics Inc., MD, USA).

Total protein measurement

Total protein concentration of the peritoneal lavage fluid was measured using the bicinchoninic acid (BCA) protein assay. Sample protein concentrations were established by comparison to a BSA standard (Sigma-Aldrich, Poole, UK) curve (0 – 1000 µg/ml). The samples were then incubated at 37oC for 30 minutes after the addition of the test reagent (1 part Cu2+ Sulphate solution (4 % w/v) to 50 parts bicinchoninic acid (Sigma-Aldrich, Poole, UK)). The absorbance was then read at 570 nm using a Synergy HT microplate reader (BioTek Instruments, Inc. VT, USA) and the sample protein concentration established via extrapolation from the BSA standard curve.

Lactate Dehydrogenase (LDH) assay

The level of cellular cytotoxicity/ cytolysis was established using a Lactate Dehydrogenase (LDH) assay (Roche Diagnostics GmbH, Mannheim, Germany). Briefly, 100 µl of lavage fluid was added in triplicate to a 96 well plate and 100 µl of the LDH test reagent (diaphorase/NAD+ mixed with iodotetrazolium chloride and sodium lactate at a ratio of 1:45) added to each well. Following a 30 minute incubation period the absorbance of each well at 490 nm wavelength was established using a Synergy HT microplate reader (BioTek Instruments, Inc. VT, USA).

Derivation of a human equivalent dose

The exposure that would have led to an equivalent human retained dose under chronic exposure conditions, to the aspirated dose used in mice was calculated for a hypothetical fibrous CNT. Assuming a mouse alveolar surface area of $0.05m^2$ [2], the 50µg dose aspirated used here would result in a normalised dose of $1000ug/m^2$ in the alveolar region (assuming 100% deposition). This would be an equivalent retained dose in the alveolar region of 102,200ug in a human taking into consideration the greater alveolar surface area of a human ($102.2m^2$) [2] The external dose which, with chronic exposure, would generate the calculated retained dose was derived by first calculating the deposited dose which would result in a retained dose of the derived value based on the clearance rate of a typical human. The clearance half time in humans is suggested to be approximately 1 year [3] for insoluble compact particles and the clearance rate is calculated by the following equation:

$k=\ln(2)/t1/2 \qquad k=\ln(2)/365= 0.0019$

The retained dose was multiplied by the clearance rate to give the deposited dose rate of 194 µg/day. The inhaled dose rate was then calculated taking into account the proportion of the inhaled dose that would deposit in the alveolar region of the lung using the Multiple-Path Particle Dosimetry

Model (MPPD). The particle physical attributes- aerodynamic diameter and density, which are required for the MPPD calculation were not known for the CNT samples and therefore were based on published data of morphologically similar fibrous CNT (Mitsui & Co MWNT-7) with a mass median aerodynamic diameter of 1.5 and GSD of 1.7 [4] (Fig 7 B). The alveolar deposition fraction for fibrous CNT was calculated to be 12.9% (Fig 7 C). The inhaled dose rate that would result in a deposited dose rate in the alveolar regions of the lung was then calculated to be 1505 µg/day assuming a deposition fraction of only 12.9% of the total inhaled fraction. In order for the inhaled dose rate to be achieved, a worker would have to be exposed over the period of a standard 8 hour shift (480 minutes) to an aerosol concentration of 150 µg/m^3 (Fig 7 A), with a respiratory minute volume of 0.0208 m^3/min [5] based on the standard parameters for a worker undertaking light activity [6] which culminates in a total inhaled volume of 9.98 m^3/day.

Supplementary material Figure 1. Determination of a human equivalent dose. Schematic diagram of the process for deriving a human equivalent exposure for the NTlong sample based on the aspirated mouse dose of 50µg (A). (B) The particle properties required for the Multiple-Path Particle Dosimetry Model (MPPD) taken from McKinney et al (28) measurements of a morphologically-similar, fibrous CNT sample. (C) Results from the MPPD computational model describing the predicted deposition fraction for the entire lung. TB= trachobronchial, P= pulmonary.

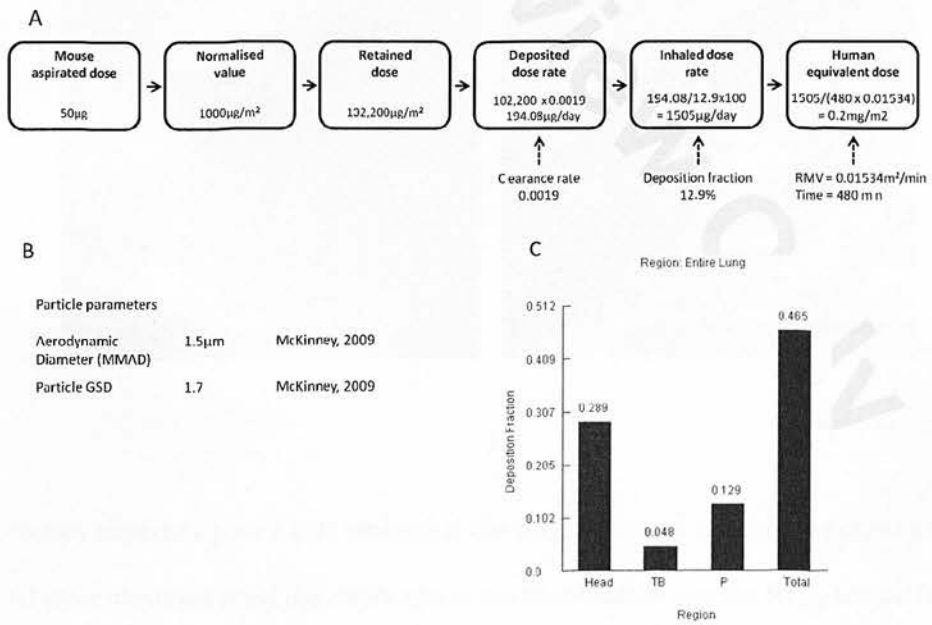

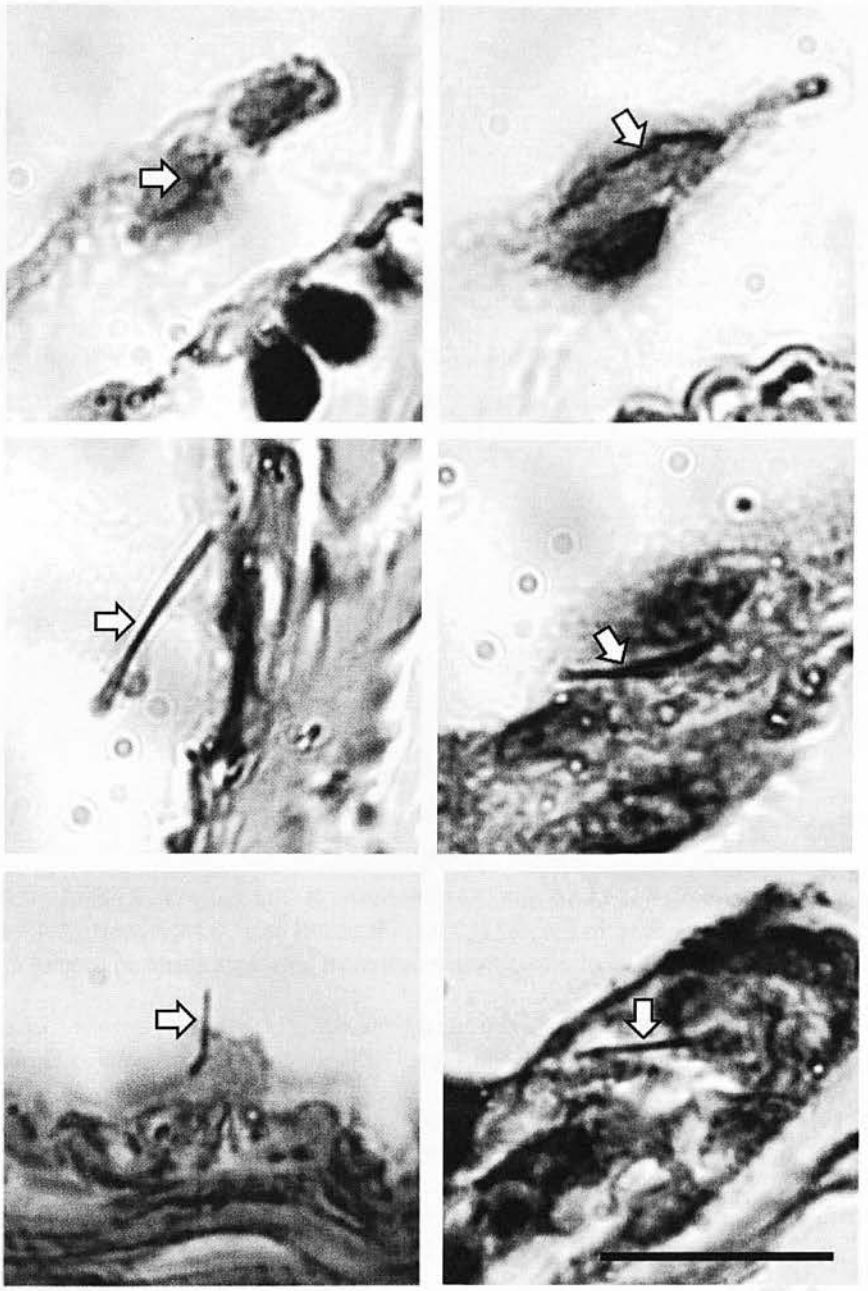

Supplemetary material Figure 2. CNT retained at the diaphragm after pulmonary exposure to CNT.

Long CNT were identified along the diaphragm of the mice treated with the NT_{long} sample (arrows).

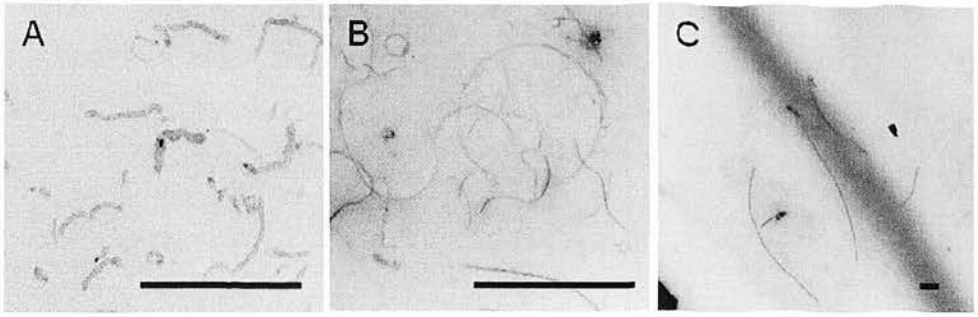

Supplementary Figure 3 TEM images of the CNT panel a) CNT_{tang} b) CNT_{short}, c) CNT_{long}. Scale bar represents 1 micron.

Reference List

1. Rao,G.V., Tinkle,S., Weissman,D.N., Antonini,J.M., Kashon,M.L., Salmen,R., Battelli,L.A., Willard,P.A., Hoover,M.D., and Hubbs,A.F. (2003) Efficacy of a technique for exposing the mouse lung to particles aspirated from the pharynx. *J.Toxicol.Environ.Health A*, **66**, 1441-1452.

2. Stone,K.C., Mercer,R.R., Gehr,P., Stockstill,B., and Crapo,J.D. (1992) Allometric relationships of cell numbers and size in the mammalian lung. *Am.J Respir.Cell Mol.Biol.*, **6**, 235-243.

3. Pauluhn,J. (2010) Multi-walled carbon nanotubes (Baytubes): approach for derivation of occupational exposure limit. *Regul.Toxicol.Pharmacol.*, **57**, 78-89.

4. McKinney,W., Chen,B., and Frazer,D. (2009) Computer controlled multi-walled carbon nanotube inhalation exposure system. *Inhal.Toxicol.*, **21**, 1053-1061.

5. Bide,R.W., Armour,S.J., and Yee,E. (2000) Allometric respiration/body mass data for animals to be used for estimates of inhalation toxicity to young adult humans. *J Appl.Toxicol.*, **20**, 273-290.

6. European Chemicals Agency. Guidance on information requirements and chemical safety assessment - Chapter R.8: Characterisation of dose [concentration]-response for human health. Version 2. http://echa.europa.eu/. 2010.

Ref Type: Generic